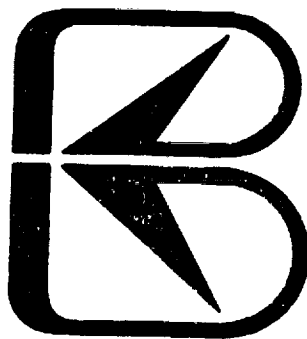


HEAT PIPE DESIGN HANDBOOK


VOLUME I

PREPARED FOR
NATIONAL AERONAUTICS AND SPACE ADMINISTRATION
GODDARD SPACE FLIGHT CENTER
GREENBELT, MARYLAND 20771



B&K ENGINEERING, INC.

SUITE 825, ONE INVESTMENT PLACE
TOWSON, MARYLAND 21204



HEAT PIPE DESIGN HANDBOOK

June 1979

Prepared for
National Aeronautics and Space Administration
Goddard Space Flight Center
Greenbelt, Maryland 20771

Under
Contract No. NAS5423406

Prepared by
B & K ENGINEERING, INC.
Suite 825, One Investment Place
Towson, Maryland 21204

Co-Authored By: Patrick J. Brennan
and Edward J. Kroliczek

F O R W A R D

This Handbook was prepared under NASA Contract NAS5-23406, "Updating of a Heat Pipe Design and Applications Handbook." The work was administered by the Goddard Space Flight Center, Greenbelt, Maryland, and Mr. Roy McIntosh was the NASA Technical Monitor.

The program was conducted by B & K Engineering, Inc., Towson, Maryland, with Mr. Patrick J. Brennan serving as Program Manager and Mr. Edward J. Kroliczek as Principal Investigator.

Special thanks are due Mrs. Dolores M. Vassallo, who typed the entire manuscript; Mr. Nam Nguyen who developed the Heat Pipe Fluid Properties Program; and Mr. Hans U. Mair, who prepared many of the figures and coordinated the final preparation of the Manual. Thanks also go to Mr. Michael R. Huber who helped prepare the first draft.

TABLE OF CONTENTS

VOLUME I

PAGE

CHAPTER 1: INTRODUCTION	1
1.1 HISTORY	1
1.2 PRINCIPLES OF OPERATION	3
1.3 TYPES OF HEAT PIPES	4
1.4 HEAT PIPE OPERATING TEMPERATURE RANGES	5
1.5 ARRANGEMENT OF THE MANUAL	5
References	5
Nomenclature	8
CHAPTER 2: FIXED CONDUCTANCE HEAT PIPE THEORY	12
2.1 HEAT PIPE OPERATION	12
2.2 FUNDAMENTAL CONSIDERATIONS	14
2.3 CAPILLARY PRESSURE	18
2.4 PRESSURE GRADIENTS IN THE LIQUID	21
2.4.1 Viscous Pressure Gradients in the Liquid	21
2.4.2 Body Forces in the Liquid	23
2.5 PRESSURE GRADIENTS IN THE VAPOR	24
2.5.1 Viscous Pressure Gradients in the Vapor	25
2.5.2 Dynamic Pressure Gradients in the Vapor	25
2.5.3 Turbulent Flow and Compressibility Effects	26
2.5.4 Body Forces in the Vapor	27
2.6 CAPILLARY HEAT TRANSPORT LIMIT	27
2.6.1 General Approach	27
2.6.2 Heat Transport Requirement and Heat Transport Capability	32
2.6.3 Closed Form Solution	36
2.7 OTHER HEAT TRANSPORT LIMITATIONS	39
2.7.1 Sonic Limit	39
2.7.2 Entrainment Limit	41
2.7.3 Heat Flux Limit	42
2.8 HEAT TRANSFER	44
References	50

TABLE OF CONTENTS (CONTINUED)

VOLUME I

	<u>PAGE</u>
CHAPTER 3: VARIABLE CONDUCTANCE HEAT PIPE THEORY	52
3.1 TECHNIQUES FOR VARYING HEAT PIPE CONDUCTANCE.	52
3.2 VARIABLE CONDUCTANCE WITH GAS-LOADED HEAT PIPES	58
3.2.1 Flat Front Theory	59
3.2.2 Types of Gas-Loaded Heat Pipes	62
3.2.3 Diffusion Effects	69
3.2.4 Gas Absorption Reservoir.	73
3.2.5 Transients with Gas-Controlled Heat Pipes	74
3.3 OTHER VARIABLE CONDUCTANCE HEAT PIPES	78
3.3.1 Excess Liquid Heat Pipe	78
3.3.2 Liquid Flow Control	80
3.3.3 Vapor Flow Control.	84
References	86
CHAPTER 4: HEAT PIPE DESIGN	88
4.1. DESIGN PROCEDURE	88
4.2 PROBLEM DEFINITION AND DESIGN CRITERIA	89
4.2.1 Operating and Non-Operating Thermal Environment	91
4.2.2 Thermal Load	91
4.2.3 Transport Length	91
4.2.4 Temperature Uniformity and Overall Temperature Drop	92
4.2.5 Physical Requirements	92
4.2.6 Acceptance and Qualification Testing	92
4.2.7 Dynamic Environment	92
4.2.8 Man Rating	92
4.2.9 Thermal/Mechanical Interface	93
4.2.10 Transient Behavior	93
4.2.11 Reliability	93
4.2.12 Temperature Control Sensitivity.	94
4.3 WORKING FLUID SELECTION	94
4.3.1 Operating Temperature Range.	108
4.3.2 Liquid Transport Factor.	108
4.3.3 Liquid Wicking Capability in a Body Force Field.	109

TABLE OF CONTENTS (CONTINUED)

VOLUME IPAGE

4.3.4	Kinematic Viscosity Ratio.	109
4.3.5	Pressure Containment	110
4.3.6	Heat Transfer.	112
4.3.7	Fluid Compatibility.	113
4.4	WICK DESIGN.	116
4.4.1	Basic Properties	116
4.4.2	Typical Wick Designs	130
4.4.3	Methods for Priming Composite Wicks.	145
4.4.4	Typical Secondary Wick Designs	153
4.4.5	Thermal Conductance.	157
4.4.6	Wick Fabrication	160
4.5	CONTAINER DESIGN	161
4.5.1	Material Selection	161
4.5.2	Structural Considerations.	166
4.5.3	Interface Design	180
4.6	FIXED CONDUCTANCE HEAT PIPE DESIGN PROCEDURE	189
	References	191

CHAPTER 5: SAMPLE DESIGN PROBLEMS 194

5.1	SAMPLE PROBLEM A - FIXED CONDUCTANCE HEAT PIPE	194
5.1.1	Step #1 - Problem Definition and Design Criteria	194
5.1.2	Step #2 - Working Fluid Selection.	196
5.1.3	Step #3 - Wick Design Selection.	196
5.1.4	Step #4 - Container Design Selection	202
5.1.5	Step #5 - Evaluate Hydrodynamic Performance Limits	203
5.1.6	Step #6 - Establish Heat Transfer Characteristics	214
5.1.7	Step #7 - Pressure Containment	216
5.1.8	Step #8 - Design Selection	221

TABLE OF CONTENTS (CONTINUED)

VOLUME I

	<u>PAGE</u>
5.2 SAMPLE PROBLEM B -- VARIABLE CONDUCTANCE HEAT PIPE.	223
5.2.1 Step #1 - Problem Definition and Design Criteria.	223
5.2.2 Step #2 - Fixed Conductance Heat Pipe Design Summary.	223
5.2.3 Step #3 - Reverse Conductance	223
5.2.4 Step #4 - Reservoir Sizing; Maximum Sink = -30°C	225
5.2.5 Step #5 - Reservoir Sizing; Maximum Sink = -10°C	226
5.3 SAMPLE PROBLEM C -- GRAVITY ASSIST HEAT PIPE	227
5.3.1 Step #1 - Problem Definition and Design Criteria	227
5.3.2 Step #2 - Heat Pipe Design Summary	227
5.3.3 Step #3 - Evaluated Hydrodynamic Performance Limits	227
5.3.4 Step #4 - Other Heat Transport Limitations	230
CHAPTER 6: HEAT PIPE MANUFACTURING	232
6.1 HEAT PIPE CONSTRUCTION	232
6.2 MANUFACTURING FLOW PLAN	236
6.2.1 Cryogenic Heat Pipes	239
6.2.2 Liquid Metal Heat Pipes	239
6.2.3 Thermal Control Heat Pipes	239
6.3 COMPONENT FABRICATION AND PROCESSING	239
6.3.1 Envelope Preparation	240
6.3.2 Wick Preparation	240
6.3.3 End Closures.	241
6.3.4 Working Fluid	242
6.4 HEAT PIPE PROCESSING AND FABRICATION	242
6.4.1 Cleaning	242
6.4.2 Heat Pipe Assembly and Closure	252
6.4.3 Evacuation and Charging	253
6.4.4 Charge Tube Pinch-Off	257
References	257

TABLE OF CONTENTS (CONTINUED)

VOLUME I

PAGE

CHAPTER 7: MATERIALS COMPATIBILITY	258
7.1 LOW TEMPERATURE CORROSION	258
7.2 HIGH TEMPERATURE CORROSION	262
7.2.1 Oxygen Corrosion	262
7.2.2 Simple Solution Corrosion	262
7.3 EXPERIMENT RESULTS	263
References	273
CHAPTER 8: HEAT PIPE TESTING	275
8.1 HEAT PIPE COMPONENT TESTS	275
8.1.1 Fluid Properties Tests.	275
8.2 WICK PROPERTY TESTS	280
8.2.1 Effective Pumping Radius	280
8.2.2 Permeability	284
8.2.3 Composite Wick Effective Capillary Pumping.	286
8.3 CONTAINER DESIGN VERIFICATION TESTS	288
8.3.1 Hydrostatic Pressure Testing	288
8.3.2 Leak Testing	290
8.4 THERMAL PERFORMANCE TESTS	297
8.4.1 Test Procedure and Data Reduction	297
8.4.2 Test Apparatus	302
8.5 THERMAL CONTROL TESTS	308
8.5.1 Gas-Loaded Heat Pipes	308
References	316
CHAPTER 9: APPLICATIONS	318
9.1 AEROSPACE	318
9.1.1 Flight Experiments -- Sounding Rockets	318
9.1.2 Flight Experiments -- Spacecraft	321
9.1.3 Flight Experiments -- Shuttle	322
9.1.4 Spacecraft Applications	325

TABLE OF CONTENTS (CONTINUED)

VOLUME I

	<u>PAGE</u>
9.2 TERRESTRIAL	329
9.2.1 Permafrost Stabilization	332
9.2.2 Deicing Systems	332
9.2.3 Heat Recovery	335
9.2.4 Electronic and Electrical Equipment	336
9.2.5 Solar Collectors	339
9.3 SPECIAL TYPES OF HEAT PIPES	341
9.3.1 Flat Plate Heat Pipe	341
9.3.2 Flexible Heat Pipe	341
9.3.3 Electrohydrodynamic Heat Pipe	344
9.3.4 Osmotic Heat Pipe	344
9.3.5 Rotating Heat Pipe	347
References	349
CHAPTER 10: BIBLIOGRAPHY	351
<i>Subject Index</i> (Volumes I and II)	369

VOLUME II

CHAPTER 1: FLUID PROPERTIES	1
References	22
CHAPTER 2: COMPUTER CODES	23
References	26
APPENDIX A. International Scientific Units and Conversion Factors	27
APPENDIX B. User's Manual for Heat Pipe Fluid Properties Program . . .	32
APPENDIX B-1. Program Listing for Heat Pipe Fluid Properties Program	43
APPENDIX C. Tabulated Fluid Property Data	54

ILLUSTRATIONS

VOLUME I

<u>Figure</u>		<u>Page</u>
1-1	Schematic Representation of Heat Pipe Operation	4
2-1	Schematic Diagram of the Principle of Operation of a Heat Pipe	13
2-2	Principal Radii of Curvature of Liquid-Vapor Interface	15
2-3	Model of Heat Pipe Hydrodynamics	15
2-4	Effective Pumping Radius in Circular Capillary	19
2-5	Effective Pumping Radius in Open Groove	19
2-6	Trapezoidal Groove Geometry	23
2-7	Conventional Heat Pipe with Uniform Heat Loads	37
2-8	Thermal Model of a Fixed Conductance Heat Pipe	45
3-1	Conductance Model of Heat Pipe	53
3-2	Gas Loaded Variable Conductance Heat Pipe	54
3-3	Schematics of Excess-Liquid Heat Pipes	54
3-4	Schematics of Liquid-Flow Modulated Heat Pipes	57
3-5	Schematics of Vapor-Flow Modulated Heat Pipes	57
3-6	Distribution of Gas and Vapor in a Gas Controlled VCHP	60
3-7	Self-Controlled VCHP with a Wicked, Uncontrolled Reservoir	64
3-8	VCHP with Reservoir Thermally Coupled to the Evaporator	68
3-9	Temperature Distribution in the Condenser for Flat Front and Diffuse Front Models	69
3-10	Effect of Axial Wall Conduction on the Condenser Temperature Profile	71
3-11	Effect of Working Fluid on the Condenser Temperature Profile	72
3-12	Effect of Operating Temperature on the Condenser Temperature Profile	72
3-13	Transient Response of Heat Source with Feedback Controlled Heat Pipe	77
3-14	Variable Conductance through Condenser Flooding with Liquid	79
3-15	Liquid Trap Diode Operation	81
3-16	Liquid Blockage Diode Operation	82

<u>Figure</u>		<u>Page</u>
3-17	Liquid Blockage of Vapor Space	83
3-18	Liquid Blockage with a Blocking Orifice	84
3-19	Vapor Flow Control using External Signal	85
3-20	Self-Controlled Vapor Modulated Heat Pipe	85
4-1	Schematic of Heat Pipe Design Procedure	89
4-2	Liquid Transport Factor: Group 1	96
4-3	Liquid Transport Factor: Group 2	97
4-4	Liquid Transport Factor: Group 3	98
4-5	Wicking Height Factor: Group 1	99
4-6	Wicking Height Factor: Group 2	100
4-7	Wicking Height Factor: Group 3	101
4-8	Kinematic Viscosity Ratio: Group 1	102
4-9	Kinematic Viscosity Ratio: Group 2	103
4-10	Kinematic Viscosity Ratio: Group 3	104
4-11	Saturated Vapor Pressure: Group 1.	105
4-12	Saturated Vapor Pressure: Group 2.	106
4-13	Saturated Vapor Pressure: Group 3.	107
4-14	Liquid Thermal Conductivity for Several Heat Pipe Working Fluids at Saturated State.	112
4-15	Nucleation Tolerance Factors of Several Commonly used Working Fluids	114
4-16	Effect of Gas Build-Up on Temperature Uniformity of Heat Pipe	115
4-17	Typical Capillary Designs	117
4-18	(f·Re) vs. Aspect Ratio for Fully Developed Laminar Flow in Rectangular Tubes	121
4-19	(f·Re) vs. Aspect Ratio for Fully Developed Laminar Flow in Circular Annuli	121
4-20	Typical Wick Designs	131
4-21	Typical Wick Area vs. Flow Optimization...Homogeneous Wicks	138
4-22	Typical Axially Grooved Heat Pipe Designs	142
4-23	Liquid-Vapor Interface in Arteries	144
4-24	Subcooling Section in a Pressure-Primed Wick	147
4-25	Menisci Coalescence for Arterial Venting	149
4-26	Minimum Pore Diameter \bar{D}_p vs. Stress $\bar{\sigma}$ with the Foil Thickness as a Parameter	150

<u>Figure</u>		<u>Page</u>
4-27	Schematic of Jet Pump Assisted Arterial Heat Pipe	152
4-28	Schematic of a Typical Secondary Wick	154
4-29	Resistance Model for a Heat Pipe's Wick System.	154
4-30	Ultimate Tensile Strength of Several Solid Materials.	163
4-31	Material Weight Parameter Versus Temperature for Several Heat Pipe Materials	163
4-32	Thermal Conductivity of Various Metals at Low Temperatures.	167
4-33	Thermal Conductivity of Several Solid Materials	168
4-34	Density of Several Solid Materials.	168
4-35	Heat Pipe Envelope Design Curves.	171
4-36	End Cap Design Detail	175
4-37	End Cap Design Curves, 6061-T6 Aluminum (as Welded)	176
4-38	End Cap Design Curves, 304 Stainless Steel (as Welded).	177
4-39	Typical Fill Tube Design.	178
4-40	Sketch of Heat Flow Through a Heat Pipe	178
4-41	Typical Uniform Heat Source/Sink Interface.	181
4-42	Typical Non-Uniform Heat Source/Sink Interface.	183
4-43	Schematic of Heat Pipe with Non-Uniform Heat Source/Sink Interface.	188
4-44	Typical Heat Pipe Interface Nodal Model	189
4-45	Heat Load Distribution in an Axially Grooved Tube	190
5-1	Sample Problem A - Fixed Conductance Heat Pipe Configuration.	194
5-2	Sample Problem A - Wick Design Options.	197
5-3	Axially Grooved Heat Pipe	224
6-1	Typical Components of a Heat Pipe	235
6-2	Gas-Controlled Variable Conductance Heat Pipe	235
6-3	Typical Wick Designs.	237
6-4	Heat Pipe Manufacturing Flow Chart.	238
6-5	Typical End Cap Weld Joints	254
6-6	Flow Chart--Heat Pipe Evacuation and Charging	256
6-7	Schematic of Heat Pipe Evacuation and Charging Station.	256

8-1	Schematic of Tilting Plate Method for Contact Angle Measurement	276
8-2	Schematic of Optical System for Contact Angle Measurement	277
8-3	Gravity Reflux Compatibility Test Capsule	279
8-4	Variations in Measured Wicking Height as a Function of Measurement Technique in Non-Uniform Wick Material	281
8-5	Advancing Liquid Front Test Set-Up for Determination of r_p and K	283
8-6	Forced Flow Permeability (K) Measurement Apparatus	285
8-7	Test Set-Up for Determination of Permeability by Gravity Flow	286
8-8	Heat Pipe Wick Static Pressure Test Set-Up	287
8-9	Hydrostatic Pressure Test Set-Up - Gas	289
8-10	Hydrostatic Pressure Test Set-Up - Liquid	289
8-11	Leakage Rates	290
8-12	Helium Leak Detection Techniques: Pressurized Pipe	292
8-13	Helium Leak Detection Techniques: Evacuated Pipe	293
8-14	Helium Leak Detection Techniques: Charged Pipe	294
8-15	General Leak Detection for any Working Fluid.	295
8-16	Typical Heat Pipe Performance Test Set-Up	297
8-17	Typical Temperature Profiles Along a Heat Pipe Under Test	298
8-18	Heat Pipe Temperature Drop versus Applied Heat Load	299
8-19	Maximum Heat Load versus Elevation	299
8-20	Types of Evaporator/Condenser Test Set-Ups	303
8-21	Thermal Control Heat Pipe Configurations and Set-Up for Cryogenic Tests	306
8-22	Typical Liquid Metal High Temperature Heat Pipe Test Set-Up	308
8-23	Gas-Controlled Heat Pipe Test Set-Up	309
8-24	Typical Temperature Profile for a Gas-Controlled Heat Pipe	310
8-25	Typical Liquid Trap Diode Heat Pipe Test Set-Up	313
8-26	Typical Liquid Trap Diode Temperature Profile	315
9-1	Ames Heat Pipe Experiment (AHPE)	323
9-2	Advanced Thermal Control Flight Experiment (ATFE).	324
9-3	Heat Pipe Experiment Package (HEPP).	326
9-4	Typical Application of Transverse Flat Plate Heat Pipe	327

<u>Figure</u>		<u>Page</u>
9-5	Primary Thermal Control System Schematic	328
9-6	Communications Technology Satellite	330
9-7	I.U.E. Heat Pipes on Lower Deck of the Spacecraft	330
9-8	Heat Pipe Thermal Control Canister	331
9-9	Heat Pipes on Trans-Alaskan Pipeline	333
9-10	Highway Ramp Heat Pipe Deicing System	333
9-11	Highway Bridge Heat Pipe Deicing System	334
9-12	Solar Powered Airport Runway Heat Pipe Deicing System	334
9-13	Heat Pipe Heat Exchanger	337
9-14	High Power Heat Sink Structure	338
9-15	Heat Pipe Heat Exchanger for Electronic Cabinet Cooling	338
9-16	Solar Electric Power Generation Station Using Heat Pipes at the Focal Axes of Parabolic Reflectors	340
9-17	Cross Section of a Flat Plate Solar Collector that uses Heat Pipes	340
9-18	Flat Plate Heat Pipe	342
9-19	Flexible Heat Pipe	343
9-20	Schematic of an EHD Heat Pipe	345
9-21	EHD Flat Plate Heat Pipe	345
9-22	Simple Osmotic Heat Pipe	347
9-23	Simple Rotating Heat Pipe	348

FigureVOLUME IIPage

1-1	Saturated Vapor Pressure: Group 1	4
1-2	Saturated Vapor Pressure: Group 2	5
1-3	Saturated Vapor Pressure: Group 3	6
1-4	Kinematic Viscosity Ratio: Group 1	7
1-5	Kinematic Viscosity Ratio: Group 2	8
1-6	Kinematic Viscosity Ratio: Group 3	9
1-7	Wicking Height Factor: Group 1	10
1-8	Wicking Height Factor: Group 2	11
1-9	Wicking Height Factor: Group 3	12
1-10	Liquid Transport Factor: Group 1	13
1-11	Liquid Transport Factor: Group 2	14
1-12	Liquid Transport Factor: Group 3	15
B-1	Main Program	36
B-2	Subroutine FITPRO	36
B-3	Subroutine LSQPOL	37
B-4	Subroutine SYMPDS	38
B-5	Subroutine ERROR	38

TABLES

VOLUME I

<u>Table</u>		<u>Page</u>
1-1	Major References	3
3-1	Room Temperature Liquid-Gas Combinations having High Solubility	75
4-1	Problem Definition and Design Criteria	90
4-2	Selected Properties of Heat Pipe Working Fluids	95
4-3	Constants for the Beattie-Bridgeman Equation of State	111
4-4	Generalized Results of Experimental Compatibility Tests	115
4-5	Capillary Properties	118
4-6	Experimentally Determined Wick Properties	122-9
4-7	Wick Selection Criteria	132
4-8	Properties of Typical Homogeneous Wicks	136
4-9	Typical Axially Grooved Heat Pipe Performance	141
4-10	Typical Heat Transfer Coefficients for Heat Pipes	159
4-11	Container Material Fabrication Properties	164
4-12	Maximum Allowable Stresses	165
4-13	Hoop and Axial Stresses	170
4-14	Stress Checklist	172
4-15	Tube Bend Radii	173
5-1	Properties of Selected Fluids	195
5-2	Material Compatibility	195
5-3	Properties of the Wick Design Option	198
5-4	Properties of Candidate Container Material	202
5-5	Wick Design Properties Summary	218
5-6	Heat Pipe Design Summary	222
6-1	Heat Pipe Manufacturers	233
6-2	Heat Pipe Materials Suppliers	234
6-3	Recommended Cleaning Procedure for Aluminum Tubes	248
6-4	Examples of Non-Etch Alkaline Cleaners	249
6-5	Examples of Chromated Deoxidizer Solutions (Immersion Type)	249

<u>Table</u>		<u>Page</u>
6-6	Recommended Cleaning Procedure for Stainless Steel Tubes	251
6-7	Examples of Passivating Solutions	251
7-1	General Compatibility Problems in Heat Pipes.	259
7-2	Relative Electrochemical Activity of some Common Materials Relative to Hydrogen	261
7-3	Generalized Results of Experimental Compatibility Tests	264
7-4	Heat Pipe Life Test Data	265-72
8-1	Variables Affecting Heat Pipe Compatibility Testing	279
8-2	Summary of Leak Detection Techniques	291
8-3	Copper Sulfate/Ethylene Glycol Leak Detection Method for NH ₃ Heat Pipes	296
9-1	Heat Pipe Applications	319
9-2	International Heat Pipe Experiment	321

VOLUME II

1-1	Selected Properties of Heat Pipe Working Fluids	2
1-2	Extrapolated Property Data	16
1-3	Constants for the Beattie-Bridgeman Equation of State	19
1-4	Tabulated Properties	20
1-5	Average Percentage Error for Fluid Property Data	21
2-1	Heat Pipe Computer Codes	24
A-1	Common Units of the International Scientific System	28
A-2	Conversion Factors	29
B-1	Input Data Description	42

INTRODUCTION

1.1 HISTORY

In 1944, Gaugler (1) patented a lightweight heat transfer device which was essentially the present heat pipe. However, the technology of that period presented no clear need for such a device and it lay dormant for two decades. The idea was resurrected in connection with the space program, first as a suggestion by Trefethen (2) in 1962 and then in the form of a patent application by Wyatt in 1963. It was not until Grover and his co-workers (3) of the Los Alamos Scientific Laboratory independently invented the concept in 1963 and built prototypes that the impetus was provided to this technology. Grover also coined the name "heat pipe" and stated, "With certain limitations on the manner of use, a heat pipe may be regarded as a synergistic engineering structure which is equivalent to a material having a thermal conductivity greatly exceeding that of any known metal."

The first heat pipe which Grover built used water as the working fluid and was followed shortly by a sodium heat pipe which operated at 1100°K. Both the high temperature and ambient temperature regimes were soon explored by many workers in the field. It was not until 1966 that the first cryogenic heat pipe was developed by Haskin (4) of the Air Force Flight Dynamic Laboratory at Wright-Patterson Air Force Base.

The concept of a Variable Conductance or Temperature Controlled Heat Pipe was first described by Hall of RCA in a patent application dated October 1964. However, although the effect of a non-condensing gas was shown in Grover's original publication, its significance for achieving variable conductance was not immediately recognized. In subsequent years the theory and technology of gas controlled variable conductance heat pipes was greatly advanced, notably by Bienert and Brennan at Dynatherm (5) and Marcus at TRW (6).

On April 5, 1967, the first "0-g" demonstration of a heat pipe was conducted by a group of engineers of the Los Alamos Scientific Laboratory. This first successful flight experiment overcame the initial hesitation that many spacecraft designers had for using this new technology to solve the ever-present temperature control problems on spacecraft. Subsequently, more and more spacecraft have relied on heat pipes either to control the temperature of individual components or of the entire structure. Past examples of this trend are the OAO-C (7) and ATS-6 (8) spacecraft. Current applications include heat pipe isothermalizers for the I.U.E. (9) and gas-controlled heat pipes on the CTS (10).

A number of different types of fixed conductance and variable conductance heat pipes are being developed or proposed for various shuttle missions including thermal canister (11), LDEF (12), and the Atmospheric Cloud Physics Lab (13), to mention a few. The Galileo Mission will use copper/water heat pipes to cool the radiator fins of the Selenide Isotope Generators (SIG) (14) which provide power for the Jupiter probe. In short, heat pipes have received broad acceptance throughout the aerospace industry.

The early development of terrestrial applications of heat pipes progressed at a much slower pace. In 1968, RCA developed a heat pipe heat sink for transistors used in aircraft transmitters. This probably represented the first commercial application of heat pipes. The early use of heat pipes for electronic cooling was prohibited by cost and the improvements were minimal because of the relatively low power densities of many of the electronic components that were available. Since that time, however, the "Energy Crisis" was experienced and the production of low cost "gravity-assist" heat pipes followed. The most notable single application is the stabilization of the permafrost in the Alyeska Pipeline (15). Heat pipe heat recovery systems also represent a substantial market which is continually growing. The demand for alternate energy sources had led to the development of innovative intermediate and high temperature heat pipes for solar collection (16, 17) and coal gasification (18). In addition, considerable development has also been conducted to utilize heat pipes for the deicing of highways (19), bridges (20), and airport runways (21).

In addition to the advancements realized from the various applications, basic research and development has also continued. Improved geometries have been developed or proposed for axially grooved heat pipes (22, 23). Graded porosity wicks have also been fabricated (24). Several priming techniques for arterial wick designs including venting foils (25), Clausius-Claperton priming (26), and jet-pump assist (27), have evolved. Control techniques including the blocking orifice diode (28), liquid trap diodes and thermal switches (29), vapor modulated variable conductance (30), and soluble gas absorption reservoirs (31), have also been developed. Finally, analytical techniques and computer programs have been developed to predict performance and establish heat pipe designs for many of the systems noted above.

Regarding the literature, the first Heat Pipe Design Handbook (32) was published for NASA Manned Spacecraft Center, Houston in August 1972. Since that time, three International Heat Pipe Conferences have been conducted, two books on heat pipes have been authored, and numerous papers have been written on the subject.

This Design Manual represents an update of the original Design Handbook. The principal reference sources that were used are listed in Table 1-1. A brief discussion of heat pipe operation is given in the next sections and then the arrangement of the Manual is defined.

TABLE 1-1. MAJOR REFERENCES

AUTHOR	TITLE	PUBLICATION DATE	REFERENCE NO.
B. D. Marcus	Theory and Design of Variable Conductance Heat Pipes	April 1972	6
W. B. Bienert and E. A. Skrabek	Heat Pipe Design Handbook	August 1972	32
F. Edelstein and Haslett	Heat Pipe Manufacturing Study	August 1974	33
P. D. Dunn and D. A. Reay	Heat Pipes	1976	34
S. W. Chi	Heat Pipe Theory and Practice	1976	35

1.2 PRINCIPLES OF OPERATION

The basic heat pipe is a closed container which contains a capillary wick structure and a small amount of working fluid which is saturated at operating conditions. The heat pipe employs a boiling-condensing cycle and the capillary wick pumps the condensate to the evaporator. This is shown schematically in Fig. 1-1.

The vapor pressure drop between the evaporator and the condenser is very small; and, therefore, the boiling-condensing cycle is essentially an isothermal process. Furthermore, the temperature losses between the heat source and the vapor and between the vapor and the heat sink can be made small by proper design. Therefore, one feature of the heat pipe is that it can be designed to transport heat between the heat source and the heat sink with very small temperature drop.

The amount of heat that can be transported as latent heat of vaporization is usually several orders of magnitude larger than can be transported as sensible heat in a conventional convective system with an equivalent temperature difference. Therefore, a second feature of the heat pipe is that relatively large amounts of heat can be transported with small light-weight structures.

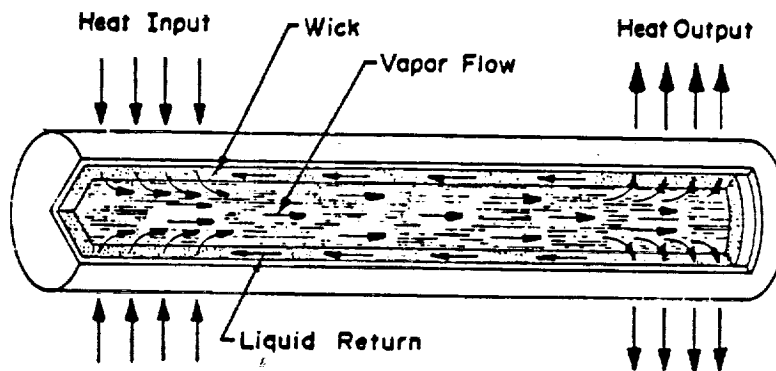


Fig. 1-1. Schematic representation of heat pipe operation

The capillary pumping head is derived from a difference in the radii of curvature of the fluid surfaces in the capillary pores in the evaporator and condenser wick sections. In order for the available capillary pumping head to be able to provide adequate circulation of the working fluid, it must be sufficient to overcome the viscous and dynamic losses of the system and it must compensate for adverse gravity effects. Capillary pumping heads are normally small when compared to the pumping heads available in dynamic systems. Therefore, certain restrictions must be imposed on the application of heat pipes in gravity environments.

1.3 TYPES OF HEAT PIPES

Heat pipes are classified into two general types--"Fixed Conductance" and "Variable Conductance." A fixed conductance heat pipe is a device of very high thermal conductance with no fixed operating temperature. Its temperature rises or falls according to variations in the heat source or heat sink.

It was recognized rather early in the history of the heat pipe research (36) that techniques could be developed which would provide for control of the effective thermal conductance of the heat pipe. This was first envisioned as blocking a portion of the condenser by a non-condensable gas. More recently several other types of control have been developed including liquid blockage and liquid and vapor modulation. Such techniques enable the device to be operated at a fixed temperature independent of source and sink conditions.

1.4 HEAT PIPE OPERATING TEMPERATURE RANGES

In this manual, the operating temperature ranges of the heat pipes are referred to as "cryogenic" (0° to 150°K) (-459° to -189°F), "low temperature" (150° to 750°K) (-189° to $+890^{\circ}\text{F}$), and "high temperature" (750° to 3000°K) (890° to 5432°F). These ranges have been defined somewhat arbitrarily such that the currently known working fluids are generally of the same type within each range, and each range is roughly four times as large as the preceding one. Working fluids are usually elemental or simple organic compounds in the cryogenic range, mainly polar molecules or halocarbons in the low temperature range, and liquid metals in the high temperature range.

1.5 ARRANGEMENT OF THE MANUAL

The new manual consists of two volumes as defined by the Table of Contents. Volume I contains ten chapters which are numbered consecutively and progress from analysis through design fabrication, test and the application of both fixed conductance and variable conductance heat pipes. Chapters 6 and 8 on Manufacturing and Testing are major new additions. Each of the chapters are independent and are arranged to permit the addition of new material as it becomes available.

Volume II contains tabulated property data for most common working fluids and summarizes the available heat pipe computer codes. It is intended to be used as a separate reference for working data.

REFERENCES

1. Gaugler, R. S., "Heat Transfer Device," U. S. Patent 2,350,348, June 6, 1944.
2. Trefethen, L., "On the Surface Tension Pumping of Liquids or a Possible Role of the Candlewick in Space Exploration," G.E. Tech. Info., Serial No. 615 D114, February 1962.
3. Grover, G. M., Cotter, T. P., and Erikson, G. E., "Structures of Very High Thermal Conductivity," J. Applied Physics, 35, 1990 (1964)
4. Haskin, W. L., "Cryogenic Heat Pipe," Technical Report AFFOL-TR-66-228, June 1967.
5. Bienert, W. B., Brennan, P. J., and Kirkpatrick J. P., "Feedback Controlled Variable Conductance Heat Pipes," AIAA Paper No. 71-42, 6th Thermophysics Conf., Tullahoma, TN., April 1971.
6. Marcus, B. D., "Theory and Design of Variable Conductance Heat Pipes," NASA CR 2018, TRW Systems Group, Redondo Beach, California, April 1972.
7. Bienert, W., and Kroliczek, E. J., "Experimental High Performance Heat Pipes for the OAO-C Spacecraft," NAS 5-11271, ASME Paper No. 71-AV-26, Dynatherm Corp., Cockeysville, MD., 1971.

References - Continued

8. Berger, M. E., and Kelly, W. H., "Application of Heat Pipes to the ATS F Spacecraft," ASME Paper No. 73-ENAS-46, Fairchild Space and Electronics Co., Germantown, MD., 1973.
9. "Technical Summary Report for I.U.E. Heat Pipe Test," NAS 5-24063, Dynatherm Corp., Cockeysville, MD., August 15, 1974.
10. Tower, L. K., and Kaufman, W. B., "Accelerated Life Tests of Specimen Heat Pipes from Communication Technology Satellite (CTS)" NASA TM-73846, 1977.
11. Harwell, W., and Canaras, T., "Transient Thermal Response of a Thermal Control Canister," NAS5-22570, Grumman Aerospace Corporation, Bethpage, New York, 1976.
12. Edelstien, F., "Transverse Flat Plate Heat Pipe Experiment," presented at 3rd International Heat Pipe Conference, May 1978.
13. "Final Definition and Preliminary Design Study for the Initial Atmospheric Cloud Physics Laboratory," Final Report for NAS8-3143, General Electric Space Division, January 1977.
14. Strazza, N. P., Brennan, P. J., and Nguyen, N. H., "Copper/Water Axially-Grooved Heat Pipes for RTG Applications," 13th Intersociety Energy Conversion Engineering Conference, August 1978.
15. Waters, E. D., Johnson, C. L., and Wheeler, J. A., "The Application of Heat Pipes to the Trans-Alaska Pipeline," 10th Intersociety Energy Conversion Engineering Conference, August 1975, p. 1496.
16. Bienert, W. B., and Wolf, D. A., "Heat Pipe Applied to Flat-Plate Solar Collectors," Final Report, Dynatherm Corp., Cockeysville, MD., Energy Research and Development Administration, May 1976.
17. Kroliczek, E. J., Yuan S. W., and Bloom, A. M., "Application of Heat Pipes to Ground Storage of Solar Energy," AIAA 12th Thermophysics Conf., Albuquerque, New Mexico, July 27-29, 1977.
18. Ranken, W. A., "Potential of the Heat Pipe in Coal Gasification Processes," Los Alamos Scientific Lab., New Mexico, 1976.
19. Bienert, W. B., "Snow and Ice Removal from Pavements Using Stored Earth Energy," Final Report, Report No. FHWA-RD-75-6, Dynatherm Corp., Cockeysville, MD., May 1974.
20. Ferrara, A. A., and Haslett, R., "Prevention of Preferential Bridge Icing Using Heat Pipes," Report No. FHWA-RD-75-111, Grumman Aerospace Corp., Bethpage, New York, July 1975.
21. Pravda, M. F., "Heating Systems for Airport Pavement Snow, Slush, and Ice Control," Final Report, Report No. FAA-RD-75-139, Dynatherm Corp., Cockeysville, MD., July 1975.
22. Harwell, W., "Analysis and Tests of NASA Covert Groove Heat Pipe," NASA CR-135156, Grumman Aerospace Corp., December 1976.
23. Kroliczek, E. J., and Jen, H., "Summary Report for Axially Grooved Heat Pipe Study," NAS5-22562, B & K Engineering, Inc., May 1977.
24. Eninger, J. E., "Graded Porosity Heat Pipe Wicks," NAS2-8310, TRW Systems Group, Redondo Beach, California, August 1974.
25. Eninger, J. E., "Menisci Coalescence as a Mechanism for Venting Non-condensable Gas from Heat Pipe Arteries," TRW Systems Group, Redondo Beach, California, 1974.

References - Continued

26. Kosson, R., et.al., "Development of a High Capacity Variable Conductance Heat Pipe," AIAA Paper No. 73-728, July 1973.
27. Bienert, W., "Development of a Jet Pump-Assisted Arterial Heat Pipe," Final Report, Dynatherm Corp., Cockeysville, MD., May 6, 1977.
28. Kosson, R., Quadrini, J., and Kirkpatrick, J., "Development of a Blocking Orifice Thermal Diode Heat Pipe," AIAA Paper No. 74-754, 1974.
29. Brennan, P. J., and Groll, M., "Application of Axial Grooves to Cryogenic Variable Conductance Heat Pipe Technology," 2nd International Heat Pipe Conference, April 1976.
30. Eninger, J. E., Fleischman, G. L., and Luedke, E. E., "Vapor-Modulated Heat Pipe Report. Flight Data Analysis and Further Development of Variable-Conductance Heat Pipes," TRW Systems Group, Redondo Beach, California, Materials Technology Dept., June 30, 1975.
31. Saaski, E. W., "Heat Pipe Temperature Control Utilizing a Soluble Gas Absorption Reservoir," NASA CR-137,792, NASA Ames Research Center, February 1976.
32. Skrabek, E. A., "Heat Pipe Design Handbook," Dynatherm Corp., NAS 9-11927, August 1972.
33. Edelstein, F., "Heat Pipe Manufacturing Study," Final Report, NAS5-23156, Grumman Aerospace Corp., August 1974.
34. Dunn, P., and Reay, D. A., "Heat Pipes," University of Reading, England and International Research and Development Co., Ltd., Newcastle-Upon-Tyne, England, 1976.
35. Chi, S. Q., "Heat Pipe Theory and Practice," The George Washington University, McGraw-Hill Book Company, New York, 1976.
36. Cotter, T. P., "Theory of Heat Pipes," Los Alamos Scientific Laboratory Report LA-3246-MS, February 1965.

NOMENCLATURE

The following pages contain a listing of the symbols used throughout this Manual.

The units for each quantity are given in both the SI system and the English Engineering Units.

<u>Symbol</u>		<u>SI Unit</u>	<u>English Units</u>
A	Area	m^2	ft^2
A, A ₀ B, B ₀	Constants for Beattie-Bridgman Equation	--	--
C	Molal Density	kg moles m^{-3}	lb mole ft^{-3}
C _p	Heat Capacity	J $kg^{-1}K^{-1}$	Btu $lbm^{-1}F^{-1}$
D	Diameter	m	ft (in)
D _i	Inside Diameter of Tube	m	ft (in)
D _o	Outside Diameter of Tube	m	ft (in)
F	Body Force	N	lbf
F ₂	Pressure Drop Ratio	--	--
G	Thermal Conductance	W K^{-1}	Btu $hr^{-1}F^{-1}$
G	Gibbs Free Energy	J kg^{-1}	Btu lbm^{-1}
H	Wicking Height Factor	m^2	ft^2
K	Permeability	m^2	ft^2
L	Length	m	ft (in)
MW	Molecular Weight	kg $kmole^{-1}$	lbm $mole^{-1}$
N	Number of Grooves	--	--
N ₂	Liquid Transport Factor	W m^{-2}	W in^{-2}
Q	Axial Heat Flow Rate	W	Btu hr^{-1}
QL	Heat Transport Factor	W m	W in
R	Principal Radius of Curvature	m	ft (in)
R	Thermal Impedance	KW ⁻¹	F W ⁻¹
Re	Reynolds Number	--	--
R _g	Gas Constant (R ₀ /M)	J $kg^{-1}K^{-1}$	ft lbf $lbm^{-1}F^{-1}$
R ₀	Universal Gas Constant	J $kmole^{-1}K^{-1}$	Btu $mole^{-1}F^{-1}$
S	Average Land Thickness	m	in
S	Crimping Factor	--	--
T	Temperature	K	F
V	Velocity	m s^{-1}	ft s^{-1}

<u>Symbol</u>		<u>SI Unit</u>	<u>English Unit</u>
V	Volume	m ³	ft ³
We	Weber Number	--	--
a	Area Per Unit Length	m	ft
a,b,c	Constants for Beattie-Bridgman Equation	--	--
b	Tortuosity Factor	--	--
d	Wire Diameter	m	in
g	Acceleration	m s ⁻²	ft s ⁻²
h	Heat Transfer Coefficient	W cm ⁻² K ⁻¹	Btu ft hr ⁻¹ F ⁻¹
h	Elevation	m	ft
k	Thermal Conductivity	W cm ⁻¹ K ⁻¹	Btu ft hr ⁻¹ ft ⁻² F ⁻¹
k	Spring Constant of Bellows	N m ⁻¹	lbf ft ⁻¹
m	Mass Flow Rate	kg s ⁻¹	lbm hr ⁻¹
p	Pressure	N m ⁻²	(psia) lbf in ⁻²
q	Radial Heat Flu /Unit Length	W m ⁻²	W in ⁻²
r	Radius	m	ft
t	Thickness	m	ft
v _n	Molal Specific Volume	m ³ mole ⁻¹	ft ³ mole ⁻¹
w	Groove Width	m	in
x	Axial Coordinate	m	ft
y	Perpendicular Coordinate	m	ft
z	Characteristic Dimension (in We)	m	in
α	Aspect Ratio	--	--
α	Fraction of Impinging Molecules Sticking to Surface	--	--
α	Groove Half Angle	rad	deg
α	Ostwald Coefficient	--	--
β	Heat Pipe Orientation with Respect to Gravity	rad	deg
γ	Ratio of Specific Heats	--	--
δ	Depth of Grooves	m	in

<u>Symbol</u>		<u>SI Unit</u>	<u>English Unit</u>
ϵ	Porosity	--	--
η	Gravity Factor	--	--
η	Liquid Void Fraction in Gas Absorption Reservoir	--	--
θ	Contact Angle	rad	deg
λ	Heat of Vaporization	J kg ⁻¹	Btu lbm ⁻¹
μ	Viscosity (dynamic)	N s m ⁻²	lbf s ft ⁻²
μ	Mesh Number (of screens)	m ⁻¹	in ⁻¹
ν	Kinematic Viscosity	m ² s ⁻¹	ft ² s ⁻¹
ρ	Density	kg m ⁻³	lbm ft ⁻³
σ	Surface Tension	N m ⁻¹	lbf ft ⁻¹
τ			
ω	Angular Velocity	rad s ⁻¹	deg s ⁻¹

Symbol

Δ	Incremental
∇	Del Operator

Subscripts

a	Active Section of VCHP
a	Adiabatic
b	Bellows
c	Condenser
cond	Condensation
e	Evaporator
en	Envelope
ev	Evaporation
ex	Excess
ext	External
h	Hydraulic
i	Inactive Section of VCHP
int	Internal
j	Counter Index
l	Liquid
max	Maximum
min	Minimum
n	Nucleation Cavity
o	Sink
p	Pore
r	Radial
r	Reservoir
s	Source
st	Storage
t	Total
v	Vapor
vap	Vaporization
w	Wick
	Parallel
⊥	Perpendicular

FIXED CONDUCTANCE HEAT PIPE THEORY

The basic heat pipe theory as first presented by Cotter (1) has remained unchanged. This Chapter presents the theory associated with the hydrodynamic and heat transfer characteristics of fixed conductance heat pipes. The hydrodynamics determines the heat transport limits of heat pipes and the heat transfer theory relates to their temperature control behavior. Basic operating principles are discussed in Section 2.1. The theory that defines a heat pipe's transport capability within the capillary pumping limit is presented in Section 2.2 through 2.6. Other heat transport limitations including sonic, entrainment, and heat flux limits are discussed in Section 2.7. The heat transfer characteristics of a heat pipe which is operating within the heat transport limits are given in Section 2.8.

2.1 HEAT PIPE OPERATION

The principle of operation of a heat pipe is best described by using the simple cylindrical geometry shown in Fig. 2-1. The essential components of a heat pipe are the sealed container, a wick and a suitable working fluid which is in equilibrium with its own vapor. When heat is applied along one section of the pipe (evaporator), the local temperature is raised slightly and part of the working fluid evaporates. Because of the saturation condition this temperature difference results in a difference in vapor pressure which, in turn, causes vapor to flow from the heated section to a cooler part of the pipe (condenser). The rate of vaporization is commensurate with heat absorbed in the form of latent heat of evaporation. The excess vapor condenses at the cooler end and releases its latent heat. During steady-state operation, conservation of energy requires that the amount of heat absorbed is identical to the heat released. Return of the liquid condensate occurs through the wick. The wick provides a flow path for the liquid and is also responsible for the pumping. During evaporation the liquid recedes somewhat into the pores of the wick thus forming menisci at the liquid-vapor interface which are highly curved. On the other hand, condensation occurs mainly on the surface of the wick with corresponding flat menisci. A pressure difference which is related to the radius of curvature exists across any curved liquid-vapor interface in thermodynamic equilibrium. Since the curvature is different at the evaporator from that at the condenser, a net pressure difference exists within the system. This capillary pumping pressure maintains circulation of the fluid against the liquid and vapor flow losses and sometimes against adverse body forces.

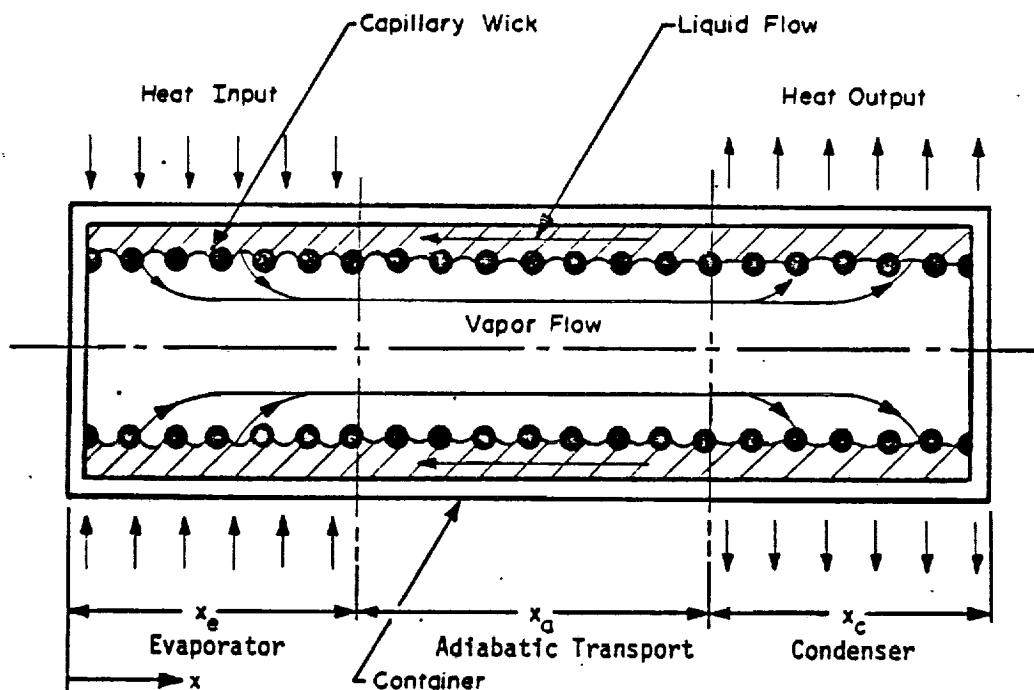


Fig. 2-1. Schematic diagram of the principle of operation of a heat pipe

In addition to an evaporator and condenser, the heat pipe frequently also has an "adiabatic" section. It is characterized by zero heat exchange with the environment. It should also be noted that the heat pipe is not limited to having only one evaporator and condenser but may have several heat input and output areas interdispersed along its length.

As generally conceived, heat pipe theory consists of the description of concurrent hydrodynamic and heat transfer processes. Hydrodynamic theory is used to describe the circulation process. Its most important function is to establish the maximum circulation and, therefore, the maximum heat transport capability of the heat pipe. It also defines and sets bounds upon various factors affecting maximum circulation.

Heat transfer theory deals essentially with the transfer of heat into and out of the heat pipe. It is used primarily to predict overall conductance. Since the heat pipe utilizes evaporation and condensation, it is subject to limitations, such as boiling, which do not apply to solid conductors. Heat transfer theory is used to investigate these limitations and also to provide a model for the overall conductance.

Fundamentally, the internal heat transport process of a heat pipe is a thermodynamic cycle subject to the First and Second Laws. A quantity of heat is applied to the system at a temperature T_1 , and the same quantity of heat is rejected at a lower temperature T_2 . "Work" is generated internally but it is completely consumed in overcoming the hydrodynamic losses of the system. The energy conversion process occurs in the phase change across the curved liquid-vapor interface, where thermal energy is converted to mechanical energy with the appearance of a pressure head. The curvature of this interface adjusts automatically, such that the capillary pumping (the "work" of the system) is just adequate to meet the flow requirement. As with every thermodynamic cycle a finite temperature difference must exist between the heat source and heat sink; that is, heat rejection must occur at a lower temperature than heat addition. In most heat pipes this ΔT associated with the circulation of the working fluid is small compared to other conductive temperature gradients. Nevertheless, even an ideal heat pipe can never be completely isothermal because this would violate the Second Law of Thermodynamics.

Although its performance does have definite limits, the heat pipe generally has very high heat transport capability. The limitations include maximum capillary pumping ability, choking of the vapor flow when it approaches sonic velocity, entrainment of liquid droplets in the vapor stream, and disruption of the liquid flow by the occurrence of boiling in the wick.

2.2 FUNDAMENTAL CONSIDERATIONS

The liquid and the vapor phases of the working fluid are in close contact with each other along the entire length of the heat pipe. Because of the circulation, the pressures in the liquid and vapor are not constant, but vary along the length of the pipe. Furthermore, the pressure difference between the liquid and the vapor is also a function of the location. In order to maintain the pressure balance between liquid and vapor, the interface separating them must be curved. Any curved liquid-vapor interface creates a pressure difference which can be expressed in terms of the surface tension and the principal radii of curvature R_1 and R_2 of the interface as given in Eqs. 2-1 and 2-2 (2). The principal radii of the surface are shown in Fig. 2-2.

$$\Delta p_1(x) = p_v(x) - p_l(x) \quad (2-1)$$

$$\Delta p_1(x) = \sigma \left(\frac{1}{R_1(x)} + \frac{1}{R_2(x)} \right) \quad (2-2)$$

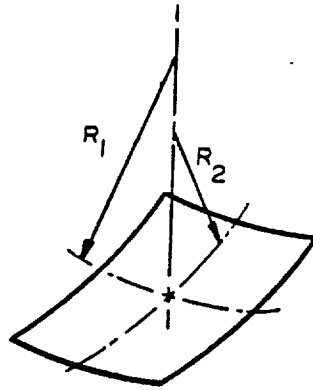


Fig. 2-2. Principal radii of curvature of liquid-vapor interface

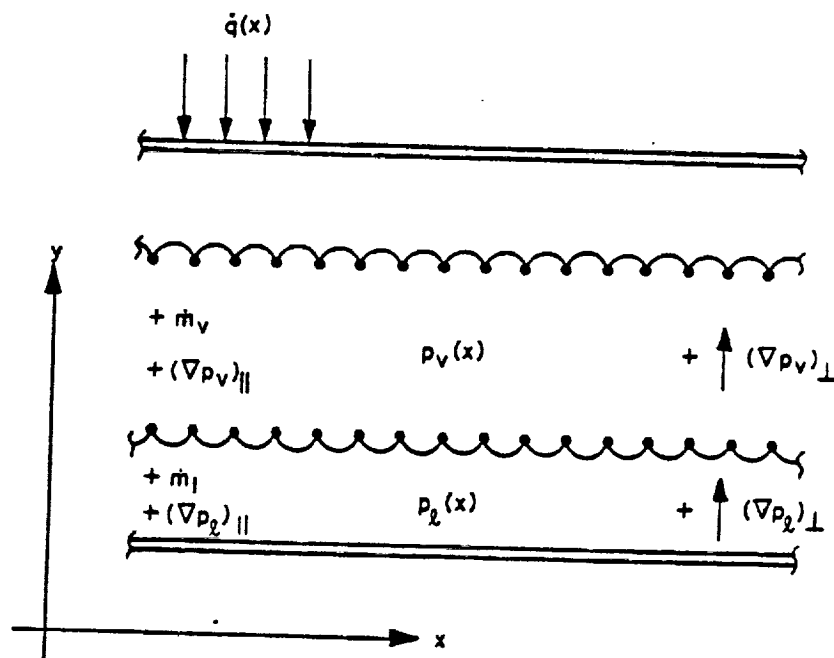


Fig. 2-3. Model of heat pipe hydrodynamics

This interfacial pressure difference Δp_i maintains the pressure balance between vapor and liquid at any point along the length of the heat pipe. Since the interfacial pressure difference varies with location, the radii of curvature of the menisci also vary along the heat pipe. If the interface is concave with respect to the vapor, the pressure in the liquid will be lower than the pressure in the vapor.

The function of the wick in a heat pipe is to provide a medium for establishing curved interfaces between liquid and vapor. It must be emphasized that the interfacial pressure difference Δp_i is independent of the wick properties and is only determined by the curvature of the interfacial surface. Wick properties such as pore size and contact angle only determine the upper bound of the interfacial pressure difference. This upper limit is frequently referred to as "capillary pressure."

In addition to pressure differences between liquid and vapor, there exist pressure gradients within both phases of the working fluid. These gradients are the result of viscous, momentum and body forces. It is convenient to group the gradients according to their origin; that is, whether they are associated with the flow or due to independent body forces.

$$\nabla p = (\nabla p)_{\text{flow}} + \frac{dF}{dV} \quad (2-3)$$

The vector Eq. 2-3 applies to both liquid and vapor phases.

For a heat pipe with one-dimensional liquid and vapor flow, the gradients are given in Eqs. 2-4 and 2-5 in terms of their axial and perpendicular components.

$$(\nabla p)_{||} = \frac{\partial p}{\partial x} = \left(\frac{\partial p}{\partial x} \right)_{\text{flow}} + \left(\frac{dF}{dV} \right)_{||} \quad (\text{Axial}) \quad (2-4)$$

$$(\nabla p)_{\perp} = \frac{\partial p}{\partial y} = \left(\frac{dF}{dV} \right)_{\perp} \quad (\text{Perpendicular}) \quad (2-5)$$

The components of the pressure gradients are shown schematically in Fig. 2-3. This figure also establishes the sign convention adopted throughout this Handbook. The "x" coordinate is parallel to the heat pipe axis, and the "y" coordinate is perpendicular to the axis. The origin of the coordinate system is located at the bottom and at the evaporator end. All vector components, such as pressure gradients, mass flow rates and body forces shall have a positive sign if they are directed in the positive "x" or "y" direction.

In some cases, a different coordinate system may be more convenient. For example, in a heat pipe with multiple evaporators and/or condensers, one might arbitrarily choose one end of the pipe as the origin of the coordinate system. All hydrodynamic equations are actually independent of the choice of the coordinate system. Care must be exercised, however, in selecting the proper sign for all vector components if a different system is selected.

Obviously the assumption of one-dimensional fluid flow does not hold in the areas where evaporation and condensation occur, or in two-or-three dimensional heat pipes such as flat plates, cavities, etc. But for most conventional heat pipes, the one-dimensional model represents a very close approximation.

The body force term in Eqs. 2-3, 2-4, and 2-5 consists of those mass action forces which are independent of flow; e.g., gravity, acceleration, and electrostatic effects. This form of the equation does not include flow dependent body forces such as arise due to magnetic effects which are generally not applicable to heat pipes.

The pressure gradients give rise to mass transfer along the heat pipe. The two axial mass-flow rates, \dot{m}_v and \dot{m}_l are related through the Continuity Eq.

$$\dot{m}_v(x) + \dot{m}_l(x) = 0 \quad (2-6)$$

Eq. 2-6 simply states that during steady-state operation mass accumulation does not occur and vapor and liquid flow rates must be equal in magnitude but opposite in direction.

Finally, the mass flow rates are related to the local heat exchange through the Energy equation:

$$\frac{d\dot{m}(x)}{dx} = \frac{1}{\lambda} \dot{q}(x) \quad (2-7)$$

Eq. 2-7 is a simplified form of the First Law of Thermodynamics where $\dot{q}(x)$ is the rate of heat addition (or removal) per unit length of the heat pipe. It is defined as positive in the case of heat addition (evaporator) and negative for heat removal (condenser). In Eq. 2-7 the effects of conduction in the axial direction are neglected. It is also assumed that sensible heat transport is negligible. In the following sections the various terms used in describing the performance of heat pipes are examined in more detail.

2.3 CAPILLARY PRESSURE

The capillary pressure is defined as the maximum interfacial pressure difference which a given wick/fluid combination can develop, or:

$$\Delta p_{\text{cap}} \equiv (\Delta p_i)_{\text{max}} \quad (2-8)$$

The capillary pressure is related to the surface tension of the liquid, the contact angle between liquid and vapor, and the effective pumping radius through (3):

$$\Delta p_{\text{cap}} = \frac{2 \sigma \cos \theta_c}{r_p} \quad (2-9)$$

With few exceptions, the wicks employed in most heat pipes very often do not have a well defined pore geometry. Therefore, it is common practice to define an effective pumping radius which is determined experimentally and which satisfies Eq. 2-9.

For some well defined wick systems analytical expressions for the effective pumping radius can be found. For a circular pore the meniscus is spherical and the two principal radii of curvature of the surface are equal. Referring to Fig. 2-4 we have:

$$(R_1)_{\text{min}} = (R_2)_{\text{min}} = \frac{r_p}{\cos \theta_c} \quad (2-10)$$

According to Eq. 2-2, the maximum interfacial pressure difference which the capillary forces are capable of handling is:

$$(\Delta p_i)_{\text{max}} = \sigma \left(\frac{1}{R_{1,\text{min}}} + \frac{1}{R_{2,\text{min}}} \right) = \left[\frac{2 \sigma \cos \theta_c}{r_p} \right] \quad (2-11)$$

A comparison of Eqs. 2-9 and 2-11, along with the identity 2-8, yields the results that for circular pores the effective pumping radius r_p is equal to the physical pore radius.

In long, open channels one of the principal radii is infinite. Using Fig. 2-5 the minimum radii can readily be calculated:

$$R_1 = \infty, (R_2)_{\text{min}} = \frac{W/2}{\cos (\alpha + \theta_c)} \quad (2-12)$$

The maximum interfacial pressure difference becomes:

$$(\Delta p_i)_{\text{max}} = \frac{\sigma \cos (\alpha + \theta_c)}{W/2} \quad (2-13)$$

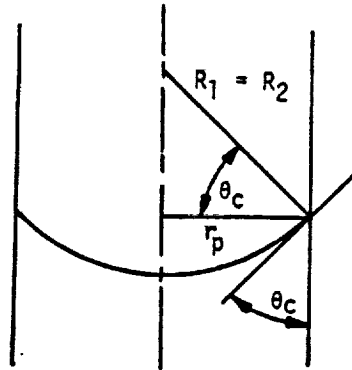
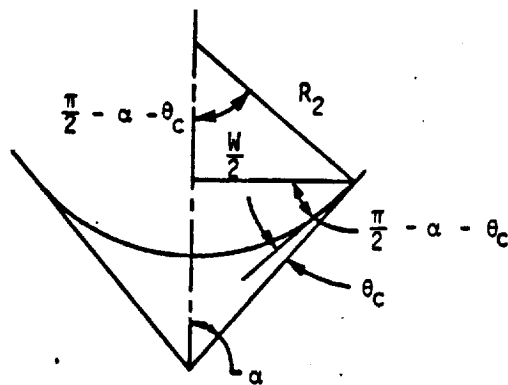


Fig. 2-4. Effective pumping radius in a circular capillary



- θ_c Contact Angle
- α Half Angle of Groove
- W Groove Width
- R_2 Minimum Radius of Curvature (Filled Groove)

Fig. 2-5. Effective pumping radius in an open triangular groove

In the limit of grooves with parallel walls ($\alpha = 0$) Eq. 2-13 reduces to:

$$(\Delta p_f)_{\max} = \frac{2 \sigma \cos \theta_c}{W} \quad (2-14)$$

If we compare Eqs. 2-14 with 2-9 along with the Identity 2-8, we see that the effective pumping radius of a rectangular groove is equal to the groove width while for circular pores it is equal to half the pore diameter. The reason for this difference is, of course, the absence of curvature in the direction of the groove length. Several methods for determining the effective radius of various wick geometries are discussed in the Design Section.

A volume of literature exists on the contact angle, and many inconsistencies in experimental results are reported. However, it has been well established now that much of the "inconsistent" behavior of the contact angle is due to very low level impurities in the liquid or on the surface being wetted. Thus, combinations of scrupulously clean surfaces and very pure liquids will exhibit no difference in advancing and receding contact angles; and water and other liquids with low surface tensions should exhibit a contact angle of approximately zero (2) on all clean metal surfaces with which they do not react chemically. The fact that much larger contact angles are often observed usually indicates the presence of absorbed impurities on the surface, which is generally more difficult to clean than the working fluid.

The capillary pressure, as defined in this section, refers to the maximum interfacial pressure difference which a given wick/liquid combination can sustain; but, as pointed out earlier, the interfacial pressure varies along the heat pipe. The upper and lower limit of the interfacial pressure difference must be known in order to determine the maximum heat transport capability. The lower limit corresponds to the maximum value of the radius of curvature of the meniscus. It can be determined that for wetting liquids the pressure in the liquid cannot exceed that of the vapor. Equal pressures in liquid and vapor correspond to an infinite radius of curvature which is equivalent to a flat meniscus. For nonwetting liquids the pressure in the liquid always exceeds that of the vapor.

The point of pressure equality in liquid and vapor represents a well-defined boundary condition for the integration of the flow equations. Frequently it is located at the end of the condenser of the heat pipe. In the presence of body forces and with complicated

heat pipe geometries or distributed heat loads, this will not necessarily be the case and a careful analysis is required to determine its location. This subject will be discussed in more detail in conjunction with the integration of the flow equations.

2.4 PRESSURE GRADIENTS IN THE LIQUID

The liquid is subjected to a number of different forces, such as the shearing forces associated with viscous flow, the forces associated with momentum in a dynamic system, and the body force effects arising from external force fields. The actions of these forces upon the liquid result in pressure gradients along the heat pipe as was indicated in Eq. 2-3.

The ratio of the dynamic-to-viscous flow pressure gradients in a capillary passage is on the order of magnitude of the Reynold's number determined using the average flow in a pore (4). Since this number will be small with respect to unity for heat pipes, the inertial (dynamic) forces in the liquid will be neglected.

2.4.1 Viscous Pressure Gradients in the Liquid

The pressure gradient resulting from viscous shear forces in an incompressible liquid with laminar flow through a porous media is given directly by Darcy's Law (5):

$$\frac{dp_l}{dx} = \frac{-\mu_l \dot{m}_l(x)}{K A_w \rho_l} \quad (2-15)$$

For some geometries where the physical dimensions of the pores are known and are well defined the permeability K may be expressed in terms of a hydraulic diameter D_h and the porosity of the wick ϵ (6):

$$K = \frac{\epsilon D_h^2}{32} \quad (2-16)$$

The hydraulic diameter D_h is defined as:

$$D_h = \frac{4A}{WP} \quad (2-17)$$

The above definition represents a good approximation for many geometries. More refined expressions for permeability are given in Chapter 4.

For cylindrical passages with diameter D , Eq. 2-17 yields for the hydraulic diameter:

$$D_h = D \quad (2-18)$$

and Eq. 2-15 reduces to a form of Poiseuille's Law:

$$\frac{dp_l}{dx} = \frac{-32 \mu_l \dot{m}_l (x)}{\varepsilon A_w \rho_l D_{h,l}^2} \quad (2-19)$$

For many wick geometries the hydraulic diameter cannot be calculated, particularly for those which involve porous materials. In these cases it is best to resort to experimental measures to obtain a value for the permeability.

When the wicking system consists of uncovered channels as in the case of axially grooved heat pipes there is a shearing effect on the liquid which results from the counterflow of the vapor. This induced liquid loss can be significant particularly at low vapor pressures or at high axial heat loads (e.g. commercial applications). Hufschmidt, et.al. (7) determined an empirical expression for a rectangular groove whose depth is greater than the groove width, which accounts for this loss.

$$\frac{dp_l}{dx} = - \frac{\mu_l \dot{m}_l (x)}{K(x) A_l (x) \rho_l} \left(1 + \frac{\phi^2 \psi}{3} \right) \quad (2-20)$$

This is basically the Hagen-Poiseuille Eq. modified by the term $(\frac{\phi^2}{3} \psi)$ to account for the liquid-vapor shear loss, where ϕ is the groove aspect ratio.

$$\phi \equiv \frac{\text{Groove width at the liquid-vapor interface}}{2 (\text{Groove depth})}$$

For the groove geometry shown in Fig. 2-6

$$\phi = \frac{(R_i + R_o) \sin \frac{\pi}{N} - R_o}{R_i - R_o} \quad (2-21)$$

The parameter ψ is dependent on whether the vapor flow is laminar or turbulent (8).

For laminar vapor flow ($Re_v < 2000$)

$$\psi = \frac{4 (R_i - R_o)}{R_o} \frac{v_v}{v_l} \frac{A_l}{A_v} \quad (2-22)$$

For turbulent vapor flow ($Re_v > 2000$)

$$\psi = 0.0328 \frac{R_i - R_o}{R_o^{0.25}} \frac{A_l}{A_v^{1.75}} \frac{\mu_v^{0.25} \dot{m}_v^{0.75}}{\rho_v v_v} \quad (2-23)$$

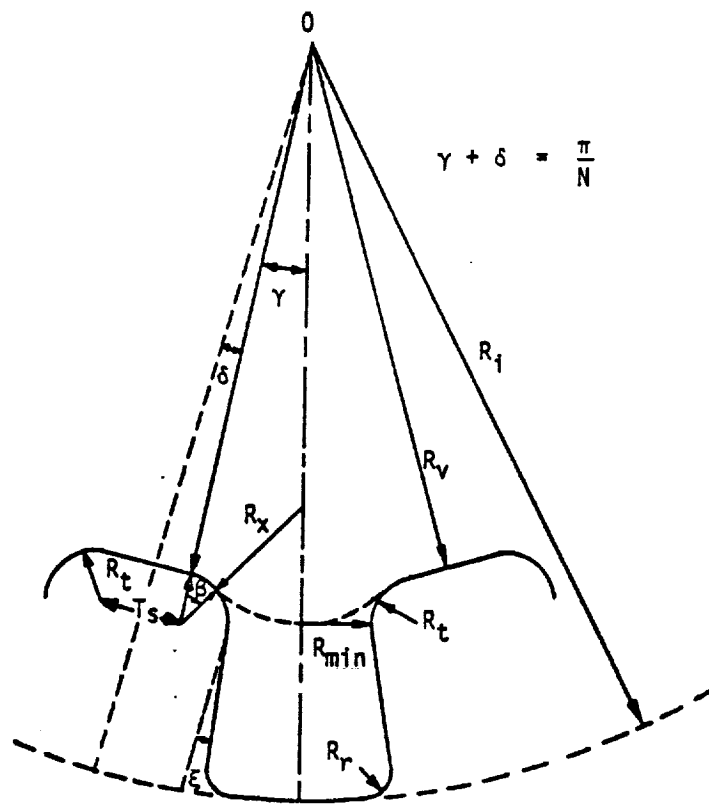


Fig. 2-6. Trapezoidal groove geometry

2.4.2' Body Forces in the Liquid

The pressure gradients in the liquid resulting from body forces can either augment or diminish the gradients associated with viscous flow. The body forces result from external fields which can be applied in any direction with respect to the heat pipe's axis. The body force can be expressed as:

$$\left(\frac{dF}{dV}\right) = \rho_l \vec{g} \quad (2-24)$$

In a gravity field the heat pipe will experience two components of body force.

The obvious body force component is the axial component which is parallel to the mass flow along the heat pipe:

$$\left(\frac{dF}{dV}\right)_{||} = \rho_l g = -\rho_l g \sin \beta \quad (2-25)$$

Depending on whether the condenser ($\beta > 0$) or the evaporator ($\beta < 0$) is elevated, the axial body force component of gravity will either augment or impede the liquid flow. Wherever possible in terrestrial applications, the heat pipe or heat pipe system is oriented to take advantage of the gravity assist to the liquid return. This mode of operation is often referred to as "refluxing." On the other hand as discussed in Chapter 8, heat pipes for aerospace applications are generally tested at a slight adverse elevation to demonstrate performance without any possible gravity assist.

Less frequently considered is the perpendicular body force component:

$$\left(\frac{dF}{dV}\right)_\perp = \rho_l g_\perp = -\rho_l g \cos \beta \quad (2-26)$$

Unlike the axial body force component, this component will always act to the detriment of heat pipe operation. It generates a pressure gradient which is perpendicular to the liquid flow (Eq. 2-5). When integrating the flow equations, it is found that this perpendicular gradient always detracts from the capillary pumping (Section 2.6).

Body forces originate not only from gravity but from any acceleration vector, \vec{g} . A typical, and frequently encountered non-gravitational body force is that resulting from acceleration due to rotation. Its vector is directed in a radial direction from the axis of rotation and its magnitude is:

$$g_{\text{rot}} = \tau \omega^2 \quad (2-27)$$

where τ is the distance between the axis of rotation and the point where the body force is encountered.

2.5 PRESSURE GRADIENTS IN THE VAPOR

The pressure gradients in the vapor will also result from a combination of flow dependent (viscous and dynamic) effects, and flow independent external force fields or body forces. However, the effects on heat pipe performance of the various pressure gradients in the vapor phase are not as easily determined as those of the liquid. Much of this difficulty is attributable to the higher flow velocities in the vapor which make it more susceptible to the effects of mass addition and removal along the length of the heat pipe, to the frequently non-negligible dynamic effects, to the existence of turbulent

flow, and to the compressibility of the vapor. All of these factors combine to produce a condition which does not permit simple, all encompassing, analytical expressions for the vapor pressure losses.

2.5.1 Viscous Pressure Gradients in the Vapor

Under conditions of low axial heat flow and high vapor density, the vapor velocity will be low and viscous forces will predominate. If laminar, non-compressible flow occurs the vapor pressure gradient can also be expressed by Darcy's Law:

$$\frac{dp_v}{dx} = \frac{-\mu_v \dot{m}_v (x)}{KA_v \rho_v} \quad (2-28)$$

Since the vapor passages are generally of a relatively simple geometry compared to those of the liquid, the concept of the "hydraulic diameter" is especially useful. Substituting the hydraulic diameter for the permeability in Eq. 2-16 the pressure gradient in the vapor becomes:

$$\frac{dp_v}{dx} = - \frac{32 \mu_v \dot{m}_v (x)}{\rho_v A_v D_{h,v}^2} \quad (2-29)$$

By the definition of the porosity ϵ --i.e., the ratio of void volume to total volume, the vapor space porosity is unity.

2.5.2 Dynamic Pressure Gradients in the Vapor

Separation of viscous and dynamic effects in the vapor flow is not really possible. If the dynamic effects cannot be neglected, Eq. 2-29 should be replaced by Eq. 2-30 (1):

$$\frac{dp_v}{dx} = - \frac{32 \mu_v \dot{m}_v}{\rho_v A_v D_{h,v}^2} \left[1 + \frac{3}{4} Re_r - \frac{11}{270} Re_r^2 + \dots \right] \quad (2-30)$$

where the radial Reynolds number, Re_r , is defined by:

$$Re_r = \frac{1}{2 \pi \mu_v} \frac{dm_v}{dx} \quad (2-31)$$

The expansion in Eq. 2-30 accounts for momentum changes due to evaporation or condensation. It obviously holds only for small rates of evaporation and condensation, i.e., for $Re_r \ll 1$. The momentum effects cause the pressure gradient in the evaporator to be higher than for viscous shear alone and the pressure gradient in the condenser to be lower due to decelera-

tion of the vapor flow. In the absence of mass addition or subtraction, as for example in the adiabatic section of a heat pipe, Eq. 2-30 reduces to that of purely viscous flow.

For high evaporation and condensation rates the pressure distribution in the vapor is considerably more complex. Analytical solutions exist only for the limiting case, where the radial Reynolds number approaches infinity. For this limit the pressure gradient is given in (9)

$$\frac{dp_v}{dx} = - \frac{S \pi \dot{m}_v}{\rho_v A_v D_{h,v}^2} \frac{d\dot{m}_v}{dx} \quad (2-32)$$

The value for the numerical constant S is 1 for evaporation and $4/\pi^2$ for condensation. Eq. 2-32 predicts approximately 40% recovery of the dynamic head in the condenser.

2.5.3 Turbulent Flow and Compressibility Effects

Little is known about the onset of turbulence in vapor flow with high radial Reynolds numbers. In the adiabatic section, where the radial Reynolds number is zero, fully developed turbulent flow will occur if the axial Reynolds number exceeds 2000. The axial Reynolds number is defined in the usual manner as:

$$Re_v = \left(\frac{D_{hm}}{A\mu} \right)_v \quad (2-33)$$

For turbulent flow the viscous pressure gradient is given by the empirical Blasius Law (5)

$$\frac{dp_v}{dx} = \frac{0.156 \mu_v^2}{\rho_v D_{h,v}^5} Re_v^{7/4} \quad (2-34)$$

In the transition region, i.e., at an axial Reynolds number of approximately 2000, Blasius' Equation holds only approximately and gives slightly different numerical values than the expression for laminar flow.

Compressibility effects can normally be ignored if the Mach number of the flow is less than approximately 0.2. This criterion applies for most heat pipes with the notable exception of liquid metal heat pipes during start-up. If compressibility effects are taken into account, the pressure recovery for high axial fluxes may be as high as 90% (10) instead of the 40% predicted by Eq. 2-32. Compressibility can certainly not be neglected when the vapor flow approaches sonic conditions. This has been considered by Levy (11) (12) and is discussed in Section 2.7.

2.5.4 Body Forces in the Vapor

The theory of body forces acting upon the vapor is identical to that of the liquid. However, because of the large difference in density between liquid and vapor (usually on the order of 10^3) the effect of body forces in the vapor is generally negligible.

2.6 CAPILLARY HEAT TRANSPORT LIMIT

2.6.1 General Approach

The rate of circulation of the working fluid is determined by a balance of capillary pumping, body forces, and viscous and dynamic flow losses. During normal operation the pumping adjusts itself to meet the circulation requirements. But since capillary pumping is limited to a maximum capillary pressure (see Section 2.3) a limit also exists for the rate of circulation and therefore for the heat transport capability.

The capillary limit is the most commonly encountered limit and it relates to the hydrodynamics previously discussed. When the required interfacial pressure exceeds the capillary pressure that the wick can sustain, the pumping rate is no longer sufficient to supply enough liquid to the evaporation sites. Consequently, more liquid is evaporated than replenished and local dryout of the wick occurs.

For high velocity vapor flows, other hydrodynamic limits may restrict the heat transport even before the capillary limit is reached. The sonic limit occurs when the vapor velocity reaches the sonic point. A further increase in the mass flow is not possible without raising the saturation vapor pressure and therefore the vapor temperature. High velocity vapor flow may also interfere with the recirculating liquid causing liquid droplets to be entrained in the vapor and preventing sufficient liquid from returning to the evaporator (entrainment limit). Finally, high local heat fluxes can lead to nucleation within the liquid and result in with dryout (boiling limit). Each one of these limitations will be discussed separately in subsequent sections.

In the preceding sections the pressures and forces affecting the circulation of the working fluid of a one-dimensional heat pipe have been presented in differential form. No restriction has been placed on the distribution of heat fluxes into and out of the heat pipe, its orientation with respect to body forces, and the geometry of the wick. In order to arrive at the capillary limit, i.e., the maximum heat transport capability of a heat

pipe, the hydrodynamic equations must be integrated. In the general case, numerical methods have to be employed and the integration constants must be chosen judiciously, particularly when body forces and more than one evaporator and condenser are involved. The following approach will always lead to the correct capillary limit and can readily be reduced to a closed form solution for uniform geometries.

The pressure distribution in liquid and vapor is obtained by integrating the axial pressure gradients.

$$p_v(x) = \int_0^x (\nabla p_v)_{II} dx + p_v(0) \quad (2-35)$$

$$p_l(x) = \int_0^x (\nabla p_l)_{II} dx + p_l(0) \quad (2-36)$$

The integration is extended from one end of the heat pipe ($x = 0$) to the specific location x . The two integration constants must be determined before the absolute values of each pressure can be calculated. The two pressures are related at every point x through the interface Eq. 2-1.

$$\Delta p_i(x) = p_v(x) - p_l(x) \quad (2-1)$$

Inserting the values for $p_v(x)$ and $p_l(x)$ from Eqs. 2-35 and 2-36 yields:

$$\Delta p_i(x) = \int_0^x [(\nabla p_v)_{II} - (\nabla p_l)_{II}] dx + p_v(0) - p_l(0) \quad (2-37)$$

Equation 2-37 gives the required interfacial pressure difference Δp_i at any axial location x to within the additive constant $[p_v(0) - p_l(0)]$.

In general, Δp_i will vary along the length of the heat pipe and at some point x' will reach its lowest, or minimum value. It is generally assumed that this minimum interfacial pressure difference is zero (equal pressure in liquid and vapor, corresponding to a "flat" meniscus). The integration constant in Eq. 2-37 may then be evaluated as follows:

$$\Delta p_i(x') = 0 \quad (2-38)$$

$$p_v(0) - p_l(0) = - \int_0^{x''} \left[(\nabla p_v)_{||} - (\nabla p_l)_{||} \right] dx \quad (2-39)$$

The interfacial pressure difference becomes:

$$\Delta p_i(x) = \int_{x'}^x \left[(\nabla p_v)_{||} - (\nabla p_l)_{||} \right] dx \quad (2-40)$$

This last equation describes the interfacial pressure difference at any location, x , of the heat pipe with respect to the reference value at x' which, conveniently, is equal to zero.

There always exists at least one axial location x'' at which the interfacial pressure difference $\Delta p_i(x)$ reaches a highest, or maximum value. Once this point has been found (either by numerical or closed form solution) the maximum interfacial pressure difference can be expressed as:

$$(\Delta p_i)_{\max} = \Delta p_i(x'') = \int_{x'}^{x''} \left[(\nabla p_v)_{||} - (\nabla p_l)_{||} \right] dx \quad (2-41)$$

In the hydrodynamic limit the pumping requirement $(\Delta p_i)_{\max}$ is equal to the maximum capillary pressure, Δp_{cap} , which the wick can develop. Proper circulation of the working fluid is assured if the pumping requirement is less than the maximum capillary pressure difference:

$$(\Delta p_i)_{\max} \leq \Delta p_{\text{cap}} \quad (2-42)$$

For a specified wick geometry and heat flux distribution, the above equation will in general be an inequality. In the course of a numerical analysis it establishes the criterion for a selected heat pipe and wick geometry to satisfy the heat transport requirement. Alternately, Eq. 2-42 may be used as an equality to determine the capillary pumping requirement. For most wicks, capillary pumping (pore size) and hydrodynamic pressure gradients are closely related. The approach is therefore to select a particular wick, compute the hydrodynamic requirements according to Eq. 2-41 and then compare the resulting $(\Delta p_i)_{\max}$ with the capillary pumping capability Δp_{cap} . If the inequality is met, the selected wick will be adequate for the given heat transport requirement.

The preceding equations express the capillary pumping requirement in terms of integrated pressure gradients within liquid and vapor. These pressure gradients are related to the corresponding mass flow rates and the body forces. The mass flow rates, in turn, are determined by the heat transport requirement.

For a specified distribution of heat input and output, $\dot{q}(x)$, the mass flow rates of vapor and liquid are obtained by integrating Eq. 2-7.

$$\frac{d\dot{m}(x)}{dx} = \frac{1}{\lambda} \dot{q}(x) \quad (2-7)$$

Integration yields:

$$\dot{m}_v(x) = \int_0^x \frac{1}{\lambda} \dot{q}(x) dx + \dot{m}_v(0) \quad (2-43)$$

The above equation gives the mass flow rate of the vapor for every axial location, x , when the integration is extended from one end of the heat pipe, ($x = 0$), to the point x . Conservation of mass requires that the integration constant, $\dot{m}_v(0)$, goes identically to zero since no vapor enters or leaves the heat pipe. Thus:

$$\dot{m}_v(0) = 0 \quad (2-44)$$

The mass flow rate of the vapor is thus uniquely determined by the heat exchange with the environment. Because of the requirement of mass continuity (Eq. 2-6), the mass flow rate of the liquid is equal in magnitude and opposite in direction to the mass flow rate of the vapor.

$$\dot{m}_l(x) = -\dot{m}_v(x) \quad (2-45)$$

The net axial heat flow rate, \dot{Q} , is related to \dot{m}_v and \dot{m}_l through

$$\dot{Q}(x) = \lambda \dot{m}_v(x) = -\lambda \dot{m}_l(x) \quad (2-46)$$

The theory as presented so far does not include the effects of perpendicular components of the body forces. Since the hydrodynamic model is one-dimensional, perpendicular body forces do not affect the axial pressure gradient. The perpendicular body forces, however, create a pressure gradient within the liquid which is perpendicular

to the flow direction. Referring to Eq. 2-26, this pressure gradient is

$$\left(\frac{dF}{dV}\right)_\perp = \rho_l g_\perp = -\rho_l g \cos \beta \quad (2-26)$$

The total pressure difference in the liquid across the heat pipe becomes:

$$(\Delta p_l)_\perp = \int_0^{D_w} \frac{\partial p_l}{\partial y} dy = -\rho_l g D_w \cos \beta \quad (2-47)$$

where the integration is extended from the bottom ($y = 0$) to the top ($y = D_w$) of the wick. Equation 2-47 holds for any axial location x . This pressure difference creates an additional capillary pumping requirement. The wick must be capable of supporting the interfacial pressure difference between any two locations within the heat pipe (including those at different vertical positions). The datum point of equal pressure in liquid and vapor will always be located at the lower liquid/vapor interface of the heat pipe ($x = x', y = 0 + t_w$). Conservatively, we locate it at the bottom of the heat pipe ($y = 0$). The point of maximum interfacial pressure difference exists at $x = x'', y = D_w$. The additional interfacial pressure difference $p_{i\perp}$ due to the perpendicular pressure gradient is given by:

$$\Delta p_{i\perp} = (p_l)_{\text{top}} - (p_l)_{\text{bottom}} = \rho_l g D_w \cos \beta \quad (2-48)$$

The amount of capillary pumping available for axial flow is therefore reduced and Eq. 2-42 must be modified as follows:

$$\begin{aligned} (\Delta p_i)_{\text{max}} &\leq \Delta p_{\text{cap}} - \Delta p_i' \\ &\leq \Delta p_{\text{cap}} - \rho_l g D_w \cos \beta \end{aligned} \quad (2-49)$$

Most aerospace heat pipes are operated very nearly in the horizontal position. In this case the value of the cosine is close to unity and the additional pumping requirement is approximately

$$\Delta p_{i\perp} \sim \rho_l g D_w \quad (2-50)$$

Although this term can be significant when operation at an adverse elevation is required, in commercial applications where a gravity assist is employed this term will generally have a negligible effect.

2.6.2 Heat Transport Requirement and Heat Transport Capability

Two very useful parameters in heat pipe design are the "Heat Transport Requirement" $(\dot{Q}L)_R$, and the "Heat Transport Capability" $(\dot{Q}L)_{\max}$. A meaningful definition of these parameters requires that:

- (1) Both liquid and vapor regimes are laminar and momentum effects are negligible.
- (2) All geometric properties of the wick and heat pipe and the fluid properties are constant along its length.
- (3) At least one of the following conditions are met:
 - (a) Body forces are absent, and/or
 - (b) The location of minimum (x') and maximum (x'') interfacial pressure are independent of $\dot{Q}(x)$.

The Heat Transport Requirement and the Heat Transport Capability shall be defined by referring to the pressure balance (Eq. 2-42) within the heat pipe. Using the applicable expressions (Eqs. 2-4, 2-20, 2-25, and 2-29) for the pressure gradients in liquid and vapor and Eq. 2-41 for the maximum interfacial pressure difference, the pressure balance (Eq. 2-42) can be written as follows:

$$\Delta p_{\text{cap}} \geq \int_{x'}^{x''} \left[\left\{ - \left(\frac{32 \mu}{\rho A D_h^2} \right) v - \left(\frac{\mu}{K(x) A(x) \rho} \right) \right. \right. \\ \left. \left. \left(1 + \frac{\phi^2}{3} \psi \right) \right\} \frac{Q(x)}{\lambda} + \rho_L g \sin \beta \right] dx \quad (2-51)$$

Using the above assumptions, Eq. 2-51 can then be rearranged to the following simplified form:

$$\Delta p_{\text{cap}} \geq - C \int_{x'}^{x''} \dot{Q} dx + \int_{x'}^{x''} \rho_L g \sin \beta dx \quad (2-52)$$

where the constant C combines the wick and working fluid properties and is given by:

$$C = \frac{1}{\lambda} \left[\left(\frac{32 \mu}{\rho A D_h^2} \right)_v + \left(\frac{\mu}{K A \rho} \right)_l \left(1 + \frac{\phi^2}{3} \psi \right) \right] \quad (2-53)$$

In both Eqs. 2-51 and 2-52, the integration is extended from the point of minimum (x') to maximum (x'') interfacial pressure difference. Further rearrangement of Eq. 2-52 yields:

$$\int_{x''}^{x'} \dot{Q}(x) dx \leq \frac{\Delta P_{cap}}{C} + \int_{x''}^{x'} \frac{\rho_l g \sin \beta}{C} dx \quad (2-54)$$

The left side of Eq. 2-54 represents the heat transport requirement; i.e., the heat transport that is determined by the axial distribution of heat flow rates. The right side of Eq. 2-54 describes the capability of the heat pipe to meet these requirements for a specified orientation.

The Heat Transport Requirement is defined as the integral on the left side of Eq. 2-54:

$$(\dot{Q}L)_R \equiv \int_{x''}^{x'} \dot{Q}(x) dx \quad (2-55)$$

It is completely described by the distribution of heat flow rates which is a function of the application only; it is independent of the heat pipe parameters and its orientation.

If Eq. 2-54 is examined, it is seen that the right side is independent of the heat transport requirement. It contains only physical heat pipe properties; i.e., wick vapor space and fluid properties and the orientation with respect to gravity. This term sets the upper limit for the Heat Transport Factor. It is therefore convenient to define the capability of the heat pipe in a form that permits a direct comparison with the requirements, namely, the heat pipes Heat Transport Capability is defined as:

$$(\dot{Q}L)_{max} \equiv \frac{\Delta P_{cap}}{C} + \int_{x''}^{x'} \frac{\rho_l g \sin \beta}{C} \quad (2-56)$$

From the definition of $(\dot{Q}L)_{max}$, it is observed that it is necessary to impose the restriction that either body forces are absent or x' and x'' are independent of $\dot{Q}(x)$. If at least one of these conditions is not met, $(\dot{Q}L)_{max}$ will be dependent on the heat transport requirement, and Eq. 2-56 will not describe the capability of the heat pipe.

Using the two definitions, Eqs. 2-55 and 2-56, the pressure balance assumes a simple form:

$$(\dot{Q}L)_R \leq (\dot{Q}L)_{\max} \quad (2-57)$$

It must be emphasized again that $(\dot{Q}L)_R$ represents the heat transport requirement as prescribed by the application and $(\dot{Q}L)_{\max}$ represents the heat pipe's transport capability to meet these requirements. The symbol $\dot{Q}L$ for both parameters has not been chosen arbitrarily, both $(\dot{Q}L)_R$ and $(\dot{Q}L)_{\max}$ are given in watt-meter or, more commonly, in watt-inches.

The significance of the Heat Transport Requirement and the Heat Transport Capability can best be realized by examining two special but very important cases.

- (1) The first case involves a heat pipe operating in a 0-g environment. No restrictions shall be placed on the shape of the heat pipe* or the distribution of evaporators and condensers. Once this distribution has been specified, the net axial heat flow rate $\dot{Q}(x)$ can be obtained from Eqs. 2-43 and 2-46. Because of the assumption of uniform wick properties and the absence of dynamic effects and body forces, the interfacial pressure difference $\Delta p_i(x)$ is proportional to $\dot{Q}(x)$. Thus the locations x' and x'' of the lowest and highest value of Δp_i are completely determined by the distribution of $\dot{Q}(x)$ and are independent of the heat pipe's geometry. The Heat Transport Requirement $(\dot{Q}L)_R$ is found from Eq. 2-55 and is also specified by the distribution of heat loads.

The Heat Transport Capability $(\dot{Q}L)_{\max}$ is given by:

$$(\dot{Q}L)_{\max} = \frac{\Delta P_{\text{cap}}}{C} \quad (2-58)$$

*As long as the one-dimensional flow model applies.

Closed form solutions for $(\dot{Q}L)_{\max}$ which apply to this special case may be found in Chapter 4. Any distribution of heat input and output which results in a $(\dot{Q}L)_R$ that is less than $(\dot{Q}L)_{\max}$ for a given heat pipe will be compatible with that heat pipe design.

- (2) Another special, but frequently encountered case is that of a straight heat pipe which is operating in a gravity field and in the "heat pipe mode." The latter shall be defined by the following two conditions:
- (a) The angle between the positive x axis and the horizontal is less than zero, i.e., evaporator above the condenser ($\beta < 0$).
 - (b) The net axial heat flow rate \dot{Q} is positive (or zero) at all axial locations x.

The above conditions state that the net axial heat flow rate should everywhere have a component in the direction of gravity. For this special case it can be shown that the points of maximum and minimum interfacial pressure are always located at the ends of the heat pipe, i.e.,

$$x'' = 0, x' = L \quad (2-59)$$

For this case, the Heat Transport Requirement becomes

$$(\dot{Q}L)_R = \int_0^L \dot{Q}(x) dx \quad (2-60)$$

The Heat Transport Capability Factor $(\dot{Q}L)_{\max}$ can be found by carrying out the integration in Eq. 2-56:

$$(\dot{Q}L)_{\max} = \frac{1}{C} (\Delta p_{\text{cap}} + \rho_2 g L \sin \beta) \quad (2-61)$$

The first term on the right side of Eq. 2-61 represents the Heat Transport Capability Factor in the absence of gravity. Eq. 2-61 can therefore be expressed as:

$$(\dot{Q}L)_{\max} = (\dot{Q}L)_{\max, 0-g} + \frac{\rho_2 g L}{C} \sin \beta \quad (2-62)$$

As expected, operation at an adverse elevation reduces the heat transport capability in 1-g. Equation 2-62 describes the reduction of the "0-g" Heat Transport Capability Factor due to a gravitational hydrostatic head.

2.6.3 Closed Form Solution

Closed form solutions of the hydrodynamic transport equations may be found for several heat pipe cases. One of the most useful is for the conventional heat pipe shown in Fig. 2-7 which has uniform heat addition and removal near the two ends, uniform wick properties along the length, and is operated in the "heat pipe mode" ($\beta < 0$, evaporator above condenser). Additional requirements necessary to obtain explicit closed form solutions are laminar flow in the liquid and the vapor and negligible momentum pressure gradients. Although the requirements of laminar flow and the absence of momentum effects appear restrictive, good design practices usually avoid these regimes altogether. Special modes of operation such as the start-up transients of liquid metal heat pipes are exceptions.

The Heat Transport Capability for this conventional heat pipe is given by Eq. 2-61. Using the appropriate expressions for the constant C (Eq. 2-53) and for Δp_{cap} (Eq. 2-9 in conjunction with Eq. 2-49), $(\dot{Q}L)_{max}$ becomes:

$$(\dot{Q}L)_{max} = \frac{2 K A_w (1 + \eta) \cos \theta_c F_l}{r_p} N_l \quad (2-63)$$

The following abbreviations have been used in Eq. 2-63

- (1) The parameter η is defined as the ratio of the sum of all pressure differences resulting from body forces to the available capillary pressure, i.e.,

$$\eta = - \left[\frac{r_p D \cos \beta}{2 H_2 \cos \theta} + \frac{r_p L \sin \beta}{2 H_2 \cos \theta} \right] \quad (2-64)$$

where H_2 is the Wicking Height Factor, and is a property of the working fluid only:

$$H_2 \equiv \frac{\sigma}{\rho_l g} \quad (2-65)$$

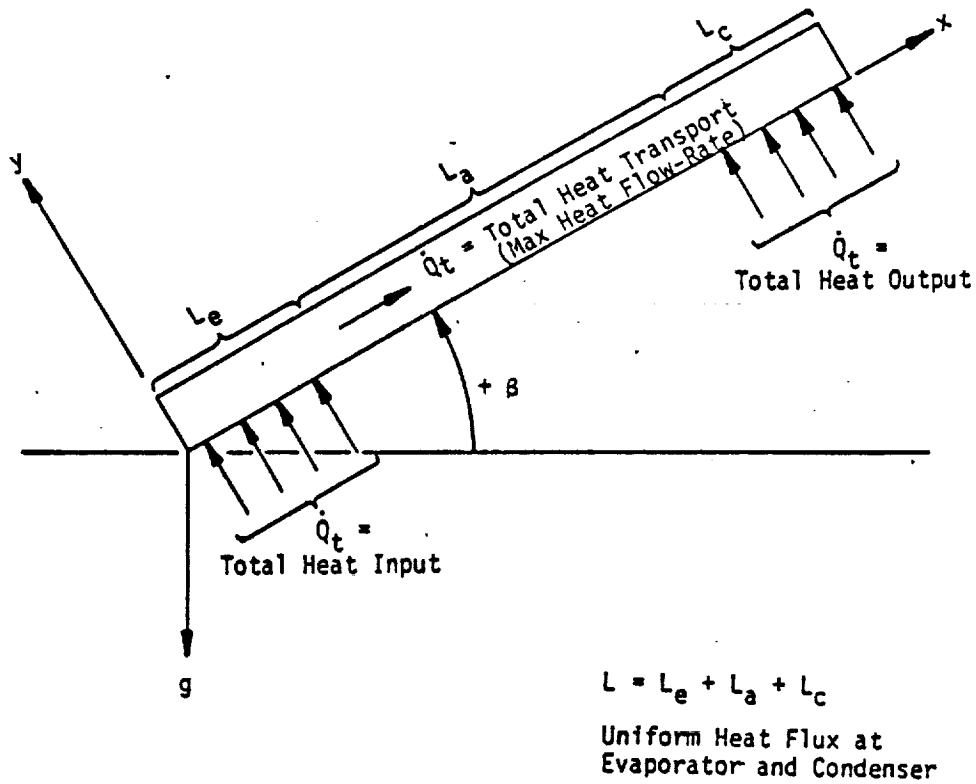


Fig. 2-7. Conventional heat pipe with uniform heat loads

- (2) The parameter F_l represents the ratio of the viscous pressure drop in the liquid to the sum of all the pressure drops in the liquid and vapor.

$$F_l = \frac{\Delta p_l}{\Delta p_l + \Delta p_{lv} + \Delta p_v} \quad (2-66)$$

$$F_l = \frac{1}{1 + \frac{\phi^2}{3} \Psi + \frac{v_v}{v_l} \frac{32 K}{D^2 h_{l,v}} \frac{A_w}{A_v}} \quad (2-67)$$

As mentioned previously, Eqs. 2-63 and 2-67 assume uniform wick properties. In the case of the axially grooved geometry the effect of meniscus recession can have a significant impact on the magnitude of the permeability K and the wick area A_w . However, as shown in Ref. 8 a closed form approximation of these parameters can be obtained. Hence the values of K , A_w , ϕ and ψ in Eqs. 2-63 and 2-67 can be taken as average values. Specific relations which define the value for a given groove geometry are presented in Chapter 4.

- (3) The Liquid Transport Factor N_L is a property of the working fluid and is defined as:

$$N_L = \left(\frac{\rho_L \lambda \sigma}{\mu_L} \right) \quad (2-68)$$

Equation 2-63 defines the maximum heat transport capability of a conventional heat pipe provided that capillary pumping is the limiting factor. Since in most applications the capillary limit is the controlling one, Eq. 2-63 is one of the most useful expressions for the design of heat pipes.

In order to obtain an expression for the maximum amount of heat which the pipe can transport, the Heat Transport Requirement is equated with the Heat Transport Capability Factor:

$$\int_0^L \dot{Q} dx = (\dot{Q}L)_{\max} \quad (2-69)$$

Referring to Fig. 2-7, the axial heat flow rate $\dot{Q}(x)$ can be expressed in terms of the total heat input \dot{Q}_t for each of the following regions:

Evaporator	$0 < x < L_e$	$\dot{Q}(x) = \dot{Q}_t x/L_e$	} (2-70)
Transport Section	$L_e < x < L_e + L_a$	$\dot{Q}(x) = \dot{Q}_t$	
Condenser	$L - L_c < x < L$	$\dot{Q}(x) = \dot{Q}_t (L - x)/L_c$	

If the integration in Eq. 2-69 is carried out, an explicit expression is obtained for the total heat transport or heat flow rate \dot{Q}_t :

$$(\dot{Q}L)_{\max} = \dot{Q}_t \left(\frac{1}{2} L_e + L_a + \frac{1}{2} L_c \right) \quad (2-71)$$

It is often convenient to define an "effective length" of the heat pipe as follows:

$$L_{\text{eff}} = \frac{1}{2} L_e + L_a + \frac{1}{2} L_c \quad (2-72)$$

Eq. 2-69 then becomes:

$$\dot{Q}_t L_{\text{eff}} = (QL)_{\text{max}} \quad (2-73)$$

Using Eqs. 2-63 and 2-73, the following expressions for the maximum heat flow rate \dot{Q}_t is obtained:

$$\dot{Q}_t = \frac{2 K A_w (1 + \eta) \cos \theta_c F_L}{r_p L_{\text{eff}}} N_L \quad (2-74)$$

It is important to note that the definition for the effective heat pipe length (Eq. 2-72) applies only for the special case of uniform heat input and heat output at two separate locations. For non-uniform heat distributions the integral of $(\dot{Q} dx)$ in Eq. 2-69 must be solved in order to obtain an applicable effective length to be used in Eqs. 2-73 and 2-74.

Since in the limit the maximum transport capability must equal the maximum transport requirement, Eq. 2-74 states that a given heat pipe geometry will satisfy any combination of total heat load \dot{Q}_t and effective length L_{eff} which results in the same product (i.e. $(\dot{Q}L)_R$).

2.7 OTHER HEAT TRANSPORT LIMITATIONS

In addition to the capillary pumping limit discussed above, the circulation of the working fluid is restricted by several other limitations.

2.7.1 Sonic Limit

The evaporator section of a heat pipe represents a constant area vapor flow duct with mass addition through the evaporation process. The vapor velocity increases steadily along the length of the evaporator section due to the progressively increasing mass flow and reaches a maximum at the evaporator exit. It can be shown (12) that the limitations of such a flow regime are comparable to that of a converging nozzle with constant mass flow. The evaporator exit corresponds to the throat of the nozzle. The maximum vapor velocity which can exist at the evaporator exit corresponds to Mach 1. This choked flow condition is a fundamental limit on the axial vapor flow in a heat pipe. This limit does

not exclude the possibility of supersonic flow in other sections of the heat pipe. In fact, Kemme (4) (13) has reported supersonic flow conditions in the condenser section of liquid metal heat pipes.

The axial heat flux for the sonic limit is obtained by calculating the mass flow rate at Mach 1:

$$\frac{\dot{Q}}{A_v} = \rho_v \lambda V_s \quad (2-75)$$

where the sonic velocity V_s is given by the familiar equation:

$$V_s = \sqrt{\frac{\gamma R_o T}{M}} \quad (2-76)$$

At the sonic limit, therefore, the mass flow rate per unit area and the corresponding axial heat flux depend only on the properties of the working fluid and in turn the operating temperature. The limiting axial heat flux has, therefore, been included as a derived fluid property in Volume II.

The axial heat flux at sonic conditions must be evaluated using the local temperature at a choking point. This temperature is considerably lower than the stagnation temperature which is measured at the entrance of the evaporator. Stagnation and local static temperature at Mach 1 are related through the expression:

$$T_{\text{stagn}} = T \left(1 + \frac{\gamma - 1}{2} \right) \quad (2-77)$$

For liquid metals with a ratio of specific heats of 5/3 the static temperature is only 75% of the stagnation temperature at $M = 1$. Levy (12) presents an equation which gives the limiting axial heat flux at sonic conditions in terms of the stagnation temperature (the temperature at the beginning of the evaporator) which is often more convenient to use:

$$\frac{\dot{Q}}{A_v} = \frac{\rho_v \lambda V_s}{\sqrt{2(\gamma + 1)}} \quad (2-78)$$

In Eq. 2-78, the fluid properties, e.g., ρ_v , λ and V_s (Eq. 2-76), are evaluated at the stagnation temperature.

When the sonic limit is exceeded, it does not represent a failure as catastrophic as exceeding the capillary limit. When the sonic limit is reached, further increase in the mass flow rate and therefore the heat transfer rate can be realized only by increasing the stagnation pressure upstream of the choking point. To some extent this will occur automatically since the evaporation temperature will rise (and with it the saturation temperature and therefore the stagnation pressure) as soon as the total heat input and total heat output begin to diverge. Operation at or near the sonic limit results in large axial temperature differences along the heat pipe.

2.7.2 Entrainment Limit

Like the sonic limit the entrainment limit is also a characteristic of high axial vapor velocities. Since liquid and vapor are in direct contact along the heat pipe, separated only by the meniscus at the wick, a mutual shear force exists between them. At low relative velocities, this shear force will only add to the viscous drag in both phases. Because the vapor velocity is usually much higher than that of the liquid, the effects will be most noticeable in the liquid phase. If the relative velocity becomes too great, the interface becomes unstable and liquid droplets are torn from the wick and "entrained" in the vapor. The first observation of this phenomenon was made at Los Alamos Scientific Laboratory through the sound made by droplets striking the condenser end of the heat pipe (14).

Entrainment may be described by the Weber number which is a ratio of the inertial forces in the vapor to the tension forces in the liquid surface. The Weber number is defined as:

$$We = \frac{\rho_v \bar{V}^2}{\sigma/z} \quad (2-79)$$

where \bar{V} is the average vapor velocity and z is a characteristic dimension for the surface. A Weber number of unity is generally believed to indicate the onset of entrainment. The corresponding axial heat flux is given by:

$$\frac{\dot{Q}}{A_v} = \left(\frac{\rho_v \sigma \lambda^2}{z} \right)^{1/2} \quad (2-80)$$

There is some uncertainty as to the proper choice of the characteristic dimension z . It is related to the wavelength of the perturbation on the liquid surface. Experimental data seems to indicate that a Weber number of unity corresponds to the onset of entrainment if z is approximately equal to the mesh size of screen material. Insufficient quantitative data is available to resolve the question of whether the characteristic dimension is related to the wire diameter (15) or the wire spacing (16). In the case of an axial groove, the groove's width has been used.

The phenomenon of entrainment reduces the amount of liquid pumped back to the evaporator by prematurely returning it to the condenser. It thus increases the circulation losses (it might be considered an internal "leak") and therein limits the amount of heat flow through the heat pipe.

2.7.3 Heat Flux Limit

In addition to the capillary, the sonic, and the entrainment limits the heat pipe performance is also limited by the evaporator heat flux. Heat is transferred into and out of the heat pipe through the pipe wall and through at least part of the wick. If the radial heat flux becomes excessive, the circulation of the working fluid can be severely affected and the heat transport capability may be controlled by the radial heat flux rather than by the axial heat transport.

The limitation of the axial heat flux is not nearly as well understood as the condenser flooding hydrodynamic limits. There appears to be no limit to the heat flux at the condenser. High condenser heat fluxes contribute, of course, directly to the heat pipe conductance but they do not affect circulation of the working fluid. The evaporator heat flux, on the other hand, has definite upper bounds which limit the axial heat transport. Unlike the previously described limits, which specify a maximum axial heat transport \dot{Q}_t , the heat flux limit specifies the maximum radial evaporator heat flux \dot{q}_e . The two quantities are related through the evaporator area A_e :

$$\dot{Q}_t = \dot{q}_e A_e \quad (2-81)$$

Thus, for a given evaporator geometry, the heat flux limit also specifies the maximum axial heat transport.

The heat flux limit is generally considered to coincide with the onset of nucleate boiling in the wick. Heat is conducted from the heat pipe wall through the wick, and evaporation is assumed to occur at the liquid-vapor interface. This model has been substantiated by extensive experimental evidence (17, 18, 19). When boiling occurs within the wick the presence of the vapor bubbles that are generated reduce the liquid flow area and consequently decrease the transport capability.

With the onset of nucleate boiling, the hydrodynamic equations previously developed are no longer applicable since they were based on one-dimensional, laminar, liquid flow in a fully saturated wick. Breakdown of the mathematical model does not necessarily indicate a heat transfer limit. Since the hydrodynamic theory does not account for boiling in the wick, it is good design practice to define the heat flux limit as the onset of nucleate boiling.

The boiling heat flux limit corresponds to the conduction heat flux which yields a "critical" super heat ΔT_{cr} in the liquid. The boiling heat flux limit is therefore:

$$q_{max} = \frac{K_{eff}}{t_w} \Delta T_{crit} \quad (2-82)$$

where K_{eff} is the effective thermal conductivity of the wick-liquid matrix. Models for the effective conductivity will be discussed in Section 2.8.

Marcus (20) has derived an expression for the critical super heat which is based on criteria similar to those which apply to nucleate boiling from planar surfaces.

$$\Delta T_{crit} = \frac{T_{sat}}{\lambda \rho_v} \left(\frac{2\sigma}{r_n} - (\Delta p_i)_{max} \right) \quad (2-83)$$

where T_{sat} is the saturation temperature of the fluid and r_n is the effective radius of the critical nucleation cavity. This equation is based on the assumption that a bubble of a certain size will grow if its internal vapor pressure associated with the local super-heat exceeds the restraining forces of saturation and capillary pressure. The radius of nucleation cavities, r_n , is a function of the boiling surface. Typical values for smooth surfaces are between 10^{-4} and 10^{-3} cm. For wicked surfaces, little is known about the critical radii of nucleation cavities but an upper bound is certainly the pore size of the wick.

The model predicts very conservative superheat tolerances. Even if the lower bound for the critical radius is used, the calculated critical superheat is sometimes one order of magnitude lower than that actually measured. Marcus (17) attributes this to the absence of a gaseous phase at the nucleation sites because heat pipes contain a highly degassed working fluid. However, incipient boiling is difficult to detect through temperature measurements alone and many wicks which provide for adequate venting of internally generated vapor can tolerate some nucleate boiling without affecting the hydrodynamic limit.

A definite upper heat flux limit exists for every wick, and it is reached when the vapor generated within the wick is at such a high rate that it cannot escape fast enough from the heated surface. This is equivalent to the inability of the capillary forces to replenish liquid at a sufficient rate. Boiling in the wick and the associated heat flux has been the subject of many investigations. Because of the present lack of a consistent theory that has been tested experimentally, it is premature to include this information in a Handbook.

2.8 HEAT TRANSFER

The preceding sections have dealt with the maximum heat transfer capability of the heat pipe. In this section the thermal conductance of a heat pipe which is operating at heat loads which are below the hydrodynamic or heat flux limits is discussed. When operated below any of its limits, the heat pipe is a thermal conductor of extremely high conductance. As mentioned previously, heat pipes are frequently referred to as isothermal devices. In reality their conductance is finite but very high. In defining the conductance of a heat pipe, one has to distinguish between its internal conductance and that of the interfaces between the heat pipe and the environment. Furthermore, the internal conductance is a composite of the radial heat transfer (at the evaporator and the condenser) and of the axial vapor mass transport. In most cases the conductance associated with the heat, input and output mechanisms (external and internal) is much lower than the one associated with axial vapor and liquid transport. The overall conductance is therefore limited by input/output conductances--a fact which is very important in heat pipe design.

The thermal model of a fixed conductance heat pipe is shown in Fig. 2-8. The total thermal resistance, R , is composed of a series of individual resistances:

$$R = R_{\text{ext},e} + R_{\text{en},e} + R_{w,e} + R_{\text{ev}} + R_v + R_c + R_{w,c} + R_{\text{en},c} + R_{\text{ext},c} \quad (2-84)$$

Frequently, it is more convenient to describe the heat transfer characteristics by a conductance, C , rather than a resistance, R . The two are related through:

$$C = \frac{1}{R} \quad (2-85)$$

In terms of conductance, Eq. 2-84 becomes:

$$\frac{1}{C_t} = \frac{1}{C_{\text{ext},e}} + \frac{1}{C_{\text{en},e}} + \frac{1}{C_{w,e}} + \frac{1}{C_e} + \frac{1}{C_v} + \frac{1}{C_c} + \frac{1}{C_{w,c}} + \frac{1}{C_{\text{en},c}} + \frac{1}{C_{\text{ext},c}} \quad (2-86)$$

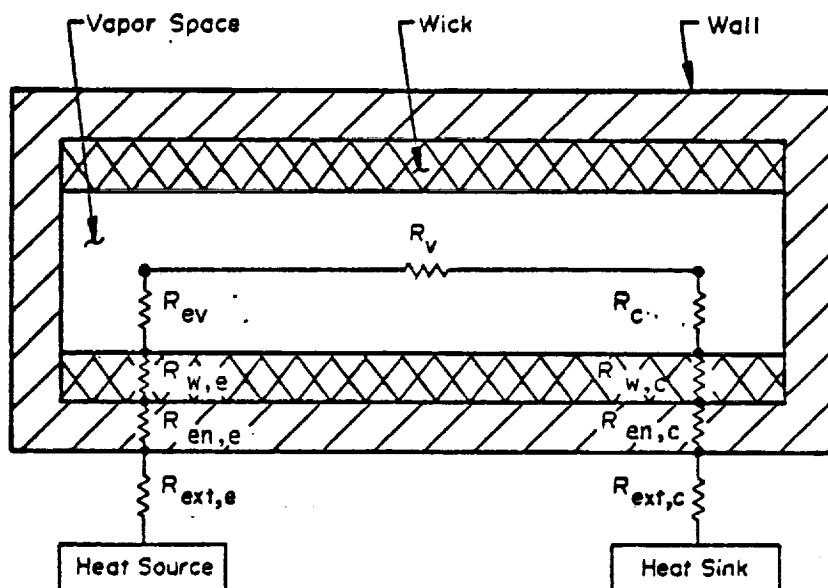


Fig. 2-8. Thermal model of a fixed conductance heat pipe

Each of the individual conductances, which are introduced by Eq. 2-86, are discussed in the following paragraphs.

- (1) $C_{\text{ext},e}$ is the conductance between the heat source and the exterior of the evaporator. Its magnitude will, in general, depend on the application of the heat pipe. When it is closely coupled to the heat source, which is most frequently the case, this conductance is directly proportional to the external evaporator area

$$C_{\text{ext},e} = h_{\text{ext},e} A_{\text{ext},e} \quad (2-87)$$

The external heat transfer coefficient, $h_{\text{ext},e}$ is a function of the type of thermal interface. Representative values can be found in Ref.(21).

- (2) $C_{\text{en},e}$ is the conductance of the heat pipe envelope (wall) at the evaporator. For cylindrical geometries

$$C_{\text{en},e} = \left(\frac{2k A}{D_o \ln \frac{D_o}{D_i}} \right)_{\text{en},e} \quad (2-88)$$

If the wall thickness is small compared to the diameter of the heat pipe this conductance reduces to:

$$C_{\text{en},e} = \left(\frac{k A}{t} \right)_{\text{en},e} \quad (2-89)$$

- (3) $C_{w,e}$ is the conductance of the wick at the evaporator. This term is usually the most difficult one to evaluate and is frequently a very significant contributor to the overall conductance. In the absence of nucleate boiling, heat is transmitted by conduction from the heat pipe wall, through the wick, and to the liquid-vapor interface which is the site of evaporation. This conduction can be expressed in terms of an internal heat transfer coefficient, $h_{\text{int},e}$:

$$C_{w,e} = (hA)_{\text{int},e} \quad (2-90)$$

$$C_{w,e} = \left(\frac{2k_w A_{int}}{D_i \ln \frac{D_i}{D_v}} \right)_{en,e} \quad (2-91)$$

The effective wick conductivity k_w has been the subject of many studies (18, 19, 22). For a porous wick saturated with liquid, the effective conductivity is bracketed by the two extremes of parallel or series conduction paths:

For metallic wicks and insulating liquids, the range of k_w covered by Eq. 2-92 is extremely broad. Conservative design would use the series conduction model. If the liquid conductivity k_2 is much lower than that of the solid, the series model essentially represents the conductivity of a liquid layer whose thickness is weighted by the porosity of the matrix. For the case of an annular wick, Eq. 2-92 gives the correct result if $\epsilon = 1$ is used.

47

circumferential grooves have been used in most of the recently developed high performance heat pipes. References (24) and (25) provide thermal analyses of circumferential grooves.

However, these models are relatively complicated and tend to over-predict the film coefficients, particularly in the evaporator. The best design approach is to use measured values wherever possible. Film coefficients that have been obtained with various fluid/wick combinations are presented in Chapter 4. Generally, these values are for equivalent film coefficients which account for the wick conductance and the evaporation or condensation process as discussed in subsequent paragraphs.

- (4) C_{ev} is the conductance associated with the vaporization process at the liquid-vapor interface. This conductance is usually very large and contributes little to the overall conductance. Cotter (1) derived an expression, based on gas kinetics, for the pressure difference between the sites of vaporization and the bulk of the vapor. This expression, in terms of a heat transfer coefficient is:

$$h = \frac{\alpha \lambda^2 \rho_v}{T} \sqrt{\frac{MW}{R_o T 2\pi}} \quad (2-93)$$

The numerical factor (α) is of the order of 1. It accounts for the probability of condensation of an impinging vapor molecule. The vaporization conductance C_{ev} is obtained from Eq. 2-93 using a relation similar to Eq. 2-90 but based on the area of the liquid-vapor interface. In the case of axially grooved heat pipes, Kamotani (26, 27) has recently developed an expression for an equivalent evaporator film coefficient as

$$h_{eq,e} = \frac{N k_l}{2\pi R_v} \frac{1}{k_f + \frac{k_l \delta}{k_w S}} \quad (2-94)$$

where:

$k_p = 0.0701$ for the evaporator, and 0.0221 for the condenser

- (5) C_v is the thermal conductance associated with the axial vapor flow. This is the only term which, because it is generally proportional to the vapor's viscous pressure drop, is also proportional to the length of the heat pipe. The temperature drop associated with this conductance is proportional to the axial heat flow whereas all other drops are proportional to the radial heat flux.

For a given vapor pressure drop, the corresponding temperature difference can be found. Based on the definition of C_v and using the Clausius-Clapeyron Equation, the following expression is obtained:

$$C_v = \frac{\lambda \rho_v}{T} \frac{\dot{Q}}{\Delta p_v} \quad (2-95)$$

If the vapor flow is predominantly viscous, Δp_v is proportional to \dot{Q} and to the length of the heat pipe. C_v then becomes a true, axial conductance which may be compared directly to that of a solid conductor. Since this term represents the minimum temperature drop that can be experienced, heat pipes have frequently been compared on this basis to other conductors. It must be noted, however, that C_v is only a small contributor to the overall heat pipe conductance and that the comparisons are therefore not very meaningful.

- (6) C_c , $C_{w,c}$, $C_{en,c}$, $C_{ext,c}$ are the conductances at the condenser end of the heat pipe and their expressions are identical to those at the evaporator. If the condenser geometry differs from that of the evaporator, the numerical values will be affected but the preceding Eqs. 2-87 through 2-94 will apply.

A combination of the individual contributions yields the overall conductance as expressed in Eq. 2-86. This expression can be simplified; since the external interfaces are not part of the heat pipe and they should be treated separately. Hence, by excluding the interface conductances and combining the contributions of wall and wick and vaporization or condensation at the evaporator or at the condenser as applicable, a simplified expression for the overall heat pipe conductance can be obtained as

$$\frac{1}{C} = \left(\frac{1}{A h_{eq}} \right)_e + \left(\frac{1}{A h_{eq}} \right)_c + \frac{1}{C_v} \quad (2-96)$$

where A_e and A_c are the external areas of the evaporator(s) and condenser(s) and $h_{eq,e}$ and $h_{eq,c}$ are the respective combined heat transfer coefficients. Since $1/C_v$ is relatively small compared to the other two terms, Eq. 2-96 illustrates that heat pipes are best utilized where heat is to be transported over relatively large distances. The evaporator and condenser conductances are independent of the heat transport length and only the relatively small term $1/C_v$ is proportional to the heat pipe. In the limit for very short heat pipes, this insensitivity to length sometimes renders the heat pipe inferior to solid conductors because the temperature drops at the evaporator and condenser can be significant depending on the radial heat flux.

REFERENCES

1. Cotter, T. P., "Theory of Heat Pipes," Los Alamos Scientific Laboratory Report LA-3246-MS, February 1965.
2. Adamson, A. W., "Physical Chemistry of Surfaces," Interscience Publishers, New York, 1960.
3. Zisman, W. A., "Contact Angle, Wettability and Adhesion," in Advances in Chemistry Series No. 43, Ed. by Fowkes, F. M., American Chemical Society, Washington, D. C., 1965, pp. 1-51.
4. Deverall, J. E., and Kemme, J. E., "High Thermal Conductance Devices Utilizing the Boiling of Lithium and Silver," Los Alamos Scientific Laboratory, LA-3211, 1965.
5. Scheidigger, A. E., "The Physics of Flow Through Porous Media," The MacMillan Co., New York, 1960.
6. Kays, W. M., "Convective Heat and Mass Transfer," McGraw-Hill Book Co., Inc., New York, 1966.
7. Hufschmidt, E. et al., "The Shearing Effect of Vapor Flow on Laminar Liquid Flow in Capillaries of Heat Pipes," NASA TT-F-16601, October 1965.
8. Jen, H. and Kroliczek, E., "Axially Grooved Heat Pipe Study," B & K Engineering, Inc. Report No. BK012-1009 for NASA Goddard Space Flight Center, Contract No. NAS5-22562, July 1977.

9. Knight, B. W. and McInteer, B. B., "Laminar Incompressible Flow in Channels with Porous Walls," LADC-5309.
10. Parker, G. H. and Hanson, J. P., "Heat Pipe Analysis," Advances in Energy Conversion Engineering ASME 1967 Intersociety Energy Conversion Conference, Miami, Florida, August 1967, p. 857.
11. Levy, E. K., "Theoretical Investigation of Heat Pipes Operating at Low Vapor Pressures," Trans. ASME, J. for Industry, November 1968, p. 547.
12. Levy, E. K., "Effects of Friction on the Sonic Velocity Limit in Sodium Heat Pipes," ASME Paper HPT-71-022.
13. Deverall, J. E., Kemme, J. E., and Florschuetz, L. W., "Sonic Limitations and Startup Problems of Heat Pipes," Los Alamos Scientific Laboratories, Report No. LA-4518, November 1970.
14. Deverall, J. E., "Capability of Heat Pipes," Heat Pipe Technology & Manned Space Station Appl. Technical Interchange, Huntsville, Alabama, May 27, 1969.
15. Kemme, J. E., "High Performance Heat Pipes," IEE 1967 Thermionic Specialist Conference, Palo Alto, California, October 1967, pp. 355-358.
16. Wright, P. E., Final Report for ICICLE Feasibility Study, Contract NAS5-21039, RCA, Camden, New Jersey.
17. Marcus, B. D., "Theory and Design of Variable Conductance Heat Pipes," NASA CR-2018, April 1972.
18. Soliman, M. M., Grauman, D. W., and Berenson, P. J., "Effective Thermal Conductivity of Saturated Wicks," ASME Paper No. 70-HT/SpT-40, 1970.
19. Ferrel, J. K., and Alievitch, J., "Vaporization Heat Transfer in Capillary Wick Structures," Chemical Eng. Prog. Symposium Series V66, Heat Transfer, Minneapolis, Minn., 1970.
20. Marcus, B. D., "On the Operation of Heat Pipes," TRW Report 9895-6001-TU-000, May 1965.
21. Wright, J. P., "Thermal Investigation and Analytical Modeling of Heat Pipe Thermal Interface Techniques," Rockwell International, June 1973.
22. Goring, R. L. and Churchill, S. W., "Thermoconductivity of Heterogeneous Materials," Chemical Engineering Prog. 57, No. 7, 53-59 (1961).
23. Saaski, E. W., and Hamasaki, R. H., "Study of a High Performance Evaporative Heat Transfer Surface," NASA CR 152008, May 1977.
24. Berger, M. E., and Feldman, K. T., Jr., "Analysis of Circumferentially Grooved Heat Pipe Evaporators," ASME Paper 73-Wa/Ht-13, 1973.
25. Schneider, G. E., and Yovanovich, M. M., "Thermal Analysis of Trapezoidal Grooved Heat Pipe Walls," Report to Department of Communications, Ottawa, Ontario, 1975.
26. Kamotani, Y., "Evaporator Film Coefficients of Grooved Heat Pipes," 3rd International Heat Pipe Conference, 1978.
27. Kamotani, Y., "Thermal Analysis Program for Axially Grooved Heat Pipes; Its Description and Capabilities," to be published.

VARIABLE CONDUCTANCE HEAT PIPE THEORY

The conventional fixed conductance heat pipe discussed in Chapter 2 is a completely passive device. It is not restricted to a fixed operating temperature but adjusts its temperature according to the heat load and the sink condition. Although its thermal conductance is very high, it is nevertheless a nearly constant parameter.

However, there are many potential heat pipe applications in which a specific operating temperature range is desired along certain portions of the pipe even though source and sink conditions are changing. In those cases, it becomes necessary to actively or passively control the heat pipe so that it maintains the desired operating temperature range. Temperature control is obtained by varying one or several of the conductances that make up the heat pipe's overall thermal conductance. Similarly there exist many applications where heat pipe operation as a (1) thermal diode or (2) a thermal switch is required. In either case, the objective is for the heat pipe to operate at the limits of variable conductance as an effective heat conductor or as a thermal insulator. Again, it is necessary to introduce an active or passive control feature to effect this behavior. Traditionally, variable conductance has been used to describe control provided by "gas-loaded" heat pipes. As discussed in the next section there are four types of variable conductance pipes: (1) gas-loaded heat pipes; (2) excess-liquid heat pipes; (3) liquid flow-modulated heat pipes; and (4) vapor flow-modulated heat pipes.

This chapter discusses the different methods for obtaining variable conductance operation and the associated theory. Fixed conductance heat pipe theory is still applicable to determine the transport capability of the heat pipe. Variable conductance theory, as presented in Sections 3.2 through 3.4, consists of the analysis and mathematical models that define the particular control technique and the associated variable conductance operation of the heat pipe.

3.1 TECHNIQUES FOR VARYING HEAT PIPE CONDUCTANCE

The basic conductance model of a heat pipe is presented in Section 2.8. For ease of reference, a slightly simplified model is shown in Fig. 3-1 in which the evaporator and condenser conductances are lumped together. In this model, C_e represents the conductance between the heat source and the vapor in the heat pipe, C_v is the internal resistance

along the length of the pipe, and C_c is the conductance between the heat pipe vapor and the ultimate heat sink. The overall conductance C between the source and the sink is given by Eq. 3-1.

$$C = \frac{1}{\frac{1}{C_s} + \frac{1}{C_c} + \frac{1}{C_v}} \quad (3-1)$$

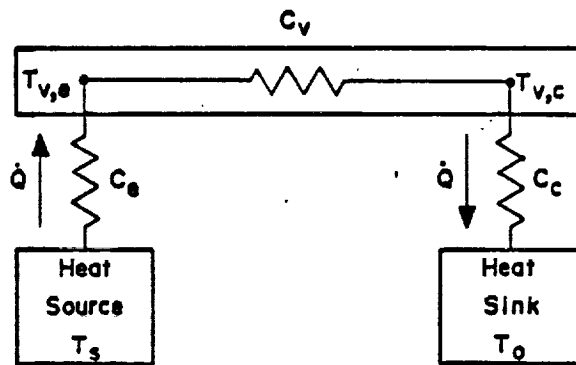


Fig. 3-1. Conductance model of heat pipe

In principle, a variable heat pipe conductance can be achieved by modulating any one or several of the individual conductances that make up the overall conductance. A number of techniques exist to achieve variable conductance, and they can be grouped into the following four categories:

1. Gas-Loaded Heat Pipe

This technique consists of introducing a fixed amount of non-condensable gas into the heat pipe which during operation will form a "plug" which blocks the vapor flow. A schematic of a gas-loaded VCHP is presented in Fig. 3-2. Typically, a reservoir is added to accommodate the gas when "full-on" heat pipe operation is required. As vapor flows from the evaporator to the condenser, it sweeps the non-condensing gas which accumulates in the cold end of the heat pipe. The gas therein forms a barrier to the vapor flow and effectively "shuts off" that portion of the condenser which it fills. The length of the plug and therefore the condenser conductance depends on such factors as the system's operating temperature, heat source and sink conditions, reservoir size

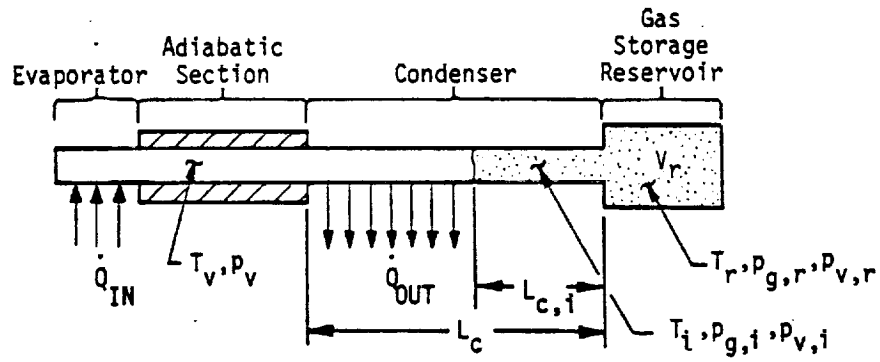


Fig. 3-2. Gas-loaded variable conductance heat pipe

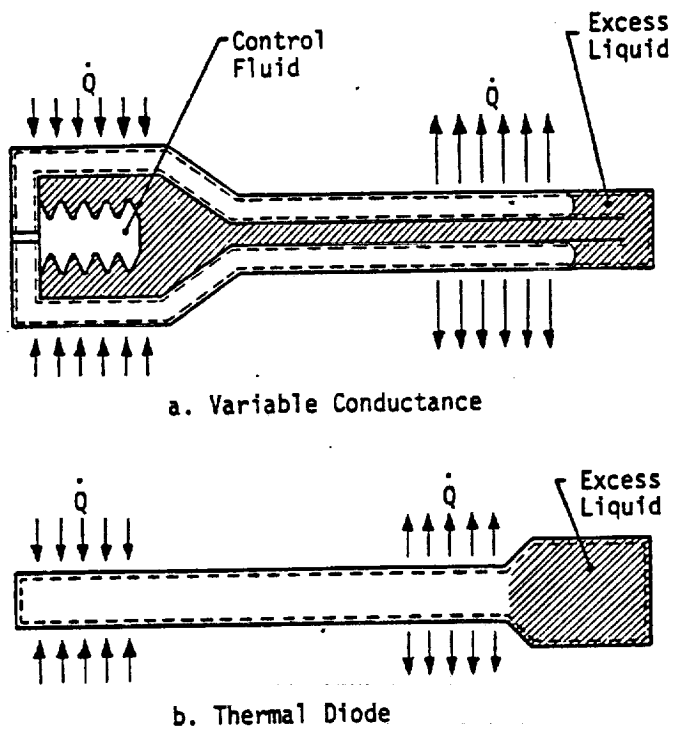


Fig. 3-3. Schematics of excess-liquid heat pipes

and reservoir temperature, etc. The influence of these parameters as well as the various methods for obtaining gas-loaded VCHP control are discussed in the next section. It should also be noted that gas blockage can also be used to effect diode and switching operations; however, the transients associated with the "shutdown" or "switching" operations can be prohibitive with a gas-loaded system (1).

2. Excess-Liquid Heat Pipe

This approach is analogous to the "gas-loaded" heat pipe except that excess liquid accumulates as a slug in the condenser end rather than a non-condensable gas. Control with this technique tends to be less sensitive to variations in sink conditions; however, the actual designs can be more difficult to implement. Fig. 3-3a shows one method for obtaining variable conductance with excess liquid. Again a reservoir is utilized and it is located inside the heat pipe envelope. The effective volume of the reservoir is varied by means of a bellows which contains an auxiliary fluid in equilibrium with its vapor. Adjustment of the bellows to changes in system temperature changes the reservoir volume therein allowing the excess liquid to move into or out of the condenser.

Fig. 3-3b illustrates a thermal diode heat pipe which utilizes liquid blockage to "shut off" the heat piping action in the reverse direction. In the normal forward mode operation the excess liquid is swept into the reservoir at the condenser end. When conditions arise (e.g. an increase in sink temperature due to orbital conditions, etc.) which cause the condenser temperature to rise above the evaporator, the direction of vapor flow is reversed. The excess liquid is then driven from the reservoir into the normal evaporator section thus blocking the vapor flow and inactivating that section for heat rejection. Thus, the heat source is insulated from the hot condenser end with the result that the heat piping action is only effective in the forward mode.

3. Liquid Flow Control

Liquid flow control involves either interrupting or impeding the condensate return in the wick in order to "dry-out" part or all of the evaporator. This technique achieves control of the evaporator conductance by affecting the

circulation of the working fluid and therein creating a hydrodynamic failure in the evaporator section.

Liquid flow control is limited generally to providing "on - off" control for diodes and thermal switches when the heat source is a dissipative one since the hydrodynamic failure will result in a non-uniform temperature distribution at the heat source. However, for fixed temperature sources, continuous modulation of the heat pipe conductance by varying the wick flow resistance is acceptable since partial evaporator dryout simply results in reduced heat transfer into the pipe.

Fig. 3-4a shows a liquid trap diode heat pipe for aerospace application. In this case, a wicked reservoir is located at the evaporator end. This reservoir does not communicate with the main wick; therefore, when the temperature gradient is reversed, liquid evaporates at the hot side of the pipe and then condenses and is trapped within the reservoir. As a result, the wick becomes partially saturated and ultimately the condensate cannot return to the heat input section and the heat piping action is effectively shut "off."

A gravity operated diode heat pipe is shown in Fig. 3-4b. Here a reversal of the temperature gradient causes the liquid to collect at the bottom of the pipe where it cannot be pumped back up against the gravitational force.

4. Vapor Flow Control

Vapor flow control involves throttling or interrupting the vapor as it proceeds from the evaporator to the condenser. This creates a pressure drop between the two sections and hence a corresponding temperature drop. A schematic of a vapor modulated variable conductance heat pipe is given in Fig. 3-5a. A bellows and auxiliary fluid are used to effect the throttling action. An increase in heat load or source temperature causes a rise in the vapor temperature which in turn causes the control fluid to expand and partially close the throttling valve therein creating a pressure differential. This method of control is substantially limited by the fact that the evaporator to condenser pressure differential must not exceed the capillary

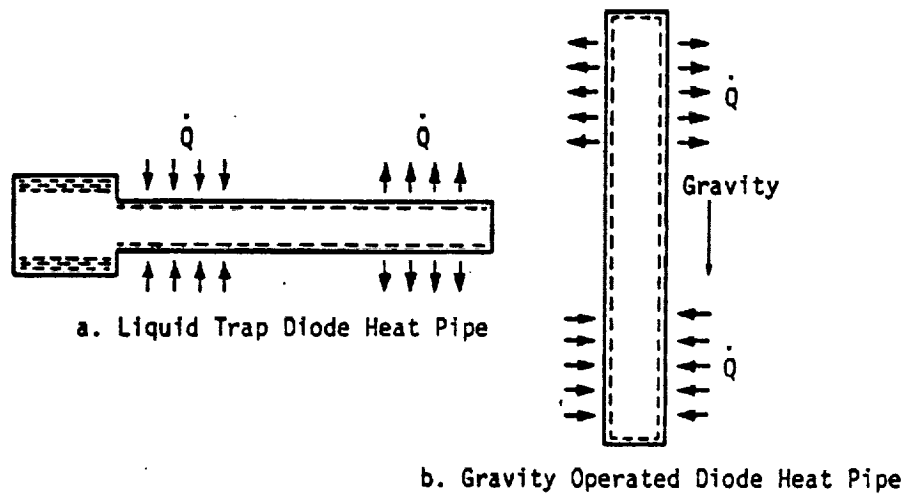


Fig. 3-4. Schematics of liquid-flow modulated heat pipes

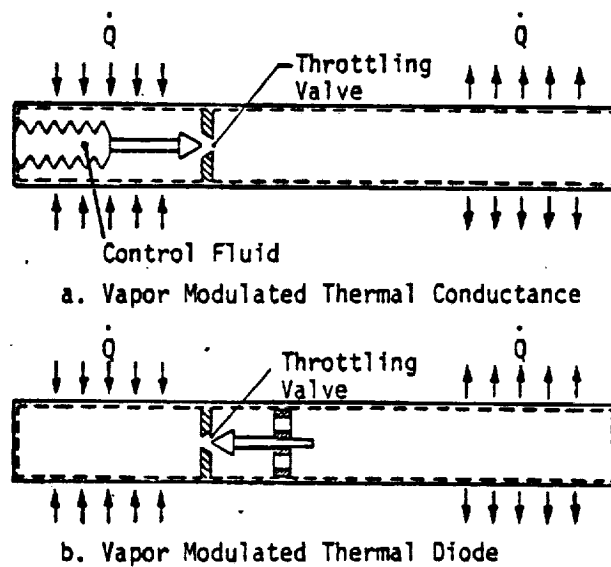


Fig. 3-5. Schematics of vapor-flow modulated heat pipes

pressure developed by the fluid/wick combination. If the valve arrangement is reversed to that shown in Fig. 3-5b, a diode action is achieved when conditions arise which reverse the normal temperature gradient.

3.2 VARIABLE CONDUCTANCE WITH GAS-LOADED HEAT PIPES

The principle of this technique is the formation of a gas plug at the condenser end of the pipe which prevents vapor from condensing in the part blocked by the gas. This plug is the result of introducing a fixed amount of a non-condensable gas into the heat pipe. In the absence of circulation of the working fluid (i.e., without heat transport) the gas is uniformly distributed within the vapor space except for a small amount which is dissolved in the liquid phase of the working fluid. During operation a steady flow of vapor exists from the evaporator to the condenser. The gas is swept by the vapor to the condenser. Unlike the vapor, it does not condense but forms a "plug" at the condenser end of the heat pipe.

Variable conductance variation through the addition of a non-condensable gas is particularly attractive because it accomplishes passive control of the vapor temperature. In a conventional (fixed conductance) heat pipe, the vapor temperature adjusts itself in order to meet the heat rejection requirements for a given sink condition. Thus, if the heat load and/or sink temperature increases, the vapor temperature will also rise. In a gas-loaded heat pipe, the fixed amount of gas occupies part of the condenser; the length of the gas plug being dependent on the vapor (and sink) temperature. If the heat load is increased, the vapor temperature tends to rise as in the fixed conductance heat pipe. However, the corresponding increase in vapor pressure of the working fluid compresses the gas plug, thereby increasing the size of the active condenser. This results in a higher conductance which effectively opposes the tendency of the vapor temperature to increase. Similarly, if the heat source and/or sink temperature decreases, the vapor temperature and pressure tend to drop which permits the gas plug to expand, the conductance of the heat pipe to decrease, and the vapor temperature decreases to be minimized. A gas-loaded heat pipe therefore reduces fluctuations of the operating temperature and behaves as a self-controlled VCHP.

3.2.1 Flat-Front Theory

A simplified model of a gas-loaded heat pipe whose condenser is partially blocked is shown in Fig. 3-6. The corresponding gas and vapor distributions that apply during operation are also presented. As indicated in this figure, the interface between the gas and vapor is not a sharp one because it is controlled by mass diffusion and axial conduction effects which are discussed in a later section. However, a good understanding of the operational characteristics, and certainly preliminary designs, can be obtained by utilizing a mathematical model which assumes that a "flat-front" exists between the vapor and gas.

The following assumptions are employed with this model:

- (1) Steady state conditions exist.
- (2) The interface between the active and shut-off portions of the pipe is very sharp.
- (3) The total pressure is uniform throughout the pipe (i.e. the vapor temperature drop is negligible).
- (4) Axial conduction can be neglected.
- (5) The gas-vapor mixture obeys the Ideal Gas Law.

In addition, if the heat transfer to the environment can be expressed in terms of a heat transfer coefficient h_c , the condenser conductance is proportional to the active condenser length $L_{c,a}$ and is defined as

$$C_c = (h P)_c L_{c,a} \quad (3-2)$$

These assumptions and the following Eqs. completely describe the operation of a gas-loaded heat pipe.

- (A) Conservation of Mass

$$m_g = m_{g,i} + m_{g,r} \quad (3-3)$$

- (B) Law of Additive Partial Pressures

$$\left. \begin{array}{ll} p_v = p_{v,i} + p_{g,i} & \text{(inactive condenser)} \\ p_v = p_{v,r} + p_{g,r} & \text{(reservoir)} \end{array} \right\} \quad (3-4)$$

(c) Ideal Gas Equation of State

$$(pV)_g = (mRT)_g \quad (3-5)$$

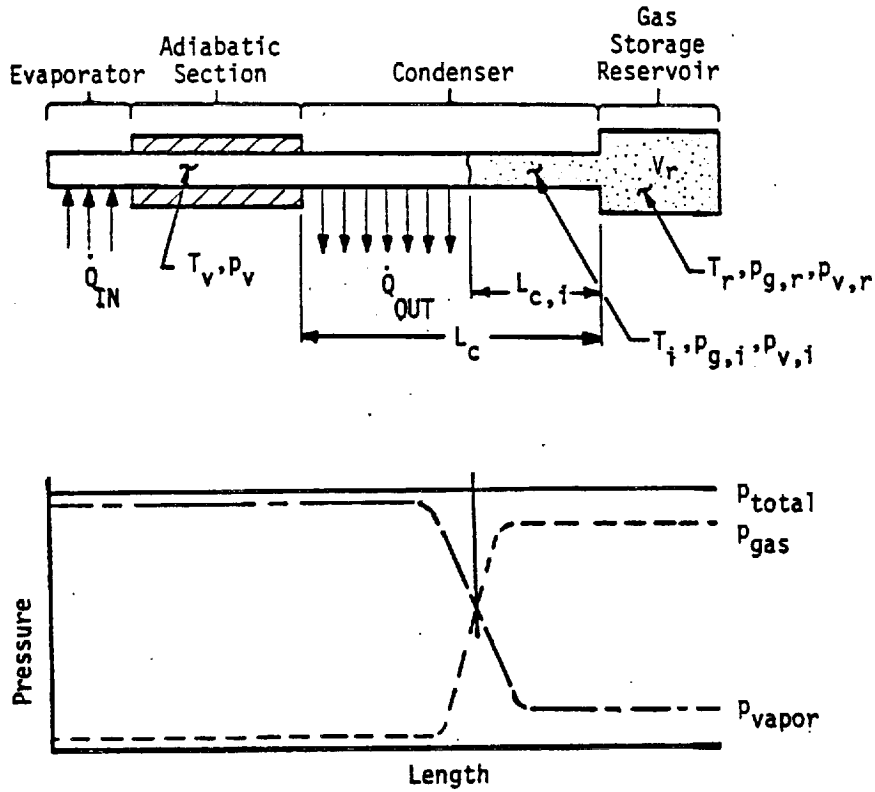


Fig. 3-6. Distribution of gas and vapor in a gas controlled VCHP

The reservoir size and gas load are determined by the following two extremes of operation:

(a) Maximum Condition -- Maximum heat load at the highest sink temperature.

Optimum operation of the heat pipe under this condition will have the heat pipe's condenser fully "open." Thus the maximum condition determines the reservoir size required to contain the non-condensable gas. Eqs. 3-4 and 3-5 can be solved to give

$$V_r = (m R)_g \left[\frac{p_v - p_{v,r}}{T_r} \right]_{\max}^{-1} \quad (3-6)$$

(b) Minimum Condition -- Minimum heat load at the lowest sink temperature.

Operation at the minimum condition requires that part or all of the heat pipe's condenser and adiabatic sections be "shut-off" consistent with the temperature control requirements. Hence, the gas load must be sufficient to block that portion of the pipe required to satisfy the minimum condition.

The solution of Eqs. 3-3 thru 3-5 gives

$$m_g = \left[\frac{p_v - p_{v,o}}{R_g T_o} \right]_{\min} V_{v,im} + \left[\frac{p_v - p_{v,r}}{R_g T_r} \right]_{\min} V_r \quad (3-7)$$

where $V_{v,im}$ is defined as the volume of the vapor space in the inactive part of the heat pipe at the minimum condition.

The following two terms are defined for the purpose of simplifying these Eqs:

$$\psi_o \equiv \frac{p_v - p_{v,o}}{T_o} ; \quad \psi_r \equiv \frac{p_v - p_{v,r}}{T_r} \quad (3-8)$$

The storage volume and gas charge required for any gas-controlled heat pipe can now be determined by the simultaneous solution of Eqs. 3-6 and 3-7 as

$$\frac{V_r}{V_{v,im}} = \frac{\psi_{o,min}}{\psi_{r,max} - \psi_{r,min}} \quad (3-9)$$

$$(m R)_g = V_r \psi_{r,max} \quad (3-10)$$

These equations apply, in general, to gas-controlled heat pipes. Before proceeding to their application to the various types of gas-controlled heat pipes, it is important to understand how they relate to temperature control.

The most important parameter in a thermal control system is the temperature control required (i.e., control sensitivity). This parameter is essentially the allowable variation in heat source temperature (ΔT_s). Once the required heat source temperature control has been defined, the corresponding maximum and minimum heat pipe vapor temperatures are determined from:

$$T_v = T_s - R_s \dot{Q} \quad (3-11)$$

For a constant resistance R_s between the heat source and heat pipe, Eq. 3-11 defines the allowable variations of T_v for variations in T_s and \dot{Q} .

The vapor pressure ($p_{v,max}$ and $p_{v,min}$) corresponding to the required vapor temperature limits are then determined from saturation conditions for the working fluid. Thus, while the temperature control required does not appear explicitly in the equations defining the storage requirements, it does enter implicitly through the heat pipe vapor pressures.

One final comment which applies to the design of gas-controlled heat pipes is that the tighter the control required, the larger the reservoir size. For a specific type of VCHP and fixed reservoir end conditions, as $p_{v,min}$ approaches $p_{v,max}$ ($\psi_{r,min}$ approaches $\psi_{r,max}$), the denominator of Eq. 3-9 decreases and the required storage volume increases. When the denominator becomes zero or negative, no further improvement in temperature control can be obtained with the type of VCHP being investigated.

Once the design has been established, the heat pipe's conductance or steady state operation for a given set of conditions can be determined from Eqs. 3-9 and 3-10 and the heat transfer requirement (Energy Eq.) which can be expressed as

$$\dot{Q} = (hP)_c L_{c,a} (T_v - T_o) \quad (3-12)$$

Since

$$L_{c,a} = L_c - L_{c,i} = L_c - \dot{V}_{v,i}/A_v \quad (3-13)$$

It follows that

$$\frac{L_{c,a}}{L_c} = \frac{\dot{Q}}{\dot{Q}_{max}} = 1 - \frac{V_r}{A_v L_c} \left[\frac{\psi_{r,max} - \psi_r}{\psi_o} \right] \quad (3-14)$$

A thermal analysis of a system which utilizes a gas-loaded heat pipe requires the simultaneous solution of the Energy Equation and the heat pipe's Mass Balance. Hence, in order to locate the gas interface for a given heat load and sink condition, one must assume a vapor temperature and then verify that Eq. 3-14 is satisfied for the specified heat load or iterate accordingly and then calculate the active length.

3.2.2 Types of Gas-Loaded Heat Pipes

A variety of different types of gas-loaded heat pipes have been developed which can be divided into wicked and non-wicked reservoir systems.

3.2.2.1 Wicked Reservoir Systems

A reservoir wick is used to provide a return path for any liquid that collects in the reservoir either through diffusion and condensation of the vapor or through accidental spillage of the working fluid. The presence of a wick saturated with liquid establishes a saturation partial vapor pressure of the working fluid which is in equilibrium with the reservoir temperature.

The reservoir wick may be an extension of the heat pipe wick or it may be an entirely different type of wick. Since the reservoir wick generally only has to satisfy a minimal heat transport requirement, a very simple design such as multiple layers of screen attached to the reservoir wall is sufficient. At the maximum condition, the vapor in the reservoir reduces the volume available for gas storage. However, at the minimum condition, the saturated vapor reduces the amount of gas required to fill the reservoir and therefore reduces the storage requirements. Several conditions can be factored into the design which affect the reservoir temperature and therefore the control characteristics of the VCHP, and they are as follows.

(a) Cold Reservoir

The simplest variable conductance heat pipe is commonly referred to as a "cold reservoir" type. As shown in Fig. 3-7, its reservoir is in thermal equilibrium with the sink condition (i.e., $T_r = T_o$). The storage volume requirement for a cold reservoir system is:

$$\frac{V_r}{V_{v,im}} = \frac{\Psi_{o,min}}{\Psi_{o,max} - \Psi_{o,min}} \quad (3-15)$$

and its gas charge requirement is:

$$(mR)_g = V_r \Psi_{o,max} \quad (3-16)$$

The location of the gas front is given by:

$$\frac{L_{c,a}}{L_c} = 1 - \frac{V_r}{A_v L_c} \left[\frac{\Psi_{r,max} - \Psi_o}{\Psi_o} \right] \quad (3-17)$$

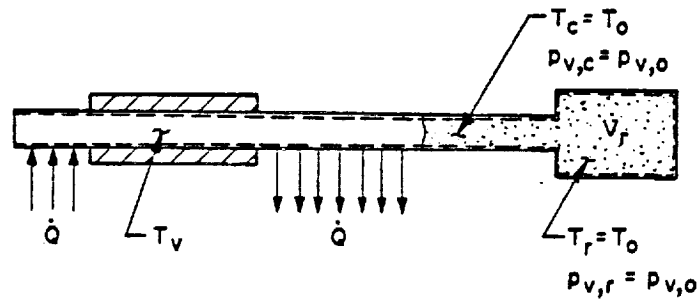


Fig. 3-7. Self-controlled VCHP with a wicked, uncontrolled reservoir

The "cold reservoir" VCHP is generally the easiest one to fabricate and integrate with another system and therefore the least expensive. However, because the reservoir has a wick and is in equilibrium with the sink temperature, its control capability is limited. In particular, unless relatively coarse temperature control is satisfactory, the cold reservoir type is suited for those applications where the maximum sink temperature is substantially less than the operating temperature and only moderate variations in heat source and sink temperature occur.

(b) Reservoir at Constant Temperature

A relatively simple extension of the cold reservoir system is one in which the reservoir is interfaced with some other component, structural member, etc., whose temperature is relatively insensitive to variations in the sink condition (i.e., $T_r = \text{constant}$). This system is capable of far greater control than an equivalent cold reservoir type. Its storage volume requirement can be determined from:

$$\frac{V_r}{V_{v,im}} = \frac{\psi_{o,min}}{\psi_{r,max} - \psi_{r,min}} \quad (3-18)$$

and its gas charge requirement is:

$$(mR)_g = V_r \psi_{r,max} \quad (3-19)$$

The location of the interface is given by Eq. 3-14, i.e.

$$\frac{L_{c,a}}{L_c} = \frac{\dot{Q}}{\dot{Q}_{\max}} = 1 - \frac{V_r}{A_v L_c} \left[\frac{\psi_{r,\max} - \psi_r}{\psi_o} \right]$$

A VCHP with a temperature controlled, wicked reservoir is far less sensitive to variations in the sink temperature than one whose reservoir is coupled to the sink temperature. Conversely, for a specified control sensitivity and sink temperature range, the VCHP with a temperature controlled reservoir will require a much smaller reservoir size. The only restriction with a controlled reservoir system is that the reservoir temperature must be less than the minimum vapor temperature.

When passive methods cannot be used to maintain the reservoir at a constant temperature, a reservoir heater can be employed. This is a type of active control wherein a feedback controller is used to regulate a reservoir heater such that the reservoir temperature is kept constant under varying sink conditions. Minimum heater power requirements result if the reservoir is maintained at a temperature just slightly above the maximum sink temperature. The equations defining the storage requirements are identical to those for the passive system; however, when active control is utilized it is generally better to control the source temperature rather than the reservoir.

(c) Feedback VCHP

Each of the preceding systems requires an infinite storage volume in order to provide absolute control of the heat pipe temperature (i.e., $\Delta T_v = 0$). Even if nearly absolute control of the vapor temperature could be obtained practically, this would not guarantee that the heat source temperature (which is really the parameter of interest) would be maintained constant. As indicated by Eq. 3-11, there is always a finite thermal impedance between the heat source and the heat pipe vapor temperature. Consequently, even though the vapor temperature is kept constant, unacceptable heat source temperature fluctuations could result from variations in the heat load.

Under these circumstances, or when the desired control cannot be obtained with practical reservoir sizes, an active feedback system can be employed. In the feedback system, the vapor temperature decreases with increasing heat load or vice versa, thereby permitting absolute control (i.e., $\Delta T_s = 0$, $\Delta T_v = -R_s \Delta Q$) of the heat source. The active feedback system is essentially the same as the heated reservoir system discussed previously, except that, instead of monitoring reservoir temperature and maintaining it constant, a controller senses the heat source temperature and regulates the reservoir temperature to derive the desired control.

In order to minimize the reservoir size, the auxiliary heater should keep the reservoir near the vapor temperature at the condition of minimum heat load and lowest sink temperature. This results in larger power requirements for the feedback system than for the heated reservoir type. However, the auxiliary power required is relatively small; its magnitude being associated primarily with the transient requirements (2). At the condition of maximum heat load and highest sink temperature, in order to achieve full utilization of the reservoir for gas storage, the reservoir temperature should approach the sink temperature. Thus, in the feedback system the reservoir temperature will vary between the maximum sink temperature and the minimum conditions. The storage requirements for a feedback system are defined by the general Eqs. 3-9 and 3-10. For the optimum steady-state case where $T_{r,min} = T_{v,min}$ and $T_{r,max} = T_{o,max}$,

$$\frac{V_r}{V_{v,im}} = \frac{\Psi_{o,min}}{\Psi_{o,max}} \quad (3-20)$$

and its gas charge requirement is:

$$(mR)_g = V_r \Psi_{o,max} \quad (3-21)$$

Again the location of the interface is determined from Eq.(3-14), i.e.

$$\frac{L_{c,a}}{L_c} = \frac{\dot{Q}}{\dot{Q}_{\max}} = 1 - \frac{v_r}{A_v L_c} \left[\frac{\psi_{r,\max} - \psi_r}{\psi_o} \right]$$

However, with a feedback system the desired temperature control is specified and therefore the required vapor temperature is known. The location of the interface and the variable conductance operation will in this case consist of determining the reservoir temperature that is needed to give the required conductance. The following analysis applies:

- (1) Solve the vapor temperature required to satisfy the specified conditions from Eq. 3-11.

$$T_v = T_s - R_s \dot{Q}$$

- (2) Solve for the corresponding conductance or interface location using Eq. 3-12.

$$L_{c,a} = \dot{Q} / (h P)_c (T_v - T_o) \quad (3-22)$$

- (3) Use Eq. 3-14 to determine the reservoir temperature that will give the required interface location.

3.2.2.2 Non-Wicked Reservoirs

One other type of gas-controlled heat pipe is a system which utilizes a non-wicked reservoir. As shown in Fig. 3-8, the reservoir is thermally coupled to the evaporator or heat source. This is done to prevent liquid from condensing in the reservoir and not being able to return because there is no capillary interconnection. The reservoir is non-wicked to avoid saturation conditions at temperatures equal to or greater than the heat pipe vapor temperature. Saturation conditions would, of course, prevent gas storage in the reservoir. Because there is no interconnection between the heat pipe wick and the reservoir, any fluid from the heat pipe that is accumulated in the reservoir, due to spillage or diffusion, must diffuse back out during start-up. This can result in relatively long start-up times (e.g., several hours) for this type of system.

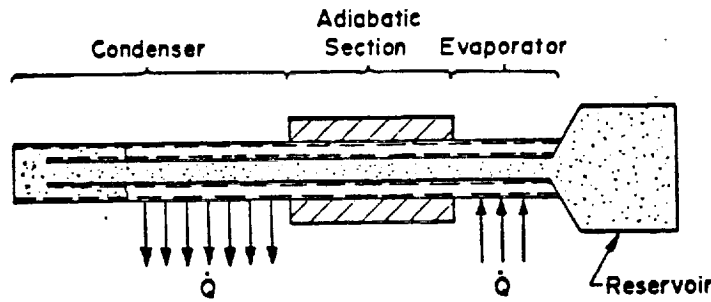


Fig. 3-8. VCHP with reservoir thermally coupled to the evaporator

Under normal operating conditions, vaporized working fluid which has diffused from the condenser will exist within the reservoir. As Marcus (3) points out, the partial pressure of this vapor will not correspond to the reservoir temperature but to the temperature at the mouth of the reservoir where the wick ends. Generally, a feeder tube which is in equilibrium with the sink condition is employed between the reservoir and the condenser section. Consequently, under the assumptions of the flat front model, the partial pressure of vapor in the reservoir corresponds to the sink temperature, i.e.

$$P_{v,r} = P_{v,o} \quad (3-23)$$

The storage volume requirement for a "hot reservoir" system is therefore:

$$\frac{V_r}{V_{v,lm}} = \frac{\psi_{o,min}}{\left[\frac{T_o}{T_r} \psi_o \right]_{\max} - \left[\frac{T_o}{T_r} \psi_o \right]_{\min}} \quad (3-24)$$

and the gas charge requirement is:

$$(mR)_g = V_r \left(\frac{T_o}{T_r} \psi_o \right)_{\max} \quad (3-25)$$

where the reservoir temperature is equal to the heat source or heat pipe evaporator temperature. Hence, the basic improvement that is realized when compared to a wicked "cold" reservoir system is that derived from compression of the gas within the reservoir.

The location of the interface is obtained from:

$$\frac{L_{c,a}}{L_c} = 1 - \frac{V_r}{A_v L_c} \frac{\left(\frac{T_o}{T_r} \psi_o \right)_{\max} - \frac{T_o}{T_r} \psi_o}{\psi_o} \quad (3-26)$$

3.2.3 Diffusion Effects

The theory of gas loaded VCHP's presented in the preceding sections is based on a sharp interface (flat front model) between active and inactive portions of the condenser. An ideal distribution does not exist in reality. The actual "front" is controlled by diffusion within the gas-vapor interface and by axial conduction in the wall. A typical diffuse front is shown in Fig. 3-9. It is seen that the "average" temperature in the inactive part of the condenser is somewhat higher than the sink temperature and that the average partial vapor pressure is higher than that corresponding to the sink temperature. This causes the temperature set point of the VCHP to be higher than predicted by "flat front" theory for the particular gas inventory.

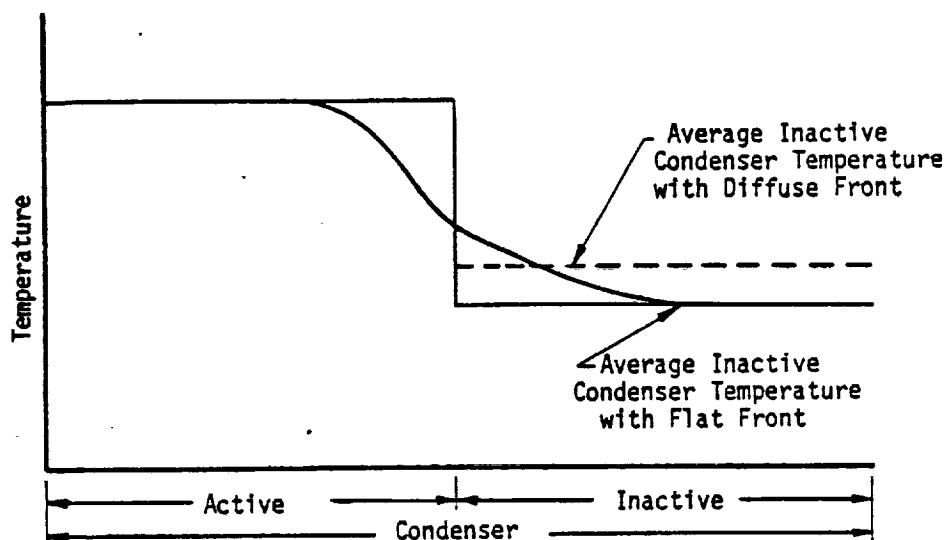


Fig. 3-9. Temperature distribution in the condenser for flat front and diffuse front models

In non-wicked reservoir heat pipes, this effect can be quite pronounced. The partial vapor pressure in a non-wicked reservoir is theoretically equal to the partial pressure in the inactive condenser section. If the interface moves close to the end of the condenser ($C_c \sim (C_c)_{\max}$), the tail of the diffuse front may extend into the reservoir and raise the vapor pressure in the reservoir. The deviation from prediction using the flat front model is more pronounced in a non-wicked reservoir heat pipe since the effects of increased partial vapor pressure involve the entire reservoir. Marcus (3) conducted experiments to test the flat front theory. He instrumented a VCHP with an internal non-wicked reservoir to measure the actual temperature profiles. Using a theoretical approach, similar to the one presented in Section 3.2.1, he computed the vapor temperature as a function of active condenser length. In order to account for the diffuse temperature distribution he integrated the molar gas density along the inactive condenser section using the actually measured temperatures. The agreement between theory and experiment is very good, indicating that the flat front model does predict the control capability of the pipe accurately provided that appropriate average temperature for the inactive portion of the condenser and the reservoir are used.

A complete model of the diffuse interface in a gas-loaded heat pipe must include: (1) heat transfer between the condenser and environment; (2) axial conduction in the walls, wicks, and fins; (3) binary mass diffusion between the vapor and gas; and (4) radial wick resistance. The theory of a diffuse gas front is rather complicated and is not included. A detailed model as well as the method of solution and numerical results are given by Marcus (3).

3.2.3.1 Numerical Analysis of Diffuse Vapor Gas Front

Marcus (3) reports the results of a parametric study which evaluates the effect of wall conductivity, working fluid, and operating temperature on the vapor-gas interface. The results can be summarized as follows:

- (1) Axial conduction in the pipe wall plays a substantial role in defining the vapor-gas interface. Typical temperature profiles along the condenser are shown in Fig. 3-10. One clearly sees that wall conductance tends to spread the front over the condenser.

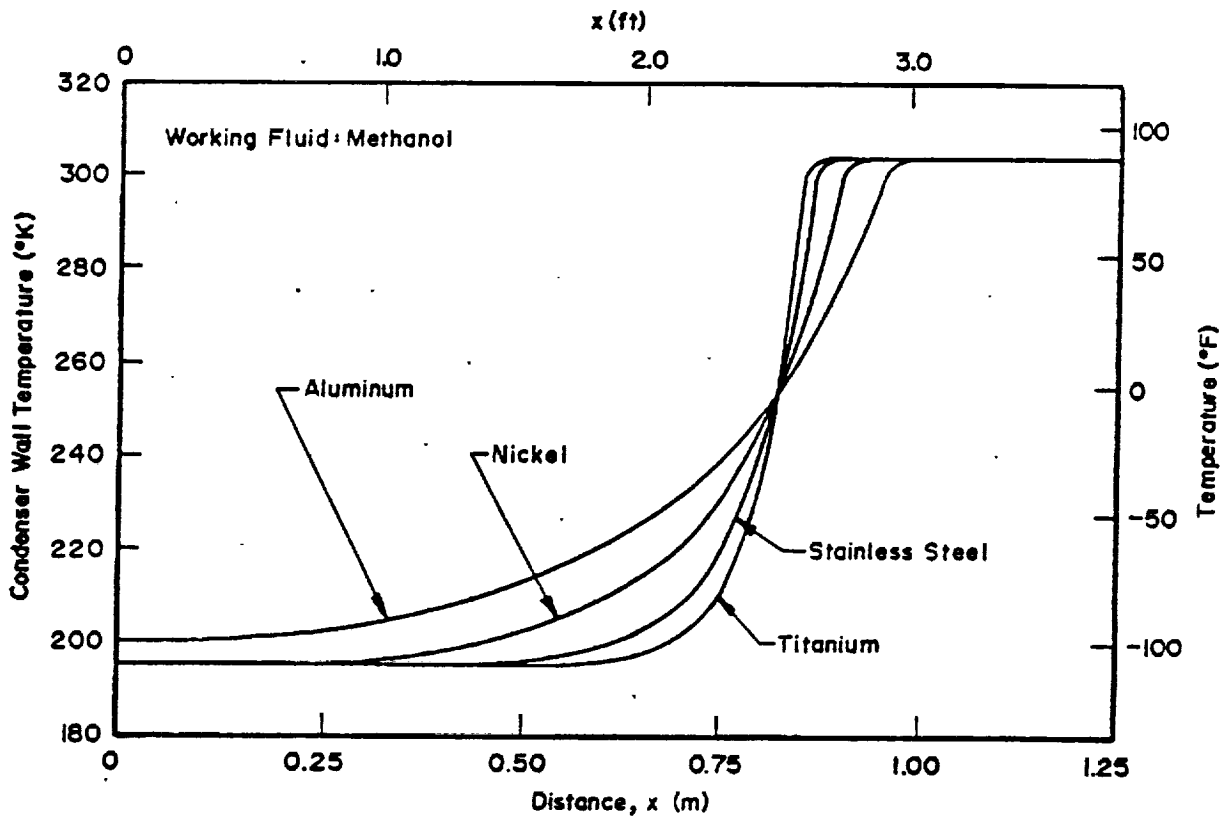


Fig. 3-10. Effect of axial wall conduction on the condenser temperature profile

- (2) The effect of working fluid on the temperature profiles is insignificant (Fig. 3-11). This suggests that heat transport by mass diffusion is minimal and that axial conduction dominates.
- (3) The operating temperature does not significantly alter the profile of the vapor-gas interface. Typical effects are shown in Fig. 3-12.

The above results are typical for heat pipes for spacecraft temperature control. There is no reason to believe that other gas controlled heat pipes would not exhibit the same qualitative behavior.

One important conclusion can be drawn from this study. Since heat transport by mass diffusion appears to be insignificant when compared to axial conduction, the temperature profile in the vicinity of the interface is determined to a first approximation by

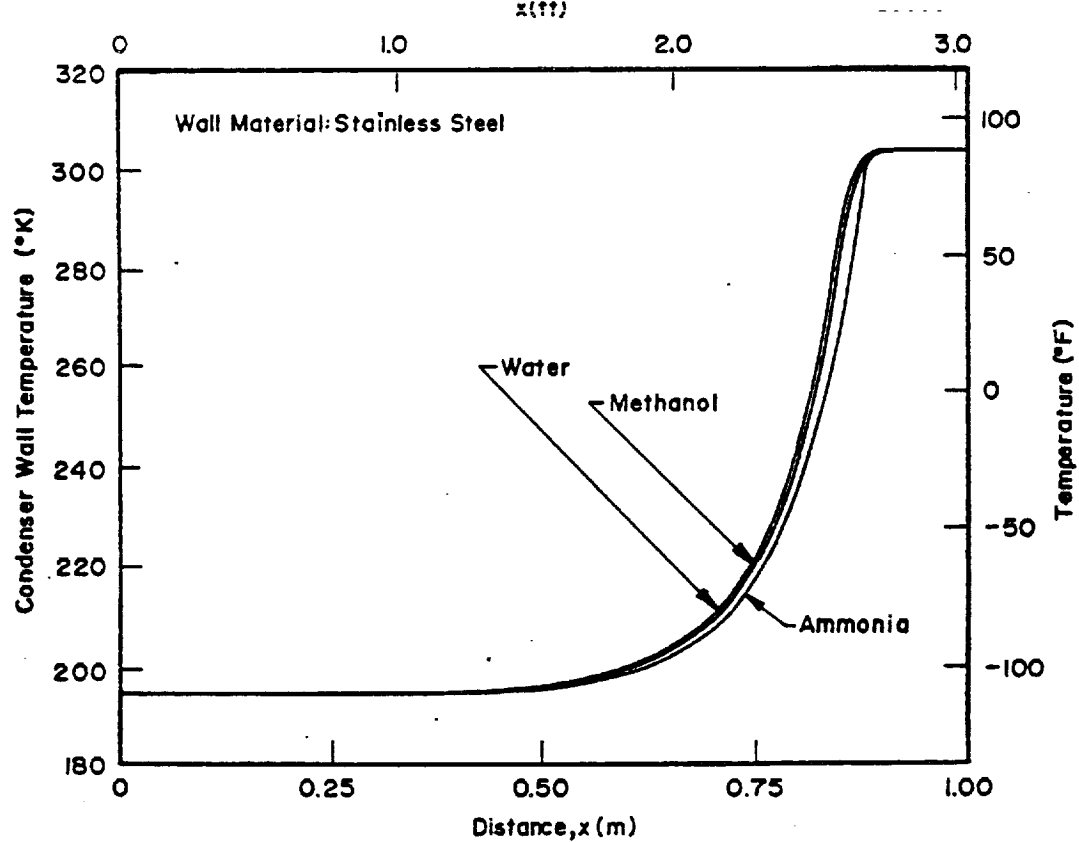


Fig. 3-11. Effect of working fluid on the condenser temperature profile

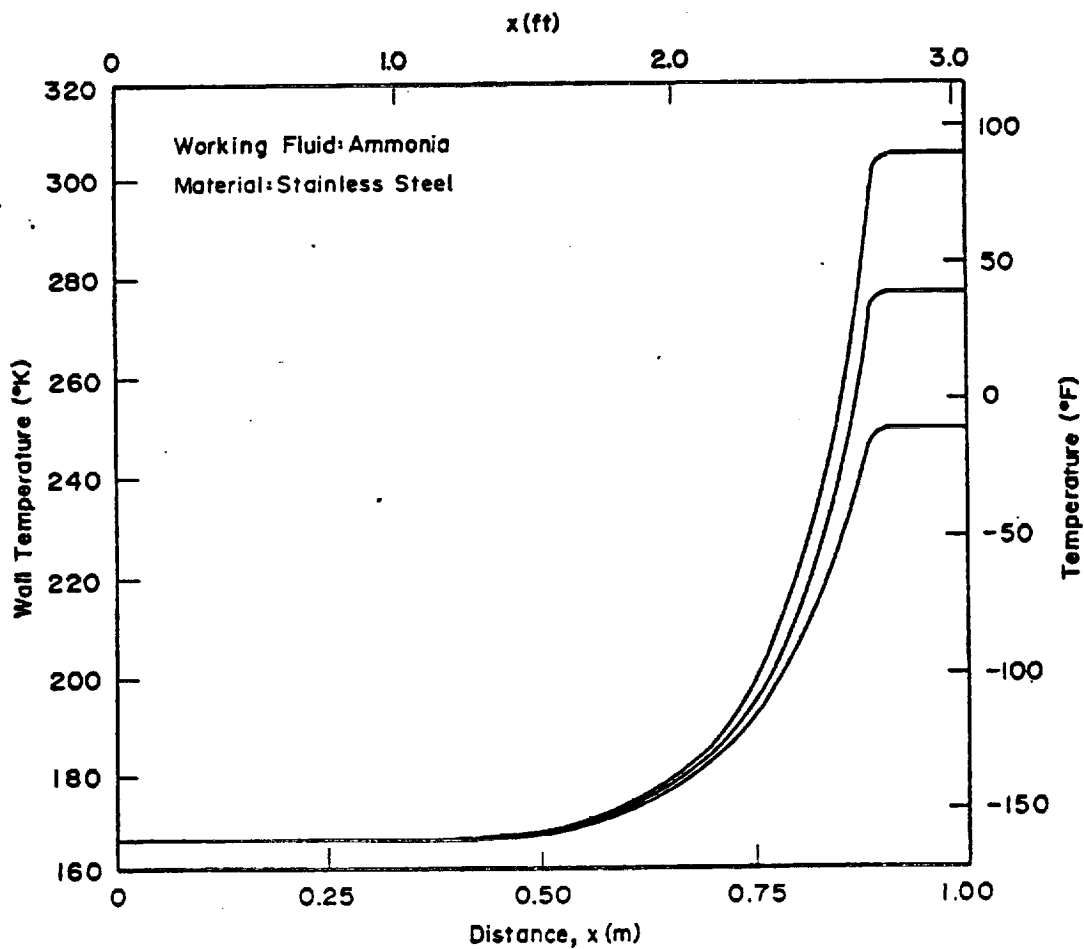


Fig. 3-12. Effect of operating temperature on the condenser temperature profile

conduction and by heat transfer to the environment. Thus, a conventional "fin" equation (4) will, in most cases, adequately describe the temperature profile along the heat pipe.

The flat front model predicts the conductance of the heat pipe satisfactorily if a realistic temperature profile is used to calculate the effective condenser temperature. Treating the inactive portions of the condenser as a fin provides an excellent approximation of the temperature profile and represents a first order refinement to the flat front model.

The detailed numerical analysis that is available with the "Gas Pipe" Program (5) provides information which cannot be obtained using the simple closed-form solution. An important example of this is the determination of the freeze-out rate of the working fluid which will occur when conditions exist which will cause the condenser and/or reservoir temperature to drop below the fluid's melting point. When this occurs a finite amount of vapor will continuously diffuse into that region and freeze there.

3.2.4 Gas Absorption Reservoir

One of the more recent innovations for improving the design of a gas-controlled heat pipe consists of replacing the gas storage volume with a much smaller gas absorption reservoir (6). For a number of gas/fluid combinations, it can be shown that it is volumetrically more efficient to store gas as a dissolved solute than dispersed as a gas in a vapor reservoir. The absorption reservoir consists of a wick matrix which supports the liquid in a 1-g environment. Under conditions of vapor-liquid equilibrium, the concentrations of non-condensable gas in the two phases are related by:

$$C_{gl} = \alpha C_{gv} \quad (3-27)$$

where:

C_{gl} = Molar gas density in the liquid phase

C_{gv} = Molar gas density in the vapor phase

The factor α is the Ostwald coefficient and is a constant for dilute solutions. Hence, the larger the Ostwald coefficient, the greater the amount of gas absorption into the liquid phase versus the vapor phase. In addition to requiring values of α which are greater than one, efficient storage volumes are realized when the volume of the liquid in the condenser is small. This is generally the case with aerospace heat pipes. If "flat-front" theory is

used, it follows that the volume required for a gas absorption reservoir in a general gas controlled application (e.g., Eq. 3-9) is given by:

$$\frac{V_{r,ga}}{V_{v,im}} = \frac{\psi_{o,min}}{\psi_{r,max} - \psi_{r,min}} \frac{\theta_c}{\theta_r} \quad (3-28)$$

where:

$$\theta_c = 1 + \beta_c (\alpha \eta_c - 1) \quad \text{and} \quad \theta_r = 1 + \beta_r (\alpha \eta_r - 1) \quad (3-29)$$

with

β_c = Fraction of condenser filled with wick/fluid composite

β_r = Fraction of reservoir filled with wick/fluid composite

η_c = Fraction of wick/fluid composite filled with liquid in the condenser

η_r = Fraction of wick/fluid composite filled with liquid in the reservoir

The void fractions η_c and η_r are generally equal to the porosity (ϵ) of the condenser and reservoir wick structures.

A comparison of Eq. 3-28 with Eq. 3-9 shows that the savings to be realized with a gas absorption reservoir are:

$$\frac{V_{r,ga}}{V_r} = \frac{\theta_c}{\theta_r} \quad (3-30)$$

In general the most efficient gas storage will be obtained with liquid-gas combinations which have large values for their Ostwald coefficient. Reservoir size reductions on the order of 1/5 to 1/10 can be realized with values of 10 to 20 for α . Unfortunately, such combinations are possible but common control gases do not satisfy this criterion. Table 3-1 lists several room temperature liquid-gas combinations which have high solubility.

3.2.5 Transients with Gas-Controlled Heat Pipes

The performance of heat pipes during transients is still only partially understood. This is particularly true for variable conductance heat pipes which represent control elements within a thermal system. A detailed discussion of transient behavior is beyond the scope of this Manual but a summary of the salient points is presented.

TABLE 3-1. ROOM TEMPERATURE LIQUID-GAS COMBINATIONS HAVING HIGH SOLUBILITY

Solvent	Solute	Temperature (°C)	Ostwald Coefficient
Hexane	n-Propane	25	23.6
Benzene	n-Propane	25	16.0
Benzene	n-Pentane	16	312.0
Methanol	Propane	25	3.4
Methanol	Carbon Dioxide	12	4.1
Methanol	Butane	12	28.0
Methanol	Sulfur Dioxide	25	83.0
Methanol	Carbon Dioxide	59	39.0
Water	Ammonia	25	40.7
Water	Sulfur Dioxide	25	34.0
Water	Methanol	100	254.0

The transient performance of fixed conductance heat pipes has been discussed by several investigators in Refs. 7 through 12. Most of this work has been concerned with the start-up dynamics of liquid-metal heat pipes whose working fluid is frozen (i.e., solid) at room temperature conditions. The presence of a non-condensing gas which reduces the transport length tends to alleviate start-up conditions associated with the low transport capability of working fluids when they are at low vapor pressures. Reference 12 treats the start-up of cryogenic heat pipes whose working fluids are supercritical at room temperature. In this case, since any non-condensable gas that might be present in the pipe is greatly compressed, its effect on start-up will be negligible.

Transient discussions of the various types of gas-loaded heat pipes can be divided into three groups--wicked reservoir, non-wicked reservoir, and feedback controlled pipes.

3.2.5.1 Wicked Reservoir Heat Pipes

The partial pressure of the vapor everywhere in a wicked reservoir heat pipe is in equilibrium with the local wick temperature. Diffusion effects may be neglected except for establishing the vapor-gas interface. The transient behavior of wicked reservoir gas-loaded pipes can therefore be adequately described by considering the sensible heat

capacities of the various heat pipe elements and the conductance between them. The position of the vapor-gas interface is assumed to be in equilibrium at all times with the pressure and temperature distributions. Consequently, transient behavior can be predicted using ordinary thermal modeling techniques.

3.2.5.2 Non-Wicked Reservoir Heat Pipes

In a non-wicked reservoir, the partial vapor pressure in the reservoir is established by diffusion. The length of the diffusion path between the nearest point of saturation, i.e., the end of the condenser and the reservoir, may be long and diffusion rates often dominate the transient response. Although the transient behavior of non-wicked reservoir heat pipes is by no means fully developed, successful correlation of the "hot" reservoir heat pipe flow in the Ames Heat Pipe Experiment (AHPE) has been obtained (13).

Another phenomenon which is peculiar to non-wicked reservoir heat pipes is the mechanism for removal of liquid working fluid from the reservoir. Ordinarily, the non-wicked reservoir contains only non-condensing gas and some working fluid vapor. Liquid may accidentally be spilled into the reservoir, as for example either as a result of handling or as a result of vibrations during launch. If the spillage occurs during handling, the bulk of the liquid can usually be removed by proper orientation. If this happens during launch and is then immediately followed by a 0-g environment, no such removal mechanism exists. In either case, some liquid will remain in the reservoir. Under these conditions, when the heat pipe is started-up, the vapor pressure in the reservoir will correspond to the saturation pressure of the liquid at the reservoir rather than the condenser temperature. Since the reservoir temperature is always higher than the condenser temperature, some of the gas will be forced out of the reservoir and the heat pipe's set point will be changed. In the extreme case, corresponding to a reservoir temperature equal to the evaporator temperature, all of the gas will be forced out. Since the reservoir volume normally exceeds the condenser volume, the latter will be completely blocked and serious overheating of the heat source may result. These abnormal conditions will prevail until the liquid is evaporated from the reservoir and recaptured by the wick.

3.2.5.3 Feedback Controlled Gas-Loaded Heat Pipes

Feedback systems exhibit a rather complex transient behavior. These systems contain all the elements of a typical control loop and are subject to the same performance characteristics. Unlike other variable conductance heat pipes, feedback systems can possess unstable

regimes in which oscillations may occur. Thermal feedback systems are more stable than electrical feedback systems; however, their stability should be established for each application.

Closely related to stability is the existence of "overshoot" and "undershoot" of the control temperature. A typical response for a feedback controlled gas-loaded heat pipe, in which the source temperature is regulated, is shown in Fig. 3-13. Changes in the heat load and/or in the sink temperature cause the source temperature to temporarily deviate from the set point. As illustrated, the feedback system regains control and the set point is restored.

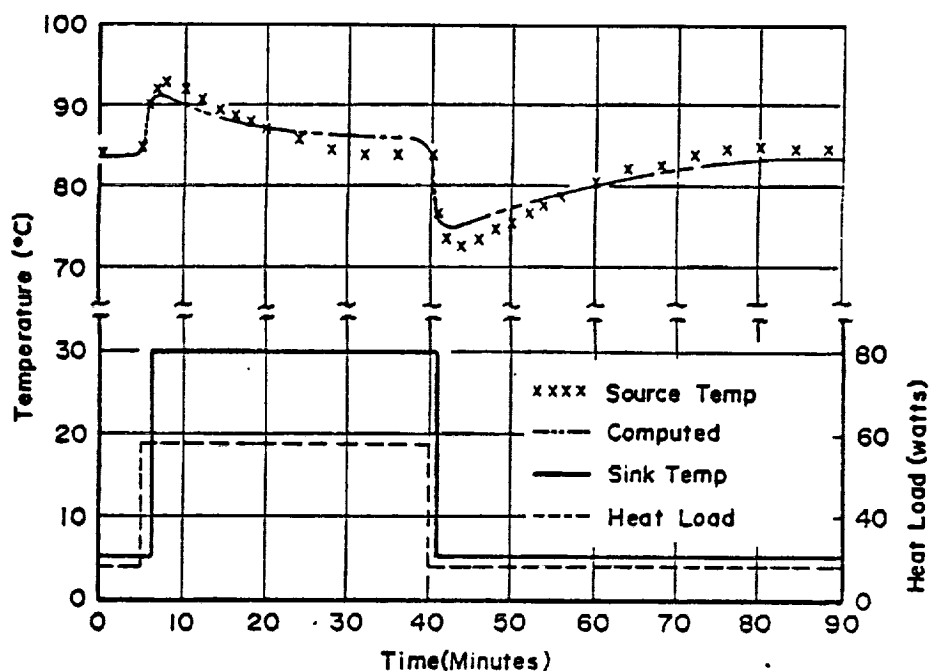


Fig. 3-13. Transient response of heat source with electrical feedback controlled heat pipe

A lumped parameter model of a heat pipe feedback loop is presented in Reference 2 which shows that the response of the heat source is controlled by the following two time constants:

$$\tau_r \equiv (m C_p R)_r$$

$$\tau_s \equiv (m C_p R)_s$$

where m_r and $C_{p,r}$ are the mass and the lumped specific heat of the reservoir, and m_s and $C_{p,s}$ are the mass and the lumped specific heat of the heat source. R_r is the thermal resistance between the reservoir and the sink, and R_s is the thermal resistance between the heat source and the heat pipe evaporator. The response time is minimized if the ratio τ_r/τ_s is small. Since the time constant of the heat source is frequently determined by the application, the only available alternative is to make τ_r as small as possible. The most desirable method of minimizing τ_r is to minimize the heat capacity m_r of the reservoir. By closely coupling (thermally) the reservoir to the sink (small R_r), a reduction in the reservoir time constant can be achieved but this is generally undesirable since it increases the auxiliary power required to maintain the reservoir at the selected temperature during steady state operation.

3.3 OTHER VARIABLE CONDUCTANCE HEAT PIPES

Most of the aerospace applications to date have utilized gas-loaded heat pipes for their thermal control requirements. However, demand for diode and switching operations is increasing, particularly for temperature control of low temperature and cryogenic detector systems (14). Although gas-loaded heat pipes can be adapted to accommodate these other thermal control functions, more efficient operation can be obtained passively by utilizing some of the other variable conductance techniques.

3.3.1 Excess Liquid Heat Pipe

This technique is closely related to non-condensing gas control. Variable conductance is achieved by inactivating part of the condenser by using an incompressible liquid. The most convenient

Fig. 3-14.

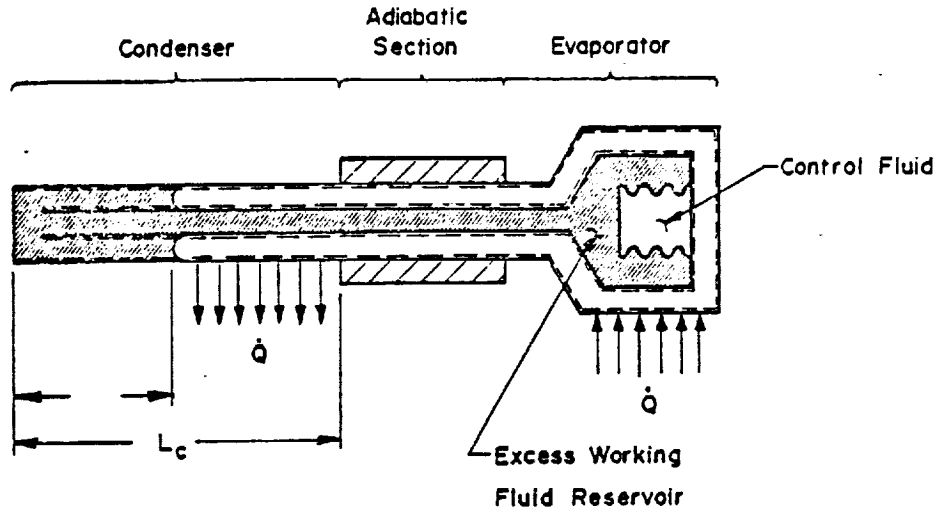


Fig. 3-14. Variable conductance through condenser flooding with liquid

Excess working fluid is contained in a reservoir which is located inside the heat pipe envelope. The effective volume of the reservoir is varied by means of a bellows which contains an auxiliary fluid in equilibrium with its vapor. Expansion of the bellows forces liquid working fluid out of the reservoir and into the condenser. This technique provides self-control of the source temperature; that is, increasing the heat source and/or the sink temperature causes the conductance to increase and this has the effect of minimizing the tendency for the source temperature to change.

The control characteristics can be developed using a model similar to the one in Section 3.2.1. Assuming that the fraction of the working fluid occupied by the wick and the vapor space is approximately constant (or negligible as in the case of the vapor), conservation of mass of the excess working fluid requires:

$$V_{ex} = V_r - V_b + A_v L_i \quad (3-31)$$

where V_r is the sum of the volumes of the reservoir and the capillary tube, V_b is the volume of the bellows containing the auxiliary control fluid, and V_{ex} is the volume of the excess fluid. Because the excess fluid is in the liquid state, conservation of mass corresponds to conservation of volumes. The volume occupied by the bellows (V_b) is related to the pressure difference between the working fluid and the auxiliary fluid through:

$$V_b = V_{bo} + \frac{A_b^2}{k} (p_a - p_v) \quad (3-32)$$

where V_{bo} is the equilibrium volume of the bellows, A_b is the bellows area, and k is the bellows spring rate.

Combining Eqs. 3-31 and 3-32 together with Eq. 3-12 yields the following expression for the active condenser length:

$$\frac{L_{c,a}}{L_c} = 1 - \frac{V_{ex} - V_r + V_{bo}}{A_v L_c} + \frac{A_b^2}{k A_v L_c} (p_v - p_a) \quad (3-33)$$

Because of the incompressibility of the liquid, this system is less sensitive to changes in the sink temperature than gas-loaded heat pipes. Good control is achieved if:

- (a) The cross-sectional area of the bellows is large
- (b) The spring rate of the bellows is small
- (c) The slope of the vapor pressure curve of the working fluid is larger than that of the auxiliary fluid

In addition to providing an insensitivity to changes in the sink temperature, temperature control using excess working fluid generally requires smaller storage reservoirs. Also, the interface between vapor and liquid is not subject to the diffusion effects. These system advantages must be weighed against some disadvantages. Gravity tends to cause the excess fluid to puddle in the condenser rather than form a well-defined interface as shown in Fig. 3-14. In addition, the sink temperature must always be above the freezing point of the working fluid because the inactive part of the condenser will be approximately at sink temperature and freezing would form a solid plug preventing any further control. Finally, sloshing of the excess fluid can be a problem, and containment of the excess fluid as well as the auxiliary fluid must be taken into account.

3.3.2 Liquid Flow Control

Liquid flow control represents probably the most viable technique for accomplishing diode and/or switching operations. Two basic methods exist: (1) the liquid trap which starves the heat pipe of its working fluid; and (2) liquid blockage which impedes the vapor flow and therefore the "heat-piping" action. A detailed summary of diode heat pipe technology is presented in Ref. 15. Significant aspects of the two techniques of liquid flow control are presented in the next sections.

3.3.2.1 Liquid Trap

The liquid trap technique is based on the tendency of liquid to accumulate at the coldest portion of the heat pipe, except as displaced by surface tension and gravity forces. The liquid trap is a reservoir provided at the evaporator end and is in good thermal contact with the evaporator to hold the liquid during and after reversal of the heat pipe operation. As shown in Fig. 3-15, the liquid trap contains a wick structure which does not communicate with the wick in the heat pipe.

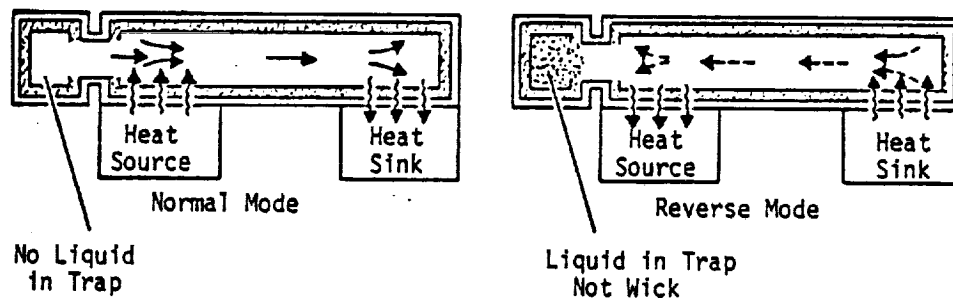


Fig. 3-15. Liquid trap diode operation

In the normal mode of operation the trap is dry. When the liquid trap end becomes the cold end of the heat pipe, condensation begins to occur within the trap, as well as in the evaporator end. As liquid accumulates in the trap, the heat pipe wick becomes underfilled causing a fairly rapid reduction in transport capability. The reduction in transport capability can be quite significant with only a few percent reduction of the liquid charge below 100% fill. This holds for both arterial wicks and axial grooves. For reduction of the transport capability to the order of less than 1% of the original value, however, it may be necessary to dry out the heat pipe wick completely, with all the liquid in the trap. Depending on the specific design the above phenomenon could also lead to a very rapid partial shutdown of the diode and a slower approach of the complete shutdown situation with minimum reverse heat flow. The trap volume should be sufficient to accommodate the entire fluid inventory of the heat pipe. Therefore, wicks having a small liquid volume are particularly attractive. The liquid trap technique combined with axially grooved wicks is an excellent combination and provides a simple and reliable design.

3.3.2.2 Liquid Blockage

The liquid blockage technique is dependent upon excess liquid shifting naturally from one end to the other as hot and cold ends are interchanged. Under reverse-mode operation, the excess liquid must have a volume sufficient to block the vapor space of the cold end and a large part of the transport section to minimize conduction heat transfer. As shown in Fig. 3-16, a reservoir is provided at the normal condenser end to obtain excess liquid under normal-mode conditions. The reservoir size must be slightly larger than the evaporator and transport section vapor space volumes, to allow for changes in liquid density with temperature. To keep the reservoir size small, the vapor space in the evaporator and adiabatic sections has to be kept small. This is automatically achieved with various arterial wicks. However, when axial grooves are intended to be used, an insert in the evaporator and at least part of the adiabatic section should be provided to reduce the vapor space. This, however, could cause a serious reduction in the forward-mode transport capability. Without an insert it would in general be impossible to hold a liquid plug in the vapor space against gravity during 1-g testing. Therefore, axial groove wicks cannot be used for the liquid blockage technique. The liquid blockage technique is most attractive for cryogenic applications where, under normal-mode operation, the evaporator is relatively short compared with the condenser and transport sections. This arrangement minimizes the excess liquid required for blockage.

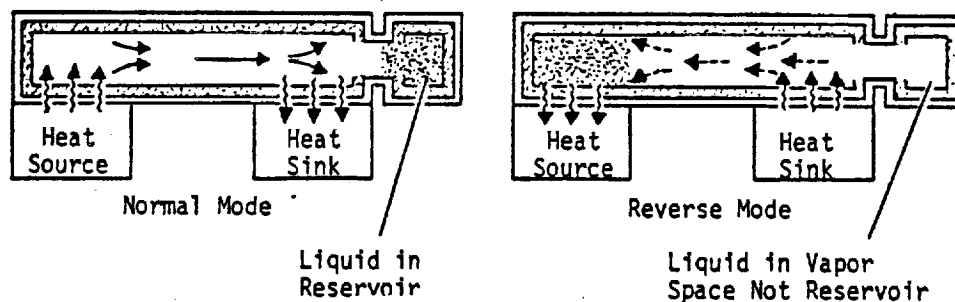


Fig. 3-16. Liquid blockage diode operation

The limitation of the liquid blockage technique is the ground testing requirement. In a gravity environment the vapor space in the blocked sections of the shutoff diode must hold the liquid. This means that the vapor space has to be small enough to insure that the respective capillary head, Δp , will support the gravity head of the liquid slug (Fig. 3-17). The condition for blockage of the vapor space in ground level testing can be derived to be:

$$\Delta p = \rho_L g D = \frac{2\sigma}{t_v} \quad (3-34)$$

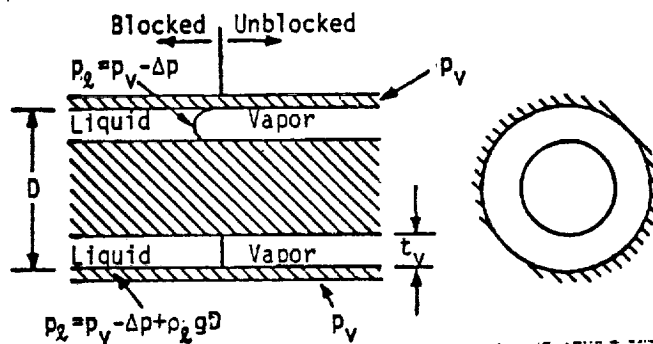


Fig. 3-17. Liquid blockage of vapor space (Ref. 16)

This requirement results in very narrow vapor spaces and consequently large vapor pressure drops during normal heat pipe operation. The heat pipe capacity is therefore limited and this type of diode is restricted to smaller heat transport applications, and the use of working fluids such as ammonia, which combine good capillary rise characteristics with small vapor losses.

One method for avoiding this problem that has been developed is referred to as a "blocking-orifice" design (16). This consists of inserting an orifice plate around the heat pipe wick at the point where blockage ends (e.g., Fig. 3-18). The opening in the orifice plate is located at the bottom of the pipe as shown in Fig. 3-18. The orifice height may be greater or less than the annular vapor passage height, t_v . The use of large vapor passage areas more than compensates for the additional vapor pressure loss introduced by the orifice.

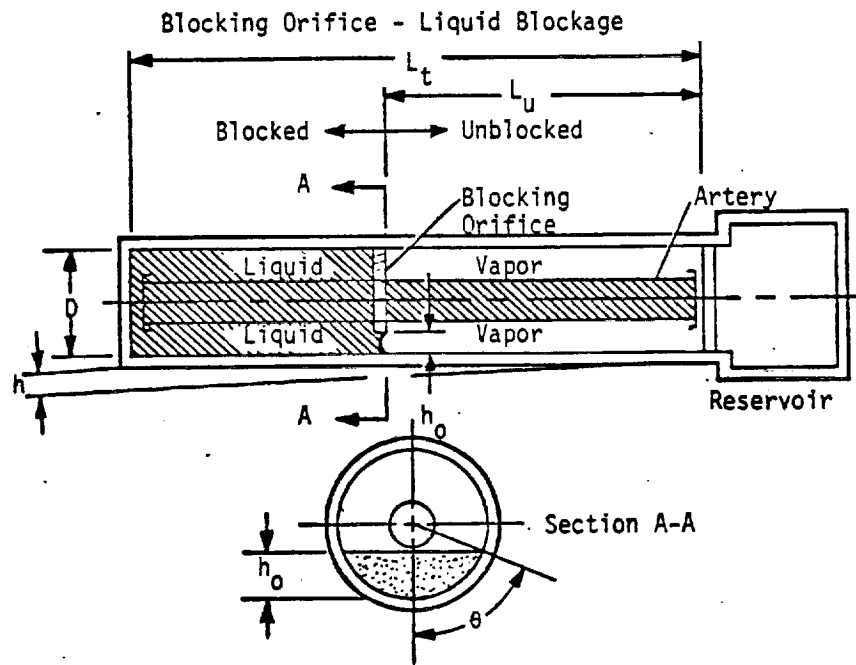


Fig. 3-18. Liquid blockage with a blocking orifice (Ref. 16)

If the pipe is tilted with the blocked end high, the equation for hydrostatic equilibrium for the design defined in Fig. 3-18 can be written as:

$$\rho_l g \left(h_o + \frac{hL_u}{L_t} \right) = \frac{2\sigma}{h_o} \quad (3-35)$$

from which the maximum orifice height can be determined as:

$$h_o = 0.5 \left\{ \left[\left(\frac{hL_u}{L_t} \right)^2 + \frac{8\sigma}{\rho_l g} \right]^{.5} - \frac{hL_u}{L_t} \right\} \quad (3-36)$$

3.3.3 Vapor Flow Control

The interruption of the vapor flow between the evaporator and condenser will result in a pressure difference in the vapor and, because of saturation conditions, a corresponding temperature difference. For a given axial heat flow rate, varying the temperature difference is equivalent to varying the heat pipe's conductance. The principle of this technique is shown schematically in Figs. 3-19 and 3-20. The vapor flow can be modulated by an external signal, e.g., the current of the electromagnet in Fig. 3-19, or the system can be self-controlled as shown in Fig. 3-20. (13).

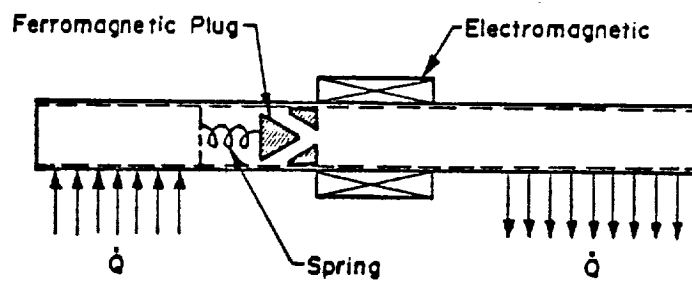


Fig. 3-19. Vapor flow control using external signal

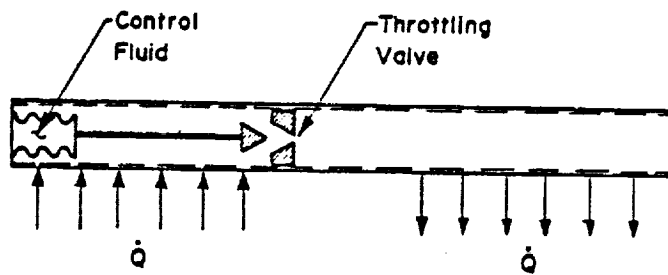


Fig. 3-20. Self-controlled vapor-modulated heat pipe

Vapor control represents a direct method of varying the axial conductance of the heat pipe. It does not, as with other techniques, render part of the condenser or evaporator ineffective. The entire evaporator and condenser are isothermal during all modes of operation since the pressure and temperature differential occurs across the throttle mechanism.

The obvious advantage is partially offset by the limited control range. The pressure difference created by the throttle must never exceed the capillary pressure of the wick. If the capillary pressure is exceeded, the vapor will "bubble" through the wick and around the throttle and the control capability will be lost. In a vapor flow-controlled heat pipe, the wick must be capable of providing sufficient capillary pressure to overcome the hydrodynamic losses and the pressure difference created for control purposes. From a hydrodynamic point of view, the wick must therefore be oversized.

The temperature difference which corresponds to a given pressure difference is obtained from the Clausius-Clapeyron equation (17).

$$\frac{\Delta T_v}{\Delta p_r} = \frac{T}{\lambda \rho_v} \quad (3-37)$$

In order to achieve large temperature differences (large variations of the conductance) with small pressure differences, the vapor density of the working fluid should be low. Vapor control is most effective if a fluid is selected which has a low vapor pressure at the operating temperature.

References

1. Brennan, P. J., and Groll, M., "Application of Axial Grooves to Cryogenic Variable Conductance Heat Pipe Technology," presented at 2nd International Heat Pipe Conference, April 1976.
2. Bienert, W. B., and Brennan, P. J., "Transient Performance of Electrical Feedback Controlled Variable Conductance Heat Pipes."
3. Marcus, B. D., "Theory and Design of Variable Conductance Heat Pipes," NASA CR-2018, April 1972.
4. Krieth, F., "Principles of Heat Transfer," International Textbook Company, Scranton, Pa., 1958.

5. Marcus, B. D., Fleishman, G. L., and Edwards, D. K., "User's Manual for the TRW GASPIPE 2 Program," NAS2-5503, October 1973.
6. Saaski, E. W., "Heat Pipe Temperature Control Utilizing a Soluble Gas Absorption Reservoir," NASA CR-137792, February 1976.
7. Cotter, T. P., "Heat Pipe Startup Dynamics," IEEE 1967 Thermionic Conversion Specialist Conference, October 1967.
8. Deverall, J. E., "Capability of Heat Pipes," Heat Pipe Technology & Manned Space Station Appl. Technical Interchange, Huntsville, Alabama, May 27, 1969.
9. Kemme, J. E., "High Performance Heat Pipes," IEEE 1967 Thermionic Specialist Conference, October 1967, pp. 355-358.
10. Kemme, J. E., "Heat Pipe Capability Experiments," Proceedings of Joint AEC/Sandia Labs., Heat Pipe Conference 1, SC-M-66-223, October 1966, pp. 11-26.
11. Shlossinger, A. P., "Heat Pipe Devices for Space Suit Temperature Control," TRW Systems Report No. 06462-6005-R0-00, November 1968.
12. Colwell, G.T. "Prediction of Cryogenic Heat Pipe Performance," Annual Report for 1975 under Grant No. NSG-2054, Feb. 1, 1976.
13. Eninger, J. E., Luedke, E. E., and Wanous, D. J., "Flight Data Analysis and Further Development of Variable-Conductance Heat Pipes," NASA CR-137782, February 1976.
14. Sherman, A., and Brennan, P. J., "Cryogenic and Low Temperature Heat Pipe/Cooler Studies for Spacecraft Application," AIAA Paper No. 74-753, July 1974.
15. Groll, M., and Munzel, W. D., "Design and Development of a Heat Pipe Diode," Phase I: Design, Prepared for ESTEC, Contract No. 2993/76/NL/PP (SC), July 1977.
16. Kosson, R. L., Quandrini, J. A., and Kirkpatrick, J. P., "Development of a Blocking-Orifice Thermal Diode Heat Pipe," AIAA Paper No. 74-754, July 1974.
17. Reid, R. C., and Sherwood, T. K., "The Properties of Gases and Liquids - Their Estimation and Correlation," McGraw-Hill Book Co., Inc., New York, 1958.

HEAT PIPE DESIGN

The development of a practical heat pipe design requires the application of the theory presented in Chapters 2 and 3 in combination with a variety of considerations including physical, thermal and mechanical constraints; application requirements; materials properties; fabrication, processing and testing limitations; as well as reliability and safety. At the outset the designer is faced with a number of optional solutions including non-heat pipe design alternatives. The objective of this chapter is to illustrate practical design procedures that are required for the successful development and application of heat pipe hardware.

4.1 DESIGN PROCEDURE

Fig. 4-1 is a flow chart of the major steps to be followed in the design of a heat pipe. The first step in the design process is to identify the performance requirements. Once the specifications for a heat pipe application have been defined, the design selection and evaluation process can be initiated. Three basic considerations are applicable to the development of any heat pipe design:

- (1) Selection of the working fluid
- (2) Selection of the wick design
- (3) Selection of the container design

For a given application, several possible combinations of working fluid, wick structure and container design can be selected to satisfy the specifications. Other considerations such as thermal control techniques (e.g., active or passive gas controlled variable conductance) will also affect the heat pipe's design. As in any design optimization, the final design represents an iteration among the various design factors, and very often an adjustment of the performance requirements or design constraints. A detailed discussion of those factors which determine a heat pipe's design is given in Section 4.2.

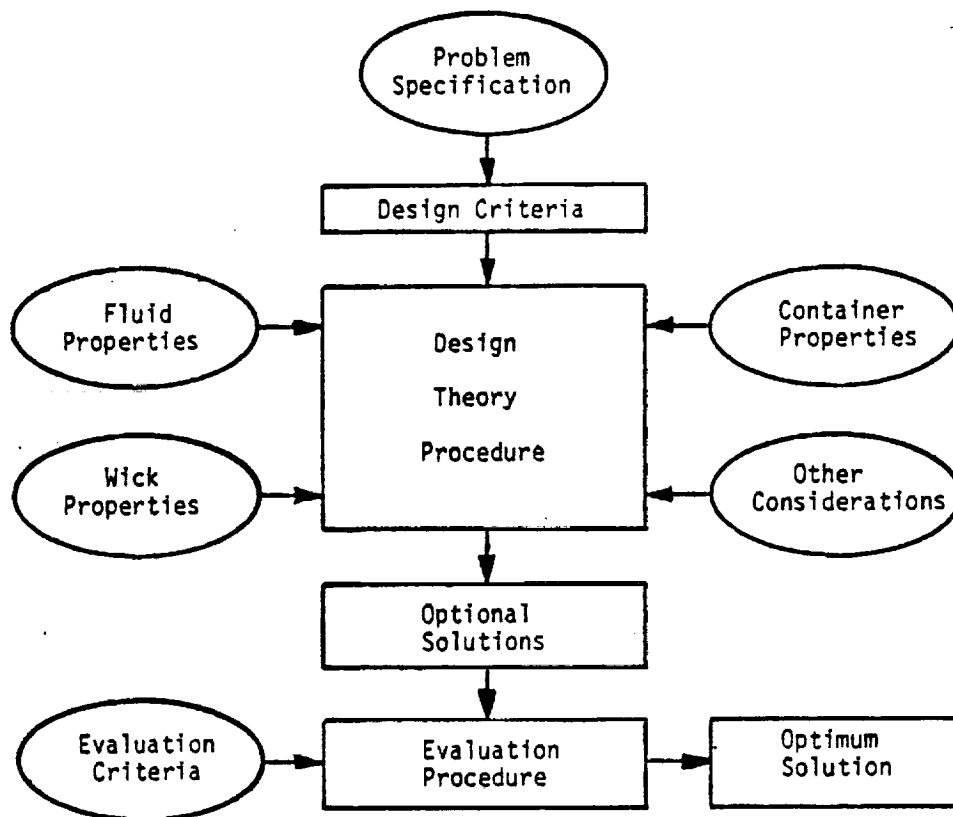


Fig. 4-1. Flow chart of heat pipe design procedure

4.2 PROBLEM DEFINITION AND DESIGN CRITERIA

The basic performance requirements of the specific application must be established before any design effort can be initiated. These parameters include operating temperature range, heat load requirements, allowable temperature drops, thermal control requirements, and size, weight and geometry limitations. In addition, design and operational constraints associated with testing, operational limits under gravitational or acceleration loads, mechanical, thermal interface requirements, storage and operational lifetimes, pressure containment specifications, toxicity requirements, and provisions for structural support must also be established. Also the type of application, aerospace or commercial, and ultimately cost must be considered. A specification should be prepared to organize and delineate the various requirements. This specification should be thorough and complete since it will be the document used for the design, development, and test efforts. A listing of the requirements which may be included in the heat pipe specification and their impact on the heat pipe design is given in Table 4-1.

TABLE 4-1 PROBLEM DEFINITION AND DESIGN CRITERIA

Requirement	Impact on Heat Pipe Design
Operating Temperature Range	Choice of working fluid; pressure retention
Thermal Load	Heat Pipe diameter, number of heat pipes, wick design, and choice of working fluid
Transport Length	Wick design
Temperature Uniformity and Overall ΔT	Evaporator and condenser wick design, conductive path length trade-off, heat pipe geometry
Physical Requirements	Size, weight structural strength and geometry
Acceptance & Quality Testing	"One-G" environment operation and correlation with "Zero-G" operation
Ground Testing	Degrees of freedom in orientation, limits on operating during testing
Dynamic Environment	Operation under acceleration loads, structural integrity
Thermal Environment	Pressure retention during non-operating temperature cycles
Man Rating	Pressure Vessel Code; Fluid Toxicity
Mechanical Interfacing	Mounting provisions, provisions for thermal interfacing
Transient Behavior	Choice of working fluid, wick design, variable conductance type
Reliability	Leak tightness requirements, material compatibility, processing care and control, redundancy

4.2.1 Operating And Non-Operating Thermal Environment

This requirement represents the primary constraint on the selection of the working fluid. Freezing point and critical temperature define the operating limits of a fluid. However, in practice, the useful temperature range must be well within these limits. Clearly defined upper and lower operating temperature bounds are therefore required for proper selection of the working fluid. In addition, it is often necessary to define maximum and minimum non-operating temperature conditions. Upper temperature limits can affect the pressure containment design and may impact working fluid degradation and materials compatibility. The minimum non-operating temperature on the other hand can affect the heat pipe's start-up behavior especially if operation is to be initiated from a frozen or low vapor temperature state at which point the pipe has negligible heat transport capacity.

Sink temperature variations and temperature control requirements are the most significant design constraints associated with thermal control heat pipes. They can affect the selection of variable conductance heat pipe design working fluids and reservoir size. For diode designs, the variation in sink temperature determines the degree of shutdown required and the maximum permissible reverse conductance.

4.2.2 Thermal Load

The specification of the thermal load consists of defining the distribution of heat addition and heat removal. Multiple heat input and heat output sections as well as adiabatic sections can exist, but a good definition of their axial and circumferential distributions must be available. This is necessary to properly evaluate their effect on the transport requirements and the heat pipe temperature drops. The power density and distribution of any heat addition will also determine whether a boiling limit could occur in the evaporator section(s). Finally, the transient nature of the heat loads should also be defined where tight temperature control and variable conductance operation are required.

4.2.3 Transport Length

The transport length is an equivalent distance over which the heat must be carried. This requirement, in combination with the thermal load distribution, determines the transport requirement $(QL)_{req}$ which directly affects the choice of working fluid and wick design.

4.2.4 Temperature Uniformity and Overall Temperature Drop

The degree of temperature uniformity and the overall heat pipe temperature drop will determine the evaporator and condenser designs as well as affecting the choice of working fluid and the wick design.

4.2.5 Physical Requirements

Size, weight, and geometry limitations as specified by the application, when considered with the performance requirements, must be such that a practical heat pipe design can be obtained.

4.2.6 Acceptance and Qualification Testing

A detailed discussion of typical heat pipe test requirements is given in Chapter 8. In addition to thermal performance tests, leak tests, compatibility tests, and pressure tests are also often required to verify that the various performance and design requirements have been attained. Thermal performance test requirements must be related to 0-g as well as 1-g behavior. When 0-g applications are specified, the test elevation for 1-g performance verification should be such that 1-g effects such as "puddling" are minimized. However, since the 1-g test elevation affects the choice of working fluid and the wick design, this elevation should not be overly prohibitive. Leak and pressure tests are generally defined as part of the fabrication process; their specified levels affect the container and closure designs.

4.2.7 Dynamic Environment

Capillary forces are relatively small, and therefore operation of a heat pipe against adverse acceleration loads is limited. The frequency and nature of acceleration loads must be defined and imposed as operational constraints on the heat pipe if operation under these conditions is required. In addition, the heat pipe may be subjected to a dynamic environment, and the heat pipe must be designed to withstand these dynamic loads without damage or degradation in performance.

4.2.8 Man Rating

Exposure to personnel during processing, testing, handling, shipping, installation and operation requires heat pipes that are safe and free of hazards. Safety standards associated with the toxicity of the working fluid, the fluid's vapor pressure, and pressure retention are additional constraints which must be placed on the heat pipe design.

Industry standards such as the ASME Boiler Code (35) for pressure vessels and safety regulations for the handling of hazardous materials are used in defining hazard-free design requirements.

4.2.9 Thermal/Mechanical Interface

Thermal/mechanical interfaces affect container design and the thermal performance of the heat pipe. To achieve good thermal interfaces, it is first necessary to define the mechanical interface requirements. The surface flatness and finish of an interface have a strong influence on the system's temperature gradients. Interface filler materials improve the performance of mechanical interfaces. However, restrictions are often imposed on their use for space applications because of the outgassing associated with many of these materials.

4.2.10 Transient Behavior

Start-up is best accomplished by using a working fluid which is initially saturated. When this is not possible, as in the case of many cryogenic or liquid metal heat pipes, the wick should be designed to give good transport during the priming operation. When a variable conductance heat pipe is required, the transient behavior will depend to a large extent on the type of VCHP employed and the choice of the working fluid.

4.2.11 Reliability

Four failure mechanisms impose limitations on the life of any heat pipe--these are fluid leakage, non-condensable gas generation, wick degradation, and fluid property degradation. The life of the heat pipe is defined as the total time span from the time of final pinch-off to the end of use as defined by application requirements. This total time span determines the minimum leak-tightness requirement. This parameter is critical since heat pipes operate with a very small fluid inventory, and small continuous leaks can cause the heat pipe to become inoperable.

The working fluid must be compatible with the container and wick materials in order to avoid generation of non-condensable gases. Again, for extended life requirements, even extremely small rates of non-condensable gas generation can be detrimental. This is especially true for heat pipes which have very small condenser regions. Non-condensable gases are swept from the evaporator to the condenser region; and, if excessive gas is generated, unacceptable condenser blockage can result.

Wicks can degrade due to erosion or an accumulation of particulate matter which impedes the liquid flow through the wick. Similarly, fluid properties can degrade due to chemical reactions. It is important that realistic lifetimes be defined so that they can be demonstrated with meaningful accelerated life tests (see Section 8.1.1.2).

4.2.12 Temperature Control Sensitivity

Temperature control requirements often determine the type of variable conductance technique that must be employed. Cold-wicked reservoir VCHP's can provide adequate temperature control for moderate heat load and sink temperature variations. A feedback controlled VCHP is capable of providing absolute temperature control for very severe variations of heat load and sink temperatures. For any variable conductance pipe, the required degree of temperature control will affect the choice of the working fluid and the reservoir size.

4.3 WORKING FLUID SELECTION

A variety of physical, chemical, and thermodynamic properties of a particular working fluid must be evaluated to determine whether or not that fluid is suitable for the specific heat pipe application. The general considerations which apply to candidate fluids are:

- (1) Operating temperature range
- (2) Liquid transport factor
- (3) Vapor phase properties
- (4) Wicking capability in body-force field
- (5) Thermal conductivity
- (6) Fluid operating pressure
- (7) Fluid compatibility and stability

A number of heat pipe fluids and their operating temperature range are summarized in Table 4-2. These are categorized into three operating temperature ranges: cryogenic (Group 1), intermediate (Group 2), and high temperature (Group 3). Properties which directly affect heat pipe design and performance are given in Figs. 4-2 through 4-13. A detailed listing of the fluid properties together with a computer program for tabulating fluid properties (HPF) is presented in Volume II of this manual. The effects of these various parameters on the selection of a working fluid are discussed below.

FLUID	FORMULA	GROUP	MOLECULAR WEIGHT	MELTING POINT		NORMAL BOILING POINT		CRITICAL TEMPERATURE		CRITICAL PRESSURE 10 ⁵ Nm ⁻² Psta	TEMPERATURE RANGE OF TABULATED DATA [°K]	REFERENCES*
				°K	°F	°K	°F	°K	°F			
1. Helium	He	1	4.0	1.3	-457.3	4.2	-452.1	5.2	-450.3	2.3	33.4	1
2. Hydrogen	H ₂	1	2.0	14.0	-434.4	20.4	-423.0	33.0	-400.3	12.9	187.2	1, 2, 7
3. Neon	Ne	1	20.2	24.5	-415.6	27.1	-410.9	44.4	-379.8	26.5	384.5	1, 3, 7
4. Oxygen	O ₂	1	32.0	54.3	-361.8	90.2	-297.3	154.8	-181.1	50.9	738.6	1, 2, 3, 7
5. Nitrogen	N ₂	1	28.0	63.1	-346.0	77.3	-320.4	126.2	-232.4	34.0	493.3	1, 2, 3, 5
6. Argon	Ar	1	39.9	83.8	-308.8	87.3	-302.5	150.9	-188.1	50.0	725.5	1, 3, 4
7. Propane	C ₃ H ₈	1	44.1	85.5	-305.8	231.1	43.7	370.0	206.3	42.6	618.1	1, 6, 9
8. Freon -14	CF ₄	1	88.0	89.4	-298.7	145.5	-197.8	227.7	-49.8	37.4	542.7	14
9. Ethane	C ₂ H ₆	1	30.1	89.9	-297.8	184.5	-127.6	305.5	90.2	49.1	712.4	1, 3, 6, 9
10. Methane	CH ₄	1	16.0	90.7	-296.4	111.4	-259.2	190.5	-116.8	46.4	673.3	1, 3, 5, 6
11. Freon -13	CClF ₃	1	104.5	93.2	-291.9	191.7	-114.6	302.3	84.5	39.0	565.9	1, 3
12. Butane	C ₄ H ₁₀	1	58.1	134.8	-210.9	282.1	48.1	451.4	362.8	38.0	550.7	1, 3, 5, 6, 9
13. Freon -21	CHCl ₂ F	1	102.9	138.2	-210.9	282.1	48.1	451.4	362.8	51.8	751.8	1, 3, 5
14. Freon -11	CCl ₃ F	1, 2	137.4	162.2	-167.8	296.9	74.7	471.2	388.5	44.1	639.9	1, 3, 5
15. Methanol	CH ₃ OH	2	32.0	175.2	-144.3	337.9	148.5	513.2	464.1	79.5	1153.0	1
16. Toluene	C ₇ H ₈	2	92.1	178.1	-139.1	383.7	133.2	593.9	609.3	41.6	603.6	1, 5, 6
17. N-Heptane	(CH ₃) ₂ CO	2	59.1	180.0	-135.7	329.4	133.2	508.2	455.1	47.6	690.0	5, 6
18. Acetone	C ₃ H ₆ O	2	100.2	182.6	-131.0	371.6	209.2	540.2	512.7	27.4	397.6	1, 5, 6
19. Ammonia	NH ₃	1, 2	17.0	195.5	-107.8	239.8	-28.0	405.6	270.4	112.9	1638.0	1, 2, 3, 5
20. M-Xylene	C ₁₀ H ₈	2	106.2	225.3	-54.1	412.3	282.5	619.2	654.9	36.5	529.6	1, 6
21. Mercury	Hg	2, 3	200.6	234.3	-37.9	630.1	674.5	1763	2714	1510	21910	1, 7, 8
22. Dowtherm E		2	147.0	273.2	32.0	453.4	356.4	690.2	785.0	40.3	584.7	13
23. Water	H ₂ O	2	18.0	278.7	42.0	373.2	212.0	647.3	705.4	221.2	3210	1
24. Benzene	C ₆ H ₆	2	78.1	285.2	53.6	531.1	176.2	562.6	553.0	49.2	713.9	1, 5
25. Dowtherm A		2	166.0	301.6	83.2	943.0	496.4	801.2	982.4	40.2	583.3	1
26. Cesium	Cs	3	132.9	336.4	145.8	1032.2	1237.8	2050	3230	117.0	1698.9	1, 7
27. Potassium	K	3	39.1	371.0	208.1	1152.2	1614.3	2250	3590	160.0	2322	1, 7
28. Sodium	Na	3	23.0	453.7	357.0	1615.0	2447.0	3600	6380	370.0	5369	1, 7
29. Lithium	Li	3	6.9	1234	1761	2450.0	3950.3	7500	13040	970.0	14074	1, 7
30. Silver	Ag	3	107.9							336.0	4875	7, 8, 12

*References for fluid properties are listed in Chapter 1 of Volume II

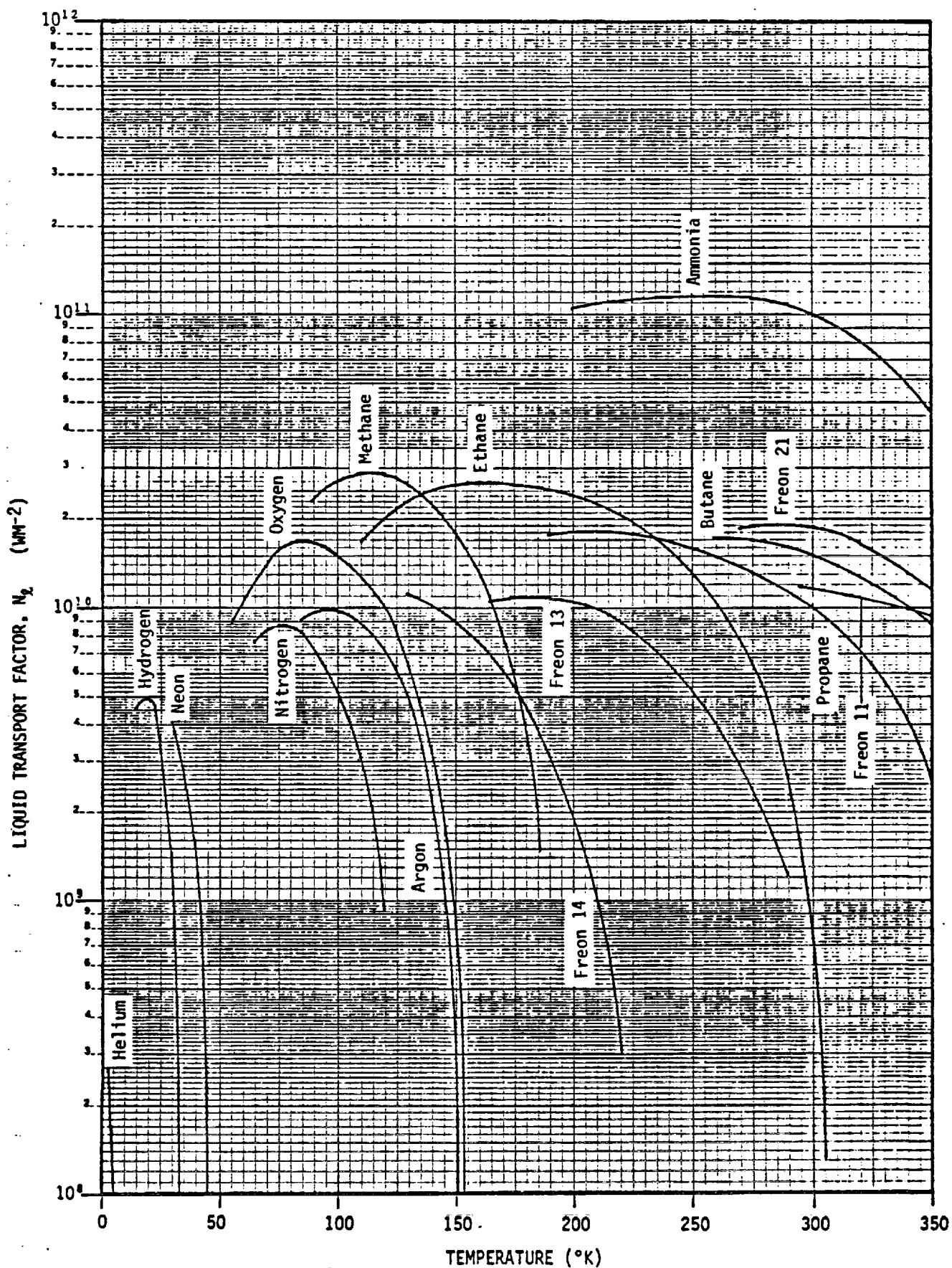


Fig. 4-2. Liquid transport factor: Group 1

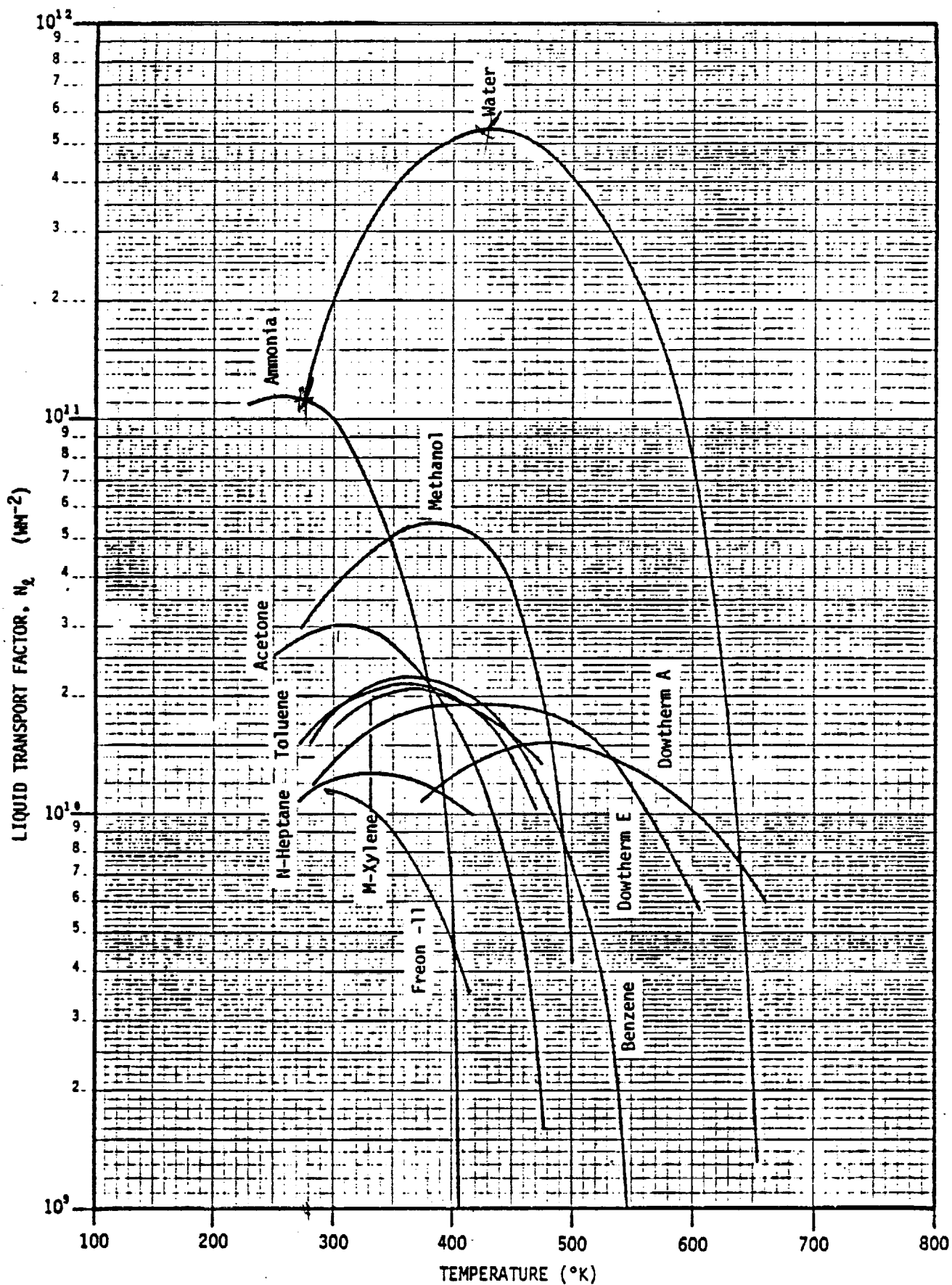


Fig. 4-3. Liquid transport factor: Group 2

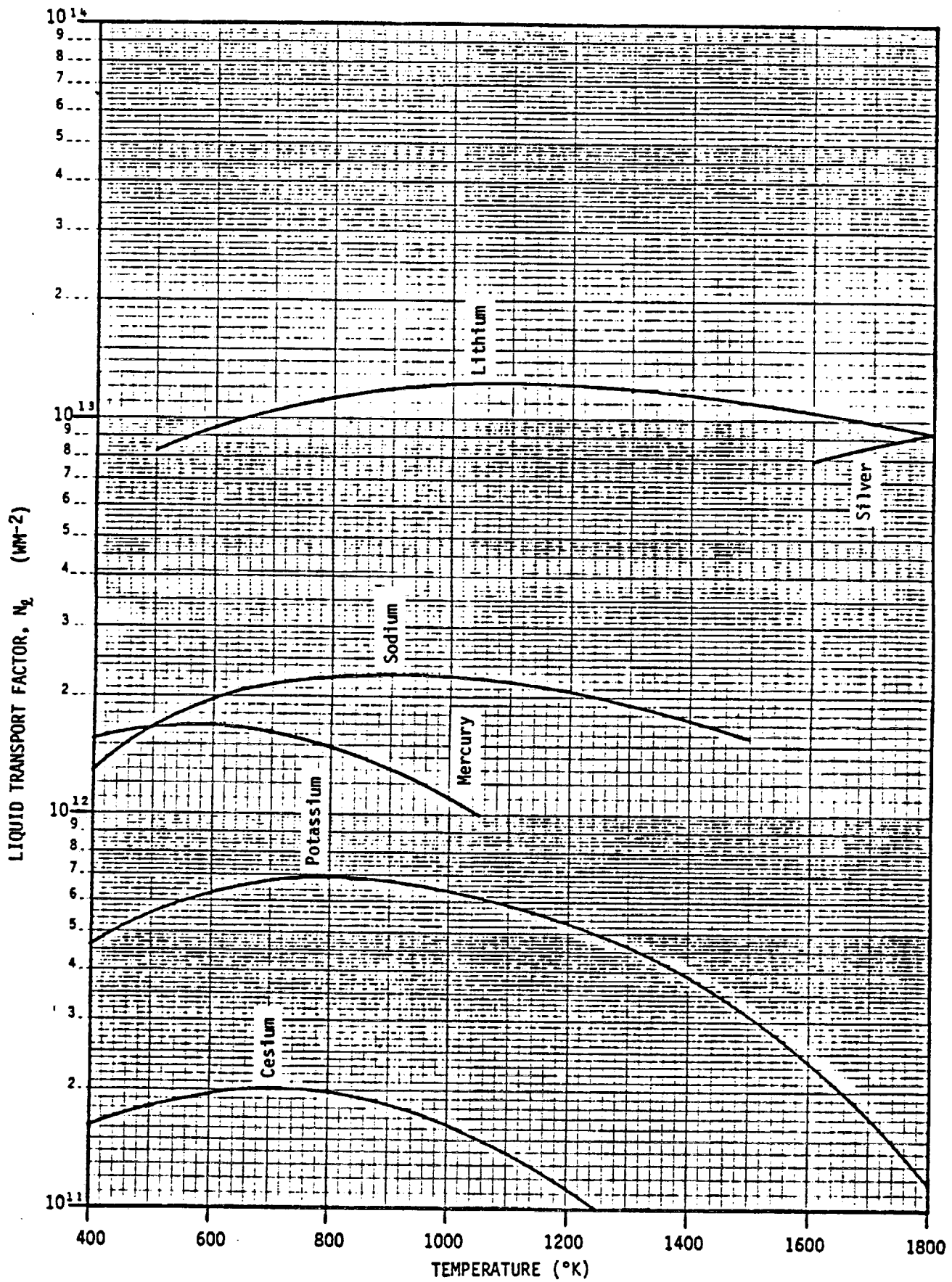


Fig. 4-4. Liquid transport factor: Group 3

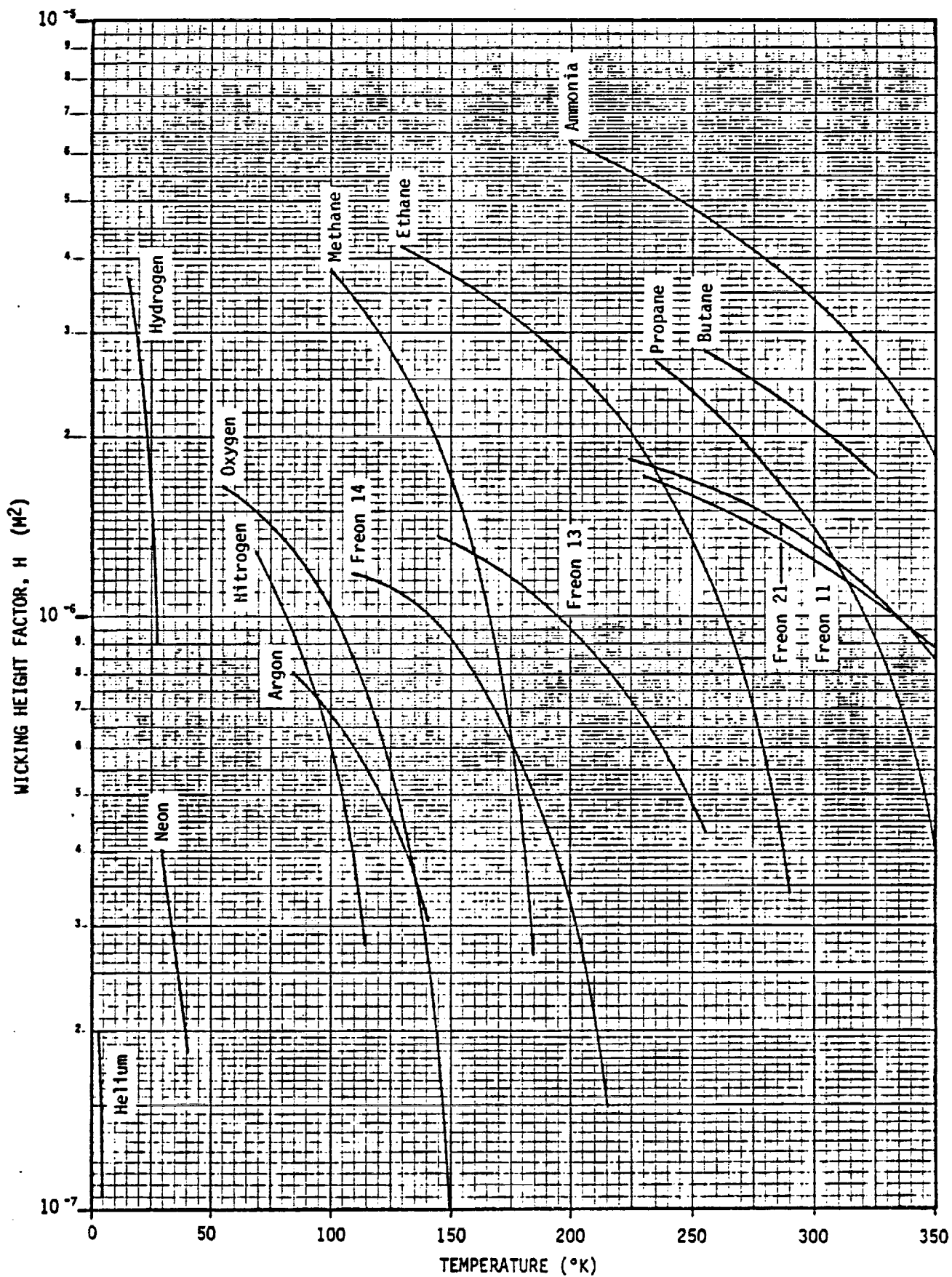


Fig. 4-5. Wicking height factor: Group 1

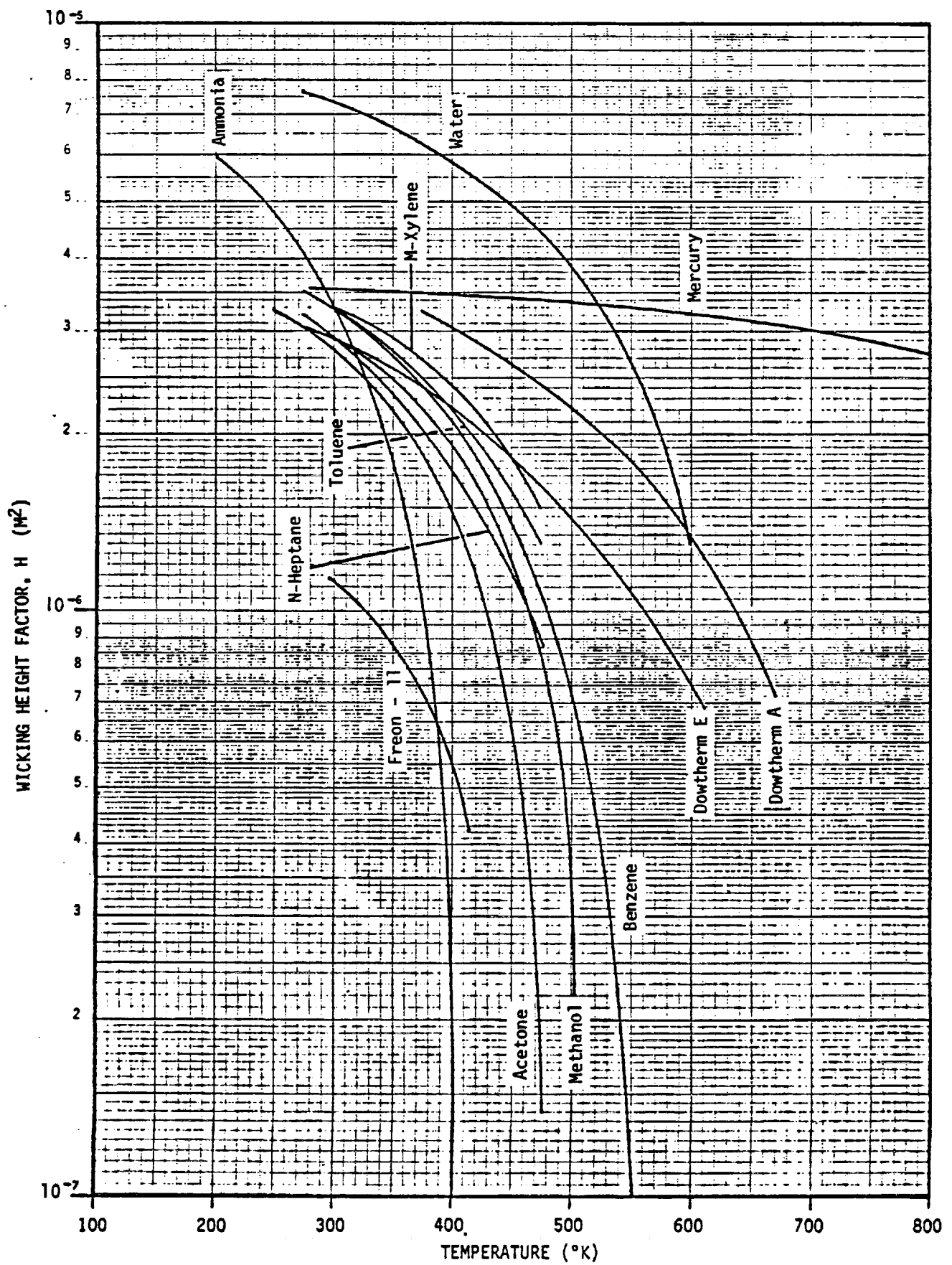


Fig. 4-6. Wicking height factor: Group 2

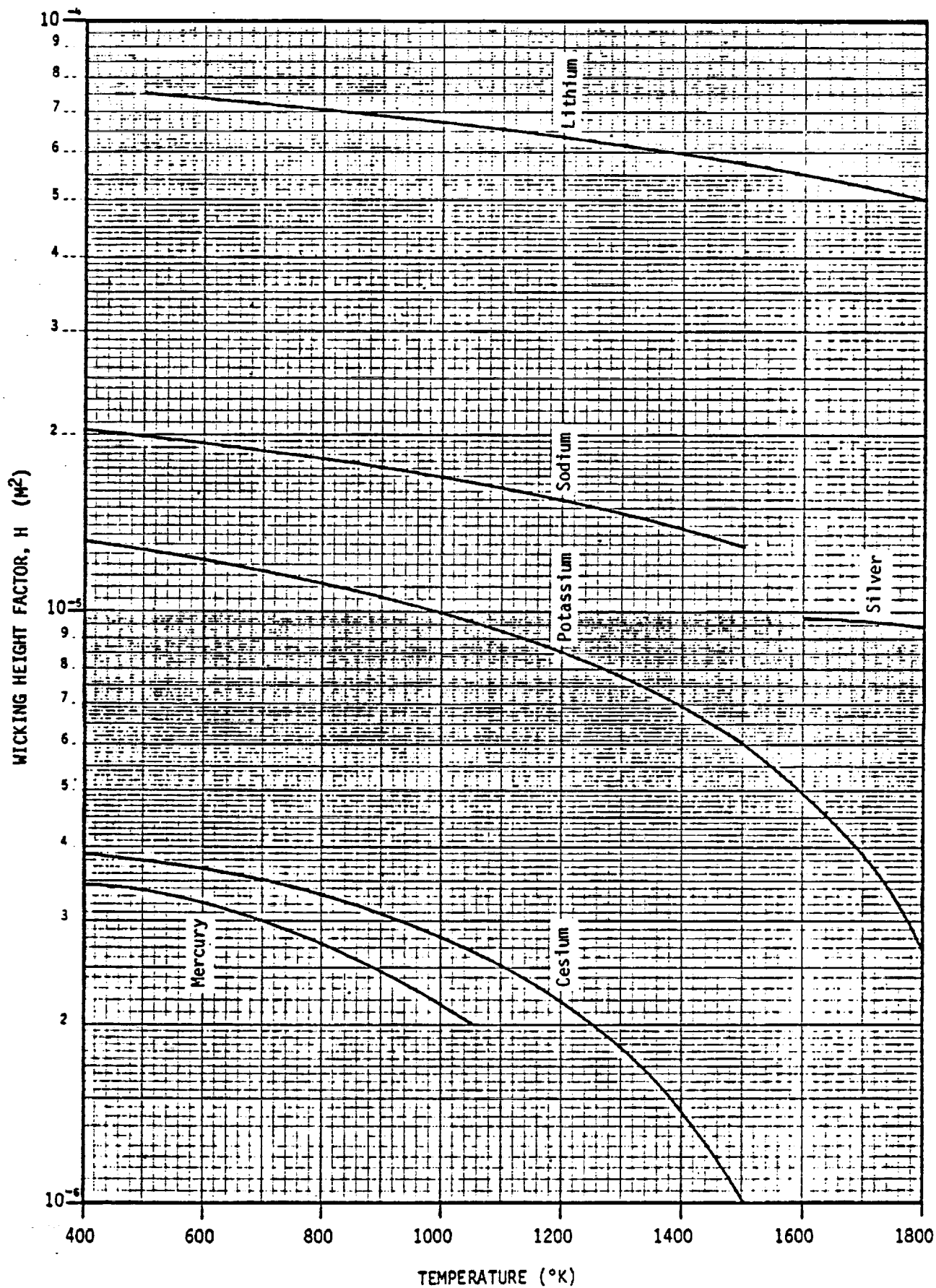


Fig. 4-7. Wicking height factor: Group 3

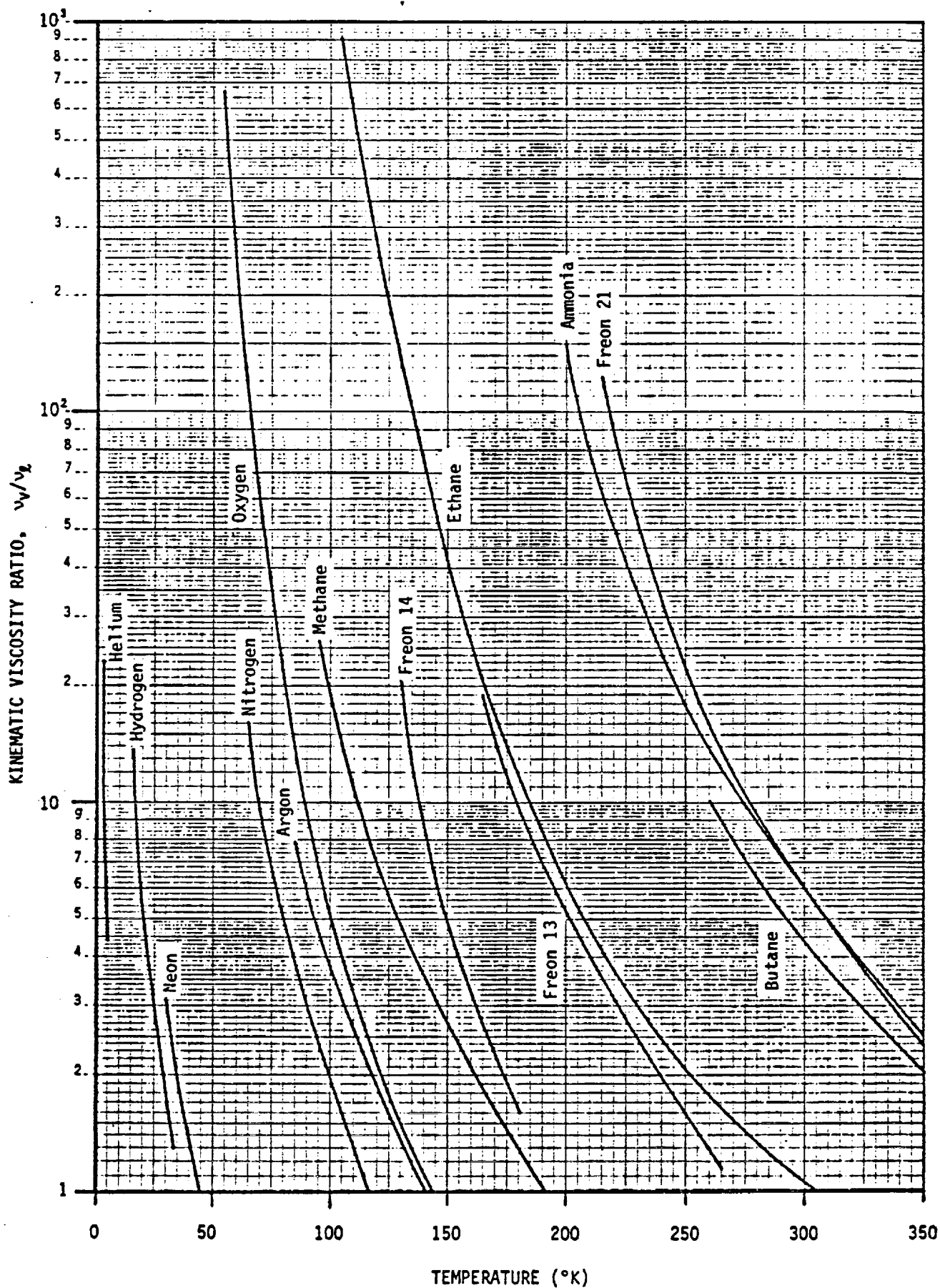


Fig. 4-8. Kinematic viscosity ratio: Group 1

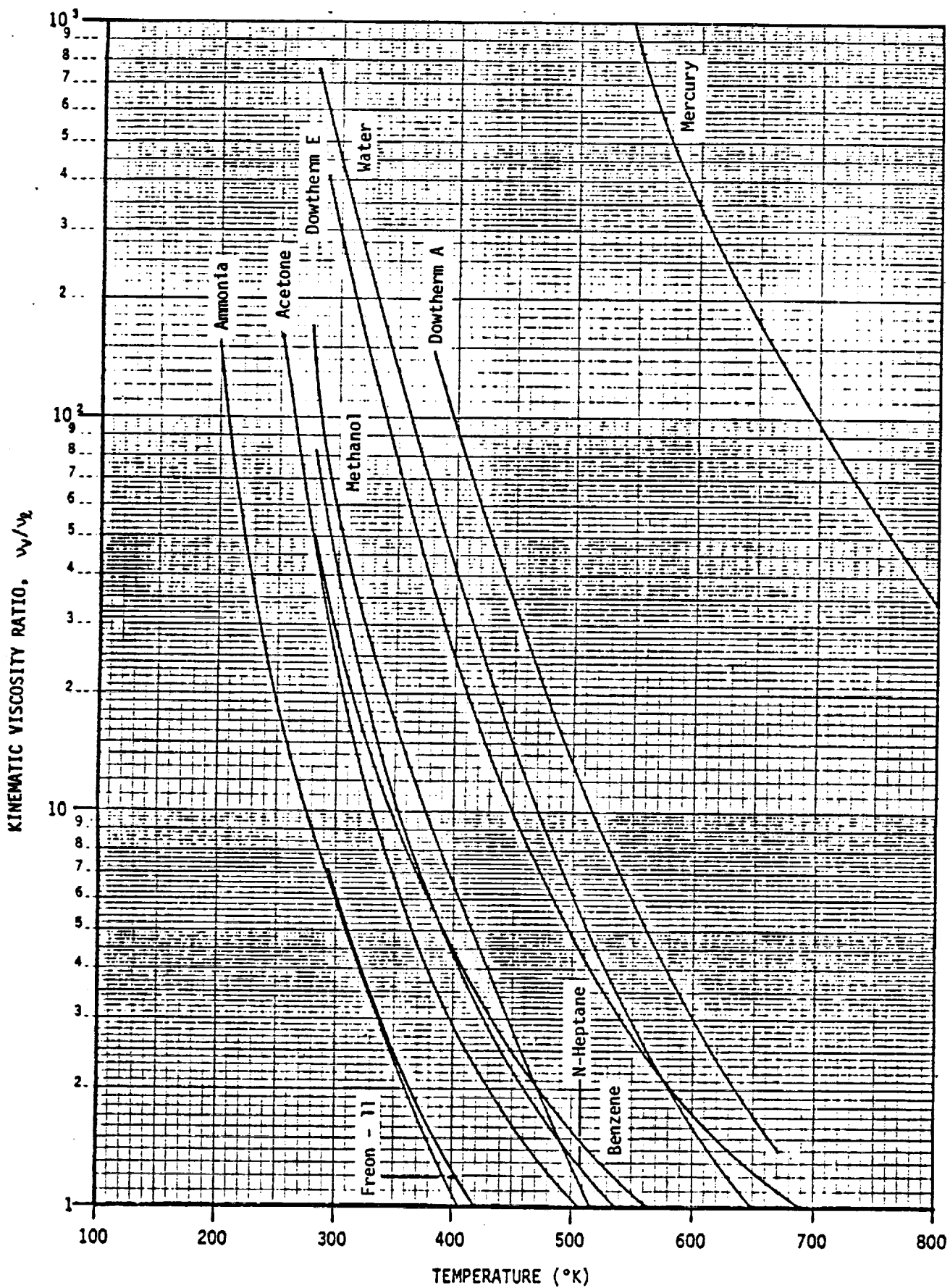


Fig. 4-9. Kinematic viscosity ratio: Group 2

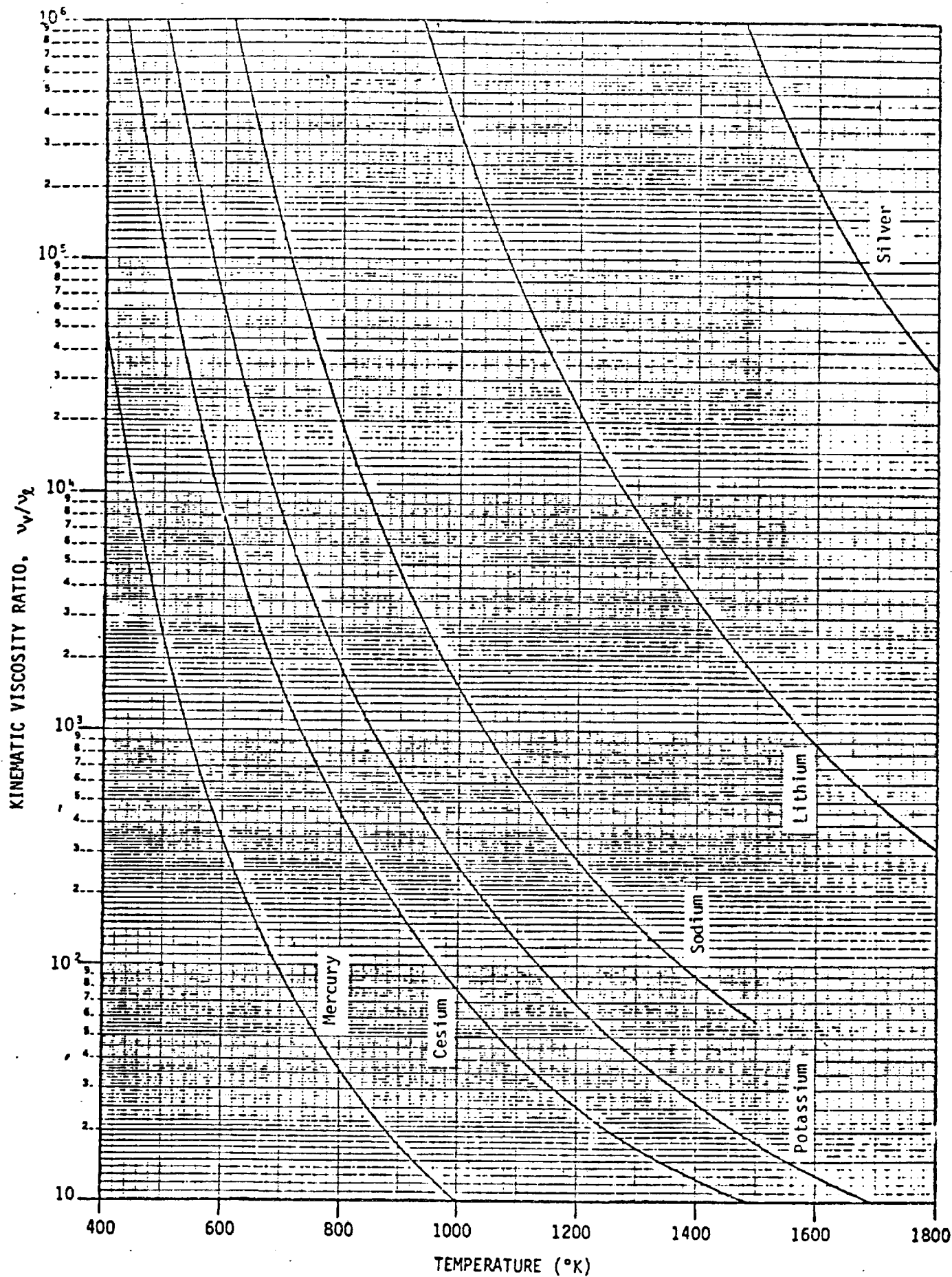


Fig. 4-10. Kinematic viscosity ratio: Group 3

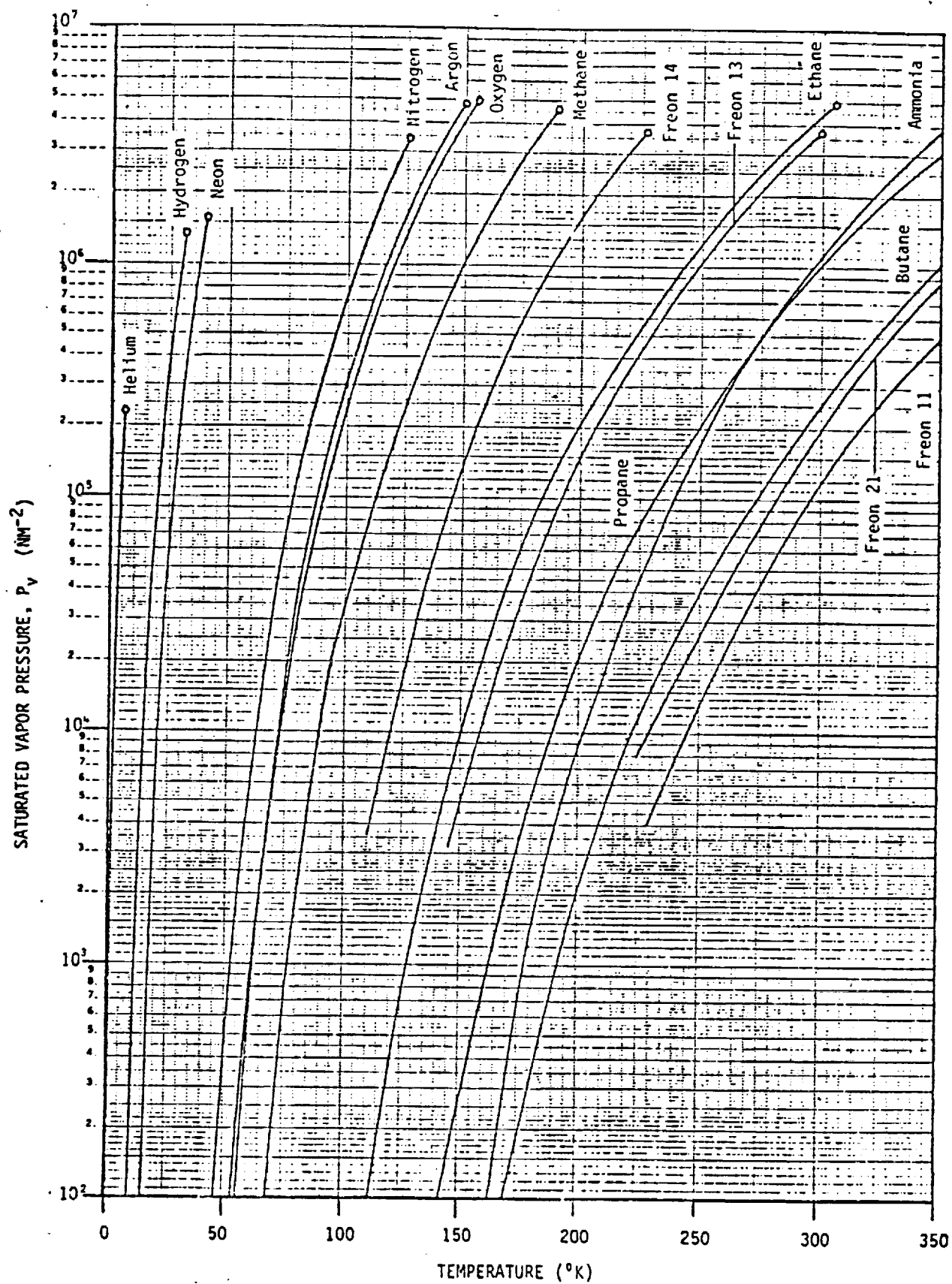


Fig. 4-11. Saturated vapor pressure: Group 1

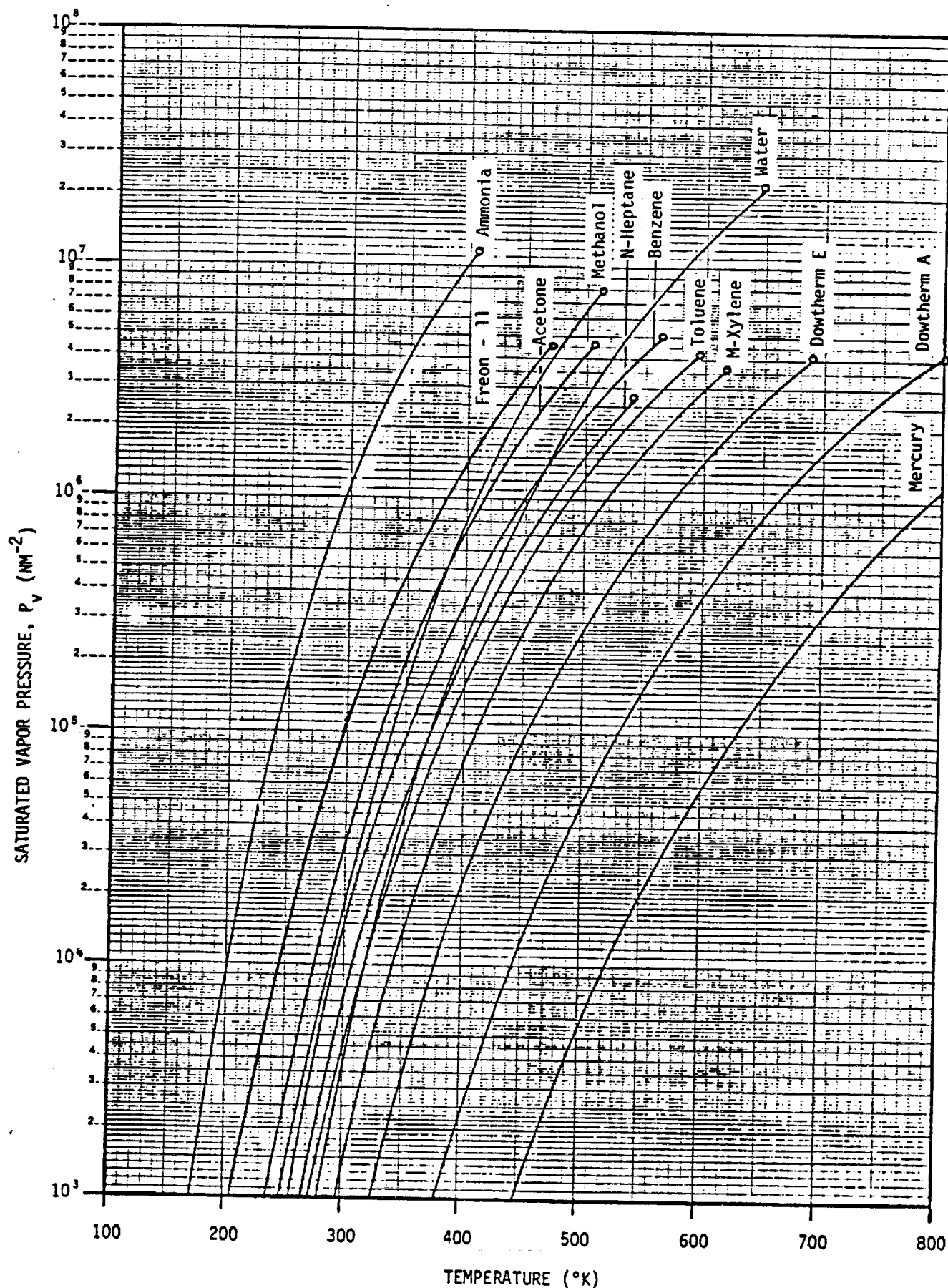


Fig. 4-12. Saturated vapor pressure: Group 2

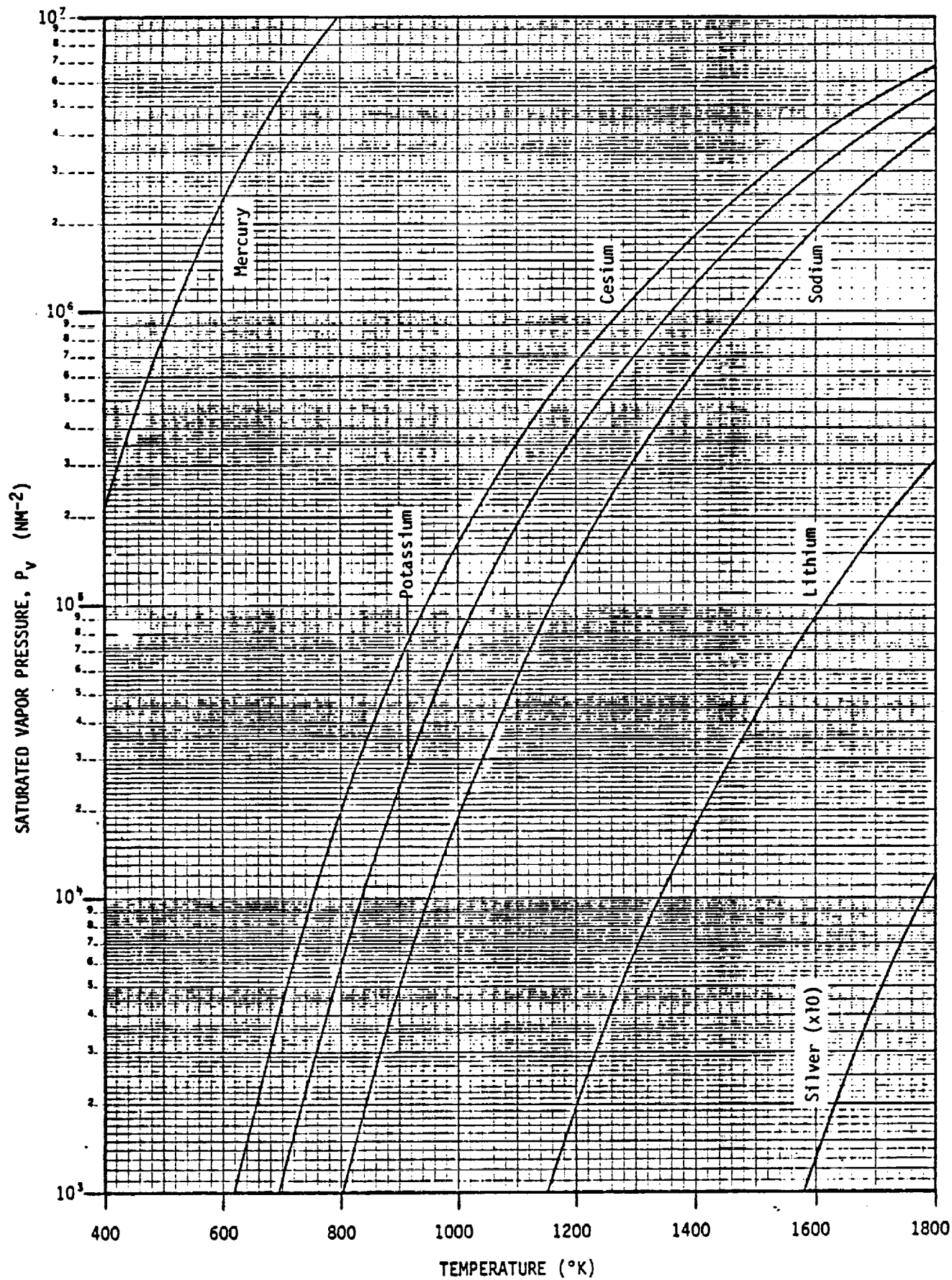


Fig. 4-13. Saturated vapor pressure: Group 3

4.3.1 Operating Temperature Range

Since a heat pipe cannot function below the freezing point or above the thermodynamic critical point of its working fluid, a fluid should be chosen whose useful temperature range spans the operating temperature limits of the heat pipe. The lower temperature limit relates to adverse vapor effects such as the sonic limit, entrainment limit, or simply excessive vapor viscous and liquid/vapor shear pressure drops. As a "rule of thumb", the lowest operating temperature should be greater than the temperature corresponding to a vapor pressure of 0.1 atmosphere. Conversely, the upper limit of the operating temperature should be kept below the critical point to avoid low values of surface tension and latent heat which result in poor capillary pumping and excessive liquid losses. Operation below the critical point will also avoid excessive containment pressure requirements.

4.3.2 Liquid Transport Factor

The capillary pumping ability of the working fluid is best described by the "Liquid Transport Factor," N_L . This factor states that the highest performance of the heat pipe is obtained with a fluid which has a high surface tension, high liquid density, high latent heat of vaporization, and a low viscosity. In Figs. 4-2 to 4-4 the Liquid Transport Factor is plotted versus temperature for selected fluids in the three basic operating temperature regions. Notice that each curve contains a rather broad maximum near the fluids normal boiling point. The decrease in the Liquid Transport Factor on the low temperature side is due to the increase in liquid viscosity. On the high temperature side, the decrease occurs because the latent heat, liquid density, and liquid surface tension all decrease more rapidly than the liquid viscosity. The Liquid Transport Factor decreases to zero at the critical temperature as the latent heat and surface tension become zero.

For heat pipes operating in the absence of body forces and for conditions where the vapor pressure drop is negligible, the capillary pumping limit is directly proportional to N_L . However, in the general design case, there is no simple grouping of fluid properties which serves as an exact basis for selection. Therefore, the N_L factor can only serve as a figure of merit for candidate heat pipe working fluids. To finalize the choice of fluid, a parametric evaluation must be conducted which includes the liquid transport factor, vapor losses, wicking height requirements, and thermal conductance.

4.3.3 Liquid Wicking Capability in a Body-Force Field

As discussed in Chapter 2, the presence of body forces can influence the relative performance of various heat pipe working fluids because:

- (1) The body-force head is subtracted from the maximum capillary head in determining the capillary pumping available to overcome flow losses.
- (2) The body-force head must be overcome by surface tension effects in order to prime the wick configuration.

Since in both cases the problem is one of surface tension forces working against body forces, the ratio of these forces represents a basis of fluid comparison. In terms of fluid properties, this ratio is proportional to the "Wicking Height Factor."

$$H_L = \frac{\sigma}{\rho_L g}$$

Thus, to minimize adverse body-force effects, the designer should select a working fluid which has a high value for this parameter. For the purpose of comparison, the Wicking Height Factor is given in Figs. 4-5 through 4-7 for various working fluids as a function of temperature. It decreases with increasing temperature since the surface tension decreases faster than the liquid density.

4.3.4 Kinematic Viscosity Ratio

The Liquid Transport Factor N_L and the Wicking Height Factor H_L defined above provide figures of merit for the liquid phase of the working fluid. The relative merit of the vapor phase can be described by the "Kinematic Viscosity Ratio."

$$\frac{v_v}{v_L} = \frac{\mu_v}{\mu_L} \frac{\rho_L}{\rho_v}$$

This parameter in combination with wick and vapor channel properties defines the proportion of viscous vapor to liquid flow losses. To minimize adverse vapor effects (viscous and shear losses), low values of this parameter are desirable. As shown in Figs. 4-8 through 4-10, the Kinematic Viscosity Ratio decreases with increasing temperature.

4.3.5 Pressure Containment

Adequate attention must be given to evaluating the heat pipe design for all possible temperature environments to which the heat pipe could be subjected. In the case of cryogenic and low temperature heat pipes, storage at ambient temperature or shipping conditions will usually result in substantial internal pressures. Similarly, there exist various applications where the heat pipe must be bonded to another system component. In many cases it is advantageous to bond the heat pipe after it has been charged. Provision must be made in the heat pipe design to contain the resulting pressure or the fabrication process must be specified to avoid this potential excessive pressure condition.

At saturation condition, the vapor pressure is readily determined (e.g., Figs. 4-11 thru 4-13). If the critical point of the fluid is exceeded, the designer can calculate an approximate pressure by using the simple equation of state for an ideal gas.

$$p V = n R T \quad (4-1)$$

This equation holds, with a fair degree of accuracy, for highly superheated vapors. In order to calculate internal pressures, which are fairly accurate throughout the entire superheated vapor region, more complex equations of state (developed from empirical data) must be utilized. One of the best known and most useful such equations is the Beattie-Bridgeman Equation of State (1). The equation is:

$$p = \frac{R T (1 - e')}{v_n^2} (v_n + B) - \frac{A}{v_n^2} \quad (4-2)$$

where:

$$\left. \begin{aligned} v_n &= \text{Specific Volume (liters/gm-mole)} \\ v_n &= (\text{Volume} \times \text{Molecular Weight})/\text{mass} \\ A &= A_0 \left(1 - \frac{a}{v_n}\right) \\ B &= B_0 \left(1 - \frac{b}{v_n}\right) \\ e' &= \frac{c}{v_n T^3} \end{aligned} \right\} \quad (4-3)$$

A_0 , a , B_0 , b , and c are constants that must be determined experimentally for each fluid. The constants for a number of fluids are given in Table 4-3. If the constants are not available for a particular fluid, it is suggested that the ideal gas equation be used and a safety factor of 2.5 to 3 be applied to the working stress of the heat pipe container material.

TABLE 4-3. CONSTANTS FOR THE BEATTIE-BRIDGEMAN EQUATION OF STATE (1)

<u>GAS</u>	<u>Ao</u>	<u>a</u>	<u>Bo</u>	<u>b</u>	<u>10⁻⁴ x c</u>
Ammonia	2.3920	0.17031	0.03415	0.19112	476.87
Argon	1.2907	0.02328	0.03931	0.0	5.99
n-Butane	17.7940	0.12161	0.24620	0.09423	350.00
Ethane	5.8800	0.05861	0.09400	0.01915	90.00
Helium	0.0216	0.05984	0.01400	0.0	0.0040
n-Heptane	54.5200	0.20066	0.70816	0.19179	400.00
Hydrogen	0.1975	-0.00506	0.02096	-0.04359	0.0504
Methane	2.2769	0.01855	0.05587	-0.01587	12.83
Methanol	33.3090	0.09246	0.60362	0.09929	32.03
Neon	0.2125	0.02196	0.02060	0.0	0.101
Nitrogen	1.3445	0.02617	0.05046	-0.00691	4.2
Oxygen	1.4911	0.02562	0.04624	0.004208	4.8
Propane	11.9200	0.07321	0.18100	0.04293	120.00

Units: Pressure in atmospheres; volume in liters/gm-mole; temperature in °K; R = 0.08206 atm-liters/gm-mole - °K

4.3.6 Heat Transfer

Although the heat pipe has been frequently considered an isothermal heat transfer device, a thermal gradient must always exist between the heat input and output regions during operation. This gradient is determined by the radial heat flux and the thermal conductance of the heat pipe wall and the wick material saturated with the working fluid. The effective conductance of various wick designs is discussed more fully in Section 4.4. As far as the selection of the working fluid is concerned, it is desirable to choose the fluid with the highest thermal conductivity since film coefficients are directly proportional to this property. Liquid phase thermal conductivities for various heat pipe fluids are given in Fig. 4-14. The thermal conductivity of a given fluid tends to decrease with increasing temperature.

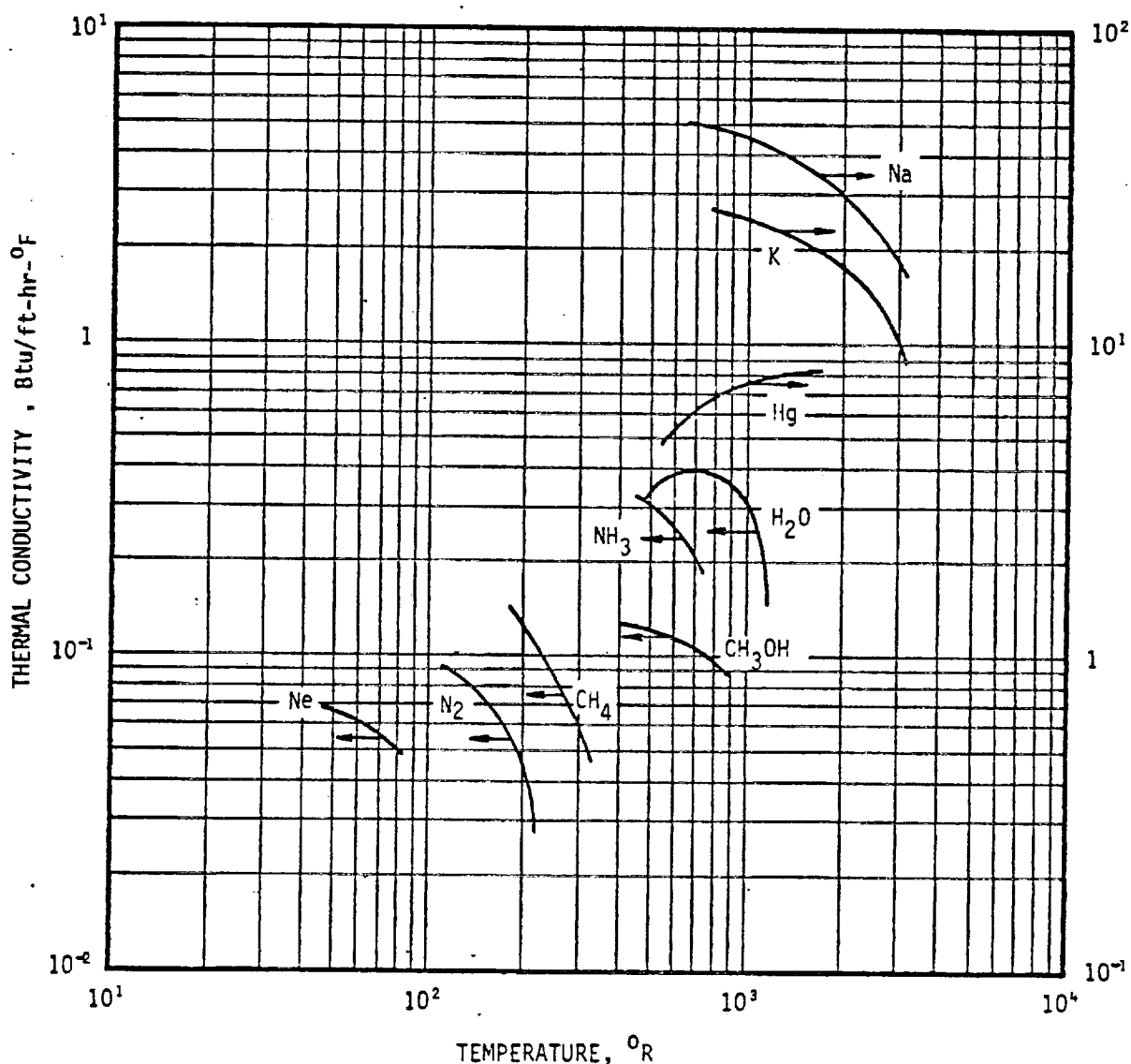


Fig. 4-14. Liquid thermal conductivity for several heat pipe working fluids at saturated state (One °R = 0.5556 °K, 1 Btu/ft-hr-°F = 1.730 W/m-°K)

The designer must also consider the radial heat transfer in the evaporator, especially if boiling would seriously degrade hydrodynamic performance. The criteria for nucleation have been discussed in Chapter 2. Assuming the critical radius in Eq. 2-83 for the critical superheat is equal to the wick pore size, the pertinent fluid property grouping for superheat tolerance is $\sigma/(\lambda \rho)_l$. This parameter, multiplied by the liquid thermal conductivity, yields a measure of the fluid's radial heat transfer tolerance with respect to nucleation. The Nucleation Tolerance Factor is defined as:

$$N_{TF} \equiv (k \sigma / \lambda \rho)_l \quad (4-4)$$

and is plotted versus vapor temperature in Fig. 4-15 for selected working fluids. The higher the value of N_{TF} the greater the heat flux that can be tolerated without nucleate boiling.

4.3.7 Fluid Compatibility

A major factor in the selection of a working fluid is its compatibility with other materials in the heat pipe system. In contrast to most corrosion problems, the structural integrity of the tube wall is not the primary consideration. One of the factors that is critical to the performance of a heat pipe is the amount of non-condensable gas that is generated. The gas could result from materials outgassing or chemical reactions. This gas collects in the condensing region and causes condenser blockage. An example of this is the hydrolysis of water which occurs in aluminum/water heat pipes.

Corrosion and erosion of the container and wick can also result in a change in the wetting angle as well as in the permeability, porosity, or capillary pore size of the wick. Solid precipitates resulting from corrosion and erosion are transported by the working fluid to the evaporator region where they are deposited when the liquid vaporizes. This leads to an increased resistance to fluid flow which results in lowering the Heat Flux Limit in the evaporator.

The compatibility and stability of working fluids and heat pipe materials at the intended operating temperatures must be established by testing. A widely used approach to compatibility testing is to employ the actual heat pipe hardware and monitor the rate of gas generated. As mentioned previously, non-condensable gas generated within a heat pipe collects at the end of the condenser, blocking vapor flow and causing a local temperature drop (see Fig. 4-16). Thus, by monitoring the temperature distribution along a heat

pipe operating at constant temperature, the rate of gas generation can be determined. Several such compatibility tests have been performed by many different experimenters and laboratories. Typical results are listed in Table 4-4.

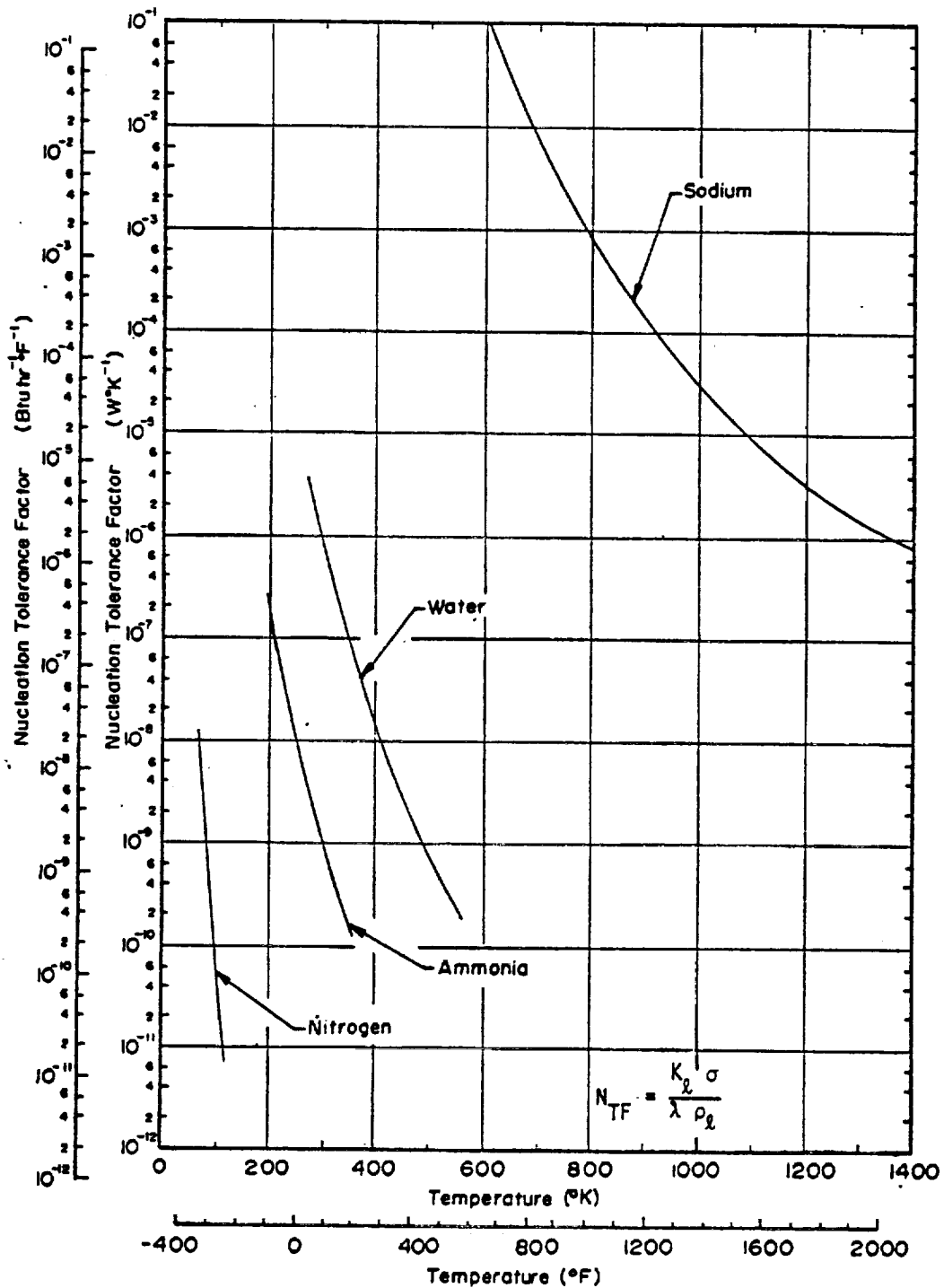


Fig. 4-15. Nucleation tolerance factors of several commonly used working fluids.

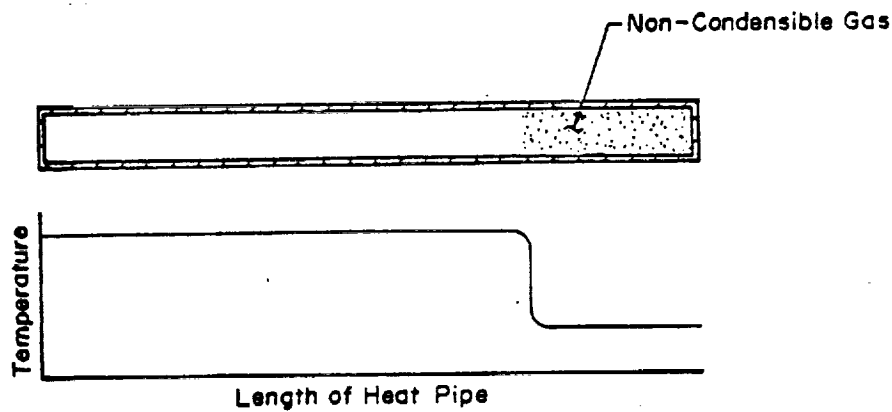


Fig. 4-16. Effect of gas build-up on temperature uniformity of heat pipe

TABLE 4-4. GENERALIZED RESULTS OF EXPERIMENTAL COMPATIBILITY TESTS *

	Aluminum	Stainless Steel	Cold rolled steel	Iron	Copper	Brass	Silica	Nickel	Inconel	Tungsten	Tantalum	Molybdenum	Rhenium	Titanium	Niobium
Water	I	C			C		C	C	I					C	
Ammonia	C	C	C	C				C							
Methanol	I	C		C	C	C	C	C							
Acetone	C	C			C	C	C								
Freon - 11	C														
Freon - 21	C			C											
Freon - 113	C														
C ₆ F ₆					C		C								
n-butane	C														
n-pentane	C	C													
n-heptane	C														
Benzene	C														
Toluene	I														
Dowtherm A		C			C		C								
Dowtherm E	I	C	I		C	I									
DC 200	C	C			C			C							
DC 209					C										
Perchloroethylene					C		C								
Dimethyl Sulfide					C		C								
Monsanto CP-9					C		C								
Monsanto CP-32(pyridene)	I				C										
Monsanto CP-34	I														
Lithium		I						I	I	C	C	C		I	C
Sodium		C						C	C					I	C
Potassium								C						I	
Cesium														C	C
Mercury		C#						I	I		I	I		I	I
Lead		I						I	I	C	C			I	I
Indium		I						I	I	I	I	I		I	
Silver										C	C		I		

C = Compatible
I = Incompatible

* Sensitive to Cleaning
I with Austenitic SS

* See Chapter 7 for detailed Compatibility Test Results

4.4 WICK DESIGN

The wick provides the necessary flow area for liquid return from the condenser to the evaporator and also provides the pores required to develop capillary pumping. The properties of the wick are characterized by the permeability K and an effective pumping radius r_p . These properties and the wick cross-sectional area A_w determine the ability of the heat pipe to overcome hydrodynamic losses.

The choice of a wick design for a specific heat pipe application is determined by trade-offs between a number of interrelated parameters. First, the wick should be capable of providing a high capillary pressure which is equivalent to processing a small effective pore radius. Second, it should be capable of supporting high flow rates which means that the wick should have a high permeability and therefore a large effective pore radius. Finally, in many designs, the wick is directly in the heat flow path and therefore its thermal conductivity is an important consideration.

4.4.1 Basic Properties

As was discussed in Chapter 2, often the only way to obtain accurate values for the various properties of wicks is by experimental measurements. However, reasonable estimates for preliminary evaluations can be made for several configurations. Various types of capillary structures which have been employed in the past are illustrated in Fig. 4-17. These include capillary cylinders (tubes) made of porous material such as wire mesh screen, rectangular and annular flow channels also made of porous material, grooves of various geometries formed in the wall of the heat pipe container, matrices of multiple layers of wire mesh screen, packed spheres, and sintered fibers. Typical wick designs employing the above are discussed in Section 4.4.2. Properties for each are summarized in Table 4-5.

Working estimates for values of the effective pore radius (r_p) and permeability can be easily determined for well defined wick geometries such as the cylindrical, rectangular and annular flow channels. These capillaries are characterized by a constant cross-sectional flow area. The effective pore radius and the permeability can be obtained from the following expressions, (2,3):

$$r_p = \frac{2A}{W_p} \quad (4-5)$$

$$K = \frac{D_h^2}{2(f \cdot Re)} \quad (4-6)$$

where:

$$D_h = \frac{4A}{W_p} \text{ Hydraulic Diameter}$$

A = Cross Sectional Flow Area of the Capillary

W_p = Wetted Perimeter

$f \cdot Re$ = The Product of the Fanning Friction Factor and the Reynolds Number

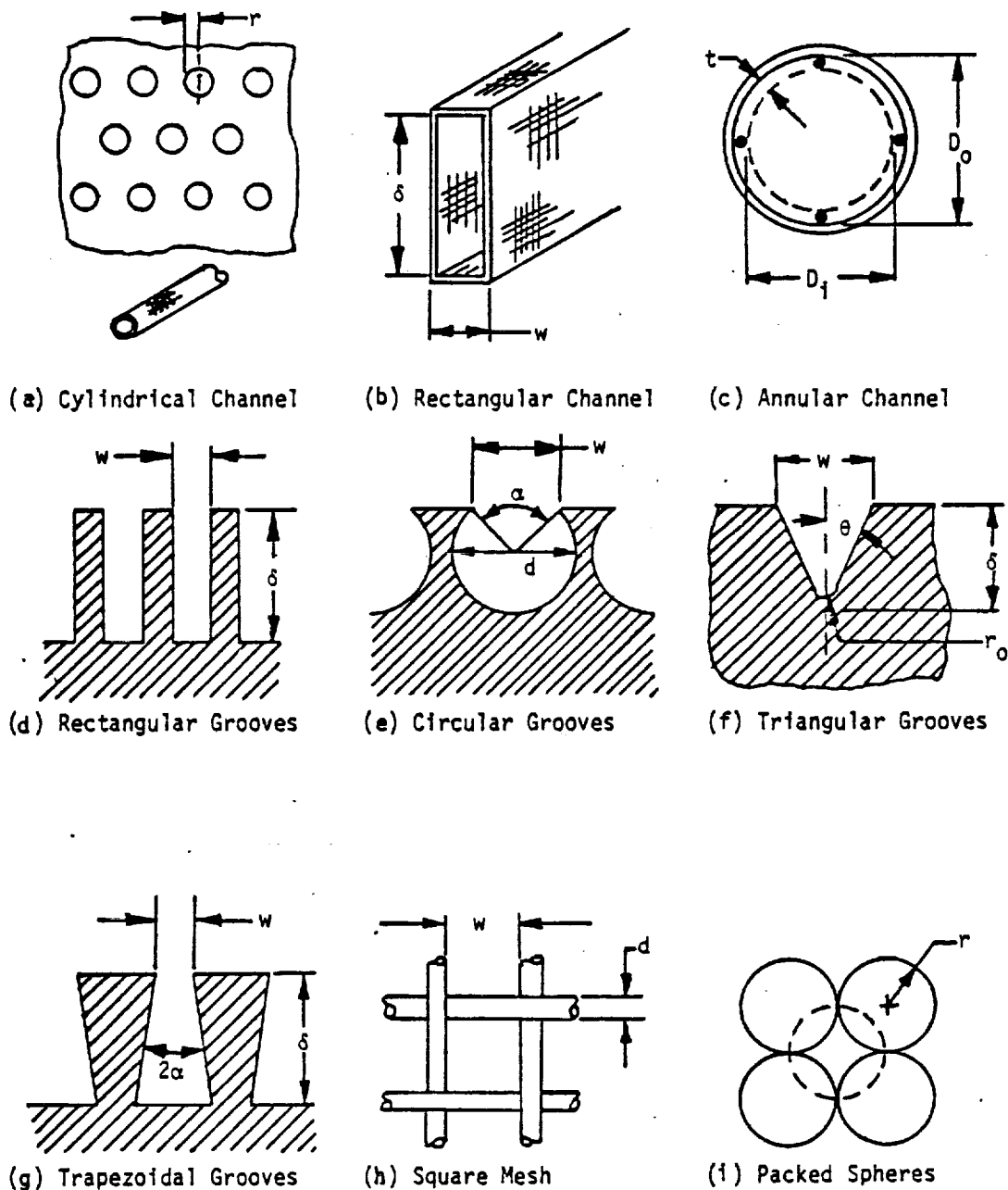


Fig. 4-17. Typical capillary wick designs

TABLE 4-5. CAPILLARY PROPERTIES

TYPE	EFFECTIVE PORE RADIUS r_p	PERMEABILITY K	COMMENTS	REFERENCE
1. Cylindrical	r	$r^2/8$	$(f \cdot Re) = 16$	2,3
2. Rectangular	$\frac{w\delta}{\delta+w}$	$\frac{2}{(f \cdot Re)} \left(\frac{w\delta}{\delta+w} \right)^2$	See Fig. 4-17 for $(f \cdot Re)$ values	2,3
3. Annular Channel	t	$\frac{2t^2}{(f \cdot Re)}$	See Fig. 4-18 for $(f \cdot Re)$ values	2,3
4. Rectangular Grooves	W	$.435 \left(\frac{\delta}{W} \right)^{2.1} \left(\frac{W}{2\delta+W} \right)^2 \frac{W^3}{\delta}$	Sharp Corner: $A_w = A'_w$; N=No. of grooves ; A'_w = Area Per Groove	4,5,6
5. Circular Grooves	w	$.0221 \frac{d^{2.2} (2\pi - \alpha + \sin \alpha)^{2.1}}{w^{0.2} (2\pi - \alpha)^2}$		4,5,6
6. Triangular Grooves	r_0	-----	No empirical values have been developed for triangular grooves	- -
7. Trapezoidal Grooves	w	$0.435 \frac{(w\delta + \delta^2 \tan \alpha)^{2.1}}{w^{0.2} \left[\frac{2\delta}{\cos \alpha} (1 + \sin \alpha) + w \right]^2}$	Sharp corner: $A_w = A'_w$; N=No. of grooves ; A'_w = Area Per Groove	4,5,6
8. Square Wire Mesh	$\frac{W+d}{2}$	$\frac{d^2 \epsilon^3}{122 (1 - \epsilon)^3}$		7,8
9. Randomly Packed Spheres	$0.41 r$	$\frac{(2r)^2 \epsilon^3}{150 (1 - \epsilon)^2}$		9,10,11
10. Fibrous Wicks	$\frac{d + \sqrt{32 K \epsilon}}{2}$	-----	Consult fibrous material suppliers for K and ϵ values	- -

For laminar flow, which always exists in the liquid phase of a heat pipe, the product $(f \cdot Re)$ is a constant and independent of flow (3) and is only a function of the channel geometry. For cylindrical channels, $(f \cdot Re)$ equals 16 and the permeability is directly proportional to the diameter of the cylinder. For rectangular channels and annuli, (3) $(f \cdot Re)$ can be obtained from Figs. 4-18 and 4-19, respectively.

Although grooves also have well defined geometries, they are open channels characterized by variable flow area and permeability along their length as the meniscus recedes to develop the required capillary pumping. In addition, grooves are also characterized by two effective pumping radii: one parallel to the flow channel and the other perpendicular to the direction of flow. In rectangular, circular and trapezoidal grooves, as illustrated in Fig. 4-17, the meniscus remains anchored at the groove opening; that is, the meniscus does not recede to the bottom of the groove to develop maximum pumping. For these types of grooves the two effective pumping radii can be determined as follows (4, 5):

$$(r_p)_I = W \quad (4-7)$$

$$(r_p)_{II} = \frac{2A}{W_p} \quad (4-8)$$

The smaller of the two values determines the capillary pumping limit unless the grooves are sealed at the end in which case $(r_p)_I$ will govern the capillary pumping limit. Note that sealed grooves can result in a composite pumping effect (see Section 4.4.2). However, this requires that the grooves be fully primed before maximum capillary pumping can be developed (5). A determination of the permeability and effective flow area is a more complex matter requiring integration along the entire length of the groove to account for meniscus recession. A capillary flow factor (N_g) which is defined by Eq. (4-9) has been developed for axial groove geometries (5). Empirical expressions have been developed for N_g using the GAP computer program (6)

$$N_g = \int_{\frac{1}{2}W}^{\infty} \frac{K_x A'_{lx}}{R_x^2} dR_x \quad (4-9)$$

Where R_x is the effective pumping radius at position x

*The two effective pumping radii should not be confused with the two principal radii of curvature which determine each effective pumping radius.

For grooves with sharp corners at the groove opening

$$N_g = 0.87 \left(\frac{A'_g}{W^2} \right)^{3.1} \left(\frac{W}{WP} \right)^2 W^3 \quad (4-10)$$

For grooves with rounded corners at the groove opening

$$N_g = \left(0.87 - 1.04 \frac{R_t}{W} \right) \left(\frac{A'_g}{W^2} \right)^{\left(3.1 + \frac{2 R_t}{3 W} \right)} \left(\frac{W}{WP} \right)^2 W^3 \quad (4-11)$$

where A'_g and W_p are the individual groove area and wetted perimeter respectively, associated with a completely filled groove with a flat meniscus. R_t is the radius at the tip of the land (See Fig. 2-6). The permeability (K) can be determined from Eqs. 4-10 and 4-11 as

$$K = \frac{N_g r_p}{2 A'_g} \quad (4-12)$$

It should be noted that if the rectangular, circular or trapezoidal grooves are open at both ends and nearly closed at the groove opening or covered with porous material such as a wire mesh screen, the effective pumping radius can be obtained from Eq. 4-8, and the permeability can be obtained from Eq. 4-6. If the grooves are sealed at both ends, a composite effect results and the minimum effective pumping radius is that of the groove opening or porous material covering. For triangular and semicircular grooves, R. G. Bressler and P. W. Wyatt (12) performed a numerical evaluation to determine the effective pore radius. Their analytical results, summarized in Table 4-5, agreed well with capillary rise experiments.

A number of variables are introduced in the properties of capillaries made of wire mesh screen, packed spheres and fibrous wicks. These variables include the porosity (ϵ), packing density, intermeshing in multilayer screens, random sphere and fiber sizes and the effect of tortuosity on flow properties. Because of these variables, properties of these types of capillaries are best established on an experimental basis. Techniques for obtaining experimental properties are discussed in Chapter 8. Table 4-6 summarizes typical data which has been obtained with those techniques.

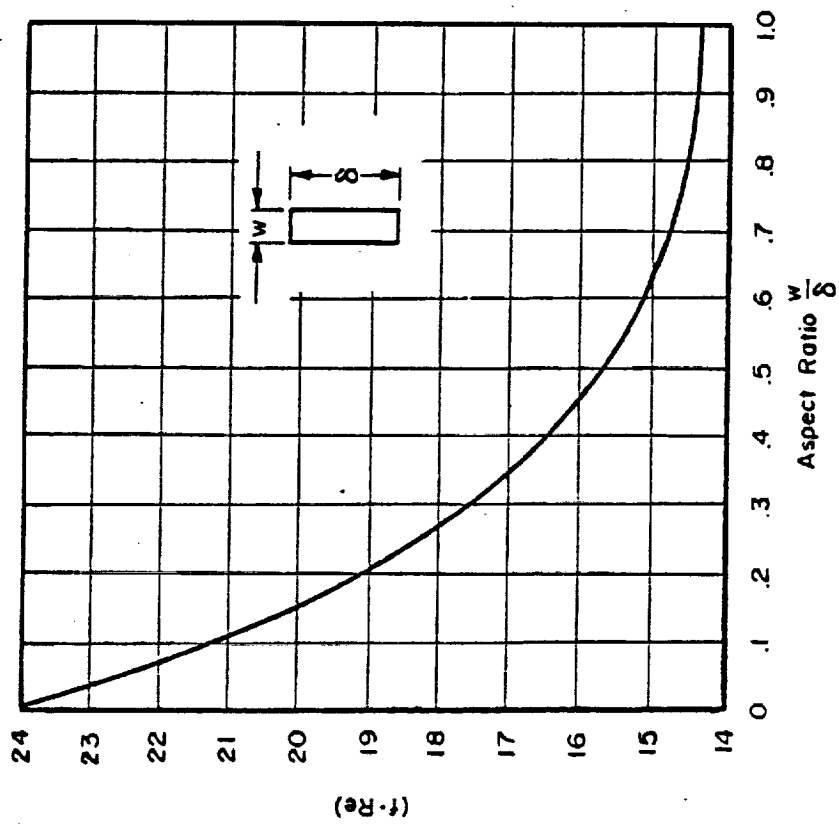


Fig: 4-18. $(f \cdot Re)$ vs. aspect ratio for fully developed laminar flow in rectangular tubes

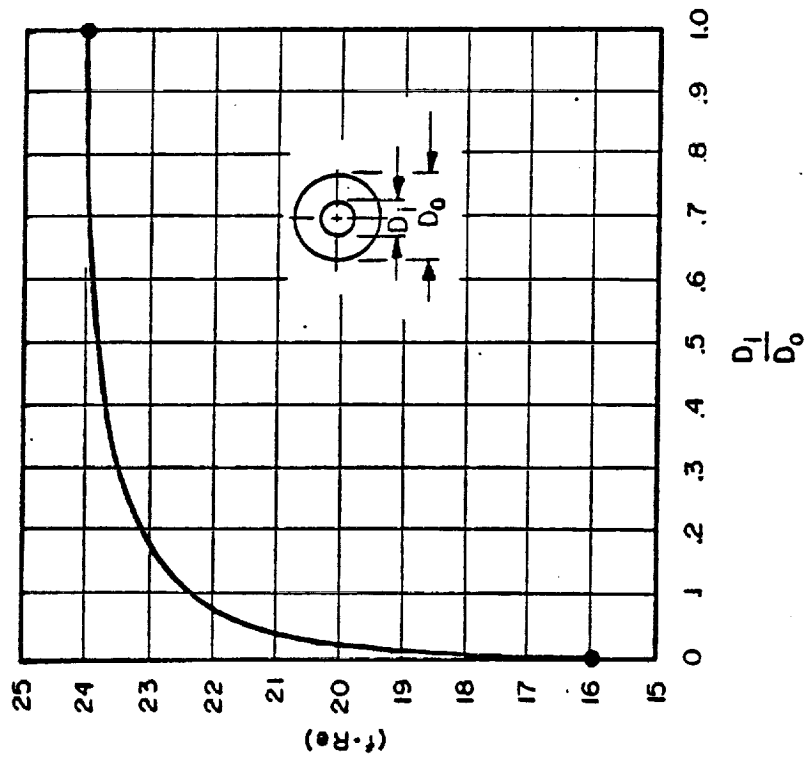


Fig. 4-19. $(f \cdot Re)$ vs. aspect ratio for fully developed laminar flow in circular annuli

TABLE 4-6. EXPERIMENTALLY DETERMINED WICK PROPERTIES							
No.	Wick Type and Description	Test Liquid	Porosity	$r_p \times 10^6$	Method	$K \times 10^{-2}$	Reference
1	Screen, SST, 120 mesh	H ₂ O		281	R1	3.02	D
2	Screen, SST, 120 mesh, oxidized at 600°C	H ₂ O		190.9	R1	1.73	D
3	Screen, SST, 200 mesh	H ₂ O	.733	58	R4	.52	B
4	Screen, SST, 200 mesh	C ₆ H ₆	.733	57	R4		B
5	Screen, SST, 200 mesh	CH ₃ OH	.733	56	R4		B
6	Screen, SST, 400 mesh	H ₂ O		29	R3		C
7	Screen, SST, 400 mesh	C ₂ H ₅ OH		30	R3		C
8	Screen, SST, 80 x 700, Double Dutch Twill	(CH ₃) ₂ CHOH		< 40	R4	.075	J
9	Screen, SST, 165 x 1400, Double Dutch Twill	(CH ₃) ₂ CHOH		< 18	R4	.044	J
10	Screen, SST, 200 x 1400, Double Dutch Twill	(CH ₃) ₂ CHOH		< 14	R4	.024	J
11	Screen, SST, 250 x 1400, Double Dutch Twill	(CH ₃) ₂ CHOH		< 12	R4	.011	J
12	Screen, SST, 325 x 2300, Double Dutch Twill	(CH ₃) ₂ CHOH		< 10	R4	.006	J
13	Screen, SST, 375 x 2300, Double Dutch Twill	(CH ₃) ₂ CHOH		< 8	R4	.006	J
14	Screen, SST, 450 x 2750, Double Dutch Twill	(CH ₃) ₂ CHOH		< 7	R4	.006	J
15	Screen, SST, 670 x 120, Reverse Dutch Twill	(CH ₃) ₂ CHOH		< 27	R4		J
16	Screen, SST, 720 x 140, Reverse Dutch Twill	(CH ₃) ₂ CHOH		< 21	R4		J
17	Screen, SST, 850 x 155, Reverse Dutch Twill	(CH ₃) ₂ CHOH		< 20	R4		J
18	Screen, Nickel, 50 mesh	H ₂ O		1813	R1	5.81	D

TABLE 4-6.- EXPERIMENTALLY DETERMINED WICK PROPERTIES (CONTINUED)							
No.	Wick Type and Description	Test Liquid	Porosity	$r_p \times 10^6$ m	Method	$K \times 10^{-2}$ m	Reference
19	Screen, Nickel, 50 mesh, oxid @ 600°C	H ₂ O		580.2	R1	6.47	D
20	Screen, Nickel, 50 mesh, sintered	H ₂ O	.625	305	R1	6.63	A
21	Screen, Nickel, 100 mesh, sintered	H ₂ O	.679	<131	R1	1.52	A
22	Screen, Nickel, 100 mesh, sintered	H ₂ O	.678	84	R1		A
23	Screen, Nickel, 200 mesh, sintered	H ₂ O	.676	64	R1	.77	A
24	Screen, Nickel, 500 mesh	H ₂ O	.60	12.5	R4		J
25	Screen, Nickel, 1000 mesh	H ₂ O	.48	13.0	R4		J
26	Screen, Nickel, 1000 mesh	CH ₃ OH	.48	10.6	R4		J
27	Screen, Nickel, 1500 mesh	H ₂ O	.36	6.7	R4		J
28	Screen, Nickel, 2000 mesh	H ₂ O	.22	6.1	R4		H
29	Screen, Nickel, 2000 mesh	CH ₃ OH	.22	5.3	R4		H
30	Screen, Copper, 60 mesh	H ₂ O		481	R1	4.20	D
31	Screen, Copper, 60 mesh, oxidized	H ₂ O		298	R1	2.38	D
32	Screen, Phosphor Bronze, 120 mesh	C ₂ H ₅ OH		102	R3		C
33	Screen, Phosphor Bronze, 120 mesh	H ₂ O		105	R3		C
34	Screen, Phosphor Bronze, 200 mesh	C ₂ H ₅ OH		54	R3		C
35	Screen, Phosphor Bronze, 200 mesh	H ₂ O		60	R3		C
36	Screen, Phosphor Bronze, 250 mesh	C ₂ H ₅ OH		51	R3		C

TABLE 4-6. EXPERIMENTALLY DETERMINED WICK PROPERTIES (CONTINUED)							
No.	Wick Type and Description	Test Liquid	Porosity	$r_p \times 10^6$ m	Method	$K \times 10^{-2}$ m	Reference
37	Screen, Phosphor Bronze, 250 mesh	H ₂ O		48	R3		C
38	Screen, Phosphor Bronze, 270 mesh	C ₂ H ₅ OH		41	R3		C
39	Screen, Phosphor Bronze, 270 mesh	H ₂ O		43	R3		C
40	Screen, Phosphor Bronze, 325 mesh	C ₂ H ₅ OH		32	R3		C
41	Screen, Phosphor Bronze, 325 mesh	H ₂ O		33	R3		C
42	Felt, Sintered, SST	H ₂ O	.822	110	R1	11.61	A
43	Felt, Sintered, SST	H ₂ O	.916	94	R1	5.46	A
44	Felt, Sintered, SST	H ₂ O	.808	65	R1	1.96	A
45	Felt, 347 SST, C38 (FM 134)	H ₂ O	.35	49	R1	1.04	L
46	Felt, 347 SST, C38 (FM 123)	H ₂ O	.35	42.5	R1	.64	L
47	Felt, SST, A-8 (FM 1101, 1106, 1111)	H ₂ O	.90	26.5	R1	.56	L
48	Felt, SST, A-8 (FM 1102, 1107, 1112)	H ₂ O	.80	13.5	R1	.087	L
49	Felt, SST, A-8 (FM 1103, 1109)	H ₂ O	.70	7.5	R1	.028	L
50	Felt, SST, A-8 (FM 1104, 1109)	H ₂ O	.60	5	R1	.013	L
51	Felt, SST, A-8 (FM 1105, 1110)	H ₂ O	.40	2.3	R1	.0009	L
52	Felt, 430 SST, B-62 (FM 1305, 1309)	H ₂ O	.95	260	R1	30.6	L
53	Felt, 430 SST, B-62 (FM 1302, 1306, 1310)	H ₂ O	.90	191	R1	18.6	L
54	Felt, 430 SST, B-62 (FM 1303, 1307, 1311)	H ₂ O	.80	120	R1	6.44	L

TABLE 4-6. EXPERIMENTALLY DETERMINED WICK PROPERTIES (CONTINUED)

No.	Wick Type and Description	Test Liquid	Porosity	$r_p \times 10^{-6}$	Method	$K \times 10^{-2}$	Reference
55	Felt, 430 SST, B-62 (FM 1304, 1308, 1312)	H ₂ O	.60	50	R1	.80	L
56	Felt, Nickel	H ₂ O	.891	165	R4	5.17	B
57	Felt, Nickel, A30	H ₂ O	.815	120	R1	.306	D
58	Felt, Nickel, A30 (FM 415)	CH ₃ OH		55.9	R1	.48	K
59	Felt, Nickel, A-16 (FM 1201, 1205, 1209)	H ₂ O	.85	40	R1	.88	L
60	Felt, Nickel, A-16 (FM 1205)	H ₂ O		37.9	R1	1.27	D
61	Felt, Sintered, Nickel	H ₂ O	.828	< 38	R1		A
62	Felt, Sintered, Nickel	H ₂ O	.868	< 37	R1	.397	A
63	Felt, Sintered, Nickel	H ₂ O	.825	< 37	R1	.337	A
64	Felt, Sintered, Nickel	H ₂ O	.689	< 37	R1	.151	A
65	Felt, Sintered, Nickel	H ₂ O	.628	< 37	R1		A
66	Felt, Sintered, Nickel	H ₂ O	.880	< 37	R1	.308	A
67	Felt, Sintered, Nickel, A30 (FM 315, 415)	H ₂ O	.85	37	R1	1.75	L
68	Felt, Sintered, Nickel	H ₂ O	.709	< 36	R1		A
69	Felt, Sintered, Nickel	H ₂ O	.626	< 35	R1		A
70	Felt, Sintered, Nickel	H ₂ O	.820	< 32	R1		A
71	Felt, Nickel, A30, oxid @ 600°C	H ₂ O		32.5	R1		D
72	Felt, Nickel, A16 (FM 1202, 1206, 1210)	H ₂ O	.80	30	R1	.48	L

TABLE 4-6. EXPERIMENTALLY DETERMINED WICK PROPERTIES (CONTINUED)							
No.	Wick Type and Description	Test Liquid	Porosity	$r_p \times 10^6 \text{ m}$	Method	$K \times 10^{-2} \text{ m}^2$	Reference
73	Felt, Nickel, A30 (FM 320, 420)	H ₂ O	.80	25.5	R1	.80	L
74	Felt, Nickel, A16 (FM 1203, 1207, 1211)	H ₂ O	.70	17	R1	.116	L
75	Felt, Nickel, A16 (FM 1204, 1208, 1212)	H ₂ O	.60	10.5	R1	.042	L
76	Felt, 347 SS, A30 (FM 627)	H ₂ O	.55	7	R1	.016	L
77	Felt, Copper	CH ₃ OH	.895	279	R3		B
78	Felt, Copper	H ₂ O	.895	229	R4	12.4	B
79	Felt, Copper	C ₆ H ₆	.895	216	R4		B
80	Felt, Copper, FM 1006	H ₂ O	.80	144	R1	.778	D
81	Felt, Copper, FM 1006, oxid @ 300°C	H ₂ O	.80	40.6	R1		D
82	Felt, OFHC Copper, A40 (FM 1006)	H ₂ O	.80	23	R1	.37	L
83	Foam, Nickel, AmPorNik 220-5	CH ₃ OH	.960	267	R3		B
84	Foam, Nickel, AmPorNik, 220-5	H ₂ O	.960	229	R4	37.2	B
85	Foam, Nickel, AmPorNik, 220-5	C ₆ H ₆	.960	216	R4		B
86	Foam, Nickel, AmPorNik, 210-5	H ₂ O	.944	229	R4	27.3	B
87	Foam, Copper, AmPorCop, 210-5	CH ₃ OH	.945	229	R3		B
88	Foam, Copper, AmPorCop, 210-5	C ₆ H ₆	.945	229	R4		B
89	Foam, Copper, AmPorCop, 210-5	H ₂ O	.945	216	R4	20.2	B
90	Foam, Copper, AmPorCop, 220-5	H ₂ O	.912	241	R4	23.2	B

TABLE 4-6. EXPERIMENTALLY DETERMINED WICK PROPERTIES (CONTINUED)

No.	Wick Type and Description	Test Liquid	Porosity	$r_p \times 10^{-6}$ m	Method	$K \times 10^{-2}$ m	Reference
91	Powder, Sintered, Nickel	H ₂ O	.696	82	R1		A
92	Powder, Sintered, Nickel	H ₂ O	.691	69	R1		A
93	Powder, Sintered, Nickel	H ₂ O	.658	61	R1	2.73	A
94	Powder, Sintered, Nickel	H ₂ O	.597	58	R1		A
95	Powder, Sintered, Nickel	H ₂ O		38.7	R1	.07	D
96	Powder, Sintered, Nickel	H ₂ O	.477	<31	R1		A
97	Powder, Sintered, Nickel	H ₂ O	.540	<36	R1	.808	A
98	Powder, Sintered, Cu	H ₂ O	.52	9.39	R1	.009	D
99	Deposited Cu		.51			.0234	G
100	Deposited Cu, Bonded		.60			.0255	G
101	Beads, Cu, 20-30 mesh, Sintered	H ₂ O		175	R1	1.11	K
102	Beads, Monel, 20-30 mesh	H ₂ O	.40	352	R2		E
103	Beads, Monel, 30-40 mesh	H ₂ O	.40	252	R2	4.12	E
104	Beads, Monel, 40-50 mesh	H ₂ O	.40	179	R2	2.31	E
105	Beads, Monel, 50-70 mesh	H ₂ O	.40	126	R2	1.25	E
106	Beads, Monel, 70-80 mesh	H ₂ O	.40	96.9	R2	.775	E
107	Beads, Monel, 80-100 mesh	H ₂ O	.40	81.5	R2	.559	E
108	Beads, Monel, 100-140 mesh	H ₂ O	.40	63.4	R2	.328	E

Notes for Table 4-6

Investigators	Ref. No.	Investigators	Ref. No.
A Kunz	13	G Gould Laboratories	18
B Phillips	14	H Dynatherm Corporation	19
C Katzoff	15	J Kressilk	20
D Freggens	16	K Marcus	7
E Ferrell	9	L Huyck Metals Company	21
F Farran	17		

Effective Pore Radius Measurement Techniques

- R1 Maximum wick height, rising meniscus
- R2 Maximum wick height, falling meniscus
- R3 Maximum supported column
- R4 Air bubble

Permeability was determined by forced flow technique except where noted:

- a Gravity flow technique
- b Plot of $\frac{dx_a}{dt}$ vs. $\frac{1}{x}$

Empirical expressions developed on the basis of available data are given in Table 4-5. For square wire mesh wicks which are often used in heat pipe design, the spacing between wires (w) is approximately equal to the wire diameter in which case the effective pore radius (r_p) and permeability (K) for this type of wick design can be expressed as (7,8):

$$r_p = d \quad (4-13)$$

$$K = 0.0122 d^2 \quad (4-14)$$

Where the porosity (ϵ) used to establish the above permeability is based on an analytical expression developed by Marcus (7) which neglects intermeshing of the wires.

$$\epsilon = 1 - \frac{\pi S N d}{4} \approx 0.6 \quad (4-15)$$

The dimensionless empirical "Crimping Factor, S " is normally unity if the screen is not tightly wound and the number of wires per inch (N) or mesh size is equal to $\frac{1}{2} d$ for $w = d$.

4.4.2 Typical Wick Designs

The capillary structures discussed in the preceeding section can be configured in a variety of ways depending on the properties desired for a particular application. Figure 4-20 illustrates some of the more commonly used wick designs, while Table 4-7 presents a "rating" of these wicks in terms of basic performance criteria.

Wick designs are divided into two basic categories: homogeneous and composite. Homogeneous wicks are isotropic structures in which the capillary pumping is derived from effective pore or channel sizes which are uniform throughout the structure. That is, the permeability (K) and the effective pumping radius (r_p) are dependent on the same characteristic property of the wick. Since high capillary pumping is equivalent to possessing small pore radii and low resistance to flow is equivalent to large pore sizes, the design of most homogeneous wicks (non-composite) requires a compromise between these conflicting requirements. Despite the performance limitations imposed by this compromise, homogeneous wick designs are widely used because of their reliability, good start-up under load characteristics, flexibility of application and cost.

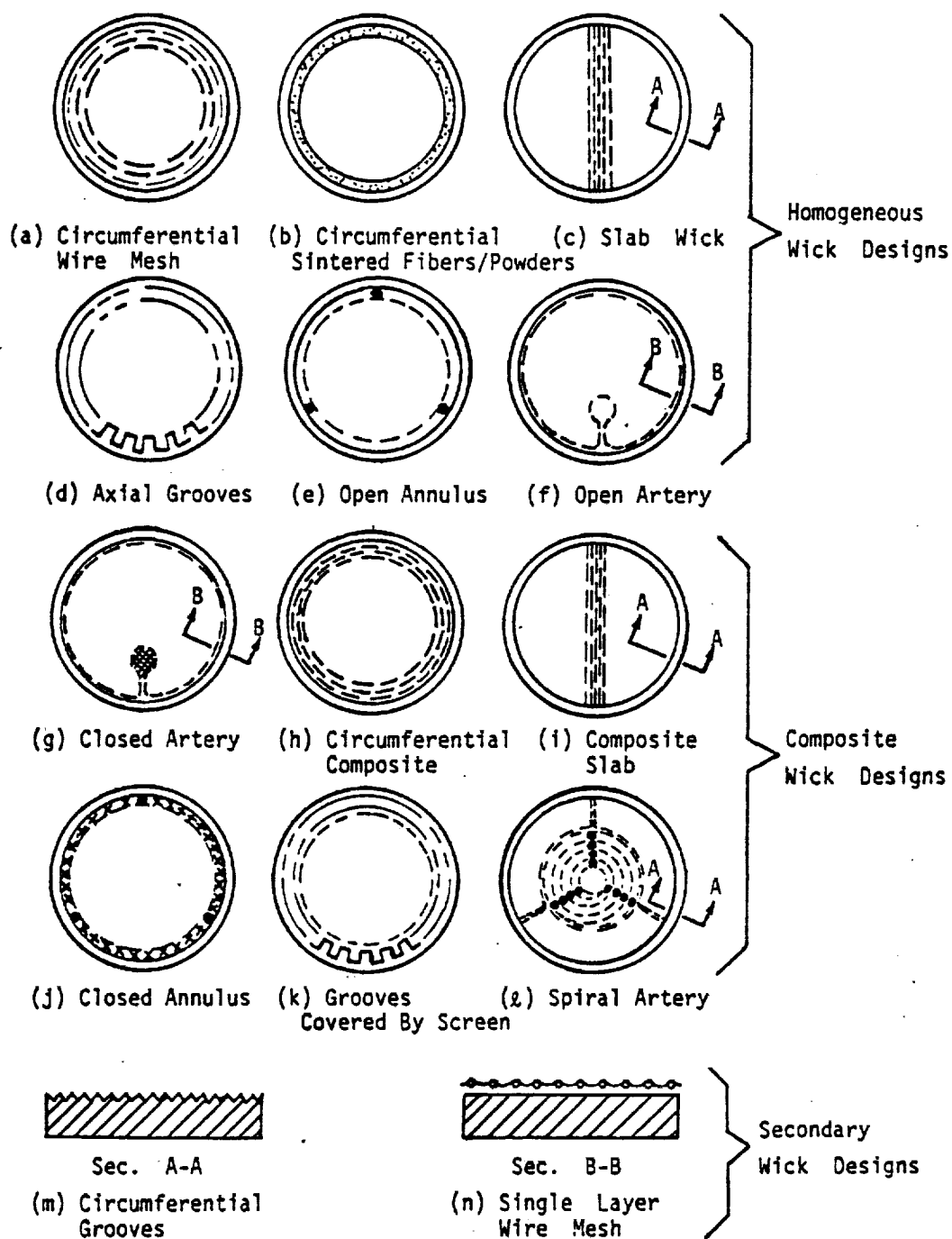


Fig. 4-20. Typical wick designs.

TABLE 4-7. WICK SELECTION CRITERIA							
	Wick Type	Permeability	Capillary Pumping	Thermal Conductance	Cost Complexity	Reliability	Comments
Homogeneous	a. Circumferential Screen	P-M	G	P	G	G	First Historical Wick
	b. Circumferential Sintered	P-M	G	M	M	G	Screen, Powder, Fiber, Spheres
	c. Slab Wick	P-M	G	G	G	G	With Screw Thread or Single Layer Screen as Circumf. Wick
	d. Axial Grooves	M-G	P	G	M	G	Not Available in All Heat Pipe Materials
	e. Open Annulus	G	P	P	M	G	
	f. Open Artery	G	P	G	M	G	
Composite	g. Closed Artery	G	G	G	P	P	Pedestal, Spiral, or Tunnel Arteries
	h. Circumferential Composite	M	G	M-P	M	P	Conductance Rating Depends on Whether Wick Sintered
	i. Composite Slab	M	G	G	G	P	Not Very Sensitive to "Perfect" Closure of Pumping Wick
	j. Closed Annulus	G	G	P	M-P	P	
	k. Grooves Covered by Screen	M-G	G	G	M-P	P	Not Reduced to Practice
	l. Spiral Artery	M-G	G	G	P	P	

G = Good M = Average P = Poor

The graded-porosity wick (22) is a non-arterial (non-composite) design which tends to offset the competing effects of permeability and pumping and results in optimized fibrous wick designs. With this design the wick porosity is varied such that at every axial location it is only as low as required to insure that the wick remains nearly saturated. Thus the permeability is everywhere as high as possible. The potential increase in capacity over a uniform porosity fibrous wick depends on the particular application, but it can be more than a factor of two greater (22).

Composite wick designs have been investigated for a number of years. Large flow channels in combination with fine capillary structures are used in composite wick designs to independently optimize capillary pumping and permeability. To achieve the resulting high performance, however, the wick structure must be completely "primed". Because vapor or non-condensable gas inclusion or a small saturation pressure differential can prevent complete priming, conventional composite wick designs have proved to be highly unreliable. Techniques to improve priming such as Clapeyron priming (23), meniscus coalescence (24), and jet pump assist (25), have met with various degrees of success as discussed in Section 4.4.2.2. Limited experience with reliable priming techniques, the high cost of such designs, together with operational limitations such as performance during start-up are factors which should be considered in the selection of composite wick designs for any application.

4.4.2.1 Homogeneous Wick Design

Permeability and capillary pumping determine the hydrodynamic heat transport capability of a wick. As stated earlier, a compromise between these two factors is often required in the design of a homogeneous wick. An examination of the equations developed in Chapter 2 for the Heat Transport Capability will show the dependence of this parameter on wick properties. The applicable Eqs. are repeated as:

$$(\dot{Q}L)_{\max} = \frac{2 K A_w (1 + \eta) \cos \theta_c F_2 N_2}{r_p} \quad (4-16)$$

where:

$$\eta = - \frac{r_p D \cos \beta}{2H_2 \cos \theta_c} + \frac{r_p L \sin \beta}{2H_2 \cos \theta_c} \quad (4-17)$$

$$F_L = \frac{1}{1 + \frac{\phi^2}{3} \Psi + \frac{v_v}{v_L} \frac{32 K}{D_{h,v}^2} \frac{A_w}{A_v}} \quad (4-18)$$

with H_L and N_L defined by equations 2-65 and 2-68, respectively.

For all homogeneous wicks except the axial groove, the wick area (A_w) is independent of the capillary properties and, as it can be seen from Table 4-5, the permeability (K) and capillary pumping radius (r_p) can be related by:

$$K \sim r_p^2$$

If vapor losses are neglected ($F_L \approx 1$), the dependence on capillary properties can be expressed as follows:

$$(QL)_{\max} = \frac{K}{r_p} (1 + \eta) = r_p \left(1 - \frac{r_p h}{2H}\right) \quad (4-19)$$

In the absence of gravity ($\eta = 0$), the wick with the largest practical capillary pore size will yield the best heat transport. For heat pipes which must be operated in gravity for performance verification or as a normal mode of operation, body-forces must be included in the selection of an optimum pore size. Differentiation of Eq. 4-19 yields the following optimum pore size for operation in a 1-g field, ($g = g_0$):

$$(r_p)_{\text{opt}} = \frac{H}{h} \quad (4-20)$$

For axial grooves, it can be shown that

$$(r_p)_{\text{opt}} = (w)_{\text{opt}} = \frac{4H}{3h} \quad (4-21)$$

Note that, since axial grooves are non-communicating:

$$h = L \sin \beta \quad (4-22)$$

where

β = heat pipe elevation angle

and that for all other wicks which communicate with the bottom of the heat pipe:

$$h = L \sin \beta + D \cos \beta \quad (4-23)$$

For a 0-g heat pipe application which must be verified in gravity, the optimum pore size should be selected for a test elevation which precludes significant puddle flow contributions. An adverse test elevation of 1.25 mm (0.050 in.) or greater is generally preferred.

Once the required capillary pore size has been identified, the type of wick design suitable for a given application can be selected. Ranges of physical pore sizes, capillary radii and permeabilities for some typical wicks are given in Table 4-8. For reference purposes, the Table also lists the maximum static wicking height $(h)_{\max}$ of water at 100°C. The designer is referred to Table 4-5 for the definition of the basic wick properties.

(a) Wire Mesh and Sintered Fibers/Powders Wick Designs

As can be seen from Table 4-8, wicks made of wire mesh screen and sintered fibers or powders can provide fine capillary pore sizes with correspondingly high static wicking heights. On the other hand, these wicks are characterized by low permeability due to the small pore sizes and the relatively tortuous path the liquid must follow. These wicks, therefore, are most suitable for applications where the heat transport capability is not too restrictive and operation against a high elevation is required. Figs. 4-20 a, b, and c, illustrate various typical wire mesh and sintered fibers/powder wick designs. The principle difference between the circumferential and the slab wicks illustrated in Fig. 4-20 is that the circumferential wick offers an ideal vapor flow channel (cylindrical) geometry but requires the heat to be transferred through the wick liquid matrix to the liquid-vapor interface at the evaporator and condenser. This type of wick, therefore, offers minimum vapor flow losses but has low heat transfer coefficients at the evaporator and condenser. The slab wick on the other hand provides efficient heat transfer at the evaporator/condenser but presents higher vapor flow losses. To enhance its heat transfer capability, the slab wick is often used in combination with circumferential grooves or a secondary wick made of a single layer of screen (Fig. 4-20, Sect. A-A & Sect. B-B).

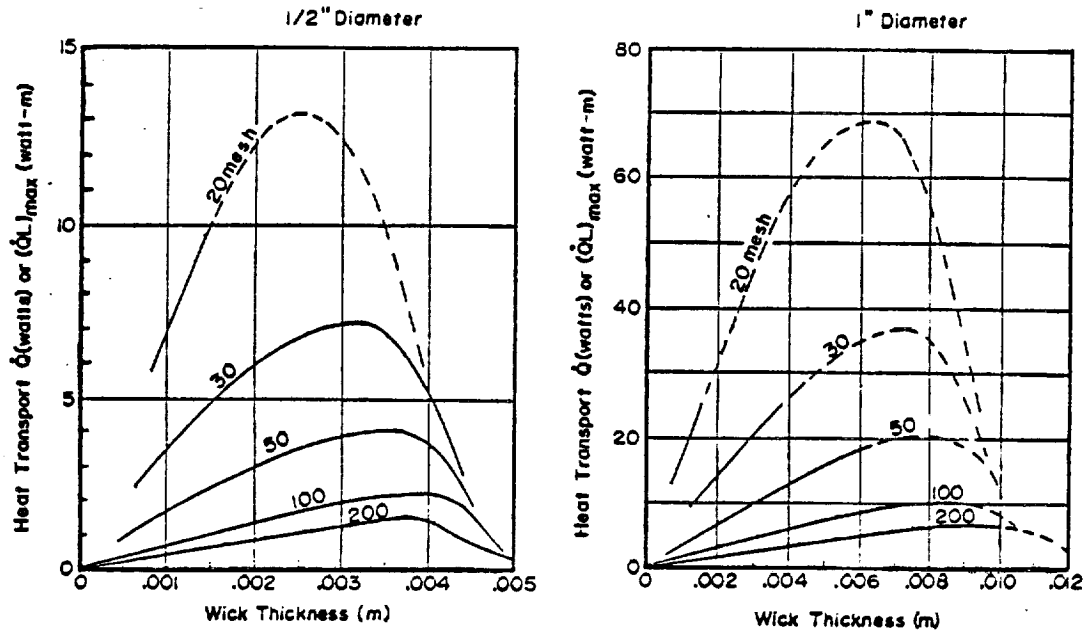
TABLE 4-8. PROPERTIES OF TYPICAL HOMOGENEOUS WICKS								
Wick Type	Characteristic Dimension		Effective Capillary Radius		Max. Wicking Height with H ₂ O at 100°C		Permeability	
	m x 10 ⁻³	in x 10 ⁻³	m x 10 ⁻³	in x 10 ⁻³	m x 10 ⁻³	inches	m ² x 10 ⁻¹⁰	ft ² x 10 ⁻¹²
30 Mesh Screen	0.50	20	0.43	16.9	29	1.14	25	2.69
100 Mesh Screen	0.14	5.5	0.12	4.7	104	4.1	1.8	0.19
200 Mesh Screen	0.07	2.75	0.063	2.5	197	7.75	0.55	0.059
Sintered Fibers/ Powders	-	-	0.01-0.1	0.4-4.0	1250-125	50-5	0.1-10	0.01-1
Axial Grooves	0.25-1.5	10-60	0.25-1.5	10-60	50-8	2-0.3	35-1250	3.8-135
Open Annulus	0.25-1.5	10-60	0.25-1.5	10-60	50-8	2-0.3	50-2000	5.4-215

With respect to vapor flow losses, the performance of the wick designs illustrated in Figs. 4-20 a, b, and c can be optimized as a function of wick area (A_w) and vapor flow losses (F_g). As can be seen, performance will be limited by liquid flow losses if the wick area is kept small. That is, the performance of the heat pipe goes to zero as the wick area goes to zero. At this point the vapor flow loss factor $F_g = 1$. As the wick area is increased, liquid flow losses are reduced but the vapor flow losses are increased.

Eventually, the vapor flow loss will dominate and the factor F_g goes to zero as the wick occupies the total cross-sectional area of the heat pipe and the performance goes to zero. Optimum wick area is dependent on a number of factors including the permeability of the wick, the vapor channel(s) geometry and the kinematic viscosity ratio, ν_v/ν_g . Optimum wick design, therefore, is not only dependent on the wick properties but is also dependent on fluid properties as a function of temperature. Figure 4-21 illustrates the optimum performance point which can be obtained with a .00127 m (1/2 inch) diameter heat pipe using ammonia at 273°K and various sizes of wire mesh screens. Optimum operating conditions for both the circumferential wick and the slab wick are illustrated. In determining the optimum wick area, the designer should keep the following points in mind:

- (1) Optimization with respect to liquid flow losses is dependent on whether the vapor flow is laminar or turbulent.
- (2) Heat pipes are typically required to operate over a temperature range. Optimization should be performed at the low end of the range. (High Vapor Flow losses.)
- (3) Fluids for low temperature applications (i.e., cryogenics) tend to have poor liquid transport properties and low kinematic viscosity ratios. Therefore, maximum transport is often achieved with large wick areas.

A. - Circumferential Wick



B. - Slab Wick

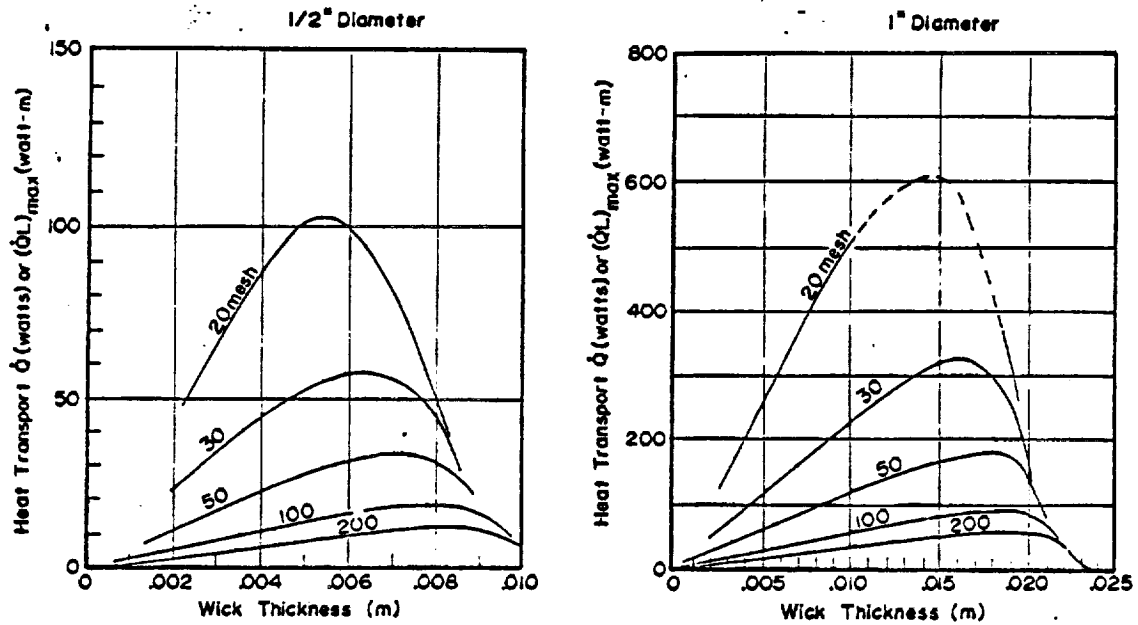


Fig. 4-2]. Typical wick area vs. vapor flow optimization...Homogeneous Wicks

(4) Fluids for high temperature applications (i.e., liquid metals) have good liquid transport properties and high kinematic viscosity ratios. Therefore, optimum performance is often achieved with large vapor flow areas.

(5) Other design considerations such as evaporator/condenser heat transfer, pressure containment and fabrication will often influence the design selected resulting in off-optimum performance. For example, a large wick area in a cryogenic heat pipe may result in an excessive pressure containment requirement.

(b) Axially Grooved Wick Designs

For applications where high elevation in gravity is not required and high heat transport performance is desirable, the designer may elect to use wick designs with large open flow channels as illustrated in Fig. 4-20 d, e, & f. The preceding discussions for optimum pore size determination, wick area optimization, and effect of wick design on thermal conductance also apply to large open flow channel wicks with the exception of axially grooved heat pipes.

The axially grooved wick design differs from other homogeneous wick designs in several important areas. The internal wick configuration consists of a series of parallel flow channels extruded or swaged as an integral part of the tube wall. Each groove is independent of the other and does not communicate with the bottom of the heat pipe. The groove size, therefore, is insensitive to the heat pipe diameter and is dependent only on the heat pipe elevation in a body-force field. Consequently, larger effective capillary sizes can be used in axially grooved designs as compared to other homogeneous wicks; and the performance of an axially grooved heat pipe is only exceeded by the more complex and less reliable composite wick structures. The integral construction also provides high conductance heat transfer paths to the liquid-vapor interface. Axially grooved heat pipes, therefore, can be classified "moderate to high conductance" wick structures.

Several factors should be considered by the designer in the development and evaluation of an axially grooved design. Axial grooves have been successfully produced in a number of materials including aluminum, copper, steel and stainless steel. However, the processes used (extruding and swaging) are limited by the size and the number of grooves that can be produced within a given envelope. Optimization with respect to vapor flow losses, therefore, is often impractical and the designer must optimize his design around fabrication limits. In addition, the axial groove is an open flow channel which is susceptible to liquid-vapor interaction at the groove opening. Finally, the open flow channel allows the liquid meniscus to recede along the length of the heat pipe resulting in a variation in the wick's cross-sectional area (A_w) and permeability (K).

The designer is referred to the results presented in Ref. (4) for an in-depth discussion of axially grooved heat pipe designs, the state-of-the-art of this technology. Extensive analytical modeling for predicting the hydrodynamic behavior including effects of fluid inventory, meniscus recession, liquid-vapor shear interaction and puddle flow effects have been developed in Ref. (6) and are summarized in Chapter 2.

Because of their versatility, simplicity of design, reliability, high heat transport, and high thermal conductance, axially grooved designs have been extensively investigated and developed for aerospace applications. They have been employed in both fixed conductance and thermal control applications including gas controlled variable conductance heat pipes (VCHP) (26), diodes (27), and thermal switches (28).

Table 4-9 summarizes the performance of several axially grooved designs which have been developed to date. Their geometries are shown in Fig. 4-22.

TABLE 4-9. TYPICAL AXIALLY GROOVED HEAT PIPE PERFORMANCE

TYPE/FLUID	TEMP. (°K)	o-g HEAT TRANSPORT CAPABILITY (W-m)	STATIC HEIGHT (cm)	FILM COEFFICIENT (W/m ² C) EVAPORATOR	CONDENSER
SWAGED ALUMINUM					
QAO Geometry					
Ammonia	295	130	1.09	7265	9480
Freon 21	295	28	0.51	1135	1700
Freon 23	295	12	0.46	653	1135
ATS Geometry					
Ammonia	310	145	0.89	5676	8515
Methane	150	18	0.52	1362	--
Nitrogen	80	16	0.30	312	1362
SWAGED COPPER					
LCHPG Geometry					
Water	363	67.6	2.8	--	--
SWAGED STAINLESS STEEL					
Approx. ATS Geometry		Performance Forthcoming			
EXTRUDED ALUMINUM					
ATS Geometry					
Ammonia	273	143	1.6	7000	13600
Methane	125	33.4	1.1	1730	6100
Ethane	200	25	1.3	1370	5900
Lewis Covert Geometry					
Ammonia	293	143	2.51	7300	20500
Methane	120	28	2.13	--	--
Ethane	180	33	2.21	--	--

4.4.2.2 Composite Wick Design

Typical composite wick designs are illustrated in Fig. 4-20. As pointed out earlier, a composite wick is one which uses both small and large capillaries in combination to avoid the compromise between the requirement for small effective pore radii for high capillary pumping and large effective pore radii for high permeability. In the case of arteries or annuli (Fig. 4-20 g, j, & l), the main flow channel is provided by the artery or annulus and the pumping is provided by the fine wire mesh screen which forms the artery or annulus. Composite wicks can also be made by combining coarse and fine wire mesh screen as illustrated in Fig. 4-20 h & i, or by covering the axial grooves with a layer of wire mesh screen. With respect to an axial groove, composite pumping can also be achieved by closing-off the groove opening. The Lewis Covert Groove (Fig. 4-20 f) is such a groove form.

Most of the considerations which are important for homogeneous wick designs also apply to composite wicks. Typical ranges for capillary pumping capability and permeability can be obtained from Table 4-8. The effective capillary radius is that of the fine mesh wick which forms the flow channel and the effective permeability is that of the channel itself. In the case of a wick formed from fine and coarse mesh screen (e.g., composite circumferential and composite slab) the permeability of the coarser screen should be used.

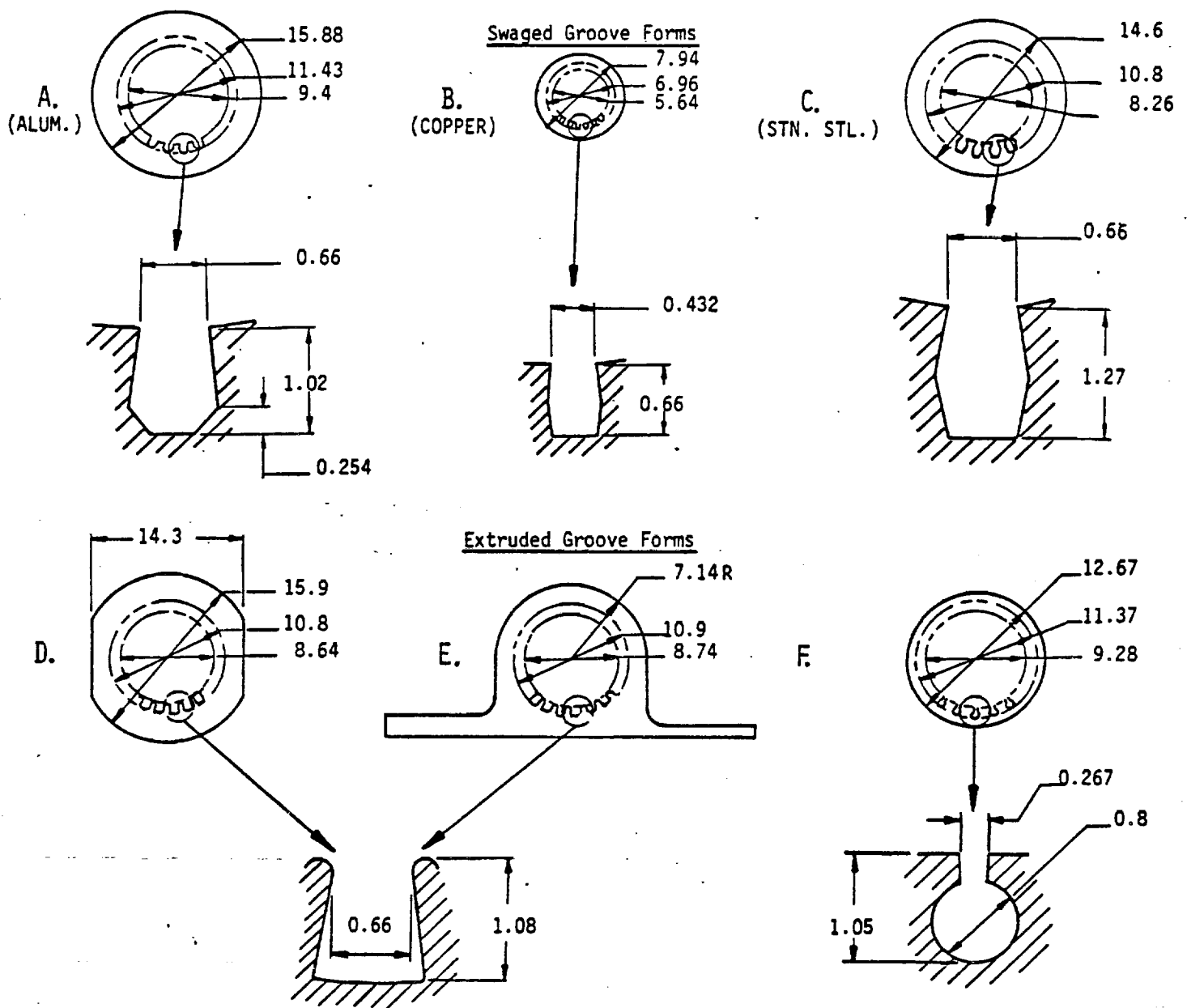


Fig. 4-22. Typical axially grooved heat pipe designs (Dimensions in. mm)

The heat transfer considerations for composite wicks are the same as for homogeneous wicks. The effective heat transfer coefficient is controlled by the thickness of the wick adjacent to the heat input/output surface. As with homogeneous wicks, secondary wicks are often used (Fig. 4-20, Sect. AA & Sect. BB) to minimize the impedance to heat flow in the evaporator and condenser regions. Such secondary wicks also affect the overall heat transport performance of the heat pipe and can become the limiting factor in composite wick designs. Their performance, therefore, should be included in the overall design of a selected wick configuration (see Section 4.4.4).

The composite wick differs from homogeneous wicks in one important aspect--they must be primed. The priming process involves saturating the wick with working fluid either during initial start-up of the heat pipe or after a dry-out. The requirements for priming are:

- (1) The capillary pumping of the large flow channel must be sufficient to fill the wick with working fluid at the particular orientation of the heat pipe in a body-force field.
- (2) The heat load during priming does not exceed the heat transport capability of the large flow channel. ✓

The self-priming requirement, therefore, establishes an upper limit for the size of the large flow channels, which is similar to the homogeneous wick. In 0-g, the composite wick will always prime as long as the second condition is not violated. But in a 1-g environment, the large flow channels must have a pumping head at least equal to the height of the wick structure. Otherwise, self-priming is impossible in any orientation.

For an annular type composite wick (Fig. 4-20, j) this requirement translates to:

$$\frac{2 \sigma \cos \theta}{\delta_{\max}} = \rho_l g D_i \quad (4-24)$$

where

δ_{\max} = the maximum permissible gap

D_i = the internal heat pipe diameter

For a pedestal artery (Fig. 4-20 g), the maximum artery diameter is given by:

$$D_{\max} = \frac{1}{2} \left(\sqrt{h^2 + \frac{8 \sigma}{\rho_l g}} - h \right) \quad (4-25)$$

where

h = the height of the pedestal

The maximum theoretical pumping capability of a composite wick can only be realized if the wick is completely filled with liquid. During a partial fill condition, a liquid-vapor interface is located inside the large flow channel. The capillary pumping is thus reduced to a value which corresponds to the effective pore radius of the large flow channel.

This effect is illustrated in Fig. 4-23 for an arterial wick. In Fig. 4-23a, the artery is completely filled with the liquid-vapor interface located in the fine screen, and the maximum capillary pumping corresponds to the pore radius of the screen. In Fig. 4-23b the artery is filled except for a small bubble. The effective pumping radius is now the radius of the bubble. In Fig. 4-23c the bubble has reached its maximum diameter and the effective pumping radius is that of the artery.

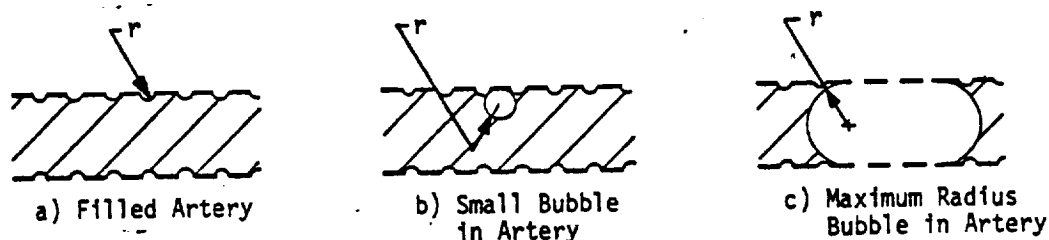


Fig. 4-23. Liquid-vapor interface in arteries

It should be emphasized that the effect of incomplete filling (bubbles) in a composite wick is much more severe than in a homogeneous wick. In the latter, internal voids simply reduce the available liquid flow area but do not affect the capillary pumping. In the composite wick, voids or bubbles will reduce the capillary pumping to a value equal to that of the large flow channel. Incomplete filling can be the result of:

- (1) An insufficient amount of working fluid
- (2) Nucleation within the composite wick due to excessive local heat fluxes
- (3) Entrapment of non-condensable gases.

The formation and stability of voids in composite wicks is not fully understood. Experience has shown that wicks consisting of different mesh size screens are less susceptible to the formation of voids than those with wide open flow channels such as arteries and annuli.

Imperfections in the pumping wick have the same general effect as incomplete filling. The maximum interfacial pressure which the wick can sustain is determined by the largest opening in the pumping wick. Since the maximum interfacial pressure difference exists at the evaporator, imperfections in that region are most damaging to the performance. Close quality control during fabrication of composite wick heat pipes is therefore very important and adds to their cost. Whenever possible, a hydrostatic pressure test should be conducted on the completed wick in order to locate and repair any imperfections.

The unreliable aspects of wick priming have been evaluated by a number of investigators and various techniques to enhance priming have been proposed.

Investigations conducted by Saaski (27) indicate that gas levels in the 10 to 100 parts per million range are sufficient to prevent reliable priming due to blockage by non-condensable gases. Saaski also demonstrated both theoretically and experimentally that the collapse of arterial gas bubble by diffusion, which depends on bubble size and particular conditions, usually takes a long time--often as long as days. Also, it has been demonstrated that under load, conditions can prevail which will cause the expansion of the gas bubbles. Since in practice it is difficult and costly to produce heat pipes with low gas contents and since the introduction of non-condensable gases is necessary in gas controlled variable conductance applications, various priming techniques have been proposed and investigated.

4.4.3 Methods for Priming Composite Wicks

A number of methods for the priming composite wicks have been developed. Pressure priming (Clapeyron priming) (23), Meniscus Coalescence (24), and the Jet Pump Assist (25) are discussed in the next sections.

4.4.3.1 Pressure (Clapeyron) Priming

Although the normal diffusion of non-condensable gas occlusions has been demonstrated as being unsatisfactory to achieve reliable priming of composite wicks, investigations conducted by Saaski indicate that sub-cooling of the condensate can significantly accelerate the loss of non-condensable gas by compressing the gas via the Clapeyron or pressure priming effect. A typical wick design suitable for pressure priming is illustrated in Fig. 4-24. It consists of several layers of fine capillary passages wrapped around a large flow channel (tunnel) wick. The fine capillary passages are sized to self-prime by surface tension even if the tunnel wick is completely drained of liquid. The wick structure is located in the center of the heat pipe envelope and webs are used to connect it with a secondary wick which lines the container wall. When heat is applied to the evaporator, the temperature in the tunnel wick is determined by the temperature of the enclosing liquid contained in the fine capillary passages. Since the liquid leaves the condenser at a sub-cooled temperature relative to the main vapor temperature, the saturation pressure within the tunnel wick is less than the pressure in the main vapor space. This pressure difference can be expressed

by the Clausius-Clapeyron equation which relates temperature and pressure along the saturation line.

$$p_v - p_{v,b} = \frac{p_v \lambda}{R T_v^2} (T_v - T_{v,b}) \quad (4-26)$$

where

- T_v = Saturation temperature in vapor space
- λ = Latent heat
- R = Gas constant
- $T_{v,b}$ = Saturation temperature in the inclusion

The pressure differential will cause the collapse of any vapor bubbles within the wicks causing the tunnel to be completely filled with liquid or it will compress any non-condensable gas which can significantly accelerate the collapse of the gas inclusion by diffusion. Pressure priming can also provide the necessary driving potential to prime large flow passages which would normally be unable to self-prime in gravity by surface tension. The degree of pressure priming that can be achieved is dependent on the amount of liquid sub-cooling in the condenser and the temperature difference which can be maintained across the wicks. To maintain the high temperature difference across the wick, multiple wraps of fine capillary passages are placed around the tunnel to achieve a high impedance to heat flow. The amount of sub-cooling achieved is dependent on conditions in the condenser. Since heat pipes are typically high conductance devices, significant sub-cooling is not achieved unless significant heat loads are applied. High heat load applications, however, cannot be satisfied until the wick is fully primed. To develop the substantial pressure differential to insure practical pressure priming, heat pipe designs with augmented cooling have been investigated (23). As illustrated in Fig. 4-24, sub-cooling can be achieved by bringing the returning condensate into contact with a secondary heat sink. The vapor phase flow is isolated from this region to insure maximum heat sinking of the liquid.

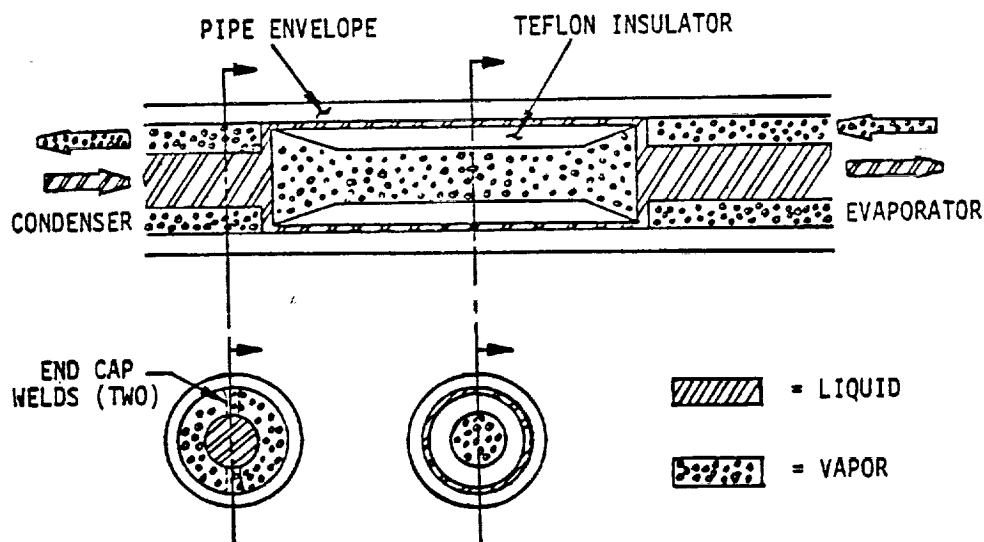


Fig. 4-24. Subcooling section in a pressure-primed wick (23)

4.4.3.2 Meniscus Coalescence

Inclusions are often trapped in a composite wick because the fine capillary structure which forms the larger flow passages will wet or glaze more rapidly than the large flow passages can self-prime. This glazing effect prevents any inclusions from venting and the large flow passages cannot fully self-prime. A method of circumventing the glazing effect is to insert a thin foil into the evaporator end of the wick. This foil contains a pattern of holes to permit venting of gas. If the foil is sized so thin that the menisci coalesce on either side of a liquid plugging the holes (see Fig. 4-25), then the liquid cannot plug the holes in the foil and venting is unimpeded during the priming of the wick (24). The maximum hole size in the priming foil is determined by the capillary pumping required to meet the desired heat pipe performance. This hole diameter in combination with the foil thickness and the diameter of the large flow channel determines the stress level required to achieve meniscus coalescence. Analytical investigations based on the governing equations defined in Fig. 4-25 (24) indicate that the stress level required to achieve meniscus coalescence can be expressed as follows:

$$\bar{\sigma} \geq \frac{2\bar{\sigma} - \left(1 - \sqrt{1 - \bar{\sigma}_p^2}\right)}{(1-2\bar{\sigma}) \left(1 - \sqrt{1 - \bar{\sigma}_p^2}\right) + 2\bar{\sigma}^2} \quad (4-27)$$

where:

$$\bar{S} = (P_{vs} - P_e)/(4 \sigma \cos \psi/D_a)$$

$$\bar{D}_p = D_p \cos \psi/D_a$$

$$\bar{\delta} = \delta \cos \psi/D_a$$

$$D_p = \text{Hole diameter in the priming foil}$$

$$D_a = \text{Diameter of the artery}$$

$$\delta = \text{Foil thickness}$$

$$\psi = \text{Wetting angle}$$

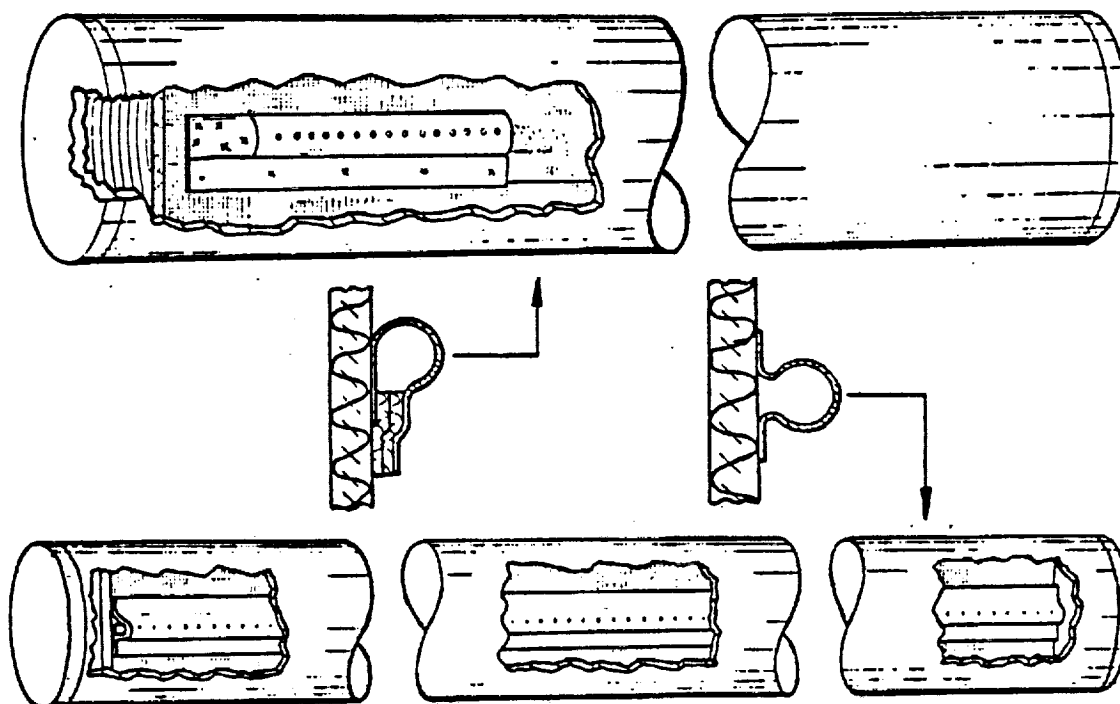
$$\sigma = \text{Surface tension}$$

The smallest critical pore diameter \bar{D}_p for which menisci coalescence will occur is given in Fig. 4-25 for given values of foil thickness $\bar{\delta}$ and stress (\bar{S}). Note that the above mentioned parameters are dimensionless and that the stress varies from zero to unit. At a value $\bar{S} = 0$, the hole is flooded. In 1-g, this corresponds to the hole just at the surface of a liquid pool. Negative values of \bar{S} correspond to the hole being submerged, and hence theoretically no venting should occur. A value $\bar{S} = 1$ corresponds to the maximum stress that the failed open artery can sustain. Thus if a bubble is entrapped and the stress must be increased greater than $\bar{S} = 1$ for menisci coalescence to occur, when it does occur, the artery will empty of liquid rather than prime.

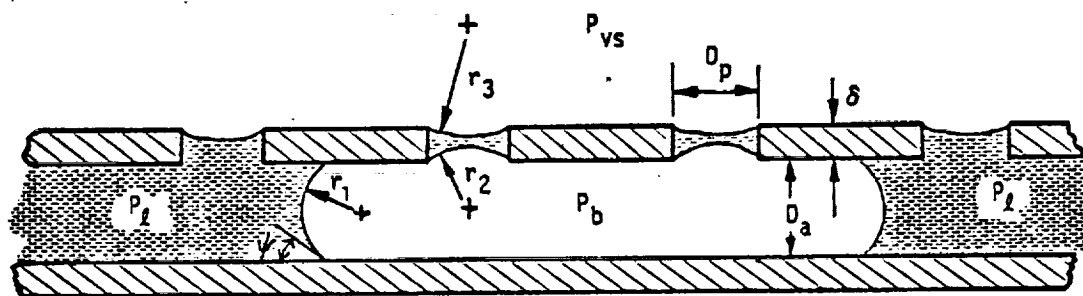
The value of \bar{S} governs the curvature of the meniscus on the outside of the potential liquid plug in the hole. Thus, for $\bar{S} = 0$ the meniscus is flat, and for $\bar{S} = 1$ the meniscus has the same radius of curvature as the inner meniscus. As a result, for a given hole size \bar{D}_p , the required foil thickness for coalescence at $\bar{S} = 0$ is one-half that for $\bar{S} = 1$, which is also apparent in Fig. 4-26.

Several experiments have been conducted to test the theory of menisci coalescence including visual experiments (24), zero gravity tests of two research heat pipes on the sounding-rocket International Heat Pipe Experiment (29), working heat pipes used for the Communications Technology Satellite (30), and a TRW Spacecraft as well as a priming study conducted with a glass heat pipe (31). Results to date indicate good agreement between priming stress factors determined experimentally and the preceding theory. Experience so far indicates that successful priming can be achieved under most but not all conditions.

Entrapment in the condenser zone is one condition under which venting of a non-condensable gas inclusion cannot be accommodated since the condenser end does not have a priming foil. Experiments were conducted with a glass heat pipe (30) to establish the ability to drive the bubble to the evaporator.



Typical Venting Foil Configurations



GOVERNING EQUATIONS:

$$\frac{2\sigma}{r_1} = \frac{2\sigma}{r_2} = P_b - P_l$$

$$\frac{2\sigma}{r_3} = P_{vs} - P_l \quad r_1 = \frac{D_a}{2 \cos \psi}$$

Fig. 4-25. Menisci coalescence for arterial venting (24)

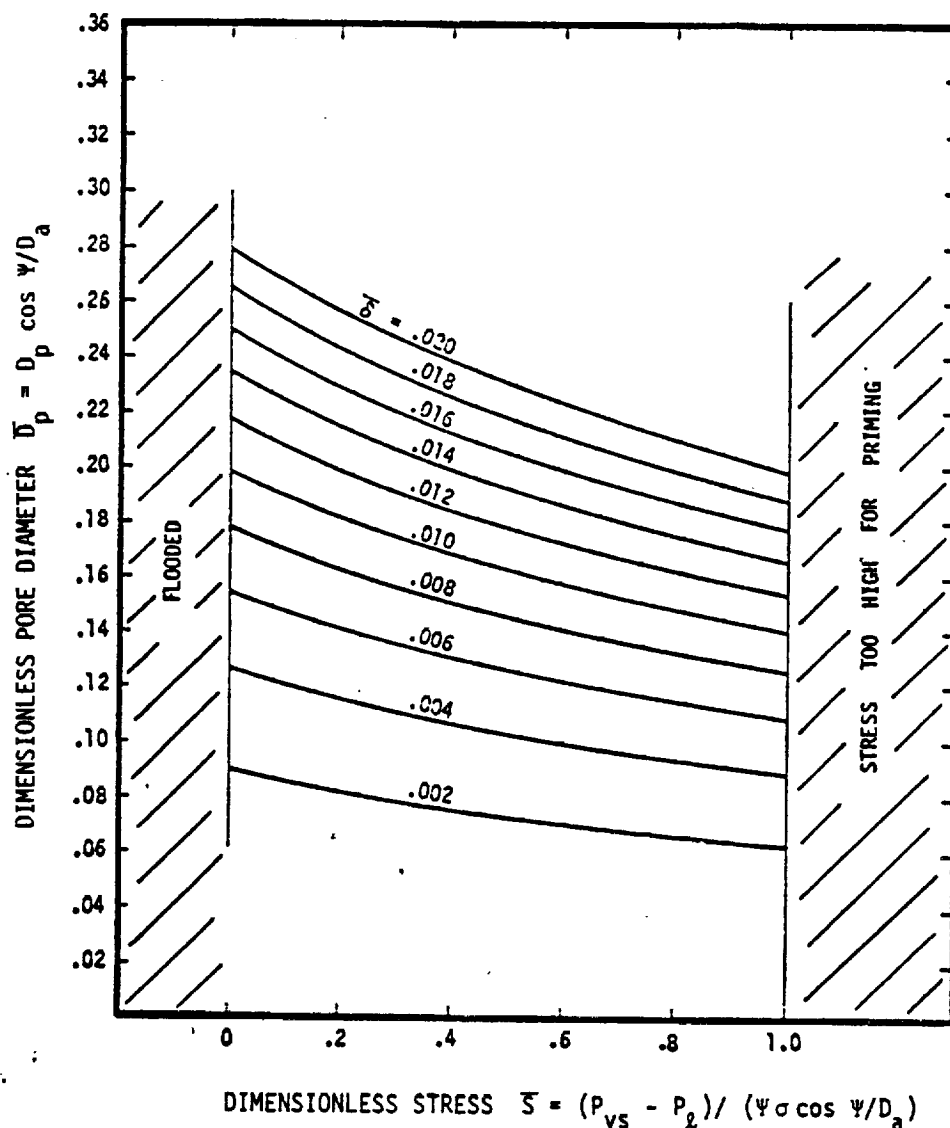


Fig. 4-26. Minimum pore diameter \bar{D}_p vs. stress $\bar{\sigma}$ with the foil thickness as a parameter (24)

Several runs were made for various heat loads and initial bubble sizes and locations. The results indicate that bubble convection was impossible at heat loads and evaporator elevations low enough for priming. Bubbles were observed to convect at heat loads greater than for priming; however, when the bubbles entered the priming foil and vented, the artery would empty of liquid.

As a consequence of these results, for actual heat pipe operation any arterial bubble that might exist would have to be cleared by applying a heat load in excess of the critical priming load, but below the maximum open artery load. Then the load is reduced sufficiently for priming. Another approach is to ignore the existence of any arterial bubble. If a bubble did exist, a burnout would result the first time the heat load was increased above the open artery capacity. Powering down below the critical priming load would result in successful priming because any bubbles would be convected to the evaporator end.

4.4.3.3 Jet Pump Assist

The suction created by a venturi can be utilized to displace and vent vapor or gas inclusions entrapped in a composite wick. Arterial heat pipe designs employing jet pump assist have been investigated by Bienert (25). Reliable operation both with and without a non-condensable gas has been demonstrated with prototype hardware. The concept of the jet pump assisted arterial heat pipe is shown in Fig. 4-27. The jet pump assembly consists of a venturi which separates the vapor in the evaporator from the vapor in the condenser, an injection port at the throat of the venturi, and a suction line which connects the artery with the injection port. During operation, the vapor flowing toward the condenser has to pass through the venturi, and its pressure drops below the saturation pressure in the evaporator. The lowest pressure exists at the throat; most of the pressure drop is recovered in the diverging section of the venturi. Since the artery is connected to the throat, its interior is exposed to the same reduced pressures and vapor and/or gas are pumped from the artery. At the same time, the reduced pressure forces liquid from the condenser into the artery. The pressure difference available for priming is a function of the vapor flow rate (which is synonymous with the heat load) and of the constriction provided by the venturi. Since the jet pump needs a finite vapor flow to generate a pressure difference, the artery must be paralleled by a priming wick. The purpose of this priming wick is to supply liquid to the evaporator before the artery is substantially primed. Sometimes the permeability of the screen from which the artery is formed suffices for this purpose. Occasionally, however, a more substantial priming wick is required.

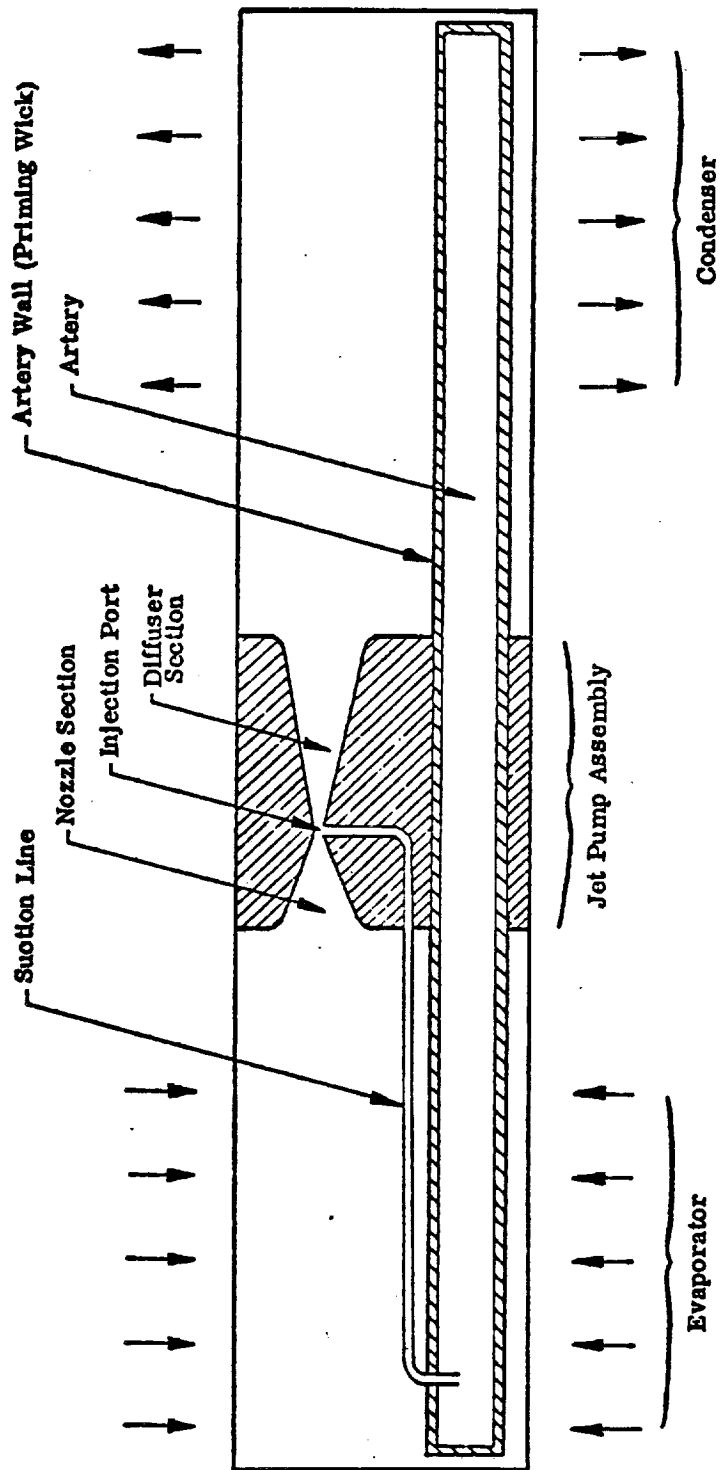


Fig. 4-27. Schematic of jet pump assisted arterial heat pipe (25)

The advantages of the jet pump assist heat pipe are:

- (1) No limitations on the artery size since self-priming by surface tension in gravity is not required.
- (2) Permits continuous venting of non-condensibles, not only during priming, but as long as vapor flows toward the condenser.
- (3) Repriming of the heat pipe can be achieved at a significant fraction of its maximum capacity.
- (4) The jet pump assist heat pipe provides stable operation at partially primed conditions.

Some of the disadvantages of the jet pump assist heat pipe are:

- (1) Cost and complexity.
- (2) Prescribed location of the evaporator/condenser region.
- (3) Pressure losses across the venturi which can significantly reduce the performance that can be achieved by capillary pumping.
- (4) The need for substantial pumping by the primary wick to provide the necessary priming potential.

4.4.4 Typical Secondary Wick Designs

Secondary wicks are often used in heat pipes to minimize temperature drops at the evaporator and condenser. Such wicks, however, can often significantly affect the performance of the heat pipe especially if they are used in combination with composite wicks. The performance characteristics of secondary wicks, therefore, should be included in the overall evaluation of a heat pipe design.

Figure 4-28 illustrates a typical secondary wick arrangement. Four equally spaced interconnecting bridges are used in the evaporator and condenser sections to interface the centrally located primary wick with the circumferential screw thread grooves on the container wall.

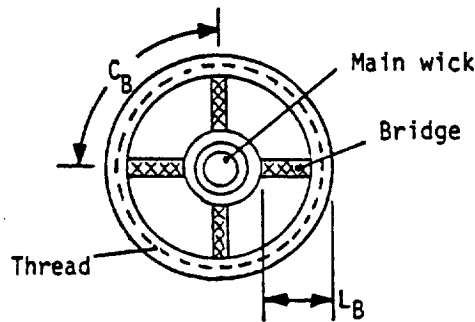


Fig. 4-28. Schematic of a typical secondary wick

In the evaluation of the overall performance of the heat pipe, the hydrodynamic flow and capillary pumping through the individual wick elements must be considered. Each component of the wick system has a characteristic permeability and an effective pumping radius which determine its hydrodynamic heat transport capability. It is seen that the heat transport capability depends on the wick properties as follows:

$$Q = \frac{K A}{L} \left(\frac{1}{r_{p1}} - \frac{1}{r_{p2}} \right) \quad (4-28)$$

The above equation is in a form which has the appearance of Ohm's law for d.c. circuits and is readily interpreted in terms of a network element resistor of resistance $\frac{L}{K A}$, through which a current Q passes because of the potential difference $\left(\frac{1}{r_{p1}} - \frac{1}{r_{p2}} \right)$. The resistance model of the heat pipe's wick system is shown in Fig. 4-29.

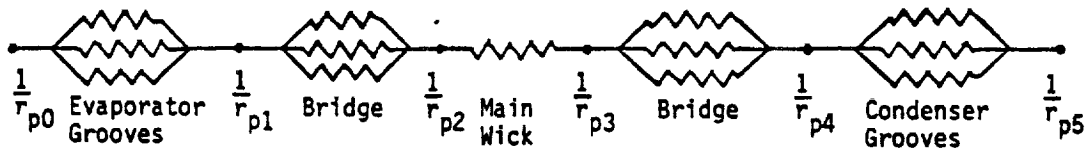


Fig. 4-29. Resistance model for a heat pipe's wick system

The total resistance R of the heat pipe can be expressed as:

$$R = R_{T,e} + R_{B,e} + R_w + R_{B,c} + R_{T,c} \quad (4-29)$$

In the evaporator, $R_{B,e}$ is the equivalent resistance of N_B bridges which can be represented as a system of $N_{B,e}$ resistance in parallel.

$$\frac{1}{R_B} = \sum_{i=1}^{N_B} \frac{1}{R_{B,i}} \quad (4-30)$$

where

$$R_{B,i} = \frac{L_{B,i}}{K_{B,i} \cdot A_{B,i}} \quad (4-31)$$

Since bridges are typically equal resistance paths, then

$$R_{B,e} = \frac{L_B}{N_{B,e} K_B A_B} \quad (4-32)$$

Similarly in the condenser $R_{B,c}$ is given by:

$$R_{B,c} = \frac{L_B}{N_{B,c} K_B A_B} \quad (4-33)$$

In the secondary wick region included between two bridges, heat can flow toward either bridge and the resistance of the region is equivalent to a system of two resistances in parallel. The resistance of each element can be expressed by:

$$R_T = \frac{1}{2} \frac{C_B}{K_T A_T N_T L_e} \quad (4-34)$$

where for a threaded secondary wick geometry

C_B = the distance between the two bridges

A_T = the cross-section area of the secondary wick

The equivalent resistance of the secondary wick in the evaporator is represented by a system of $2N_B$ resistances R_T in parallel and is given by:

$$R_{T,e} = \frac{R_T}{2N_{B,e}} = \frac{C_{B,e}}{4N_{B,e} K_T A_T N_T L_e} \quad (4-35)$$

Similarly, the equivalent resistance of the secondary wick in the condenser is expressed by:

$$R_{T,c} = \frac{C_{B,c}}{4N_{B,c} K_T A_T N_T L_c} \quad (4-36)$$

The resistance of the main wick is given as:

$$R_w = \frac{L_{eff}}{K_w A_w} \quad (4-37)$$

where

$$L_{eff} = \frac{1}{2} L_e + L_a + \frac{1}{2} L_c$$

The heat transport capability of the heat pipe is defined by the simultaneous solution of the system of individual transport equations. As illustrated in the wick system schematic in Fig. 4-29, the pumping radii of the various wick elements are equal at common interfaces. Additionally, these radii adjust to provide uniform heat transport across each element within the system, therefore:

$$\begin{aligned} Q = \frac{2N_B}{R_T} \left(\frac{1}{r_{p0}} - \frac{1}{r_{p1}} \right) = \frac{N_B}{R_B} \left(\frac{1}{r_{p1}} - \frac{1}{r_{p2}} \right) = \frac{1}{R_w} \left(\frac{1}{r_{p2}} - \frac{1}{r_{p3}} \right) \\ = \frac{N_B}{R_B} \left(\frac{1}{r_{p3}} - \frac{1}{r_{p4}} \right) = \frac{2N_B}{R_T} \left(\frac{1}{r_{p4}} - \frac{1}{r_{p5}} \right) \end{aligned} \quad (4-38)$$

If the maximum heat transport of the wick system requires a pumping radius at the bridge interface (r_{p1}) which is greater than the pore radius of the fine mesh screen used for the bridges and the main wick envelope, the secondary wick is limiting. If the secondary wick is capable of providing the maximum heat pipe transport with a value of (r_{p1}) which is less than the fine mesh pore radius, the main wick is limiting.

4.4.5 Thermal Conductance

As indicated above, thermal conductance is an important factor in the selection of a wick design. The third column in Table 4-9 rates the various wicks in terms of thermal conductance. The primary concern is the heat transfer at the evaporator and condenser since the temperature drop within the vapor is usually negligible. The thermal conductance is not only a property of the wick but also depends directly on the thermal conductivity of the working fluid. With respect to their conductivity, all fluids can be divided into two groups--non-conducting fluids and liquid metals. The range of thermal conductivities for both groups is:

Low Conductivity Fluids: 0.1 - 0.7 W/m-°K (0.06 - 0.04 Btu/Hr-Ft-°F)

Liquid Metals : 10 - 200 W/m-°K (5.8 - 115 Btu/Hr-Ft-°F)

Because the difference in thermal conductivities between low conductivity fluids and liquid metals is more than an order of magnitude, different considerations apply to the two groups. In liquid metal heat pipes, one is seldom concerned with the conductance of the wick itself since the high conductivity of the fluid provides for high heat transfer coefficients even for fairly thick layers of wick. But for heat pipes containing low conductivity fluids, the effective conductance is strongly dependent on the wick design.

A simplified model for the heat transfer process at the evaporator and the condenser assumes that heat is conducted through the heat pipe wall and through the wick/liquid matrix to the liquid-vapor interface where evaporation occurs. More complex models, such as the recession of the liquid-vapor interface into the wick and/or nucleate boiling within the wick, have been proposed but are not sufficiently refined to be used for design purposes.

The conduction model can be used to calculate an effective heat transfer coefficient at the evaporator and condenser which is, (excluding the contribution of the wall):

$$h_{int} = \frac{k_{eff}}{t} \quad (4-39)$$

where

k_{eff} = The effective thermal conductivity of the wick liquid matrix

t_w = Wick thickness

From Eq. 4-39 it is evident that high conductance can only be achieved if the thickness of the wick adjacent to the evaporation and condensation surfaces is kept at a minimum. This requirement has led to the development of "high conductance" wick structures in which the main transport wick is removed from the wall and only a thin secondary wick is used for circumferential distribution of the working fluid. Examples of such high conductance wicks are: the porous slab and the arterial wick, in both the conventional and the composite configuration.

The effective thermal conductivity of the wick/liquid matrix is bracketed by the series and the parallel path conduction models (Section 2.8) which is repeated here for easy reference:

$$K_w = \frac{K_s K_l}{\epsilon K_s + (1 - \epsilon) K_l} \quad (\text{Series Paths}) \quad (4-40)$$

$$K_w = (1 - \epsilon K_s) + \epsilon K_l \quad (\text{Parallel Paths}) \quad (4-41)$$

As a general rule, the series path conduction model will apply for wicks which are only in mechanical contact; e.g., wraps of screen, packed particles, fibers, or spheres. Sintered wicks, on the other hand, will have an effective conductivity which is better approximated using the parallel path model. Typical heat transfer coefficients for heat pipes containing non-conduction working fluids are summarized in Table 4-10.

The effective conductance of grooves, which are integral parts of the heat pipe envelope, are not described by either of the above models.

For axial grooves, Kamotani (32) suggests the following:

$$h_e = \frac{N K_l}{2\pi R_v} \frac{1}{.0701 + \frac{K_l \delta}{K_w \bar{t}_f}} \quad (\text{Evaporator}) \quad (4-42)$$

$$h_c = \frac{N K_l}{2\pi R_v} \frac{1}{.0221 + \frac{K_l \delta}{K_w \bar{t}_f}} \quad (\text{Condenser}) \quad (4-43)$$

where:

- K_L = Liquid thermal conductivity
 K_W = Thermal conductivity of pipe wall
 N = Number of grooves
 δ = Groove depth
 \bar{t}_f = Average land thickness

TABLE 4-10. TYPICAL HEAT TRANSFER COEFFICIENTS FOR HEAT PIPES				
Wall Material/Type		Heat Transfer Coefficients		Comments
		$W/m^2-^{\circ}K$	$Btu/Hr-Ft^2-^{\circ}F$	
Heat Pipe Envelope	Aluminum	173,000	100,000	$0.89 \times 10^{-3} m$ (0.035 in) wall
	Copper	440,000	250,000	$0.89 \times 10^{-3} m$ (0.035 in) wall
	Stainless 316	24,000	14,000	$0.89 \times 10^{-3} m$ (0.035 in) wall
	Molybdenum	154,000	89,000	$0.89 \times 10^{-3} m$ (0.035 in) wall
Wicks	Multilayer Screen	600-1000	100-170	$10^{-3} m$ (0.040 in) Thick SST Wick - Non-Conducting Fluid
	Sintered Wick	4700-6700	830-1180	$2.25 \times 10^{-3} m$ (0.09 in) Circular Wick - Water (10)
	Secondary Wick (Single Layer)	3000-9000	350-1600	200 Mesh Screen Non-Conducting Fluid
	Grooves	3000-15000	500-2500	Aluminum Wall 20-200 Grooves/inch

4.4.6 Wick Fabrication

One final important criterion (last column, Table 4-7) for selecting a wick is its fabricability and the corresponding cost to manufacture. This criterion is highly subjective since its importance depends a great deal on the application. For example, in a heat pipe which is intended to protect a vital component of an expensive spacecraft, cost will be of secondary importance when judged against performance and reliability. On the other hand, heat pipes which are designed for mass production must contain wicks which can be manufactured at low cost.

As a general rule, those wicks which are simple to install and do not require precise process control to manufacture are usually the least expensive. Multiple wraps of screen, layers of fibrous material, or slabs of porous material fall into this category. Wicks which are individually assembled such as arteries, annuli, etc., are high cost wicks. Sintered wicks are medium cost wicks, and their cost will depend to a large extent on the available process. They are expensive in small quantities but can be much less expensive when mass produced. The cost of grooved tubing is determined by the material and the groove geometry. Grooves can be extruded or swaged rather inexpensively in aluminum, copper and other ductile materials. Grooved aluminum tubing is moderately expensive in small quantities because of prorated die costs, while in large quantities it can be produced inexpensively.

For axially grooved tubing, experience to date indicates that the extrusion process is the best method for producing aluminum tubing. Well defined groove forms and good dimensional control have been achieved. Mounting flanges can be extruded as an integral part of the tubing which can simplify interfacing in many applications. In addition, the ability to produce complex groove forms has been demonstrated by the NASA Lewis Covert Groove extrusion which should lead to higher performance and greatly reduce sensitivity to 1-g testing. For the intermediate to high temperature range, however, axially grooved tubing of materials such as copper and its alloys, stainless steel, carbon steels and super alloys are required, and the swaging process is the only known process which can effectively be used today to produce axially grooved tubing in these materials on a cost effective basis.

4.5 CONTAINER DESIGN

The heat pipe container is a leak tight enclosure which isolates the working fluid from the outside environment, mechanically retains the wick structure in position and provides the necessary interface with the heat source and heat sink. A variety of shapes, sizes, and configurations have been developed for different applications including flat plates, rectangular shapes, conical and annular geometries. The tubular geometry made of tubing or pipe materials is the most common configuration employed in heat pipe designs and the following section addresses itself primarily to this cross-section. The design considerations discussed, however, are basic and can be applied to the design of any shape or geometry. The basic container design considerations are as follows:

- (1) Structural integrity and leak tight containment of the working fluid
- (2) Compatibility with the working fluid and the external environment
- (3) External interfacing with the heat source(s) and heat sink(s)
- (4) Internal size and geometry suitable for liquid and vapor flow requirement
- (5) Fabrication considerations including machining, forming, cleaning, welding and charging
- (6) Heat transfer consideration as it applies to the external interface, conduction through the container wall and the evaporator/condensation processes within the heat pipe

The size and internal geometry of the container is dependent on the requirements of the selected wick structure, the vapor flow area requirement, heat transfer considerations, external interface requirements and leak tight pressure containment of the working fluids. Design considerations with respect to container material selection, pressure retention and external interface are discussed in the next sections.

4.5.1 Material Selection

The material selected for the construction of the heat pipe container must be compatible with the working fluid and the external environment. In addition, the material must provide sufficient strength for the retention of the vapor pressure, good thermal conductivity and it must provide satisfactory fabrication properties.

Since leak tight pressure retention of the working fluid is paramount to reliable, long-term operation of the heat pipe, the material selected must provide adequate strength, it must be non-porous to prevent diffusion of gases or working fluid vapor and it must be easily sealed. The strength properties of typical heat pipe container materials are summarized in Fig. 4-30 (33). Joining (welding, brazing, etc.) characteristics are summarized in Table 4-11. For applications where the container must retain substantial internal pressure and where personnel safety is critical, such as heat pipes shipped via commercial carriers, it is recommended (34) that the ASME Boiler and Pressure Vessel Code, 1965 (35) be the principal source of material properties and allowable stresses for use in the structural analysis and design of heat pipes. Additional information can be obtained from sources such as MIL-HDBK-5B (36) the American Society Metals Handbook (37) and the Mechanical Engineers' Handbook (38).

The ASME code specifies that the maximum allowable stress at any temperature be one-quarter of the material's ultimate tensile strength F_{tu} , at that temperature. Material properties and allowable stresses for the two most commonly used heat pipe materials (6061-T6 aluminum alloy and 304 stainless steel) are given in Table 4-12. These values were excerpted from the ASME Code; similar tables can be constructed for other ductile materials listed in MIL-HDBK-5B for military or aerospace applications. For reference purposes, maximum allowable stresses as a function of temperature for various materials are given in Fig. 4-30.

Allowable stresses for welded tubing are also given in Table 4-12. The ASME Code specifies that welds of the type which would be used on heat pipes shall be double-welded (i.e., both sides), fully radiographed butt joints. The allowable stresses in Table 4-12 refer to this type of weld. The code permits the use of single-welded, fully radiographed butt joints if they can be shown to be of the same quality as the double-welded joints. Since the quality of single-welded joints in thinner gauge materials can be shown to have the same quality as the double-welded (and since double welding is completely impractical on small-diameter tubes), single-welded, fully radiographed butt joints discussed in Section 4.5.2.3 are considered to have a strength equal to that of a double-welded joint.

Normally, the temperature drop through a heat pipe wall is negligible even if low conductivity materials are used because the conductance path (wall thickness) is often very small. However, if thick walls are required for pressure retention and if the application consists of concentrated local heat loads, a high thermal conductivity material may be

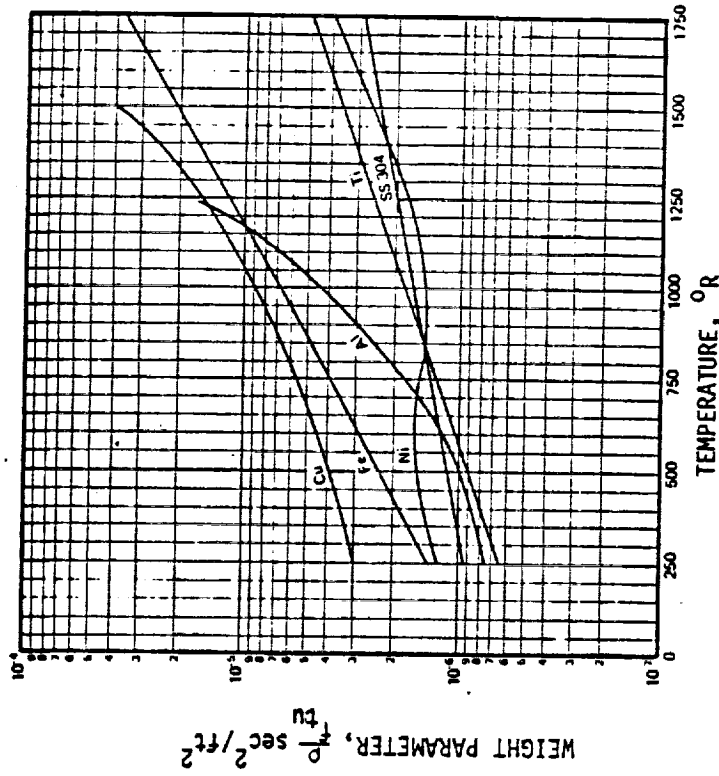


Fig. 4-31. Material weight parameter versus temperature for several heat pipe materials ($1 \text{ sec}^2/\text{ft}^2 = 10.76 \text{ sec}^2/\text{m}^2$; $1 ^{\circ}\text{R} = 0.5556^{\circ}\text{K}$) (33)

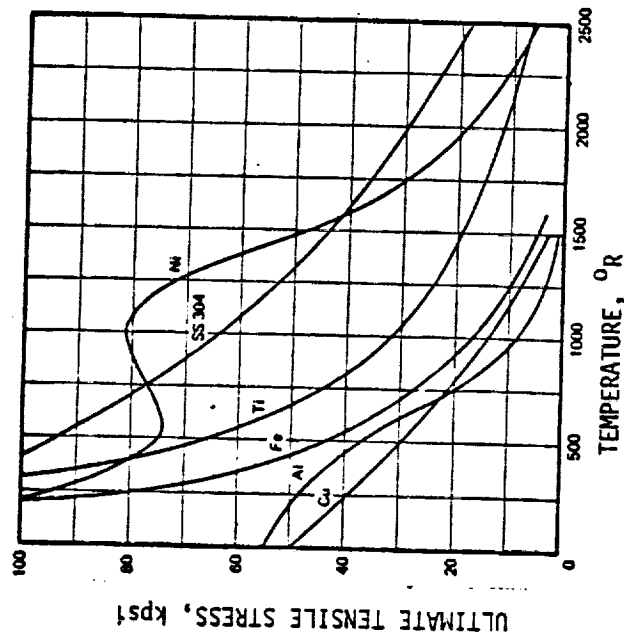


Fig. 4-30. Ultimate tensile strength of several solid materials, ($10^6 \text{ R} = 0.5556 ^{\circ}\text{K}$, $1 \text{ kpsi} = 6.895 \times 10^6 \text{ N/m}^2$) (33)

TABLE 4-11. CONTAINER MATERIAL FABRICATION PROPERTIES

MATERIAL	MACHINABILITY	WELDING	JOINING	FORMING
6063 Aluminum	Good	Good	Poor	Good
6061 Aluminum	Good	Good	Poor	Good
304 Stainless Steel	Fair	Good	Good	Poor
316 Stainless Steel	Fair	Good	Good	Poor
A-178 Carbon Steel	Good	Good	Good	Fair
Copper (CDA-101)	Fair	Good	Good	Fair/Good

TABLE 4-12. MAXIMUM ALLOWABLE STRESSES (34)							
	Ultimate tensile strength, F_u at 100°F	Tensile yield strength, F_y at 100°F	Maximum allowable stress at temperature, ksi				Modulus of elasticity, E
			100°F	150°F	200°F	400°F	
Aluminum drawn tube (seamless) ^a	42 ksi	35 ksi	10.5	10.2	9.9	—	10.5×10^6 psi 13.0×10^{-6} in./°F
• 6061-T6							
• 6061-T6 welded ^b	24	(14) ^d	6.0	5.9	5.7	—	
• 6063-T6	33	28	8.25	7.8	7.5	—	
• 6063-T6 welded ^b	17	(11) ^d	4.25	4.20	4.0	—	10.5×10^6 psi 13.0×10^{-6} in./°F
Aluminum seamless pipe and extruded tube							
• 6061-T6	38 ksi	35 ksi	9.5	9.2	9.0	—	
• 6061-T6 welded ^b	24	(14) ^d	6.0	5.9	5.7	—	
• 6063-T6	30	25	7.5	7.1	6.8	—	29×10^6 psi 8.5×10^{-6} in./°F
• 6063-T6 welded ^b	17	(11) ^d	4.25	4.2	4.0	—	
High alloy steel ^c seam- less pipe and tube							
• TP 304 (18-8)	75 ksi	35	18.75	17.85	17.00	15.45	
• TP 304L (18-8)	70	35	17.50	17.25	17.00	15.00	

^a Excerpted from Table UNF-23 of Section VIII, ASME Unfired Pressure Vessels (ref. 22)

^b These allowables apply to doubled welded, fully radiographed butt joints as per the ASME code. Refer to discussion in materials section.

^c Excerpted from Table UHA-23 of Section VIII

^d From reference 29

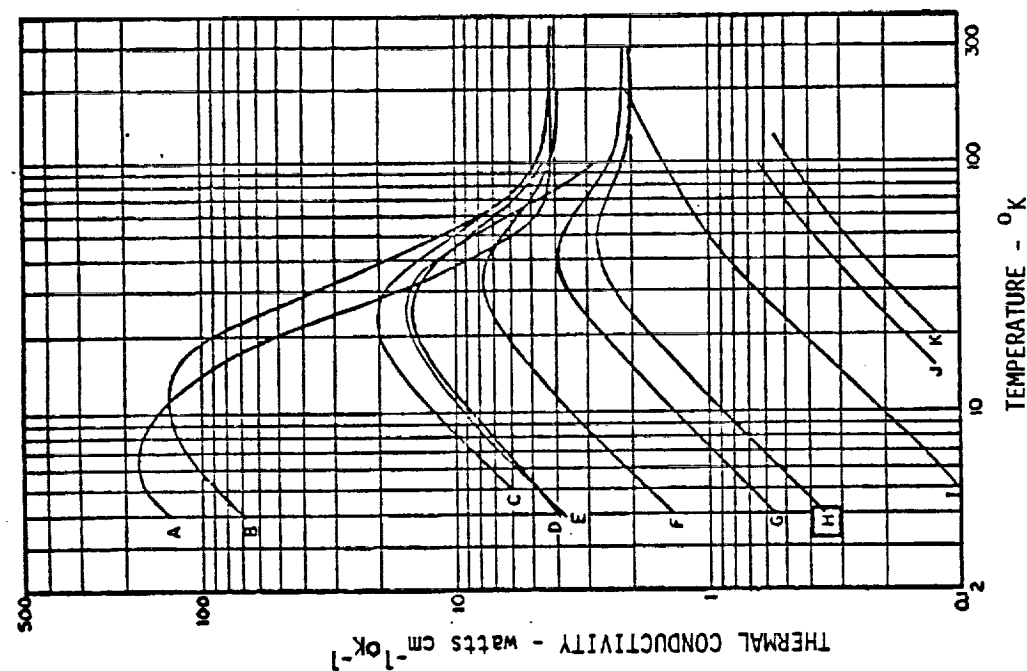
preferred. Fig. 4-32 summarizes typical thermal conductivities of various metals as a function of temperature. Note that the thermal conductivity of various metals is affected differently by temperature and that the most significant change in properties occurs in the cryogenic temperature range. Other material properties such as weight to strength ratio (weight parameter) and density are given in Figs. 4-31 and 4-34, respectively.

Fabrication of the container must be considered in the selection of the materials. Joining (welding, brazing, etc.), machining, forming, extruding, sintering, and cleaning are typical processes employed in the manufacturing of the heat pipe. The relative workability of typical heat pipe container materials is given in Table 4-11. For certain heat pipe designs, such as axially grooved tubing, fabrication is the dominant factor affecting the performance that can be realized. The extrusion process is typically used to form axial grooves in aluminum alloys and swaging has been successfully employed in forming grooves in aluminum alloys, copper and its alloys, stainless steels, carbon steels and super alloys.

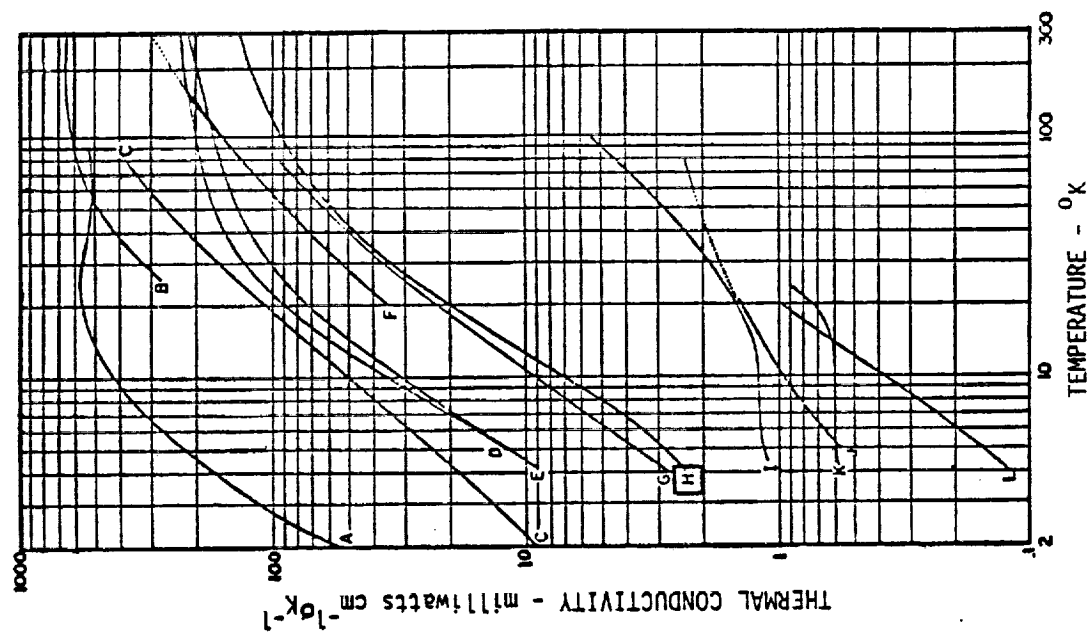
4.5.2 Structural Considerations

The primary structural considerations which must be evaluated in the heat pipe container design are its ability to withstand internal pressure and temperature, and external (induced) loads. The internal pressure of the heat pipe is dependent on the maximum temperature during processing, handling, storage, shipping, or during its operational lifetime. This maximum temperature also determines the strength of the container material. In addition to the stresses associated with the internal pressure, the heat pipe may also be subjected to externally induced environmental loads including pressure loads, acceleration, vibration and shock. The externally induced loads can occur during shipment, handling, and operation or may be caused by such factors as differential expansion loads due to mounting restraints within the system. From the structural analysis view point, the externally induced loads are equivalent to axial and bending stresses which the heat pipe must be able to sustain in combination with internally induced pressure loads.

A comprehensive analysis by a cognizant stress engineer should be performed to insure proper heat pipe structural design. Methods which can be applied to the preliminary structural design of heat pipes have been developed in the "Heat Pipe Manufacturing Study" (34). Recommended structural analysis procedures applicable to strength calculations for heat pipes developed in this study are summarized in the following sections.



Low-temperature thermal conductivities of some materials having relatively high conductivities. A, silver 99.999% pure (39); B, high purity copper (42); C, coalesced copper (42); D, copper, electrolytic tough pitch (42); E, aluminum single crystal (43); F, free-machining tellurium copper (42); G, aluminum, 1100 F (43); H, aluminum, 6063-T5 (43); I, copper, phosphorous deoxidized (42); J, aluminum, 2024-T4 (43); K, free-machining leaded brass (42).



Low-temperature conductivities of some solids with relatively low conductivities. A, 50-50 lead-tin solder (44); B, steel, SAE 101 (39); C, beryllium copper (44); D, constantan (39); E, Monel (39); F, fused quartz (39); G, polymer fluoroethylene Teflon (41); H, polymer fluoroethylene Teflon (39); I, polymer fluoroethylene Teflon (39); J, polymer fluoroethylene Teflon (39); K, polymer fluoroethylene Teflon (39); L, nylon (44).

Fig. 4-32. Thermal conductivity of various metals at low temperatures

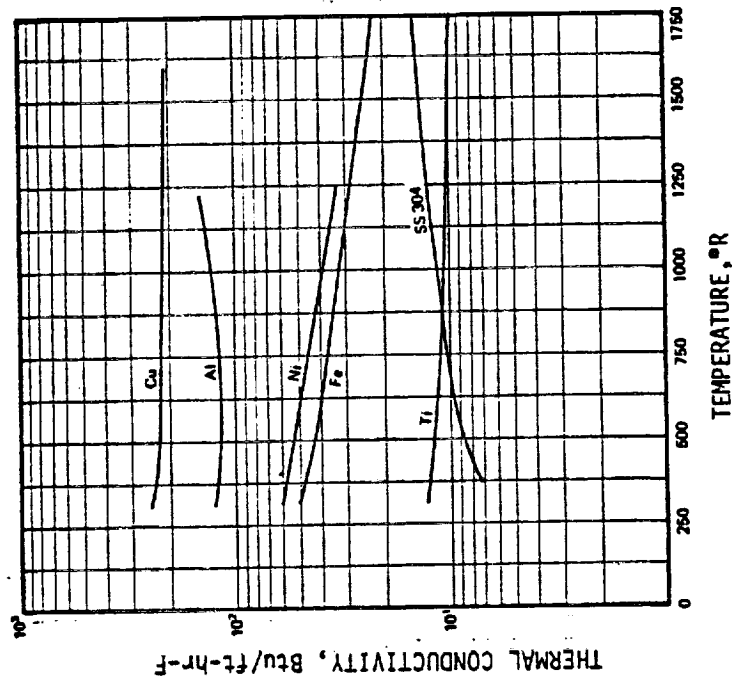


Fig. 4-33. Thermal conductivity of several solid materials, (1 deg R = 0.556 deg K, 1 Btu/ft-hr-F = 1.730 W/m-K) (33)

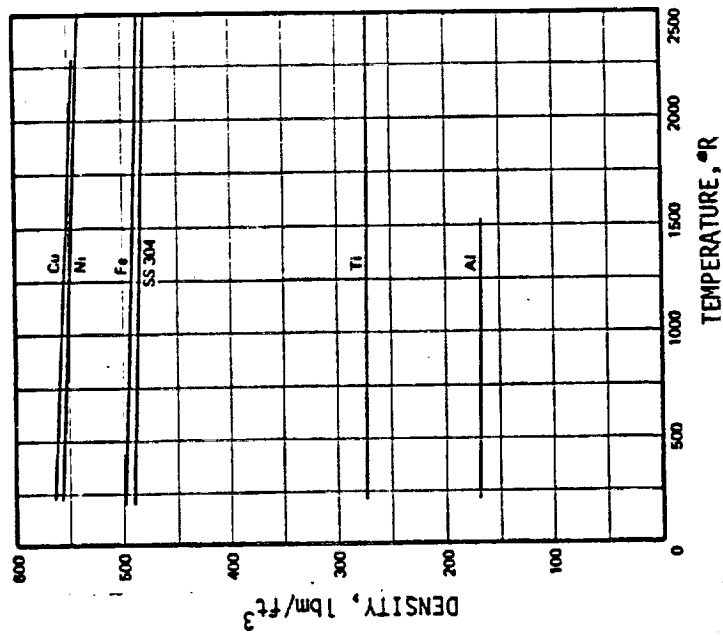


Fig. 4-34. Density of several solid materials, (1 deg R = 0.556 deg K, 1 lbm/ft³ = 16.02 kg/m³) (33)

4.5.2.1 Pressure Containment

As a ground rule, the design approach for tubes subject to internal pressurization follows that of the ASME Boiler and Pressure Vessel Code, 1965 - Section VIII, "Unfired Pressure Vessels" (35). The code is recommended as a design guide on the basis of its general acceptance in commercial and governmental areas of pressure vessel application.

As per this reference, a factor of safety of 4 on ultimate strength is used. Although some NASA criteria do specify lower factors of safety, it is recommended that the higher safety factor be used because of certain heat pipe characteristics which are different from the usual aerospace structures. First, heat pipes are handled and transported in the charged condition, and Federal regulations (39, 40) require that pressurized container shipped by commercial transportation conform to the ASME Code. Second, heat pipes are generally not "high technology" items and consequently, extensive structural analysis, design verification testing, and manufacturing quality assurance are not performed, as is the case with the typical aerospace structure. The ASME code also provides a method for experimentally determining the allowable operating pressure when the strength is difficult to calculate (as, for example, pinched-off fill tubes).

4.5.2.2 Tubular Container Design

The ASME Pressure vessel code limits the maximum operating pressure in a vessel to the pressure at which the most critical part reaches one quarter of the material's ultimate tensile strength, F_{tu} . The vessel can have different operating pressures at different temperatures. Each vessel must also be tested (proof pressure) to 1.5 times this maximum operating pressure without observable deformation or leaks. In addition, the code lists formulae for use in calculating allowable pressures and stresses. These relations are modifications to the thick-walled (Lame) solution for cylinders and spheres (41). The thick-walled solutions are listed in Table 4-13, and then reduced to the simplified thin-walled formulae which are sufficiently accurate for the geometries usually encountered in heat pipes, although they are somewhat different than those listed in the code. In these equations, the dimensions resulting in the minimum net section should be used including allowances for corrosion, threading or grooving and manufacturing tolerances. Figure 4-35 contains typical container design requirements for 6061 and 6063 aluminum and 304 stainless steel based on the hoop stress. Allowances for corrosion, threading, grooving and manufacturing tolerances are not included in these curves. The curves can be used to quickly determine required tube size when the maximum operating pressure is known.

TABLE 4-13. HOOP AND AXIAL STRESSES

Internal Pressure Hoop Stress

$$f_{hoop\ max} = p(R_2^2 + R_1^2)/(R_2^2 - R_1^2) \quad \text{(Thick-walled cylinder)} \quad (4-44)$$

$$f_{hoop} = \frac{pR}{t} \quad \text{(Thin-walled cylinder)} \quad (4-45)$$

$$R = 1/2 (R_2 + R_1) \quad (R_2/R_1 < 1.25)$$

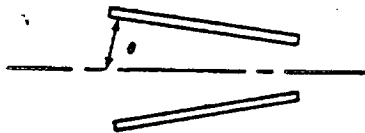
$$t = R_2 - R_1$$

Internal Pressure Axial Stress

$$f_{axial} = \frac{pR}{2t} \quad \text{(Thin-walled cylinder)} \quad (4-46)$$

Transition Section

The hoop and axial stresses due to internal pressures in a thin-walled conical shell (e.g., a reducer) are given by the relations:






$$f_{hoop} = pR/t \cos \theta \quad \text{(Conical shell)} \quad (4-47)$$

$$f_{axial} = pR/2t \cos \theta \quad (4-48)$$

Stress Due to Bends in a Tube

Between 10% of the yield and 20% of the ultimate strength

Stress Due to End Caps

MAXIMUM BENDING STRESSES		f_{bend}	
	CYLINDER ATTACHED TO A HEMISPHERE	$0.03 pR/2t$	(4-49)
	CYLINDER ATTACHED TO A 2/1 ELLIPSE	$1.18 pR/2t$	(4-50)
	RIGID END CAP	$3.10 pR/2t$	(4-51)

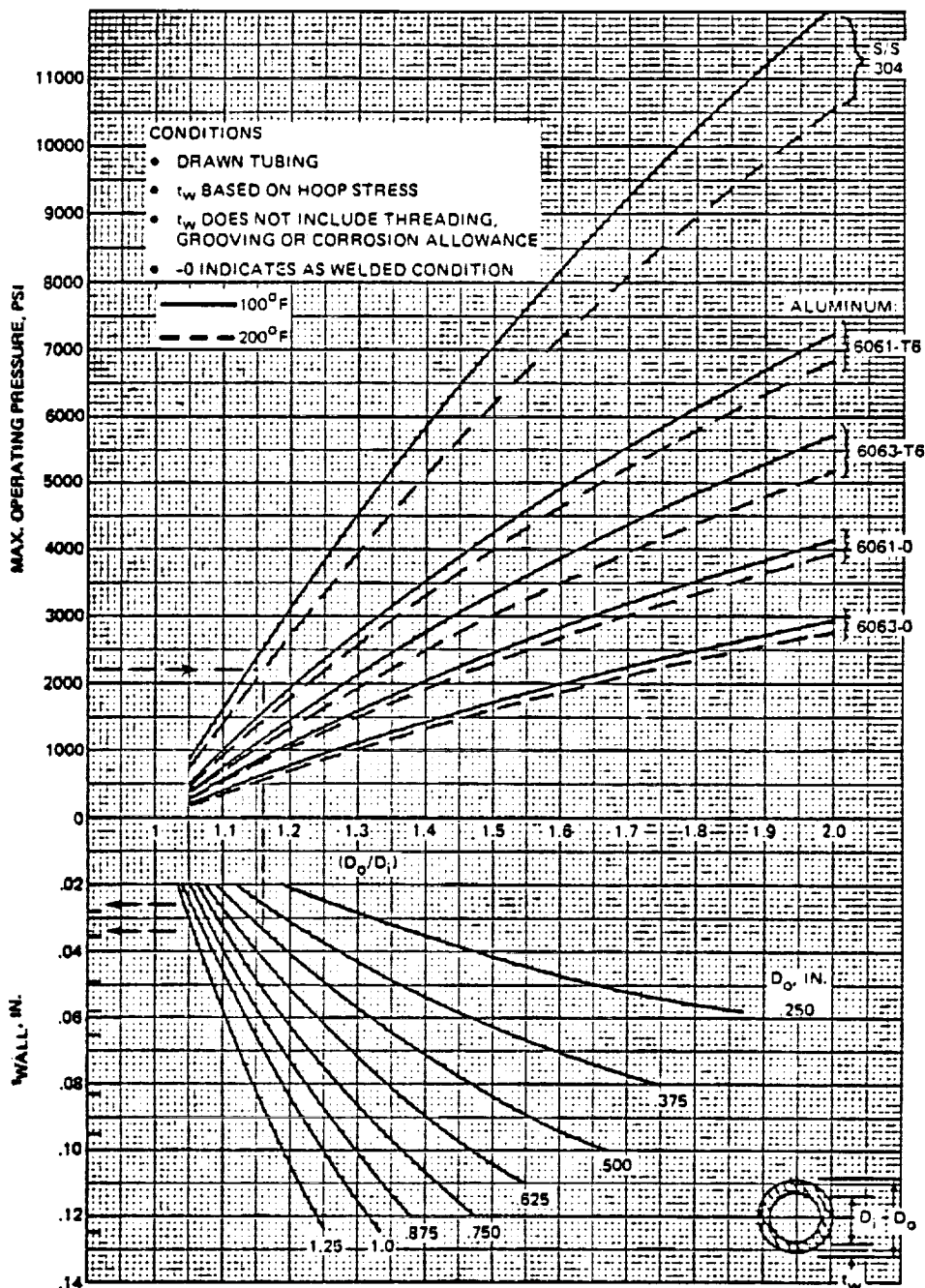


Fig. 4-35. Heat pipe envelope design curves (34)

In addition to the familiar hoop stress and axial stress, various localized axial stresses due to bends, end caps, saddles, restrained thermal expansion and dynamic (vibration) loading should be included in the structural analysis. Table 4-14 summarizes the various stress combinations that must be checked to determine the maximum operating stress in a heat pipe. The checkmarks in each column indicate the stresses that are additive for a particular situation. Although the major contributors are given, the Table is not all inclusive and it is conceivable that other combinations can occur that are not listed.

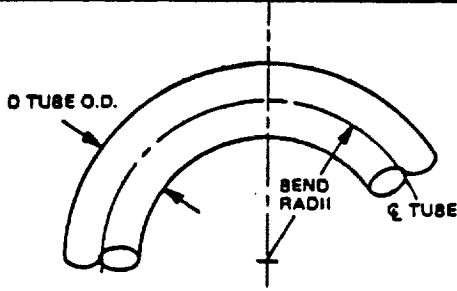
TABLE 4-14. STRESS CHECKLIST (34)

Stress	Reference section	Possible stress combinations					Design criteria
Hoop	5.2.4.1	✓					• f_{\max} = largest of the possible combinations
Axial	5.2.4.1		✓	✓	✓	✓	• $f_{\max} \leq 1/4 F_{tu}$
Bends	5.2.4.3		✓				
End caps	5.2.4.4			✓			
Saddles	5.2.4.5				✓		
Thermal expansion	5.2.4.6				✓		
Dynamic loading	5.2.4.7					✓	

Localized axial stresses due to bends and end caps can be estimated using the expressions summarized in Table 4-13. It is suggested in Ref.34 that 10% of the yield strength and 22% of the ultimate strength of the material be used to obtain a conservative estimate of the residual bending stresses in thin-walled tubes. The actual residual stress lies somewhere between these two values and acts in the axial direction. The foregoing criterion assumes a smooth-walled tube. In actual practice, the tube may be threaded or grooved and higher than average local strain could be developed in the thinner sections. In such cases, it is recommended that bend samples be made to determine the minimum bend radius and the proper bending speed. Table 4-15, extracted from Military Standard MS33611 (ASG), can be used as a guide to establish allowable bend radii.

The presence of a cap at the pipe end restrains the radial expansion which occurs in the pipe wall away from the ends. This restraint results in local bending stresses which are maximum at the restraint and die out with increasing distance away from the restraint. The maximum bending stresses for various types of end restraints are determined in Ref. 34, and are summarized in Table 4-13. These local bending stresses are additive to the basic pressure vessel axial stresses. This sum should be less than $F_{tu}/4$ for the design criteria to be satisfied. Also, the end cap region is an area of the pipe where "as welded" material properties must be used unless subsequent heat treatment is done after welding.

TABLE 4-15. TUBE BEND RADII



TUBE O.D.	SPECIAL BEND RADII SEE NOTE ^a		RECOMMENDED BEND RADII SEE NOTE ^b		ADDITIONAL RADII SEE NOTE ^c
	1-1/2D	2D	3D	4D	6D
1/8	0.188	0.250	0.375	0.500	0.750
3/16	0.281	0.375	0.563	0.750	1.125
1/4	0.375	0.500	0.750	1.000	1.500
5/16	0.469	0.625	0.938	1.250	1.875
3/8	0.563	0.750	1.125	1.500	2.250
7/16	0.656	0.875	1.312	1.750	2.625
1/2	0.750	1.000	1.500	2.000	3.000
5/8	0.938	1.250	1.875	2.500	3.750
3/4	1.125	1.500	2.250	3.000	4.500
7/8	1.3125	1.750	2.625	3.500	5.250
1	1.500	2.000	3.000	4.000	6.000
1-1/8	1.688	2.250	3.375	4.500	6.750
1-1/4	1.875	2.500	3.750	5.000	7.500
1-3/8	2.063	2.750	4.125	5.500	8.250
1-1/2	2.250	3.000	4.500	6.000	9.000
1-5/8	2.438	3.250	4.875	6.500	9.750
1-3/4	2.625	3.500	5.250	7.000	10.500
1-7/8	2.813	3.750	5.625	7.500	11.250
2	3.000	4.000	6.000	8.000	12.000
2-1/4	3.375	4.500	6.750	9.000	13.500
2-1/2	3.750	5.000	7.500	10.000	15.000
3	4.500	6.000	9.000	12.000	18.000

NOTES:

- Use of special bends (1-1/2D to 2D) in fluid systems with working pressures of 1500 psi or greater require the approval of the procuring service. Flatness, wrinkle and scratch requirements shall be as specified in Notes (d) and (e).
- Recommended bends (3D and 4D) require no approval and shall be used wherever possible. Flatness, wrinkle and scratch requirements shall be as specified in Notes (d) and (e).
- Additional bends (6D) shall be used only where fabrication or design difficulties preclude the use of recommended bends. Applications do not require specific approval and are limited only by the flatness, wrinkle and scratch requirements provided in Notes (d) and (e).

(d) Flatness limitations

- Flatness in the area of a tube bend shall be defined by the formula:

$$\text{Flatness} = \frac{\text{Max OD} - \text{Min OD}}{\text{Nominal OD}} \times 100 \text{ percent}$$

- Tube flatness for fluid systems with working pressures of 1000 psi or greater shall not exceed 5 percent
- Tube flatness for fluid systems with working pressures less than 1000 psi shall not exceed 10 percent

(e) Wrinkles and scratches:

- For fluid systems with working pressures 500 psi or greater, there shall be no wrinkles or kinks deeper than 1 percent of tube OD and no scratches deeper than 5 percent of the nominal wall thickness.
- For fluid systems with working pressures of less than 500 psi there shall be no wrinkles or kinks deeper than 2 percent of tube OD and no scratches deeper than 10 percent the nominal wall thickness.

Bend radii for tube diameters other than those specified may be established by multiplying the tube outside diameter by the appropriate numerical prefix noted in the table for the class bend desired.

Present bending dies may be used until such time as tools must be replaced.

[Ref: Mil-STD MS 33611 (ASG)]

Analyses to determine localized axial stresses due to saddles, restrained thermal expansion and dynamic loads are rather complicated and should be performed by a cognizant stress engineer. Analytical methods suitable to heat pipe designs can be found in Ref. 34.

4.5.2.3 End Cap Design

The ASME Code, 1965, describes two configurations, designated here as Type I and Type II, for welded flat circular heads that are recommended for heat pipe use. Design details are given in Fig. 4-36. The wall thickness, t_s , is the minimum net section after all allowances for corrosion, threading, or grooving have been made.

For these designs, the minimum required end cap thickness (t_{ec}) is specified in the ASME code as:

$$t = D \sqrt{4 C p_m / F_{tu}} \quad (4-52)$$

where:

- C = A factor obtained from Fig. 4-36
- D = 2R is the average diameter of the pipe
- p_m = internal pipe pressure

Figures 4-37 and 4-38 show typical variations in required thickness, t_s , with internal pipe pressure, p_m , for 6061-T6 aluminum and 304 stainless steel, respectively. These curves assume a value of 0.5 for the factor C, which gives conservative results.

4.5.2.4 Fill Tube Design

The design of fill tubes is similar to that of tubes and end caps with the exception of the fill tube pinch-off itself. A typical fill tube design is shown in Fig. 4-39.

Since this is a region of the heat pipe for which strength cannot be calculated with satisfactory accuracy, the maximum operating pressure should be determined experimentally (see Section 4.5.2.5).

In practice, the fill tube dimensions are determined by how tight a mechanical seal or crimp can be achieved prior to welding. A large inside diameter with a narrow wall will have good pump-down characteristics, but poor crimping properties - cracks are easily developed when the material is deformed. Too narrow an opening with a thick wall will have poor pump-down characteristics.

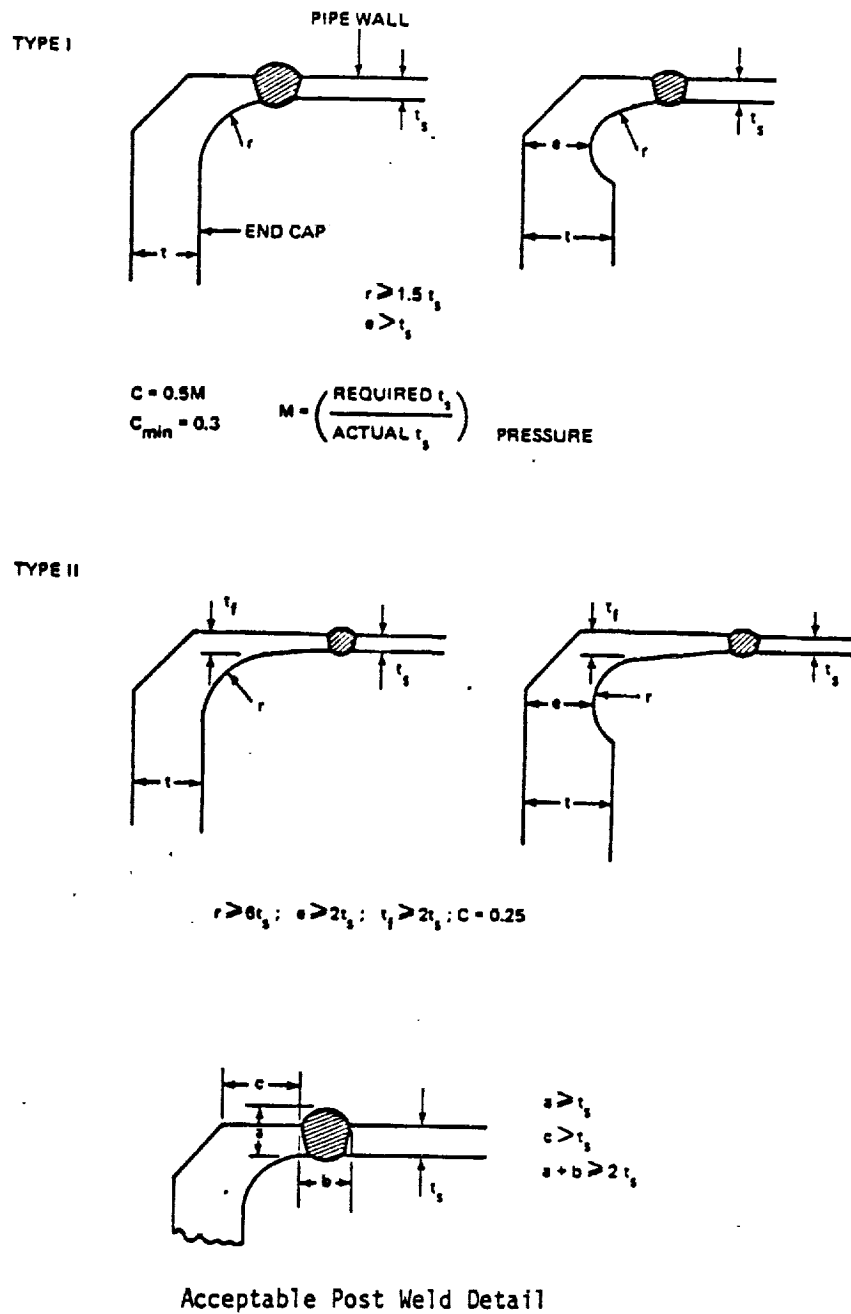


Fig. 4-36. End cap design detail (34)

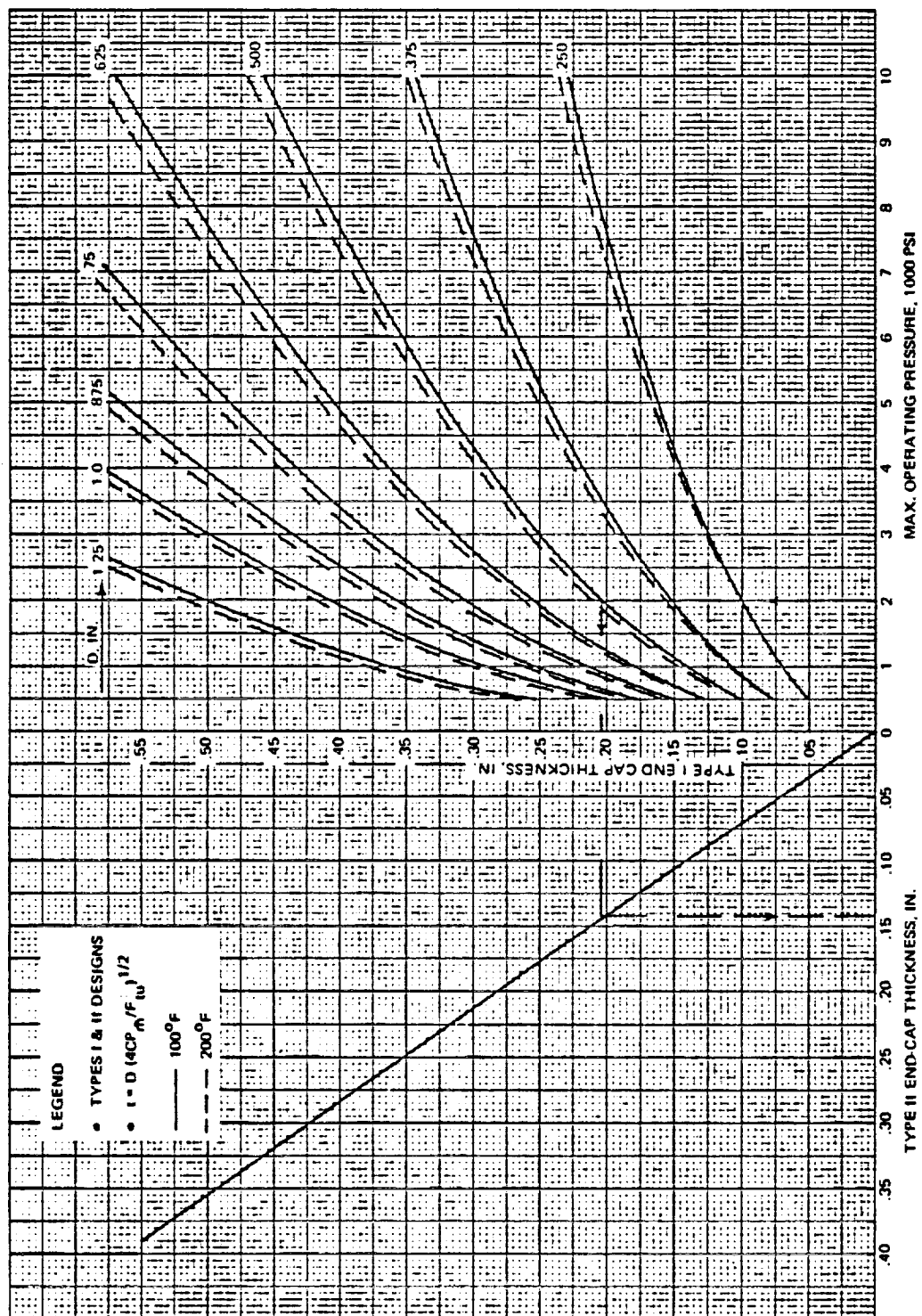


Fig. 4-37. End cap design curves, 6061-T6 aluminum (as welded) (34)

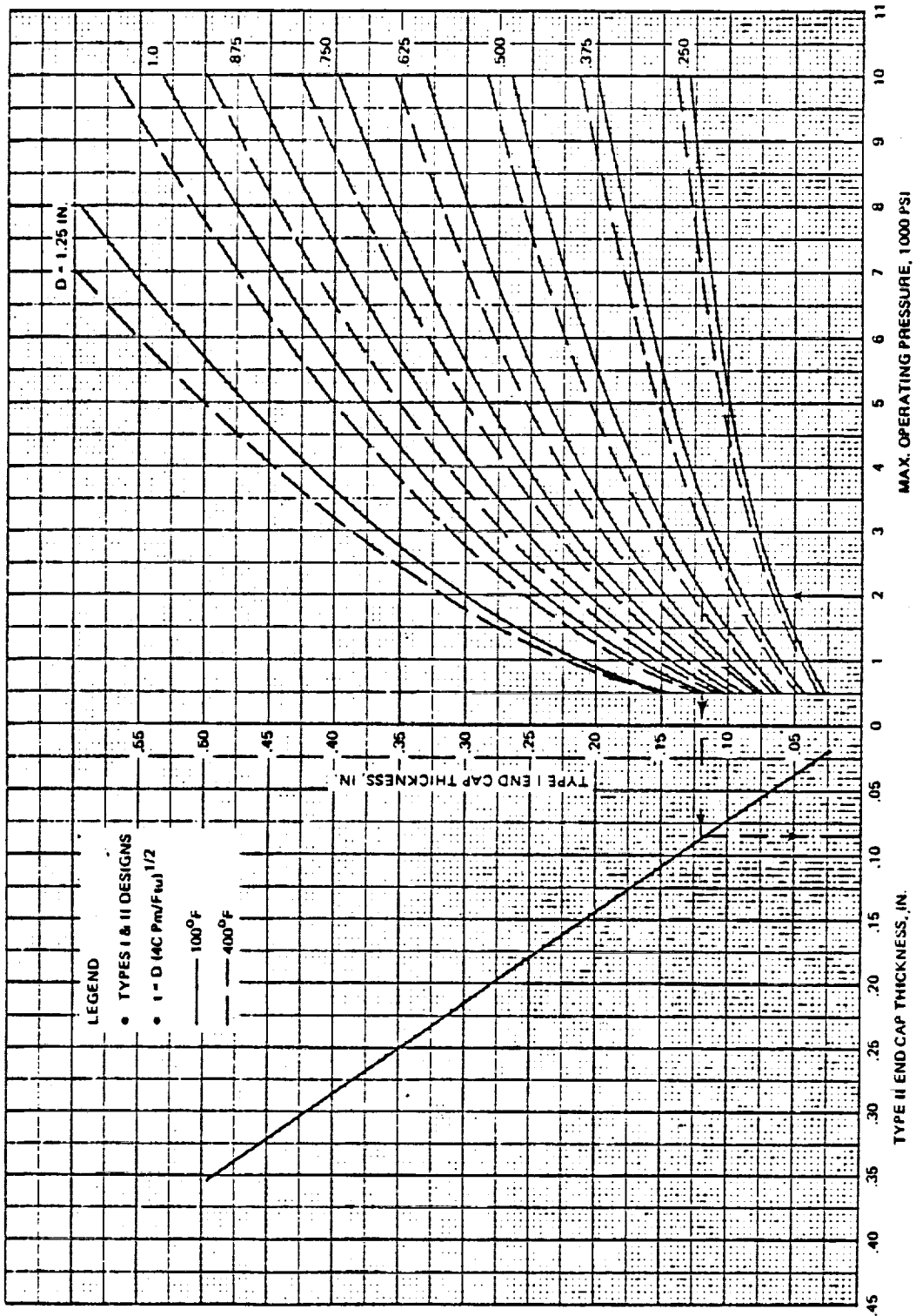


Fig. 4-38. End cap design curves, 304 stainless steel (as welded) (34)

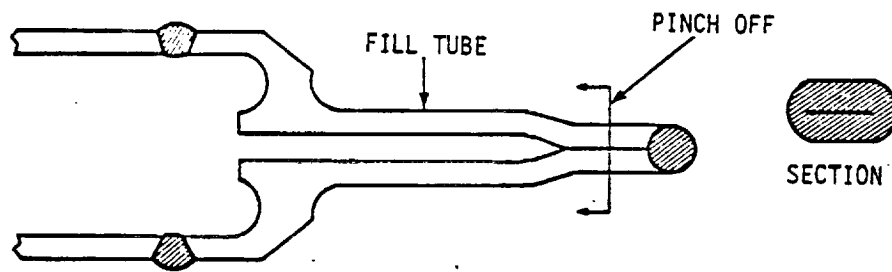


Fig. 4-39. Typical fill tube design (34)

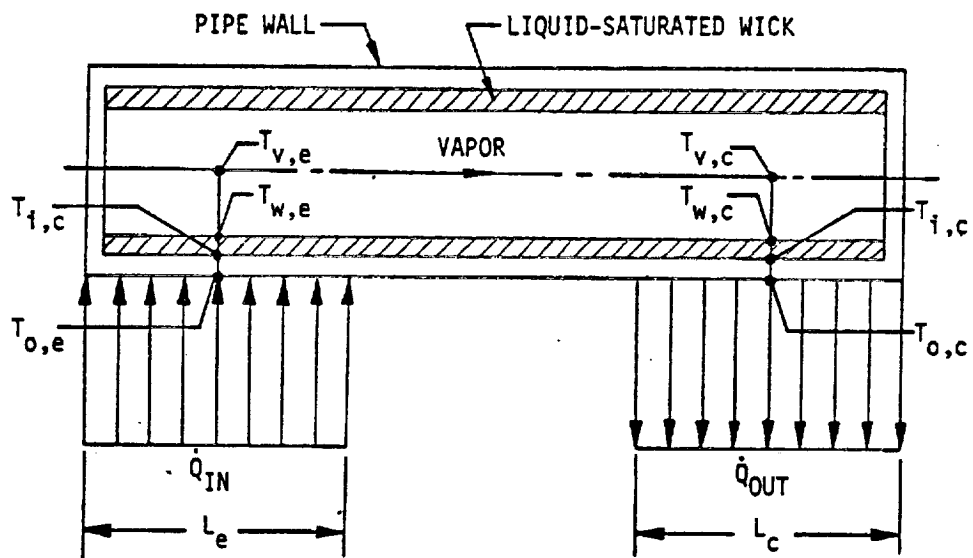


Fig. 4-40. Sketch of heat flow through a heat pipe

One fill-tube geometry that has been favored by a number of heat pipe fabricators uses a 3/16 to 1/4 in. (0.476 cm to 0.635 cm) o.d. tube with a 1/16 in. (0.159 cm) i.d. hole. It produces reasonable pump-down times ($\approx 1/2$ hr.) and repeatable crimp closures, in both stainless steel and aluminum. Burst test samples with aluminum charge tubes have given 3100 psi (2.137×10^7 newt/m²) for a fully annealed condition and 7500 psi (5.171×10^7 newt/m²) for -T6 tubes that were heated to 600°F (316°C) for 1 min. and air cooled to room temperature prior to pinch off.

4.5.2.5 Experimental Pressure Containment Verification

The ASME Code also provides a means of experimentally determining the maximum operating pressure of vessels for which the strength cannot be calculated with a satisfactory assurance of accuracy. These tests cannot, however, be used to obtain a higher value of maximum operating pressure than would be obtained for a vessel for which the strength can be calculated. There are two types of tests which can be used - a proof test, and a burst test. If the material yield strength, F_{ty} , is less than 0.625 of the material ultimate strength, F_{tu} , a burst test must be performed.

The maximum operating pressure can be obtained from the results of a single destructive burst test by the relation:

$$p_m = p_B F_{tu} / 5F_a \quad (4-53)$$

where:

p_m = maximum operating pressure

p_B = actual burst pressure

F_a = average tensile strength of four test specimens taken from the part after failure or from the same billet as the test specimen; or the maximum tensile strength in the material specification

F_{tu} = material tensile ultimate strength

The maximum operating pressure can be obtained non-destructively from the results of a proof test by the relation:

$$p_m = p_P F_{ty} / 2F_{ay} \quad (4-54)$$

where:

p_p = proof pressure

F_{ay} = average yield strength of four specimens taken from the part after test
or from the same billet

F_{ty} = material tensile yield strength

If no material property tests are performed, the maximum operating pressure may be obtained from:

$$p_m = 0.4 p_p \quad (4-55)$$

where the proof pressure, p_p , is defined as the pressure at which permanent set occurs and is determined using strain, or displacement measurements. In this test, strain gages are affixed to the vessel in the hoop direction and the strain is recorded as a function of internal pressure, or the change in diameter at various locations is recorded as a function of internal pressure to the point of permanent set.

When a corrosion, "threading" or "grooving" allowance has been included in the wall thickness, the proof or burst test result shall be multiplied by $(t - c)/t$ where t is the total wall thickness and c is the corrosion, "threading", and/or "grooving" allowance.

The test results can be corrected for temperature using the relation

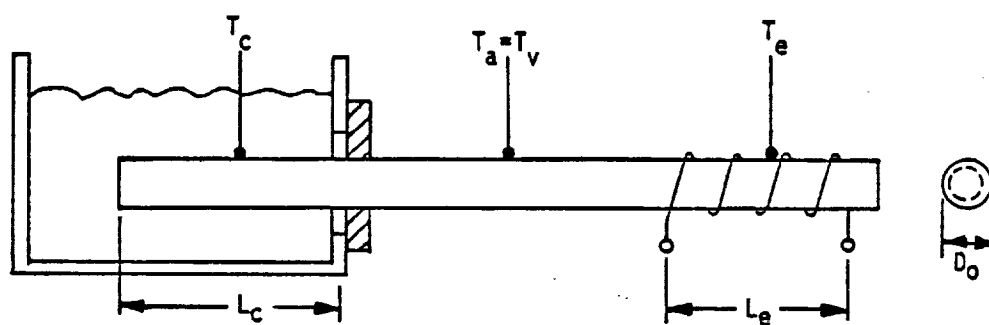
$$p_o = p_t F_o/F_t \quad (4-56)$$

where the subscripts t and o refer to test and operating conditions, respectively.

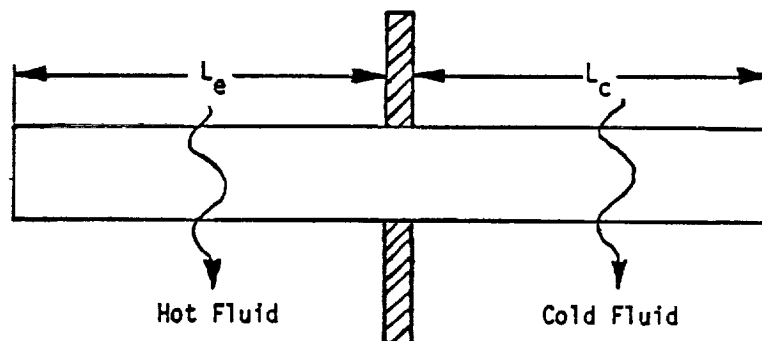
4.5.3 Interface Design

The external heat pipe container configuration is determined by mechanical and thermal interface considerations. Mechanical constraints, in addition to being associated with thermal interface requirements, generally relate to structural requirements and affect primarily the method of attachment of the heat pipe to the rest of the system. Thermal interface requirements, on the other hand, can affect the heat pipe's performance and therefore its design. The various implications of the thermal interface on heat pipe design are discussed in this section.

The simplest type of thermal interface condition is illustrated in Fig. 4-41. It consists of uniform heat input and heat removal. This condition is used very often in heat pipe performance test set-ups where heat is applied uniformly with a wrap-around heater and removed uniformly by a well stirred coolant bath. In some applications, uniform heat input/output conditions can occur when a heat pipe is used to transfer heat from a hot to a cold fluid as in heat pipe heat recovery systems.



(a) Typical Heat Pipe Performance Test Set-Up



(b) Heat Transfer Between Two Fluids

Fig. 4-41. Typical uniform heat source/sink interface

In many applications, however, the heat input/output may be non-uniformly applied around the heat pipe (e.g., Fig. 4-42).

In either case, the heat transfer capability of the heat pipe is determined by the thermal conductance of the container, the evaporator and condensation heat transfer characteristics of the fluid/wick combination and the size, geometry and length of the evaporator and condenser sections. The thermal conductances associated with both uniform and non-uniform heat loads are defined in the next sections.

4.5.3.1 Uniform Heat Loads

The primary heat transfer mechanisms in heat pipes with uniform heat addition and removal are: heat conduction across the pipe wall and the liquid-saturated wick at the evaporator section; axial transport of heat from the evaporator to the condenser by the latent heat of vaporization and heat conduction across the liquid-saturated wick and the pipe wall at the condenser. Heat conduction in the wall and in the wick can be described by Fourier's Law, whereas the temperature difference in the vapor phase between the evaporator and the condenser sections can be described by the Clausius-Clapeyron relationship. The temperature difference between the vapor and the liquid at the liquid-vapor interface in both the evaporator and condenser is generally small and can be neglected (42). The overall heat pipe conductance can be expressed as follows (see Fig. 4-40):

$$(UA)_{H.P.} = \dot{Q} / (T_{o,e} - T_{o,c}) \quad (4-57)$$

where:

\dot{Q} = heat flow rate

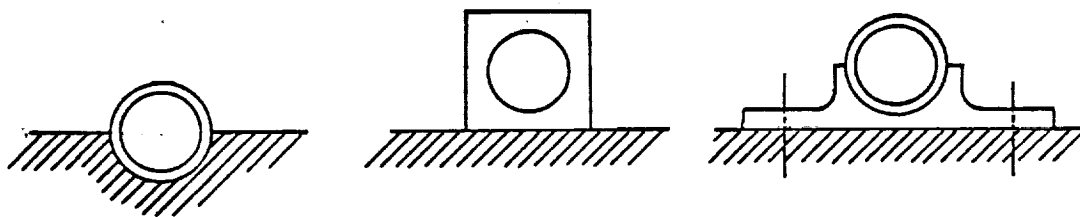
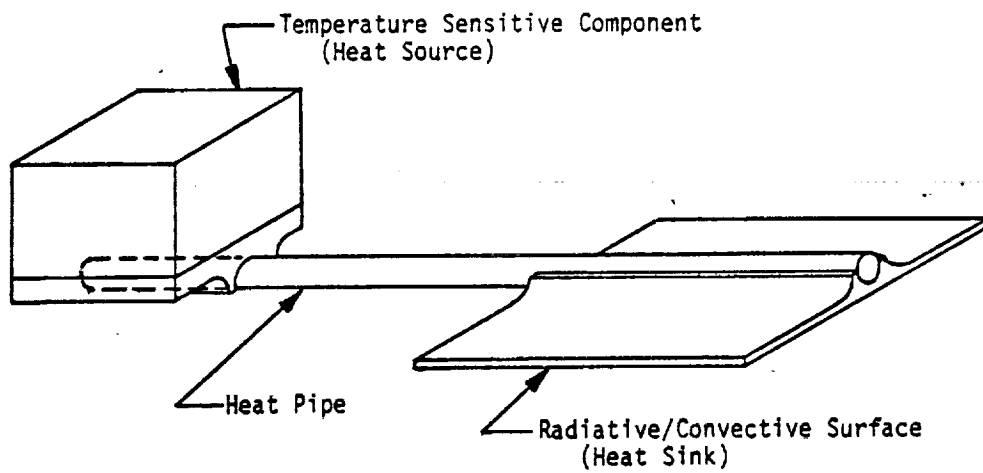
$T_{o,e}$ = external surface temperature of the envelope at the evaporator

$T_{o,c}$ = external surface temperature of the envelope at the condenser

Since all the conductive paths within the heat pipe are in series, the overall temperature drop across the heat pipe ($T_{o,e} - T_{o,c}$) is the sum of individual temperature drops within the heat pipe. If the temperature drop at the liquid/vapor interface is neglected,

$$T_{w,e} = T_{v,e}$$

$$T_{w,c} = T_{v,c}$$



a) Grooved Source/Sink Interface

b) Heat Pipe With Flat External Geometry

c) Heat Pipe With Mounting Saddle

Typical Source/Sink Interface Conditions

Fig. 4-42. Typical non-uniform heat source/sink interface

and the individual temperature drops can be expressed as follows:

$$T_{o,e} - T_{i,e} = \dot{Q} \frac{\ln (r_o/r_i)}{2\pi L_e K_t} \quad (4-58)$$

$$T_{i,e} - T_{v,e} = \dot{Q} \frac{\ln (r_i/r_v)}{2\pi L_e K_{w,e}} \quad (4-59)$$

$$T_{v,e} - T_{v,c} = \dot{Q} \frac{T_v (P_{v,e} - P_{v,c})}{\rho_v \lambda J Q} \quad (4-60)$$

$$T_{v,c} - T_{i,c} = \dot{Q} \frac{\ln (r_i/r_v)}{2\pi L_c K_{w,c}} \quad (4-61)$$

$$T_{i,c} - T_{o,c} = \dot{Q} \frac{\ln (r_o/r_i)}{2\pi L_c K_t} \quad (4-62)$$

The heat pipe conductance can then be expressed as follows:

$$(UA)_{H.P.} = \left[\frac{\ln (r_o/r_i)}{2\pi L_e K_t} + \frac{\ln (r_i/r_v)}{2\pi L_e K_{w,e}} + \frac{T_v (P_{v,e} - P_{v,c})}{\rho_v \lambda J Q} + \frac{\ln (r_i/r_v)}{2\pi L_c K_{w,c}} + \frac{\ln (r_o/r_i)}{2\pi L_c K_t} \right]^{-1} \quad (4-63)$$

The temperature drop in the vapor phase ($T_{v,e} - T_{v,c}$) can be determined by solving the hydrodynamic flow equation for the vapor phase (see Chapter 2). If the vapor flow is laminar and incompressible with dynamic effects, Chi (33) suggests a closed form solution as follows:

$$(P_{v,e} - P_{v,c}) = F_v Q \left(\frac{L_e}{6} + L_a + \frac{L_c}{6} \right) \quad (4-64)$$

where:

$$F_v = \frac{2 (f_v R_{ev}) u_v}{D_{h,v}^2 A_v \rho_v \lambda}$$

However, with the exception of gravity assisted heat pipes and high temperature heat pipes operating at the low end of their operating temperature range, (e.g., liquid metal heat pipes operating near their freezing point) the temperature drop in the vapor phase is negligible. That is, since the pressure differences that can be typically sustained by the capillary structure are small, the only way significant vapor temperature differences can be developed is at high absolute vapor temperatures (T_v) in combination with small vapor densities (ρ_v) which is the case for liquid metals operating at the low end of their operating temperature range.

For most heat pipes including liquid metal types, this term can be neglected and Eq. 4-63 reduces to:

$$(UA)_{H.P.} = \left[\frac{\ln(r_o/r_i)}{2\pi L_e K_t} + \frac{\ln(r_i/r_v)}{2\pi L_e K_{w,e}} + \frac{\ln(r_i/r_v)}{2\pi L_c K_{w,c}} + \frac{\ln(r_o/r_i)}{2\pi L_c K_t} \right]^{-1} \quad (4-65)$$

For thin walled tubes Eq. 4-65 can be expressed as:

$$(UA)_{H.P.} = \left[\frac{t}{2\pi L_e r_o K_t} + \frac{\ln(r_i/r_v)}{2\pi L_e K_{w,e}} + \frac{\ln(r_i/r_v)}{2\pi L_c K_{w,c}} + \frac{t}{2\pi L_c r_o K_t} \right]^{-1} \quad (4-66)$$

Finally, in most heat pipe designs with the exception of liquid metal heat pipes, the thermal conductivity of the container is much greater than the conductivity of liquid/wick combination. In such cases, the heat pipe conductance can be expressed as:

$$(UA)_{H.P.} = \left[\frac{\ln(r_i/r_v)}{2\pi L_e K_{w,e}} + \frac{\ln(r_i/r_v)}{2\pi L_c K_{w,c}} \right]^{-1} \quad (4-67)$$

The above equations were derived for a cylindrically shaped wick held against the internal diameter of a tubular container. Since there are a variety of wick designs with different heat transfer properties, it is convenient to reduce the conductance through the liquid/wick combination to an equivalent film coefficient and the overall heat pipe conductance (excluding the container wall and vapor temperature drop) can be written as follows:

$$(UA)_{H.P.} = \left[\frac{1}{h_e A_e} + \frac{1}{h_c A_c} \right]^{-1} \quad (4-68)$$

A_e and A_c are the liquid/vapor interface areas in the evaporator and condenser, respectively. For the above example, the terms in Eq. 4-68 can be defined as follows:

$$h_e = \frac{K_{w,e}}{r_v \ln(r_i/r_v)} \quad (4-69)$$

$$A_e = 2\pi r_v L_e \quad (4-70)$$

$$h_c = \frac{K_{w,c}}{r_b \ln(r_i/r_v)} \quad (4-71)$$

$$A_c = 2\pi r_v L_c \quad (4-72)$$

Note that in order to solve the above equations it is necessary to develop the equivalent thermal conductivity for the liquid/wick combination. Methods of estimating this equivalent thermal conductivity are discussed in Section 4.4.5. Whenever possible, measure data for equivalent film coefficients are recommended.

4.5.3.2 Non-Uniform Heat Loads

In many applications the heat is applied to or removed from only a portion of the heat pipe's circumference. Most aerospace applications fall into this category. Typically, heat from a source (such as an electronic component) is conducted to a heat pipe which in turn transports the heat to a heat rejection system such as a space radiator as illustrated in Fig. 4-42. A conductive plate (cold plate) is usually used to conduct the heat from the source to the heat pipe. Evaporator and condenser interfaces are usually achieved either by clamping or bonding the heat pipe as shown in Fig. 4-42.

A non-uniform heat input/output condition can be represented schematically as shown in Fig. 4-43. If the conductance of the source/sink plate is much larger than the conductance around the container wall, a uniform temperature distribution at the interface can be assumed and the conductance of the heat pipe can be determined by assuming radial conduction through the container wall at the interface and circumferential heat flow in the container wall around the remainder of the heat pipe periphery. If the radial

conductance of the container wall is large compared to the internal conductance of the heat pipe, then Eq. 4-67 can be applied in determining the conductance of the interface zone (Sector I) as follows:

$$(UA)_{H.P.,I} = \left[\frac{1}{h_e A_e} \frac{2\pi}{\theta_e} + \frac{1}{h_c A_c} \frac{2\pi}{\theta_c} \right]^{-1} \quad (4-73)$$

The conductance over the remainder of the heat pipe (Sector II) can be determined on the basis of the fin equation.

$$(UA)_{H.P.,II} = \left[\frac{1}{\eta_e h_e A_e} \frac{2\pi}{(2\pi - \theta_e)} + \frac{1}{\eta_c h_c A_c} \frac{2\pi}{(2\pi - \theta_c)} \right]^{-1} \quad (4-74)$$

Since the heat flows in Sector II from two directions and since heat flows from one side of the tube container into the heat pipe, the fin efficiency (η) can be expressed as follows (43):

$$\eta_e = \frac{\tanh(w_e \sqrt{h_e/K_T t})}{w_e \sqrt{h_e/K_T t}} \quad (4-75)$$

$$\eta_c = \frac{\tanh(w_c \sqrt{h_c/K_T t})}{w_c \sqrt{h_c/K_T t}} \quad (4-76)$$

Also, since heat paths in Sector I and Sector II are in parallel, the overall conductance of the heat pipe is the sum of the two.

$$(UA)_{H.P.} = \left[\frac{1}{h_e A_e} \frac{2\pi}{\theta_e} + \frac{1}{h_c A_c} \frac{2\pi}{\theta_c} \right]^{-1} + \left[\frac{1}{\eta_e h_e A_e} \frac{2\pi}{(2\pi - \theta_e)} + \frac{1}{\eta_c h_c A_c} \frac{2\pi}{(2\pi - \theta_c)} \right]^{-1} \quad (4-77)$$

In many applications the temperature drop in the interface plate is significant (such as weight optimized aerospace system) or in more complex geometries such as illustrated in Fig. 4-42, the above simplified model for non-uniform heat input is no longer adequate and more complex thermal models are required. A numerical analysis using a nodal network as shown in Fig. 4-44 and a thermal computer code will then be required. The heat load distribution corresponding to the thermal model defined by Fig. 4-44 is presented in Fig. 4-45.

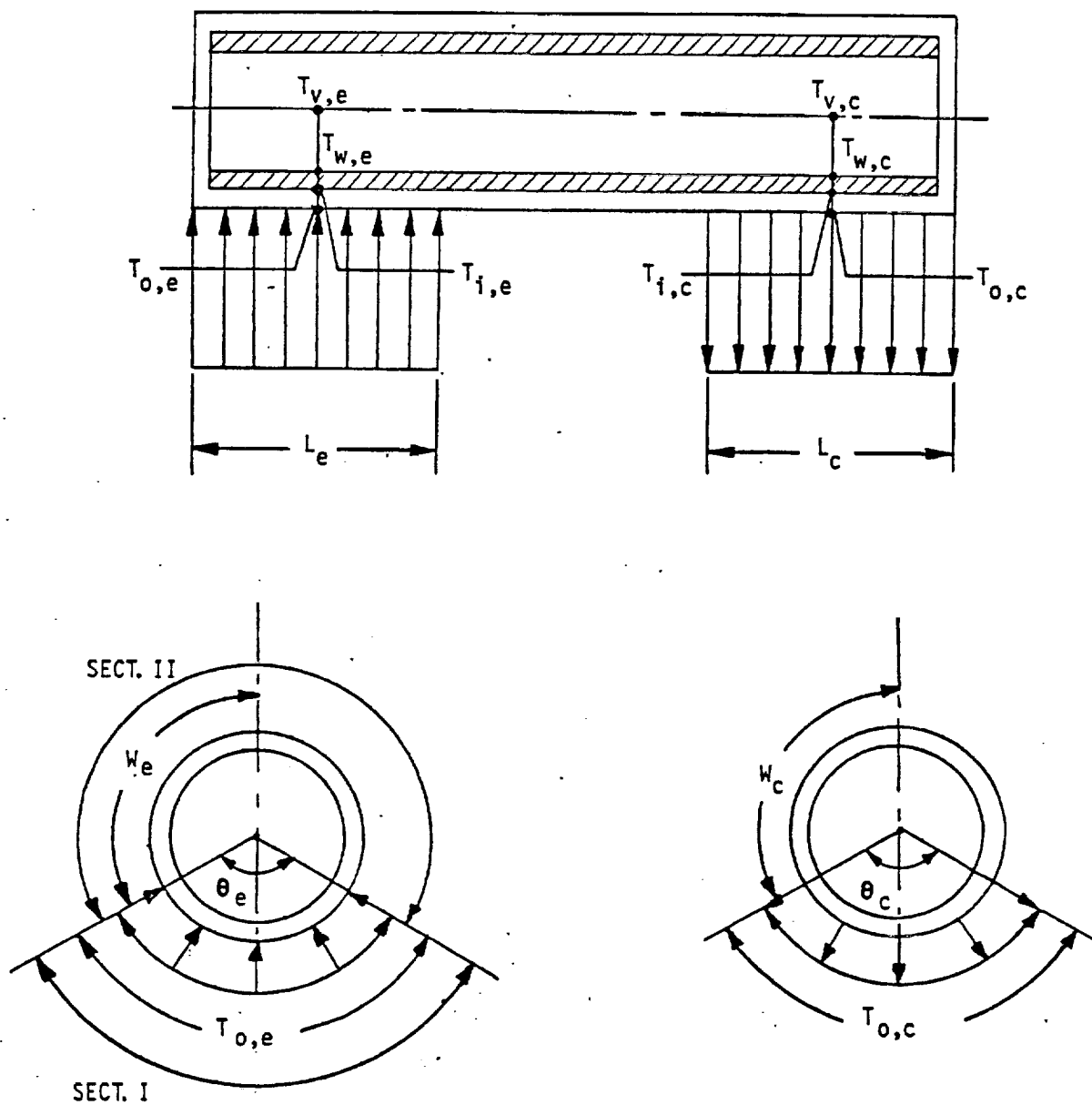


Fig. 4-43. Schematic of heat pipe with non-uniform heat source/sink interface

Heat throughput: 205.04 BTU/hr = 60 W
 Evaporator film coefficient: 1600 BTU/hr ft²
 Condenser film coefficient: 3120 BTU/hr ft²
 Aluminum Thermal Conductivity: 90 BTU/hr ft°F
 Copper Thermal Conductivity: 219 BTU/hr ft°F

Evaporator Length: 5 inches
 Condenser Length: 30 inches
 Heat Pipe Wall Thickness: 0.02 inches

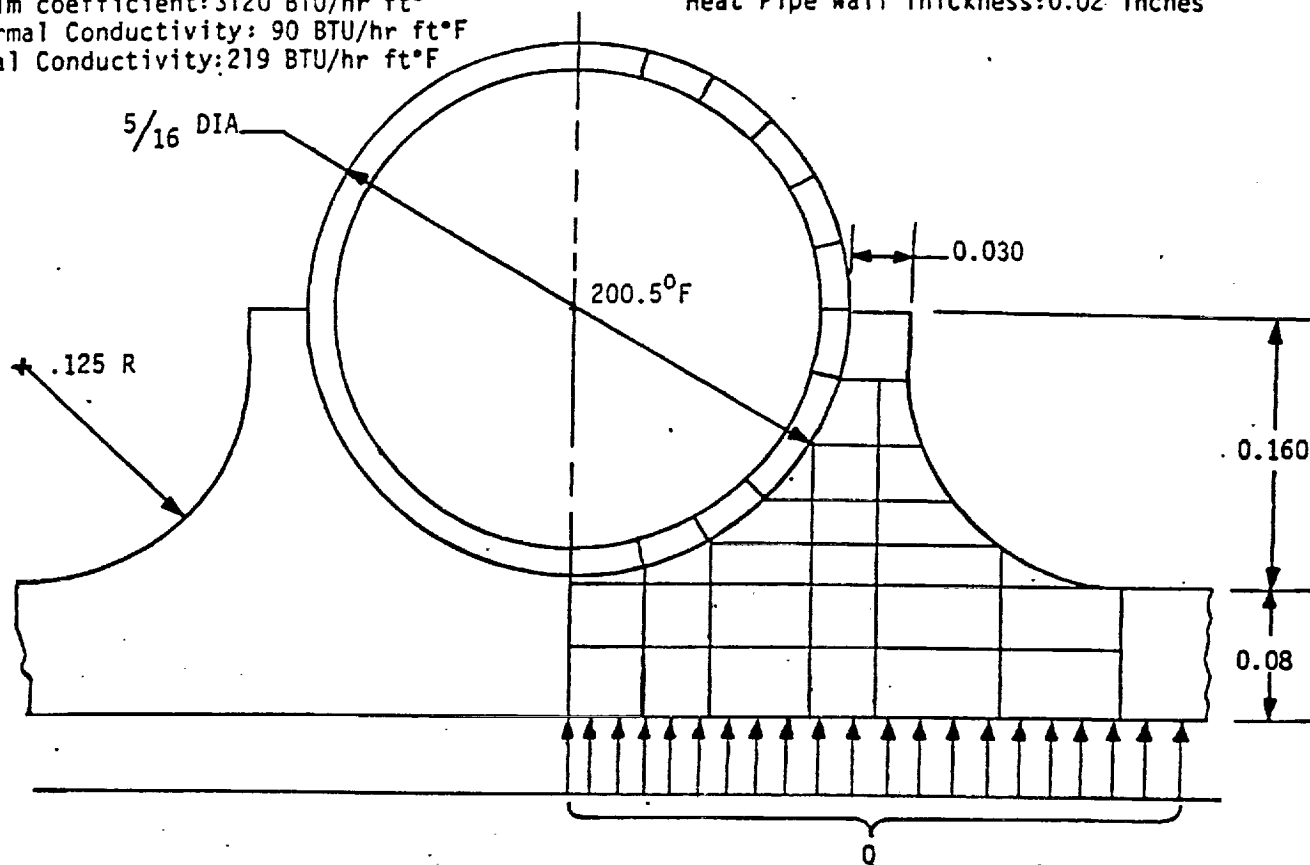


Fig. 4-44. Typical heat pipe interface nodal model

4.6 FIXED CONDUCTANCE HEAT PIPE DESIGN PROCEDURE

The design of a heat pipe is dependent on the various factors discussed in the preceding sections. From the design viewpoint, it is convenient to separate the types of heat pipes into two categories: fixed conductance (conventional) heat pipes and variable conductance heat pipes. The design procedure for the fixed conductance heat pipe is outlined in this section.

The variety and very often the interdependence of the different factors to be considered, as well as the qualitative, and in some cases the complexity of the mathematics, precludes the definition of a rigid design procedure. In general, however, the design of any fixed conductance heat pipe will follow the procedure outlined in Fig. 4-1. The major steps in this procedure and the applicable sections in this chapter which discuss each of these steps are as follows:

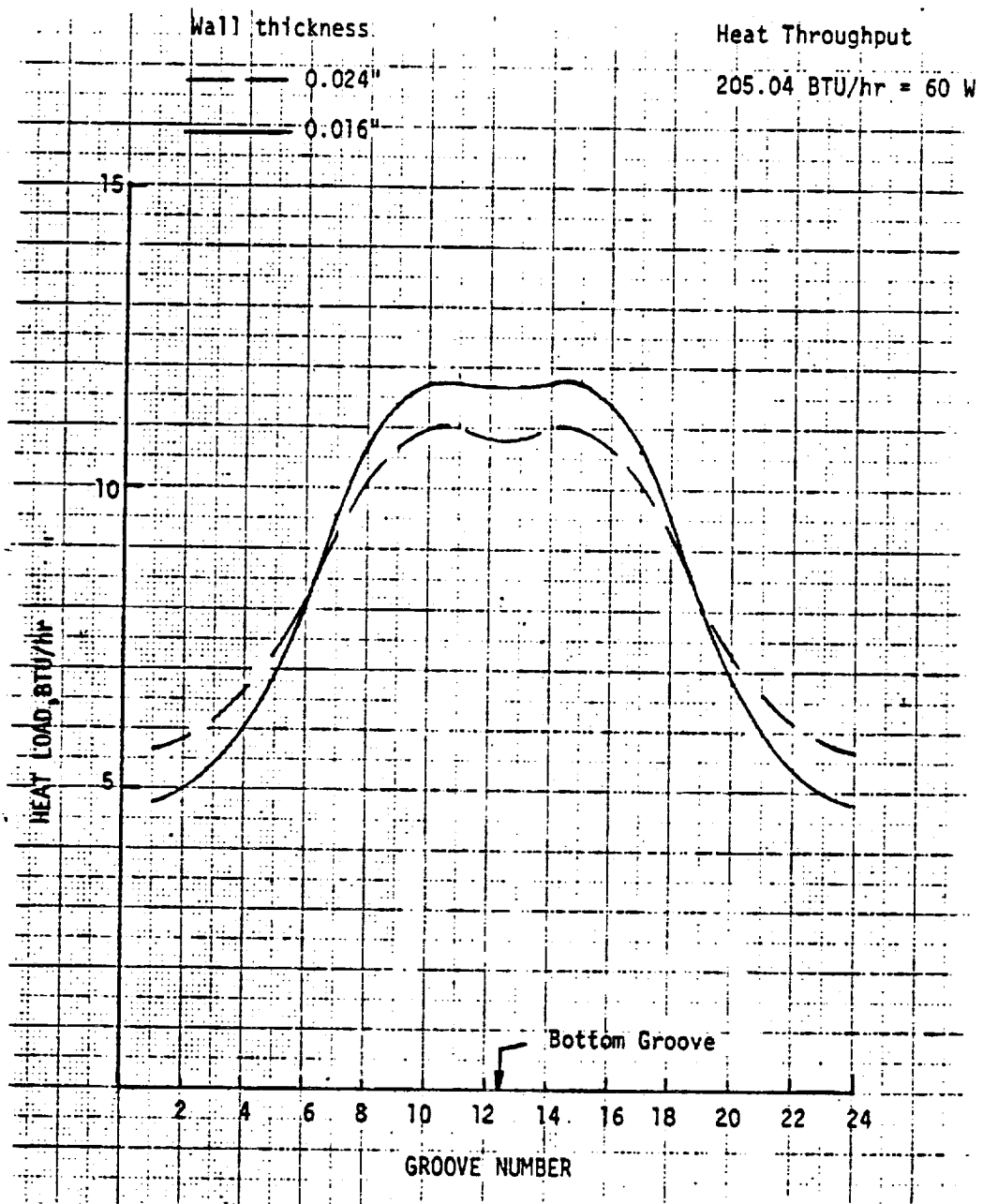


Fig. 4-45. Heat load distribution in an axially grooved tube

STEP	DESCRIPTION	REF. SECTION
1	Establish the Design Parameters	4.2
2	Select the Working Fluid	4.3
3	Select the Wick Design	4.4
4	Select the Container Design	4.5
5	Determine the Hydrodynamic Performance Limits	Chapter 2
6	Verify Container Structural Integrity	4.5
7	Establish the Heat Transfer Characteristics	4.5
8	Select the Optimum Design	

The application of this procedure to the preliminary design of a fixed conductance heat pipe is illustrated in Chapter 5.

REFERENCES

1. Van Wylen, Gordon J., "Thermodynamics," John Wiley & Sons, Inc., New York, 1959.
2. Sears, F. W., Zemansky, M. W., "University Physics," Addison-Wesley Publishing Company, Inc., Massachusetts, 1957.
3. Kays, W. M., "Convective Heat and Mass Transfer," McGraw-Hill, Co., Inc., New York, 1966.
4. Kroliczek, E. J., and Jen, H., "Axially Grooved Heat Pipe Study," B & K Engineering, Inc., 1977.
5. Brennan, P. J., et.al., "Axially Grooved Heat Pipes - 1976," AIAA 12th Thermophysics Conference, Albuquerque, New Mexico, Paper No. 77-747, June 27-29, 1977.
6. Jen, H., and Kroliczek, E. J., "User's Manual for Groove Analysis Program (GAP)," BK012-1007, B & K Engineering, Inc., June 1976.
7. Marcus, B. D., "Theory and Design of Variable Conductance Heat Pipes," No. 1 TRQ 1311-RO-00, Contract NAS 2-5503, April 1971.
8. Cosgrove, J. H., Ferrell, J. K., and Carnesle, A. J., Nuclear Energy 21, pp. 547-558 (1967).
9. Ferrell, J. K., and Alleavitch, J., "Vaporization Heat Transfer in Capillary Wick Structure," Chemical Eng. Prog. Symp. Series, Vol. 66, Heat Transfer Minneapolis, Minn., 1970.
10. Luikov, A., "Heat and Mass Transfer in Capillary-Porous Bodies," Pergamon Press, New York, 1966.
11. Scheidegger, A. E., "The Physics of Flow Through Porous Media," The MacMillan Co., New York, 1960.

References - Continued

12. Bressler, R. G., and Wyatt, P. W., "Surface Wetting Through Capillary Grooves," Trans, ASME, J. Heat Transf., pp 126-132 (1970).
13. Kunz, H. R., Langston, L. S., Holton, B. H., Wyde, S. S. and Nashick, G. H., "Vapor-Chamber Fin Studies," NAS CR-812, June 1967.
14. Phillips, E. C., "Low Temperature Heat Pipe Research Program," NASA CR-66792, June 1969.
15. Katzoff, S., "Heat Pipes and Vapor Chambers for Thermal Control of Spacecraft," Thermophysics of Spacecraft and Aeronautics, V. 20, Academic Press, New York, 1968, pp. 761-818.
16. Freggens, R. A., "Experimental Determination of Wick Properties for Heat Pipe Applications," Proc. of 4th Intersociety Energy Conversion Conference, Washington, D. C., September 1968, pp. 888-897.
17. Farran, R. A., and Starner, K. E., "Determining Wick Properties of Compressible Materials for Heat Pipe Applications," Annual Aviation and Space Conference, Beverly Hills, California, June 1968, pp. 659-669.
18. Gould Inc., Gould Laboratories, Brochure GLMT-101.
19. Marjon, P. L., 12th Monthly Progress Report, DOT Contract No. FH-11-7413, Dynatherm Corporation, November 1971.
20. "Metal Filter Cloth, Technical and Performance Data," Kressilk Products, Inc., Monterey Park, California, June 23, 1969.
21. "Manual - Feltmetal Fiber Metal," Huyck Metals Company (now Brunswick Corporation, Technical Division).
22. Eninger, J. E., "Graded Porosity Heat Pipe Wicks," NAS2-8310, TRW Systems Group, Redondo Beach, California, August 1974.
23. Kosson, R., Hambach, R., Edelstein, F., and Loose, J., "Development of a High Capacity Variable Conductance Heat Pipe," AIAA 8th Thermophysics Conference, Paper No. 73-728, Palm Springs, California, July 16-18, 1973.
24. Eninger, J., "Menisci Coalescence as a Mechanism for Venting Non-condensable Gas from Heat Pipe Arteries," Final Report, 99900-7742-RU-00, TRW Systems Group, 1974.
25. Bienert, W. B., "Development of a Jet Pump-Assisted Arterial Heat Pipe, Final Report, NASA CR-152, 015, Dynatherm Corp., Cockeysville, MD., May 6, 1977.
26. Harwell, W., and Ball, T., "Thermal Vacuum Tests on a Thermal Controlled Canister Breadboard," NAS5-22980, Grumman Aerospace Corp., Bethpage, New York, 1976.
27. Brennan, P. J., and Groll, M., "Application of Axial Grooves to Cryogenic Variable Conductance Heat Pipe Technology," 2nd International Heat Pipe Conference, April 1976.
28. Saaski, E. N., "Investigation of Bubbles in Arterial Heat Pipe," NAS CR-114,531, December 1972.
29. Eninger, J. E., "Sounding-Rocket Heat Pipe Experiment," TRW Report No. 26263-6008-RU-00, December 30, 1974.
30. Mock, P. R., Marcus, B. D., and Edelman, E. A., "Communications Technology Satellite: A Variable-Conductance Heat Pipe Application," AIAA Paper No. 74-749, July 1974.
31. Eninger, J. E., "Priming Studies with a Glass Heat Pipe," Contract NAS 2-8310, Materials Technology Department, TRW Systems Group, January 8, 1975.

References - Continued

32. Kamotani, Y., "Thermal Analysis Program for Axially Grooved Heat Pipes, Its Description and Capabilities," to be published.
33. Chi, S. W., "Heat Pipe Theory and Practice," The George Washington University, Hemisphere Publishing Company, Washington, 1976.
34. "Heat Pipe Manufacturing Study," Final Report, NAS 5-23156, Grumman Aerospace Corp., Bethpage, New York, August 1974.
35. ASME Boiler and Pressure Vessel Code, 1965. Section VIII Unfired Pressure Vessels, Section II Material Specifications.
36. MIL-HDBK-5B, Metallic Materials and Elements for Aerospace Vehicle Structures, Department of Defense, September 1971 (MD).
37. Lyman, T., "Metals Handbook," 8th Edition, American Society for Metals, Metals Park, Ohio, 1961.
38. Marks, L. S., "Mechanical Engineers Handbook," McGraw-Hill, New York, 1967.
39. U. S. Civil Aeronautics Act, Title XIII.
40. Code of Federal Regulations. Title 49, Parts 100 to end.
41. Seely, F. G., and Smith, J. O., J. Wiley & Sons: Advanced Strength of Materials, Second Ed., 1963 (MD).
42. Cotter, T. P., Theory of Heat Pipe, Los Alamos Scientific Laboratory, Rept. No. LA-3246-MS, February 1965.
43. Kreith, F., "Principles of Heat Transfer," Second Edition, International Textbook Company, Scranton, Pennsylvania, 1966.

SAMPLE DESIGN PROBLEMS

This chapter presents an example of the analyses and procedures which are employed in determining the preliminary design of a fixed conductance heat pipe. The final design will of course be dependent upon test results obtained with breadboard or prototype hardware.

5.1 SAMPLE PROBLEM A -- FIXED CONDUCTANCE HEAT PIPE

5.1.1 Step #1 - Problem Definition and Design Criteria

A heat pipe is required which will be capable of transferring a minimum of 15-W at an operating temperature between 0 and 40°C. The overall length of the heat pipe is 100 cm with one evaporator and one condenser section each 8 cm long, located at each end of the heat pipe. To minimize cost and delivery time, a straight tubular geometry is desired. The heat pipe will be attached by epoxy bonding into a semi-circular groove to be provided in the heat source and the heat sink. The maximum allowable temperature drop between the outside wall of the evaporator and the outside wall of the condenser is 6°C. Heat is to be applied and removed uniformly along the entire length of the evaporator and condenser sections. Bonding must be performed after the heat pipe is charged at a temperature of 170°C (337°F). Because of weight and volume limitations, a maximum heat pipe diameter of 1.27 cm is desired. Finally, for ground demonstration purposes it is desired to demonstrate the performance at a test elevation of 1 cm and any composite wick design must be able to demonstrate self-priming at this elevation. The desired heat pipe design is illustrated in Fig. 5-1.

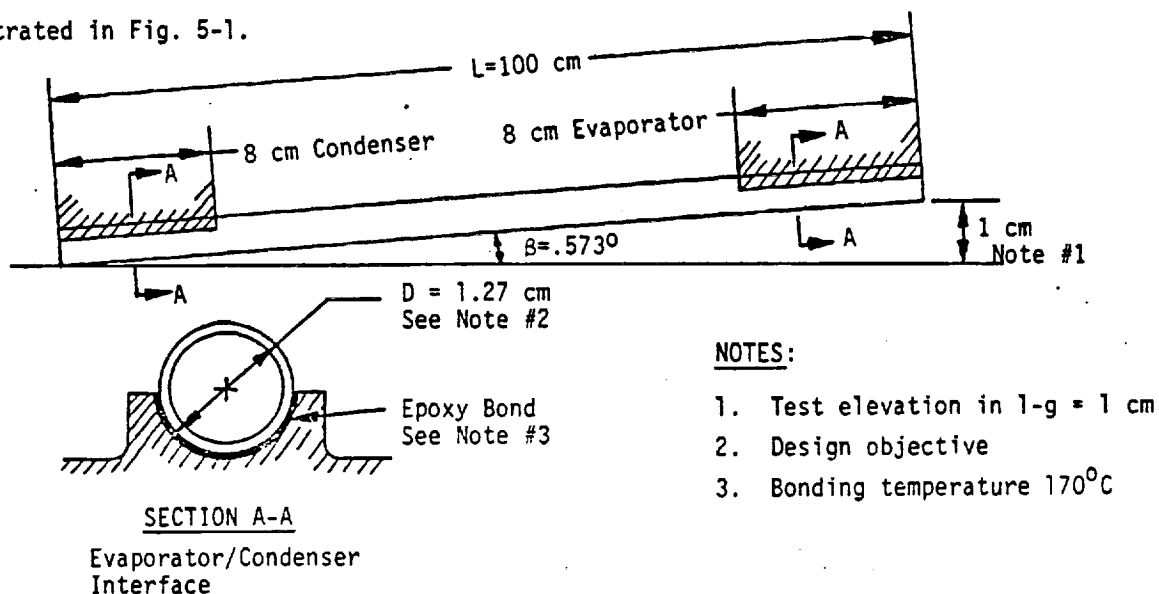


Fig. 5-1. Sample problem A - fixed conductance heat pipe configuration

TABLE 5-1. PROPERTIES OF SELECTED FLUIDS
SAMPLE PROBLEM A

FLUID	N_L (w/m^2)		H (m^2)		ν_v/ν_L		P_v @170°C N/m^2	K ($w/m-k$)
	0°C	40°C	0°C	40°C	0°C	40°C		
Ammonia	1.25×10^{11}	9.0×10^{10}	4.2×10^{-6}	2.9×10^{-6}	11.0	5.1	*	0.449 - 0.54
Methanol	2.955×10^{10}	4.246×10^{10}	3.070×10^{-6}	2.762×10^{-6}	169.7	41.3	2.161×10^6	0.198 - 0.21
Acetone	2.761×10^{10}	3.0×10^{10}	3.142×10^{-6}	2.736×10^{-6}	78.0	16.3	1.649×10^6	0.163 - 0.182
Freon 21	1.845×10^{10}	1.766×10^{10}	1.546×10^{-6}	1.227×10^{-6}	10.96	4.841	4.588×10^6	0.109 - 0.095

*Above the critical temperature

TABLE 5-2. MATERIAL COMPATIBILITY

SAMPLE PROBLEM A

CONTAINMENT MATERIALS

FLUID OPTION	ALUMINUM	STAINLESS STEEL	COPPER
Ammonia	Compatible	Compatible	Incompatible
Acetone	Compatible	Compatible	Compatible
Methanol	Incompatible	Compatible	Compatible
Freon 21	Compatible	Compatible	Compatible

5.1.2 Step #2 - Working Fluid Selection

As discussed in Section 4.3, the choice of working fluid depends on a number of considerations including working pressure, fluid properties as they affect the capillary pumping limit and other performance limits, thermal conductivity, compatibility with the wick and container material, and stability at elevated temperatures. Table 5-1 summarizes several candidate working fluids and their properties. Table 5-2 summarizes the compatibility of the candidate working fluids with several commonly available container materials.

A review of Tables 5-1 and 5-2 shows that ammonia offers the best overall combination of thermophysical and derived properties with the exception of its working pressure. The bonding temperature of 170°C is above its critical temperature and a significant weight penalty may be required to contain the pressure during bonding. On the other hand, its superior fluid properties (high liquid transport factor, high wicking height and low kinematic viscosity ratio) will require a smaller heat pipe diameter which will compensate for the pressure. Furthermore, ammonia is compatible with aluminum which is a weight effective material. Finally, ammonia has a high thermal conductivity which can be an important factor with respect to the 6°C maximum allowable temperature drop.

The next best choices are acetone and methanol. Of the two, acetone would be selected on the basis of low kinematic viscosity ratio and its compatibility with aluminum. If methanol were selected, copper would have to be considered as the container material since heat input is over only half of the heat pipe circumference. If stainless steel were used the second half of the heat pipe circumference would become ineffective because of its low thermal conductivity.

In the remainder of this sample problem, ammonia will be used as the reference working fluid since it does illustrate pressure containment above the critical point which is a typical problem in the design of many heat pipes.

5.1.3 Step #3 - Wick Design Selection

Three basic wick designs could be considered to meet the performance requirements: homogeneous wire mesh screen; composite wire mesh screen; and axial grooves. The homogeneous wire mesh wick design offers the ability of providing fine capillary sizes to achieve high static height to meet 1-g test conditions but with a correspondingly low permeability factor. The composite wire mesh wick design avoids the compromise between fine and coarse capillaries but presents a priming reliability problem. To minimize the

problem with bubble entrapment, alternate layers of coarse and fine wire mesh can be used to disperse any inclusions, and the composite ratio can be held to a minimum consistent with performance objectives. Finally, the axially grooved design offers large open flow channels which are sensitive to gravity.

Fig. 5-2 illustrates the three types of wick designs. Both the homogeneous and composite wicks are centrally located, spirally wound geometries. This arrangement which removes the main wick from the wall provides optimum heat transfer at the evaporator and condenser sections to achieve the 6°C requirement. Bridges that are used to interface the main wick with the secondary wick would be either circumferential grooves or a single layer of wire mesh screen pressed against the wall (e.g., Fig. 5-2). For the axially grooved wick design, a rectangular groove is selected since it most closely approximates what can be achieved by extruding or swaging. An extrusion would be used if the selected container material is aluminum. For copper or stainless steel the swaging process would be required to fabricate the axially grooved tubing.

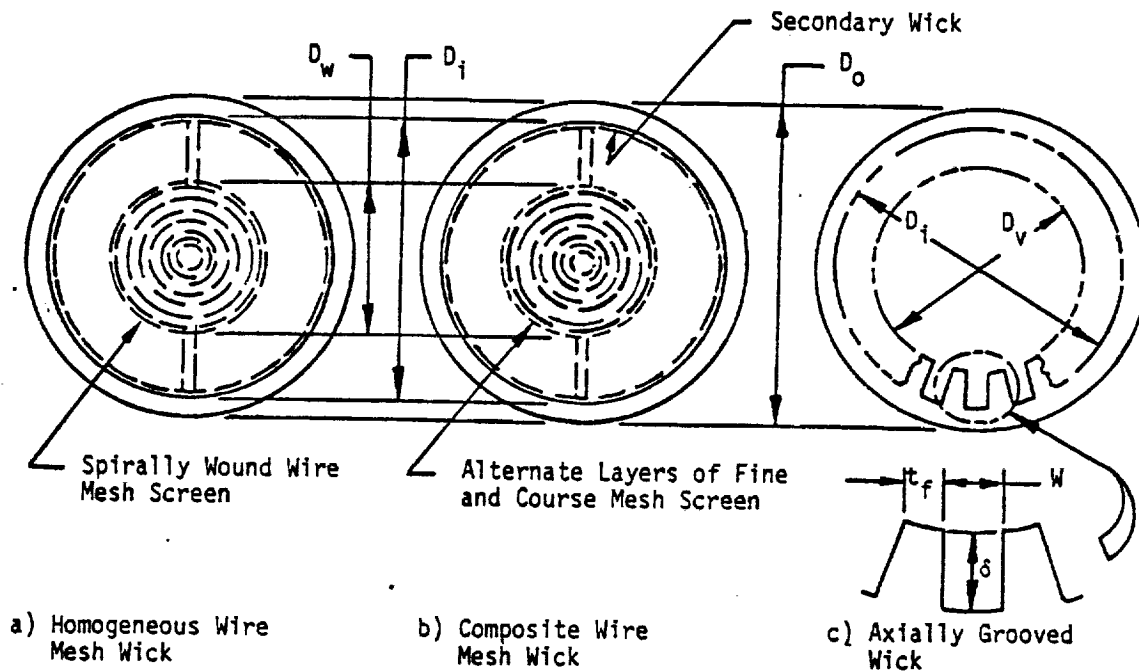


Fig. 5-2. Sample problem A - wick design options

Near perfect wetting can be assumed for ammonia (i.e., $\cos \theta = 1$), and the required capillary sizes should be determined on the basis of demonstrating the transport requirement at a 1 cm test elevation in 1-g. The resulting wick properties, as determined below, are summarized in Table 5-3. A preliminary wick evaluation of the selected design can be

TABLE 5-3. PROPERTIES OF THE WICK DESIGN OPTION*

SAMPLE PROBLEM A

I HOMOGENEOUS WIRE MESH WICK

Effective Pumping Radius (r_p)	$1.28 \times 10^{-4} \text{ m}$
Equivalent Square Mesh Size	<u>100</u>
Composite Factor (S)	1.0
Permeability	$2.0 \times 10^{-10} \text{ m}^2$
K/r_p Ratio	$1.56 \times 10^{-6} \text{ m}$

II COMPOSITE WIRE MESH WICK

Effective Pumping Radius of the Coarse Mesh ($r_{p \text{ max}}$)	$2.56 \times 10^{-4} \text{ m}$
Equivalent Square Mesh Size (coarse)	<u>50</u>
Effective Pumping Radius of the Fine Mesh Screen (r_p)	$6.4 \times 10^{-5} \text{ m}$
Equivalent Square Mesh Size (fine)	<u>200</u>
Composite Factor (S)	4
Effective Permeability (K_{eff})	$6.4 \times 10^{-10} \text{ m}^2$
K/r_p Ratio (primed)	$1.0 \times 10^{-5} \text{ m}$

III AXIAL GROOVE WICK (RECTANGULAR)

Effective Pumping Radius (r_p)	$3.87 \times 10^{-4} \text{ m}$
Groove Width (w)	$3.87 \times 10^{-4} \text{ m}$
Groove Depth (δ)	$7.74 \times 10^{-4} \text{ m}$
Groove Flow Factor - Sharp Corner (N_g)	$1.73 \times 10^{-11} \text{ m}^3$
Composite Factor (S)	0.8
Permeability (K).	$1.12 \times 10^{-8} \text{ m}^2$
K/r_p Ratio	2.89×10^{-5}

* The values of r_p and K are calculated for each wick design in Steps (a) through (c) which follow.

obtained from this table. On the basis of the k/r_p ratio, a 4:1 wire mesh composite wick will provide 6.4 times greater 0-g performance than the homogeneous wick. The choice between the two options could be resolved at this point if the relative importance of size and weight versus reliability were known. The axially grooved design on the other hand can provide 18.5 times greater 0-g performance than the homogeneous wick and 2.89 times greater 0-g performance than the composite wick. However, the number of grooves that can be located in a given diameter is limited by fabrication constraints (i.e., the fin thickness between groove). In addition, cost factors must also be considered, and therefore the complete heat pipe design is required to make a final choice. Steps (a) through (c) which follow illustrate the calculation of the values of the wick properties presented in Table 5-3.

(a) Homogeneous Wick Capillary Sizing

The optimum mesh size for the homogeneous wick can be determined from Eq. 4-20 using the minimum wicking height associated over the operating temperature range (i.e., at 40°C in this case):

$$(r_p)_{\text{opt}} = \frac{H}{h_c} = \frac{2.9 \times 10^{-6} \text{ m}^2}{2.27 \times 10^{-2} \text{ m}} = 1.28 \times 10^{-4} \text{ m}$$

the static head (h_c) is the sum of the test elevation (h) and the internal heat pipe static head ($D_f \cos \beta$).

$$h_c = h + D_f \cos \beta = 1 \text{ cm} + 1.27 \text{ cm} \cos (.573^\circ) = 2.27 \text{ cm}$$

An internal diameter of 1.27 cm is selected on the basis of the stated problem objective for the heat pipe size. If the required heat pipe size is determined to be significantly larger or smaller, then a design iteration(s) will be required to refine the selection of the homogeneous wick capillary size. Also, as illustrated in Fig. 5-2, the main wick does not extend the full height of the internal diameter. For optimum design, an iteration with respect to this effect would also be required once the relative size of the heat pipe design is established. For square mesh screens, the spacing between wires is approximately equal to the wire diameter ($w \approx d$) and $d = r_p$ (see Section 4.4.1). In

this case the permeability of the screen (K) can be determined from Eq. 4-14:

$$K = .0122 d^2 = .0122 (1.28 \times 10^{-4} \text{ m})^2 = 2.0 \times 10^{-10} \text{ m}^2$$

(b) Composite Wick Capillary Sizing

For the composite wick design, the coarse mesh is only restricted by the self priming requirement. Since self priming at the test elevation of 1 cm is required, the maximum capillary size can be determined from:

$$(r_p)_{\max} = \frac{2H}{h_c} = \frac{2 (2.9 \times 10^{-6} \text{ m}^2)}{2.27 \times 10^{-2} \text{ m}} = 2.56 \times 10^{-4} \text{ m}$$

If square mesh screen is employed as discussed above, the permeability of the coarse screen is:

$$K = .0122 d^2 = .0122 (2.56 \times 10^{-4} \text{ m})^2 = 8.0 \times 10^{-10} \text{ m}^2$$

No restrictions are imposed on the fine mesh screen with the exception that experience has shown that low composite factor wicks prime more reliably and that the fine mesh screen does occupy a finite amount of space which reduces the effective area of the wick. For illustration purposes a composite factor of 4 is selected. For the fine mesh screen then:

$$r_p = 6.4 \times 10^{-5} \text{ m} \text{ and } K = 5.0 \times 10^{-13} \text{ m}^2$$

Since alternate layers of coarse and fine mesh screen are to be used, the fraction of the wick area occupies by the fine mesh screen can be expressed as follows:

$$\begin{aligned} \frac{\text{Area of the Fine Mesh}}{\text{Total Wick Area}} &= \frac{\text{Fine Mesh Wire Diameter}}{\text{Coarse Mesh Wire Diameter} + \text{Fine Mesh Wire Diameter}} \\ &= \frac{6.4 \times 10^{-5} \text{ m}}{2.56 \times 10^{-4} \text{ m} + 6.4 \times 10^{-5} \text{ m}} \\ &= .20 \end{aligned}$$

Based on parallel flow circuits, the effective permeability of the composite wick can be determined as follows:

$$K_{eff} = .2 (5 \times 10^{-13} \text{ m}^2) + .8 (8 \times 10^{-10} \text{ m}^2) = 6.4 \times 10^{-10} \text{ m}^2$$

Note that the contribution of the fine mesh screen is insignificant compared to the coarse mesh screen.

(c) Axial Groove Capillary Sizing

For an axial groove operating in 1-g, the optimum groove size can be determined from Eq. 4-21:

$$w = (r_p)_{opt} = \frac{4H}{3h_c} = \frac{(4) (2.9 \times 10^{-6} \text{ m}^2)}{(3) 1 \times 10^{-2} \text{ m}} = 3.87 \times 10^{-4} \text{ m}$$

Since axial grooves are non-communicating, their performance in 1-g is independent of heat pipe diameter. In this example, the elevation (h_c) is the test elevation (1 cm).

Typically the groove depth is limited to twice the groove width for the extrusion and the swaging process (i.e., $\delta = 2w$). For grooves with sharp corners at the groove opening, the groove permeability can be determined from Eqs. 4-10 and 4-12.

$$N_g = 0.87 \left(\frac{A_g'}{w^2} \right)^{3.1} \left(\frac{w}{WP} \right)^2 w^3$$

$$N_g = .87 \left\{ \frac{3 \times 10^{-7} \text{ m}^2}{(3.87 \times 10^{-4} \text{ m})^2} \right\}^{3.1} \left\{ \frac{3.87 \times 10^{-4} \text{ m}}{1.94 \times 10^{-3} \text{ m}} \right\}^2 \times$$

$$(3.87 \times 10^{-4} \text{ m})^3 = 1.73 \times 10^{-11} \text{ m}^3$$

where

$$A_g' = 2 w^2 = 2 (3.87 \times 10^{-4} \text{ m})^2 = 3 \times 10^{-7} \text{ m}^2$$

$$WP = w + 2\delta = 1.94 \times 10^{-3} \text{ m}$$

$$\delta = 2w = 7.74 \times 10^{-4} \text{ m}$$

$$K = \frac{N_g r_p}{2 A_g'} = \frac{(1.73 \times 10^{-11} \text{ m}^3) (3.87 \times 10^{-4} \text{ m})}{(2) (3 \times 10^{-7} \text{ m}^2)}$$

$$= 1.12 \times 10^{-8} \text{ m}^2$$

In the above analysis, both the permeability (K) and the groove flow factor (N_g) are determined. In most design analyses, it is convenient to only calculate the groove flow factor since it can be applied directly into the capillary pumping limit equation.

5.1.4 Step #4 - Container Design Selection

The container shape, maximum size and geometry have already been specified as part of the problem statement. With respect to shape, the tubular design is the most commonly used configuration because it is the most efficient configuration from a pressure containment point of view. Round tubes and pipes of many materials are readily available, and most manufacturing processes, such as groove forming, can most easily be applied to this shape. Candidate container materials with demonstrated compatibility with the selected working fluid have also been identified in Step #2. Other properties such as strength, weight to strength ratio, density and thermal conductivities of the candidate container materials are summarized in Table 5-4. The strength data is for the 170°C bonding temperature since this condition will apply.

TABLE 5-4. PROPERTIES OF CANDIDATE CONTAINER MATERIALS SAMPLE PROBLEM A				
Material	Ultimate Tensile Strength, F_{tu} @170°C (Ref. Fig. 4-30) (ksi)	Weight Parameter ρ/F_{tu} @170°C (Ref. Fig. 4-31) (sec ² /ft ²)	Density ρ @20°C (Ref. Fig. 4-34) (lbm/ft ³)	Thermal Conductivity @20°C (Ref. Fig. 4-33) (Btu/ft-hr-F)
Aluminum	20	2×10^{-6}	170	122
Copper	18	5×10^{-5}	563	225
Stainless Steel	74	1.5×10^{-6}	487	9

As mentioned in Step #2, thermal conductivity is an important criteria since heat is being applied and removed from only half the heat pipe circumference. On this basis, copper is the best choice and stainless steel the worst. However, weight and material strength are important parameters in view of the high pressure containment required to bond at 170°C and the stated problem objective to minimize weight. On a weight to

strength basis (Table 5-4, Column 2) stainless steel is the lowest with aluminum a close second and copper the worst. Aluminum, therefore, appears to be the best compromise if a compatible fluid can be used.

With respect to end closures and the fill tube, the designer is directed to Section 4.5.2 for detailed designs. Once the heat pipe diameter is established (Step #5), the designer can determine the end closure thickness required.

5.1.5 Step #5 - Evaluate Hydrodynamic Performance Limits

This problem example is to establish a heat pipe size consistent with the stated objective of a minimum capacity of 15 watts at a test elevation of 1 cm. The heat pipe size has not been specified but the objective is to stay within a 1.27 cm diameter and as low a weight as possible. Since a 15 watt minimum is specified, a design margin should be introduced. For the purpose of this example the objective will be to maintain a 1.2 to 1.3 design margin. There is no established criteria for the design margin, it must be based on experience primarily with the wick's performance and on the criticality of the application. The ability to achieve the required performance with the margin applied must also be recognized. In other words, overdesigning can lead to an impossible requirement. To establish the design requirements of the three types of heat pipes, the capillary pumping limit is used as discussed below. Results are summarized in Table 5-5.

(a) Capillary Pumping Limit

Since the evaporator and the condenser are at opposite ends of the heat pipe with the evaporator up and since it is advisable to design a heat pipe with the vapor in the laminar flow regime, the closed form solutions for the capillary pumping limit, as discussed in Chapter 2, can be used. First, transport requirements can be established on the basis of a 1.3 design factor and Eqs. 2-72 and 2-73 as follows:

$$L_{\text{eff}} = \frac{1}{2} L_e + L_a + \frac{1}{2} L_c = \frac{1}{2} (8 \text{ cm}) + 84 \text{ cm} + \frac{1}{2} (8 \text{ cm}) = 92 \text{ cm}$$

$$(\dot{Q}L)_{\text{max}} = 1.3 \times 15 \text{ watts} \times 92 \text{ cm} = 1794 \text{ w-cm} = 17.94 \text{ w-m}$$

For the homogeneous wick, this requirement is equal to QL_{eff} in Eq. 2-63:

$$(\dot{Q}L)_{max} = 17.94 \text{ w-m} = \frac{2K A_w (1 + \eta) \cos \theta_c F_l}{r_p} N_l$$

For perfect wetting, $\cos \theta_c = 1$ and from Eq. 2-64:

$$\begin{aligned} 1 + \eta &= 1 - \left[\frac{r_p L \sin \beta}{2H \cos \theta} + \frac{r_p D_i \cos \beta}{2H \cos \theta} \right] \\ &= 1 - \frac{r_p}{2H \cos \theta} (L \sin \beta + D_i \cos \beta) \\ &= 1 - \frac{1.28 \times 10^{-4} \text{ m}}{(2) (2.9 \times 10^{-6} \text{ m}^2) (1)} (1 \text{ m} \sin .573^\circ + \\ &\quad 1.27 \times 10^{-2} \text{ m} \cos .573^\circ) \end{aligned}$$

$$1 + \eta = .5$$

For the selected homogeneous wick properties (Table 5-3) and minimum liquid transport factor (40°C for ammonia), the combination of wick area (A_w) and friction factor (F_l) required to meet the desired performance is:

$$\begin{aligned} A_w F_l &= \frac{(\dot{Q}L)_{max} r_p}{2K (1 + \eta) \cos \theta_c N_l} \\ &= \frac{(17.94 \text{ w-m}) (1.28 \times 10^{-4} \text{ m})}{(2) (2.0 \times 10^{-10} \text{ m}^2) (.5) (1) \left(9 \times 10^{10} \frac{\text{W}}{\text{m}^2} \right)} \\ &= 1.28 \times 10^{-4} \text{ m}^2 \end{aligned}$$

For the Selected Wick Geometry

$$A_w = \frac{\pi}{4} D_w^2$$

$$A_v = \frac{\pi}{4} (D_i^2 - D_w^2)$$

$$D_{H,v} = \frac{4 \times \text{Area}}{\text{Wetted Perimeter}} = \frac{4 \times \frac{\pi}{4} (D_i^2 - D_w^2)}{\pi (D_i + D_w)} = D_i - D_w$$

where the bridge wick is assumed to have a negligible effect on vapor flow losses. The vapor flow factor (F_2) can be determined from Eq. 2-67 using the capillary properties from Table 5-3 and the wick and vapor area properties as defined above. If the maximum value of the kinematic viscosity ratio is used, a conservative estimate will result.

$$\begin{aligned} F_2 &= \left[1 + \frac{\nu_v}{\nu_l} \frac{32K}{D_{H,v}^2} \frac{A_w}{A_v} \right]^{-1} \\ &= \left[1 + (11) \frac{(32) (2.0 \times 10^{-10} \text{ m}^2)}{(D_i - D_w)^2} \frac{\frac{\pi}{4} D_w^2}{\frac{\pi}{4} (D_i^2 - D_w^2)} \right]^{-1} \\ &= \left[1 + 7.04 \times 10^{-8} \frac{D_w^2}{(D_i - D_w)^2 (D_i^2 - D_w^2)} \right]^{-1} \end{aligned}$$

A number of combinations of wick diameter (D_w) and internal diameter (D_i) will satisfy the ($A_w F_2$) requirement. To achieve minimum size and minimum weight, however, an optimization is required. The optimum condition can be determined by parametric analysis with the aid of a simple computer model.

As a first approximation, the minimum wick diameter (D_w) based on $F_2 = 1$ is used:

$$\begin{aligned} D_w)_{\min} &= \left(\frac{4}{\pi} A_w \right)^{1/2} = \left(\frac{4}{\pi} \times \frac{1.28 \times 10^{-6}}{1.0} \text{ m}^2 \right)^{1/2} \\ D_w)_{\min} &= 1.28 \times 10^{-2} \text{ m} \end{aligned}$$

Note that this diameter is greater than the desired 1.27×10^{-2} m heat pipe diameter. However, we shall continue with the homogeneous wick design to show its relative merits with respect to other wick designs.

Also, since it is desirable to maintain laminar vapor flow ($Re_v \leq 2000$)

$$\begin{aligned} Re_v &= \frac{V_v \rho_v D_{H,v}}{\mu_v} = \frac{Q D_{H,v}}{\lambda \mu_v A_v} \\ &= \frac{4Q}{\lambda \mu_v \pi (D_i + D_w)} \end{aligned}$$

As a matter of practical consideration, a vapor space size of 1.65×10^{-3} m (.065 inches) is initially assumed. A smaller vapor space would be too small to consider since it would be difficult to control its size. On that basis and on the basis of the minimum wick diameter determined above:

$$D_{iv \min} = 1.28 \times 10^{-2} \text{ m}$$

$$D_i = 1.62 \times 10^{-2} \text{ m}$$

The vapor flow condition based on ammonia properties at 0°C (see Volume II - Tabulated Properties) and a design margin of 1.3:

$$\begin{aligned} R_{ev} &= \frac{4Q}{\pi \lambda \mu_v (D_i + D_v)} \\ &= \frac{(4) (15 \text{ watts}) (1.3)}{\pi (1.27 \times 10^6 \frac{\text{J}}{\text{kg}}) (.92 \times 10^{-5} \frac{\text{kg}}{\text{m} \cdot \text{sec}}) (2.9 \times 10^{-2} \text{ m})} \\ &= 73 \end{aligned}$$

Since the vapor flow is well within the laminar flow range, the vapor flow factor (F_L) can be determined as follows:

$$\begin{aligned} F_L &= 1 + \frac{(7.04 \times 10^{-8}) (1.28 \times 10^{-2} \text{ m})^2}{[1.62 \times 10^{-2} \text{ m} - 1.28 \times 10^{-2} \text{ m}]^2 [(1.62 \times 10^{-2} \text{ m})^2 - (1.28 \times 10^{-2} \text{ m})^2]} \quad -1 \\ F_L &= .99 \end{aligned}$$

Since this value of the vapor flow factor is approximately equal to unity, the design margin of 1.2 to 1.3 is satisfied on the basis of minimum fluid properties except for the fact that the internal diameter is larger than originally assumed and the gravity loss will be larger than determined above. Performance at

the two temperature extremes of the operating temperature range can now be determined as follows.

At 0°C

$$\begin{aligned}
 1 + \eta &= 1 - \left[\frac{r_p}{2H \cos \theta_c} \left(L \sin \beta + \left(D_i - \frac{D_i - D_w}{2} \right) \cos \beta \right) \right] \\
 &= 1 - \left[\frac{1.28 \times 10^{-4} \text{ m}}{(2) (4.2 \times 10^{-6} \text{ m}) (1)} (1 \text{ m} \sin .573 + 1.45 \times 10^{-2} \text{ m} \cos .573) \right] \\
 &= .64
 \end{aligned}$$

where the internal wick elevation is taken from the bottom of the heat pipe to the top of the internal wick core.

$$\begin{aligned}
 F_L &= \left[1 + \frac{v}{v_L} \frac{32K}{(D_i - D_w)^2} \frac{D_w^2}{(D_i^2 - D_w^2)} \right]^{-1} \\
 &= \left[1 + (11.0) \frac{(32) (2 \times 10^{-10}) (1.28 \times 10^{-2})^2}{(1.62 \times 10^{-2} - 1.28 \times 10^{-2})^2 [(1.62 \times 10^{-2})^2 - (1.28 \times 10^{-2})^2]} \right]^{-1} \\
 &= .99
 \end{aligned}$$

The transport capability at the 1 cm test elevation and 0°C is:

$$\begin{aligned}
 QL)_{\max} &= \frac{2K A_w (1 + \eta) \cos \theta_c F_L N_L}{r_p} = \frac{2K A_w N_L}{r_p} \\
 &= \frac{(2) (2 \times 10^{-10} \text{ m}) \left(\frac{\pi}{4} \right) (1.28 \times 10^{-2} \text{ m})^2 (.64) (1) (.995) (1.25 \times 10^{11} \text{ W/m}^2)}{1.28 \times 10^{-4} \text{ m}} \\
 &= 32 \text{ W-m}
 \end{aligned}$$

At 40°C

$$\begin{aligned}
 1 + \eta &= 1 - \left[\frac{1.28 \times 10^{-4} \text{ m}}{(2) (2.9 \times 10^{-6} \text{ m}) (1)} \times (1 \text{ m} \sin .573^\circ + 1.45 \times 10^{-2} \text{ m} \cos .573^\circ) \right] \\
 &= .451 \\
 F_L &= \left[1 + \frac{(5.1) (32) (2 \times 10^{-10})}{(1.62 \times 10^{-2} - 1.28 \times 10^{-2})^2} \frac{(1.28 \times 10^{-2})^2}{[(1.62 \times 10^{-2})^2 - (1.28 \times 10^{-2})^2]} \right]^{-1} \\
 &= .995
 \end{aligned}$$

The transport capability at the 1 cm test elevation and 40°C is:

$$QL_{\max} = \frac{(2) (2 \times 10^{-10} \text{ m}^2) \left(\frac{\pi}{4}\right) (1.28 \times 10^{-2} \text{ m})^2 (.451) (1) (.99)}{1.28 \times 10^{-4} \text{ m}} \times 9 \times 10^{10} \frac{\text{W}}{\text{m}^2}$$

$$= 16.2 \text{ W-m}$$

Note that as a result of adjusting for the selected internal diameter which is larger than originally assumed, the gravity loss factor is larger and a performance margin of only 1.17 is achieved versus the design objective of 1.2. A slight iteration on the design (i.e., a wick diameter increase of $1.2/1.17 = .025$) would allow the homogeneous wick to meet the design objective.

(b) Composite Wick Design

A similar design procedure as outlined above for the homogeneous wick is also applicable to the composite wick design with the exception of the wick properties. Once primed, the gravity loss factor in Eq. 2-63 for the selected homogeneous wick design and for minimum ammonia properties is:

$$1 + \eta = 1 - \left[\frac{6.4 \times 10^{-5} \text{ m}}{(2) (2.9 \times 10^{-6} \text{ m}^2) (1)} \times (1 \text{ m} \sin .573^\circ + 1.27 \times 10^{-2} \text{ m} \cos .573^\circ) \right]$$

$$= .75$$

The combined wick area (A_w) and friction flow (F_ℓ) required to meet the desired performance is then:

$$A_w F_\ell = \frac{(17.94 \text{ W-m}) (6.4 \times 10^{-4} \text{ m})}{(2) (6.4 \times 10^{-10} \text{ m}^2) (.75) (1) (9 \times 10^{10} \frac{\text{W}}{\text{m}^2})}$$

$$= 1.33 \times 10^{-4} \text{ m}^2$$

Since the specified geometry is the same as that of the homogeneous wick, the minimum wick diameter based on $F_L = 1$ is:

$$D_{w,min} = \left(\frac{4}{\pi} \times 1.33 \times 10^{-5} \text{ m}^2 \right)^{1/2}$$

$$= 4.12 \times 10^{-3} \text{ m}$$

Handwritten notes:
 1.33×10^{-5}
 10^{-5}
 10^{-5}
 10^{-5}

And, since it is also desirable to maintain laminar flow in the composite wick design:

$$D_{t,min} = \frac{4 (15 \text{ watts}) (1.3)}{\pi (2000) \left(1.27 \times 10^6 \frac{\text{J}}{\text{kg}} \right) \left(.92 \times 10^{-5} \frac{\text{kg}}{\text{m} \cdot \text{sec}} \right)} + 4.12 \times 10^{-3} \text{ m}$$

$$= 5.18 \times 10^{-3} \text{ m}$$

As in the case of the homogeneous wick, the annular vapor space ($5.3 \times 10^{-4} \text{ m} = .021 \text{ inches}$) is too small to be considered in a practical heat pipe design. For the same annular vapor space thickness as the homogeneous wick ($1.65 \times 10^{-3} \text{ m} = .065 \text{ inches}$) and on the basis of the minimum wick diameter:

$$D_{w,min} = 4.12 \times 10^{-3} \text{ m}$$

$$D_i = 7.42 \times 10^{-3} \text{ m}$$

Using the viscosity ratio at 0°C it follows that:

$$F_L = \left[1 + \frac{(11) (32) (6.4 \times 10^{-10}) (4.12 \times 10^{-3} \text{ m})^2}{(7.42 \times 10^{-3} \text{ m} - 4.12 \times 10^{-3} \text{ m})^2 [(7.42 \times 10^{-3} \text{ m})^2 - (4.12 \times 10^{-3} \text{ m})^2]} \right]^{-1}$$

$$F_L = .991$$

Again, since the vapor flow factor (F_L) is approximately unity, vapor flow losses are negligible, the design margin of 1.2 to 1.3 should be satisfied especially since the internal diameter is smaller than initially assumed and the gravity loss factor should be less than determined above. Performance at the two temperature extremes of the operating temperature range for the selected wick diameter ($D_w = 4.12 \times 10^{-3} \text{ m}$) and the selected internal heat pipe

diameter ($D_1 = 7.42 \times 10^{-3} \text{ m}$) can be determined as follows:

At 0°C

$$1 + \eta = 1 - \left[\frac{6.4 \times 10^{-5} \text{ m}}{(2) (4.2 \times 10^{-6} \text{ m}^2) (1)} (1 \text{ m} \sin .573^\circ + 9.07 \times 10^{-3} \text{ m} \cos .573^\circ) \right]$$

$$= .855$$

$$F_L = \left[1 + \frac{(11) (32) (6.4 \times 10^{-10}) (4.12 \times 10^{-3})^2}{(7.42 \times 10^{-3} - 4.12 \times 10^{-3})^2 (7.42 \times 10^{-3})^2 - (4.12 \times 10^{-3})^2} \right]^{-1}$$

$$= .991$$

The corresponding maximum transport capability at the 1 cm test elevation and at 0°C is:

$$QL)_{\max} = \frac{(2) (6.4 \times 10^{-10} \text{ m}^2) \left(\frac{\pi}{4}\right) (4.12 \times 10^{-3} \text{ m})^2 (.855) (.991)}{6.4 \times 10^{-5} \text{ m}} \times 1.25 \times 10^{11} \frac{\text{W}}{\text{m}^2}$$

$$= 28.4 \text{ W-m}$$

At 40°C

$$1 + \eta = 1 - \left[\frac{6.4 \times 10^{-5} \text{ m}}{(2) (2.9 \times 10^{-6} \text{ m}^2) (1)} (1 \text{ m} \sin .573^\circ + 9.07 \times 10^{-3} \text{ m} \cos .573^\circ) \right]$$

$$= 0.790$$

$$F_L = \left[1 + \frac{(5.1) (32) 6.4 \times 10^{-10}}{(7.42 \times 10^{-3} - 4.12 \times 10^{-3})^2 \{(7.42 \times 10^{-3})^2 - (4.12 \times 10^{-3})^2\}} \frac{(4.12 \times 10^{-3})^2}{\{(7.42 \times 10^{-3})^2 - (4.12 \times 10^{-3})^2\}} \right]^{-1}$$

$$= 0.996$$

The corresponding maximum transport capability at the 1 cm test elevation at 40°C is:

$$QL)_{\max} = \frac{(2) (6.4 \times 10^{-10} \text{ m}^2) \left(\frac{\pi}{4}\right) (4.12 \times 10^{-3} \text{ m})^2 (.790) (.996)}{6.4 \times 10^{-5} \text{ m}} \times 9 \times 10^{10} \frac{\text{W}}{\text{m}^2}$$

$$= 18.87 \text{ W-m}$$

(c) Axial Groove Design

Three major factors distinguish the axial groove design from the homogeneous and composite wicks discussed above.

- (1) The gravity loss factor ($1 + \eta$) is independent of tube diameter since the grooves do not communicate.

- (2) The liquid/vapor shear effect must be taken into account in the design of grooves.
- (3) The number of grooves that can be located around the periphery of the heat pipe is fixed by the groove width (w), depth (δ), and the fin thickness (t_f).

For the selected axial groove design, the gravity loss factor at minimum working fluid properties is:

$$1 + \eta = 1 - \left[\frac{3.87 \times 10^{-4} \text{ m}}{(2) (2.9 \times 10^{-6} \text{ m}^2)} (1 \text{ m} \sin .573^\circ) \right]$$

$$= .333$$

The maximum transport performance for the axial groove design can be determined from Eq. 2-63 as follows:

$$QL)_{\max} = N N_g (1 + \eta) F_\ell N_\ell$$

For negligible vapor flow losses ($F_\ell = 1$), the selected groove properties (Table 5-3) and minimum fluid properties; the minimum number of grooves required for a design margin of 1.3 is:

$$N)_{\min} = \frac{(QL)_{\max}}{N_g (1 + \eta) F_\ell N_\ell}$$

$$= \frac{(1.3) (15 \text{ watts}) (.92 \text{ m})}{(1.73 \times 10^{-11} \text{ m}) (.333) (1) (9 \times 10^{10} \frac{\text{W}}{\text{m}^2})}$$

$$= 35$$

In both the extrusion and the swaging processes, a typical fin thickness (t_f) of approximately one-half (1/2) the groove width can be achieved. The minimum vapor core diameter required to accommodate 35 grooves is therefore:

$$D_v)_{\min} = \frac{N)_{\min} \times 1.5w}{\pi} = \frac{(35) (1.5) (3.87 \times 10^{-4} \text{ m})}{\pi}$$

$$= 6.45 \times 10^{-3} \text{ m}$$

The vapor Reynolds number (Re_v) for the minimum flow diameter and a design factor of 1.3 is:

$$Re_v = \frac{Q D_{H,v}}{\lambda \mu_v A_v} = \frac{(1.3) (15 \text{ watts}) (6.45 \times 10^{-3} \text{ m})}{(1.27 \times 10^6 \frac{\text{J}}{\text{kg}}) (.92 \times 10^{-5} \frac{\text{kg}}{\text{m sec}}) \frac{\pi}{4} (6.45 \times 10^{-3} \text{ m})^2}$$

$$= 329$$

Since the vapor flow is laminar, it only remains to establish the vapor flow loss factor (F_{lv}) and compensate accordingly:

$$F_{lv} = \left[1 + \frac{v_v}{v_l} (f_v + f_{lv}) \right]^{-1}$$

$$\text{where: } f_v = \frac{4}{\pi} \frac{N N_g}{\left\{ \frac{R_1}{w} - \alpha \right\}^4 w^3}$$

$$= \frac{4}{\pi} \frac{(35) (1.73 \times 10^{-11} \text{ m}^3)}{\left\{ \frac{4.0 \times 10^{-3} \text{ m}}{3.87 \times 10^{-4} \text{ m}} - 2 \right\}^4 (3.87 \times 10^{-4} \text{ m})^3}$$

$$= 2.75 \times 10^{-3}$$

$$f_{lv} = \frac{N}{3\alpha\pi} \frac{A'_l}{w^2} \left\{ \frac{R_1}{w} - \alpha \right\}^{-3}$$

$$f_{lv} = \frac{35}{(3) (2) (\pi)} (2) \left\{ \frac{4 \times 10^{-3} \text{ m}}{3.87 \times 10^{-4} \text{ m}} - 2 \right\}^{-3}$$

$$f_{lv} = 6.41 \times 10^{-3}$$

$$R_1 = \frac{1}{2} D_v + \delta = \frac{1}{2} 6.45 \times 10^{-3} \text{ m} + (7.74 \times 10^{-4} \text{ m})$$

$$= 4.0 \times 10^{-3} \text{ m}$$

$$\alpha = \frac{\delta}{w} = \frac{7.74 \times 10^{-4}}{3.87 \times 10^{-4}} = 2$$

$$\frac{A'_l}{w^2} = \frac{\delta w}{w^2} = \frac{2w^2}{w^2} = 2$$

Using the maximum viscosity ratio (0°C) it follows that

$$F_L = \left[1 + (11) (2.75 \times 10^{-3} + 6.41 \times 10^{-3}) \right]^{-1}$$

$$= .91$$

Since a value of 0.92 for F_L will give the desired design margin of 1.3, the axial groove design is satisfactory as developed above.

If the vapor had been more significant, the number of grooves and the vapor space diameter would have been increased until satisfactory performance was achieved. For the selected vapor core diameter ($D_v = 6.45 \times 10^{-3} \text{ m}$), internal diameter ($D_i = 8 \times 10^{-3} \text{ m}$), and the properties of the selected groove design, performance at the two extremes of the operating temperature range will be:

$$\frac{\text{At } 0^{\circ}\text{C}}{1 + \eta} = 1 - \left[\frac{3.87 \times 10^{-4} \text{ m}}{(2) (4.2 \times 10^{-6} \text{ m}^2)} (1 \text{ m} \sin .573^{\circ}) \right]$$

$$= .54$$

$$F_L = \left[1 + (11) (2.75 \times 10^{-3} + 6.41 \times 10^{-3}) \right]^{-1}$$

$$= .91$$

The maximum transport capability at the 1 cm test elevation and 0°C is therefore $QL_{\text{max}} = (35) (1.73 \times 10^{-11} \text{ m}^2) (.54) (.91) (1.25 \times 10^{11} \frac{\text{W}}{\text{m}^2})$

$$= 37.2 \text{ W-m}$$

$$\frac{\text{At } 40^{\circ}\text{C}}{1 + \eta} = 1 - \left[\frac{3.87 \times 10^{-4} \text{ m}}{(2) (2.9 \times 10^{-6} \text{ m}^2)} (1 \text{ m} \sin .573^{\circ}) \right]$$

$$= .333$$

$$F_L = \left[1 + (5.1) (2.75 \times 10^{-3} + 6.41 \times 10^{-3}) \right]^{-1}$$

$$= .955$$

The maximum transport capability at the 1 cm test elevation and 40°C is therefore $QL_{\text{max}} = (35) (1.73 \times 10^{-11} \text{ m}^2) (.333) (.955) (9 \times 10^{10} \frac{\text{W}}{\text{m}^2})$

$$= 17.3 \text{ W-m}$$

(d) Static Wicking Height

The static wicking height for each of the preceeding wick designs can be determined by setting $(1 + \eta = 0)$, in which case:

For both the homogeneous and composite wick

$$h_{\max} \approx \frac{2H}{r_p} - \left\{ \frac{D_i - D_w}{2} + D_w \right\}$$

For example, at 0°C the maximum static height for the homogeneous wick is:

$$\begin{aligned} h_{\max} &= \frac{(2) (4.2 \times 10^{-6} \text{ m}^2)}{1.28 \times 10^{-4} \text{ m}} - 1.45 \times 10^{-2} \text{ m} \\ &= 5.11 \times 10^{-2} \text{ m} \end{aligned}$$

For the axial groove:

$$h_{\max} = \frac{2H}{r_p}$$

At 0°C

$$\begin{aligned} h_{\max} &= \frac{(2) (4.2 \times 10^{-6} \text{ m}^2)}{3.87 \times 10^{-4} \text{ m}} \\ &= 2.17 \times 10^{-2} \text{ m} \end{aligned}$$

5.1.6 Step #6 - Establish Heat Transfer Characteristics

For illustration purposes, it is assumed that the secondary wick for both homogeneous and the composite wick consists of a single layer of fine mesh screen: for example, 200 mesh screen with $6.35 \times 10^{-5} \text{ m}$ wire diameter. The effective thermal conductivity of screen wicks can be approximated with a series model (Eq. 4-40)

$$K_w = \frac{K_s K}{\epsilon K_s + (1 - \epsilon) K}$$

With ammonia as the working fluid, aluminum wick material and a square mesh ($\epsilon \approx .6$)

$$K_w = \frac{(70.5 \frac{\text{W}}{\text{m}^\circ\text{C}}) (.45 \frac{\text{W}}{\text{m}^\circ\text{C}})}{(.6) (70.5) + (1 - .6) (.45)} = .75 \frac{\text{W}}{\text{m}^\circ\text{C}}$$

Since the total wick thickness is approximately equal to twice the wire diameter, the equivalent film coefficient can be expressed as:

$$h_e = h_E = \frac{k_w}{t_w} = \frac{.75 \frac{W}{m^2 \cdot ^\circ C}}{(2) (6.35 \times 10^{-5} m)} = 5.9 \times 10^3 \frac{W}{m^2 \cdot ^\circ C}$$

In this problem, the evaporator and condenser are of equal length (8 cm) and the heat input is over half the circumference. If the heat conductance over the second half of the circumference is neglected:

$$A_E = A_e = \frac{1}{2} \pi D_i \times 8 \times 10^{-2} m$$

For the homogeneous wick design:

$$A_E = A_e = (\frac{1}{2} \pi) (1.62 \times 10^{-2} m) (8 \times 10^{-2} m) = 2.03 \times 10^{-3} m^2$$

$$\begin{aligned} \Delta T_{H.P.} &= 2 \frac{Q}{h_E A_E} = 2 \frac{Q}{h_C A_C} \\ &= \frac{(2) (15 \text{ watts})}{\left(5.9 \times 10^3 \frac{W}{m^2 \cdot ^\circ C}\right) (2.03 \times 10^{-3} m^2)} \\ &= 2.5 ^\circ C \end{aligned}$$

For the composite wick design:

$$A_E = A_e = (\frac{1}{2} \pi) (7.42 \times 10^{-3} m) (8 \times 10^{-2} m) = 9.32 \times 10^{-4} m^2$$

$$\Delta T_{H.P.} = \frac{(2) (15 \text{ watts})}{\left(5.9 \times 10^3 \frac{W}{m^2 \cdot ^\circ C}\right) (9.32 \times 10^{-4} m^2)} = 5.46 ^\circ C$$

Both the homogeneous wick and the composite wick designs meet the design performance of $6^\circ C$. If higher conductances were desired, a threaded secondary wick instead of a single layer of screen could be used. Also it should be noted that the results are conservative since only 50% of the tubes circumference was used. These could be modified by applying a fin efficiency to this 50%, once the wall thickness has been determined based on pressure retention requirement (Section 5.1.7).

For the axial groove, the evaporator and the condenser film coefficients can be determined from Eqs. 4-42 and 4-43, respectively. For aluminum, with ammonia as the working fluid, a groove depth of $7.74 \times 10^{-4} m$, a land thickness of $1.94 \times 10^{-4} m$, a

vapor core diameter of 6.45×10^{-3} m ($R_v = 3.23 \times 10^{-3}$ m) and 35 grooves:

$$\begin{aligned}
 h_e &= \frac{N K_e}{2\pi R_v} \frac{1}{.0701 + \frac{K_e \delta}{K_w t_f}} \\
 &= \frac{35 \times .45 \frac{W}{m^2 \cdot ^\circ C}}{2\pi (3.23 \times 10^{-3} m)} \frac{1}{.0701 + \frac{.45 \frac{W}{m^2 \cdot ^\circ C} \cdot 7.74 \times 10^{-4} m}{70.5 \frac{W}{m^2 \cdot ^\circ C} \cdot 1.94 \times 10^{-4} m}} \\
 &= 8.12 \times 10^3 \frac{W}{m^2 \cdot ^\circ C} \\
 h_c &= \frac{N K_e}{2\pi R_v} \frac{1}{.0221 + \frac{K_e \delta}{K_w t_f}} \\
 &= \frac{(35) (.45)}{2\pi (3.23 \times 10^{-3})} \frac{1}{.0221 + \frac{.45 \cdot 7.74 \times 10^{-4}}{70.5 \cdot 1.94 \times 10^{-4}}} \\
 &= 1.63 \times 10^4 \frac{W}{m^2 \cdot ^\circ C}
 \end{aligned}$$

For the axial groove heat pipe, considering heat into half of the circumference:

$$\begin{aligned}
 \Delta T_{H.P.} &= T_E + T_C = \frac{Q}{h_E A_E} + \frac{Q}{h_C A_C} \\
 &= \frac{15w}{\left(8.12 \times 10^3 \frac{W}{m^2 \cdot ^\circ C}\right) (8.1 \times 10^{-4} m^2)} + \frac{15w}{\left(1.63 \times 10^4 \frac{W}{m^2 \cdot ^\circ C}\right) (8.1 \times 10^{-4} m^2)} \\
 &= 3.42 ^\circ C
 \end{aligned}$$

Hence, the axial groove design also meets the $6^\circ C$ requirement.

5.1.7 Step #7 - Pressure Containment

Maximum containment pressure will occur at a specified bonding temperature of $170^\circ C$ ($337^\circ F$). This temperature exceeds the critical temperature of ammonia and the internal pressure can be determined by using the Beattie-Bridgeman Equation of State (Eq. 4-2). To obtain the pressure from this equation it is necessary to establish the wick volume, vapor channel volume and the total fluid inventory. Once the internal pressure is determined, the required wall thickness can be established on the basis of the thick-walled Lamé solution (Table 4-13) and the properties of the selected container material (Table 5-4). For the

design properties of the three types of heat pipes that are summarized in Table 5-5, pressure containment requirements are as follows.

I. Homogeneous Wick Design

The homogeneous wick is made of multiple wraps of square wire mesh, the porosity (ϵ) is approximately 0.6 (Eq. 4-15) and the wick volume is:

$$V_w = \epsilon A_w L_{H.P.} = (.6) (1.29 \times 10^{-4} \text{ m}^2) (1 \text{ m})$$

$$V_w = 7.74 \times 10^{-5} \text{ m}^3$$

The vapor channel volume is:

$$V_v = \frac{\pi}{4} (D_1^2 - D_w^2) = \frac{\pi}{4} \left[(1.62 \times 10^{-2} \text{ m})^2 - (1.28 \times 10^{-2} \text{ m})^2 \right]$$

$$V_v = 7.74 \times 10^{-5} \text{ m}^3$$

For ammonia the maximum fluid inventory is determined at 0°C. The required inventory for the homogeneous wick is therefore

$$m = \left(642.4 \frac{\text{kg}}{\text{m}^3} \right) (7.74 \times 10^{-5} \text{ m}^3) + \left(3.391 \frac{\text{kg}}{\text{m}^3} \right) (7.74 \times 10^{-5} \text{ m}^3)$$

$$m = 4.99 \times 10^{-2} \text{ kg}$$

The pressure containment requirement based on the Beattie-Bridgeman Equation is:

$$P = \frac{RT (1 - e')}{v_n^2} (v_n + B) - \frac{A}{v_n^2}$$

$$v_n = \frac{(1.55 \times 10^{-4} \text{ m}^3)(1000 \text{ l/m}^3) \times 17 \frac{\text{gm}}{\text{gm-mole}}}{4.99 \times 10^{-2} \text{ kg} \times 1000 \frac{\text{gm}}{\text{kg}}} = 5.28 \times 10^{-2} \frac{\text{l}}{\text{gm-mole}}$$

$$M = \text{Molecular Weight } (17 \frac{\text{gm}}{\text{gm-mole}} \text{ for ammonia})$$

$$v = V_w + V_v$$

$$T = 170^\circ\text{C} = 443^\circ\text{K}$$

$$A = A_0 \left(1 - \frac{a}{v_n} \right) = 2.392 \left(1 - \frac{0.17031}{5.28 \times 10^{-2}} \right)$$

$$B = B_0 \left(1 - \frac{b}{v_n} \right) = .03415 \left(1 - \frac{.19112}{5.28 \times 10^{-2}} \right)$$

TABLE 5-5. WICK DESIGN PROPERTIES SUMMARY

SAMPLE PROBLEM A

I. HOMOGENEOUS WICK

Wick Diameter (D_w)	$1.28 \times 10^{-2} \text{ m}$
Wick Area (A_w)	$1.29 \times 10^{-4} \text{ m}^2$
Internal Diameter (D_i)	$1.62 \times 10^{-2} \text{ m}$
Transport Capacity at 1.0 cm Elevation	
$QL)_{\max}$ @ 0°C	32 W-m
$QL)_{\max}$ @ 40°C	16.2 W-m
Design Margin	
At 0°C	2.2
At 40°C	1.17
Static Wicking Height (h_{\max})	
At 0°C	$5.10 \times 10^{-2} \text{ m}$
At 40°C	$3.1 \times 10^{-2} \text{ m}$
Composite Factor (S)	1.0

II. COMPOSITE WICK DESIGN

Wick Diameter (D_w)	$4.12 \times 10^{-3} \text{ m}$
Wick Area (A_w)	$1.33 \times 10^{-5} \text{ m}^2$
Internal Diameter (D_i)	$7.42 \times 10^{-3} \text{ m}$
Transport Capacity at 1.0 cm Elevation (primed)	
$QL)_{\max}$ @ 0°C	28.4 W-m
$QL)_{\max}$ @ 40°C	18.9 W-m
Design Margin	
At 0°C	2.06
At 40°C	1.37
Static Wicking Height (h_{\max}) (primed)	
At 0°C	$11.7 \times 10^{-2} \text{ m}$
At 40°C	$7.6 \times 10^{-2} \text{ m}$
Composite Factor (S)	4.0

III. AXIAL GROOVE DESIGN

Vapor Core Diameter (D_v)	$6.45 \times 10^{-3} \text{ m}$
Internal Diameter (D_i)	$8.0 \times 10^{-3} \text{ m}$
Number of Grooves (N)	35
Area Per Groove (A_g)	$3 \times 10^{-7} \text{ m}^2$
Transport Capacity at 1.0 cm Elevation	
$QL)_{\max}$ @ 0°C	38.4 W-m
$QL)_{\max}$ @ 40°C	17.6 W-m
Design Margin	
At 0°C	2.78
At 40°C	1.28
Static Wicking Height (h_{\max})	
At 0°C	$2.17 \times 10^{-2} \text{ m}$
At 40°C	$1.50 \times 10^{-2} \text{ m}$
Composite Factor (S)	0.8

$$B = 8.95 \times 10^{-2}$$

$$e' = \frac{c}{v_n T^3} = \frac{476.87 \times 10^4}{(5.28 \times 10^{-2})(443)^3}$$

$$e' = 1.04$$

Where A_0 , a , B_0 , b and c are constants as defined in Table 4-3 for ammonia.

$$p = \frac{(0.08206)(443)(1 - 1.04)}{(5.28 \times 10^{-2})^2} (5.28 \times 10^{-2} - 8.95 \times 10^{-2})$$

$$+ \frac{5.32}{(5.28 \times 10^{-2})^2}$$

$$p = 1090 \text{ atm.} \approx 28,000 \text{ psia}$$

As can be seen, the internal pressure associated with the homogeneous wick design is excessive. Based on the thick-walled Lamé solution, the wall thickness requirement is:

$$R_o^2 = \frac{F_{tu} + p}{F_{tu} - p} R_i^2$$

Even with stainless steel ($F_{tu} = 74,000 \text{ psi}$), an ASME safety factor of 4 on ultimate could not be satisfied (i.e., $\frac{1}{4} F_{tu} < p$). For a safety factor of 2, which could be acceptable for the bonding process

$$R_o^2 = \frac{\left(\frac{1}{2}\right)(74,000) + 28,000}{\left(\frac{1}{2}\right)(74,000) - 28,000} \left(\frac{1}{2} \times 1.62 \times 10^{-2} \text{ m}\right)^2$$

$$R_o = 2.17 \times 10^{-2} \text{ m}$$

Note that aluminum cannot satisfy the pressure containment requirement ($F_{tu} = 20,000 @ 170^\circ\text{C}$) under any condition.

II. Composite Wick Design

A similar analysis as described above can be followed to determine the internal pressure associated with the composite wick design. Since the wick material selected is also square mesh screen ($\epsilon \approx .6$), the following volumes, inventories and pressure containment requirement would apply to the composite wick:

$$V_w = 8.0 \times 10^{-6} \text{ m}^3$$

$$V_v = 3.0 \times 10^{-5} \text{ m}^3$$

$$m = 5.24 \times 10^{-3} \text{ kg}$$

$$v_n = 0.123 \text{ l/gm-mole}$$

and therefore

$$p = 199 \text{ atm} \approx 2900 \text{ psia}$$

Note that the fluid inventory required for the composite wick is an order of magnitude less than for the homogeneous wick. Also, the percentage of vapor volume to total volume for the composite wick is much larger than for the homogeneous wick. If a safety factor of 2 were to be applied on pressure containment, the required external diameter for stainless steel would be:

$$R_o^2 = \frac{\left(\frac{1}{2}\right)(20,000) + 2900}{\left(\frac{1}{2}\right)(20,000) - 2900} \left(\frac{1}{2} \times 7.42 \times 10^{-3} \text{ m}\right)^2$$

$$R_o = 5 \times 10^{-3} \text{ m}$$

Since the pressure containment is sufficiently low a safety factor of 4 could have been used for pressure containment in which case for stainless steel:

$$R_o = 4.35 \times 10^{-3} \text{ m}$$

And for aluminum

$$R_o = 7.20 \times 10^{-3} \text{ m}$$

III. Axial Groove Wick Design

The wick's volume in an axially grooved design is the volume of the grooves and therefore, the following volumes, inventories and pressure containment requirements apply:

$$V_w = NA_2 L_{H.P.} = (35) (3 \times 10^{-7} \text{ m}^2) (1 \text{ m})$$

$$V_w = 1.05 \times 10^{-5} \text{ m}^3$$

$$V_v = \frac{\pi}{4} D_v^2 L_{H.P.} = \frac{\pi}{4} (6.45 \times 10^{-3} \text{ m})^2 (1 \text{ m})$$

$$V_v = 3.27 \times 10^{-5} \text{ m}^3$$

$$m = 6.85 \times 10^{-3} \text{ kg}$$

$$v_n = 0.1072$$

The internal pressure is therefore

$$p = 247 \text{ atm} \approx 3600 \text{ psia}$$

For a safety factor of 4:

$$R_o = 4.87 \times 10^{-3} \text{ m} \quad \text{For Stainless Steel}$$

$$R_o = 9.91 \times 10^{-3} \text{ m} \quad \text{For Aluminum}$$

5.1.8 Step #8 - Design Selection

Table 5-6 summarizes the significant performance and design factors of the three selected wick designs. As can be seen, the homogeneous wick can be excluded on the basis of size, pressure containment requirement and weight. Of the two remaining design options, the composite wick offers higher performance, smaller size and lower weight. However, composite wicks are known to be unreliable. If high reliability is required, the axial groove would be a better choice at a size and weight penalty. In both cases it can be seen that the weight is governed by the 170°C bonding requirement. To achieve more optimum weight, a larger heat pipe diameter (larger total internal volume) or the addition of a reservoir could be considered. Also, charging after the bonding operation would provide a significant weight savings.

TABLE 5-6. HEAT PIPE DESIGN SUMMARY (AMMONIA)

SAMPLE PROBLEM A

	<u>Homogeneous Wick</u>	<u>Composite Wick</u>	<u>Axial Groove</u>
<u>Performance @ 40°C</u>			
Transport @ 1.0 cm Elev. $(QL)_{\max}$ (W-m)	16.2	18.9	17.6
Static Wicking Height (h_{\max}) (m)	3.1×10^{-2}	7.6×10^{-2}	1.50×10^{-2}
Composite Factor	1.0	4.0	0.8
Design Margin ΔT (°C)	1.17	1.37	1.28
Pressure @ 170°C (atm)			
Aluminum Containment at a Safety Factor of 2			
Outer Diameter (D_o) (m)	--	1.0×10^{-2}	1.17×10^{-2}
Weight (kg)	--	0.131*	0.176
Stainless Steel Containment at a Safety Factor of 2			
Outer Diameter (D_o) (m)	4.34×10^{-2}	8.02×10^{-3}	8.82×10^{-3}
Weight (kg)	10.9*	0.094*	0.149
Aluminum Containment at a Safety Factor of 4			
Outer Diameter (D_o) (m)	--	1.44×10^{-2}	1.982×10^{-2}
Weight (kg)	--	.365*	.735
Stainless Steel Containment at a Safety Factor of 4			
Outer Diameter (D_o) (m)	--	8.7×10^{-3}	9.74×10^{-3}
Weight (kg)	--	0.167*	0.260
Temperature Drop (ΔT) (°C)	2.5	5.46	3.42

*Heat pipe weight based on stainless steel wire mesh wick

5.2 SAMPLE PROBLEM 8 -- VARIABLE CONDUCTANCE HEAT PIPE

5.2.1 Step #1 - Problem Definition and Design Criteria

A gas controlled variable conductance heat pipe is required to maintain the temperature of a package on-board a satellite in the range of 0 to 10°C with variation in sink temperatures between -60°C and -30°C. At the minimum sink temperature it is desired that the heat pipe be sufficiently shut down to allow the package to be maintained at 0°C with a maximum power input of 2.0 watts. It is also desirable to provide sufficient flexibility in the design to accommodate an alternate position on the spacecraft where maximum sink temperature may be as high as -10°C.

Condenser length, evaporator length and overall length are to be the same as specified in Sample Problem A. To minimize development, an existing fixed conductance heat pipe design as defined in Sample Problem A is required.

5.2.2 Step #2 - Fixed Conductance Heat Pipe Design Summary

The axially grooved heat pipe design as developed in Sample Problem A is shown in Fig. 5-3. Pertinent physical properties are summarized in Table 5-7. The principle difference between this heat pipe and the heat pipe in Sample Problem A is the wall thickness. In this case a 9×10^{-4} m (.035 inch) wall thickness is specified to minimize reverse conductance. Pressure containment is not a problem since the reservoir will significantly reduce internal pressure at high temperatures.

5.2.3 Step #3 - Reverse Conductance

The first step in establishing the variable conductance heat pipe (VCHP) is to determine the amount of blockage beyond the end of the condenser required under minimum sink condition to accommodate the specified maximum power input of 2.0 watts. In this region, heat will be conducted through the aluminum wall of the heat pipe. Including the fins between the grooves, the total cross-sectional area is:

$$\begin{aligned} A &= \frac{\pi}{4} (D_o^2 - D_v^2) - A_G \\ &= \frac{\pi}{4} [(9.8 \times 10^{-3} \text{ m})^2 - (6.45 \times 10^{-3} \text{ m})^2] - (35)(3.87 \times 10^{-4} \text{ m})(7.74 \times 10^{-4} \text{ m}) \\ &= 3.23 \times 10^{-5} \text{ m}^2 \end{aligned}$$

TABLE 5-7. CHARACTERISTICS OF THE AXIALLY GROOVED DESIGN

Number of grooves	35
Vapor core diameter (D_v)	$6.45 \times 10^{-3} \text{ m}$
Inner diameter (D_i)	$8 \times 10^{-3} \text{ m}$
Effective pumping radius (r_p)	$3.87 \times 10^{-4} \text{ m}$
Groove width (w)	$3.87 \times 10^{-4} \text{ m}$
Groove depth (δ)	$7.74 \times 10^{-4} \text{ m}$
Groove area (A_g)	$1.048 \times 10^{-5} \text{ m}^2$
Groove flow factor - sharp corner (N_g)	$1.73 \times 10^{-11} \text{ m}^3$
Permeability (k)	$1.12 \times 10^{-8} \text{ m}^2$

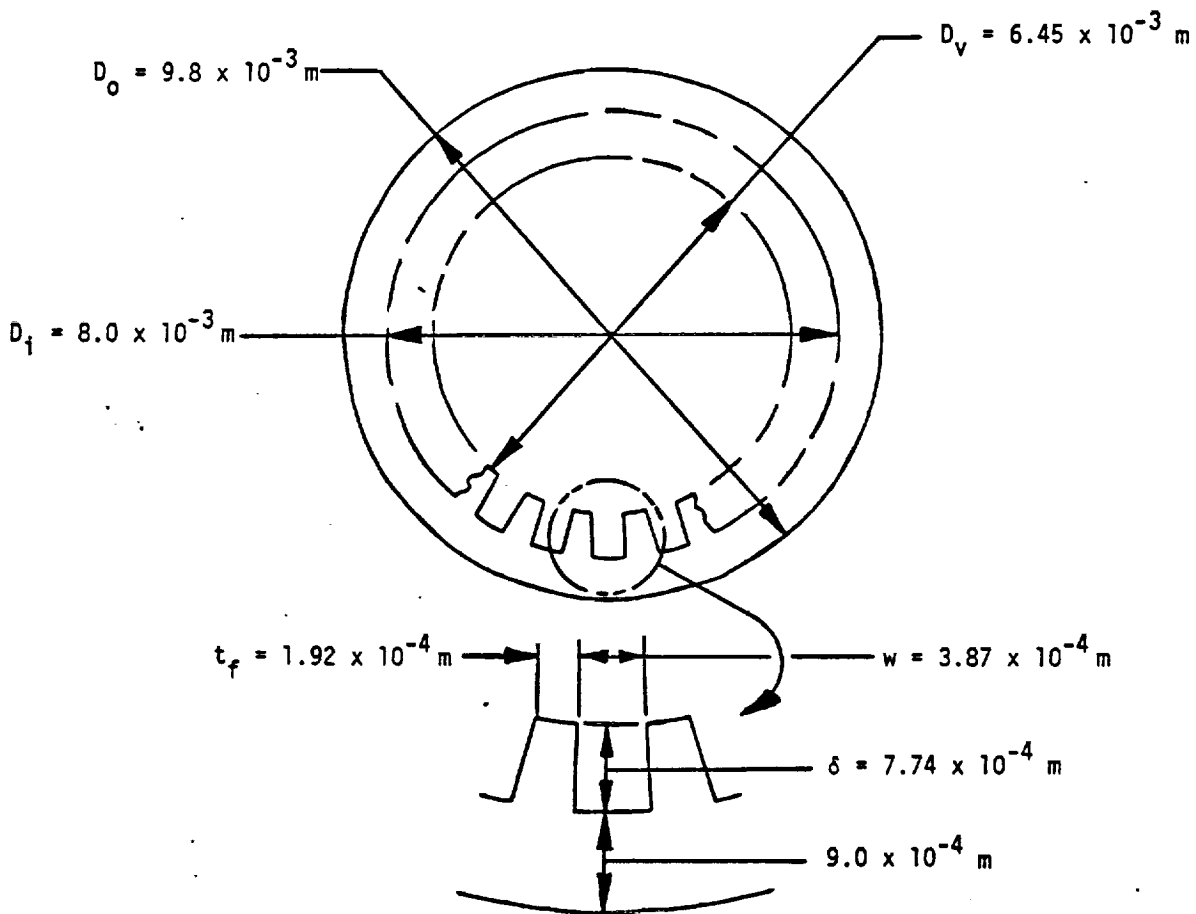


Fig. 5-3. Axially grooved heat pipe

For aluminum the reverse conductance can be expressed as:

$$\begin{aligned}\frac{Q \Delta x}{\Delta T} &= KA = \left(211 \frac{\text{watt}}{\text{m} \cdot ^\circ\text{C}} \right) (3.23 \times 10^{-5} \text{m}^2) \\ &= 6.82 \times 10^{-3} \frac{\text{watt-m}}{^\circ\text{C}}\end{aligned}$$

For a maximum of 2.0 watt input at the minimum sink of -60°C and a vapor temperature of 0°C

$$\begin{aligned}\Delta x &= \frac{KA \Delta T}{Q} = \frac{(6.82 \times 10^{-3} \frac{\text{watt-m}}{^\circ\text{C}}) 60^\circ\text{C}}{2 \text{ watt}} \\ &= .205 \text{ m}\end{aligned}$$

To achieve sufficient shutdown, therefore, the gas interface must recede the entire length of the condenser (0.08 m) plus the above distance. The volume of the vapor space in the inactive part of the heat pipe at the minimum condition is:

$$\begin{aligned}V_{v,im} &= \frac{\pi}{4} D_v^2 (L_c + \Delta x) \\ &= \frac{\pi}{4} (6.45 \times 10^{-3} \text{m})^2 (.08 \text{m} + .205 \text{m}) \\ &= 6.81 \times 10^{-6} \text{m}^3\end{aligned}$$

5.2.4 Step #4 - Reservoir Sizing; Maximum Sink = -30°C

The simplest type of VCHP that can be employed is the "cold reservoir" type as defined in Section 3.2.2. For this type of design, the reservoir size can be determined from Eq. 3-15.

$$\frac{V_r}{V_{v,im}} = \frac{\psi_{o,min}}{\psi_{o,max} - \psi_{o,min}}$$

From Eq. 3-8 and ammonia vapor pressure properties (Ref. Volume II)

$$\begin{aligned}\psi_{o,min} &= \frac{P_v - P_{v,o}}{T_o} \min = \frac{.427 \times 10^6 \text{ N/m}^2 - .217 \times 10^5 \text{ N/m}^2}{213 \text{ K}} \\ &= 1903 \frac{\text{N}}{\text{m}^2 \cdot \text{K}} \\ \psi_{o,max} &= \frac{P_v - P_{v,o}}{T_o} \max = \frac{.612 \times 10^6 \text{ N/m}^2 - .119 \times 10^6 \text{ N/m}^2}{243 \text{ K}} \\ &= 2029 \frac{\text{N}}{\text{m}^2 \cdot \text{K}}\end{aligned}$$

$$\frac{V_r}{V_{v,min}} = \frac{1903}{2029 - 1903} = 15.1$$

The required reservoir volume is:

$$V_r = (15.1)(6.81 \times 10^{-6} \text{ m}^3) = 1.03 \times 10^{-4} \text{ m}^3$$

And the gas charge required is (Eq. 3-10):

$$\begin{aligned} (mR)_g &= V_r \psi_{r,\max} = V_r \psi_{o,\max} \\ &= (1.03 \times 10^{-4} \text{ m}^3) \left(2029 \frac{\text{N}}{\text{m}^2 \cdot \text{K}} \right) \\ &= .209 \text{ N} \cdot \text{m} / \text{K} \end{aligned}$$

Where R , the universal gas constant is equal to $8.31 \times 10^3 \frac{\text{N} \cdot \text{m}}{\text{kg-mole K}}$. The required non-condensable gas charge is:

$$m_g = 2.52 \times 10^{-5} \text{ kg - mole}$$

5.2.5 Step #5 - Reservoir Sizing; Maximum Sink = -10°C

For a -10°C sink temperature, the "cold reservoir" cannot satisfy the control requirement. In this case $\psi_{o,\min}$ is the same as determined above and:

$$\begin{aligned} \psi_{o,\max} &= \frac{.612 \times 10^6 \text{ N/m}^2 - .290 \times 10^6 \text{ N/m}^2}{263 \text{ K}} \\ &= 1224 \frac{\text{N}}{\text{m}^2 \cdot \text{K}} \end{aligned}$$

and

$$\frac{V_r}{V_{v,1m}} = \frac{1903}{1224 - 1903} = -2.8$$

The negative value for $\frac{V_r}{V_{v,1m}}$ indicates that even an infinite volume would not satisfy the control requirement. In this case, therefore, the reservoir temperature must be controlled and a design such as the feedback VCHP as described in Section 3.2.2 is required. In a feed-fabk system the reservoir temperature varies between the maximum sink temperature and the maximum conditions as determined by the reservoir heater and controller. Since control bands of only a few degrees are easily achieved with typical electronic controllers, an optimum reservoir for feedback control can be determined from Eq. 3-18:

$$\frac{V_r}{V_{v,1m}} = \frac{\psi_{o,\min}}{\psi_{o,\max}} = \frac{1903}{1224} = 1.55$$

In this case the reservoir volume is:

$$V_r = (1.55)(6.81 \times 10^{-6} \text{ m}^3) = 1.06 \times 10^{-6} \text{ m}^3$$

The required non-condensable gas charge can be determined in the same fashion as in the case of the "cold reservoir" as illustrated above.

5.3 SAMPLE PROBLEM C -- GRAVITY ASSIST HEAT PIPE

5.3.1 Step #1 - Problem Definition and Design Criteria

It is desired to utilize the axially grooved heat pipe design developed in Sample Problem A in a system for ground application. The heat pipes are to be operated with a .153 m (6 in.) positive tilt. Total system heat load is 250 watts at a nominal operating temperature of 0°C. Heat input (evaporator), heat output (condenser) and overall heat pipe length are to be the same as specified in Sample Problem A. The working fluid is to be ammonia. A minimum number of heat pipes is desired to minimize system cost.

5.3.2 Step #2 - Heat Pipe Design Summary

The axially grooved heat pipe design as developed in Sample Problem A is shown in Fig. 5-3. Pertinent physical properties are summarized in Table 5-7.

5.3.3 Step #3 - Evaluate Hydrodynamic Performance Limits

When a heat pipe is operated at a positive elevation in a gravity field, the condensate return to the evaporator occurs with the help of gravity. The total performance of the heat pipe is, therefore, in excess of its performance associated with capillary pumping limit.

As a first approximation, the laminar vapor flow is assumed. The maximum transport performance for the axial groove design can be determined from Eq. 2-63 as follows:

$$Q)_{\max} = NN_g (1 + \eta) \frac{F_L N_L}{L_{\text{eff}}}$$

$$\text{where } 1 + \eta = 1 - \frac{r_p L \sin \beta}{2H_L} = 1 - \frac{3.87 \times 10^{-4} \text{ m}}{2 \times 4.2 \times 10^{-6} \text{ m}^2} [1 \text{ m} \sin (-8.7^\circ)]$$

$$= 8$$

Note that the sign of the tilt angle is negative for a reflux mode of operation resulting in a $(1 + n)$ term greater than unity.

$$\text{For } L_{\text{eff}} = .92 \text{ m}$$

$$\text{and } F_L = .91 \quad (\text{see Sample Problem A})$$

$$\begin{aligned} Q)_{\text{max}} &= 35 \times 1.73 \times 10^{-11} \text{ m}^3 \times 8 \times .91 \times 1.25 \times 10^{11} \frac{\text{W}}{\text{m}^2} \times \frac{1}{.92 \text{ m}} \\ &= 599 \text{ watt} \end{aligned}$$

The corresponding vapor Reynolds number (Re_v) is:

$$\begin{aligned} Re_v &= \frac{Q D_{h,v}}{\lambda \mu_v A_v} = \frac{(599 \text{ W})(6.45 \times 10^{-3} \text{ m})}{(1.27 \times 10^6 \text{ J/kg})(.92 \times 10^5 \text{ kg/m-sec}) \frac{\pi}{4} (6.45 \times 10^{-3} \text{ m})^2} \\ &= 10,128 \end{aligned}$$

Since the vapor flow is turbulent, Eq. 2-23 and 2-34 apply

$$\begin{aligned} \frac{dP_v}{dx} &= \frac{.156 \mu_v^2 Re_v^{7/4}}{\rho_v D_{h,v}^3} \\ &= \frac{.156 (.92 \times 10^{-5} \text{ kg/m-sec})^2 (10,128)^{7/4}}{(3.391 \text{ kg/m}^3) (6.45 \times 10^{-3} \text{ m})^3} = 158 \text{ N/m} \\ \psi &= 0.0328 \frac{R_i - R_v}{R_v^{.25}} \frac{A_L}{A_v^{1.75}} \frac{\mu_v}{\rho_v \nu_v} \dot{m}^{.75} \end{aligned}$$

Eq. 2-23 can also be written as:

$$\begin{aligned} \psi &= .0195 \frac{R_i - R_v}{R_v} \frac{A_L}{A_v} R_v^{.75} \\ &= .0195 \frac{7.74 \times 10^{-4}}{3.225 \times 10^{-3}} \frac{1.048 \times 10^{-5}}{\pi (3.225 \times 10^{-3})^2} 10,128^{.75} \\ &= 15.6 \end{aligned}$$

The liquid loss is determined by Eq. 2-20

$$\frac{dP_L}{dx} = - \frac{N_L \dot{m}_L(x)}{k(x) A_L(x)}$$

$$\frac{dP_l}{dx} = \frac{-(2.87 \times 10^{-7} \text{ m}^2/\text{sec})(599 \text{ W})}{(1.12 \times 10^{-8} \text{ m}^2)(1.048 \times 10^{-5} \text{ m}^2)(1.27 \times 10^6 \text{ J/kg})}$$

$$= 1153 \text{ N/m}$$

The liquid vapor shear loss can be determined by:

$$\frac{dP_{lv}}{dx} = \frac{\phi^2}{3} \psi \frac{dP_l}{dx} = \frac{.374}{3} (15.16) (1153 \text{ N/m}) = 815 \text{ N/m}$$

$$\phi = \frac{(R_v + R_t) \sin(\pi/N) - R_t}{R_l - R_v}$$

Neglecting the land tip corner radius ($R_t = 0$)

$$\phi = \frac{R_v \sin(\pi/N)}{R_l - R_v} = \frac{3.225 \times 10^{-3} \sin(\pi/35)}{7.74 \times 10^{-4}} = 0.374$$

The parameter F_l which represents the ratio of the viscous pressure drop in the liquid to the sum of all the pressure drops in the liquid and vapor can be determined from:

$$F_l = \frac{\Delta P_l}{\Delta P_l + \Delta P_{lv} + \Delta P_v} = \frac{1153}{1153 + 815 + 158} = .542$$

The maximum transport performance of the heat pipe on the basis of $F_l = .542$ is:

$$Q_{\max} = \frac{NNQ}{L_{\text{eff}}} (1 + \eta) F_l N_l = 357 \text{ watt}$$

The corresponding vapor Reynolds number is 6,036. The next step is to iterate the calculations based on the new Reynolds number. The iteration process is repeated until the final Reynolds number is equal to the initial value. The final iteration gives:

$$Q_{\max} = 404 \text{ watt}$$

The performance based on hydrodynamic limits is in excess of the required performance. Therefore, only a single heat pipe would be required. However, other heat transport limitations should be checked because of the high capacity achieved with gravity assist.

5.3.4 Step #4 - Other Heat Transport Limitations

Other factors which may effect the performance of the gravity assist heat pipe are vapor entrainment, sonic limit and boiling limitation. For the above design, these can be determined as follows:

(a) Sonic Limit:

The limiting axial heat flux associated with the sonic limit are included in Volume II as a derived fluid property. For ammonia at 0°C:

$$\frac{\dot{Q}}{A_v} = .834 \times 10^9 \text{ watt/m}^2$$

For the axially grooved design, the vapor flow channel diameter is $6.45 \times 10^{-3} \text{ m}$ and:

$$\begin{aligned}\dot{Q} &= \frac{\pi}{4} (6.45 \times 10^{-3} \text{ m})^2 (.834 \times 10^9 \text{ watt/m}^2) \\ &= 27,250 \text{ watts}\end{aligned}$$

(b) Entrainment Limit:

The entrainment limit can be derived from Eq. 2-80:

$$\begin{aligned}\dot{Q} &= A_v \left(\frac{\rho_v \sigma \lambda^2}{Z} \right)^{\frac{1}{2}} \\ &= \frac{\pi}{4} (6.45 \times 10^{-3} \text{ m})^2 \left[\frac{(3.391 \text{ kg/m}^3)(.026 \text{ N/m})(1.27 \times 10^6 \text{ J/kg})^2}{3.87 \times 10^{-4} \text{ m}} \right]^{\frac{1}{2}} \\ &= 626 \text{ watts}\end{aligned}$$

Where the characteristic dimension Z is assumed to be equal to the groove width.

(c) Boiling Limit

A first approximation of the boiling limit can be determined by combining Eqs. 2-82 and 2-83:

$$\left(\frac{\dot{Q}}{A} \right)_{\max} = \frac{K_{\text{eff}}}{t_w} \frac{T_{\text{sat}}}{\lambda \rho_v} \left[\frac{2\sigma}{r_n} - (\Delta P_f)_{\max} \right]$$

For ammonia at 0°C and the axially grooved design and Eq. 2-14:

$$(\Delta P_1)_{\max} = \frac{2 \sigma \cos \theta_c}{w} = \frac{2 (.206 \text{ N/m})(\cos 0^\circ)}{3.87 \times 10^{-4} \text{ m}}$$

$$= 1.34 \times 10^{-2} \text{ N/m}^2$$

where a zero wetting angle is assumed for ammonia. The ratio of the effective thermal conductance (K_{eff}) of the wick-liquid matrix and the wick thickness (t_w) is equivalent to the evaporator film coefficient. As determined in Sample Problem A, this value is:

$$\frac{K_{\text{eff}}}{t_w} \approx h_L = 8.12 \frac{\text{W}}{\text{m}^2 \cdot \text{K}}$$

Therefore, the maximum evaporator power density based on the boiling limit is:

$$\left(\frac{Q}{A}\right)_{\max} = 8.12 \times 10^3 \frac{\text{W}}{\text{m}^2 \cdot \text{K}} \left[\frac{273 \text{ K}}{(1.27 \times 10^6 \text{ J/kg})(3.391 \text{ kg})} \right] \left[\frac{2 (.206 \text{ N/m}^2)}{10^{-5} \text{ m}} - 1.34 \times 10^2 \text{ N/m}^2 \right]$$

$$= 2.67 \times 10^4 \text{ W/m}^2$$

For an evaporator length of .08 m and the vapor diameter of $6.45 \times 10^{-3} \text{ m}$, the area (A) is $1.62 \times 10^{-3} \text{ m}^2$ and the maximum input power is:

$$Q_{\max} = (2.67 \times 10^4 \text{ W/m}^2)(1.62 \times 10^{-3} \text{ m}^2)$$

$$= 43.3 \text{ watts}$$

Since this limit is lower than the required 250 W, boiling could be the limiting factor in this application. However, as pointed out in Section 2.7.3, the calculated critical superheat is sometimes one order of magnitude lower than actually measured. Test verification, therefore, would be required to determine whether this limit applies.

HEAT PIPE MANUFACTURING

Manufacturing is the single most critical step in the development of successful heat pipe hardware. Although many schemes and designs have been proposed in the past to achieve enhanced performance, very few have been successfully implemented into reliable products which can be repeatedly produced at reasonable cost. The manufacture of heat pipes embraces a number of processes and operations which are dependent on the type of heat pipe (fixed conductance, thermal control, commercial, etc.), the operating temperature of the heat pipe, the design selected and the application. The major factors which influence manufacturing processes include leak tight containment of the fluid, pressure containment, as-fabricated wick properties, materials compatibility, cleanliness, fluid purity and charge requirements. Although manufacturers are currently using a number of independent procedures, the basic processing of heat pipes is very similar. This chapter outlines the basic elements of heat pipe fabrication. A significant portion was extracted from Ref. 1 which discusses manufacturing procedures in detail. A list of heat pipe manufacturers and materials suppliers is given in Tables 6-1 and 6-2, respectively.

6.1 HEAT PIPE CONSTRUCTION

Heat pipe designs fall into two general categories: fixed conductance and thermal control. The fixed conductance heat pipe is composed essentially of five elements as shown in Fig. 6-1, namely, the envelope (or container), wick, end cap, fill tube, and working fluid. Thermal control heat pipes are special adaptations of the fixed conductance heat pipe with modifications designed to accomplish a variety of thermal control functions. Gas controlled variable conductance heat pipes, as illustrated in Fig. 6-2 require the addition of a non-condensable gas, a reservoir, and in most cases a reservoir wick to prevent liquid entrapment. Transition sections and low conductivity (Low K) sections may also be employed. Diode heat pipes will generally include a reservoir to accommodate the blocking fluid or to trap the working fluid inventory. Finally, some of the more complicated systems such as passive feedback controlled and vapor modulated heat pipes will employ a bellows reservoir and an auxiliary fluid.

TABLE 6-1. HEAT PIPE MANUFACTURERS

<u>MANUFACTURER</u>	<u>LOCATION</u>	<u>AEROSPACE</u>	<u>COMMERCIAL</u>
B & K Engineering, Inc.	Towson, Md. 21204	X	X
Dynatherm Corporation	Cockeysville, Md. 21230	X	X
Energy Conversion Systems, Inc.	Albuquerque, N.M. 87112		X
General Electric Co.	Valley Forge, PA. 19101	X	
Grumman Aerospace Corp.	Bethpage, N.Y. 11714	X	
Heat Pipe Corp. of America	Newark, N. J. 07060		X
Hughes Electron Dynamics Div.	Torrance, CA. 90509	X	X
Isothermics, Inc.	Augusta, N.J. 07822		X
McDonnell Douglas Corp.	St. Louis, MO. 63166	X	
Noren Products, Inc.	Redwood City, CA. 94062		X
Perkin Elmer	Danbury, CT. 06810	X	
Power Technology, Corp.	Ann Arbor, MI. 48103		X
Q-Dot Corporation	Dallas, Texas 75247		X
Rockwell International, Space Division	Seal Beach, CA. 90740	X	
Sigma Research Corp.	Richland, WA. 99352	X	
Thermoelectron Corp.	Waltham, MA. 02154		X
TRW Systems Group	Redondo Beach, CA. 90278	X	
Xerox Corporation/ Electro-Optical Systems	Pasadena, CA. 91107	X	

TABLE 6-2. HEAT PIPE MATERIALS SUPPLIERS

Metal Foams

Astro Met Associates, Inc.
95 Barron Drive
Cincinnati, Ohio 45215

General Electric Company
Metallurgical Products Department
Box 237, General Post Office
Detroit, Michigan 48238

Gould, Inc.
Gould Laboratories
540 East 105th Street
Cleveland, Ohio 44108

Union Carbide Corporation
12900 Snow Road
Parma, Ohio

Metal Felts

Astro Met Associates, Inc.
95 Barron Drive
Cincinnati, Ohio 45215

Brunswick Corporation*
Technical Division
1 Brunswick Place
Skokie, Illinois
*Formerly Huyck Metals Company

Wire Mesh

Cambridge Wire Cloth
P. O. Box 399
Cambridge, Maryland 21613

Michigan Wire Cloth Company, Inc.
2100 Howard Street
Detroit, Michigan 48216

Newark Wire Cloth Company
351 Vernon Avenue
Newark, New Jersey 07104

Tobler, Ernst and Traver, Inc.
420 Saw Mill River Road
Elmsford, New York 10523

Composite Screen

Aircraft Porous Media, Inc.
32 Sea Cliff Avenue
Glen Cove, New York 11542

Finned Tubing

Micro Extrusions
2871 LaMesa Avenue
Anaheim, California 94806

Minalex Corporation
Coddington Road
Whitehouse Station, New Jersey 08889

Noranda Metal Industries, Inc.
French Tube Division
P. O. Box 558
Newtown, Connecticut 06470

Porous Metals

Union Carbide Corporation
Satellite Division
1020 West Park Avenue
Kokomo, Indiana 46901

Bi-Metallic Transitions

Bi-Braze Corp.
4 Railroad Avenue
Glen Head, New York 11545

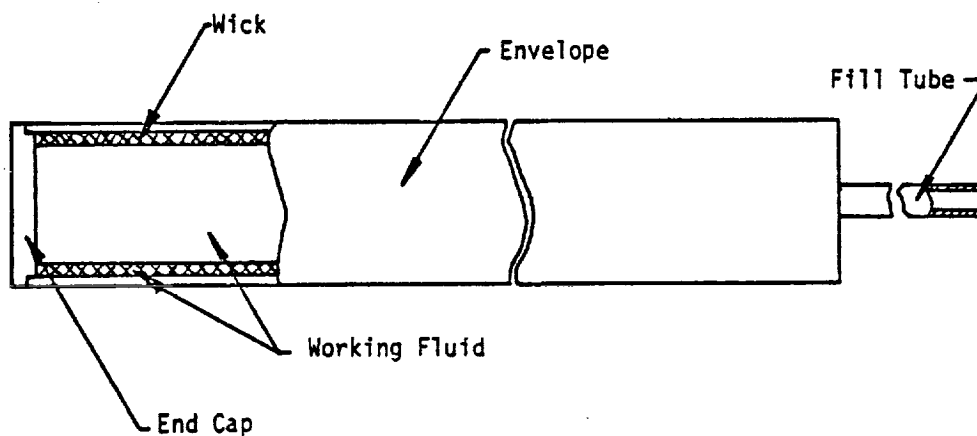


Fig. 6-1. Typical components of a heat pipe

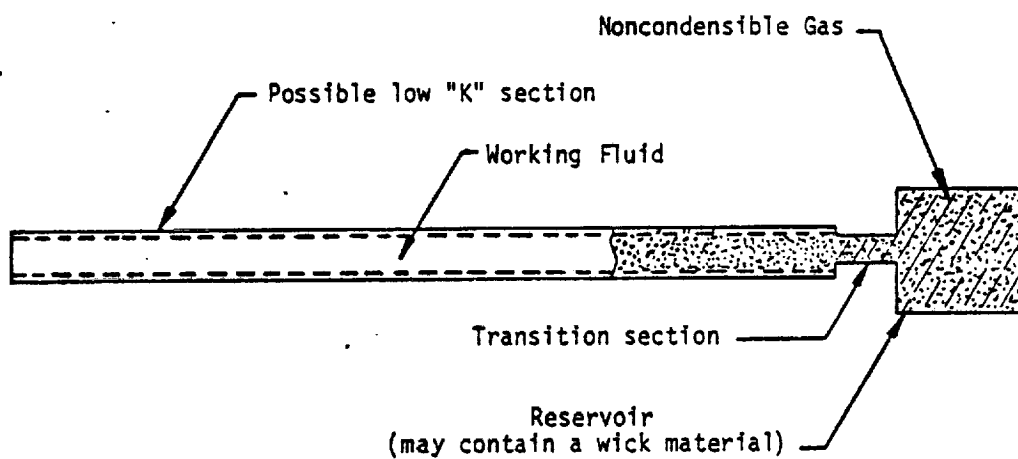


Fig. 6-2. Gas-controlled variable conductance heat pipe.

The heat pipe construction may be of any cross section required by the application (e.g. circular, square, flat plate, etc.); it may contain external flanges to simplify installation and improve thermal interfaces; and it may be bent into various shapes to accommodate system design. The internal construction can consist of an integral wick such as axial grooves extruded into the envelope, or separate wick assemblies made of wire mesh, sintered screen, or sintered fibers. Other designs include integral circumferential grooves in combination with a separate central core wick assembly. Several homogeneous and composite wick structures are presented in Fig. 6-3.

A variety of working fluids from the cryogenics to liquid metals can be used in the design of heat pipes. Envelope, wick, end cap, and fill tube materials used are selected on the basis of compatibility with the working fluid, leak tight pressure containment, fabricability, cost, availability, etc. Typical materials used in heat pipe fabrication include aluminum alloys, copper alloys, stainless steels, and carbon steels. For high temperature liquid metal applications, super-alloys and refractory metals are also employed.

6.2 MANUFACTURING FLOW PLAN

The large variety of heat pipe shapes, configurations, wick constructions, working fluids, and materials preclude the specification of a single manufacturing process and procedure. However, there is sufficient similarity to define a typical flow plan that can be employed in any heat pipe fabrication. A typical manufacturing flow chart for a fixed conductance heat pipe is illustrated in Fig. 6-4. The process consists of the fabrication and preparation of the various components, cleaning (and sometimes surface coating or passivation), assembly, welding of the end closures (end cap and fill tube), verification of mechanical integrity (leak tightness and possible pressure containment), working fluid preparation, heat pipe evacuation and charging with the working fluid and final closure of the fill tube.

Specific procedures used during each of the major steps outlined above are dependent on the shape and geometry of the heat pipe, the wick designs, materials employed for the envelope, wick and end closures and the type of working fluid. Typical procedures and manufacturing processes are outlined in the following sections. Noteworthy differences between the various types of heat pipes are as follows.

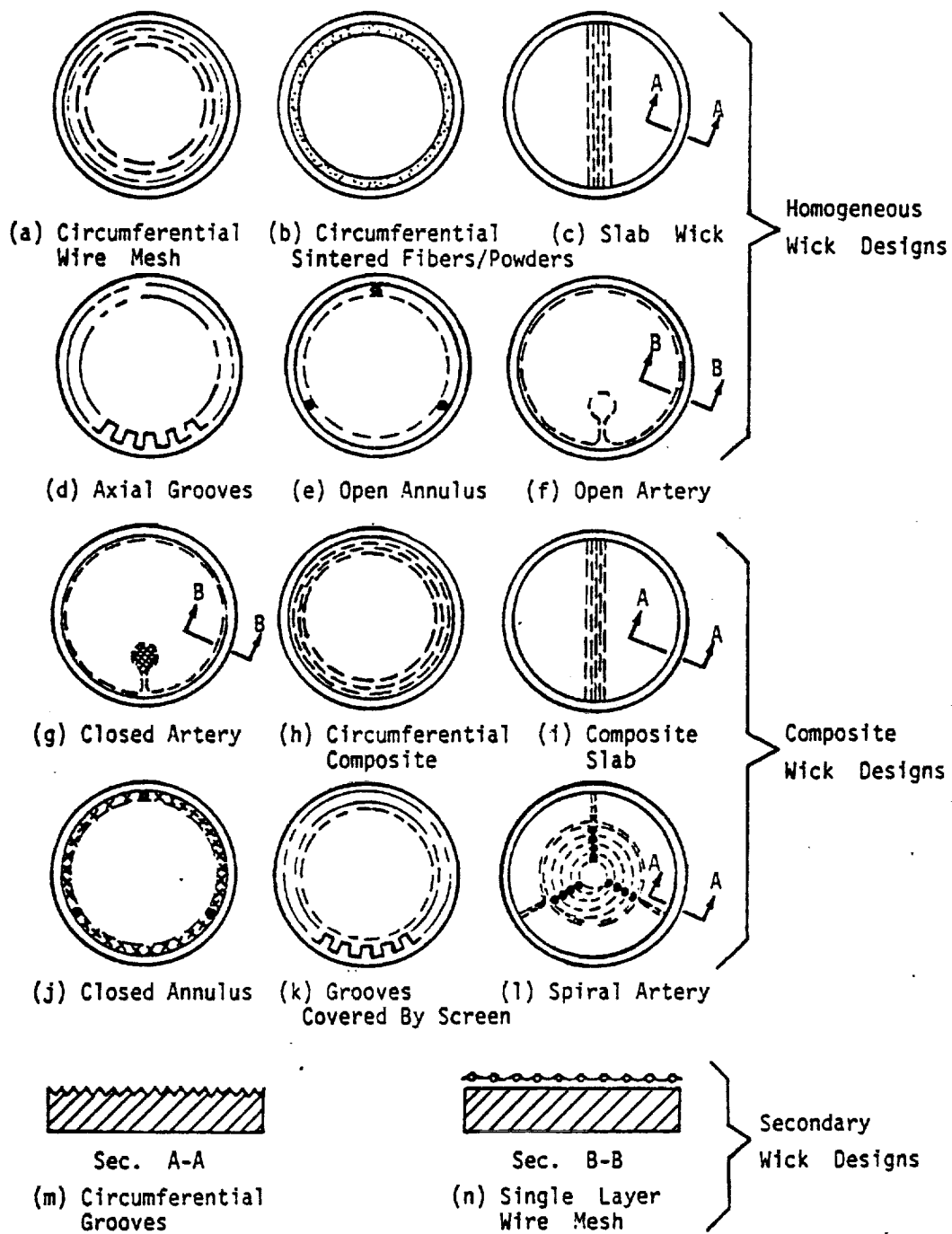


Fig. 6-3. Typical wick designs

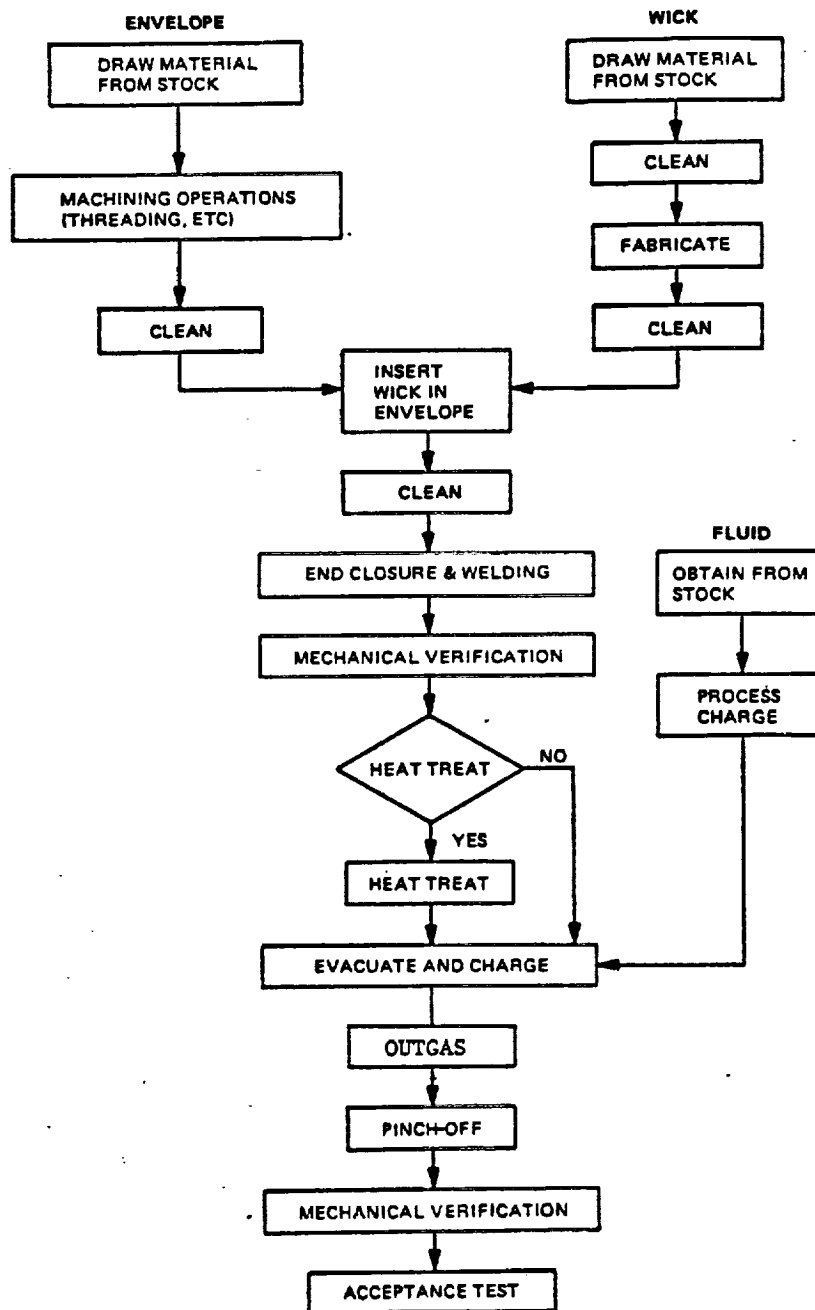


Fig. 6-4. Heat pipe manufacturing flow chart

6.2.1 Cryogenic Heat Pipes

Working fluids for cryogenic and low temperature heat pipes are very often in the gaseous state at room temperature. This requires the charging and handling of heat pipes with high internal pressures. Proof pressure tests and burst samples are generally specified, and proper safety precautions should be implemented. In addition, the charging process consists of the transfer of the fluid in a gaseous state with subsequent condensation in the heat pipe.

6.2.2 Liquid Metal Heat Pipes

All liquid metals except for mercury are solid at room temperature. The charging of liquid metal heat pipes requires a transfer station wherein the working fluid is melted under an inert environment or vacuum. In addition, special fittings and valves, etc. are needed to accommodate liquid metals. Safety precautions are also required because of the potential fire hazards.

6.2.3 Thermal Control Heat Pipes

The manufacture of thermal control heat pipes generally requires the fabrication and processing of liquid or gas reservoirs and associated wicks together with the standard components of the fixed conductance heat pipes. Gas controlled heat pipes also require the addition of a non-condensable gas prior to final closure. Thermal control heat pipe designs may also require the fabrication and processing of low thermal conductance sections (Low K) between the evaporator and condenser and/or between the heat pipe and the reservoir. A low-K section can consist of a filament wound reinforced section of the envelope whose wall thickness has been reduced to minimize axial conductance. Bi-metallic transition sections (such as aluminum to stainless steel) are also utilized to provide low conductance between an aluminum heat pipe and a gas reservoir (2).

6.3 COMPONENT FABRICATION AND PROCESSING

The manufacture of a heat pipe begins with the procurement of raw materials in accordance to the requirements of the design and commercial availability. Raw material control is required to insure working fluid compatibility and leak tight and pressure tight containment. Materials certification and verification as well as working fluid purity are dependent on the level of the desired product reliability which should be determined during the heat pipe design development phase. After the desired materials have been procured, the individual components are processed as defined in the following sections.

6.3.1 Envelope Preparation

Although heat pipe envelopes can be made of different cross-sectional shapes, commercially available round tubing is the most common configuration. If no integral grooves are used, envelope preparation simply consists of cutting the tube to the desired length. For designs requiring circumferential grooves, a threading operation employing a fine thread tap is often used. Special tools which offset rather than thread the material have also been developed (3).

Extrusion or swaging processes are normally employed to produce axially grooved tubing. Grooves have also been milled in flat stock which is then rolled and butt welded into a tube form. Experience to date indicates that the extrusion process is the best method for producing aluminum axially grooved tubing. Well defined groove forms and good dimensional control have been achieved. Mounting flanges can be extruded as an integral part of the tubing which can simplify interfacing in many applications. In addition, the ability to produce complex groove forms with aluminum has also been demonstrated with the extrusion process (4). For the intermediate to high temperature range, materials such as copper and its alloys, stainless steels, carbon steels and super alloys are required. The swaging process is the only known process which can be used effectively today to produce axially grooved tubing in these materials on a cost effective basis.

6.3.2 Wick Preparation

If the wick structure is an integral part of a heat pipe (e.g. axial grooves), separate operations for the preparation of the wick are not needed. The other wick designs illustrated in Fig 6-3 require separate manufacturing and processing prior to insertion into the envelope. Typically such wicks are either made of wire mesh, sintered screen or sintered metal fibers and powders. The processing of a wire mesh wick consists of cutting commercially available screen (see Table 6-2) to size and then form rolling or stacking multiple screen layers to achieve the desired wick geometry. Wicks fabricated of stainless steel screen are usually spotwelded together prior to insertion into the envelope. Precautions must be taken in the cleaning process to remove any contaminants (e.g. copper) introduced by the spotwelding operation. Materials that cannot be easily spotwelded such as copper or aluminum are usually rolled or formed to a geometry that can be mechanically held together when inserted into the envelope.

Wicks can also be fabricated from multiple screen layers which have been sintered together to form a slab. Slabs or tubular wick shapes can also be produced by sintering metal fibers or metal powders. Fiber and powder wicks have also been sintered directly to the envelope wall.

The important factors to be controlled during wick manufacturing are:

- (a) Cleanliness should be maintained throughout processing to avoid the introduction of contaminants.
- (b) Forming or sintering processes should be controlled to achieve the desired wick properties repeatedly (e.g. permeability and effective pumping pore size). The proximity of wire mesh screen layers and intermeshing can significantly affect the properties of this type of wick. Similarly, the compacting of fibers or powders in sintered felts also affect wick properties. Wick designs which employ wire mesh screen to form liquid flow channels such as arteries, annuli, etc., must also be controlled to meet design performance.
- (c) The size, shape and geometry of the wick design must be controlled to allow easy insertion into the envelope while providing sufficient rigidity to maintain the wick in place. "Bridges" are used to hold wick assemblies in the envelope as illustrated in Fig. 6-3 (1).
- (d) Composite wicks, such as arteries, must be properly sealed (usually by spotwelding) to achieve the desired pumping. Integrity of such wicks can be verified with hydrostatic tests as described in Chapter 8.

6.3.3 End Closures

Typical end closures (end cap and fill tube) are designed to fit the size and shape of the envelope, to provide the desired joint for welding, to give adequate strength for pressure retention and to provide access to the heat pipe for evacuation and fluid charging (fill tube). A number of end closure designs including butt joint, lipped butt joint, fillet joint and lap joint have been used. Fill tubes with various diameters are dependent on the weld process and end closure techniques employed. End closures are produced

generally by machining round stock material. The following items are critical in producing satisfactory end closures:

- (a) Dimensional control for proper fit with the envelope and also to provide the proper thickness ratio for welding.
- (b) The surface finish condition on the inside of the fill tube should be controlled to achieve a leak tight mechanical seal during closure.

6.3.4 Working Fluid

Working fluids can either be procured to the desired purity or they must be processed to remove gaseous and dissolved impurities. Fluid processing typically consists of distillation to eliminate solids and high boiling point liquids. Gases and low boiling point liquids can be eliminated by refluxing and venting or freeze/thaw cycles. The amount of refluxing or number of freeze/thaw cycles is dependent on the desired purity level.

6.4 HEAT PIPE PROCESSING AND FABRICATION

The processing and fabrication of a heat pipe includes cleaning the envelope, wick, end closure and reservoir materials; wick insertion; attachment of the end closures; possible coating or surface preparation; forming; evacuation and fluid charging. In addition, a number of in-process tests as described in Chapter 7 can be performed at various stages to verify wick properties and system integrity.

6.4.1 Cleaning

Just as extreme care is required in selecting proper heat pipe materials to avoid compatibility problems, cleaning of the component heat pipe parts is critical to avoid similar consequences. As seen in the heat pipe manufacturing cycle in Fig. 6-4, contaminants can be introduced into the heat pipe through a dirty wick, dirty envelope, impurities in the working fluid, etc. In fact, every operation that is not performed properly can be a source of contamination. A summary of problems that can arise due to improper cleaning techniques is as follows:

- (a) Physical clogging of wall and wick capillary surfaces can impair both heat pipe transport and conductance.

- (b) Non-condensable gas generation reduces both heat pipe conductance (loss of condensation area) and transport capacity (bubbles in arterial wicks).
- (c) A decrease in the wettability of the wick and corresponding loss of pumping.
- (d) Adverse changes in fluid properties, such as surface tension, wetting angle, and viscosity.
- (e) The loss of structural integrity of the container wall due to galvanic corrosion, crevice corrosion, and porosity.

Unfortunately, many of these problems cannot be uncovered until the pipe is charged, sealed and tested. In some cases a long time can elapse until degradation is noticed. By then, it is usually too late to provide corrective action. Hence, thorough cleaning procedures must be included in any heat pipe fabrication to prevent these problems from occurring and to produce a more reliable product. Moreover, to be cost effective and reliable, the cleaning procedure should also be simple and as free as possible from human error.

6.4.1.1 Cleaning the Envelope

The heat pipe tube or envelope receives its primary cleaning after dirty operations (such as machining) have been completed. Machining will involve cutting the tube to length and preparing the ends for welding, and in some cases cutting threads into the inside surface to provide a circumferential wick. An assortment of debris such as metal chips, cutting oil, grease, moisture, etc., can be expected after machining. The cleaning operation, therefore, has a number of aims, namely to:

- (a) Mechanically remove particulate matter, such as metal chips which may clog the porous wick material and/or damage the periphery during subsequent wick insertion.
- (b) Remove water that can cause corrosion, attacking both aluminum and stainless steel, as well as providing a galvanic coupling between the envelope and wick if dissimilar materials are used. A buildup of

particulate reaction products as well as gas generation are the principal results. Loss of container structural integrity due to crevice corrosion and porosity may also result from the presence of water.

- (c) Remove contaminants, not necessarily corrosive, but which may impair fluid properties and the heat pipe wick. Examples of these contaminants are the variety of oils and greases used in metal cutting and removal operations, extruding, forming, etc. These contaminants may coat the internal surfaces and increase the contact angle, or may dissolve in the working fluid and change its transport properties.
- (d) Chemically clean and prepare the surface so as to be nonreactive with subsequent manufacturing environments, the wick, and the working fluid.

6.4.1.2 Cleaning of the Wick

Wick cleaning and pretreatment is at least as important as the need for envelope cleaning. Obviously gas generation is just as likely to come from a "dirty" wick as from other improperly cleaned parts. Oil and grease imbedded in either the fine wire mesh or sintered screen material used to construct wicks must be removed to assure proper heat pipe performance. Foreign substances conducive to gas generation might be introduced in the construction process therein requiring that a cleaning process be employed following the wick's fabrication. For example, if a copper electrode is used to assemble a stainless steel wick with tack-welds, some copper particles may become imbedded in the screen. To remove this material, which is incompatible with ammonia, a nitric acid rinse would be required. However, it is preferable to eliminate this potential problem by using tungsten electrodes. Once the wick has been cleaned, surface passivation and/or pretreatment is also often required for both the wick and the container to avoid reaction with the working fluid or to enhance wetting.

6.4.1.3 General Cleaning Procedures

A variety of methods are currently employed to clean heat pipe envelopes. These include solvent cleaning, vapor degreasing, alkaline cleaning, acid cleaning, passivation, pickling, ultrasonic cleaning, and vacuum firing. More than one technique may be used in a particular cleaning operation. A brief description of some of these techniques follows. A more complete presentation may be found in Ref. 1.

Vapor Degreasing

Vapor degreasing is a generic term applied to a cleaning process that typically employs the hot vapors of a chlorinated solvent to remove residue - particularly oils, greases and waxes. Trichloroethylene is a common solvent.

A vapor degreasing unit consists of an open steel tank with a heated solvent reservoir, or sump at the bottom and a cooling zone near the top. Sufficient heat is introduced into the sump to boil the solvent and generate hot vapor. Because the vapor is heavier than air, it displaces the air and fills the tank up to the cooling zone where it condenses, thus maintaining a fixed level and creating a thermal balance. The condensation of the vapor on the cool workpiece and the return of the liquid acts to dissolve and remove any grease or residue.

Some degreasing units are also equipped with facilities for immersing the work in warm or boiling solvent and for spraying workpiece surfaces with clean solvent as a supplement to vapor cleaning. The efficiency of the liquid phase of the cleaning cycle can be further augmented by the application of ultrasonic energy.

Solvent Cleaning

Solvent cleaning is a process of removing oil, grease, loose metal chips, and other contaminants from the surfaces of metal parts by the use of common organic solvents, such as aliphatic petroleums, chlorinated hydrocarbons, or blends of these two classes of solvents. Cleaning is usually performed at, or slightly above, room temperature. Parts are cleaned by being immersed and soaked in the solvent, with or without agitation. Parts that are too large to be immersed are sprayed or wiped with the solvent.

Ultrasonic vibration is sometimes used in conjunction with solvent cleaning to loosen and remove residue from deep recesses or other difficult-to-reach areas. This reduces the time required for solvent cleaning of complex shapes.

Although some of the solvents used in solvent cleaning are the same as those used in vapor degreasing, solvent cleaning differs in that it is commonly performed at room temperature. In vapor degreasing, parts may be degreased by exposure to the solvent vapor as well as by immersion in the hot solvent; drying is accomplished by evaporating the solvent from the parts while they are suspended in the hot vapor. In solvent cleaning, parts are dried at room temperature or by the use of external heat, centrifuging, or an absorptive medium.

Alkaline Cleaning

Alkaline cleaning is employed for the removal of oily, semi-solid or solid materials from metals before they are electroplated, conversion coated, or otherwise finished or processed. To a great extent, the solutions used in alkaline cleaning depend on their detergent properties for cleaning action and effectiveness. Agitation of the solution and movement of the workpieces through it, although important, are secondary in their effect.

The principal methods employed in alkaline cleaning are soaking, spraying, and electrolytic. Other methods are variations incorporating the essential features of these three.

A universal (or all-purpose) cleaner is not available because the requirements for various cleaning jobs are too diverse and are not mutually compatible. Therefore, compromises are made in formulations to fit particular applications. The cleaning effectiveness of alkaline compounds is attributed mainly to the action of "builders," which are the principal bulk components of the formulation. Most builders are sodium compounds (carbonates, phosphates, silicates, and hydroxides), which provide alkalinity and other desirable properties at low cost.

Acid Cleaning

Acid cleaning is a process in which a solution of a mineral acid, organic acid, or acid salt (possibly in combination with a wetting agent and detergent) is employed to remove oxide, shop soil, oil, grease, and other contaminants from metal surfaces, with or without the application of heat. The distinction between acid cleaning and acid pickling is a matter of degree, and there is often some overlapping in the usage of these terms. In general, however, acid pickling refers to a more severe treatment for the removal of scale from semi-finished mill products, forgings, and castings. Acid cleaning is the term most frequently used when the acid solution is employed for final or near-final preparation of metal surfaces prior to plating, painting, or storage.

Ultrasonic Cleaning

Ultrasonic energy can be used in conjunction with several types of cleaners, but it is most commonly applied to chlorinated hydrocarbon solvents, water, and water with surfactants. Ultrasonic cleaning, however, is more expensive than other methods because of the higher initial cost of equipment and higher maintenance cost. Consequently, the use of this process is largely restricted to applications in which other methods have proved inadequate.

Passivation

Treatment of stainless steels after fabrication with oxidizing chemicals is known as chemical cleaning, or passivation. If iron particles or other substances have become embedded in the surface during fabrication or polishing operations, they must be removed. Otherwise, these minute foreign particles can promote discoloration, rusting, or even pitting. Besides dissolving such particles, the oxidizing action of the bath also tends to enhance the corrosion resistance of stainless steels by fortifying the passive natural surface film.

Passivation is done generally by immersing the stainless steel part in a nitric acid solution and then rinsing in clear running water, and drying. If immersion is impractical the acid solution may be applied with a suitable swab and then removed by rinsing with water. Nitric acid is recommended because it will dissolve any iron or copper particles and leave the stainless steel unaffected. It is necessary that the surface of the steel be free of scale, heavy grease, and oil if the chemical treatment is to be effective.

6.4.1.4 Sample Cleaning Procedures

This section presents sample cleaning procedures for aluminum and stainless steel heat pipes that have been utilized in NASA flight hardware during the past four years or more.

Aluminum Tubes

NASA Goddard Space Flight Center conducted an extensive development effort to qualify axially grooved aluminum heat pipes for the ATS-6 spacecraft (5). As part of this effort, cleaning and heat treating procedures were established for the aluminum tubing. This procedure, which is listed in Table 6-3 with slight modifications, is recommended for 6061 and 6063 aluminum axially grooved or circumferentially threaded envelopes. The procedure is relatively simple, employs equipment generally available to the industry and if properly implemented, it will provide a consistently clean surface.

The procedure requires an initial mechanical brush cleaning with 1,1,1 trichloroethane of the as received, or threaded tube. This operation is used to dislodge the larger particles which subsequent flushing may not accomplish. The solvent, 1,1,1 trichloroethane, is safer to use than trichloroethylene, which has already been disallowed in many states. It is also convenient to use, particularly in a through-the-tube flushing operation. A non-etch alkaline cleaner (cf. Table 6-4) is next used followed by a chromated deoxidizer (cf. Table 6-5). In contrast to a nitric acid/sodium sulfate deoxidizer, the chromated deoxidizer is less aggressive and provides a more corrosion-free surface. The tubing is

TABLE 6-3. RECOMMENDED CLEANING PROCEDURE FOR ALUMINUM TUBES

(Applicability - Aluminum 6061 or 6063 axially grooved or radially threaded tubes)

Procedure

1. Clean in cold 1,1,1 trichloroethane with bristle brush or wire extension. Periodically clean brush between strokes.
2. Flush internal surface with cold trichloroethane; dry with filtered air and cap pipe ends.
3. Immerse in non-etch alkaline cleaner for 5 mins. (minimum). Refer to Table 6-4 for materials, and temperature.
4. Follow with a two min. tap water rinse, raising and lowering tube during rinsing.
5. Immerse in chromated deoxidizer. Refer to Table 6-5 for material, time and temperature.
6. Follow with a two min. tap water rinse, raising and lowering tube during rinsing.
7. Thoroughly dry inside surface with forced filtered air.
8. Rinse with anhydrous isopropyl alcohol.
9. Force dry with clean, filtered, dry nitrogen heated to 160°F.
10. Cap pipe ends.
11. If applicable, insert the wick, rinse with isopropyl alcohol and dry as in Step 9.
12. If applicable, vacuum outgas tube/wick assembly at elevated temperature after welding.
13. If heat treating is required after welding:
 - (a) Evacuate pipe for 4 hrs. at 600°F and leak check (Note: This will accomplish vacuum outgassing of Step 12.)
 - (b) Seal evacuated heat pipe.
 - (c) Perform heat treat operations on sealed pipe.

TABLE 6-4. EXAMPLES OF NON-ETCH ALKALINE CLEANERS		
Material	Concentration	Temperature, °F
Ridoline No. 53 (Amchem Products Co.)	2-10 oz/gal	140-180
Oakete No. 164 (Oakite Products Co.)	2-10 oz/gal	140-180
Kelite spray white (Kelite Corp)	40-60% by volume	Ambient
A-38 (Pennwatt Corp)	4-8 oz/gal	160-180

TABLE 6-5. EXAMPLES OF CHROMATED DEOXIDIZER SOLUTIONS (IMMERSION TYPE)			
Material	Concentration	Temperature, °F	Immersion time
Mixture of: Chromated deoxidizer replenisher No. 17 ^a (Amchem Products Co.)	2-6 oz/gal	Ambient to 120	5 to 30 min
Nitric Acid 42° Be	10-20% by volume		
Mixture of: Chromated deoxidizer replenisher No. 17 ^a	2-6 oz/gal	Ambient	5 to 30 min
Sulfuric acid 66° Be	4-7% by volume		

^aDeoxidizer make up No. 7 to be used for initial makeup

then dried with forced, filtered air; followed by an anhydrous isopropyl alcohol rinse; followed again by drying with clean, filtered and heated nitrogen to assure complete water removal.

At this point, if applicable, wick may be inserted into the envelope. Depending on the type of wick design and the cleanliness associated with its installation, an alcohol rinse may be appropriate. In applications where the operating temperature may be 50°C or higher, vacuum outgassing at a temperature above the operating condition is recommended to remove absorbed gases. If the aluminum tube is to be heat treated after welding operations, Steps 13a, b, and c of the procedure are recommended.

The foregoing procedure is based, in part, on facilities being available for the tube lengths and/or configurations being processed. For example, immersion tanks may not be available for exceptionally long tubes, and their cost for a "one shot deal" would not be justified. Alternate methods such as flushing can be equally effective, but should be reviewed by qualified personnel before implementation.

Stainless Steel Tubes

Although the experience with stainless steel is somewhat limited, it would appear that all the processes described in the literature are adequate in that gas generation is insignificant for most working fluids, with water being the major exception. However, long-term gas generation, particularly at lower temperatures, has not been analyzed as extensively for stainless steel envelopes as it has for aluminum envelopes.

An examination of the various procedures indicates that ultrasonic cleaning and vacuum firing may not be as economical as passivation treatments. Therefore, a passivation treatment is recommended for stainless steels principally because of their general use and availability in industry. The procedure, given in Table 6-6, is derived from Ref. 1. Table 6-7 lists examples of passivating solutions.

Note that even though the presence of water on stainless steel is not as corrosive as it is on aluminum, extensive drying operations have still been included as an assurance against possible contamination later on in the manufacturing process.

Wick Assemblies

There is little information available on the cleaning of wicks. Wherever possible, the wick material should be the same material or at least come from the same generic group as the envelope. This is required to avoid galvanic corrosion within the heat pipe assembly.

TABLE 6-6. RECOMMENDED CLEANING PROCEDURE FOR
STAINLESS STEEL TUBES

[Applicability - Stainless Steel 300 series, radially threaded tubes]

Procedure:

1. Clean in cold 1,1,1 trichloroethane with bristle brush on wire extension. Periodically clean brush between strokes
2. Flush internal surface with cold trichloroethane, dry with filtered air and cap pipe ends
3. Immerse in passivating solution. Refer to Table 6-7 for materials, temperature, and time
4. Follow with a two min tap water rinse, raising and lowering tube during rinsing
5. Thoroughly dry inside surface with forced filtered air
6. Rinse with anhydrous isopropyl alcohol
7. Force dry with clean, filtered, dry nitrogen heated to 160°F
8. Cap pipe ends
9. If applicable, insert wick, rinse with isopropyl alcohol and dry as in step 7

TABLE 6-7. - EXAMPLES OF PASSIVATING SOLUTIONS

Material	Concentration	Temperature	Immersion time
Nitric acid	35-65% by volume	Ambient	30 min to 2 hr
Mixture of: sodium dichromate or potassium dichromate	1 - 4 oz/gal	Ambient	30 min to 2 hr
Nitric acid	15-30% by volume		

In all cases, unless the wick is integral with the container, it should be cleaned prior to insertion into the tube. Generally the cleaning procedure employed for the tube material will be applicable to the wick. If the wick is a spotwelded assembly, a nitric acid cleaning may be required to remove residual copper deposited by the electrodes. Once inserted into the tube a degrease or alcohol rinse can be used depending on the amount of handling that was required.

One final note, whenever an item has been cleaned it should be stored in a plastic bag until it is required for further use. The bag should be either backfilled with an inert gas or kept in a clean room to avoid contamination from the ambient environment. In general, the various operations should be performed in fairly rapid sequence to avoid storage for long duration where the possibility of contamination is increased. Similarly, the individual operations should be done in proximity to one another to lessen the danger of contamination during transportation.

6.4.2 Heat Pipe Assembly and Closure

Assembly of heat pipe parts includes welding the end cap and fill tube, and forming and inserting the wick if applicable. Since parts have been thoroughly cleaned, they should be assembled immediately following the cleaning if practical. Otherwise, cleaned heat pipe parts should be stored in a clean dry atmosphere to prevent contamination by vapor, smoke, and dust suspended in air. Clean gloves should be worn while handling parts to prevent contamination by skin oils and acids.

6.4.2.1 Wick Forming and Insertion

Manual forming and insertion of wrapped-screen wicks can be accomplished as follows. The assembled wick must not contain wrinkles. To prevent this, the screen can be wrapped on a clean mandrel. The total diameter of mandrel and wrapped screen should be only slightly less than the heat pipe inside diameter so that the residual stress in the coiled screen will force it against the pipe wall when it is released from the mandrel. Also, the screen ends must be even, and the screen must be positioned properly so the installation of end caps will not interfere with or crush the screen. To insure physical contact between the screen layers and the pipe wall, a tapered plug or ball may be forced through the wick. A helical spring with an unstretched diameter slightly larger than the wick inside diameter is sometimes used to hold the screen layers in contact. It can also be installed with the aid of a mandrel. The length of the stretched spring must not greatly

exceed that of the installed length or when it is released from the mandrel, axial forces may displace the screen. With the wick properly positioned in the pipe, the end caps are then welded on.

6.4.2.2 End Closure Welding

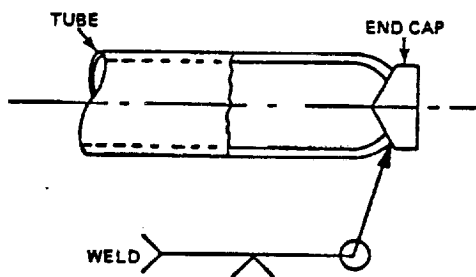
If the fill tube is not an integral part of the end cap, it should first be welded to its end cap. End caps with or without a fill tube are usually welded to the pipe ends. High quality welded joints are required at all seams since porosity or cracks in the weld can lead to a loss of the working fluid. To minimize the probability of this failure, inspections should be performed to verify the adequacy of the seal. A number of welding techniques are available. However, gas torch welds, e.g., using oxyacetylene gases, are generally not recommended because of the presence of flux. Oxygen and filler metals tend to recontaminate the cleaned parts; tungsten inert gas welding (TIG), either manual or automatic, and electron beam welding (EBW) have been found to be satisfactory for heat pipe welding.

TIG welding is an electric arc welding process which uses a sharp tipped tungsten electrode surrounded by an annular shield of inert gas flowing from a torch tip. Filler metals are not generally used for heat pipe welding, but they may be integral parts of the end caps, e.g., the lip of the lipped butt joint shown in Fig. 6-5 can serve as filler metal. This process does not employ a flux and therefore, TIG welding does not contaminate the cleaned heat pipe part. The EB weld is made in a vacuum chamber, and it eliminates the formation of the surface compounds from the metal and air. In addition, it enables one to produce a welded joint with a minimum heat affected zone, and consequently, the joint properties may approach those of the parent metal. Although ideal for heat pipe welding, the investment cost in equipment for EBW may exceed that for automatic TIG by more than 100% and that for manual TIG by an order of magnitude. Hence, the choice of the welding process is dependent upon the available equipment; and the investment in equipment depends greatly upon the quantity of production and the required quality of the products.

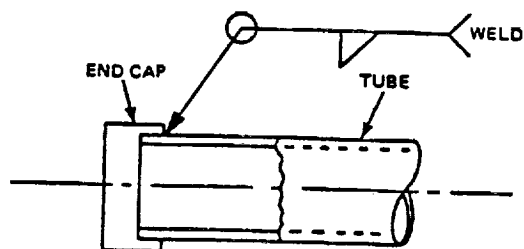
6.4.3 Evacuation and Charging

6.4.3.1 Outgassing Process

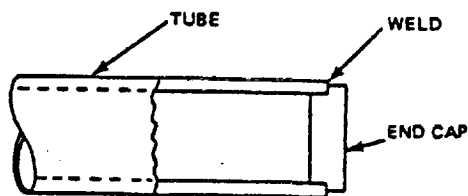
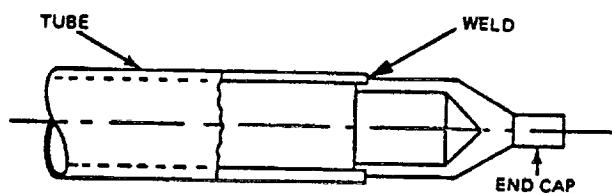
Prior to charging, a heat pipe must be evacuated to remove materials that may subsequently appear as unwanted non-condensibles, or that will chemically react with the working fluid to form undesirable corrosion products. The non-condensibles are due not only to the



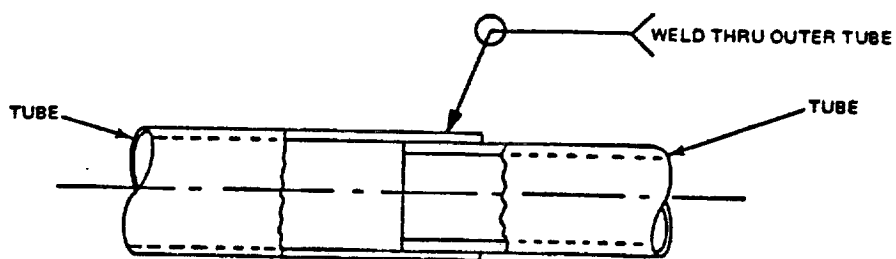
a. 15-Degree Bevel Joint Design



b. Fillet Joint Design



c. Square Butt and Fillet Joint Design



d. Lap Joint Design

Fig. 6-5. Typical end cap weld joints

free gas in the pipe but also to the molecules absorbed on the metal surface. Removal of free gases in the pipe can be done simply by pumping down with a vacuum pump. Removal of absorbed gas requires the evacuation of the pipe at elevated temperatures. The time required to desorb surface contaminants is usually reduced with increased temperature. However, metals may lose their strength at high temperature. For example, if the loss of strength cannot be tolerated, aluminum should not be evacuated at a temperature higher than 350°F (450°K). The minimum evacuation temperature for stainless steel has been suggested to be 400°F (478°K). However, if stainless steel is used for a liquid-metal heat pipe, the heat pipe operating temperature may greatly exceed 400°F (478°K). A general rule is to evacuate the pipe at a temperature greater than the heat pipe operating temperature. The evacuation time should be of sufficient duration to achieve a vacuum level of less than 10^{-2} microns.

6.4.3.2 Evacuation and Flushing

Evacuation and charging are two processes that are closely related. Fig. 6-6 shows a flow chart for an evacuation and charging procedure used by many heat pipe manufacturers (1). The close relation between evacuation and charging can be seen in this chart, and these processes are often performed within the same equipment set-up. Figure 6-7 shows a schematic of a station for both evacuation and charging. A typical procedure is as follows: with valve B closed and valves A and C open, the pipe is first pumped down at the ambient temperature; and then, the pumping is continued while the pipe is heated. The temperature of the heat pipe and the pumping time depend, of course, on the pipe material and its eventual operating temperature as described in the previous paragraph. This process is sometimes called vacuum bakeout. After completion of this vacuum bakeout process, the pipe is flushed with a small amount of fluid. For this purpose, the fluid in the charge bottle is first heated above the temperature of the heat pipe. Momentary opening of valve B then allows a small amount of flush charge to be dumped into the pipe. After the pipe is flushed in this manner once or twice, the pipe is ready for charging.

6.4.3.3 Fluid Charging

Details of the charging process depend on the state of the working fluid at the ambient temperature. If the fluid is in the gaseous state at room temperature, such as the case for the cryogenic heat pipe fluid, the charge can be introduced from a cylinder containing gas of high quality. The amount of charge can be measured by the gas pressure in the pipe at room temperature. Hence, the charging process consists of closing valve A

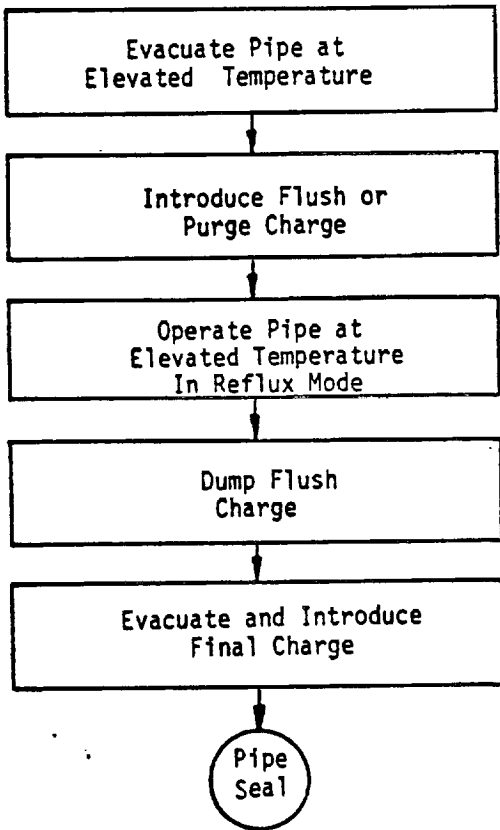


Fig.6-6. Flow chart -- heat pipe evacuation and charging

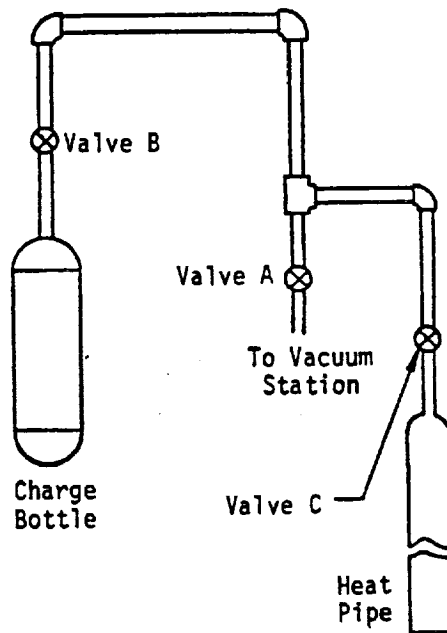


Fig. 6-7. Schematic of heat pipe evacuation and charging station

and opening valves B and C. When the required amount of fluid has been transferred into the pipe, valves B and C are closed. The pipe is then ready for pinch-off and final sealing.

If the charge fluid is a liquid, volumetric displacement or distillation of a known amount of fluid is employed. Solids are generally melted and distilled into the heat pipe in applications that require high purity and quality. Liquid metals and some other fluids may require refluxing at a temperature above the normal operating range, and subsequent bleeding before sealing. In some commercial applications, the liquid or solid may be poured into the tube and then the system is evacuated prior to the final closure. This method can result in a loss of working fluid, and some means of control, such as weight verification might be needed.

6.4.4 Charge Tube Pinch-Off

The manufacture of the heat pipe is essentially completed with the exception that the pipe has a closed valve attached to the fill tube. It is necessary to sever the pipe from the valve and to form a permanent seal. In this process, no gas must enter the pipe and no fluid should be lost from the pipe. A closure technique, which has proven both economical and reliable, consists of:

1. Crimp seal (flatten and pinch) the fill tube to form a temporary leak-proof closure.
2. Sever the valve from the pipe by making a cut in the flattened area of the fill tube on the valve side of the crimp seal.
3. Weld the cut end of the fill tube by TIG or EB welding and remove the crimping tool.

REFERENCES

1. Edelstein, F., "Heat Pipe Manufacturing Study," Grumman Aerospace Corp., Final Report to NASA, NAS5-23156, August 1974.
2. Harwell, W., and Canaras, T., "Feasibility Study to Use Heat Pipes to Control Temperatures of SIPS Canister," Concept Evaluation Phase for NASA, NAS5-2234, August 1975.
3. Wright, J. P., "Flexible Cryogenic Heat Pipe Development Program" CR-152027, July 1977.
4. Harwell, W., "Covert Axially Grooved Heat Pipe Analyses and Test Data," CR-135156, December 1976.
5. Berger, M. E., and Kelly, W. H., "Application of Heat Pipes to the ATS F Spacecraft," ASME Paper No. 73-ENAS-46, July 1973.

MATERIALS COMPATIBILITY

Long system lifetimes can be insured only by selecting envelope, wick and welding or brazing materials which are compatible with each other and with the working fluid. Performance and system degradation can occur as a result of chemical reaction or decomposition of the working fluid and corrosion or erosion of the container or wick. The most common types of heat pipe compatibility problems are listed in Table 7-1. It can be seen that certain basic questions should be asked when evaluating material fluid combinations.

- (1) Do they react chemically with each other at the operating temperature?
(This includes the formation of alloys and intermetallic compounds.)
- (2) Will they tend to set up a galvanic cell?
- (3) Are any of the materials soluble in the working fluid at the operating temperature?
- (4) Will any of the structural materials catalyze the decomposition of the working fluid at the operating temperature?

The following sections cover the most common types of compatibility problems. However, since the level of corrosion which can be tolerated in a heat pipe is extremely small, the results of most ordinary corrosion studies can be used only as a guide to the intelligent selection of heat pipe materials. Each new combination must still be proved by performing life tests.

7.1 LOW TEMPERATURE CORROSION

Most metals are found in nature as ores, and energy must be supplied to reduce them to the metallic state. This suggests that the metallic state is a high energy state; and, consequently, metals will generally combine with other substances to revert to a lower energy state. This basic process is generally referred to as corrosion. According to thermodynamics, the driving force is the difference between the Gibbs Free Energies, ΔG , of the reactants and products (1). For any reaction, ΔG is related to the equilibrium constant, K_e , for the reaction:

$$\Delta G = - R T \ln K_e \quad (7-1)$$

TABLE 7-1. GENERAL COMPATIBILITY PROBLEMS IN HEAT PIPES	
Effects	Causes
Decrease in Heat Pipe Conductance	Noncondensing gas reaction product
	Outgassing of container, wall, wick, or fluid
	Decomposition of working fluid generating noncondensing gas
Decrease in Heat Pipe Transport Capability	Wick plugged with solid precipitate and unable to transport working fluid
	Fluid flow disrupted by gas bubbles in wick
	Decrease of wick wettability due to chemical reactions
	Decrease in surface tension of liquid due to dissolved reaction products
	Increase in viscosity of fluid due to dissolved reaction products
	Wick dissolved and unable to transport working fluid
Failure of Container Wall	Galvanic corrosion of container wall
	Solubility of container wall in working fluid

The reactions involve the transfer of electrons between the chemical species. A definite electromotive force is associated with such an exchange between two species. The emf is related to the Gibbs Free Energy by:

$$\Delta G = - n F E \quad (7-2)$$

where F is the Faraday number and n is the number of electrons transferred. The combination of Eqs. 7-1 and 7-2 yields:

$$E = \frac{R T}{n F} \ln K_e \quad (7-3)$$

For the reaction,



Eq. 7-3 would be expressed as:

$$E = \frac{R}{n} \frac{T}{F} \ln \frac{(C)(D)}{(A)(B)} \quad (7-5)$$

Thus, if the reaction expressed by Eq. 7-4 proceeds to the right, the product of the concentrations of C and D are larger than the product of the concentrations of A and B. The electromotive force, E, is then positive. Similar reasoning shows that if the reactants are present to a greater extent than the product at equilibrium (the reaction does not occur) the emf will be negative.

Extensive tables which list the characteristic emf for different electrochemical reactions in various solutions are presented in References (1), (2), and (3). A short list of some common materials in the order of their decreasing activity in aqueous solutions is given in Table 7-2. The reader is referred to Ref. (1) for a thorough discussion of the utilization of such data. Special attention must be given to determine whether the tables being used give oxidation or reduction reactions in their format, since the emf's are of opposite sign in the two cases. The farther apart two materials are in this table, the more likely they are to cause a corrosion reaction if they are exposed to a common liquid bath.

The fact that the emf indicates that a reaction can take place does not necessarily mean that it will occur. In electrochemical reactions, the rate is generally determined by the current flow; and this is subject to many variables (4), e.g., surface configuration, deposition of products, diffusion rates of current carrying species, etc. Thus, even though thermodynamic considerations indicate that the reaction should proceed spontaneously, kinetic factors may cause it to proceed at an extremely slow rate. Emf differences can occur between different concentrations of a single species as well as between separate species (1). Different concentrations of a single species occur in a heat pipe between the condenser and the evaporator because of the concentrating effect of the evaporator process on dissolved materials.

In water heat pipes the presence of a small amount of dissolved air is very detrimental, not only because the air is swept to one end of the heat pipe to act as a gas plug, but also because the presence of oxygen in aqueous solutions generally increases the reaction rate of galvanic processes (4).

Some metals owe their stability to the presence of a continuous coat of oxide, usually amorphous, on their surfaces (5). This is the case for aluminum, stainless steel, and the super-alloys (Inconel, Hastelloy; etc.). Aluminum is protected by a tightly adhering layer of aluminum oxide, while the alloys are covered with an amorphous layer of chromium oxide. As long as these coatings remain intact the metals tend to be very unreactive. But, if they are exposed to substances which dissolve the oxide, they generally corrode rapidly. (For instance, aluminum is attacked rapidly when exposed to a sodium hydroxide solution.)

TABLE 7-2. RELATIVE ELECTROCHEMICAL ACTIVITY OF SOME COMMON MATERIALS RELATIVE TO HYDROGEN					
EMF	Material	Alloys/Condition	EMF	Material	Alloys/Condition
2.34	Magnesium		0.23	Lead	
0.76	Zinc		0.23	Tin	
0.63	Alclad 3003	Clad with 6061, 7075	0.20	Nickel	Active
0.54	Aluminum Alloys	5056, 3003, 1100, 6061-T6	0.20	Inconel	Active
0.49	Cadmium		-0.18	Copper	
0.48	Aluminum Alloys	7075, 6061-T4	-0.20	Bismuth	
0.45	Aluminum Alloys	2014-T6, 2024-T3	-0.24	Stainless Steel	304 (Passive)
0.40	Steel	Mild	-0.24	Stainless Steel	316 (Passive)
0.40	Iron	Wrought	-0.24	Nickel	Passive
0.35	Iron	Cast	-0.24	Inconel	Passive
0.25	Stainless Steel	410 (Active)	-0.79	Silver	
0.25	Solder	50% Tin, 50% Lead	-0.82	Chromium	Complete Surface Oxide
0.25	Stainless Steel	304 (Active)	-1.3	Gold	
0.25	Stainless Steel	316 (Active)	-1.3	Platinum	

7.2 HIGH TEMPERATURE CORROSION

7.2.1 Oxygen Corrosion

If a metal does not form a tightly adhering coating of oxide, it will often corrode in air at an accelerating pace as the temperature is increased. This is due to the direct oxidation of the base metal. The exact mechanism of attack is still argued (4) (6).

The presence of oxides (or other impurities) can also affect the corrosion resistance in other ways. Some oxides (especially alkalies) can dissolve a protective coating off the base metal and thus increase the rate of reaction, while other oxides can form tightly bound barrier coatings and thus inhibit corrosion. Brewer (7) gives thermodynamic data on many oxides. From the values of the free energies of formation, estimates can be made of the relative stabilities of the oxides of the fluid and the structural materials (8) (9). Use of these properties has been made in the purification of some liquid metal heat pipes as discussed in Refs. (10) and (11).

7.2.2 Simple Solution Corrosion

A common phenomenon is the formation of a simple solution of the container material in the liquid. This type of corrosion leads to uniform thinning of the wall unless some constituents of the alloy are preferentially dissolved. In this latter case the surface becomes pitted. Attempts have been made to treat such solution attacks theoretically, but the rather involved equations which result are usually of such a nature that errors of a few percent in some of the physical properties used result in errors of orders of magnitude in the prediction of the solution rates (12).

Normally, the rate of solution is limited by the mechanisms involved in transferring the solid atoms (molecules) into the bulk of the solvent. This transfer involves two steps: the crossing of a surface barrier, and the diffusion through the boundary layer in the liquid. If the first step is the controlling one, then the rate of corrosion will be independent of the rate of circulation of the work fluid. However, if the second mechanism is controlling, the hydrodynamic conditions can have a more pronounced effect on corrosion rates. Thus, if the flow rate is such that diffusion will not occur against it, the solution will become saturated at the evaporator as the solvent continues to become vapor and solute particles will precipitate out. Normally, the most significant effect of this type of corrosion is the plugging of the flow channels rather than loss of metal at the opposite end of the heat pipe. With low flow rates, a reverse effect can be observed

in which the wall material dissolves readily at the hot end; but diffusion results in a solution at the lower temperatures of the condenser, which then becomes plugged.

Another type of concentration gradient mass transfer can occur if metals which can form alloys or compounds are used in the heat pipe. Then, if one metal dissolves and is transferred in the fluid to where it can form an alloy or compound, it will never build up to a high enough concentration in the liquid to slow or stop the rate of solution; and thus failure will occur as a result of the destruction of the wick or the formation of a hole in the container wall.

7.3 EXPERIMENTAL RESULTS

The discussions earlier in this chapter have indicated some basic compatibility considerations which must be taken into account to narrow down the list of candidate materials for use in particular heat pipe design. However, it has been found through experience that many supposedly minor factors can profoundly affect the compatibility. Therefore, experimental results remain an important part of heat pipe materials technology.

Table 7-3 summarizes currently available experimental findings for various material combinations. Some of the tests which were used to establish this reference chart are summarized in Table 7-4. In Test Number 9, deoxidized Nb-1Zr wall was prepared by cutting off the evaporator section after the heat pipe had operated 95 hours at 1500°C. The "deoxidized" pipe which was thus formed showed very little corrosion other than some Zr depletion. Some grain growth occurred and the evaporator section exhibited some swelling, but this is a phenomenon separate from that of corrosion.

Experiments 13-22 represent the suggested technique of adding, to the working fluid, metals which exhibit higher free energies of formation for their oxides so as to "getter" the oxygen in the system. Except for calcium, all of the additives apparently accelerated the corrosion process. This is rather surprising since all of these materials have ΔG 's of -130 to -144 kcal/mole of oxygen. Some penetration of lithium into the Nb walls was also found in these tests.

The highest operating temperature thus far attained has been 2000°C with Re/Ag and W-26 Re/Ag heat pipes (Numbers 43 and 44). The latter exhibited negligible corrosion after 1000 hours. The rhenium pipe failed after only 365 hours, but the evidence points to the presence of foreign inclusions in the Re as the cause of failure. If this is so, pure Re pipes would seem to be capable of extended operation at 2000°C.

TABLE 7-3. GENERALIZED RESULTS OF EXPERIMENTAL COMPATIBILITY TESTS

	Aluminum	Stainless Steel	Cold rolled steel	Iron	Copper	Brass	Silica	Nickel	Inconel	Tungsten	Tantalum	Molybdenum	Rhenium	Titanium	Niobium
Water	I	C*													
Ammonia	C	C	C	C			C	C	I					C	
Methanol	I	C		C	C	C	C	C							
Acetone	C	C			C	C	C								
Freon - 11	C														
Freon - 21	C			C											
Freon - 113	C														
C ₆ F ₆					C		C								
n-butane	C														
n-pentane	C	C													
n-heptane	C														
Benzene	C														
Toluene	I														
Dowtherm A		C			C		C								
Dowtherm E	I	C*	I		C	I									
DC 200	C	C			C			C							
DC 209					C										
Perchloroethylene					C		C								
Dimethyl Sulfide					C		C								
Monsanto CP-9					C		C								
Monsanto CP-32(pyridene)	I				C										
Monsanto CP-34	I														
Lithium	I							I	I	C	C	C		I	C
Sodium	C							C	C					I	C
Potassium								C						I	
Cesium														C	C
Mercury	C#							I	I		I	I		I	I
Lead	I							I	I	C	C			I	I
Indium	I							I	I	I	I	I			I
Silver										C	C		I		

C = Compatible
I = Incompatible

* Sensitive to Cleaning
I with Austenitic SS

TABLE 7-4. HEAT PIPE LIFE TEST DATA						
No.	Wall Material	Fluid	Test Temp. (°C)	Hours of Operation	Ref.	Remarks
1	CVD1-W	Li	1600	1,000	12	No failure
2	W-26Re	Li	1600	10,000	13	No failure
3	TZM ²	Li	1560	4,600	14	Evaporator leak
4	TZM	Li	1500	10,526	15	Weld leak
5	TZM	Li	1500	10,400	16	Weld failure in end cap
6	TZM	Li	1500	9,800	16	Weld failure in end cap
7	Nb-1Zr	Li	1600	132	17	
8	Nb-1Zr	Li	1500	9,000	12	
9	Nb-1Zr deoxidized	Li	1500	1,000	18	Grain growth, Zr loss, swelling
10	Nb-1Zr	Li	1350	2,300	19	
11	Nb-1Zr	Li	1100	4,300	20	
12	Nb-1Zr	Li	1000	3,670	12	
13	Nb-1Zr	Li-13Ca	1500	1,000	21	Grain growth, Zr loss, swelling
14	Nb-1Zr	Li-40Pr	1500	52	21	Evaporator leak
15	SGS ³ -Ta	Li	1600	1,000	22	No failure
16	Ta	Li-13Ca	1600	208	21	Evaporator leak
17	Ta	Li-40Pr	1600	94	21	Evaporator leak
18	Ta	Li-0.5Y	1600	21	21	Evaporator leak

TABLE 7-4. HEAT PIPE LIFE TEST DATA (Continued)

No.	Wall Material	Fluid	Test Temp. (°C)	Hours of Operation	Ref.	Remarks
19	Ta	Li-3Y	1600	607	21	Evaporator leak
20	Ta	Li-15Y	1600	146	21	Evaporator leak
21	Ta	Li-0.55 Sc	1600	357	21	Evaporator leak
22	Ta	Li-15 Sc	1600	16	21	Evaporator leak
23	Nb-1Zr	Na	1000	1,000	12	No failure, terminated
24	Nb-1Zr	Na	850	16,000	13	Continuing
25	304 SST	Na	800	12,760	16	No failure, terminated
26	316 SST	Na	771	11,860	16	Failed, pinhole in evaporator
27	347 SST	Na	750	1,500	11	No failure, terminated
28	304 SST	Na	732	11,500	22	No failure, terminated under program
29	Ni	Na	800	13,755	16	No failure, terminated
30	Haynes 25	Na	732	12,000	22	No failure, terminated under program
31	Hastelloy-X	Na	715	33,100	16	
32	347 SST	K	510	6,500	11	No failure, terminated
33	Ni	K	600	41,000	16	Gas controlled
34	Ni	K	600	10,000	16	Gas controlled No failure, terminated under contract
35	Ni	K	600	6,000	16	Gas controlled No failure, terminated under contract
36	Nb-1Zr	Cs	1000	1,000	12	Terminated, no failure

TABLE 7-4. HEAT PIPE LIFE TEST DATA (Continued)

No.	Wall Material	Fluid	Test Temp. (°C)	Hours of Operation	Ref.	Remarks
37	Nb-1Zr	Cs	850	5,000	13	
38	Tl	Cs	400	2,000	20	No failure, terminated
39	Ta-10W	Ca	1700	1,000	23,24	Reflux capsule
40	304 SST	Hg	340	32,000	16	
41	347 SST	Hg	330	10,000	11	No failure, terminated
42	Re	Ag	2000	365	25	Evaporator leak
43	W-26Re	Ag	2000	1,000	13	No failure
44	W	Ag	1900	335	26	
45	Ta	Ag	1900	100	20	
46	Ta	Ag	1900	1,000	26	W wick, no failure
47	Ta	Pb	1600	1,000	12	No failure
48	CVD-W	Pb	1600	1,000	12	No failure
49	Nb	Pb	1600	3	17	Failed
50	Nb-1Zr	Pb	1615	23	17	Failed
51	Nb-1Zr	Pb	1600	19	17	Failed
52	NB-1Zr	Pb	1570	51	17	Failed
53	W	In	1900	75	20	
54	Cu	H ₂ O	150	20,420	16	Continuing

TABLE 7-4. HEAT PIPE LIFE TEST DATA (Continued)

No.	Wall Material	Fluid	Test Temp. (°C)	Hours of Operation	Ref.	Remarks
55	Cu	H ₂ O	130	> 1,400	27	Cu bronze wick, Continuing
56	Cu	H ₂ O	115	> 2,100	27	Cu bronze wick, Continuing
57	Cu	H ₂ O	100	19,490	16	Continuing
58	Cu (OFHC)	H ₂ O	33	4,000	28	Triply distilled H ₂ O, Continuing
59	Cu	H ₂ O	80	21,360	16	Continuing
60	Cu	H ₂ O	34	13,200	29	Continuing
61	321 SST	H ₂ O	164	570	29	Gas generated, corrosion on walls (but see #62)
62	347 SST	H ₂ O	91	15,000	30	Terminated
63	SST	H ₂ O	65	8,500	22	Gas generated
64	SST	H ₂ O	135	26,244	31	Much gas, Refrasil wick
65	SST	H ₂ O		3,744	31	Refrasil wick, terminated
66	304 SST	H ₂ O	35	7,000	28	KOH passivated, much gas generated
67	Ni (oxidized)	H ₂ O	38	7,000	28	Much gas generated
68	Inconel 600	H ₂ O	38	14,000	28	Gas generated (oxidized Inconel)
69	Titanium	H ₂ O	35	14,000	28	No wick (oxidized Ti), Continuing
70	Cu	Methanol	70	> 700	27	Cu Bronze wick, Continuing
71	Cu	Methanol	74	24,158	31	Refrasil wick, Continuing
72	Brass	Methanol	60	> 800	27	Cu Bronze wick, Continuing

TABLE 7-4. HEAT PIPE LIFE TEST DATA (Continued)						
No.	Wall Material	Fluid	Test Temp. (°C)	Hours of Operation	Ref.	Remarks
73	Al 6061-T6	Methanol	46	4,000	28	Gas generated, SST wick
74	Al 6061-T6	Methanol	--	--	32	Generated gas during setup
75	304 SST	Methanol	62	>14,250	29	Continuing
76	304 SST	Methanol	40	16,000	28	Specially dried Methanol, Continuing
77	304 SST	Methanol	40	16,000	28	Spectrophotometric Methanol, Continuing
78	304 SST (oxid.)	Methanol	40	16,000	28	Spectrophotometric Methanol, Continuing
79	316 SST	Methanol	46	8,000	28	Slight gas generation
80	SST	Methanol	60	> 1,650	27	Continuing
81	Fe	Methanol	33	> 8,250	29	Continuing
82	Nickel 200	Methanol	35	6,000	28	Specially dried Methanol, Continuing
83	SST	Ethanol	60	> 1,550	27	Continuing
84	Al 6061-T6	NH ₃	71	500	32	Al wick, no failure, terminated under contract
85	Al 6061-T6	NH ₃	47	10,800	29	SST artery wick, radial grooves
86	Al 6061-T6	NH ₃	42	2,373	29	No failure, terminated under contract
87	Al 6061-T6	NH ₃	49	14,000	28	SST wick, 99.999% NH ₃ , Continuing
88	Al	NH ₃	48	18,120	31	Al felt wick, Continuing
89	Al	NH ₃	48	18,120	31	Ni felt wick, Continuing
90	SST	NH ₃	46	18,900	31	

TABLE 7-4. HEAT PIPE LIFE TEST DATA (Continued)

No.	Wall Material	Fluid	Test Temp. (°C)	Hours of Operation	Ref.	Remarks
91	SST	NH ₃	47	18,900	31	
92	Fe	NH ₃	35	>18,300	29	Continuing
93	Cu	Acetone	74	24,158	31	Some gas, Refrasil wick, Continuing
94	Brass	Acetone	60	> 800	27	Continuing
95	Al	Acetone	110	1,700	16	Continuing
96	Al	Acetone	71	9,936	31	SST, fiber wick, no failure, terminated
97	Al 6061-T6	Acetone	33	4,000	28	Gas generated
98	304 SST	Acetone	87	14,500	16	Continuing
99	SST	Acetone	60	1,500	27	Continuing
100	Al 6061-T6	n-Butane	66	500	32	Al wick, no failure, terminated
101	Al 6061-T6	n-Pentane	158	570	32	Al wick, slight fluid discoloration, terminated
102	SST	Hexane	60	> 1,200	27	Continuing
103	Al 6061-T6	n-Heptane	161	600	16	Al wick, no failure, terminated
104	Al 6061-T6	Benzene	158	570	16	Al wick, no failure, terminated
105	Al 6061-T6	Toluene	162	600	32	Small ΔT developed, terminated
106	Cu	C ₆ F ₆	100	24,980	31	Refrasil wick, Continuing
107	Al 6061-T6	Freon 11	106	500	32	No failure, terminated
108	Al 6061-T6	Freon 11	69	500	32	No failure, terminated

TABLE 7-4. HEAT PIPE LIFE TEST DATA (Continued)						
No.	Wall Material	Fluid	Test Temp. (°C)	Hours of Operation	Ref.	Remarks
109	Al 6061-T6	F-21	41	10,000	28	Slight gas generation
110	Al 6061-T6	Freon 113	107	500	32	No failure, terminated
111	Al 6061-T6	Freon 113	69	500	32	No failure, terminated
112	Cu	Dow-A	160	20,500	31	No failure, terminated for exam., Refrasil wick
113	Cu	Dow-A	156	26,830	31	Refrasil wick, Continuing
114	Cu	Dow-A	149	26,644	31	Refrasil wick, Continuing
115	SST	Dow-A	150	22,376	31	Refrasil wick, Continuing
116	Brass	Dowtherm E	121	20,500	29	Gas generated after 5850 hours
117	Steel cold rolled	Dowtherm E	121	20,500	29	Gas generated after 4680 hours
118	Cu	Dowtherm E	110	>20,500	29	Continuing
119	SST	Dow-E	128	31,098	31	No failure, removed for analysis
120	Cu	Dow-E	~140	31,270	31	Sintered Cu wick, Continuing
121	Cu	Dow-E	182	41,460	31	SST wick, Continuing
122	Cu	DC-200	168	23,000	31	SST wick, very slight mass transfer to evap. No failure, terminated for examination
123	Al	DC-200	104	18,021	31	Ni wick, Continuing
124	Cu	Dow-209	110	40,414	31	Sintered Cu wick, Continuing
125	Cu	CP-9	149	33,460	31	Refrasil wick, Continuing
126	Cu	Pyridene CP-32	98	10,810	31	Cu felt wick, Continuing

TABLE 7-4. HEAT PIPE LIFE TEST DATA (Continued)						
No.	Wall Material	Fluid	Test Temp. (°C)	Hours of Operation	Ref.	Remarks
127	Al 6061-T6	Pyridene CP-32	159	550	32	Δ T developed, deposits, discolored
128	Al 6061-T6	Monsanto CP-34	160	550	32	Gas generated, discolored fluid
129	Cu	Perchloro-ethylene	93	16,670	31	Refrasil wick, Continuing
130	Cu	Dimethylsulfide	100	15,634	31	Some gas, Refrasil wick, Continuing

Notes to Table 7-4

¹CVD = chemical vapor deposition

²TZM = Mo-0.8Zr-0.5Ti-0.03C

³SGS = stabilized grain size

In the intermediate temperature range (500 - 1000°C), sodium has been amply demonstrated to be compatible with stainless steels, nickel, and several of the super-alloys (Numbers 25 - 31). Also in this temperature range is the longest successful life test reported to date--nearly five years of continuous operation for a Ni/K system at 600°C (Number 33).

In the low and intermediate ranges and in some cases up to 700°C, the available data indicate that nearly unlimited operation can be obtained with a whole series of materials, provided care is taken to eliminate impurities from the system. This is demonstrated rather graphically by a comparison of Numbers 61 and 62. In the first case, gas began to appear in the system soon after the start of the test; but, when the system was very thoroughly cleaned and outgassed, no signs of deterioration were observed after 3000 hours of testing. Other very good systems in this temperature range are 304 SST/Hg, Cu/H₂O, Al or Fe/NH₃, SST or Fe/Methanol, Cu/Dowtherm E, and Al/Freons.

REFERENCES

1. Moelwyn-Hughes, E. A., "Physical Chemistry," 2nd Ed., Pergamon Press, New York (1964).
2. Lange, N. A., "Handbook of Chemistry," 9th Ed., Handbook Publishers, Inc., Sandusky, Ohio, 1956.
3. Lyman, T., "Metals Handbook," 8th Ed., American Society for Metals, Metals Park, Ohio (1961).
4. LaQue, F. L. and Copson, H. R. (Eds), Corrosion Resistance of Metals and Alloys, 2nd Ed., American Chemical Society Monograph Series No. 158, Reinhold Publishing Corp., New York, 1963.
5. MacLennan, McMillan and Greenblatt, "Corrosion of Aluminum and Aluminum Alloys in High Temperature Water," 1st Int'l. Congress on Metallic Corrosion, London, April 1961.
6. Wagner, C. J., J. Electrochem Soc. 99, 369 (1952).
7. Brewer, L., "The Thermodynamic Properties of the Oxides and Their Vaporization Processes," Chemical Reviews - 1-75, 1953.
8. Margrave, J. L., "Thermodynamic Calculations, 1. Free Energy Functions and Heat Content Functions," J. Chem. Education 32, 520-4 (1955).
9. Margrave, J. L., "High Temperature - A Tool for the Future," Stanford Research Inst., Palo Alto, Calif. (1956), pp. 87-106.
10. Kemme, J. E., "Heat Pipe Capability Experiments," Los Alamos Scientific Lab. Rept. LA-3585-MS, Oct. 1966.
11. Kemme, J. E., "Quarterly Status Report on Space Electric Power R&D Program, July 31, 1971," Los Alamos Scientific Lab. Rept. LA-4746-MS.
12. Busse, C. A., Geiger, G., Quantaert, D., Potzschke, M., "Heat Pipe Life Tests at 1600°C and 1000°C," 1966 IEEE Thermionic Specialist Conference, Houston, Texas, pp. 149-58.

13. Busse, C. A., "Heat Pipes for Thermionic Space Power Supplies," Proc. 3rd International Conference on Space Technology, Rome (1971).
14. Shefsiek, P. K. and Ernst, D. M., "Heat Pipe Development for Thermionic Application," 4th Intersociety Energy Conversion Conference, Washington, D. C. (1969, pp. 879-887).
15. Rouklove, P., Comment in Proceedings of 2nd International Conference on Thermionic Electrical Power Generation, Stresa, Euratom Rept. EUR 4210, f.e., Ispra; Italy (1968), p. 494.
16. Eastman, G. Y., "The Heat Pipe - A Progress Report," 4th Intersociety Energy Conversion Engineering Conference, Washington, D. C., September 1969, pp. 873-8.
17. Busse, C. A., Caron, R. and Cappelletti, C., "Prototype of Heat Pipe Thermionic Converters for Space Reactors," Proc. of 1st International Conference of Thermionic Electrical Power Generation, London, 1965.
18. Busse, C. A., Geiger, F., Quataert, D., "Status of Emitter Heat Pipe Development at Ispra," IEEE Con. Record of Thermionic Specialist Conference, 1970.
19. Harbaugh, W. E., "The Development of an Insulated Thermionic Converter Heat Pipe Assembly," RCA Rept. AF APL TR-67-45 (1967).
20. Ranken, W. A. and Kemme, J. E., "Survey of Los Alamos and Euratom Heat Pipe Investigations," IEEE Conference Record of 1965 Thermionic Conversion Specialist Conf., San Diego, California, October 1965, pp. 325-336.
21. Busse, C. A., "Heat Pipe Thermionic Converter Research in Europe," 4th Intersociety Energy Conversion Engineering Conference, Washington, D. C., September 1969.
22. Busse, C. A., Geiger, F., Strub, H., Potzschke, M. and Kraft, G., "High Temperature Lithium Heat Pipes," 2nd International Conference on Thermionic Electrical Power Generation, Euratom, Euratom Rept. EUR 4210 f.e., 1968, pp. 495-506.
23. Johnson, G. D., "Compatibility of Various High Temperature Heat Pipe Alloys with Working Fluids," IEEE 1968 Thermionic Conversion Specialist Conf., Framingham, N.Y. (1968), pp. 258-65.
24. Johnson, G. D., "Corrosion Studies of Liquid Metal Heat Pipe System at 1000°C to 1800°C." In Draley, J. E., and Weeks, J. R., "Corrosion by Liquid Metals," Plenum Press, N. Y. (1970), pp. 321-37.
25. Kemme, J. E., Quarterly Status Report on Space Electric R & D Program for period ending January 31, 1969, Pt. 1, Los Alamos Scientific Laboratory Rept. LA-4109-MS.
26. Grover, G. M., Kemme, J. E., and Keddy, E. S., "Advances in Heat Pipe Technology," Proceedings 2nd International Conference Thermionic Electrical Power Generation, Stresa, Euratom Rept. EUR-4210, f.e., Ispra, Italy, 1968.
27. Groll, M., Brost, O., Kreeb, H., Schubert, K. and Zimmerman, P., "Power Limits, Technology, and Application of Low Temperature Heat Pipes," Forschung im Ingenieurwesen 37, 33-37 (1971).
28. Marcus, B. D., Private Communications, April 1972.
29. Dynatherm Corporation, Unpublished Data.
30. Deverall, J. E. and Kemme, J. E., "Satellite Heat Pipe," Los Alamos Scientific Laboratory Report LA-3278-MS, January 1965.
31. Basiulis, A. and Filler, M., "Operating Characteristics and Long Life Capabilities of Organic Fluid Heat Pipes," AIAA 6th Thermophysics Conference, April 26-28, 1971. (AIAA Paper No. 71-408).
32. Gerrels, E. E. and Larson, J. W., "Brayton Cycle Vapor Chamber (Heat Pipe) Radiator Study," NASA CR-1677, February 1971.

HEAT PIPE TESTING

A variety of tests are required to evaluate the performance characteristics of a heat pipe and to establish the reliability of a given design. Tests with individual elements of a heat pipe such as the fluid, wick, and container are often conducted as part of the heat pipe development to establish properties such as effective pumping, permeability, and burst pressure, etc. Once prototype designs have been developed various aspects of quality assurance are generally imposed. Leak tests and proof pressure tests are conducted to insure component integrity. After the heat pipe assembly has been completed, thermal performance tests are conducted to establish heat transport and heat transfer characteristics. Additional tests are required to verify the different control features of variable conductance heat pipes. Finally, life tests are also conducted in many cases to establish materials compatibility and operating lifetime. This chapter summarizes the different test methods and test set-ups and equipment that have been used in the development of heat pipes.

8.1 HEAT PIPE COMPONENT TESTS

The ability of a heat pipe to meet performance objectives is dependent on a number of factors as discussed in Chapters 2 through 4. Often, only limited data is available to evaluate the performance of the selected fluid/wick/container combination. Component level tests which are performed to determine applicable fluid, wick or container properties are discussed below.

8.1.1 Fluid Properties Tests

The properties of any fluid can be obtained from a number of standard test methods. The thermophysical properties of most fluids are usually well documented in the literature (see Volume II) and basic property measurements are not required. However, two factors which are often not readily available in the literature are the wetting behavior (contact angle) and compatibility of the working fluid with wick and/or container materials.

8.1.1.1 Contact Angle Measurement

The contact angle is dependent on a number of factors including surface tension, material properties, surface preparation and cleaning. Several methods exist for measuring contact angle including sessile drop (1, 2, 3), tilting plate (4, 5, 6), porous plug (7),

cylinder (8), and wetting balance techniques (9). One of the most accurate and reproducible techniques is the tilting plate method which is illustrated schematically in Fig. 8-1. Typically, a plate several centimeters wide is dipped into the test liquid and rotated until the liquid level remains perfectly horizontal up to the surface of the plate. For this condition the inclination of the plate relative to the liquid surface is the contact angle.

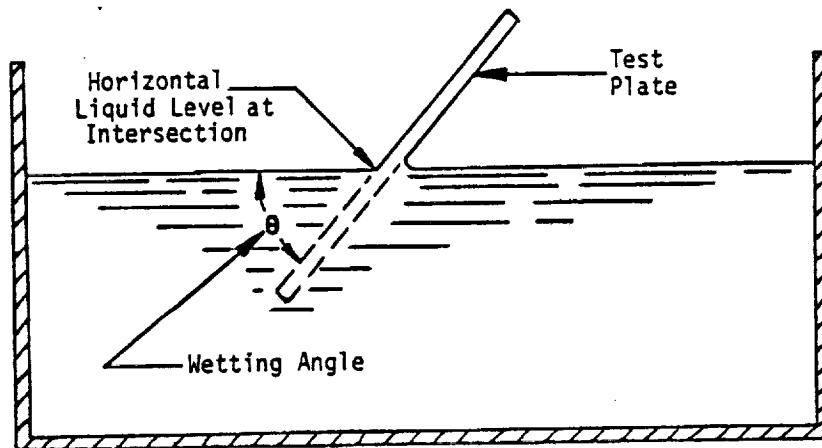


Fig. 8-1. Schematic of tilting plate method for contact angle measurement

An advantage of this test method is that it can be readily adopted to measure contact angle with a variety of fluids including cryogenic liquids. Figure 8-2 illustrates a test set-up which was successfully used to measure wetting angles of cryogenic fluids (10). Basically it consists of dewar with viewing ports which allow isolation of the test specimen and working fluid from the environment. The dewar is vacuum insulated and equipped with cooling coils to maintain the desired test temperature. An optical system which permits viewing of the contact angle within the enclosed dewar consists of a light source and slit, condensing lens, objective lens and a screen mounted on two optical benches. The image of the slit is focused on the surface of the liquid at approximately the center of the sample. The surface of the liquid refracts the image which is then projected into a ground glass screen. The resultant image on the screen is that of the liquid surface shape at the sample interface. With this method, contact angles can be determined by both direct observation using only the condenser lens and indirect observations wherein the image on the screen is used to establish when the liquid surface is horizontal at its point of intersection with the solid.

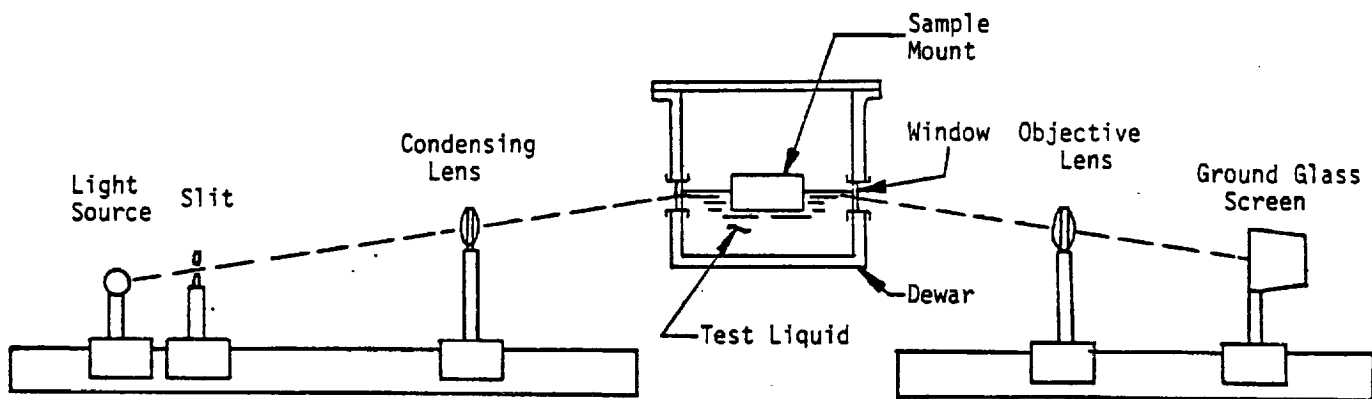


Fig. 8-2. Schematic of optical system for contact angle measurements

8.1.1.2 Materials Compatibility Test

Since the level of corrosion which can be tolerated in a heat pipe is extremely small, the results of most available corrosion studies can only be used as a guide in the selection of compatible heat pipe materials. In order to insure long system lifetime, compatibility must be established for any given material combination at operating conditions which are representative of typical heat pipe applications. Materials compatibility and stability may affect the performance of the heat pipe in various ways. In most instances, an internal reaction will result in the production of a non-condensable gas which will separate from the working fluid vapor phase and collect in the condenser. This effectively reduces the condenser heat transfer area and results in a non-isothermal temperature profile. Since even small quantities of non-condensable gas can result in measurable temperature differences at the end of the condenser, non-condensable gas generation can be used as one method to determine materials compatibility.

Heat pipe material compatibility tests are performed very often with gravity reflux test capsules as illustrated in Fig. 8-3. The capsule is fabricated of the same material as the heat pipes and processed in the same manner. Wick material is also introduced in these capsules to establish representative heat pipe design conditions. Testing consists of applying heat at the bottom of the capsule and removing it from the top. Heat is usually applied with an electrical heater wound around the test capsule and is removed by natural or

forced air convection; or by means of clamp-on chill blocks depending on the desired operating temperature and heat flux conditions. Thermocouples are attached along the length of the heat pipe to measure the temperature profile as a function of time. The adiabatic section thermocouples (T_a) provide the saturated vapor temperature of the working fluid from which the saturation pressure inside the capsule can be established. The condenser thermocouples (T_c) establish the location of the non-condensable gas interface and the temperature profile of the blocked condenser section. With these measurements, the amount of gas generated can be determined from the Ideal Gas Law:

$$m_g = \left(\frac{p_v V_{bc}}{R T_{bc}} \right) \quad (8-1)$$

where:

- m = Amount of gas generated (gm-mole)
- p_v = Internal pressure based on the working fluid property and adiabatic section temperature (T_a) (N/m^2)
- V_{bc} = Volume of the blocked condenser region (m^3)
- R = Universal gas constant ($J/gm-mole - ^\circ K$)
- T_{bc} = Average temperature of the blocked condenser section ($^\circ K$)

If the thermal conductance of the sample is significant, a representative average temperature of the blocked region may not be readily obtained and an integrated value may be required to accurately establish the amount of gas generated. Also, if the internal pressure at the selected test temperature is significant, or when gas generation rates are very small, test specimens are often cycled down in temperature to establish a sufficiently large blocked condenser region for easier or more accurate temperature profile measurements.

A large number of factors, as summarized in Table 8-1, can influence the results of compatibility tests. The type of materials used, the fluid purity, and the cleaning and processing procedures should be representative of typical heat pipe designs and fabrication processes. The container, including any valve retained for gas sampling, should be leak tight to avoid loss of any generated non-condensable gas. Permeability of the container wall material to gases (i.e., hydrogen) should be considered especially if any decreasing rate of gas evaluation is noted (11). Finally, reaction rate dependence on both the heat flux and the operating temperature have been well demonstrated (12, 13). The test capsule, therefore, should be operated at heat loads and temperatures which are typical of the heat

pipe application. Elevated temperatures may also be included in a test program to obtain accelerated test conditions for long life compatibility predictions (14).

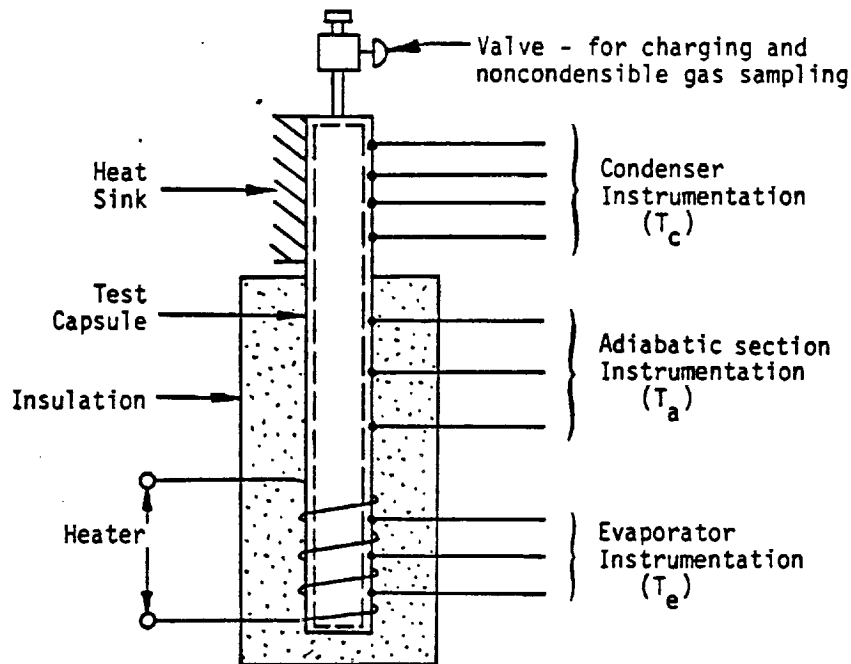


Fig. 8-3. Gravity reflux compatibility test capsule

TABLE 8-1. VARIABLES AFFECTING HEAT PIPE COMPATIBILITY TESTING

WORKING FLUID

- Purity
- Solubility
- Stability at Temperature

WICK

- Material Make-up
- Surface Condition
- Cleanliness

CONTAINER

- Material Make-up
- Surface Condition
- Cleanliness
- Leak Tightness
- Gas Permeability

TEST CONDITION

- Test Temperature and Pressure
- Heat Flux
- Instrumentation Accuracy

8.2 WICK PROPERTY TESTS

As discussed in Chapter 4, the wick permeability (K) and effective pumping radius (r_p) can be accurately predicted for well defined capillary structures such as cylindrical, rectangular, annular and axially grooved flow channels. For wire mesh screen and wicks fabricated of fibers or powders, experimental data is required to ascertain wick properties. Much of the available wick test data summarized in Table 4-6 was obtained by various techniques as discussed below.

8.2.1 Effective Pumping Radius

Several investigators (15, 16, 17, 18) have used the technique of measuring the maximum height (h) to which a liquid will rise in a wick material when the bottom of the material is immersed in the liquid. The effective pore radius can then be determined using:

$$r_p = \frac{2 \sigma \cos \theta}{\rho_l g h} \quad (8-2)$$

This method measures the smallest pore size present and thus tends to predict higher capillary pressures than will be representative of a non-homogeneous wick having varying pore sizes.

Variations of up to 25% have been found (16) between the maximum heights attained with rising liquid levels in a dry wick and falling liquid levels in a saturated wick. This effect has been attributed to the existence of unevenly sized passages in the wick (sections of predominantly "large" passages interspersed with other sections of predominantly "small" passages, as illustrated in Fig. 8-4). The maximum rising height is reached when a section of "large" passages is encountered. However, the falling liquid in a saturated wick can form menisci with smaller radii at a higher height and thereby maintain a liquid column at this height even though a section of "too large" pores exists at a lower height. Thus, two measurements of the maximum wicking height on the same wick sample can yield very different values for the effective capillary radius, and care must be exercised before applying the data to the design of heat pipes. The conservative approach is to use the effective pore radius corresponding to the rising liquid level.

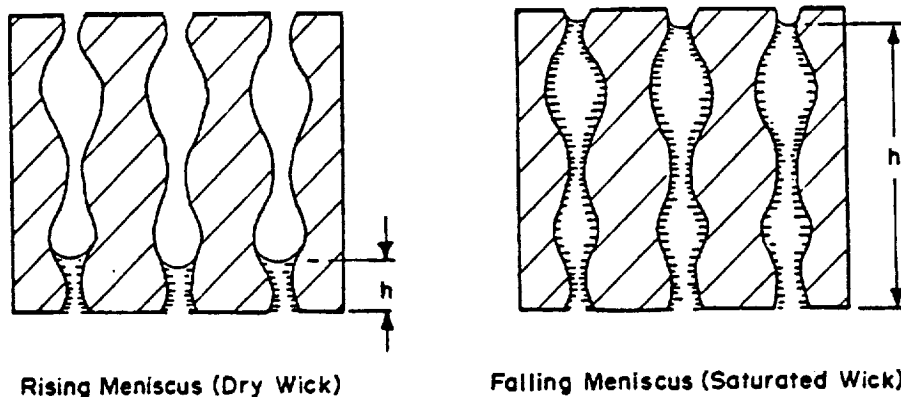


Fig. 8-4. Variations in measured wicking height as a function of measurement technique in non-uniform wick material

It is also important when making these measurements to enclose the wick material in a saturated atmosphere to avoid attaining too low a maximum height which can result from evaporation. A modification of this technique has been used by several investigators (16, 19, 20). This involves fastening a thin section of wick material over the end of a nonporous tube and then filling the tube with test liquid and either raising the tube or lowering a reservoir to a level at which the wick can no longer support the column of liquid. Equation 8-2 is then used to obtain the effective pore radius. The maximum height can be obtained in a much shorter time than with the previous technique (which may require a period of more than one week).

Another measurement technique, called the bubble method, employs a section of wick over the end of a tube in contact with a column of test liquid. Instead of measuring the height of the column of liquid which can be supported, the overpressure, p , required to force a bubble of air through the wick is determined (19,20) and then the following relationship is applied:

$$r_p = \frac{2 \sigma \cos \theta}{p} \quad (8-3)$$

This technique also gives the value for the largest pore size present in the wick. It has been reported (19) that this technique gives essentially the same result as the preceding method. However, the test used to establish this equivalence utilized a 200-mesh stainless steel screen (which has very little variation in pore size); thus, both test methods would be expected to yield similar values for r_p .

The rate of rise of liquid in the wick can be used to determine the effective capillary radius and also the permeability (17, 18, 21). This technique is discussed to illustrate the application of the equations developed in Chapter 2. If one end of the test wick is placed in the fluid, as indicated in Fig. 8-5 then the rate dx_a/dt of the advancing front is related to the mass flow of the liquid through:

$$\dot{m}(x) = \epsilon \rho_l A_w \frac{dx_a}{dt} \quad (8-4)$$

Combining Eq. 8-4 with the equations for the pressure gradients (2-4, 2-15 and 2-25) gives:

$$\frac{dp_l}{dx} = - \frac{\epsilon \mu_l dx_a/dt}{K} - \rho_l g \sin \beta \quad (8-5)$$

Integration along the column of liquid yields the pressure at the advancing interface:

$$p_l(x_a) = \int_0^{x_a} \frac{dp_l}{dx} dx + p_l(0) \quad (8-6)$$

The capillary pressure developed at the advancing interface is given by:

$$\Delta p_{cap} = \Delta p_i(x_a) = \frac{2 \sigma \cos \theta}{r_p} = p_v(x_a) - p_l(x_a) \quad (8-7)$$

But since this system is open to the atmosphere:

$$p_v(x_a) = p_v(0) = p_l(0) \quad (8-8)$$

Combining Eqs. 8-5, 8-6, and 8-8 with 8-7 gives:

$$\frac{2 \sigma \cos \theta}{r_p} = p_l(0) - \int_0^{x_a} \left(- \frac{\epsilon \mu_l dx_a/dt}{K} - \rho_l g \sin \beta \right) dx - p_l(0) \quad (8-9)$$

Integrating and rearranging yields:

$$\frac{dx_a}{dt} = \frac{K}{\epsilon \mu_l} \frac{2 \sigma \cos \theta}{r_p} \frac{1}{x_a} - \frac{K}{\epsilon \mu_l} \rho_l g \sin \beta \quad (8-10)$$

Thus, a plot of dx_a/dt vs. $1/x_a$ is a straight line and the permeability is determined from the intercept and r_p is determined from the slope. In the horizontal (minimum g) case, Eq. 8-10 reduces to the simple form:

$$\frac{2 \sigma \cos \theta}{r_p} = \frac{\epsilon \mu_l x_a}{K} \frac{dx_a}{dt} \quad (8-11)$$

which integrates to:

$$t_a = \frac{r_p \mu_l \epsilon}{4 K \sigma \cos \theta} x_a^2 \quad (8-12)$$

where t_a is the time required for the front to reach an axial location x_a . This has been verified experimentally with twenty inch lengths of SiO_2 fabric wicks (18).

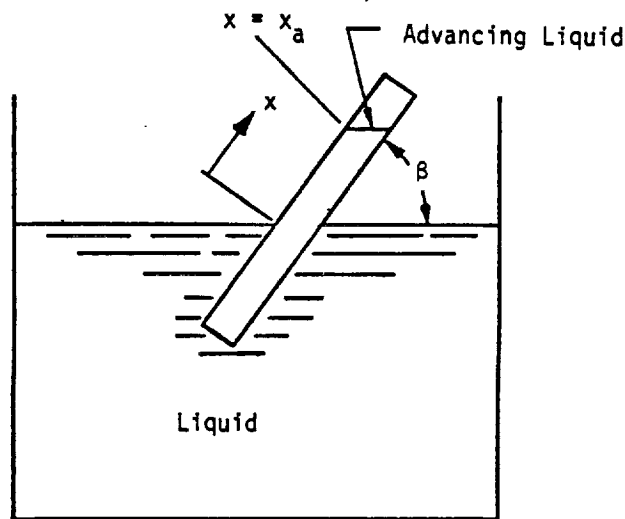


Fig. 8-5. Advancing liquid front test set-up for determination of r_p and K

It is difficult to obtain reproducible data with this approach due to the difficulty in making precise measurements of the motion of the liquid front; this is especially true during the early rise above the surface of the reservoir. Much of this difficulty is associated with the ability to see the actual leading edge of the liquid. The addition of coloring and/or fluorescing agents has been considered, but the fluid properties may be changed and the results thereby invalidated. Other techniques suggested include the placement of indicating papers (such as litmus) at intervals along the wick or the insertion

of wire electrodes (in non-metallic wicks) at intervals along the wick. Any such external indicators suffer from the problem that they are discontinuous and that they bias the time of liquid front passage by the indicator reaction time. Thus, all of the rise time experiments show only approximate adherence to the above formulas.

8.2.2 Permeability

As with the determination of the effective pumping radii, several techniques of varying complexity are available for the determination of the permeability of wick materials. All methods involve the measurement of the pressure gradient along the wick concurrently with a determination of the flow rate of the test fluid.

The simplest technique (generally only applicable to fairly thick wick samples) involves the clamping of the test specimen in a chamber of dimensions such that all surfaces are in tight contact in order to prevent the fluid from bypassing the sample. A fluid flow under a constant pressure head is then maintained until a constant pressure profile is established across the sample. The pressure profile is measured using a series of pressure probes as indicated in Fig. 8-6. The equilibrium flow rate is determined by weighing the amount of fluid collected over a specific period of time. The permeability can then be calculated from Eq. 8-13.

$$K = \frac{L}{\Delta p_2} \frac{\mu_2 \dot{m}_2}{A_w \rho_2} \quad (8-13)$$

where L is the length of the sample and Δp_2 is the pressure drop as measured along this length. Equation 8-13 follows directly by integration of Darcy's Law (Eq. 2-15). The data obtained using this experimental method are usually reproducible. Unfortunately, this technique does not duplicate the condition inside a heat pipe where one surface of the wick is free to permit the formation of menisci of various shapes. Katzoff (16) has suggested that this can reduce the apparent permeability of the wick since the effective flow area is reduced.

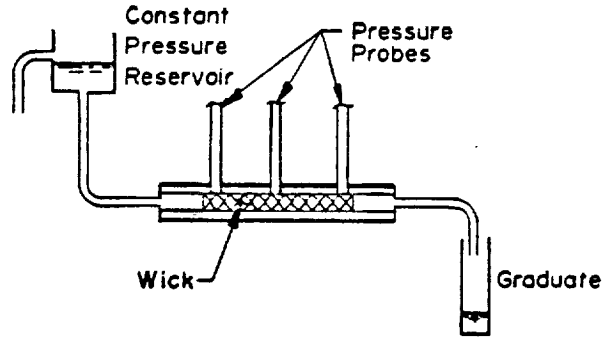


Fig. 8-6. Forced flow permeability (K) measurement apparatus

A modification of the above technique has been used to obtain permeability measurements under conditions more closely resembling those in a heat pipe (20). In this case, the pressure probe taps are placed under the wick and a vapor space is left in the test chamber above the wick. The test fixture is tilted in such a manner that gravity aids the liquid flow. The tilt is adjusted so that the pressure due to viscous drag is exactly balanced by the gravity pressure gradient (Fig. 8-7). For these test conditions, Eqs. 2-4, 2-15 and 2-25 yield the following relation:

$$\frac{\mu_l \dot{m}_l}{K A_w \rho_l} - \rho_l g \sin \beta = 0 \quad (8-14)$$

and

$$K = \frac{\mu_l \dot{m}_l}{A_w \rho_l^2 g |\sin \beta|} \quad (\beta < 0) \quad (8-15)$$

The effective radius r_{eff} of the meniscus between liquid and vapor can be determined from:

$$\frac{2 \sigma \cos \theta}{r_{eff}} = p_v - p_l \quad (8-16)$$

where p_v and p_l are the pressures in the vapor and the liquid phases, respectively. This effective meniscus may be varied by adjusting the pressure in the vapor space above the wick. The recession of the meniscus into the wick modifies the flow pattern and reduces the cross-sectional area available for liquid flow. Both of these effects reduce permeability

over that of a completely filled wick. This technique, although it provides useful information, has proved difficult to control experimentally. As a result, most experimenters have utilized the forced flow method.

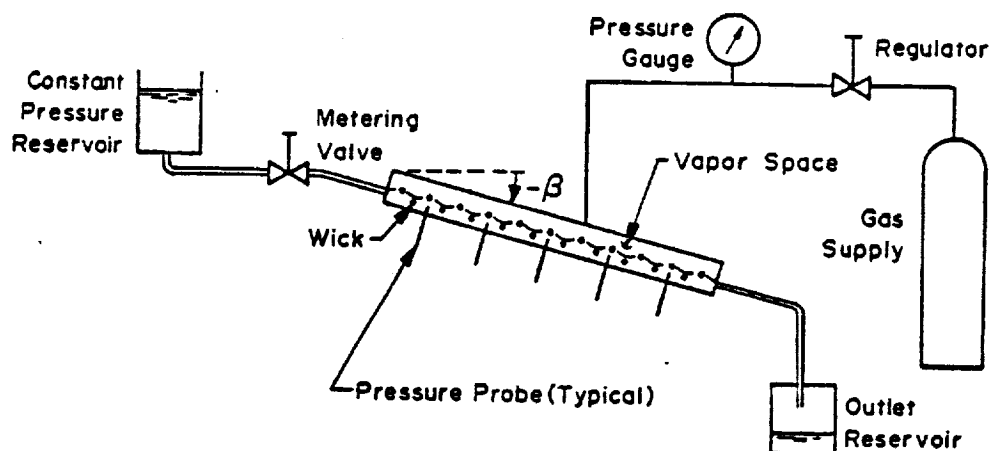


Fig. 8-7. Test setup for determination of permeability by gravity flow

Measurements have also been made of pressure gradients in actual operating heat pipes. Presumably, these tests should yield the most representative data. However, serious problems with vapor bubbles in the pressure probes have severely limited the reproducibility of data from such tests (19).

8.2.3 Composite Wick Effective Capillary Pumping

The composite wick combines the high permeability of channel flow together with the high pumping capacity of fine pore wick materials. The permeability of the composite wick can be determined by techniques similar to those discussed in Section 8.2.2. The maximum pumping that can be developed is determined by the smallest opening in the pumping wick. When the wick consists of alternate layers of screen, the maximum pumping that is developed can be measured using the receding meniscus techniques discussed in Section 8.2.1. For composite wicks made of large open flow channels such as arterial composite wicks, the maximum pumping can be determined by hydrostatic pressure testing as illustrated in Fig. 8-8 (22).

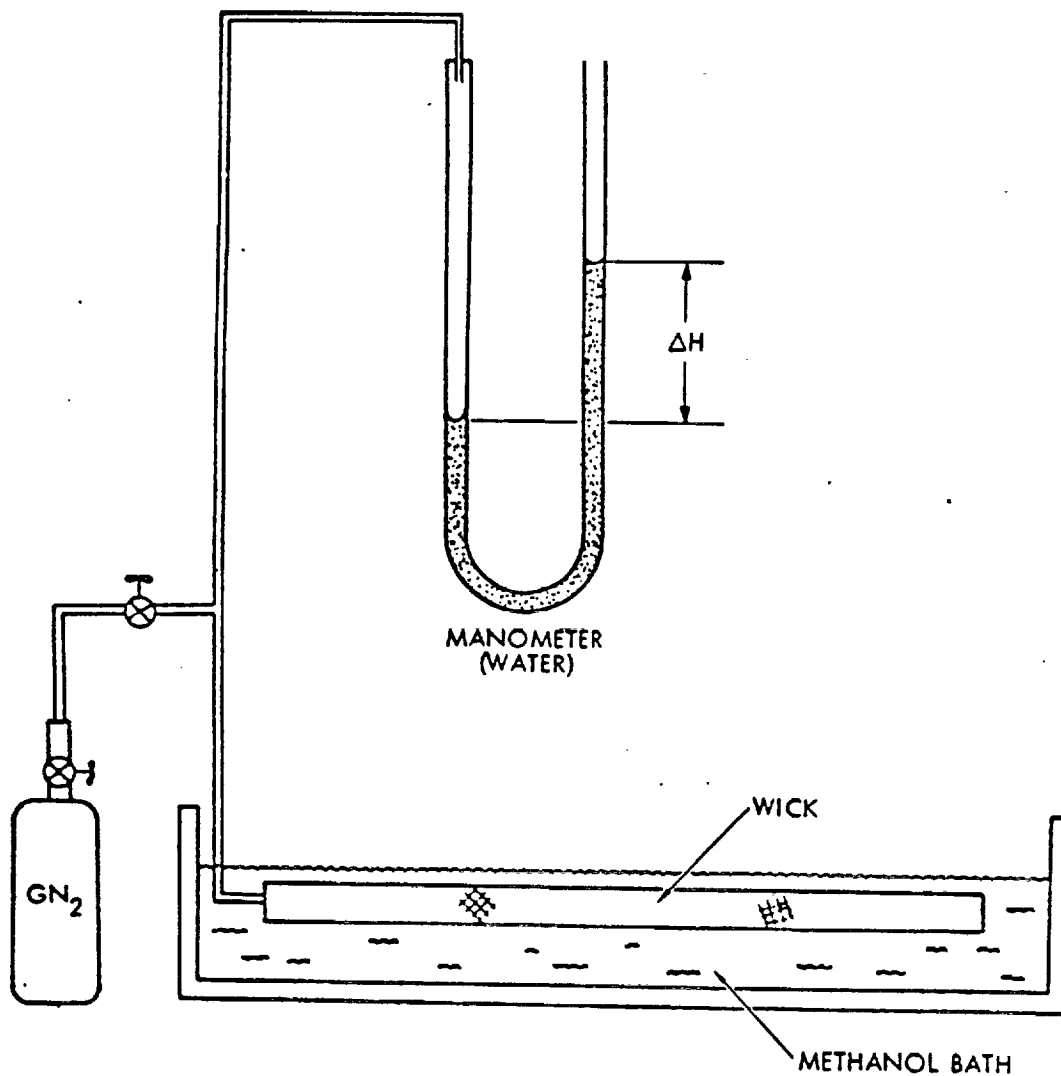


Fig. 8-8. Heat pipe wick static pressure test set-up

This hydrostatic pressure test set-up consists of a methanol bath in which the wick is immersed, a regulated gaseous nitrogen supply, a micrometer needle valve, and an open U-tube manometer. The wick is held level just below the surface of the methanol. Pressure is gradually increased and read on the manometer. When the first leak (bubble) occurs, the pressure is reduced slightly, stable hydrostatic pressure retention is verified and a final reading on the manometer is obtained. The effective pumping radius which will establish the maximum pumping capability of the wick can then be determined from Eq. 8-2.

8.3 CONTAINER DESIGN VERIFICATION TESTS

Pressure containment integrity and leak tightness are required in the container design to insure long term reliable performance of the heat pipe. Both of these factors can be verified with tests as described below.

8.3.1 Hydrostatic Pressure Testing

Pressure containment integrity is verified prior to charging of the working fluid by introducing a pressurized fluid into the heat pipe either in the gaseous form (Fig. 8-9) or in the liquid form (Fig. 8-10).

The advantages of gas pressure testing are that it minimizes potential internal heat pipe contamination and it can be combined with pressurized leak testing as discussed in Section 8.3.2. Once testing is completed, the test gas can be easily evacuated. The disadvantages of gas pressure testing are safety and limited pressure levels that can be achieved with standard pressurized gas supply cylinders. For these reasons, gas pressure hydrostatic tests are typically performed where contamination is critical, where non-destructive proof pressure tests are required and where the test pressures are sufficiently low as not to create a safety hazard.

Much higher test pressures can safely be achieved with liquid hydrostatic pressure testing. This test method, therefore, is often used when safety can be a problem, such as burst pressure tests, and where potential contamination is not a problem. Liquids which do not leave a residue when the heat pipe is evacuated are used to minimize potential contamination (i.e., alcohol).

Two types of hydrostatic pressure tests that are performed are proof pressure tests and burst pressure tests. Proof pressure tests are usually performed at 1.5 times the maximum expected pressure to conform with ASME pressure vessel codes. Dimensional measurements are made at controlled locations on the heat pipe both before and after proof pressure testing to determine any material yield which would indicate non-conformance with the ASME Code.

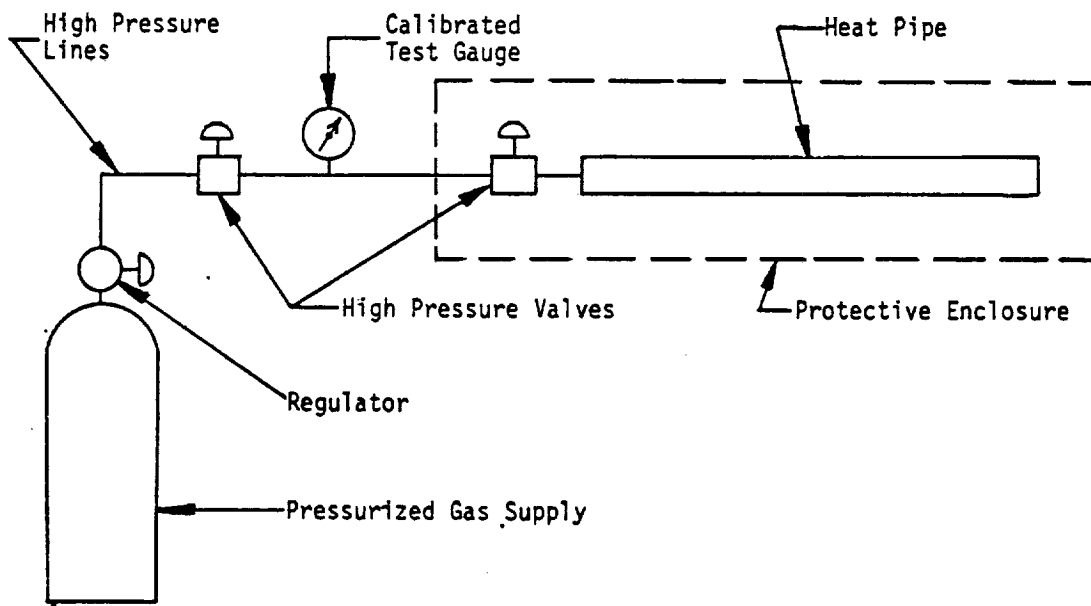


Fig. 8-9. Hydrostatic pressure test set-up: Gas

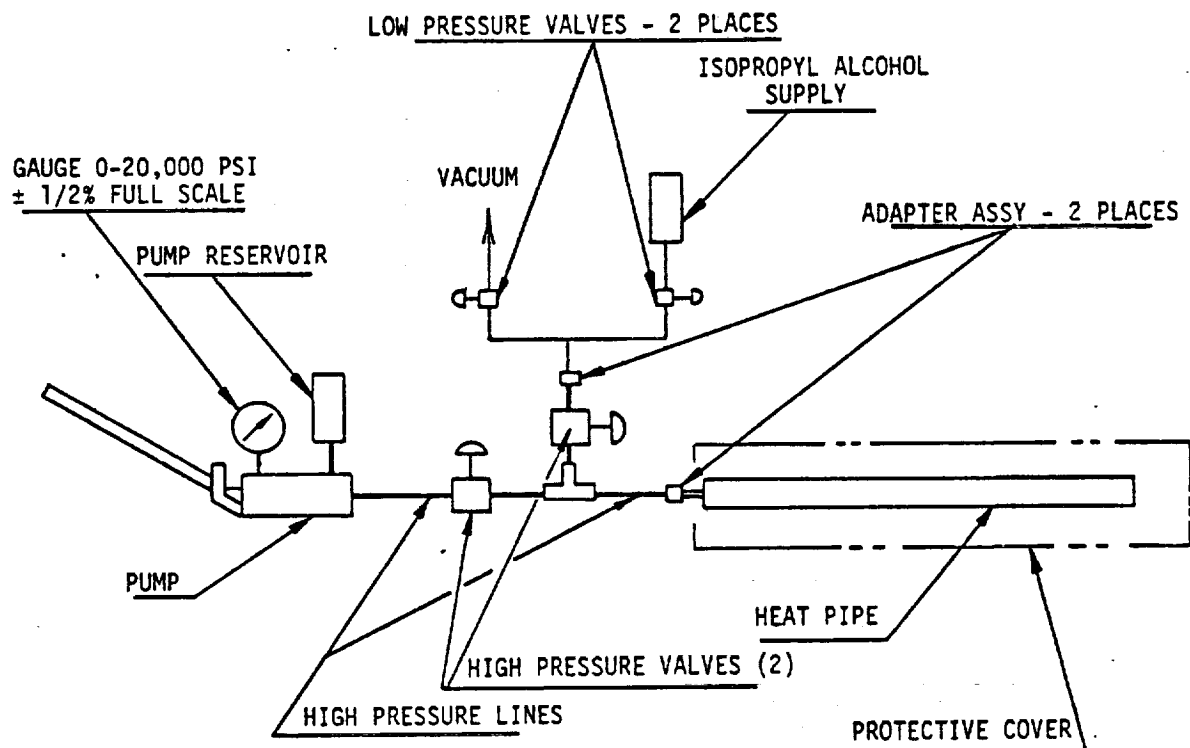


Fig. 8-10. Hydrostatic pressure test set-up: Liquid

8.3.2 Leak Testing

Numerous techniques which cover broad ranges of sensitivity and cost can be used to measure leakage rates in a heat pipe container. Table 8-2 summarizes some of the most commonly used detection techniques. Before determining which technique is applicable to a particular heat pipe design, it is necessary to establish tolerable leakage rates to avoid unwarranted costs. Once a heat pipe design is established, the maximum loss of fluid inventory that can be tolerated can be calculated on the basis of allowable performance degradation. A leak rate can then be determined based on the design lifetime of the heat pipe. Figure 8-11 relates leakage rates of various heat pipe fluids from standard cubic centimeters/sec (std cc/sec) to equivalent loss on a gram per year basis.

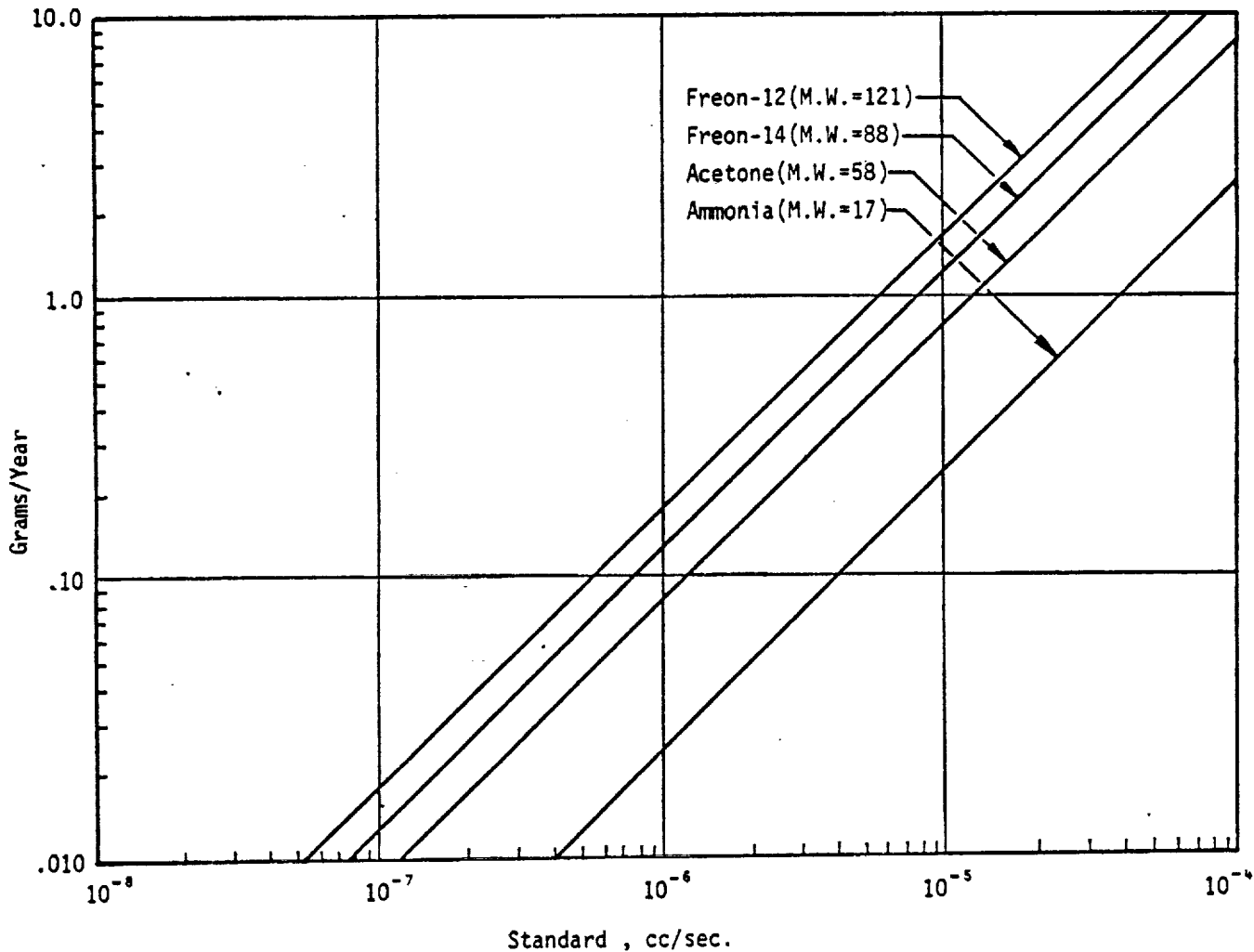


Fig. 8-11. Leakage rates (23)

TABLE 8-2. SUMMARY OF LEAK DETECTION TECHNIQUES (23)				
Leak detection technique	Sensitivity	Special equipment	Comments	
Precharging				
Penetrant method	Poor	None	Requires additional verification	
Radiography (X-ray)	Poor	X-ray machine	Not conclusive	
Nitrogen pressurization under water	10 ⁻⁴ std cc/sec	N2 bottle, water tank	Conclusive, quick and inexpensive	
Helium detectors	10 ⁻¹¹ std cc/sec	He mass spectrometer, vacuum chamber	Much equipment required	
Mass spectrometer	10 ⁻¹¹ std cc/sec	Mass spectrometer, vacuum station	Much equipment required	
Halogen leak detector	10 ⁻⁷ std cc/sec	Leak detector	Quick and inexpensive	
Post-charging				
Phenolphthalein (litmus paper)	Go/no go	None	Ammonia heat pipes, quick and inexpensive	
Copper Sulfate/ethylene glycol	10 ⁻⁷ - 10 ⁻⁸ std cc/sec	Chemical solutions	Ammonia heat pipes, 4 hrs	
Hot filament ionization gauge	10 ⁻⁹ std cc/sec	Ionization gauge	Ammonia heat pipes, quick	
Halogen leak detector	10 ⁻⁷ std cc/sec	Leak detector	Freon heat pipes, quick	
Solution PH	10 ⁻⁷ std cc/sec	PH indicator	Ammonia heat pipes, quick	
Mass spectrometer	10 ⁻¹¹ std cc/sec	Mass spectrometer, vacuum station	Much equipment required, applicable to any working fluid	

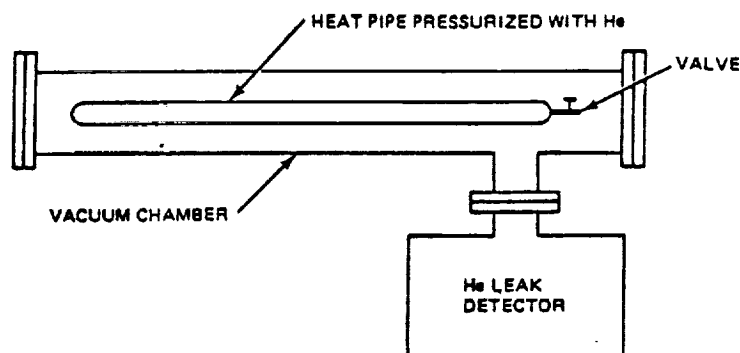
Once the desired maximum leak rate has been established, an appropriate leak test method can be selected from Table 8-2. The features of these leak detection techniques are discussed in detail in Ref. (23). Since most heat pipe applications require extended lifetime and since most designs involve only small fluid inventories, sensitive leak detection techniques, such as helium leak detectors, are often used to verify leak tightness prior to charging the heat pipe with a working fluid. After charging and pinch-off, any number of tests, as summarized in Table 8-2, can be used. The most commonly used leak detection methods listed in Table 8-2 are discussed in the following paragraphs.

8.3.2.1 Helium Detector Techniques

Techniques that use helium gas in conjunction with helium mass spectrometers offer much more sensitive, but more expensive, methods of leak detection. One type of procedure involves pressurizing the inside of a pipe with helium and measuring the leakage on the outside, giving an integrated leak rate. Figure 8-12 shows a typical set-up where the pressurized pipe is placed in a vacuum chamber attached to the leak detector/pumping station. Calibration of the system with a known leak is necessary before and after use. This technique allows the pipe to be leak checked at its operating (or proof) pressure and temperature, and depending on the equipment used, can detect leakage rates in the range of 10^{-11} std cc/sec.

GENERAL METHODS:

1. SNIFF OUTSIDE WITH He SNIFFER IN AMBIENT (METER, AUDIO DETECTOR).
2. PLACE IN EVACUATED CHAMBER AND CALIBRATE SYSTEM WITH STANDARD He LEAK RATE SOURCE



3. PLACE PIPE IN SEALED AIR ENCLOSURE AND PERIODICALLY MEASURE THE He CONTENT OF AIR SAMPLES

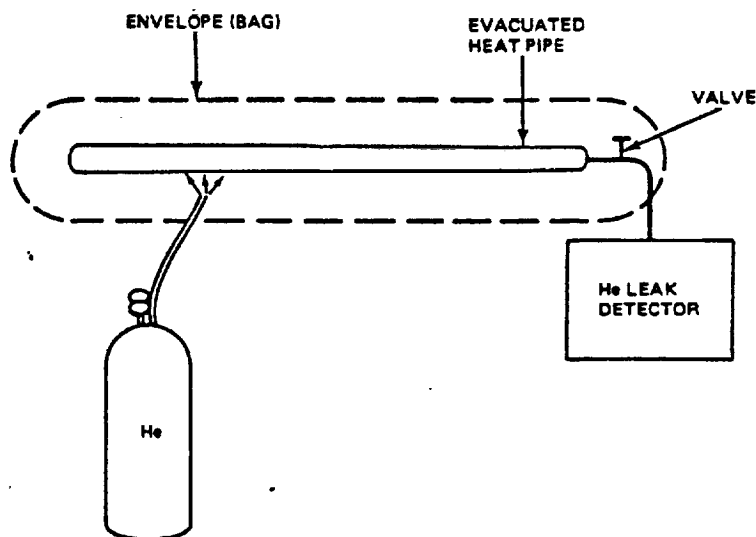
COMMENTS:

- ALLOWS PIPE TO BE PRESSURIZED TO SAME LEVEL AS OPERATING PRESSURE (AND TEMPERATURE)

Fig. 8-12. Helium leak detection techniques: Pressurized Pipe (23)

A somewhat less sensitive, but time saving, alternative is to use a portable helium sniffer in ambient air, thereby avoiding the use of the chamber. The sniffer is directed over specific areas of the pipe and can be used to pinpoint leakage sites. A number of small leaks may be acceptable if the total leakage is less than the specified value. Hence, a detector at least one order of magnitude more sensitive than the specified total leak is required. One method which also avoids the use of a vacuum chamber is to place the helium pressurized pipe in a sealed air enclosure and periodically sample the air for the presence of helium.

Figure 8-13 depicts another variation. The pipe is evacuated through a helium leak detector while helium is directed over the outside of the pipe. This can be done through an envelope (or bag) to determine gross leakage, followed by local impingement to identify the faulty area. The disadvantage with this technique is that the helium pressure difference across the pipe (high outside, low inside) is opposite to the normal pipe pressure gradient (high inside, low outside). In addition, the leak is simulated with only a 14.7 psi (1.014×10^5 newt/m²) pressure differential which may be many times smaller than would actually exist.



PROCEDURE:

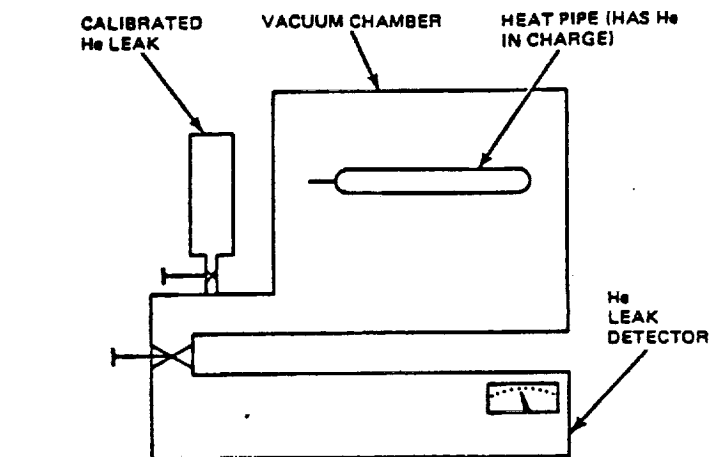
- (a) DETERMINE GROSS LEAKAGE BY PRESSURIZING ENVELOPE
- (b) ISOLATE LEAK BY DIRECTING He TO LOCAL AREAS

COMMENTS:

- CAN ONLY PRESSURIZE TO A DIFFERENCE OF PRESSURE OF 14.7 PSI, WHICH MAY BE MUCH LESS THAN ACTUAL PIPE OPERATING PRESSURE
- PRESSURE DIFFERENCE IS IN WRONG SENSE (SHOULD BE HIGHER INSIDE THAN OUTSIDE)

Fig. 8-13. Helium leak detection techniques: Evacuated Pipe (23)

A third helium detection technique, employed by Ames Research Center (24) for use with VCHP's, is described in Fig. 8-14. The technique is similar to that shown in Fig. 8-12, except the pipe is a gas controlled variable conductance heat pipe which has helium as part of the control gas charge. This technique has the benefit of leak testing a completely charged pipe at its anticipated operating temperature, including the pinch-off tube, a feature not found with the other helium techniques. It is limited to gas controlled VCHP's or heat pipes which can tolerate trace amounts of helium.



PROCEDURE:

- (a) EVACUATE CHAMBER TO 10^{-4} TORR OR LESS (NOTHING IN CHAMBER)
- (b) CALIBRATE DETECTOR WITH KNOWN SOURCE
- (c) INSTALL PIPE, PUMP DOWN TO 10^{-4} , READ LEAKAGE
- (d) REMOVE PIPE AND RECALIBRATE WITH KNOWN SOURCE
- (e) COMPARE PIPE LEAKAGE WITH PRE- OR POST-TEST CALIBRATED LEAK

COMMENTS:

- TECHNIQUE LIMITED TO GAS-CONTROLLED VCHP'S OR PIPES WITH TOLERABLE He IMPURITY
- CHECKS ENTIRE PIPE INCLUDING PINCHOFF TUBE
- WILL NOT PINPOINT LEAK

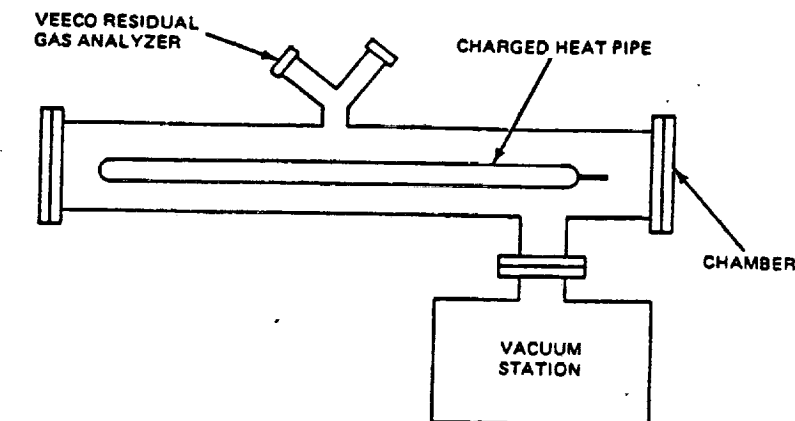
Fig. 8-14. Helium leak detection techniques: Charged Pipe (23)

8.3.2.2 Halogen Leak Detector for Freon Heat Pipes

Halogen leak detectors provide a fast, accurate method of checking Freon heat pipes. They are small, portable, relatively inexpensive units that use a pencil probe to pinpoint leaks. They can typically measure absolute leak level on the order of 10^{-7} std cc/sec. Detailed specifications are readily available from any of the manufacturers.

8.3.2.3 Mass Spectrometer

A general leak detection technique that can also be used on a completely sealed pipe with any working fluid is shown in Fig. 8-15. It employs a mass spectrometer, e.g. Residual Gas Analyzer, from which leak rates can be calculated. A problem with this procedure is its relative cost. Also, long pump-down times are required and there is difficulty in distinguishing compounds with similar molecular weights, e.g., water, 18 and ammonia, 17.



GENERAL PROCEDURE:

- (a) DO IMPURITY TRACE OF SYSTEM WITHOUT PIPE
- (b) INSERT PIPE
- (c) DO IMPURITY TRACE AT VARIOUS TIMES

$$\text{LEAK RATE} = \frac{\Delta \text{MASS}}{\Delta \text{TIME}}$$

SENSITIVITY: CAN DETECT 10^{-13} TORR OF NITROGEN

COMMENTS:

- CAN LEAK TEST CHARGED PIPE INCLUDING PINCHOFF TUBE
- CERTAIN ELEMENTS MAY BE DIFFICULT TO DISTINGUISH, SUCH AS H_2O (MOLECULAR WT = 18) AND NH_3 (MOLECULAR WT = 17)

Fig. 8-15. General leak detection for any working fluid

8.3.2.4 Copper Sulfate/Ethylene Glycol for NH_3 Heat Pipes

A relatively inexpensive but sensitive (3×10^{-8} std cc/sec) method for leak checking ammonia heat pipes has been developed by NASA/GSFC. It involves soaking filter paper in a copper sulphate/ethylene glycol solution, wrapping it around the weldment and enclosing it in an air-tight bag. After four hours, a simple visual inspection for the absence of dark blue spots will provide a 3.3×10^{-7} std cc/sec leak sensitivity measurement. If no dark blue spots are visible, applying a few drops of Nessler's reagent, and looking for dark

brown spots, can increase the sensitivity to about 3×10^{-8} std cc/sec. Reasonable care must be exercised to avoid false results from contamination of surfaces and reagents. The complete details of this procedure, as contained in OAO Document EX-D-1019-C (25), is given in Table 8-3.

TABLE 8-3. COPPER SULFATE/ETHYLENE GLYCOL LEAK DETECTION METHOD FOR NH₃ HEAT PIPES

Equipment Required - The equipment required to perform this ammonia leak test includes:

- Filter paper - Wattman No. 120 or equal
- Reagent solution (by weight) - 3% copper sulfate ($\text{CuSO}_4 \cdot 5\text{H}_2\text{O}$) and 10% ethylene glycol in distilled water
- Small plastic bags to cover ends of pipe after filter paper has been laid down
- Rubber band (or adhesive-backed tape) to hold plastic bags in place
- Nessler's reagent in dropping bottle

Procedure - The following procedure should be followed when leak checking heat pipes containing ammonia:

- Prepare filter paper as follows:
 - Soak one sheet of filter paper in reagent (copper sulfate) solution.
 - Blot wet filter paper between two sheets of dry filter paper.
 - Place wet filter paper in air-tight container (to prevent evaporation) until ready for use.
 - Cut filter paper into sheets approximately 1-1/2 in. (3.810 cm) by 2 in. (5.080 cm).
 - Wrap filter paper (prepared previously) around ends of pipes.
 - Cover ends of pipe and filter paper with small plastic bag and secure with rubber band or adhesive-backed tape.
 - Leave ends of pipe covered for at least four hours. This should provide a leak sensitivity of approximately 3.3×10^{-7} std cc/sec.
 - After at least four hours, remove plastic bag and filter paper and observe filter paper for dark blue spots. If these spots are visible, a leak rate of $\approx 3.3 \times 10^{-8}$ std cc/sec was exceeded. Note that dark brown spots may have resulted from the aluminum-copper sulfate reaction before the application of the Nessler's reagent and should be disregarded.

8.4 THERMAL PERFORMANCE TESTS

The thermal performance limits of the heat pipe, described in Chapter 2, can be investigated using a test set-up illustrated schematically in Fig. 8-16. The heat pipe is held at any desired orientation with respect to gravity with a supporting fixture. Heat is applied to one end of the heat pipe with an electrical heater and is removed from the opposite end by a coolant. Thermocouples are attached along the length of the heat pipe to measure the axial wall temperature along the heat pipe at different power inputs. The heat pipe is usually insulated to minimize parasitic heat losses or inputs. A typical test procedure, definition of terms, data reduction and special test considerations for cryogenic, intermediate temperature and liquid metal heat pipes are discussed in the next section.

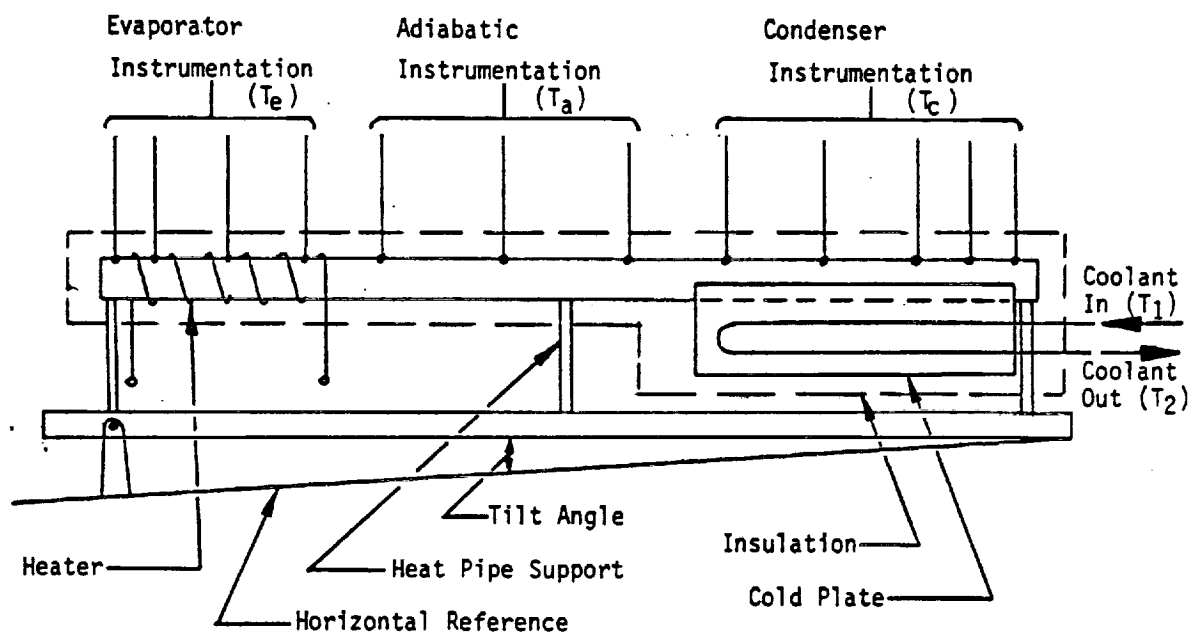


Fig. 8-16. Typical heat pipe performance test set-up

8.4.1 Test Procedure and Data Reduction

A typical test procedure consists of elevating the heat pipe to the desired test elevation, applying heat to the evaporator in predetermined increments and recording the resulting temperature profile as illustrated in Fig. 8-17. Sufficient time is allowed between power increments (typically 10 - 15 minutes) to allow the heat pipe to reach steady-state. Power is increased until the transport limit of the heat is reached. At this point the temperature at the end of the evaporator rises suddenly above the other

temperatures. This sudden rise in temperature indicates a "dry-out" condition. That is, the internal liquid flow rate required to accommodate the rate of heat input is in excess of the heat pipe's pumping capacity.

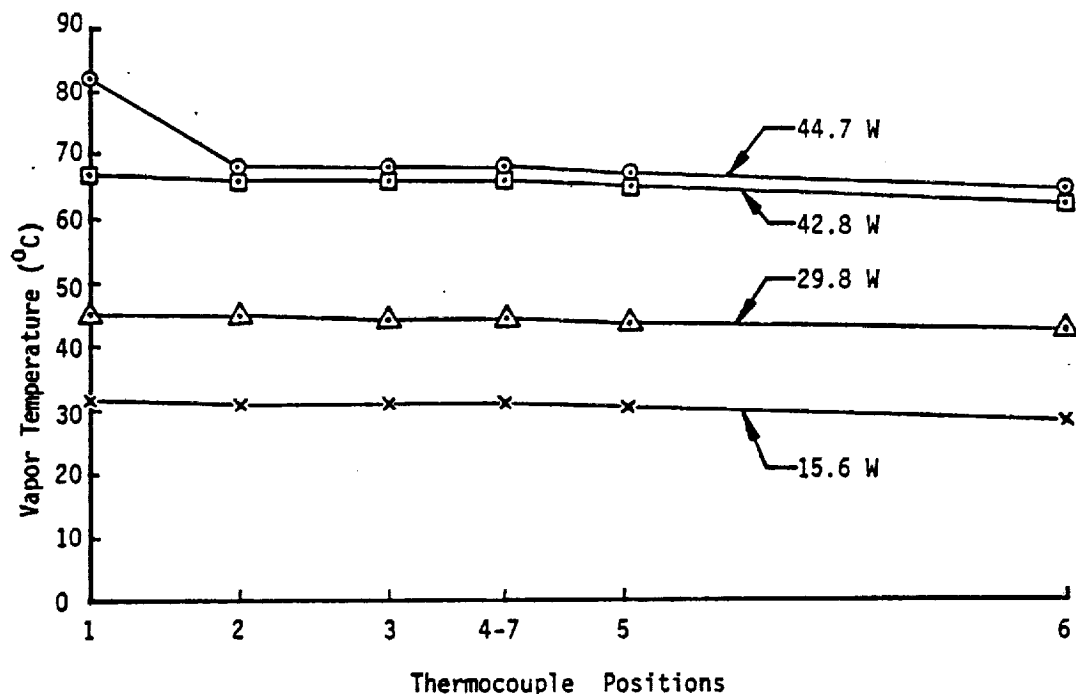


Fig. 8-17. Typical temperature profiles along a heat pipe under test.

Accurate determination of the dry-out point can be influenced by a number of factors including axial conduction along the wall of the heat pipe. For this reason and to minimize the amount of test data point plotting, it is convenient to plot the temperature difference between the end of the evaporator and the vapor temperature (adiabatic temperature) as illustrated in Fig. 8-18. Since the internal heat transfer coefficient in the evaporator is approximately constant, the temperature drop between evaporator and the vapor is a linear function of power input. When partial dry-out is reached, the effective evaporator area is reduced and the slope of the temperature drop versus power is changed. The point of significant change in slope establishes the dry-out point.

Once the dry-out point has been reached, the usual procedure is to reduce the power until complete recovery has been achieved. Heat pipe recovery can be used to confirm the dry-out point in homogeneous wick designs. In composite wick designs, complete power shut-down and a reduction in elevation may be required.

The above procedure is repeated at various elevations and a plot of the maximum (dry-out) heat load versus elevation can be developed as illustrated in Fig. 8-19. The following performance data can be obtained from the plots presented in Fig. 8-17, 8-18, and 8-19.

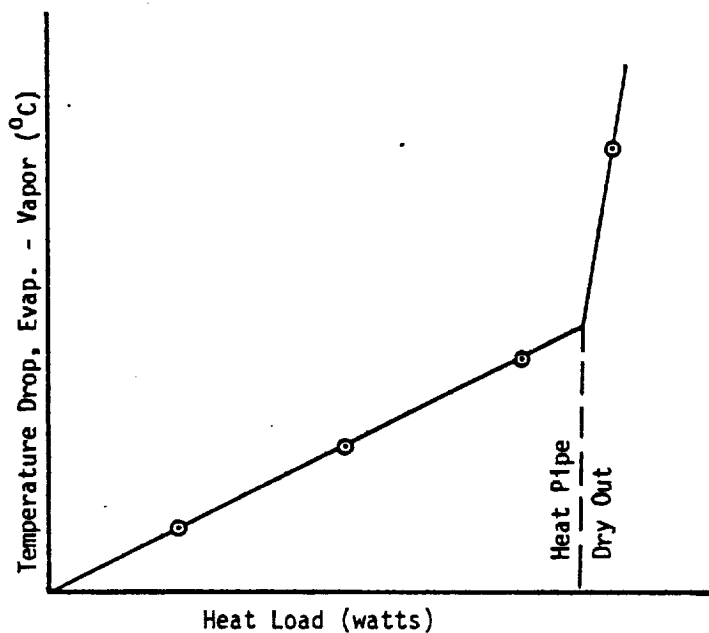


Fig. 8-18. Heat pipe temperature drop versus applied heat load

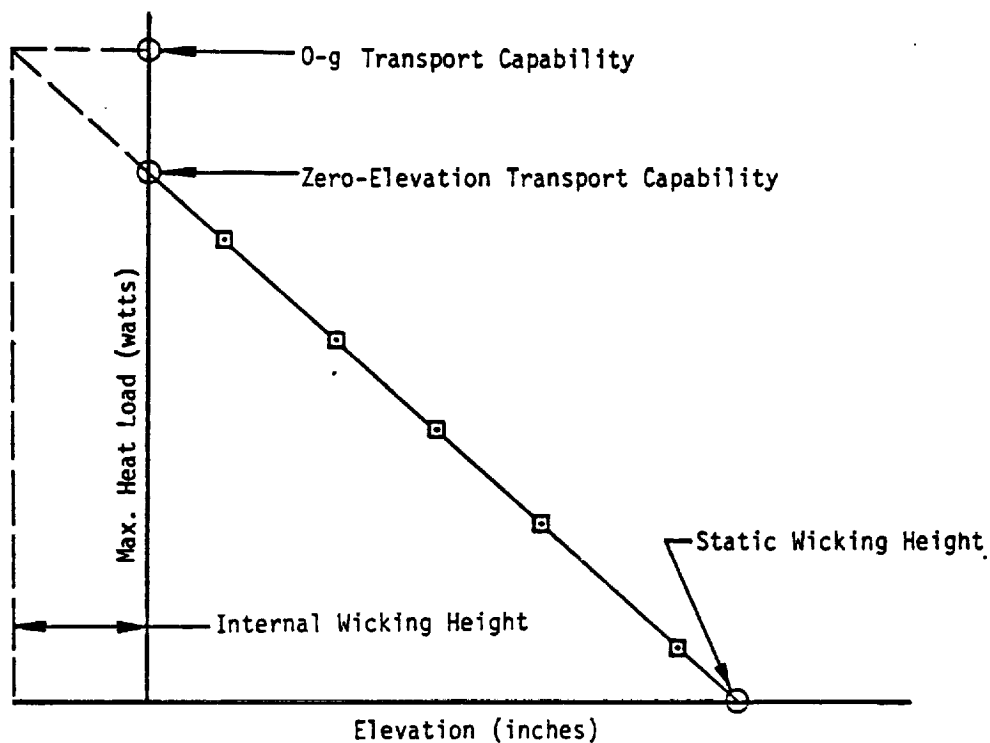


Fig. 8-19. Maximum heat load versus elevation

8.4.1.1 Dry-Out Heat Transfer Rate

Dry-out is defined as the heat load which causes a significant change of slope in the evaporator ΔT versus Q curve (e.g. Fig. 8-18). The evaporator ΔT is defined as the maximum temperature drop between the evaporator (usually the end thermocouple) and the vapor (average adiabatic) temperature. Dry-out is reached when the performance limits as defined in Chapter 2 are exceeded.

8.4.1.2 Heat Transport Capacity

Heat transport capacity is the maximum heat load that the heat pipe can carry over a given distance and at a given elevation and operating temperature. Heat transport capacity is often defined in terms of watt-inches or watt-meters. For uniform heat input and removal as illustrated in the test set up shown in Fig. 8-16, the effective transport length is defined as:

$$L_{\text{eff}} = \frac{1}{2} L_e + L_a + \frac{1}{2} L_c \quad (8-17)$$

And the heat transport capability can be defined as:

$$(QL)_{\text{max}} = Q_{\text{max}} \times L_{\text{eff}} \quad (8-18)$$

Where Q_{max} is the dry-out heat load. The heat transport capability can be applied to establish heat pipe performance for applications with various heat load/heat sink combinations as long as the liquid and vapor flows are in the laminar regime and the limiting performance is due to the capillary pumping limit.

Tests at a horizontal elevation are not usually performed in order to avoid any significant performance contribution due to puddle flow inside the heat pipe. The curve in Fig. 8-19, however, can be extrapolated to obtain zero-elevation transport capability which in turn can be used to establish "0-g" performance. If the internal wicking height (circumferential wicking height) of the heat pipe is not significant, extrapolated zero-elevation capability can be used to directly estimate "0-g" performance. If the internal wicking height is significant, it must be included in the performance extrapolation as shown in Fig. 8-19.

8.4.1.3 Static Wicking Height

The static wicking height can also be determined from the plot of Q_{\max} versus evaporator tilt. The static wicking height is the extrapolated elevation which corresponds to zero power input as shown in Fig. 8-19. This value can be used to determine the effective pumping radius of the wick.

8.4.1.4 Thermal Conductance

The thermal conductance of the heat pipe can be determined from temperature profiles obtained during heat transport tests. The thermal conductance is the slope of the curve generated by plotting heat load (Q) versus temperature drop. Averages of all the evaporator temperature readings (T_e), adiabatic temperature readings (T_a), and active condenser readings (T_c) are used typically to obtain the conductance in each section. Curves, similar to Fig. 8-18, are plotted based on average evaporator temperature drops ($T_e - T_a$) and the slope of the curves ($Q/\Delta T_e$ and $Q/\Delta T_c$) are obtained. Equivalent evaporator and condenser film coefficients

$$\bar{h}_e = \frac{Q}{\Delta T_e} \times \frac{1}{A_e} \quad (8-19)$$

$$\bar{h}_c = \frac{Q}{\Delta T_c} \times \frac{1}{A_c} \quad (8-20)$$

where A_e and A_c are the active liquid/vapor interface areas in the evaporator and condenser, respectively. The internal tube circumference is generally used in calculating the area. Any blocked condenser zone or partially dried-out evaporator zone is excluded from the above thermal conductance determination.

8.4.1.5 Condenser Blockage

If sufficient instrumentation is placed at the end of the condenser, blockage due to non-condensable gasses or excess liquid can be detected. Condenser blockage can be used to determine if the heat pipe has been properly processed and charged or if compatible materials have been used. Gas blockage can be distinguished from liquid blockage by the fact that the length of non-condensable gases blocked region will compress or expand depending on the operating temperature. Liquid blockage will not. If liquid blockage is detected, charge calculations and procedures can be checked to remedy the problem. To determine if gas blockage is due to processing or incompatibilities, heat pipe life tests similar to the compatibility tests defined in Section 8.1.1.2 are required.

If the gas blockage continues to increase over a period of time, the selected materials are incompatible or contaminants have been introduced during processing. If the amount of gas blockage remains constant, the heat pipe or the working fluid were not properly outgassed during processing.

8.4.2 Test Apparatus

The apparatus shown in Fig. 8-16 can be used, with appropriate modification, to test any heat pipe design under various types of test conditions. Typical test set-ups are discussed below. These can be applied to most intermediate temperature heat pipes. Special considerations for cryogenic and liquid metal temperature heat pipes are also discussed.

8.4.2.1 Heat Input

Heat can be applied in any of several forms including electrical heaters wound around the evaporator or with a heater block containing cartridge or strip heaters as illustrated in Fig. 8-20. The latter is often used to simulate actual interface conditions actually encountered in many applications. For higher power requirements, it is convenient to use eddy current heating (Fig. 8-20c) in combination with a calorimeter located at the condenser. For electrical resistance heating, wattmeters covering the anticipated power range, and a variac for close power control are used.

8.4.2.2 Heat Removal

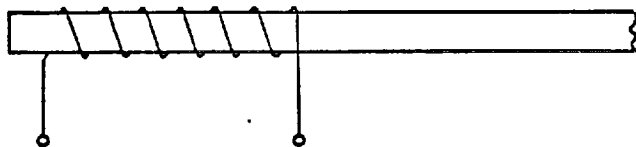
Heat from the condenser can be removed by direct cooling with a coolant bath, forced air cooling or the heat pipe may be attached to a cold plate equipped with cooling coils and a trim heater for temperature control as illustrated in Fig. 8-20. The test temperature of the heat pipe is always controlled by varying the cooling rate at the condenser. This is accomplished by controlling the temperature of the coolant and/or its flow rate. Electrical trim heaters, as illustrated in Fig. 8-20c, are often used to obtain accurate control of the test temperatures.

8.4.2.3 Instrumentation

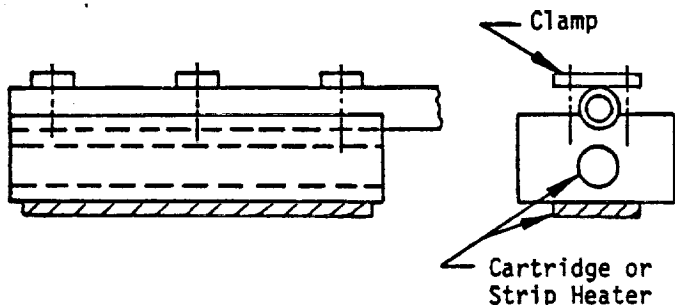
Instrumentation usually consists of a series of thermocouples of the type appropriate for the desired test temperature. They can be either strapped-on, spot welded, epoxy bonded, or held by pressure contact against the heat pipe container. The important factors in proper instrumentation are:

- Thermocouples and instrumentation should be calibrated for accurate temperature readings.

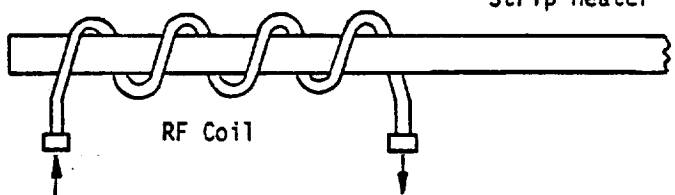
A. EVAPORATOR HEATERS



a. Electrical Heater Winding

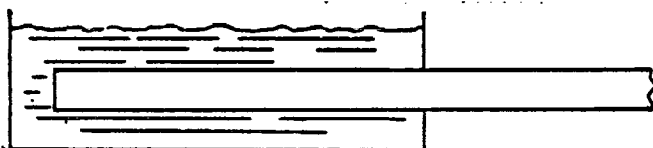


b. Heater Block

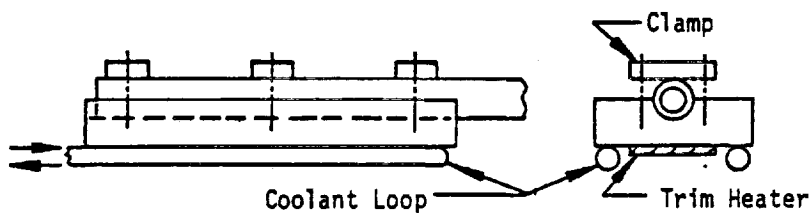


c. Eddy Current Heating

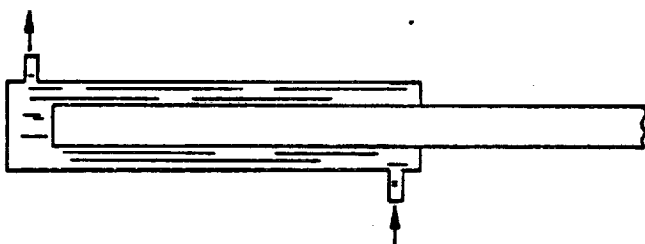
B. CONDENSER COOLERS



d. Bath



e. Cold Plate



f. Calorimeter

Fig. 8-20. Types of evaporator/condenser test apparatus

- Good contact between the thermocouple and the heat pipe is necessary to avoid measurement errors.
- Thermocouples should be located as close as possible to the actual heat input/output area.

The last requirement often presents a problem in the evaporator area since a thermocouple and the heater cannot be physically located in the same area at the same time. The thermocouple should be located as close to the heater as possible; however, care should be exercised to avoid direct contact with the heater since this can result in excessively high temperature readings.

8.4.2.4 Heat Pipe Leveling

A support fixture is required to maintain the proper heat pipe orientation. This fixture can be as simple as a series of ringstands. Adequate support, however, must be provided to achieve accurate elevations since the heat pipe is typically made of a long slender tube. Tilt tables with a series of stand-offs are often used in heat pipe test set-ups. The heat pipe is mounted to the stand-offs which are designed to locate the heat pipe parallel to the plane of the tilt table. The heat pipe elevation is then controlled by varying the tilt in the table. Elevation of the heat pipe is determined either by measuring the angle of tilt or by measuring the elevations of the table at controlled points. A commonly used elevation measurement technique involves the use of a machinist scale in combination with a transit. With this method, accurate elevations of the tilt table or the heat pipe itself can accurately be determined at any number of desired points as long as the location can be sighted with the transit.

8.4.2.5 Intermediate Temperature Test Apparatus

Intermediate temperature testing is usually performed in a laboratory environment with no special test set-up considerations except those discussed above. Once the heat pipe is set up on its test fixture, instrumented and leveled, a blanket of insulation is applied around the heat pipe to minimize parasitic heat losses. The type of insulation used is dependent on the operating temperature. For below ambient temperature tests, closed cell foam insulation can be used to minimize water condensation; above ambient temperature, conventional fiberglass is used. At elevated temperatures, care should be taken in select-

ing the appropriate type of insulation since they contain binders which can vaporize if used at higher than recommended temperatures.

With respect to the cooling of the condenser, a number of coolants such as water, water-glycol, high temperature fluids such as Dowtherm, or forced air cooling may be used depending on the test temperature and the selected design of the test fixture.

8.4.2.6 Cryogenic Temperature Test Apparatus

The principal difference between cryogenic heat pipe tests and those at ambient temperature is that a vacuum chamber (as illustrated in Fig. 8-21) is required for cryogenic temperatures, to avoid excessive parasitic heat inputs. Two reasons dictate this requirement. First, cryogenic heat pipes have relatively low heat transport performance and, hence, parasitic heat input can significantly affect performance measurements since typical test heat loads are low. Second, expensive coolants such as liquid nitrogen or liquid helium are required. Minimum expenditures of the coolant materials is desirable for cost effective testing.

Multilayer insulation (MLI) blankets, consisting of alternate layers of aluminized mylar and nylon netting are used to obtain the required insulation properties for cryogenic testing. To achieve the full potential of this type of insulation, contamination should be kept to a minimum, the insulation should be well vented and loosely wrapped with no direct radiation paths between the heat pipe test set-up and the chamber, and a hard vacuum should be provided. To provide the necessary vacuum level a diffusion pump in combination with a mechanical roughing pump is desirable.

In addition to proper insulation, the heat pipe test apparatus must be carefully designed to provide accurate support of the heat pipe with conduction heat leaks kept to a minimum. Support provisions should be made of low conductivity materials (e.g. plastics such as lexan) and the conduction path should be kept as long as possible. Accurate location of the heat pipe on the test fixture is required since sighting (leveling) of the heat pipe cannot be performed directly once the chamber is closed. Leveling and accurate elevation measurements are especially critical since cryogenic fluids have relatively low static heights.



Fig. 8-21. Thermal control heat pipe configurations and set-up for cryogenic tests

Other test apparatus used in the testing of cryogenic heat pipes include:

(1) hermetically sealed feed-through for both instrumentation and power leads; (2) liquid nitrogen or liquid helium supplies for the cooling of the vacuum chamber; and (3) trim heaters on the cold plate for temperature control adjustment.

8.4.2.7 Liquid Metal Temperature Test Apparatus

Material stability at high temperatures and the relatively large heat transport capability of liquid metal heat pipes are the principal factors affecting high temperature testing. Liquid metal heat pipes made of stainless steel or super alloys such as Inconel can be tested in air since they do not present an oxidation problem. Heat pipes made of refractory metals, however, must be either tested in an inert environment or in a vacuum chamber similar to cryogenic heat pipes. If the heat pipe is tested in a vacuum chamber, similar considerations apply as discussed above for the cryogenic heat pipe. The difference, of course, being that the type of insulation and heat pipe support materials must be consistent with the operating temperature. Nickel foil, for example, can be used to insulate the heat pipe and cooling can be provided by radiation to a cold shroud or to the ambient if a glass chamber is used.

As indicated above, many of the liquid metal heat pipes do not require an inert environment or a vacuum for testing. Test apparatus for these heat pipes, however, do require some special considerations. For example, electrical resistance heaters are limited both in operating temperature and power density. Cooling is also limited to radiation, conduction through gases or convection. For these reasons, it is often convenient to test liquid metal heat pipes with eddy current heating and removing the heat with a gas-gap calorimeter as illustrated in Fig. 8-22. This method of heating can provide high power density while maintaining the heating element (RF Coil) cool. Direct power measurement cannot be obtained since this is dependent on the coupling efficiency between the coil and the heat pipe. To determine heat transfer rates, a calorimeter with a gas-gap is often used. The gap thickness and the type of gas used are selected to reduce the temperature to a level where conventional coolants can be employed. The heat flow is determined from the rate of coolant flow and its temperature rise in the calorimeter. By varying the gap size and/or the type of gas used, heat flow rates can be varied.

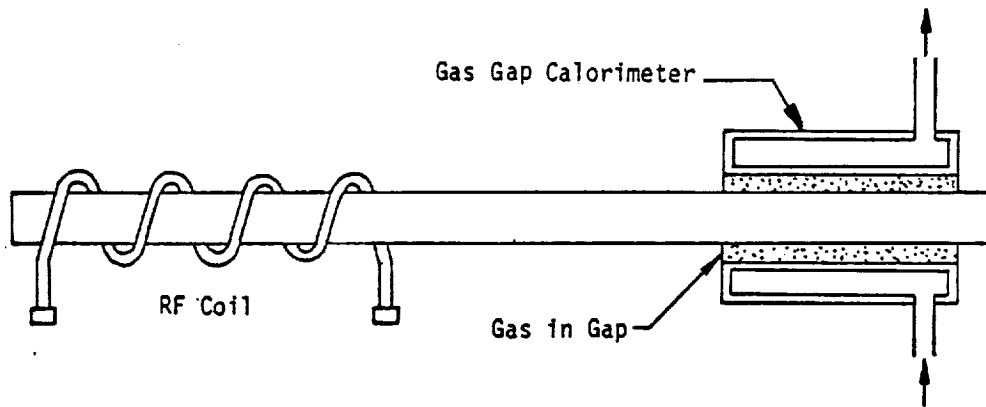


Fig. 8-22. Typical liquid metal high temperature heat pipe test set-up

8.5 THERMAL CONTROL TESTS

Test set-ups and procedures for thermal control heat pipes are similar to fixed conductance heat pipes with the added requirement for testing to evaluate the various control features. Requirements for gas-loaded variable conductance heat pipes and diodes are discussed below.

8.5.1 Gas-Loaded Heat Pipes

Figure 8-23 illustrates a typical test set-up for determining the variable conductance behavior of a gas-loaded heat pipe. It is similar to a fixed conductance heat pipe set-up with the addition of a thermal link between the gas reservoir and the coolant loop. A separate trim heater is provided in this region to allow independent control of the reservoir temperature. Test procedures and test data reduction are discussed below.

8.5.1.1 Thermal Performance Test

Thermal performance tests of gas-loaded variable conductance heat pipes are performed in a similar fashion as described for the fixed conductance heat pipe with the exception that the sink (coolant) temperature conditions must be maintained such that the gas interface resides in the condenser region. For the maximum transport length condition, the interface is maintained close to the reservoir. Expansion of the interface into the reservoir should be avoided to prevent liquid entrapment and premature dry-out of the heat pipe. Dry-out tests are also often performed with the gas interface at other locations in the condenser region to determine the effects of gas loading on heat pipe performance.

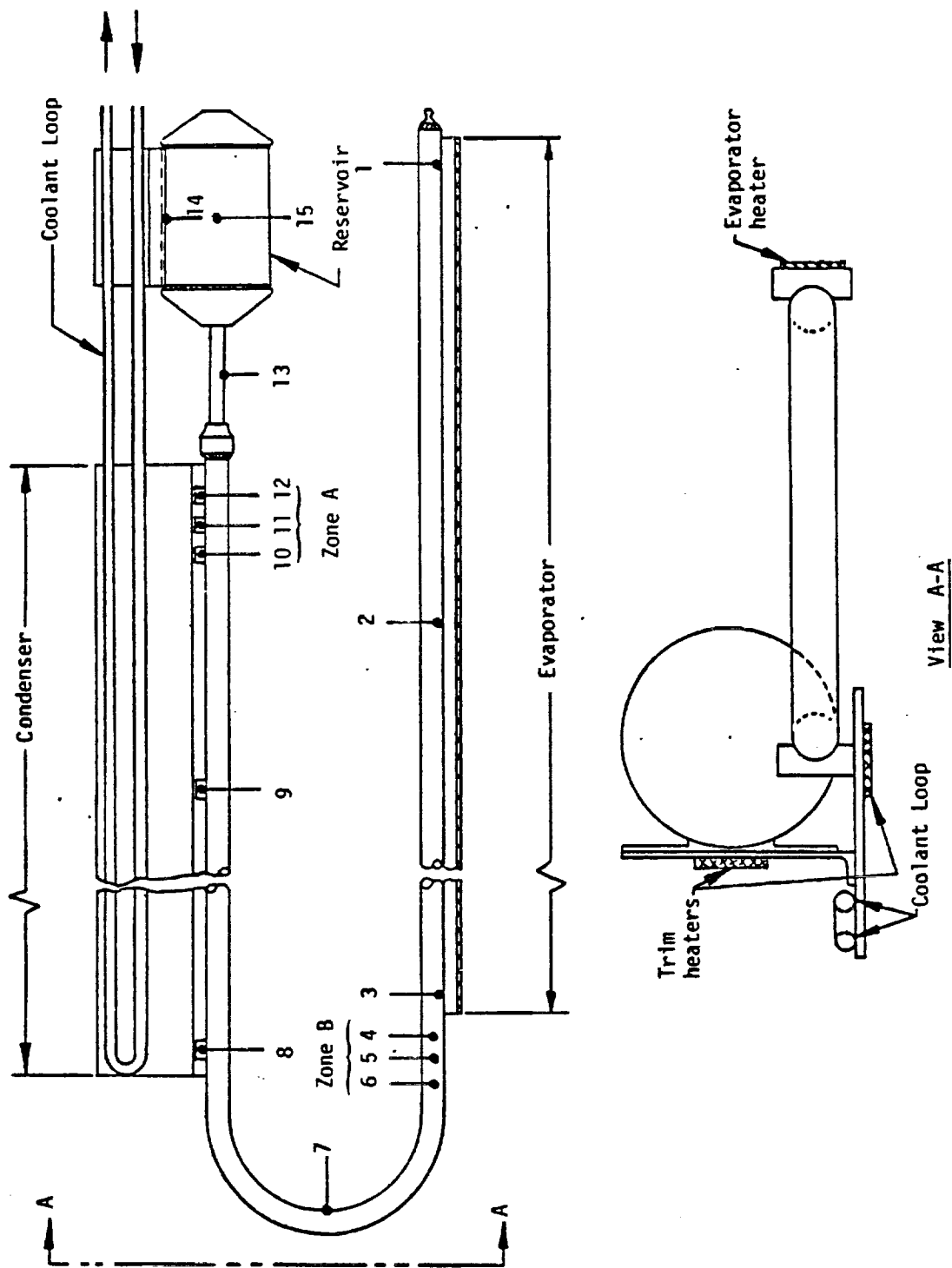


Fig. 8-23. Gas-controlled heat pipe test set-up

8.5.1.2 Thermal Control Tests

Thermal tests are also performed to determine the control characteristics of the variable conductance heat pipe. The general objective of these tests is to observe the response of the heat source or evaporator temperature to variations in the heat load and/or sink conditions. Results from the tests are used to establish the degree of temperature control that can be obtained. Test data can also be used to establish the gas charge, the "OFF conductance" and in the case of diode operation, the shutdown energy. For example, the sink (coolant) condition may be held constant while the power is increased. At each power increment, a temperature profile can be obtained and plotted to determine source, evaporator and/or vapor temperature as a function of power input as illustrated in Fig. 8-24. The test can be repeated for various sink temperature conditions until the thermal control characteristics are established over an entire range of operating conditions.

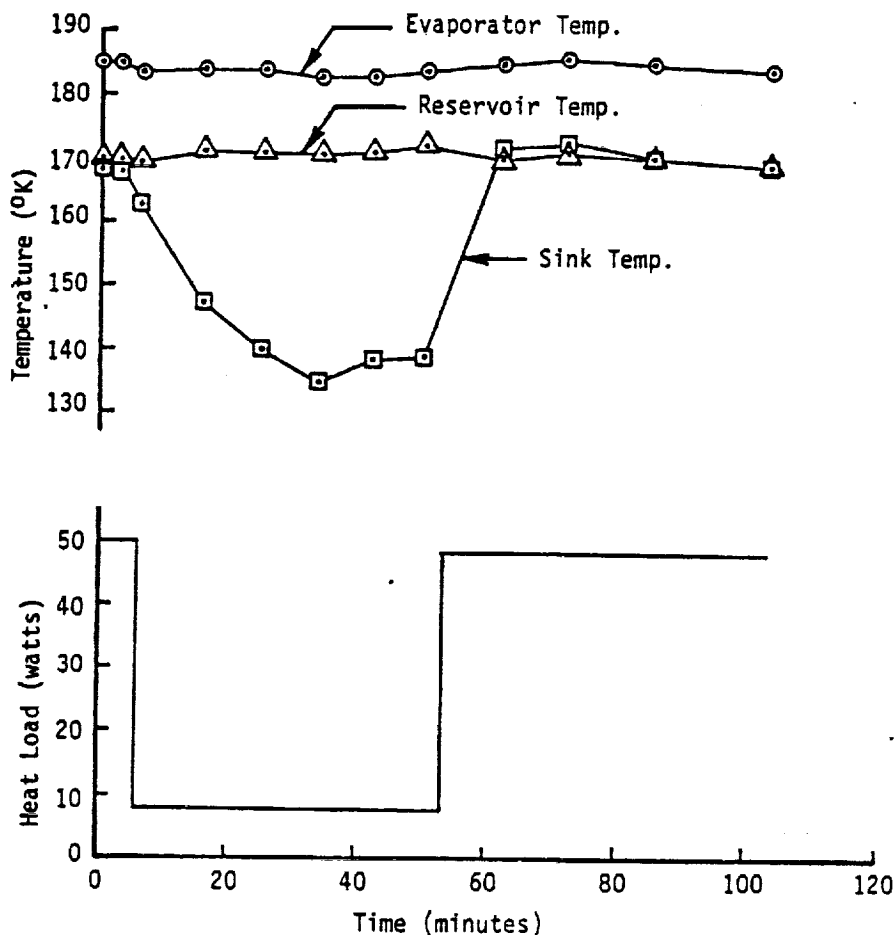


Fig. 8-24. Typical temperature profile for a gas-controlled heat pipe

In most instances, a VCHP can be adequately characterized by measuring its performance at maximum and minimum design conditions. Maximum test conditions consist of applying the maximum amount of power to be controlled by the VCHP with the sink (coolant) condition set at the maximum anticipated operating temperature. After steady state is achieved, the temperature profile is recorded. Minimum test conditions consist of lowering the sink (coolant) temperature to the minimum anticipated operating condition. The power input is also lowered to the minimum value expected during operation. Automatic recording equipment (e.g., a stripchart recorder) can be used to establish VCHP response characteristics between maximum and minimum operating conditions and vice versa. The response characteristics obtained, however, are meaningful only if the rate of sink temperature change, rate of power change and the thermal mass of the test set-up are representative of the actual application.

The following VCHP performance characteristics can be established.

(1) Minimum Set Point

The minimum set point of a gas-loaded heat pipe is the condition at which complete shutdown occurs. It is defined as the lowest acceptable evaporator or heat source temperature which corresponds to the minimum heat load and minimum sink temperature. Generally, the interface is located within the adiabatic section at the evaporator end for this condition. Complete shutdown occurs when the interface moves into zone B in the heat pipe shown in Fig. 8-23. Tests at this condition consist of establishing that the evaporator temperature does not drop below the specified value for the minimum heat load and sink temperature. The test procedure involves applying the minimum heat load and then reducing the sink temperature until the evaporator temperature drops below the control range. Results from this test will determine the adequacy of the gas charge and the "OFF" conductance. It could happen that the gas charge calculated from the data does not agree with the measured value. An undercharge of gas would result in inadequate shutdown at the minimum condition.

(2) Maximum Set Point

The maximum set point is the highest allowable heat source or evaporator temperature. It is the condition at which the condenser is fully active (i.e. interface is in zone A in Fig. 8-23), corresponding to the maximum heat load and sink temperature. Tests at this condition consist of establishing that the evaporator temperature does not rise above the specified upper limit when the maximum heat load and sink temperature are applied as boundary conditions. The test procedure involves applying the maximum heat load and then raising the sink temperature until the evaporator temperature exceeds the control range. Results from this test will determine the adequacy of the reservoir or whether an overcharge of gas exists.

8.5.2 Diode Heat Pipes

Fig. 8-25 illustrates a test apparatus for a liquid trap diode. It is virtually identical to the fixed conductance set-up except that provision must be made to incorporate a simulated thermal mass which is thermally coupled to the evaporator and reservoir. The purpose of the thermal mass is to absorb the shutdown energy and the reverse mode heat leak. Generally, a solid metal block is used (26), although phase change materials have been proposed. In any case, the thermal mass should simulate the thermal interfaces and the actual heat capacitance that are envisioned for the final application. The test apparatus for a liquid blockage design includes the thermal mass and must also have provision to couple the liquid reservoir to the effective sink condition.

8.5.2.1 Diode Thermal Performance Test

Forward mode thermal performance tests with a diode heat pipe are identical to tests with fixed conductance heat pipes. The data obtained can be reduced in the same fashion to determine dry-out, heat transport capability, static wicking height, and forward mode thermal conductance. During forward mode testing, care should be exercised to insure that the test set-up results in proper reservoir temperatures. In the case of the liquid trap, the reservoir temperature must be at or above the vapor temperature to avoid fluid inventory depletion. In the case of a liquid blockage design the reservoir should be below the vapor temperature to avoid excess liquid in the heat pipe.

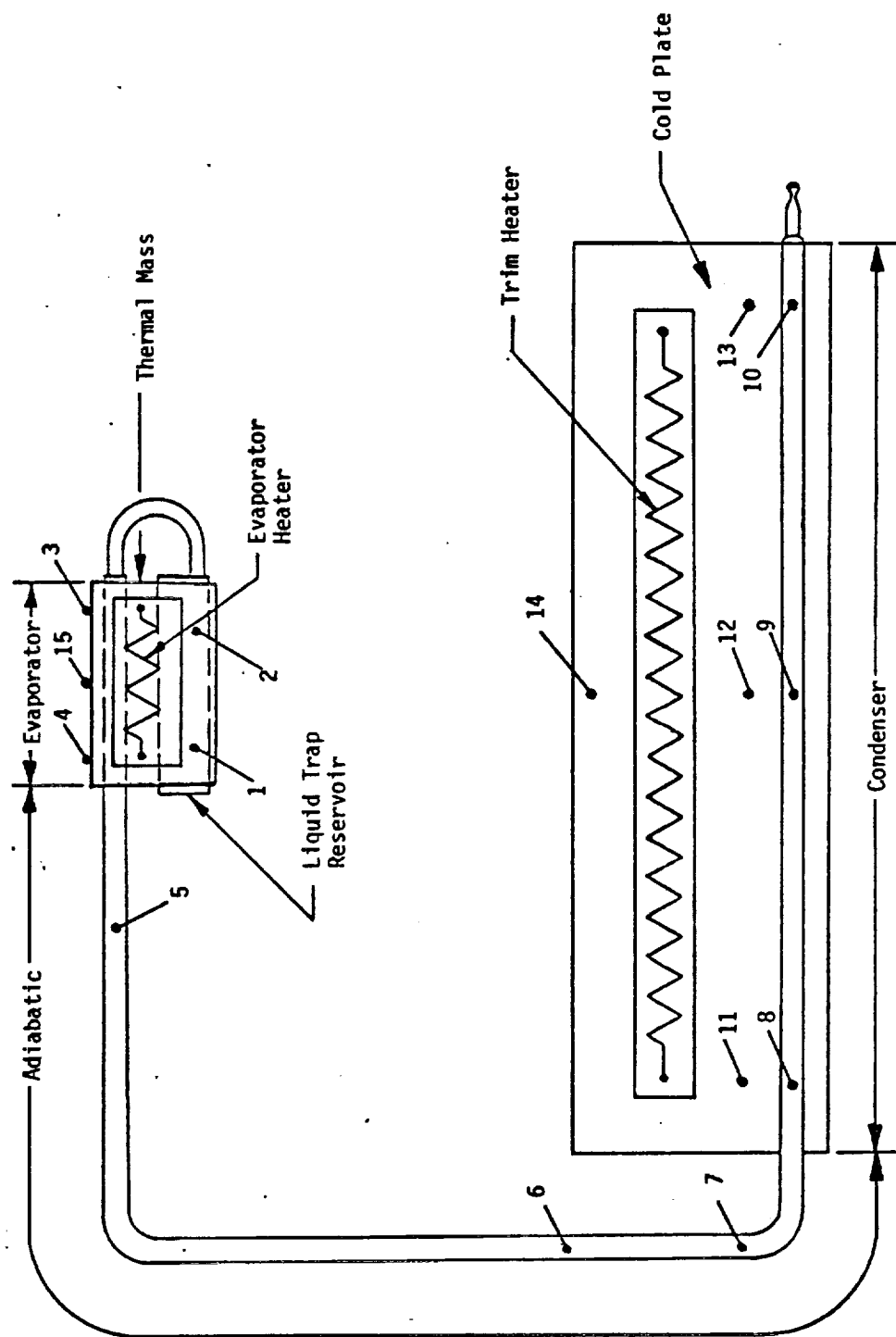


Fig. 8-25. Typical liquid trap diode heat pipe test setup

8.3.2.2 Diode Thermal Control Test

The purpose of the diode thermal control test is to establish reverse mode behavior of the heat pipe when the sink temperature rises above the forward mode operating temperature. The test sequence is normally initiated from a nominal forward mode condition with some heat being applied to the evaporator. Once conditions have been stabilized in the forward mode, power is applied to the cold plate trim heater such that the condenser temperature begins to increase at a rate which is typical of a given application. Heater power is maintained on the cold plate until a maximum temperature is achieved within a desired period of time. Power is then removed from the trim heater until complete recovery (i.e. forward mode) is achieved.

A typical test profile for a liquid trap diode is illustrated in Fig. 8-26 (27). As can be seen during the initial stages of reversal, the entire system rises at the same temperature rate as the cold plate. After a short period of time (i.e. minutes), the reservoir partially depletes the fluid inventory, the heat pipe no longer functions efficiently and the rate of temperature rise of the heat pipe begins to decline as compared to the cold plate temperature. Eventually, the heat pipe liquid inventory becomes completely depleted and the heat pipe ceases to function. At this point a significant temperature rise develops between the thermal mass and the adiabatic sections. "OFF" conductance and shutdown energy are determined from the data as follows.

(a) "OFF" Conductance

Once complete shutdown has been established, the reverse mode conduction heat leak (\dot{Q}_{RM}) from the "hot" condenser section to the heat source can be determined from the rate of temperature rise of the thermal mass. Generally, parasitic heat loads must be added or subtracted in order to establish an accurate estimate of the OFF conductance. The "OFF" conductance (C_{RM}) is then determined from

$$C_{RM} = \frac{\dot{Q}_{RM}}{T_C - T_{HS}} \quad (8-21)$$

where:

T_C = Temperature of the condenser after equilibrium condition
have been achieved in the reverse mode

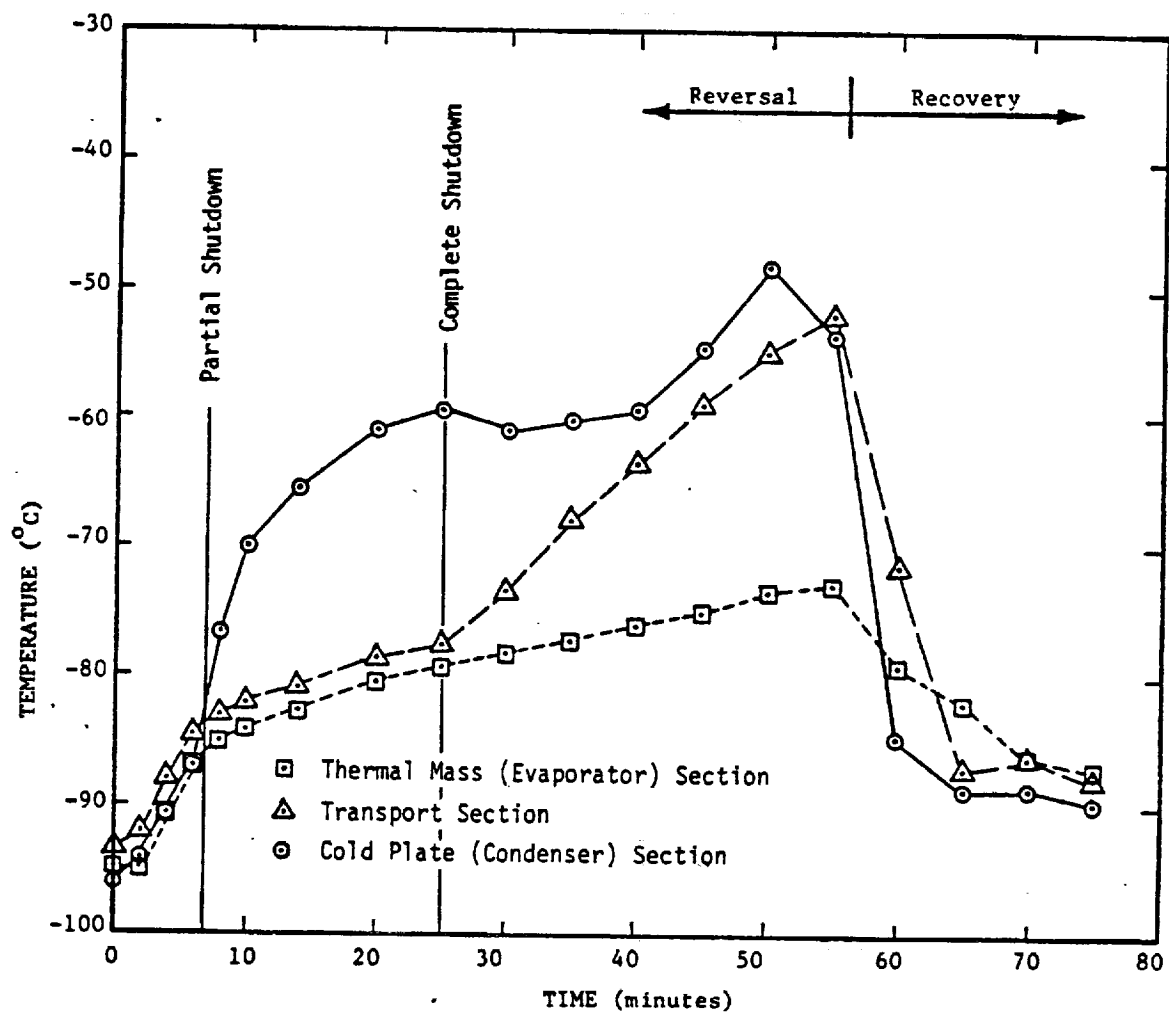


Fig. 8-26. Typical liquid trap diode temperature profile

T_{HS} = Temperature of the heat source (thermal mass) after equilibrium conditions have been achieved in the reverse mode

(b) Shutdown Energy

The shutdown energy (E_{SD}) is defined as the energy that the heat source received during the time between the start of the reverse mode and the time when complete shutdown is achieved. During this period there is a diminishing heat pipe action that exists between the "hot" condenser section and the heat source (thermal mass). Shutdown energy can be determined by establishing the rates of rise of the temperature of thermal mass during the shutdown period and over an interval after shutdown has occurred. Integration of the difference between the two rates over the shutdown period then gives the shutdown energy.

REFERENCES

1. Bickerman, J. J. Ind. Eng. Chem., Anal. Ed. 13, 1941. p. 443.
2. Rebinder, P., et. al., Kolloid Z. 65, 1933. p. 268.
3. Bigelow, W. C., et. al., Jour. Coll. Sci. 1, 1946. p. 513.
4. Adam, N. K., Jessup, G. Jour. Chem. Soc. 1925. p. 1863.
5. Fowkes, F. M., Haskins, W. D. Jour. Am. Chem. Soc. 62, 1940. p. 3377.
6. Spreece, A. L., et. al., Rev. Sci. Instr. 28, 1957. p. 636.
7. Bartell, F. E., Walton, C. W., Jr. Jour. Phys. Chem. 38, 1934. p. 503.
8. Ablett, R. Phil. Mag. 46, 1923. p. 244.
9. Guastalla, J. Proc. 2nd Int'l. Congr. Surface Activity. V. 3, London, 1957. p. 143.
10. "Design and Development of a Prototype Static Cryogenic Heat Transfer System," NAS5-21191, Dynatherm Corp., Cockeysville, Md. August 1971.
11. Saaski, E. W. and Owzarski, P. C., Two-Phase Working Fluids for the Temperature Range 50° to 350°C," Sigma Research, Inc., Richland, Wash., June 1977.
12. Dunn, P. and Reay, D. A., Heat Pipes, Pergamon Press, New York, 1976.
13. Eninger, J. E., Fleischman, G. L., Luedke, E. E., "Heat Pipe Materials Compatibility," Final Report, TRW Systems Group, Calif., Jan. 1976.
14. Baker, E., "Prediction of Long-Term Heat Pipe Performance from Accelerated Life Tests," AIAA Journal, Vo. II, No. 9, Sept. 1973.

15. Kunz, H. R., Langston, L. S., Hilton, B. H., Wyde, S. S. and Nashick, G. H., "Vapor-Chamber Fin Studies," NASA CR-812, June 1967.
16. Katzoff, S., "Heat Pipes and Vapor Chambers for Thermal Control of Spacecraft," Thermophysics of Spacecraft and Aeronautics, V.20, Academic Press, New York, 1968, pp. 761-818.
17. Freggens, R. A., "Experimental Determination of Wick Properties for Heat Pipe Applications," Proc. of 4th Intersociety Energy Conversion Conference, Washington D.C., September 1968, pp. 888-897.
18. Farran, R. A. and Starner, K. E., "Determining Wicking Properties of Compressible Materials for Heat Pipe Applications," Annual Aviation and Space Conference, Beverly Hills, California, June 1968, pp. 659-669.
19. Phillips, E. C., "Low Temperature Heat Pipe Research Program," NASA CR-66792, June 1969.
20. Marjon, P. L., 12th Monthly Progress Report, DOT Contract No. FH-11-7413, Dynatherm Corporation, November 1971.
21. Ginwala, K., Blatt, T. A., and Bilger, R. W., "Engineering Study of Vapor Cycle Cooling Components for Space Vehicles," Tech. Doc. Rept. ASD-TDR-63-582, Wright-Patterson Air Force Base, Ohio, September 1963.
22. "Flexible Cryogenic Heat Pipe Development Program," Final Report, NASA CR 152027, NAS2-8830, Rockwell International, July 1977.
23. "Heat Pipe Manufacturing Study," Final Report, NAS5-23156, Grumman Aerospace Corp., Bethpage, New York, August 1974.
24. Environmental Test Procedure for Leak Test - Ames Heat Pipe Experiment, R & QA Document No. PERS-P-1051-A, NASA AMES Research Center, Moffett Field, Calif. (MV).
25. "Procedure for Leak Checking Heat Pipes Containing Ammonia," OAO Document, EX-D-0109C, NASA Goddard Space Flight Center, Greenbelt, Maryland, May 1971.
26. Kroliczek, E. J., "Definition of a Cryogenic Heat Pipe Experiment," 2nd International Heat Pipe Conference, Bologna, Italy, March 31 - April 2, 1976, pp. 673-682.
27. "HEPP/LDEF Axially Grooved Heat Pipe," Test Report, BK042-1011, NAS2-9613, B & K Engineering, Inc., Towson, Maryland, June 1978.

APPLICATIONS

Numerous applications of heat pipes have evolved since 1964 when the concept was first applied. Initially, liquid metal heat pipes were developed for cooling thermionic devices and for nuclear reactors. Now the list of applications spans the cryogenic through liquid metal temperature range. Many of the applications that have been considered to date are listed in Table 9-1 (1). This Chapter discusses flight experience obtained with heat pipes and planned aerospace activities. The more noteworthy terrestrial applications are also presented. As the demand for heat pipes increases, the number of different requirements also goes up. Special types of heat pipes that have evolved to meet these demands are discussed in the last section.

9.1 Aerospace

NASA sponsored activities have pioneered the development of heat pipes for spacecraft use. The approach to date has been a program wherein heat pipes have been developed in the laboratory and flown first as experiments aboard such satellites as the Orbiting Astronomical Observatory (OAO-III) (2), and sounding rockets (3,4,5) followed by a commitment to a spacecraft thermal design as in the ATS-6 (6).

9.1.1 Flight Experiments -- Sounding Rockets

Sounding rockets have been used to demonstrate basic heat pipe operating principles in the 6 - 8 minutes of 0-g time that is typically available.

The first Sounding Rocket Experiment (3) was used to demonstrate the performance of three different wick geometries with ammonia at ambient temperature: an axially grooved heat pipe, a pedestal artery, and a spiral artery. Each of these heat pipes was identical in cross-section to the 3 isothermalizer heat pipes flown on the OAO-III (2). All pipes performed as expected; however, full composite pumping could not be demonstrated for the arterial pipes because of limited battery power.

TABLE 9-1 HEAT PIPE APPLICATIONS (Ref. 1)

<u>Heating</u>	<u>Cooling</u>	<u>Temperature Control, Isothermalization, Other</u>
Thermal recovery units	Air conditioning precoolers	Crystal oscillator ovens
Space heating from flue-gas, fireplaces	Electric motors, transformers	Inertial guidance gyros
Industrial process heat recycle.	Switchgear, circuit breakers, starters	Electroplating baths
Aircraft wing deicing	Electric bus bars	Temperature regulation for data processing electronics
Warming carburetors, air intakes	Storage batteries, fuel cells	Coating rolls and rotor blades
Stirling engines, Brayton cycle engines	High power electron tubes, TWT's	Isothermal furnaces, semiconductor diffusion
Deicing highway bridges, intersections	Power rectifiers, SCR's, transcalent rectifiers	Black-body radiation cavities
Solar energy collectors	Electronic rack cooling, high density packaging	Spacecraft structures, isothermalization
Geothermal energy recovery	Turbine shafts and blades	Isothermal mounting plates for electronics
Thermoelectric hot shoes	Lathe cutting tools, drills	Telescopes, optical equipment
Thermionic emitters	Foundry and die casting molds	Surgical cryoprobe, dermatology, etc.
Coal gasification	Injection molding machines and dies	Infra-red detector cryogenic cooling
Chemical reaction vessels	Disc brakes, auto and aircraft	Laser mirror cooling, laser tuning
Heat recuperators, air preheaters	Motorcycle crankcase cooling	Directional casting, heat treating
Mobile home furnace/hot water heater combination units	Fission product storage vaults	
	Space suit temperature control	

A total of seven heat pipes were flown aboard the second Sounding Rocket Experiment (4):

- 3 ATS-6 type axially grooved ammonia heat pipes
- 1 pedestal artery ammonia heat pipe
- 1 spiral artery ammonia heat pipe
- 1 tunnel artery acetone heat pipe with glass tubes at each end of the pipe beyond the condenser and evaporator end sections
- 1 control pipe filled with enough ammonia to wet all internal surfaces to a depth of 0.254 mm but with no internal wick

The following test objectives were accomplished:

- (1) The fill criteria and corresponding analytical model developed for axially grooved heat pipes was evaluated for overfilled and underfilled conditions.
- (2) Liquid slug formation in the condenser section of the overfilled axially grooved pipe was studied.
- (3) The performance of the two ammonia/arterial heat pipes was demonstrated with high evaporator heat fluxes (123 watts per cm^2) and large heat transport loads (up to 230 watt-m).
- (4) Heat pipe startup from an unprimed condition was accomplished by launching the payload with all evaporators up and also by applying a thermal load to the evaporator of several of the pipes prior to entering 0-g. The subsequent isothermalization of the heat pipes as compared to the large temperature gradient measured across the control pipe demonstrated the heat pipe startup capability.
- (5) A 16 mm motion picture camera and appropriate optics were used to observe the liquid distribution and arterial priming through the glass ends of the acetone heat pipe.

The International Heat Pipe Experiment (IHPE) (5) was launched on October 4, 1974.

Approximately six minutes of 0-g time was provided for a total of ten separate heat pipe experiments. The individual experiments are listed in Table 9-2. In addition to its technical merits, the IHPE brought together many participants from the U.S.

TABLE 9-2 INTERNATIONAL HEAT PIPE EXPERIMENT

Experiment	Experimenter		Number of Pipes
	Agency	Manufacturer	
Ambient Temperature Control Pipe	NASA/GSFC	Grumman	1
Grooved Extrusion Pipe	NASA/GSFC	Grumman	2
Flat Plate HP	NASA/GSFC	TRW	1 Pipe + 1 Control
Ames HP	NASA/Ames	TRW	2
Slab Wick HP	NASA/GSFC	TRW	2
Hughes HP	Hughes	Hughes	2
ESRO HP	ESRO	IKE	2
GFW HP	GFW	Dornier	1 Plate + 1 Pipe
Cryogenic HP	NASA/GSFC	Grumman	1 Pipe + 1 Control
Photographic HP	NASA/GSFC	Grumman	1

and European heat pipe communities and laid the ground work for further cooperative programs in the era of the Space Lab.

9.1.2 Flight Experiments -- Spacecraft

Several flight experiments have been flown which have demonstrated both fixed conductance and variable conductance operation at ambient temperatures.

Flight data from the OAO-III (4) which was launched in August, 1972 continues to give confidence in long term heat pipe performance. The spacecraft provided a test bed for three fixed conductance pipes and a variable conductance heat pipe system. Each of the fixed conductance pipes had a different wick design: an axially grooved tube, a pedestal artery, and a spiral artery. All of these pipes were charged with ammonia for operation between 0 - 20°C. No detectable evidence of degradation has been noted on any of the heat pipes.

The variable conductance heat pipe is part of the Ames Heat Pipe Experiment (AHPE) system which was used to provide temperature control for the On-Board-Processor electronic package. A wire mesh kidney-shaped homogeneous wick was used with methanol as the working fluid. The AHPE is shown schematically in Fig. 9-1. Nitrogen is used as the control gas in a "hot" non-wicked reservoir. Analysis of the data (7) has demonstrated temperature control at $20 \pm 5^\circ\text{C}$ for more than six years.

The Advanced Thermal Control Flight Experiment (ATFE) (8) was launched aboard the Applications Technology Satellite-6 (ATS-6) on May 30, 1974. The ATFE which is shown in Fig. 9-2 has demonstrated the long-term temperature control capability of a thermal diode, an electrical feedback controlled heat pipe (FCHP) and a phase-change material. The experiment was designed to permit evaluation of these components on an individual basis and as an integrated thermal control system.

The heat pipes were designed for nominal operation at 28°C . Ammonia was used in the diode and methanol in the FCHP. Liquid blockage was incorporated with a spiral artery wick design to accomplish the diode operation. Shutdown with more than a 90°C temperature difference was demonstrated. Temperature control to within $\pm 2^\circ\text{C}$ was demonstrated with the FCHP which utilized a composite slab wick design. The same pipe when operated as a passive VCHP provided $\pm 10^\circ\text{C}$ temperature control with the same test conditions.

9.1.3 Flight Experiments -- Shuttle

The advent of the shuttle will afford additional opportunities for demonstrating heat pipe principles as well as their behavior as part of a temperature control system. Experiments that are currently planned include the Heat Pipe Experiment Package (HEPP) (Ref. 9) and the Transverse Flat Plate Heat Pipe Experiment (Ref. 10). Both Experiments will be flown aboard the Shuttle-launched Long Duration Exposure Facility (LDEF). They are each self-sufficient with respect to electrical power and data storage and utilize their own battery, signal conditioning equipment, data multiplexer, encoding and timing systems, and tape recorder. Pre-programmed electrical heaters provide the heat loads for the various operational modes. After 6 - 9 months, LDEF will be retrieved from orbit and the data from the experiments will be analyzed to evaluate their performance. Additional experiments are also being planned to plug in the pressurized module of Spacelab as part of a cooperative effort between NASA and ESA.

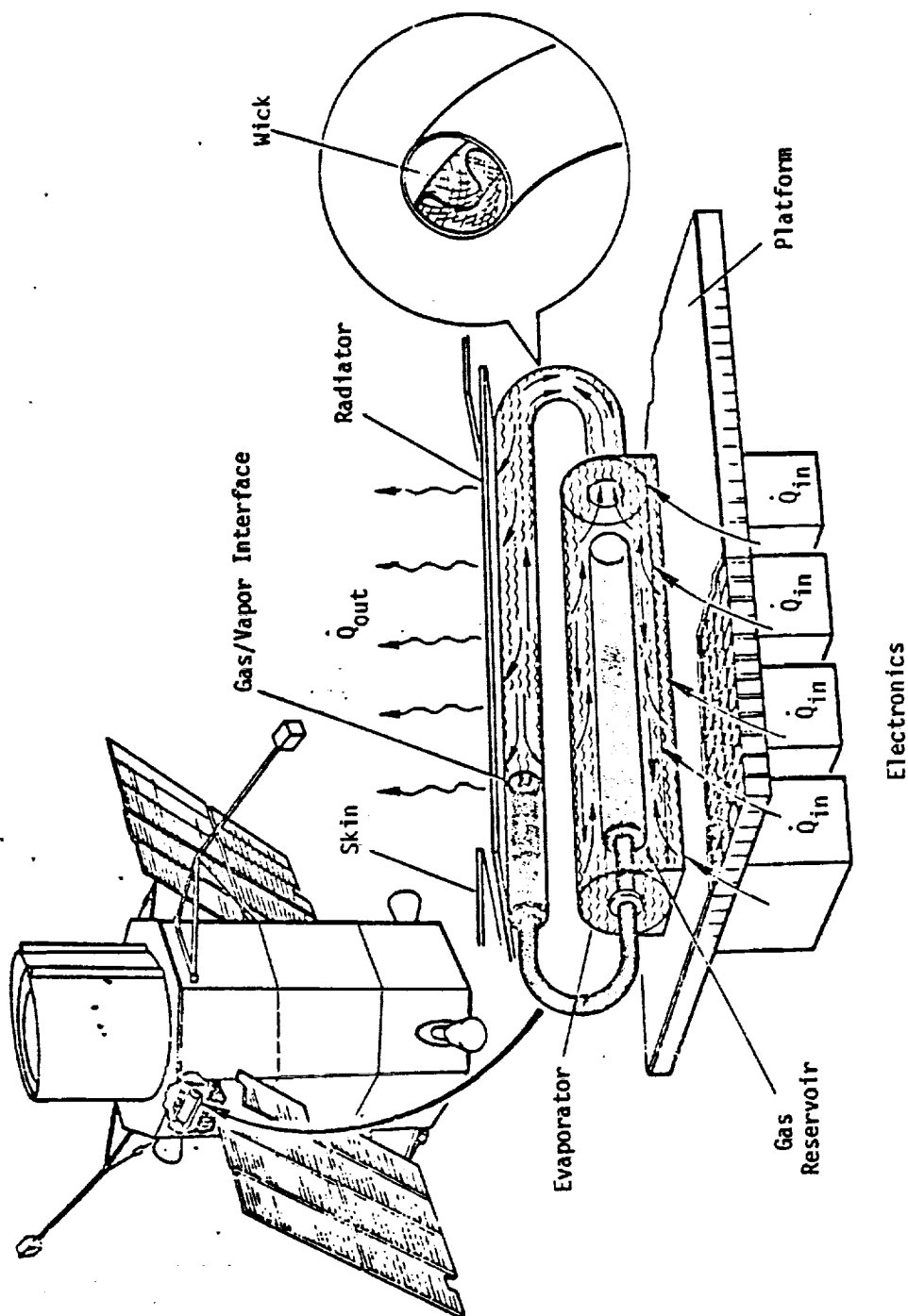


Fig. 9-1 Ames Heat Pipe Experiment (AHPE)

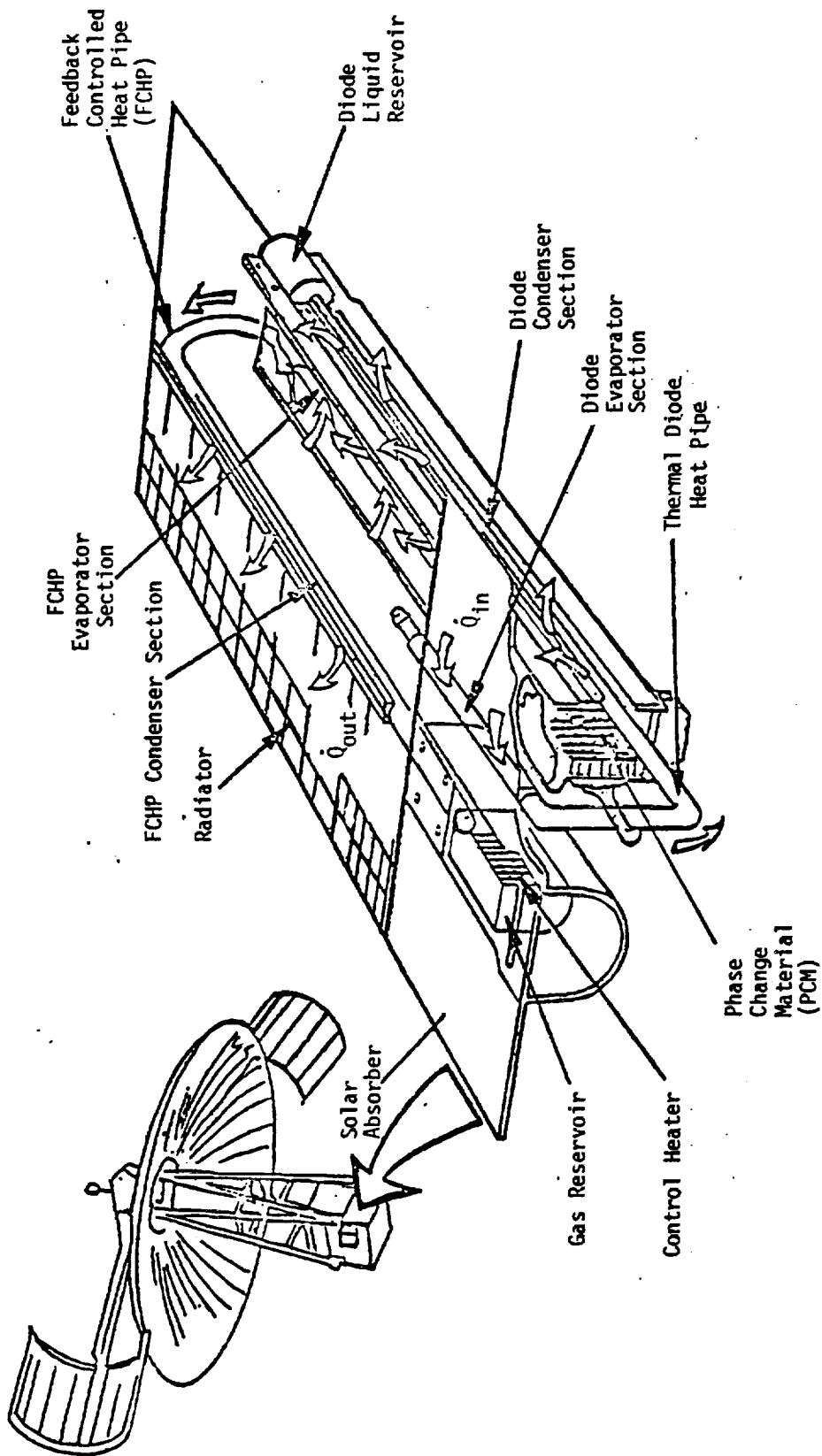


Fig. 9-2 Advanced Thermal Control Flight Experiment (ATFE)

A schematic of the HEPP is presented in Fig. 9-3. This experiment is designed to demonstrate low temperature ($< 200^{\circ}\text{C}$) heat pipe operation. This system contains an axially grooved aluminum ATS extrusion which will be operated as a fixed conductance heat pipe, and a stainless steel axially grooved liquid trap diode design. Ethane is used as the working fluid. Heptane is utilized in the phase change material canister which is integrated with the main radiator. The canister is designed to provide approximately 25 W-hr of temperature stability during forward mode transport tests.

The Transverse Heat Pipe Experiment consists of four transverse flat plate modules which are mounted together to form a temperature control panel (cp. Fig. 9-4). In the basic design of a transverse heat pipe (11), liquid flows in a direction which is perpendicular to the vapor flow. Temperature control is achieved by using conventional gas control techniques. This experiment is designed to demonstrate variable conductance temperature control for high heat loads suitable for space radiator applications. On the inboard side of the modules, heaters are mounted to simulate electronic equipment while the opposite side serves as a radiator whose active surface is controlled by the action of the non-condensable gas. Methanol is used as the working fluid with nitrogen as the control gas. The maximum heat load will be 160 watts.

9.1.4 Spacecraft Applications

Ambient temperature heat pipes have been used successfully in a number of spacecraft applications over the past six years. Their acceptance as a reliable aerospace component is continually increasing as more experience is gained and as additional applications emerge.

The most extensive use to date of heat pipes aboard an operational spacecraft has been on the Applications Technology Satellite (ATS-6) launched in May 1974. A total of fifty-five heat pipes were placed in equipment panels (Fig. 9-5) to carry solar and internal power loads to radiator surfaces. Ammonia was used with aluminum axially grooved tubing. Data taken over a 24-hour orbital period shows a maximum gradient of 3°C existed from one side of the spacecraft to the other. To date, no degradation in the thermal design has been seen.

The Communications Technology Satellite shown in Fig. 9-6 utilizes three gas-controlled heat pipes to provide temperature control of a traveling wave tube (12). A cold wicked reservoir design is utilized with methanol as the working fluid and a 10% helium/10% nitrogen gas mixture. The helium is included for the purpose of leak testing. A stainless steel felt

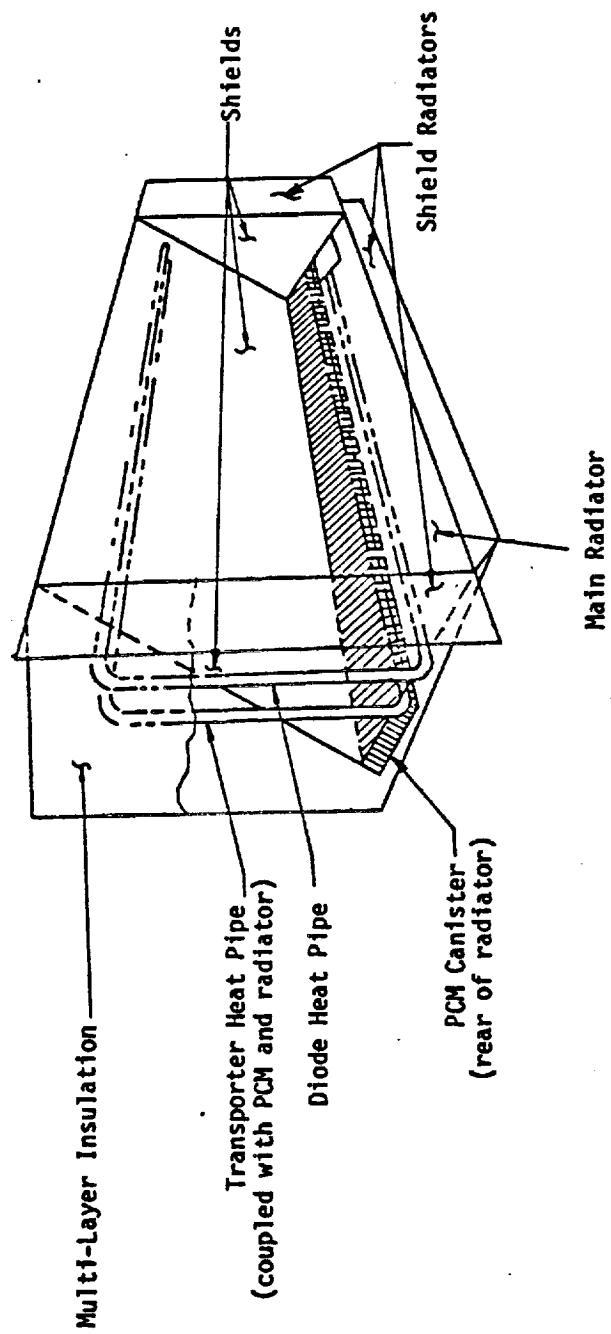


Fig. 9-3 Heat Pipe Experiment Package (HEPP)

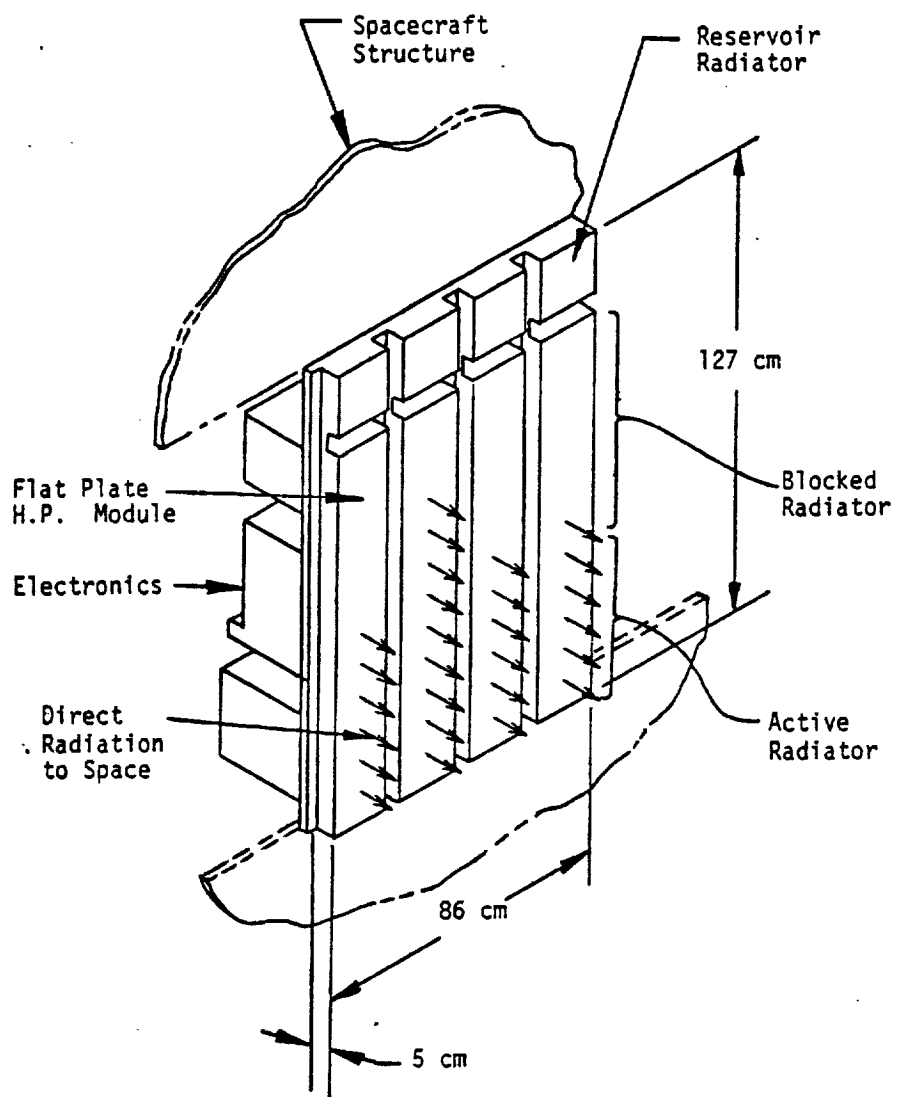


Fig. 9-4 Typical application of transverse flat plate heat pipe

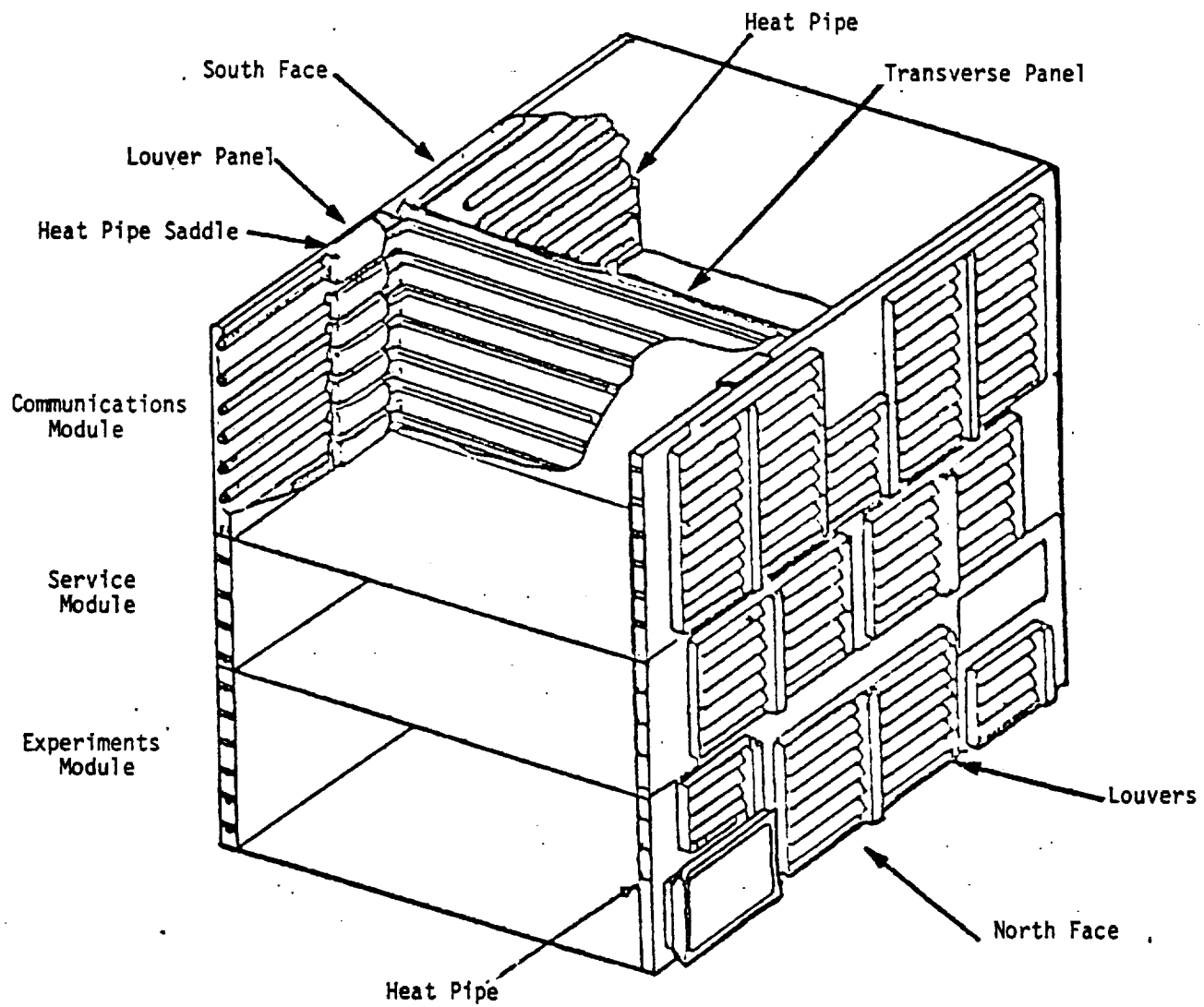


Fig. 9-5 Primary thermal control system schematic

metal slab with two arteries attached comprises the primary wick design. The heat pipes have been operating continuously on a daily cycle carrying up to 200 watts each at a nominal operating temperature of approximately 50°C.

Axially-grooved aluminum extrusions with ammonia working fluid are used to isothermalize the equipment platform of the International Ultraviolet Explorer (13) as shown in Fig. 9-7.

The advent of the Space Shuttle and Spacelab offers an opportunity to fly a wide variety of scientific instruments at a relatively low cost. Instruments normally flown on balloons, sounding rockets as well as spacecraft will have to be protected from the harsh thermal environment of space. The problem is compounded by the fact that Shuttle heat rejection services are quite limited and orientations may be random due to operational considerations. The variability of the instruments with regard to size, geometry, power dissipations and temperature requirements, has led to the development of a canister for thermal protection (14,15). Such a canister is shown in Fig. 9-8 utilizing fixed conductance as well as variable conductance heat pipes. The heat pipes in the walls absorb heat generated by instruments within the canister and transfer it to radiators mounted outside with a good view to space.

Feedback variable conductance heat pipes control either the wall temperature, or a specific point within the instrument to $20 \pm 1^\circ\text{C}$. A power range of 100 - 400 watts with a 1 W/cm^2 power density will be accommodated. The size will house up to $1 \text{ m} \times 1 \text{ m} \times 3 \text{ m}$ instrument of 340 kg weight. An added flexibility will be that the system will be able to be "shut down" during adverse periods such as re-entry where heat soak back will occur, by activating the reservoir heater on command and forcing gas into the heat pipe. This will decouple the canister from its radiators which will rise in temperature during re-entry. Axially grooved aluminum extrusions charged with ammonia are used throughout.

9.2 TERRESTRIAL

The potential of heat pipes as an efficient heat transfer device has been demonstrated in a number of terrestrial applications. Significant improvements over conventional systems have been realized in such applications as highway deicing (16,17) and energy recovery (18). Heat pipes have also been used to resolve numerous electronics and electrical cooling problems (19). Recently heat pipes have been applied to the stabilization of the perma-frost in the

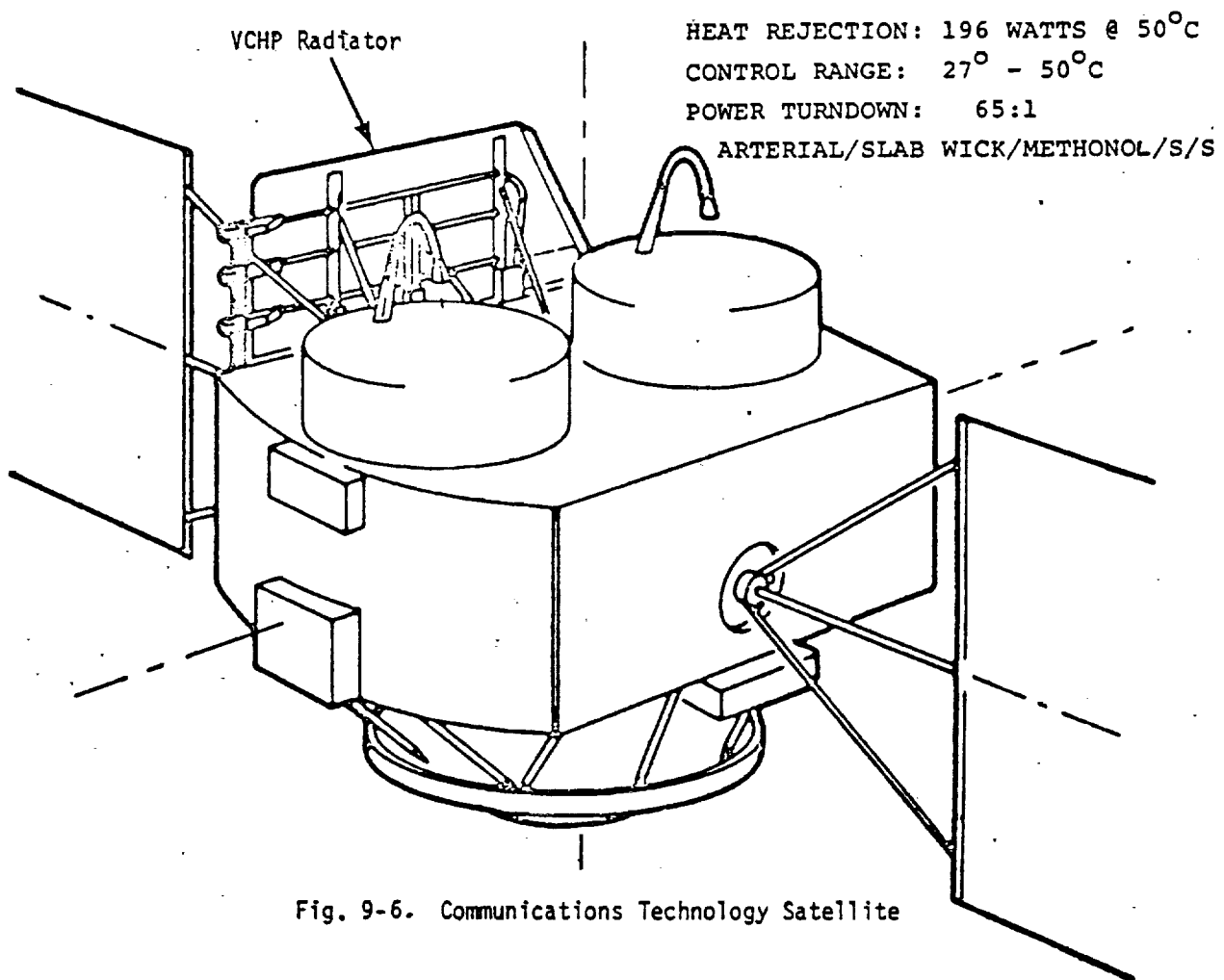


Fig. 9-6. Communications Technology Satellite

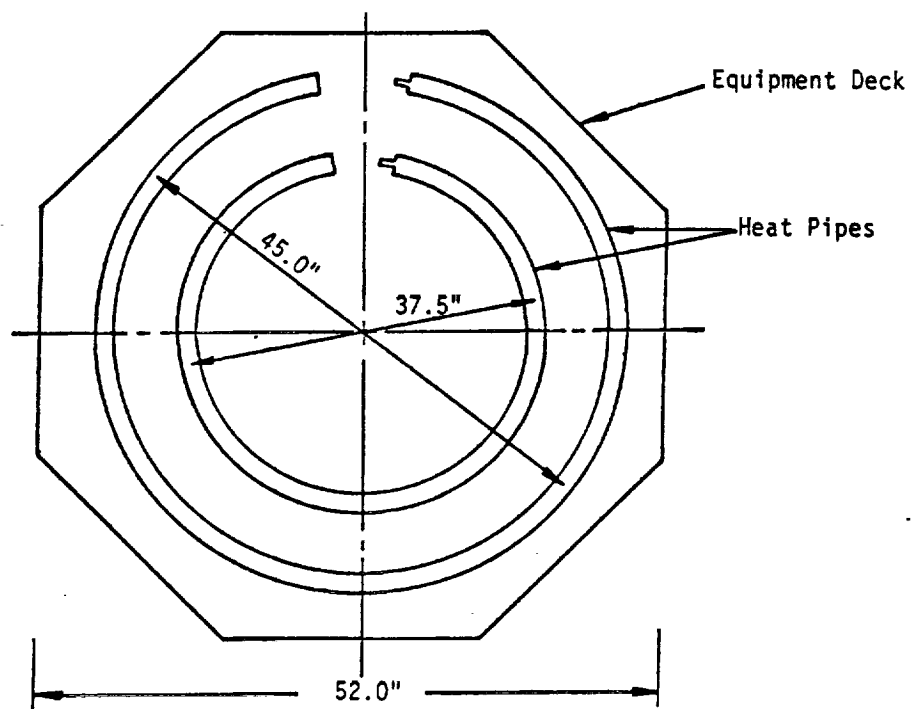


Fig. 9-7. I.U.E. Heat Pipes on lower deck of the spacecraft

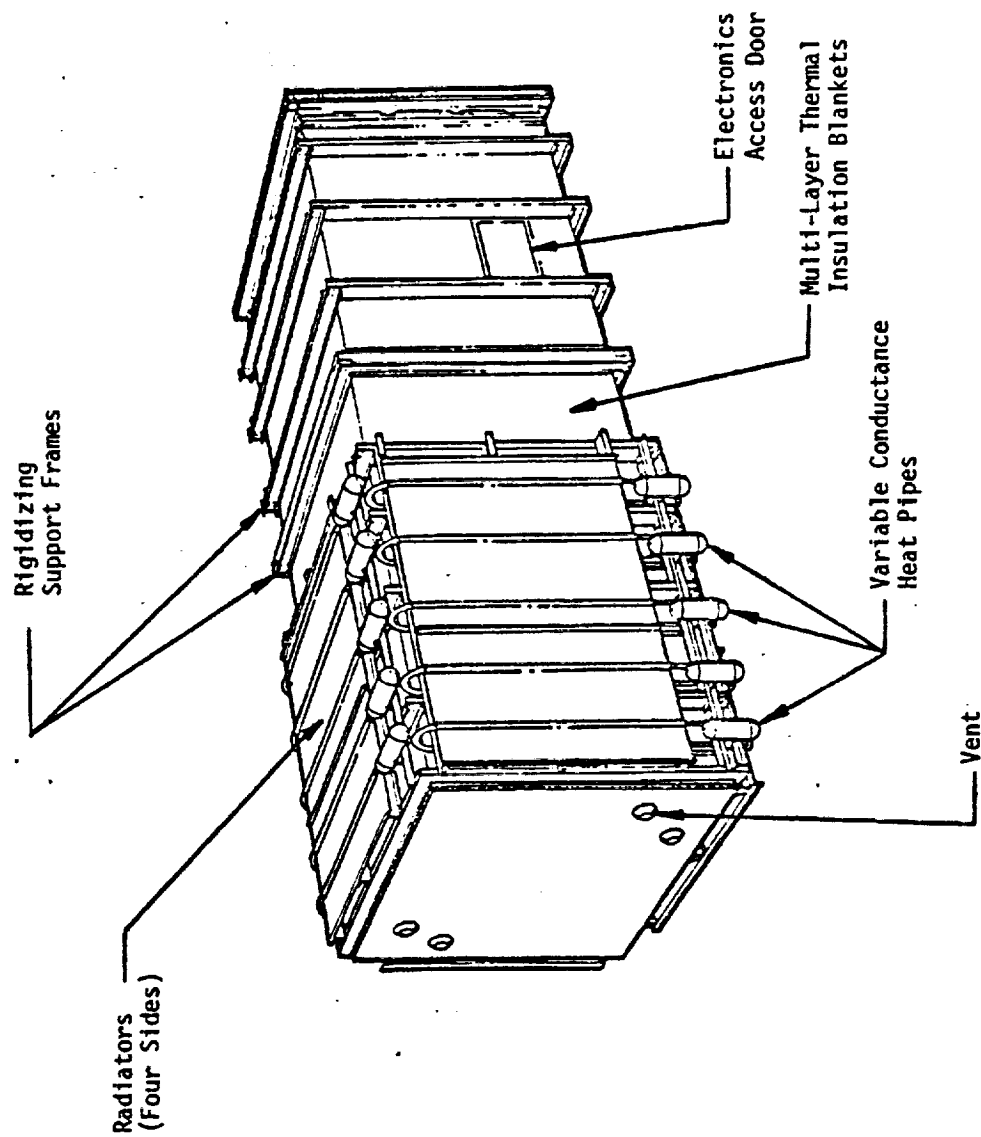


Fig. 9-8. Heat pipe thermal control canister

Trans-Alaskan pipeline (20). Other applications which have been investigated include solar energy systems where efficient heat transfer is a necessity. Some of the more significant terrestrial applications are discussed below.

9.2.1 Permafrost Stabilization

The most significant commercial application of heat pipes to date has been their use in the Trans-Alaskan pipeline (20) to stabilize the permafrost. Approximately 150,000 heat pipes with a total cost of over 20 million dollars were installed as shown in Fig. 9-9. The heat pipes are used to remove heat from the concrete piles and dissipate it to the ambient air in order to prevent thawing of the permafrost. Accelerated life tests at elevated temperature were used to demonstrate a 30-year life for this ammonia/steel tubing heat pipe system.

9.2.2 Deicing Systems

Heat pipe deicing systems have been investigated by the U. S. Department of Transportation for application in locations where frozen pavement surfaces cause a high safety risk. In particular, deicing of access ramps, dangerous sections of roads and highways, bridges and airport runways have been considered. Various systems have been investigated including systems which utilize stored earth energy (Figs. 9-10 and 9-11) and augmented systems such as the solar powered system illustrated in Fig. 9-12. In all such systems, the heat pipe is used as a reliable and efficient means of heat transfer to collect, transport and distribute thermal energy.

Systems which utilize stored earth energy typically consist of a series of heat pipes which operate in a reflux-boiler mode (Fig. 9-10). As the temperature of the pavement surface drops below that of the ground, the two-phase energy transport mechanism of the heat pipe is initiated. Energy from the higher temperature (ground) region evaporates the heat pipe working fluid and is transported as latent heat of vaporization to cooler (pavement) zones where it is released through condensation. Liquid is then returned to the higher temperature region via gravity reflux. Heat pipes used in deicing applications (21) have been constructed of black iron pipe (1 in.) charged with ammonia. The vertical leg has ranged from 10-15 m and the pavement portion is typically 4-6 m long. Heat loads are on the order of 150 watts with an overall conductance of about 100 W/°C.

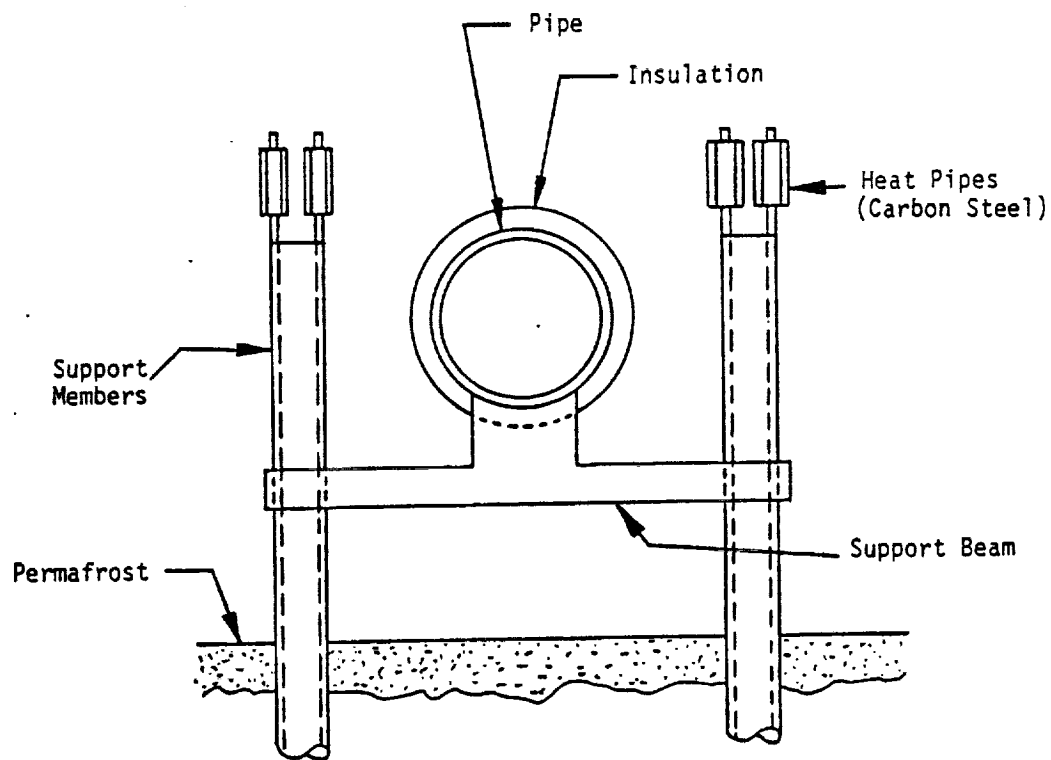


Fig. 9-9 Heat pipes on Trans-Alaskan Pipeline

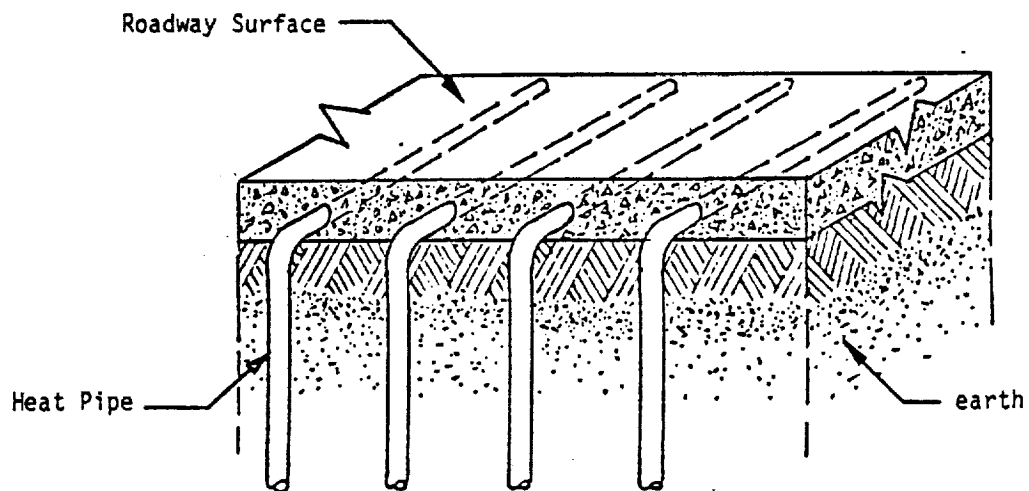


Fig. 9-10 Highway ramp heat pipe deicing system

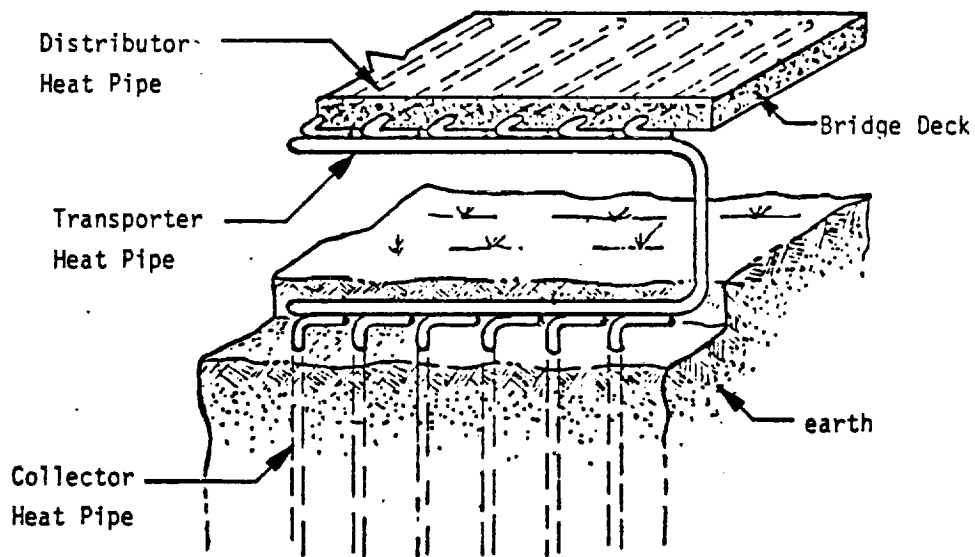


Fig. 9-11 Highway bridge heat pipe deicing system

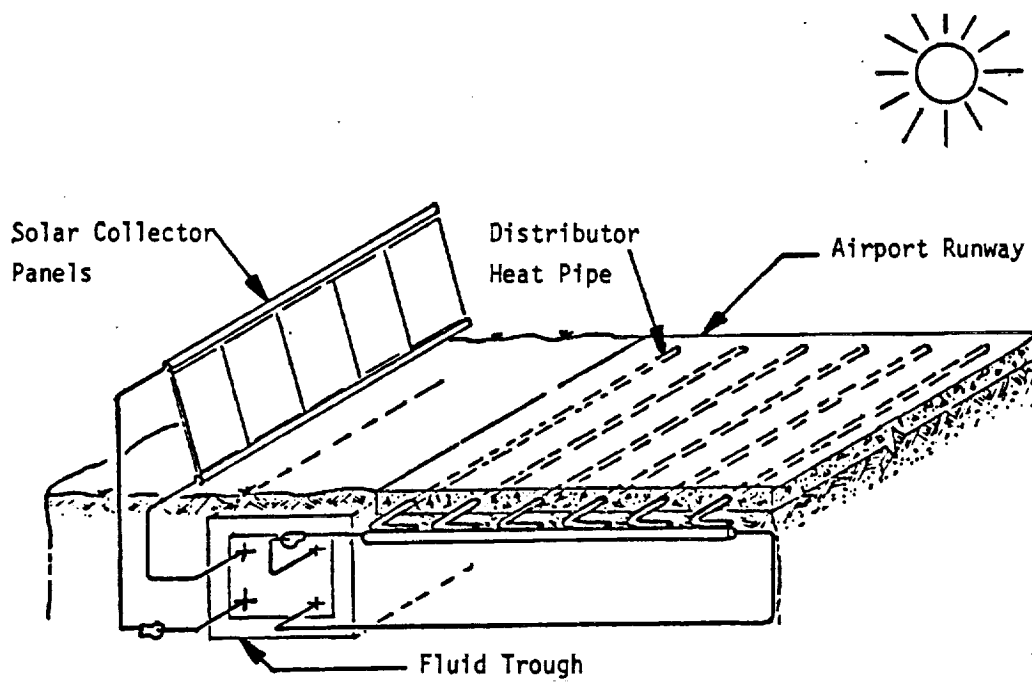


Fig. 9-12 Solar powered airport runway heat pipe deicing system

Extraction of earth stored energy with heat pipes has been evaluated at the U. S. Department of Transportation's Fairbank Highway Research Station (FHRS) (21). Six concrete test panels measuring 2.44 by 3.66 m contain embedded heat pipes on 10, 15 and 20-cm centers. Three panels melted snow with the earth heat extracted by vertical in-ground legs of 9.15 and 12.19 m. The other three panels used electrical heaters to power the in-concrete heat pipes.

Tests performed during two major snowfalls confirmed that earth heat extraction with heat pipes is a viable technique for pavement deicing. During one test, 22-cm of snow was deposited on the surrounding ground with temperatures dropping to a low of -8°C and wind gusts up to 45 kph. The earth heat pipe test panels were capable of melting most of the incident snowfall. Extensive drifting, combined with a wicking of melt water, contributed to ice ridge formation in some areas. However, the ice did not adhere to the pavement surface. In highway applications, normal traffic flow should dislodge ice ridges and contribute to melting.

Another test was conducted when 15-cm of snow fell in a period of 12 hours, while the air temperature hovered between -6 and -4°C and winds were variable up to 17 kph gusts. The earth heat pipe panels were capable of maintaining a clean surface, except for some isolated areas. During the same tests, the electrically powered test panels, which had an average heat input of 107 W/m^2 , also melted all incident snowfall.

More recently, utilization of heat pipe extracted ground stored energy has been evaluated at a highway range in West Virginia with excellent results. Studies have also been conducted to determine the applicability of heat pipe systems for the deicing of bridges (17) and airport runways (22).

9.2.3 Heat Recovery

Extensive application developments have been underway for several years in the utilization of heat pipes to reclaim the thermal energy of exhaust air in heating, ventilation and air conditioning (HVAC) systems and from exhaust gases in industrial processes.

Typical heat pipe heat recovery units consist of a grouping of heat pipe elements illustrated in Fig. 9-13. The heat pipe elements are usually externally finned to provide efficient heat transfer to and from the exhaust and intake streams. In a typical application, a portion of the heat pipes extends into a hot air stream while the other portion of the heat pipes extends into a cold air stream. Heat is transferred from the hot air stream to the evaporator section of the heat pipe via the external fins. This heat is then transported, by the evaporation/condensation process, from the evaporator to the condenser section of the heat pipe. There, the heat is transferred through the external fins in that section to the cold air stream.

The advantages of heat pipe heat recovery units are many including wide flexibility of packaging resulting from the self contained nature of each heat pipe element. This packaging flexibility allows optimization with respect to counterflow heat exchange, air stream flow rates and fin spacing. In addition, the heat pipes can be made of a variety of materials suitable for any application.

By combining a few to several hundred heat pipes with extended area fins into a heat pipe module, a thermal path between two counter-flow air streams is created which allows large quantities of heat to be transferred from one region to another with low temperature drops.

9.2.4 Electronic and Electrical Equipment

Application of heat pipes to cool electronic and electrical equipment have been many and varied. Heat pipes have been utilized to cool individual, high power-dissipating components (Fig. 9-14), and electronic components such as P. C. boards as well as an entire system such as the electronic cabinet cooler illustrated in Fig. 9-15.

In individual component cooling the heat pipe serves to lower the resistance between the heat dissipating component and the environment. The heat pipe provides increased efficiency in air-cooled applications requiring large heat sinks. It also allows remote location of the heat sink in high density packaging.

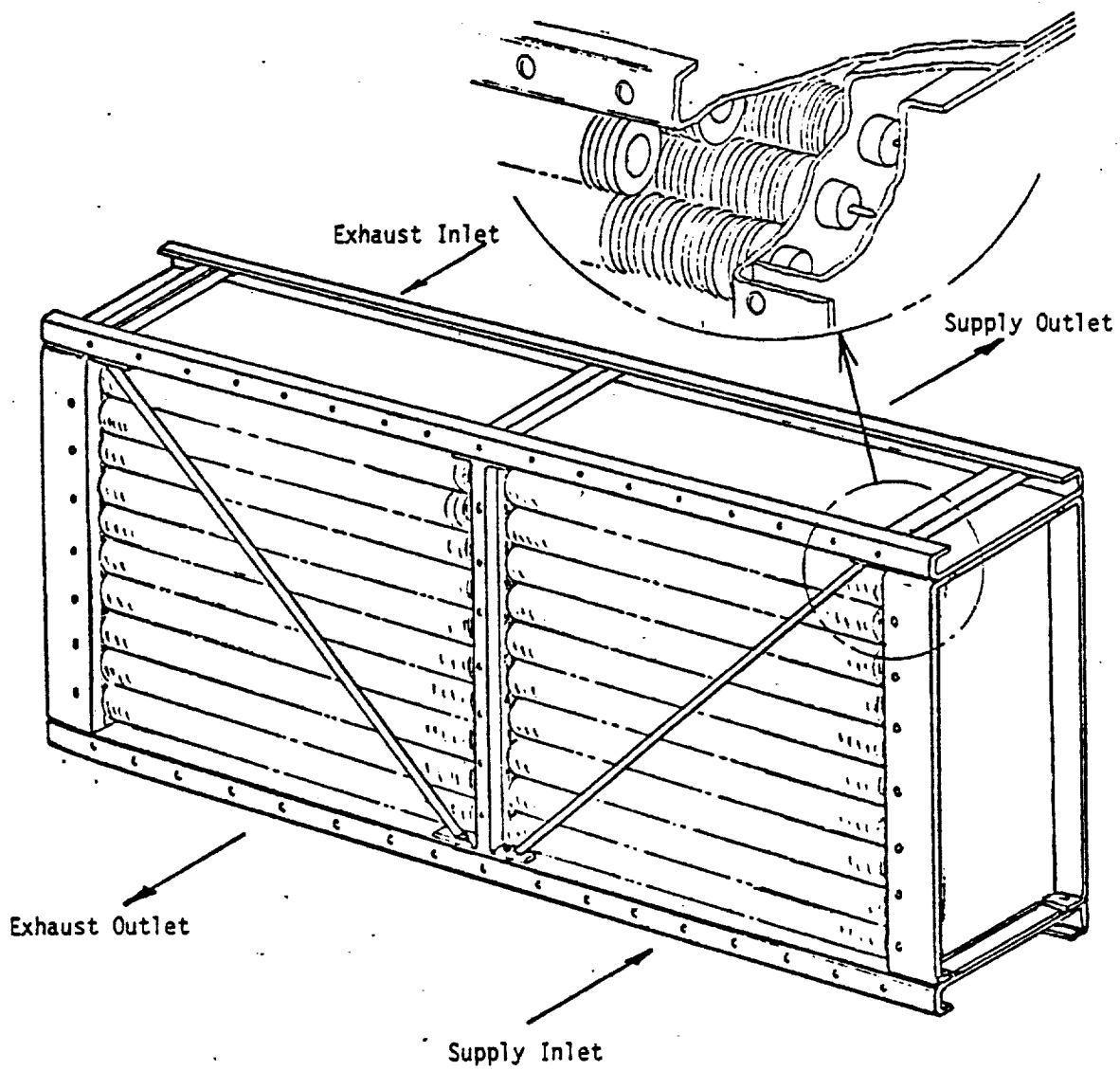


Fig. 9-13. Heat pipe heat exchanger

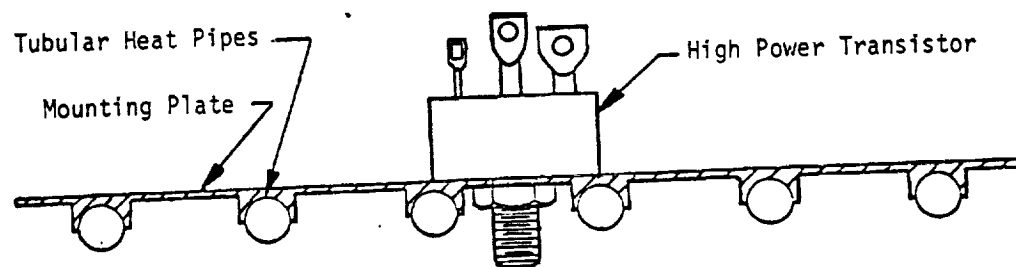


Fig. 9-14 High power heat sink structure

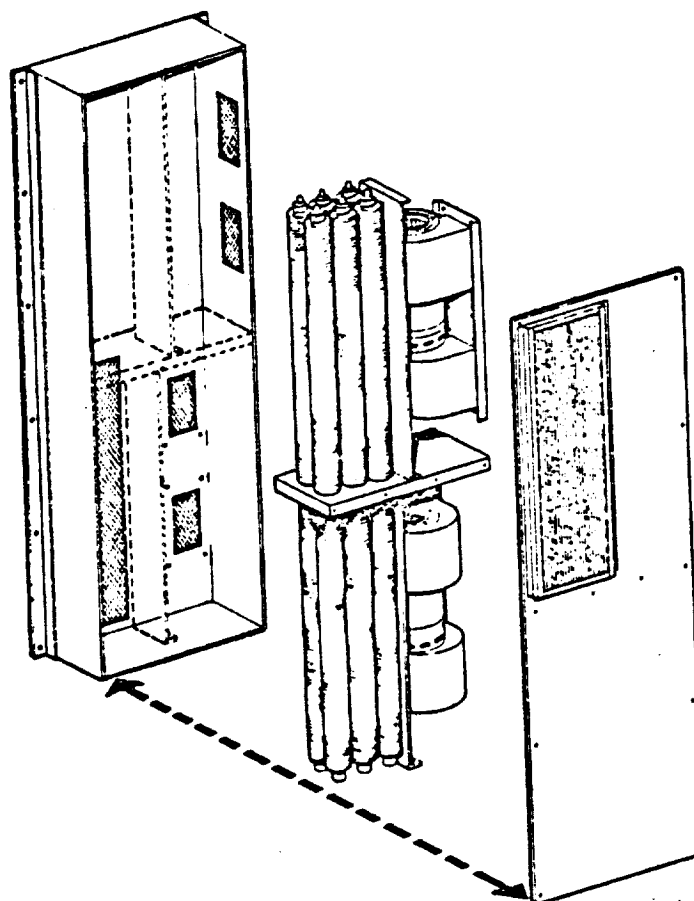


Fig. 9-15 Heat pipe heat exchanger for electronic cabinet cooling

For total system cooling, the heat pipe provides a self-contained heat exchanger package which can efficiently transfer heat from the clean internal air of an electronic enclosure to cooler external ambient air from a harsh environment such as encountered by on-line industrial equipment. Complete isolation between air streams provides contamination free operation of the electronic enclosure.

Heat pipes have been found to be especially suitable for applications where water cooling is inconvenient and the complexity and cost of air conditioners are prohibitive. In such applications, the capacity of the heat pipe is limited only by available space for air heat exchange surface and the temperature of the environment. A variety of heat pipe designs suitable for electronic cooling application are available from a number of vendors.

9.2.5 Solar Collectors

Solar energy systems require efficient heat transfer from collectors to the energy storage areas and points of utilization. Heat pipes have been under investigation for several years for applications with large solar collectors (23).

Fig. 9-16 illustrates a typical solar collector for an electrical power generation station. The solar collector consists of a parabolic reflector rotating with the sun, a heat pipe in a glass envelope, an energy storage unit and a steam generator. A prototype study (24) has shown that a heat pipe of 0.09 m (3.5-in.) diameter and 11 m (36 ft.) long can collect 18,000-W peak load while operating at 573 K (571°F).

Flat plate collectors utilizing heat pipes (Fig. 9-17) have also been investigated for heating of residences and large buildings. In such a design the heat pipe is used to collect the solar energy from a large area and transfer it to a small area where an energy storage liquid is heated.

The flat-plate solar collector using heat pipes has the advantage of eliminating the liquid which is circulated under the large collector plates. Also, its heat pipes can be operated as diodes to cut off the loss of heat from the storage liquid to the atmosphere when the collector plate is at a lower temperature.

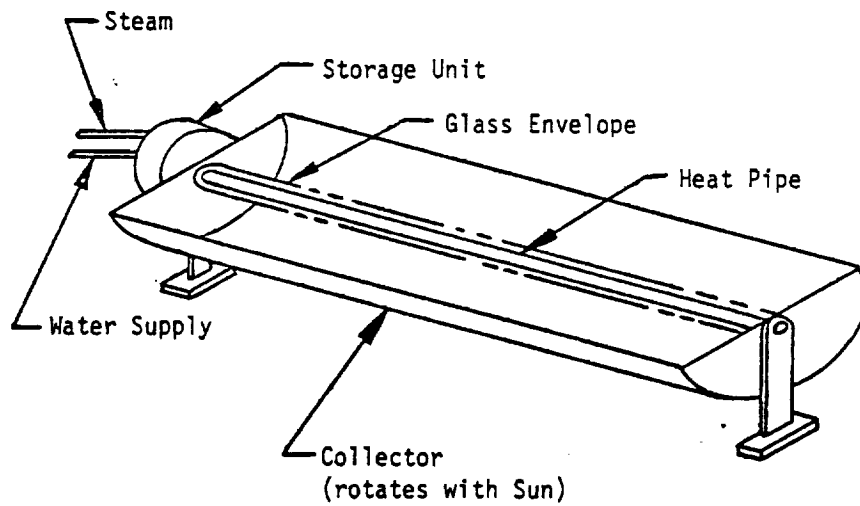


Fig. 9-16 Solar electric power generation station using heat pipes at the focal axes of parabolic reflectors

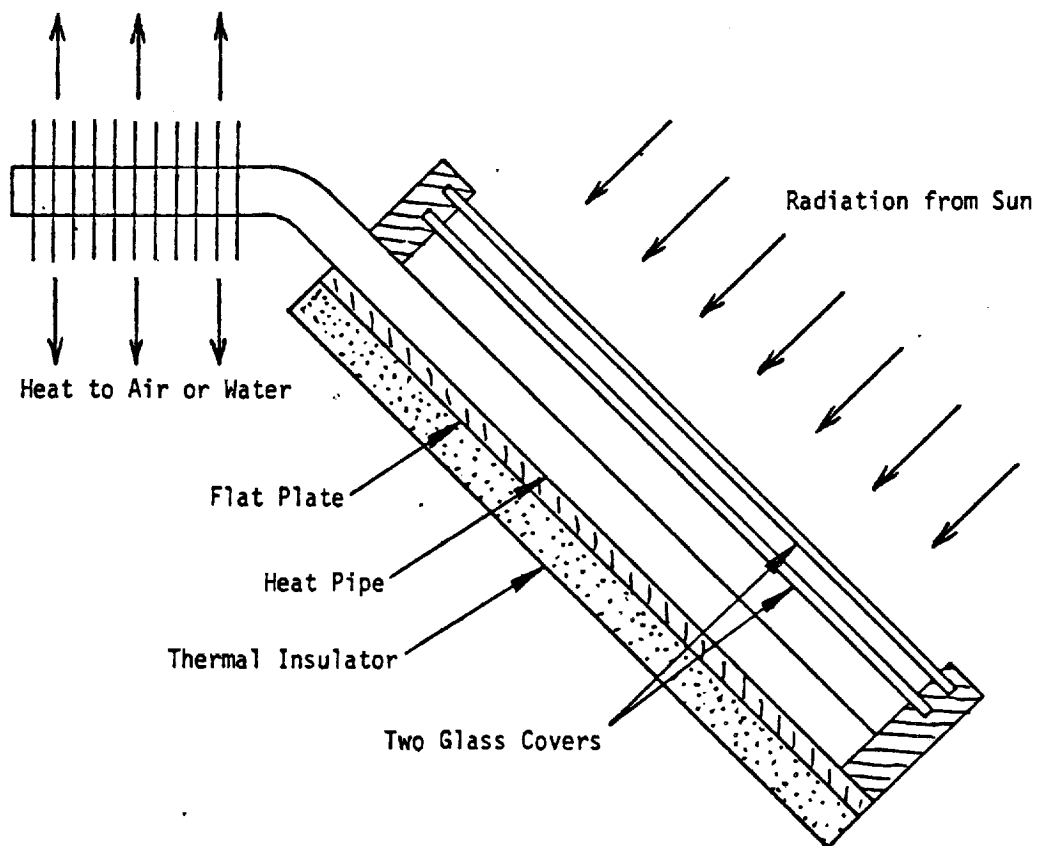


Fig. 9-17 Cross section of a flat plate solar collector that uses heat pipes

9.3 SPECIAL TYPES OF HEAT PIPES

There are obviously a multiplicity of applications of heat pipes to temperature control and heat transfer systems. In many cases special heat pipe designs which incorporate the basic two-phase heat exchanger are required to satisfy the particular application. Flat plate vapor chambers are required when uniform temperature surfaces are specified as in the case of the Atmospheric Cloud Physics Lab. Flexible heat pipes have been developed for application to detector systems. In addition, various methods have been devised to provide circulation of the working fluid in applications where capillary pumping is inadequate. This section describes several of the more significant special heat pipe designs now in use or under development.

9.3.1 Flat Plate Heat Pipes

A number of flat plate vapor chambers whose design is similar to that shown in Fig. 9-18 have been developed over the past few years (19,25). The major characteristic of this design is its ability to provide a surface with a very high thermal conductance. Care must be taken in providing adequate pressure containment for the working fluid. In general, the internal surface of each face is wicked to accommodate either evaporation or condensation. Transverse wick bridges are used to provide a return path for the liquid between the plates and also along the plate. Internal structural supports can be employed to strengthen the unit or to provide for attachment of external components.

9.3.2 Flexible Heat Pipes

Flexible heat pipes are desirable in applications where the assembly prohibits incorporation of a rigid heat pipe or where flexibility is needed to accommodate vibration or temperature cycling. Flexibility is also required to permit in-orbit deployment, and orientation or scanning of detector systems. A typical flexible heat pipe design which was developed for detector cooling (25) is presented in Fig. 9-19. Flexibility in the container design is obtained by employing a bellows system which can be reinforced with an external steel braid material. Flexibility in a screen wick is obtained by orienting the crossmembers or fibers on a bias relative to the longitudinal axis of the wick to avoid normal compression of the fibers in bending. With square mesh screens that are commonly used, bias angles between 30 and 60 degrees provide the greatest flexibility. In addition this also provides the axial pliability needed for expansion and contraction. Maximum flexure in all directions requires a wick which

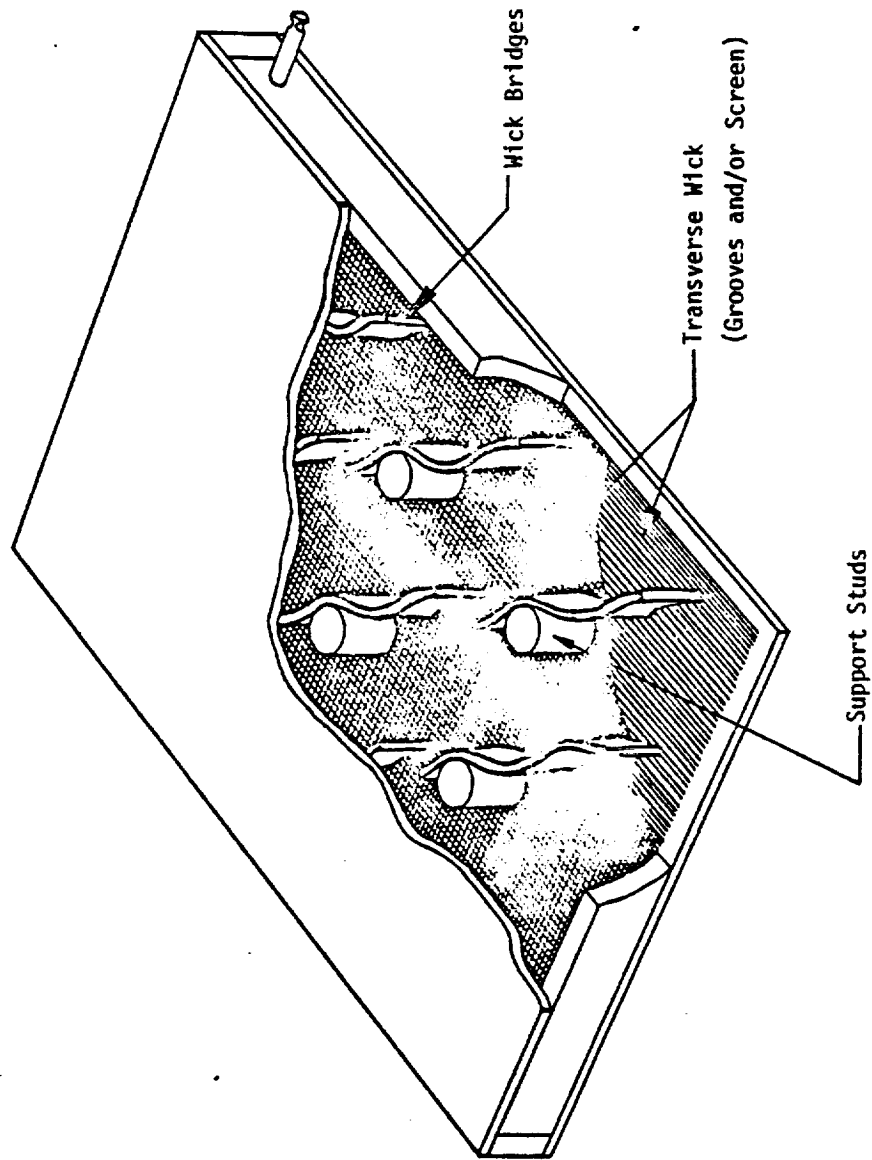


Fig. 9-18. Flat plate heat pipe

has a circular or annular cross-section and is concentric with the container. The cross-section should be as small as possible, consistent with transport and wicking height requirements.

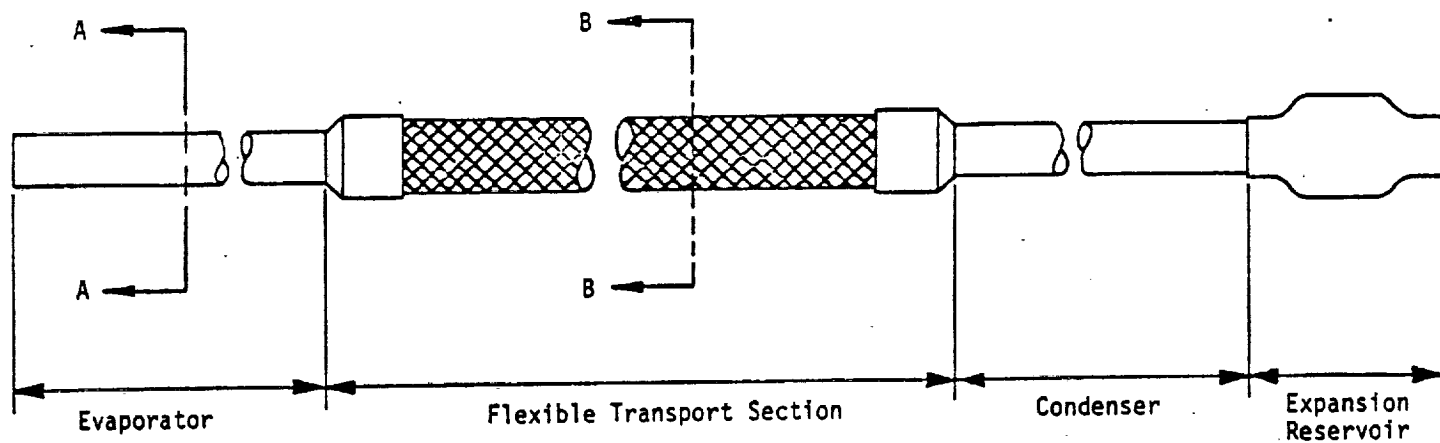
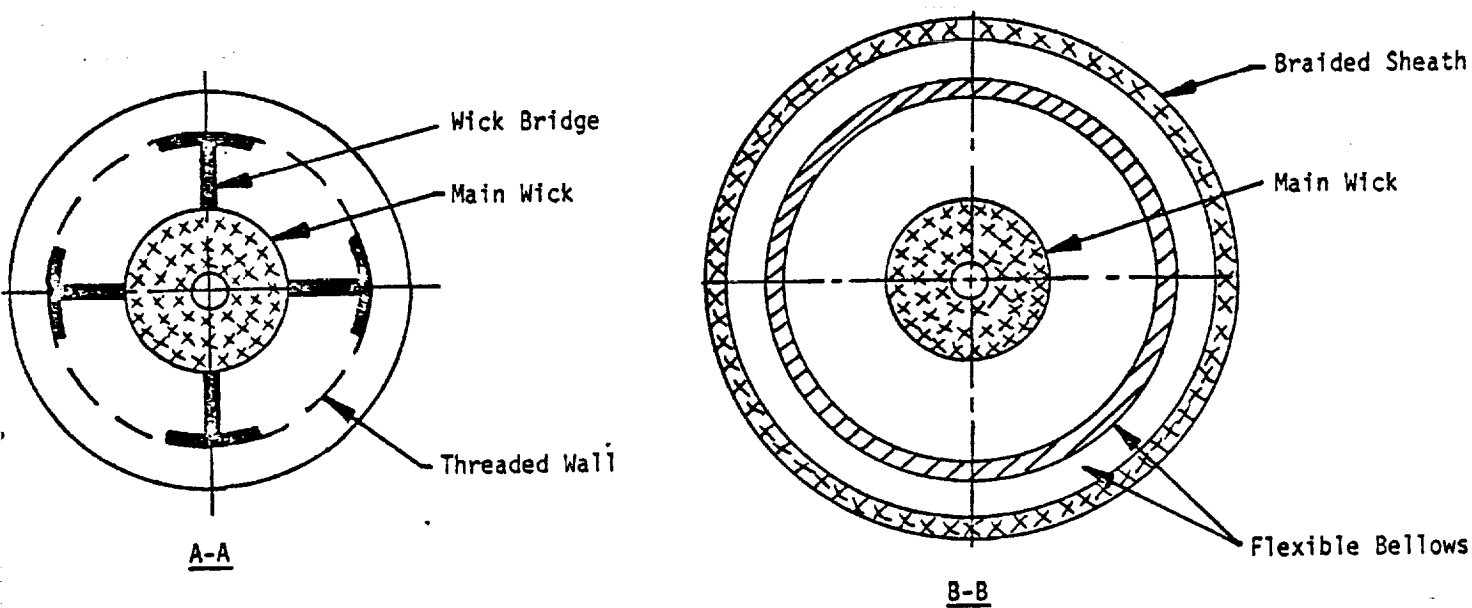


Fig. 9-19. Flexible heat pipe



9.3.3 Electrohydrodynamic Heat Pipes

One method for improving the liquid pumping capability which has been successfully demonstrated (27) with heat pipes is the application of electrostatic forces to collect, guide, and pump the liquid condensate. The basic concept is to replace the capillary wick of a conventional heat pipe with an electrode structure as shown in Fig. 9-20 and to utilize a dielectric working fluid. This concept can be employed in flat plate configurations as illustrated in Fig. 9-21.

The electrohydrodynamic heat pipe developed by Jones (27) consists of a thin-walled tube of aluminum, with end caps made of an insulating material such as plexiglass. A thin ribbon electrode is stretched and fixed to the end caps in such a way that a small annulus is formed between it and the heat pipe wall over the complete length of the heat pipe. This annulus is only confined to about 20 percent of the heat pipe circumference, and provision must be made for distributing the liquid around the evaporator by conventional means.

When a sufficiently high voltage is applied, the working fluid collects in the high electric field region between the electrode and the heat pipe wall, forming a type of tent as shown in Figs. 9-20 and 9-21. Evaporation of the liquid causes a net recession at the evaporator, whereas cooling at the condenser causes an outward bulging of the liquid interface. This creates an inequality in the electromechanical surface forces acting normal to the liquid surface, causing a negative pressure gradient between condenser and evaporator. Thus a liquid flow is established between the two ends of the heat pipe.

A pumping capability which is up to two times greater than that developed by capillary action can be obtained with this technique. Electrostatic pumping has also been considered for arterial priming and is a means to achieve variable conductance.

9.3.4 Osmotic Heat Pipe

An osmotic heat pipe differs from a conventional heat pipe in that a semipermeable membrane is used to circulate the liquid instead of a capillary wick. A simple osmotic heat pipe is shown in Fig. 9-22. A binary mixture of solvent and solute is required along with a semipermeable membrane. Application of heat to the working solution causes it to evaporate to a pure solvent which enters the vapor passage and flows to the condenser section where it

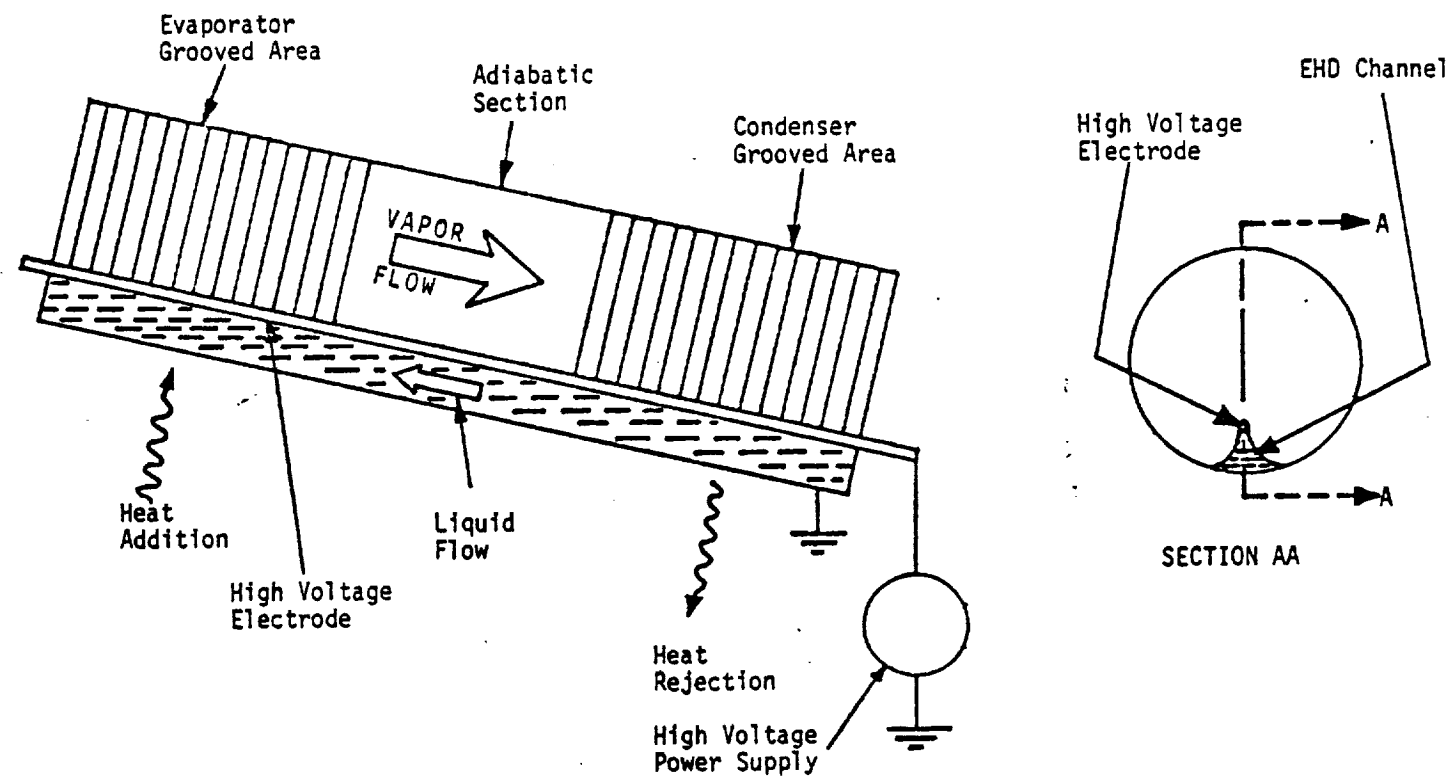


Fig. 9-20 Schematic of an EHD heat pipe

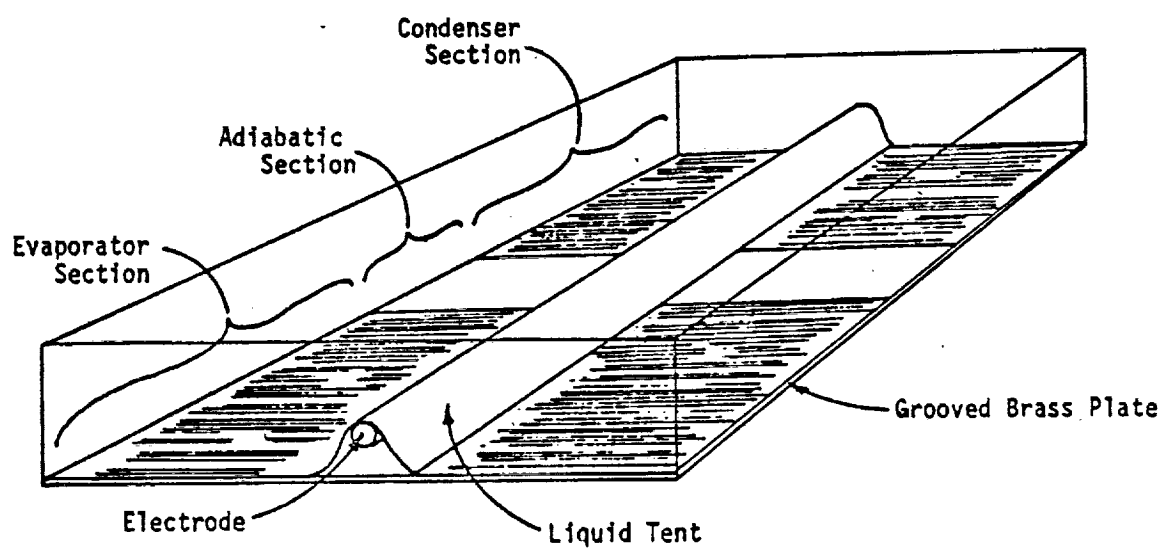


Fig. 9-21 EHD flat plate heat pipe

condenses and flows into the semi-permeable membrane. The pure liquid solvent then passes through the membrane into solution in the return channel. The passage of the solvent through the membrane creates an osmotic pressure which can be several orders of magnitude greater than capillary heads. Since this pressure is considerably greater than the hydrostatic head of the solution in the return channel, a flow of solution to the evaporator is effected and the heat piping process is accomplished.

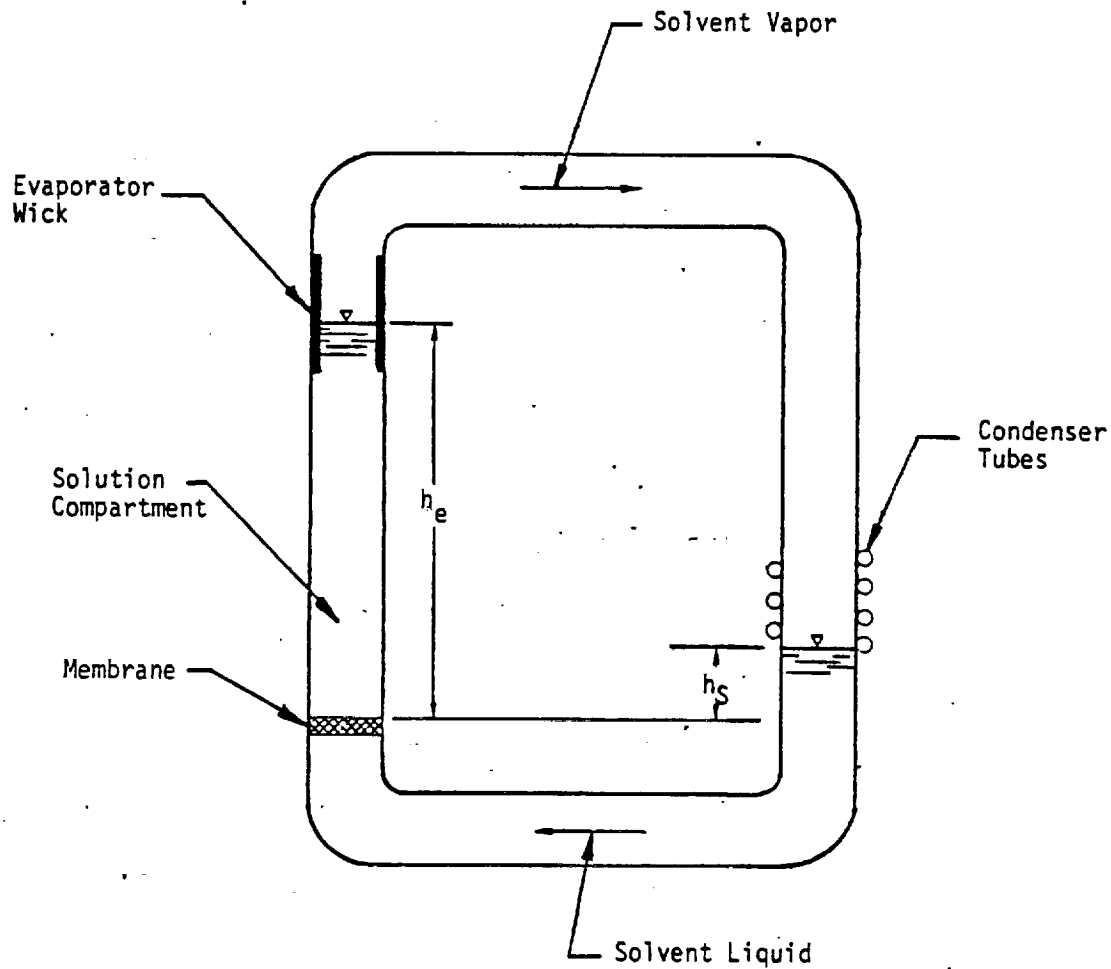


Fig. 9-22 Simple osmotic heat pipe

One method of improving upon the performance of rotating machinery components is to provide internal cooling using the rotating, wickless heat pipe which is shown schematically in Fig. 9-23. It consists of a sealed hollow shaft, having a slight internal taper from one end to the other, and containing a fixed amount of working fluid. When the shaft is rotated at high speed about its longitudinal axis, the working fluid collects as an annulus at the large end. The diameter may be stepped at this end to provide a larger liquid reservoir. Heat added to this end of the shaft (evaporator) evaporates the working fluid, generating vapor which then flows axially toward the other end. Heat removed from this end of the shaft (condenser) condenses the vapor. The centrifugal forces accelerate the liquid condensate back to the evaporator to complete the cycle. Since it has no wick structure, the rotating heat pipe can operate at substantially higher heat fluxes than a conventional, capillary heat pipe. Its performance is controlled primarily by the thermal resistance due to condensation.

Experimental results presented in Ref. (28) show that the evaporator performs better at higher heat loads because of the well-known pressure effect upon nucleate boiling. Care must be exercised in designing a rotating heat pipe to insure that the internal condensation resistance is of the same order as the condenser wall resistance, and outside convection resistance. Performance can be improved by operating at higher rotational speeds, by using thin-walled, high-conductivity condensers and by promoting dropwise condensation.

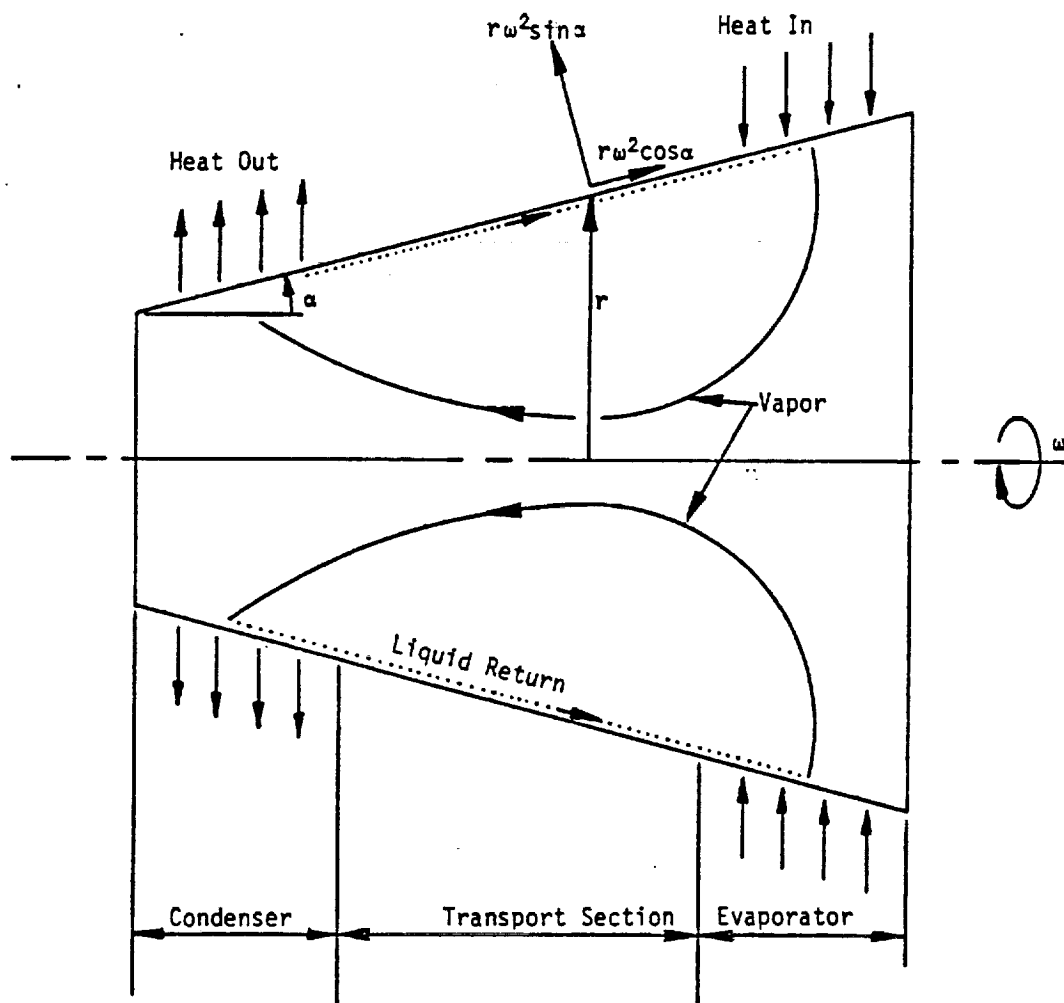


Fig. 9-23 Simple rotating heat pipe

References

1. "Heat Pipes," Final Report prepared by Midwest Research Institute, NASA CR-2508, January 1975.
2. Harwell, W. F., et.al., "OAO Heat Pipe Performance Data," AIAA Paper No. 73-758.
3. McIntosh, R., Knowles, G., and Hembach, R., "Sounding Rocket Heat Pipe Experiment," AIAA Paper No. 72-259.
4. Ollendorf, S., McIntosh, R., and Harwell, W., "Performance of Heat Pipes in Zero Gravity," Paper 9-5, International Heat Pipe Conference, October 1973.
5. McIntosh, R., Ollendorf, S., and Harwell, W., "The International Heat Pipe Experiment," 2nd International Heat Pipe Conference, April 1976.
6. Berger, M. E. and Kelly, W., "Application of Heat Pipes to the ATS-F Spacecraft," ASME Paper No. Enas-46, July 1973.
7. Wanous, D. J., and Marcus, B. D., "A Variable Conductance Heat Pipe Experiment - Performance In Space," AIAA Paper No. 75-725, 1975.
8. Kirkpatrick, J. P., and Brennan, P. J., "Long Term Performance of the Advanced Thermal Control Experiment," 2nd International Heat Pipe Conference, April 1976.
9. Suelau, H. J., Brennan, P. J., and McIntosh, R., "HEPP - A Low Temperature Heat Pipe Experiment Package Developed for Flight On-Board the Long Duration Exposure Facility (LDEF)," 3rd International Heat Pipe Conference, May 1978.
10. Edelstein, F., "Transverse Flat Plate Heat Pipe Experiment," 3rd International Heat Pipe Conference, May 1978.
11. Edelstein, F., "Transverse Header Heat Pipe," AIAA Paper 75-656, 1975.
12. Mock, P., Marcus, B. D., and Edelman, E. A., "Communications Technology Satellite: A Variable Conductance Heat Pipe Application," AIAA/ASME Thermophysics Conference, July 1974.
13. Skladany, J. T., "Thermal Control of the International Ultraviolet Explorer," ASME Paper No. 76-Enas-38, 1976.
14. Harwell, W., and Ollendorf, S., "Instrument Canister Thermal Control," AIAA Paper 77-761, 1977.
15. McIntosh, R., and Ollendorf, S., "A Thermal Canister Experiment for the Space Shuttle," 3rd International Heat Pipe Conference, May 1978.
16. Bienenert, W. B., et.al., "Snow and Ice Removal from Pavements Using Stored Earth Heat Energy," FHWA-RD-75-6, 1974.
17. Ferrara, A., and Haslett, R., "Prevention of Preferential Bridge Icing Using Heat Pipes," U. S. Department of Transportation Contract No. DOT-FH-11-8545, 1975.
18. Ruch, M. A., Grover, G. M., "Heat Pipe Thermal Recovery Unit Applications," 2nd International Heat Pipe Conference, 1976.
19. Basulius, A., and Formilles, D. J., "Emerging Heat Pipe Applications," 3rd International Heat Pipe Conference, 1976.
20. Waters, E. D., "Heat Pipes for the Trans-Alaskan Pipeline," 2nd International Heat Pipe Conference, 1976.

References - Continued

21. Kroliczek, E. J., et.al., "Application of Heat Pipes to Deicing Systems," 2nd International Heat Pipe Conference, 1976.
22. Pravda, M. F., Trimmer, D. C., and Wolf, D. A., "Airport Pavement Heating System for Removing Snow, Slush and Ice," U. S. Department of Transportation Contract No. DOT-FA 74 WA-3421, 1975.
23. Bienert, W., "Heat Pipes for Solar Energy Collectors," International Heat Pipe Conference, 1973.
24. Ramsey, J. W., Gupta, B. P. and Knowles, G. P., "Experimental Evaluation of a Cylindrical Parabolic Solar Collector," ASME Paper 76 WA/HT-13.
25. Fleishman, G. L., Marcus, B. D., et.al., "Flat Plate (Vapor Chamber) Heat Pipes," AIAA Paper No. 75-728, 1975.
26. Wright, J. P., "Flexible Cryogenic Heat Pipe Development Program," NASA CR-152027, July 1977.
27. Jones, T. B., and Perry, M. P., "Electrohydrodynamic Heat Pipe Research," Research Report No. 4, NASA CR-114646, July 1973.
28. Marto, P. J., "Performance Characteristics of Rotating Wickless Heat Pipes," 2nd International Heat Pipe Conference, April 1976.

BIBLIOGRAPHY

A list of pertinent heat pipe references is presented on the following pages. The references are listed by year and in alphabetical order within each year. One exception is the International Heat Pipe Conference Proceedings which are listed as the first reference of 1973, 1976 and 1978.

For a very thorough bibliography on heat pipes, the user is referred to the NASA sponsored "Heat Pipe Technology - A Bibliography with Abstracts" published periodically by the Technology Application Center at the University of New Mexico, Albuquerque, New Mexico.

Another thorough bibliography on heat pipes can be obtained from the Small Business Administration, Philadelphia Regional Office, 646 West Lobby, One Bala Cynwyd Plaza, 231 St. Asaphs Road, Bala Cynwyd, Pennsylvania 19004. This bibliography is divided into three parts: COMPENDEX, ISMEC, and NTIS and is researched by Documentation Associates, 11720 West Pico Boulevard, Los Angeles, California 90064. An excerpt from this listing is shown below.

ACCESSION NUMBER	PATENT-3 935 063
TITLE	Emergency Heat Removal System for a Nuclear Reactor
TITLE NOTE	Patent
AUTHORS	Dunckel, T. L.
ORGANIZATIONAL SOURCE	to Energy Research and Development Administration.
PAGINATION/DATE	Filed 28 Nov 73. Patented 27 Jan 76; 10p
ISSUE	U7702
NTIS PRICES	NTIS Prices: PC A02/MF A01
AVAILABILITY	This Government-owned invention available for U.S. licensing and, possibly, for foreign licensing. Copy of patent available Commissioner of Patents, Washington, D.C. 20231 \$0.50.
REPORT NOS.	PAT-APPL-419 832
CATEGORY CODES	18I; 77H; 90C
INDEX TERMS	*Bwr type reactors; *Eccs; *Heat pipes; *Lmfr type reactors; *Pwr type reactors; .Configuration; Heat transfer; Performance
SUPPLEMENTARY TERMS	ERDA/210100; ERDA/210200; ERDA/210500; *Patents: NTISGPERDA; NTISERDA
ABSTRACT	A heat removal system for nuclear reactors serving as a supplement to an Emergency Core Cooling System (ECCS) during a Loss of Coolant Accident (LOCA) comprises a plurality of heat pipes having one end in heat transfer relationship with either the reactor pressure vessel, the core support grid structure or other in-core components and the opposite end located in heat transfer relationship with a heat exchanger having heat transfer fluid therein. The heat exchanger is located external to the pressure vessel whereby excessive core heat is transferred from the above reactor components and dissipated within the heat exchanger fluid. (ERA citation 01:023239)

BIBLIOGRAPHY

1964

1. Grover, G. M., Cotter, T. P. and Erikson, G. F., "Structures of Very High Thermal Conductivity," J. Appl. Phys., 35, 1990 (1964).

1965

2. Busse, C. A., Caron, R. and Cappelletti, C., "Prototype of Heat Pipe Thermionic Converters for Space Reactors," Proc. of 1st Int'l. Conf. on Thermionic Electrical Power Generation, London, 1965.
3. Cotter, T. P., "Theory of Heat Pipes," Los Alamos Scientific Laboratory Report LA-3246-MS, February 1965.
4. Deverall, J. E. and Kemme, J. E., "High Thermal Conductance Devices Utilizing the Boiling of Lithium and Silver," Los Alamos Scientific Laboratory, LA-3211, 1965.
5. Deverall, J. E. and Kemme, J. E., "Satellite Heat Pipe," Los Alamos Scientific Laboratory Report LA-3278-MS, January 1965.
6. Marcus, B. D., "On the Operation of Heat Pipes," TRW Report 9895-6001-TU-000, May 1965.
7. Ranken, W. A. and Kemme, J. E., "Survey of Los Alamos and Euratom Heat Pipe Investigations," IEEE Conf. Record of 1965 Thermionic Conversion Specialist Conf., San Diego, California, October 1965, pp. 325-336.
8. Wyatt, T., "A Controllable Heat Pipe Experiment for the 5E-4 Satellite," Appl. Phys. Lab., Johns Hopkins University, SDO-1134 (1965).

1966

9. Busse, C. A., Geiger, G., Quataert, D., Potzschke, M., "Heat Pipe Life Test at 1600°C and 1000°C," 1966 IEEE Thermionic Specialist Conference, Houston, Texas, pp. 149-58.
10. Kemme, J. E., "Heat Pipe Capability Experiments," Los Alamos Scientific Laboratory Rept. LA -3585-MS, October 1966.
11. Kemme, J. E., "Heat Pipe Capability Experiments," Proceedings of Joint AEC/Sandia Labs., Heat Pipe Conf. 1, SC-M-66-223, October 1966, pp. 11-26.
12. Luikov, A., "Heat and Mass Transfer in Capillary-Porous Bodies," Pergamon Press, New York, 1966.

1967

13. American Society of Heating, Refrigeration, and Air Conditioning Engineers, "Handbook of Fundamentals," 1967.
14. Anand, D. K. and Hester, R. B., "Heat Pipe Application for Spacecraft Thermal Control," Tech Memo DDC AD 662 24, NASA NG8-15338, 1967.

1967 - Continued

15. Cosgrove, J. H., Ferrell, J. K and Carnesle, A., J. Nuclear Energy 21, pp. 547-558, 1967.
16. Cotter, T. P., "Heat Pipe Startup Dynamics," IEEE 1967 Thermionic Conversion Specialist Conference, Palo Alto, California, Oct. 30, 1967.
17. Deverall, J. E., Salmi, E. W. and Knapp, R. J., "Orbital Heat Pipe Experiment," Los Alamos Scientific Laboratory Report LA-3714, June 5, 1967.
18. Ernst, D. M., "Evaluation of Theoretical Heat Pipe Performance," Thermionic Conversion Specialist Conference, Palo Alto, California, October 30 - November 1, 1967, pp. 349-354.
19. Frank, S., Smith, J. T. and Taylor, K., "Heat Pipe Design Manual," Martin Marietta Corporation, Nuclear Division Report 3288, 1967.
20. Harbaugh, W. E., "The Development of an Insulated Thermionic Converter-Heat Pipe Assembly," RCA Rept. AF APL TR-67-45, 1967.
21. Kemme, J. E., "High Performance Heat Pipes," IEEE 1967 Thermionic Specialist Conference, Palo Alto, California, October 1967, pp. 355-358.
22. Kunz, H. R., Langston, L. S., Hilton, B. H., Wyde, S. S. and Nashick, G. H., "Vapor-Chamber Fin Studies," NASA CR-812, June 1967.
23. Parker, G. H. and Hanson, J. P., "Heat Pipe Analysis," Advances in Energy Conversion Engineering ASME 1967 Intersociety Energy Conversion Conference, Miami, Florida, August 1967, p. 857.
24. Schins, H. E. J., "Liquid Metals for Heat Pipes, Properties, Plots, and Data Sheets," Euratom Report EUR 3653e, 1967.
25. Smithells, C. J., "Metals Reference Book," Vol. 3, Plenum Press, New York, 1967.

1968

26. Busse, C. A., Geiger, F., Strub, H., Potzschke, M. and Kraft, G., "High Temperature Lithium Heat Pipes," 2nd Int'l. Conf. on Thermionic Electrical Power Generation, Euratom Report. EUR 4210 f.e., 1968, pp. 495-506.
27. Farran, R. A. and Starner, K. E., "Determining Wicking Properties of Compressible Materials for Heat Pipe Applications," Annual Aviation and Space Conference, Beverly Hills, California, June 1968, pp. 659-669.
28. Freggens, R. A., "Experimental Determination of Wick Properties for Heat Pipe Applications," Proc. of 4th Intersociety Energy Conversion Conference, Washington, D. C., September 1968, pp. 888-897.
29. Grover, G. M., Kemme, J. E., and Keddy, E. S., "Advances in Heat Pipe Technology," Proceedings 2nd Int'l. Conf. Thermionic Electrical Power Generation, Stresa, Euratom Rept. EUR-4210, f.e., Ispra, Italy, 1968, pp. 477-90.
30. Johnson, G. D., "Compatibility of Various High Temperature Heat Pipe Alloys with Working Fluids," IEEE 1968 Thermionic Conversion Specialist Conf., Framingham, N. Y., 1968, pp. 258-65.
31. Katzoff, S., "Heat Pipes and Vapor Chambers for Thermal Control of Spacecraft," Thermophysics of Spacecraft and Aeronautics, V. 20, Academic Press, New York, 1968, pp. 761-818.

1968 - Continued

32. Levy, E. K., "Theoretical Investigation of Heat Pipes Operating at Low Vapor Pressures," Trans. ASME, J. for Industry, November 1968, p. 547.
33. Rouklove, P., Comment in Proceedings of 2nd Int'l. Conf. on Thermionic Electrical Power Generation, Stresa, Euratom Rept. EUR 4210, f.e., Ispra, Italy 1968, p. 494.
34. Shlossinger, A. P., "Heat Pipe Devices for Space Suit Temperature Control," TRW Systems Rept. No. 06462-6005-RO-00, November 1968.
35. Varljen, T. C., "A Computer - Subroutine to Generate the Thermophysical Properties of Space-Power System Working Fluids," WANL-TME-1838, November 1968.

1969

36. Busse, C. A., "Heat Pipe Thermionic Converter Research in Europe," 4th Intersociety Energy Conversion Engineering Conference, Washington, D. C., September 1969.
37. Deverall, J. E., "Capability of Heat Pipes," Heat Pipe Technology & Manned Space Station Appl. Technical Interchange, Huntsville, Alabama, May 27, 1969.
38. Eastman G. Y., "The Heat Pipe - A Progress Report," 4th Intersociety Energy Conversion Engineering Conference, Washington, D. C., September 1969, pp. 873-8.
39. Kemme, J. E., Quarterly Status Report on Space Electric R&D Program for period ending Jan. 31, 1969, Pt. 1, Los Alamos Scientific Laboratory Rept. LA-4109-MS.
40. Moritz, K. and Pruschek, R., "Energy Transport Limits in Heat Pipes," Chemie Ingenieur Technik 41, 30, 1969.
41. Phillips, E. C., "Low Temperature Heat Pipe Research Program," NASA CR-66792, June 1969.
42. Shesiek, P. K. and Ernst, D. M., "Heat Pipe Development for Thermionic Application," 4th Intersociety Energy Conversion Conference, Washington, D.C., 1969, pp. 879-887.

1970

43. Bienert, W. B., "Study to Evaluate the Feasibility of a Feedback Controlled Variable Conductance Heat Pipe," Contract No. NAS 2-5722, Dynatherm Corporation Rept. DTM-70-4, September 1970.
44. Bressler, R. G. and Wyatt, P. W., "Surface Wetting Through Capillary Grooves," Trans. ASME, J. Heat Transf., pp. 126-132, 1970.
45. Busse, C. A., Geiger, F., Quataert, D., "Status of Emitter Heat Pipe Development at Ispra," IEEE Con. Record of Thermionic Specialist Conference, 1970.
46. Chi, S. W. and Cygnarowicz, T. A., "Theoretical Analyses of Cryogenic Heat Pipes," 1970 Space Technology and Heat Transfer Conference, January 1970.
47. Chi, S. W., "Mathematical Modeling of Cryogenic Heat Pipes," Final Report NASA Grant No. NGRO9-005-071, Catholic University of America, Sept. 1970.
48. Deverall, J. E., "Mercury as a Heat Pipe Fluid," Los Alamos Scientific Laboratory, LA-4300-MS, January, 1970.

1970 - Continued

49. Deverall, J. E., Kemme, J. E., and Florschuetz, L. W., "Sonic Limitations and Startup Problems of Heat Pipes," Los Alamos Scientific Laboratory, LA-4518, November 1970.
50. Ferrel, J. K. and Alleavitch, J., "Vaporization Heat Transfer in Capillary Wick Structures," Chemical Eng. Prog. Symposium Series V66, Heat Transfer, Minneapolis, Minn., 1970.
51. Freggens, R. A. and Langsderff, R. W., "Development of High Performance Sodium/Nickel Heat Pipes," Intersociety Energy Conversion Engineering Conference, Las Vegas, Nevada, September 1970.
52. Johnson, G. D., "Corrosion Studies of Liquid Metal Heat Pipe Systems at 1000°C to 1800°C." In Draley, J. E., and Weeks, J. R., "Corrosion by Liquid Metals," Plenum Press, N. Y., 1970, pp. 321-37.
53. Marcus, B. D. and Fleischmann, G. L., "Steady State and Transient Performance of Hot Reservoir Gas Controlled Heat Pipes," ASME 1970 Space Techn. and Heat Transf. Conf., Los Angeles, California, June 1970.
54. Soliman, M. M., Grauman, D. W. and Berenson, P. J., "Effective Thermal Conductivity of Saturated Wicks," ASME Paper No. 70-HT/SpT-40, 1970.

1971

55. Basiulis, A. and Filler, M., "Operating Characteristics and Long Life Capabilities of Organic Fluid Heat Pipes," AIAA 6th Thermophysics Conference, April 26-28, 1971, (AIAA Paper No. 71-408).
56. Bienert, W. B. and Brennan, P. J., "Transient Performance of Electrical Feedback Controlled Variable-Conductance Heat Pipes," ASME Paper 71-Av-27, SAE/ASME/AIAA Life Support and Environmental Control Conference, San Francisco, California, July 12-14, 1971.
57. Bienert, W. B., Brennan, P. and Kirkpatrick, J. P., "Feedback Controlled Variable Conductance Heat Pipes," AIAA Paper No. 71-42, 6th Thermophysics Conf., Tyllahoma, Tenn., April 1971.
58. Bienert, W. B. and Kroliczek, E., "Experimental High Performance Heat Pipes for the OAO-C Spacecraft," SAE/ASME/AIAA Life Support and Environmental Control Conference, July 1971, San Francisco, California, ASME 71-Av-26.
59. Brennan, P. J., Trimmer, D. S., Sherman, A. and Cygnarowicz, T., "Arterial and Grooved Cryogenic Heat Pipes," ASME, Heat Transfer Div., Winter Meeting November 28, 1971, ASME Paper 71-WA/HT-42.
60. Busse, C. A., "Heat Pipes for Thermionic Space Power Supplies," Proc. 3rd Int'l. Conf. on Space Technology, Rome, 1971.
61. Chi, S. W., "Introduction to Heat Pipe Theory," George Washington University, Washington, D. C., 1971.
62. Dynatherm Corporation, Cockeysville, Md., "Design, Fabrication and Qualification of Heat Pipes for ATS F&G," 2nd Monthly Progress Report. Contract SC 68280 (Fairchild Industries), June 9, 1971.
63. Edwards, D. K., Fleischman, G. L., and Marcus, B. D., "User's Manual for the TRW GASPIPE Program," NASA CR-114306, April 1971.

1971 - Continued

64. Feldman, K. T., Jr., Ed., "Heat Pipe Technology - A Bibliography with Abstracts," Technology Application Center, University of New Mexico, Albuquerque, New Mexico, Published Quarterly, 1971.
65. Gerrels, E. E. and Larson, J. W., "Brayton Cycle Vapor Chamber (Heat Pipe) Radiator Study," NASA CR-1677, February 1971.
66. Groll, M., Brost, O., Kreeb, H., Schubert, K. and Zimmerman, P., "Power Limits, Technology, and Application of Low Temperature Heat Pipes," *Forschung im Ingenieurwesen* 37, pp. 33-37, 1971.
67. Kemme, J. E., Quarterly Status Report on Space Electric Power R&D Program, July 31, 1971, Los Alamos Scientific Laboratory Rept. LA-4746-MS.
68. Levy, E. K., "Effects of Friction on the Sonic Velocity Limit in Sodium Heat Pipes," ASME Paper HPT-71-022.
69. Marcus, B. D., "Theory and Design of Variable Conductance Heat Pipes," NASA CR-2018, July 1971.
70. Quataert, D., "Investigations of the Corrosion Mechanism in Tantalum-Lithium High Temperature Heat Pipes by Ion Analysis," *Forsch. Ing. Wes.* 37, pp. 37-38, 1971.
71. Reiss, F. E. and Schretzmann, K., "Boiling Tests with an Open Grooved Capillary Evaporator," *Forschungen im Ingenieurwesen* 37, pp. 55-58, 1971.
72. Winter, E. R. F. and Barsch, W. O., "The Heat Pipe," in *Advances in Heat Transfer*, Vol. 7, Ed. by Irvine, T. F. and Hartnett, J. P., Academic Press, New York, 1971.

1972

73. Alario, J. P., Prager, R. C., "Space Shuttle Orbiter Heat Pipe Applications. Volume 1 Synopsis," Grumman Aerospace Corp., 30 April 1972.
74. Alario, J. P., Prager, R. C., "Space Shuttle Orbiter Heat Pipe Applications. Volume 2 Final Report," Grumman Aerospace Corp., April 1972.
75. Bacigalupi, R. J., "Fabrication and Evaluation of Chemically Vapor Deposited Tungsten Heat Pipe," National Aeronautics and Space Administration, Lewis Research Center, 1972.
76. Edwards, D. K., Fleischman, G. L., Marcus, B. D., "Theory and Design of Variable Conductance Heat Pipes Steady State and Transient Performance," TRW Systems Group, Dec. 1972.
77. Eliseev, V. B., Sergeev, D. I., "Heat Pipe: New High-Temperature Heat-Transfer Device," Joint Publications Research Service.
78. Feldman, K. T., Jr., "A Study of Optimum Wick Design in Water Heat Pipes," New Mexico Univ. Albuquerque Bureau of Engineering Research.
79. Fraas, A. P., Samuels, G., "Isotope Kilowatt Program Quarterly Progress Report for Period Ending December 31, 1971," Oak Ridge National Lab.
80. Fraas, A. P., Samuels, G., "Isotope Kilowatt Program Quarterly Progress Report for Period Ending March 31, 1972," Oak Ridge National Lab.

1972 - Continued

81. Garg, S. C., "Investigation of Heat Pipe Technology for Naval Applications," Naval Civil Engineering Lab., Port Hueneme, Calif., Feb. 1972.
82. Hanke, H., "Design and Optimization of a Fast Heat Pipe Thermionic Reactor," Vols. 1 and 2, Scientific Translation Service, Santa Barbara, Calif., Feb. 1972.
83. Hitschke, U., "Study of the Possible Application of Heat Pipes in Steam Generators of Sodium-Cooled Reactors," Kernforschungszentrum, Karlsruhe (West Germany) Institut fuer Reaktorentwicklung, December 1972.
84. Hollister, M. P. and Ekern, W. F., "Performance of a Precision Thermal Control System Using Variable Conductance Heat Pipes," AIAA 7th Thermophysics Conc., San Antonio, April 1972.
85. Jones, T. B., Perry, M. P., "Entrainment in Electrohydrodynamic Heat Pipes," Colorado State University, Fort Collins, Dept of Electrical Engineering, Aug. 1972..
86. Jones, T. B., and Perry M. P., "Experiments with an Electrohydrodynamic Heat Pipe," Colorado State University, Fort Collins Dept. of Electrical Engineering, Sept. 1972.
87. Kosson, R., Hemback, R., Edelstein, F. and Tawil, M., "A Tunnel Wick 100,000 Watt-Inch Heat Pipe," AIAA Thermophysics Conference, San Antonio, Texas, April 1972.
88. Kroeger, E. W, Ward, J. J. and Breitwieser, R., "An out-of-Core Version of a Six Cell Heat-Pipe Heated Thermionic Converter Array," National Aeronautics and Space Administration, Lewis Research Center, 1972.
89. "Quarterly Status Report on the Space Electric Power R&D Program for the Period Ending January 31, 1972," Los Alamos Scientific Lab., N. Mex., Feb. 1972.
90. Marcus, B. D., "Ames Heat Pipe Experiment (Ahpe) Experiment Description Document," TRQ Systems Group, Redondo Beach, Calif., Materials Science Staff, Jan. 1972.
91. Marcus. B. D., "Theory and Design of Variable Conductance Heat Pipes," NASA CR-2018, TRW Systems Group, Redondo Beach, Calif., April 1972.
92. Marshburn, J. P., "Heat Pipe Investigations," NASA / Goddard Space Flight Center, May 1972.
93. Marshburn, J. P., "Techniques Associated with Thermal-Vacuum Testing of the Oao C Heat Pipes," NASA/Goddard Space Flight Center, Aug. 1972.
94. Marto, P. J., "An Analytical and Experimental Investigation of Rotating, Non-Capillary Heat Pipes," Naval Postgraduate School, Monterey, Calif., Dept. of Mechanical Engineering, Nov. 30, 1972.
95. McKechnie, J., "The Heat Pipe: A List of Pertinent References," National Engineering Lab, East Kilbride (Scotland), Mar. 1972.
96. Mortimer, A. R, "Cryogenic Heat Pipe: A Review of Work at the Rutherford Laboratory," Rutherford High Energy Lab., Chilton (England), Aug. 1972.
97. "Heat Pipe Technology. A Bibliography with Abstracts. Cumulative Volume through Dec. 31, 1972," New Mexico Univ., Albuquerque, Technology Application Center, Dec. 31, 1972.
98. Reynolds, K. E., "Investigation of the Performance of a Gas-Loaded Variable Conductance Heat Pipe," Naval Postgraduate School, Monterey, Calif., Dec. 1972.

1972 - Continued

99. Saaski, E. W., "Investigation of Bubbles in Arterial Heat Pipes," McDonnell-Douglas Astronautics Co., Richland, Wash., Dec. 1972.
100. Skrabek, E. A. and Biernert, W. B., "Heat Pipe Design Handbook," NASA Contract NAS9-11927, Dynatherm Corporation Report No. 72-3, August 1972.
101. Steininger, Jacques and Reed, Thomas B., "Application of Heat Pipe Technology to Crystal Growth," (Reprint), Massachusetts Inst. of Tech., Lexington, Lincoln Lab., 1972.
102. Swerdling, B. and Kosson, R., "Design, Fabrication and Testing of a Thermal Diode," Final Report, 1 Jul 1971 - 15 Nov. 1972, Grumman Aerospace Corp., Bethpage, N.Y., Nov. 1972.
103. Werner, R. W., "Heat Pipes as a Means of Energy Removal from Thermonuclear Reactor Vacuum Walls," California Univ., Livermore, Lawrence Livermore Lab., July 24, 1972.
104. Woodard, J. S., "The Operation of Rotating Non-Capillary Heat Pipes," Naval Postgraduate School, Monterey, Calif., March 1972.
105. Wright, J. P., "Computer Program for the Design and Analysis of Heat Pipes," North American Rockwell, Space Division, Report No. SD72-SA-001, Jan. 1972.

1973

106. "International Heat Pipe Conference Proceedings, October 15-17, 1973," Stuttgart, Federal Republic of Germany.
107. Alario, J., "Space Shuttle Heat Pipe Thermal Control Systems," Final Report, Jun. 1972 - Oct. 1973, Grumman Aerospace Corp., Bethpage, N.Y., Oct. 1973.
108. Anand, D. K., "Heat Pipe Symposium/Workshop held at College Park, Maryland on 5 - 6 November 1973," Science Foundation, Washington, D. C., Nov. 1973.
109. Birnbreier, H., Gammel, G., Heidtmann, U., Joens, M., and Pawlowski, P. "A Novel Method of Cooling Semiconductor Devices for Power Electronics," Brown, Boveri and Cie, A. G., Heidelberg, West Germany, Apr. 1973.
110. Busse, C. A., "Material Problems for High Temperature Heat Pipes," Scientific Translation Service, Santa Barbara, Calif., Feb. 7, 1973.
111. Chimenti, R. J., "Heat Pipe Copper Vapor Laser," Semi-Annual Technical Rept. 1 Feb. - 30 Sept. 1973, Esso Research and Engineering Co. Linden, N. J., Government Research Lab., Oct. 8, 1973.
112. Depew, C. A., Sauerbrey, W. J., and Benson, B. A., "Construction and Testing of a Gas-Loaded Passive-Control, Variable-Conductance Heat Pipe," Washington Univ., Seattle, Dept. of Mechanical Engineering, April 1973.
113. Edwards, D. K., Fleischman, G. L., and Marcus, B. D., "User's Manual for the TRW GASPIPE 2 Program: A Vapor-Gas Front Analysis Program for Heat Pipes Containing Non-Condensable Gas," TRW Systems Group, Redondo Beach, Calif., Oct. 1973.
114. Feldman, K. T., Jr., and Berger, M. E., "Analysis of a High-Heat-Flux Water Heat Pipe Evaporator," New Mexico Univ., Albuquerque Bureau of Engineering Research, Sept. 1973.
115. Fraas, A. P., and Samuels, G., "Isotope Kilowatt Program Quarterly Progress Report for Period Ending December 31, 1972," Oak Ridge National Lab., Tenn., May 1973.

1973 - Continued

116. Fraas, A. P., and Samuels, G., "Isotope Kilowatt Program Quarterly Progress Report for Period Ending March 31, 1973," Oak Ridge National Lab., Tenn. Sept. 1973.
117. Humphreys, W. I., "Investigation of Gravitational Effects on the Performance of a Variable Conductance Heat Pipe," Naval Postgraduate School, Monterey, Calif., Dec. 1973.
118. Jacobson, D. L., "An Intercell Heat Pipe for Fuel Cell and Battery Cooling," Final Report, June 1972 - July 1973, Arizona State Univ., Tempe Dept. of Mechanical Engineering, Dec. 1973.
119. Jones, T. B., and Perry M. P., "Electrohydrodynamic Heat Pipe Research," Colorado State Univ., Fort Collins, July 1973.
120. Kemme, J. E., Deverall, J. E., Keddy, E. S., Phillips, J. R., and Ranken, W. A., "Performance Tests of Gravity-Assist Heat Pipes with Screen-Wick Structures," Los Alamos Scientific Lab., N. Mex., 1973.
121. Kirkpatrick, J. P., "Variable Conductance Heat Pipes from the Laboratory to Space," NASA Ames Research Center, Moffett Field, Calif., July 1973.
122. Lloyd, D. B., "Test of a Combined Heat Pipe -- Thermoelectric Module," Oak Ridge National Lab., Tenn., April 1973.
123. Marcus, B. D., Edwards, D. K., and Anderson, W. T., "Variable Conductance Heat Pipe Technology," TRW Systems Group, Redondo Beach, Calif., Dec. 1973.
124. Marshburn, J. P., "Heat Pipe Investigations," NASA/Goddard Space Flight Center, Aug. 1973.
125. Marto, P. J., "An Analytical and Experimental Investigation of Rotating, Non-Capillary Heat Pipes," Naval Postgraduate School, Monterey, Calif., Sept. 1973.
126. "Design, Fabrication, Testing, and Delivery of Shuttle Heat Pipe Leading Edge Test Modules. Volume 1: Executive Summary," (Final Report) McDonnell-Douglas Astronautics Co., St. Louis, Mo., April 20, 1973.
127. "Design, Fabrication, Testing, and Delivery of Shuttle Heat Pipe Leading Edge Test Modules. Volume 2: Technical Report," (Final Report) McDonnell-Douglas Astronautics Co., St. Louis, Mo., April 20, 1973.
128. Morris, J. F., "Figure-of-Merit Calculation Methods for Organic Heat Pipe Fluids," NASA Lewis Research Center, Nov. 1973.
129. "Heat Pipe Stability. -1: A Preliminary Investigation into Thermally Assisted Cavitation," NASA/Goddard Space Flight Center, July 1973.
130. "Heat Pipe Technology. A Bibliography with Abstracts," Annual Supplement. New Mexico Univ., Albuquerque. Technology Application Center, 1973.
131. Raspet, D., "Thermophysical and Optical Evaluation of Heat Pipe Cooled Laser Mirrors," Air Force Inst. of Tech., Wright-Patterson AFB, Ohio School of Engineering, June 1973.
132. Reiss, F. E., "Application of the Heat Pipe Principle to Avoid the Error Due to the Emergent Stem in Liquid-in-Glass Thermometers," Kernforschungszentrum Karlsruhe, Federal Republic of Germany, Inst. Fuer Neutronenphysik und Reaktortechnik, Dec. 1973.

1973 - Continued

133. Reiss, F. E., "Heat Pipe With an Electrostatic Pump," Kernforschungszentrum Karlsruhe, Federal Republic of Germany, Inst. Fuer Neutronenphysik und Reaktortechnik, Aug. 1973.
134. Saaski, E. W., "Heat Pipe Thermal Conditioning Panel," Detailed Tech. Report, June 28, 1972 - Aug. 12, 1973, McDonnell-Douglas Astronautics Co., Richland, Wash., Sept. 1973.
135. Schlitt, K. R., "Design and Testing of a Passive, Feedback-Controlled, Variable Conductance Heat Pipe," NASA Ames Research Center, Aug. 1973.
136. Sockol, P. M., "Startup Analysis for a High Temperature Gas Loaded Heat Pipe," NASA Lewis Research Center, July 1973.
137. Swerdling, B., and Alario, J., "Heat Pipe Radiator," Final Report, June 1972 - Sept. 1973, Grumman Aerospace Corp., Bethpage, N.Y., Oct. 1973.
138. Tower, L. K., "Theoretical Analysis of Oxygen Diffusion at Startup in an Alkali Metal Heat Pipe with Gettered Alloy Walls," NASA Lewis Research Center, May 1973.
139. Vidal, C. R., "Spectroscopic Observations of Subsonic and Sonic Vapor Flow Inside an Open-Ended Heat Pipe." (Reprint) Final Rept. Sept. 1971 - Apr. 1972, National Bureau of Standards, Washington, D. C., 1973.
140. "Study of the Collector/Heat Pipe Cooled Externally Configured Thermionic Diode," Final Report. Westinghouse Electric Corp., Pittsburgh, Pa., March 6, 1973.

1974

141. Abhat, A., and Hage, M., "Constant Temperature Heat Pipe," Final Report, Stuttgart Univ. (West Germany), Abteilung Energiewandlung, Oct. 1974.
142. Anderson, W. T., Edwards, D. K., Eninger, J. E., and Marcus, B. D., "Variable Conductance Heat Pipe Technology," Final Research Report, March 1974.
143. Bienert, W. B., "Development of Electrical Feedback Controlled Heat Pipes and the Advanced Thermal Control Flight Experiment," Technical Summary Report, Dynatherm Corp., May 1974.
144. Chimenti, R. J. L., "Heat Pipe Copper Vapor Laser," Final Tech. Report, Feb. 1, 1973 - June 30, 1974, Exxon Research and Engineering Co., Linden, N.J., Nov. 1974.
145. Edelstein, F., "Heat Pipe Manufacturing Study," Final Report, Grumman Aerospace Corp., Bethpage, N. Y., Aug. 1974.
146. Eninger, J. E., "Computer Program Grade for Design and Analysis of Graded-Porosity Heat Pipe Wicks," TRW Systems Group, Redondo Beach, Calif., Aug. 1974.
147. Lantz, G., Breitwieser, R., and Niederauer, G. F., "Development Concept for a Small, Split-Core Heat Pipe Cooled Nuclear Reactor," NASA Lewis Research Center, April 1974.
148. Nakashima, A. M., and Kikin, G. M., "A Homogeneous Heat Pipe Design Code," Jet Propulsion Lab., Calif. Inst. of Tech., Pasadena, Jan. 15, 1974.
149. Nelson, L. A., "Development of Heat Pipe Cooled Anode for Xenon Arc Lamp," Final Report Jan. 1973 - Jan. 1974, Hughes Aircraft Co., Fullerton, Calif. Ground Systems Group, Mar. 1974.
150. "Heat Pipe Technology. A Bibliography with Abstracts," Quarterly Update, New Mexico Univ., Albuquerque, Technology Application Center, 1974.

1974 - Continued

151. Pittinato, G. F., "The Elimination or Control of Material Problems in Water Heat Pipes," Semi-Annual Progress Rept., Jan. 1 - June 30, 1974, McDonnell-Douglas Astronautics Co., West Huntington Beach, Calif., July 31, 1974.
152. Pittinato, G. F., "The Elimination or Control of Material Problems in Water Heat Pipes," Quarterly Progress Report No. 3, July 1 - Sept. 30, 1974, McDonnell-Douglas Astronautics Co., West Huntington Beach, Calif., Nov. 1974.
153. Quadrini, J., and Kosson, R., "Design, Fabrication, and Testing of a Cryogenic Thermal Diode," Interim Research Report, Grumman Aerospace Corp., Bethpage, N.Y., Dec. 1974.
154. Ranken, W. A., "Conceptual Design of a Heat Pipe Methanator," Los Alamos Scientific Lab., N. Mex., April 1974.
155. Richter, R., "Solar Collector Thermal Power System. Volume II, Development, Fabrication, and Testing of Fifteen Foot Heat Pipes," Final Report, Aug. 16, 1971 - June 28, 1974, Xerox Corp./Electro-Optical Systems, Pasadena, Calif., Nov. 1974.
156. Richter, R., "Solar Collector Thermal Power System. Volume III. Basic Study and Experimental Evaluation of Thermal Train Components," Final Report, Aug. 16, 1971 - June 28, 1974, Xerox Corp./Electro-Optical Systems, Pasadena, Calif., Nov. 1974.
157. Saaski, E. W., "Investigation of Arterial Gas Occlusions," Final Report, May 22, 1973 - Jan. 22, 1974, McDonnell-Douglas Astronautics Co., Richland, Wash., March 1974.
158. Sasin, V. I., and Shelginsky, A. I., "Heat Transfer Intensity in the Condensation Section of a Heat Pipe," Techtran Corp., Glen Burnie, Md., April 1974.
159. Schuchardt, J. M., "Heat Pipe Cooled Microwave Window," Final Report, Georgia Inst. of Tech., Atlanta, Feb. 1974.
160. Sellers, J. P., "Steady-State and Transient Operation of a Heat Pipe Radiator System," Technical Report, Jan. - Aug. 1974, Tuskegee Inst., Ala. School of Mechanical Engineering, Dec. 1974.
161. Smith, B. L., Bassett, H. L., Schuchardt, J. M., and Colwell, G. T., "A Microwave Transparent Method of Cooling Microwave Components, with Practical Results," Army Advanced Ballistic Missile Defense Agency, Huntsville, Ala., 1974.
162. Stadelmann, M., "Gas-Fired Heat Pipe Vacuum Furnace," Jan. 17, 1974.
163. Strimbeck, D. C., Sherren, D. C., and Keddy, E. S., "Process Environment Effects on Heat Pipes for Fluid-Bed Gasification of Coal," Los Alamos Scientific Lab., N. Mex., 1974.
164. "Function of Heat Pipes. Progress Report," Stuttgart Univ. (West Germany), Inst. fuer Kernenergetik, Oct. 1974.
165. Trimmer, D. S., "Design, Development and Testing of a Cryogenic Temperature Heat Pipe for the Icicle System," Final Report, Dynatherm Corp., Cockeysville, Md., May 31, 1974.
166. Tucker, R. S., "Heat Transfer Characteristics of a Rotating Two-Phase Thermosyphon," Naval Postgraduate School, Monterey, Calif., Sept. 1974.

167. Bader, E. E., "Heat Pipes as a Method of Heat Recovery," March 6, 1975.
168. Batts, W. H., Jr., "Investigation of Gravitational Effects on a Variable Conductance Heat Pipe Utilizing Liquid Crystal Thermography," Naval Postgraduate School, Monterey, Calif., Dec. 1975.
169. Bienert, W. B., and Wolf, D. A., "Heat Pipes Applied to Flat-Plate Solar Collectors," Annual Progress Report, Dynatherm Corp., Cockeysville, Md., Jan. 31, 1975.
170. Brennan, P. J., "Analysis of Fourth Sounding Rocket Heat Pipe Experiment," Summary Report, March - June 1974, April 1975.
171. Brennan, P. J., and Kroliczek, E. J., "Erts-C (Landsat 3) Cryogenic Heat Pipe Experiment Definition," Final Report, B & K Engineering, Inc., Towson, Md., March 1975.
172. Carbone, R. J., "Laser Application of Heat Pipe Technology in Energy Related Programs," Los Alamos Scientific Lab., N. Mex., 1975.
173. Deveral, J. E., Keddy, E. S., Kemme, J. E., and Phillips, J. R., "Gravity Assist Heat Pipes for Thermal Control Systems," Los Alamos Scientific Lab., N. Mex., June 1975.
174. Edelstein, F., "Deployable Heat Pipe Radiator," Final Report, Grumman Aerospace Corp., Bethpage, N. Y., April 1975.
175. Edelstein, F., "Large Variable Conductance Heat Pipe. Transverse Header," Final Report, Grumman Aircraft Engineering Corp., Bethpage, N.Y., 1975.
176. Eninger, J. E., Fleischman, G. L., and Luedke, E. E., "Vapor-Modulated Heat Pipe Report. Flight Data Analysis and Further Development of Variable-Conductance Heat Pipes," TRW Systems Group, Redondo Beach, Calif., Materials Technology Dept., June 30, 1975.
177. Ferrara, A. A., and Haslett, R., "Prevention of Preferential Bridge Icing Using Heat Pipes," Interim Report, July 1974 - July 1975, Grumman Aerospace Corp., Bethpage, N.Y., July 1975.
178. Groll, M., Pittman, R. B., and Eninger, J. E., "Parametric Performance of Circumferentially Grooved Heat Pipes with Homogeneous and Graded-Porosity Slab Wicks at Cryogenic Temperatures," NASA Ames Research Center, Moffett Field, Calif., Dec. 1975.
179. Hermann, E., Koch, H., Kreeb, H., and Perdu, M., "Handbook of Grooved Heat Pipes," Final Report, Dornier-System G. M. B. H., Friedrichshafen (Germany, F. R.), Sept. 2, 1975.
180. Hufschmitt, T. W., Burck, E., Dicola, G., and Hoffman, H., "The Shearing Effect of Vapor Flow on Laminar Liquid Flow in Capillaries of Heat Pipes," Kanner (Leo) Associates, Redwood City, Calif., Oct. 1975.
181. Kemme, J. E., Deverall, J. E., Keddy, E. S., Phillips, J. R., and Ranken, W. A., "Temperature Control with High Performance Gravity-Assist Heat Pipes," Los Alamos Scientific Lab., N. Mex., 1975.
182. Kraft, G. A., "Preliminary Evaluation of a Heat Pipe Heat Exchanger on a Regenerative Turbofan," NASA Lewis Research Center, Cleveland, Ohio, Dec. 1975.

1975 - Continued

183. Kreeb, H., "Design and Development of a Gas Controlled Heat Pipe Radiator for Communication Spacecraft Applications," Phase 1 Report, Nov. 1974 - May 1975, Dornier-System G.M.B.H., Friedrichshafen (West Germany), May 1975.
184. Loehrke, R. I., and Sebits, D. R., "Flat Plate Electrohydrodynamic Heat Pipe Experiments," Colorado State Univ., Fort Collins Dept. of Mechanical Engineering, July 1975.
185. "Heat Pipes," Final Report, Midwest Research Inst., Kansas City, Mo., Jan. 1975.
186. Naydan, T. P., "Investigation of a Variable Conductance Heat Pipe," Naval Postgraduate School, Monterey, Calif., March 1975.
187. "Heat Pipe Technology. A Bibliography with Abstracts," Quarterly Update, March 31, 1975, New Mexico Univ., Albuquerque, Technology Application Center, 1975.
188. "Heat Pipe Technology. A Bibliography with Abstracts," Quarterly Update, Sept. 30, 1975, New Mexico Univ., Albuquerque, Technology Application Center, 1975.
189. Pittinato, G. F., "The Elimination or Control of Material Problems in Water Heat Pipes," Semi-Annual Progress Report, Jan. 1 - June 30, 1975, McDonnell-Douglas Astronautics Co., West Huntington Beach, Calif., National Science Foundation, Washington, D. C., Div. of Advanced Energy Research and Technology, July 1975.
190. Pittinato, G. F., "The Elimination or Control of Material Problems in Water Heat Pipes," Quarterly Progress Report, July 1 - Sept. 30, 1975, McDonnell-Douglas Astronautics Co., West Huntington Beach, Calif., National Science Foundation, Washington, D. C., Research Applied to National Needs, Oct. 31, 1975.
191. "Spacecraft Thermal Control Design Data, Volume 2," Polytechnical Univ. of Madrid (Spain). School of Aeronautics, May 1975.
192. Potapov, Yu. F., "Determination of the Permissible Heat Flows in Heat Tubes with Capillary System in the Form of Longitudinal Rectangular Channels," Foreign Technology Div. Wright-Patterson AFB, Ohio, Jan. 15, 1975.
193. Reed, W. E., "Heat Pipes," Volume 1, 1964-1972 (A Bibliography with Abstracts), National Technical Information Service, Springfield, Va., Feb. 1975.
194. Reed, W. E., "Heat Pipes," Volume 2, Rept. for 1973 - Dec. 1974, (A Bibliography with Abstracts), National Technical Information Service, Springfield, Va., Feb. 1975.
195. "Solar Electric Propulsion System Thermal Analysis," Final Report, Dec. 27, 1973 - Feb. 1975, Rockwell International Corp., Downey, Calif., Space Div., Feb. 28, 1975.
196. Saaski, E. W., "Investigation of an Inverted Meniscus Heat Pipe Wick Concept," Sigma Research, Inc., Richland, Wash., Aug. 1975.
197. Sakurai, K., and Broida, H. P., "Chemically Reacting Bismuth and Nitrous Oxide in a Heat Pipe Oven," California Univ., Santa Barbara, Dept. of Physics, Sept. 29, 1975.
198. Suelau, H. J., "Examination of Earth Heat Pipes at Fairbanks Highway Research Station," Final Report, Jan. - July 1975, B & K Engineering, Inc., Towson, Md., July 1975.
199. "Low Cost High Performance Generator Technology Program, Volume 5, Heat Pipe Topical, Appendices," Teledyne Energy Systems, Timonium, Md., Energy Research and Development Administration, July 1975.

200. "2nd International Heat Pipe Conference Proceedings, March 31 - April 2, 1976," European Space Agency, Volumes 1 and 2.
201. Bienert, W. B., and Wolf, D. A., "Heat Pipe Central Solar Receiver," Semi-Annual Progress Report, March 1 - Aug. 31, 1976; Dynatherm Corp., Cockeysville, Md., Energy Research and Development Administration, Nov. 1976.
202. Bienert, W. B., and Wolf, D. A., "Heat Pipe Applied to Flat-Plate Solar Collectors," Final Report, Dynatherm Corp., Cockeysville, Md., Energy Research and Development Administration, May 1976.
203. "Design and Analysis of a Cryogenic Variable Conductance Axial Grooved Heat Pipe," B & K Engineering, Inc., Towson, Md., March 1976.
204. Blaser, P., Hauser, G., and Strittmatter, R., "Development and Qualification of PCM Thermal Capacitors. Part II. Development of PCM Thermal Capacitor Platforms and PCM Thermal Capacitor Radiators," Dornier-System G.M.B.H., Friedrichshafen (West Germany), Dec. 1976.
205. Chi, S. W., "Heat Pipe Theory and Practice," McGraw-Hill Publishing Co., New York, 1976.
206. Colwell, G. T., "Prediction of Cryogenic Heat Pipe Performance," Annual Report, 1975, Georgia Inst. of Tech., Atlanta, School of Mechanical Engineering, Feb. 1, 1976.
207. Corley, R. D., "Heat Transfer Analysis of a Rotating Heat Pipe Containing Internal, Axial Fins," Master Thesis, Naval Postgraduate School, Monterey, Calif., June 1976.
208. Depau, J. F., Reader, K. E., and Staskus, J. V., "Test Program for Transmitter Experiment Package and Heat Pipe System for Communications Technology Satellite," NASA Lewis Research Center, Nov. 1976.
209. Deverall, J. E., and Keddy, E. S., "Helical Wick Structures for Gravity-Assist Heat Pipes," Los Alamos Scientific Lab., N. Mex., 1976.
210. Dunn, P., Reay, D. A., "Heat Pipes," University of Reading, England and International Research and Development Co., Ltd., Newcastle-Upon-Tyne, England, 1976.
211. Eninger, J. E., and Edwards, D. K., "Computer Program Grade 2 for the Design and Analysis of Heat Pipe Wicks," TRW Defense and Space Systems Group, Redondo Beach, Calif., Nov. 1976.
212. Enginer, J. E., Luedke, E. E., and Wanous, D. J., "Flight Data Analysis and Further Development of Variable Conductance Heat Pipes for Aircraft Control," TRW Systems Group, Redondo Beach, Calif., Feb. 1976.
213. Eninger, J. E., Edwards, D. K., and Luedke, E. E., "Flight Data Analysis and Further Development of Variable Conductance Heat Pipes," TRW Systems Group, Redondo Beach, Calif., Nov. 1976.
214. Eninger, J. E., Fleischman, G. L., and Luedke, E. E., "Heat Pipe Materials Compatibility," (Final Report), TRW Systems Group, Redondo Beach, Calif., Jan. 1976.
215. Feldman, K. T., "Investigation of Performance Limits in Axial Groove Heat Pipes," (Final Report) New Mexico Univ., Albuquerque, Dept. of Mechanical Engineering, July 1976.
216. Ferrara, A. A., and Yenetchi, G., "Prevention of Preferential Bridge Icing Using Heat Pipes," (Final Report Aug. 1975 - Sept. 1976) Grumman Aerospace Corp., Bethpage, N.Y., Sept. 1976.

1976 - Continued

217. Fivel, H. J., and Lang, G. P., "Graphite Curtain Vacuum Outgassing and Heat Transfer," (Quarterly Progress Report No. 3, July 1, 1976 - Sept. 30, 1976), McDonnell-Douglas Astronautics Co., St. Louis, Mo., Energy Research and Development Administration, 1976.
218. Galzin, F., "Faust Program Heat Pipe Experiment: General Summary of Flight Results Experience," Centre National d'Etudes Spatiales, Toulouse (France), Oct. 1976.
219. "Analysis and Tests of NASA Coverted Groove Heat Pipe," (Final Report), Grumman Aerospace Corp., Bethpage, N. Y., Dec. 1976.
220. Hage, M., "IKEPIPE - A Programme for the Calculation of Heat Pipes," Stuttgart Univ. (West Germany), Inst. fuer Kernenergetik, July 1976.
221. Haller, F. B., Hessel, M. M., Neef, W., Lai, W., and Lohr, H., "Concentric Heat Pipe Cavity for E-Beam Excited Lasers," California Univ., Livermore, Lawrence Livermore Lab., 1976.
222. Harwell, W., and Canaras, T., "Transient Thermal Response of a Thermal Control Canister," NAS5-22570, Grumman Aerospace Corporation, Bethpage, N. Y., 1976.
223. Hermann, E., Koch, H., Kreeb, H., and Perdu, M., "Handbook of Grooved Heat Pipes," (Final Report), Dornier-System G.M.B.H., Friedrichshafen (West Germany), Dec. 1976.
224. Jen, H. F., and Kroliczek, E. J., "User's Manual for Groove Analysis Program (GAP)," BK012-1007, B & K Engineering, Inc., June 1976.
225. Kemme, J. E., "Vapor Flow Considerations in Conventional and Gravity-Assist Heat Pipes," Los Alamos Scientific Lab., N. Mex., 1976.
226. Kirkpatrick, J. P., and Groll, M., "Heat Pipes for Spacecraft Temperature Control: An Assessment of the State-of-the-Art," NASA Ames Research Center, Moffett Field, Calif., Jan. 1976.
227. Koenig, D. R., "Heat Pipe Nuclear Reactor for Space Power," Los Alamos Scientific Lab., N. Mex., 1976.
228. Kroliczek, E. J., "Heat Pipe Heat Rejection System for Electrical Batteries," (Final Report), Dyantherm Corp., Cockeysville, Md. 1976.
229. Molt, W., "Calculation of the Major Material Parameters of Heat Carriers for Cryogenic Heat Pipes," Stuttgart Univ. (TH) (Germany, F. R.), Inst. fuer Kernenergetik, July 1976.
230. Molt, W., "Studies on Capillary Structures with Regard to Their Use in Cryogenic Heat Pipes," Stuttgart Univ. (TH) (Germany, F.R.), Inst. fuer Kernenergetik, July 1976.
231. Muenzel, W. D., "Performance Evaluation of the ESA Heat Pipes Included in the International Heat Pipe Experiment (IHPE)," (Final Report), June 1976.
232. "Heat Pipe Technology. A Bibliography with Abstracts," New Mexico Univ., Albuquerque, Technology Application Center, 1976.
233. Ranken, W. A., "Ceramic Heat Pipe Heat Exchangers," Los Alamos Scientific Lab., N. Mex., Sept. 1976.
234. Ranken, W. A., "Potential of the Heat Pipe in Coal Gasification Processes," Los Alamos Scientific Lab., N. Mex., 1976.

1976 - Continued

- 235. Reed, W. E., "Heat Pipes," Volume 1, 1970 - 1973 (Citations from Engineering Index), National Technical Information Service, Springfield, Va., March 1976.
- 236. Reed, W. E., "Heat Pipes," Volume 2, Feb. 1974 - 1976 (Citations from Engineering Index), National Technical Information Service, Springfield, Va., March 1976.
- 237. Reed, W. E., "Heat Pipes," Volume 1, 1964 - 1972 (Citations from the NTIS Data Base), National Technical Information Service, Springfield, Va., March 1976.
- 238. Reed, W. E., "Heat Pipes," Volume 2, Feb. 1973 - 1976 (Citations from the NTIS Data Base), National Technical Information Service, Springfield, Va., March 1976.
- 239. "Flexible Cryogenic Heat Pipe Development," (Final Report) Rockwell International Corp., Downey, Calif., Space Div., July 1976.
- 240. Saaski, E. W., and Hanson, R. J., "An Investigation of Condensation Heat Transfer in a Closed Tube Containing a Soluble Non-Condensable Gas," Washington State Univ., Pullman Dept. of Computer Science, 1976.
- 241. Saaski, E. W., "Heat Pipe Temperature Control Utilizing a Soluble Gas Absorption Reservoir," Sigma Research, Inc., Richland, Wash., Feb. 1976.
- 242. Sellers, J. P., "Heat Pipe Radiators for Space," (Annual Report), Tuskegee Inst., Ala. School of Mechanical Engineering, Jan. 1976.
- 243. Wagenseil, L. L., "Heat Transfer Performance of Various Rotating Heat Pipes," Naval Postgraduate School, Monterey, Calif., Dec. 1976.
- 244. Wright, J. P., and Wilson, D. E., "Development of Thermal Control Methods for Specialized Components and Scientific Instruments at Very Low Temperatures," (Final Report, March 31 - Nov. 1976), Rockwell Int'l. Corp., Canoga Park, Calif., Space Div., Nov. 1976.

1977

- 245. Arcella, F. C., "The Heat Pipe Heat Bridge and Thermal Controller," AIAA 12th Thermophysics Conference, Albuquerque, N. Mex., June 27-29, 1977.
- 246. Beam, J. E., and Mahefkey, T., "Demonstration Testing of a Vuilleumier Cryocooler with an Integral Heat Pipe/Thermal Energy Storage Unit," (Final Report Sept. - Dec. 1976) Air Force Aero Propulsion Lab, Wright-Patterson AFB, Ohio, June 1977.
- 247. Bienert, W. B., Ducao, A. S. and Trimmer, D. C., "Development of a Jet Pump-Assisted Arterial Heat Pipe," (Final Report) Dynatherm Corp., Cockeysville, Md., May 6, 1977.
- 248. Brennan, P. J., Kroliczek, E. J., Jen, H., and McIntosh, R., "Axially Grooved Heat Pipes - 1976," AIAA 12th Thermophysics Conf., Albuquerque, N. Mex., June 27-29, 1977.
- 249. Camarda, C. J., "Analysis and Radiant Heating Tests of a Heat Pipe Cooled Leading Edge," NASA Langley Research Center, Langley Station, Va., Aug. 1977.
- 250. Deverall, J. E., "Gas-Interface Studies in Large Horizontal Heat Pipes," Los Alamos Scientific Lab., N. Mex., Jan. 1977.
- 251. "Design and Development of a Heat Pipe Diode," (Final Report) Institut Fuer Kernenergetik, Univ. of Stuttgart (West Germany) July 1977.
- 252. Jacobson, D. L., "Material Selection Considerations for Fluoride Thermal Energy Storage Containment in a Sodium Heat Pipe Environment," (Final Report June 1 - Aug. 1976) Purdue Univ., Lafayette, Ind., May 1977.

1977 - Continued

253. Jen, H., and Kroliczek, E. J., "Summary Report for Axially Grooved Heat Pipe Study," NAS5-22562, B & K Engineering, Inc., July 1977.
254. Kelleher, M. D., "Effects of Gravity on Gas-Loaded Variable Conductance Heat Pipes," (Final Report for FY 75-76) Naval Postgraduate School, Monterey, Calif., March 25, 1977.
255. Koenig, D. R., Ranken, W. A., and Salmi, E. W., "Heat Pipe Reactors for Space Power Applications," Los Alamos Scientific Lab., N. Mex., 1977.
256. Kreeb, H., "Design and Development of a Gas Controlled Heat Pipe Radiator for Communication Spacecraft Applications, Phase 2," Dornier-System, G.M.B.H., Friedrichshafen (West Germany), Feb. 1977.
257. Kroliczek, E. J., Yuan, S. W. and Bloom, A. M., "Application of Heat Pipes to Ground Storage of Solar Energy," AIAA 12th Thermophysics Conf., Albuquerque, N. Mex., July 27-29, 1977.
258. Lehtinen, A. M., "Controllability Analysis for Passively and Actively Controlled Heat Pipes," AIAA 12th Thermophysics Conf., Albuquerque, N. Mex., June 27-29, 1977.
259. Loehrke, R. I., "An Investigation of Electrohydrodynamic Heat Pipes," (Final Report), Colorado State Univ., Fort Collins Dept. of Mechanical Engineering, March 1977.
260. "Thermal Control of Power Supplies with Electronic Packaging Techniques Using Low Cost Heat Pipes," (Final Report) Martin Marietta Corp., Denver, Colo., Feb. 1977.
261. McKee, H. B. and Steele, W. H., "A Precise Satellite Thermal Control System Using Cascaded Heat Pipes," AIAA 12th Thermophysics Conf., Albuquerque, N. Mex., June 27-29, 1977.
262. "Heat Pipe Technology. A Bibliography with Abstracts," (Quarterly Reports) New Mexico Univ., Albuquerque, Technology Application Center, NASA, Washington, D. C. 1977.
263. Owendoff, R. S., "Gravitational Effects on the Operation of a Variable Conductance Heat Pipe," Naval Postgraduate School, Monterey, Calif., March 1977.
264. Reed, W. E., "Heat Pipes," Volume 2, Feb. 1973 - 1976 (Citations from the NTIS Data Base), National Technical Information Service, Springfield, Va., May 1977.
265. Reed, W. E., "Heat Pipes," Volume 2, March 1974 - 1977 (Citations from the Engineering Index Data Base) National Technical Information Service, Springfield, Va., May 1977.
266. Reed, W. E., "Heat Pipes," Volume 3, March 1976 - 1977 (Citations from the NTIS Data Base) National Technical Information Service, Springfield, Va., May 1977.
267. Richter, R., "Thermal Energy Storage Demonstration Unit for Vuilleumier Cryogenic Cooler," (Interim Report June 2, 1975 - Aug. 31, 1976) Xerox Corp./ Electro-Optical Systems, Pasadena, Calif., Feb. 1977.
268. Roberts, C. C., "A Zero-G Variable Conductance Heat Pipe Using Bubble Pump Injection," AIAA 12th Thermophysics Conf., Albuquerque, N. Mex., June 27-29, 1977.
269. Saaski, E. W., and Hamasaki, R. H., "Study of a High Performance Evaporative Heat Transfer Surface," *SIGMA Research, Inc., Richland, Wash., May 27, 1977, *NAS2-9120.
270. Tantrakul, C., "Condensation Heat Transfer Inside Rotating Heat Pipes," Naval Postgraduate School, Monterey, Calif., June 1977.

1977 - Continued

271. Tower, L. K., and Kaufman, W. B., "Accelerated Life Tests of Specimen Heat Pipe from Communication Technology Satellite (CTS) Project," NASA Lewis Research Center, Dec. 1977.
272. "Study of an Sln-Test Platform for Thermal Components (Heat Pipes and Latent Heat Accumulators)," Transemantics, Inc., Wash., D. C., March 1977.
273. Vasilyev, L. L., and Konev, S. V., "Heat Transmitting Tubes," Foreign Technology Div., Wright-Patterson AGB, Ohio, March 17, 1977.
274. Wayner, P. C., Jr., "The Effect of the Liquid-Solid System Properties on the Interline Heat Transfer Coefficient," Rensselaer Polytechnic Inst., Aug. 1977.
275. Williams, R. J., "Parametric Performance of a Spiral Artery, Liquid-Trap-Diode Heat Pipe," NASA Ames Research Center, Oct. 1977.
276. Wright, J. P., "Flexible Cryogenic Heat Pipe Development Program," NAS2-8830, Rockwell Int'l., Space Division, Downey, Calif., July 1977.

1978

277. "3rd International Heat Pipe Conference Proceedings, May 22-24, 1978," American Institute of Aeronautics and Astronautics.